

# AGARD

ADVISORY GROUP FOR AEROSPACE RESEARCH & DEVELOPMENT

7 RUE ANGELLE 92 NEUILLY SUR SEINE FRANCE

AD 688921

## The Aerodynamics of V/STOL Aircraft



MAY 1968

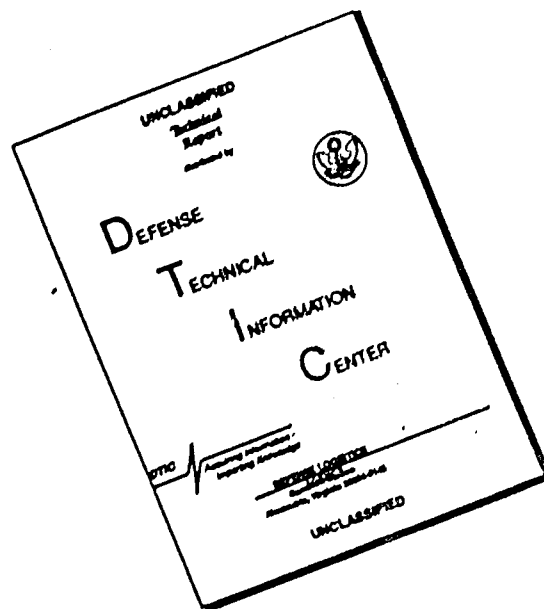
*Handwritten signature or initials.*

NORTH ATLANTIC TREATY ORGANIZATION



This document is for publication distribution

# DISCLAIMER NOTICE



THIS DOCUMENT IS BEST QUALITY AVAILABLE. THE COPY FURNISHED TO DTIC CONTAINED A SIGNIFICANT NUMBER OF PAGES WHICH DO NOT REPRODUCE LEGIBLY.

**BLANK PAGES  
IN THIS  
DOCUMENT  
WERE NOT  
FILMED**

NORTH ATLANTIC TREATY ORGANIZATION  
ADVISORY GROUP FOR AEROSPACE RESEARCH AND DEVELOPMENT  
(ORGANISATION DU TRAITE DE L'ATLANTIQUE NORD)

THE AERODYNAMICS OF V/STOL AIRCRAFT

These Papers were presented at a Lecture Series jointly sponsored  
by AGARD and the von Kármán Institute, held at the Institute,  
Rhode-Saint-Genèse, Belgium, May 13-17, 1968.



533.652.6



*Printed by Technical Editing and Reproduction Ltd  
Harford House, 7-9 Charlotte St. London. W1P 1HD*

## FOREWORD

This publication contains the lecture notes prepared for the AGARD-VKI Lecture Series on "The Aerodynamics of V/STOL Aircraft" which took place at the von Kármán Institute, Rhode-Saint Genèse, Belgium, from May 13 to 17, 1968.

The lecture series was designed to provide an up-to-date account of special aerodynamic problems and aerodynamic requirements for V/STOL aircraft, including a discussion of the present state of knowledge, novel aerodynamic advances, important areas for research and development, experimental and theoretical treatments as well as immediate and long-term V/STOL aircraft prospects. It was intended for aeronautical engineers with a need to acquire a more adequate background on V/STOL aerodynamics.

The course was divided into nine sessions of approximately a half day each. The introductory session was followed by seven lectures dealing with the different types of V/STOL aircraft classified on the basis of their lifting system and with the problems of model and flight testing. The last session, introduced with an informal talk on the critical factors for the specification and assessment of V/STOL aircraft, was organized as a seminar with the participation of the audience.

The lecture series was well attended as regards both the number and the quality of the participants. Ninety-nine people representing ten different countries registered at VKI for the course, which was organized under the auspices and with the support of AGARD, in collaboration with the von Kármán Institute who had the responsibility for the general administration and local organization.

We are grateful to Messrs. Ph. Poisson-Quinton, M. Wanner and G. Ville of France with whom discussions at an early stage were very useful in the formulation of the final programme.

A special tribute must be paid to the lecturing staff not only for the quality of their presentations and the comprehensive and valuable information contained in their lecture notes but also for making these notes available for reproduction in time for them to be distributed to the participants at the start of the course.

Our thanks also go to the official and private organizations through whose courtesy it was possible to form a distinguished group of lecturers.

The Course Directors

P. E. Colin and J. Williams  
V. K. I.                      R. A. E.

## CONTENTS

	Page
<b>FOREWORD</b>	<b>iii</b>
<b>PAPER</b>	
<b>A INTRODUCTION TO V/STOL AIRCRAFT CONCEPTS AND CATEGORIES'</b> by Ph. Poisson-Quinton (France)	<b>1</b>
<b>B PURE AND COMPOUND HELICOPTERS</b> by P. F. Yaggy (USA)	<b>51</b>
<b>C BASIC AERODYNAMICS OF CONVERTIBLE ROTOR/PROPELLER AIRCRAFT</b> by W. Z. Stepniewski (USA)	<b>149</b>
<b>D AERODYNAMICS OF SHROUDED PROPELLERS</b> by M. Lazareff (France)	<b>237</b>
<b>E TURBO-JET/TURBO-FAN AIRCRAFT</b> by J. Williams (UK)	<b>291</b>
<b>F BOUNDARY LAYER AND CIRCULATION CONTROL FOR STOL AIRCRAFT</b> by F. Thomas (Germany)	<b>349</b>
<b>G TECHNIQUES FOR THE AERODYNAMIC TESTING OF V/STOL MODELS</b> by W. J. G. Trebble (UK)	<b>383</b>
<b>H FLIGHT TESTING AND V/STOL HANDLING REQUIREMENTS</b> by P. F. Yaggy (USA)	<b>429</b>

PAPER A

INTRODUCTION TO V/STOL AIRCRAFT CONCEPTS AND CATEGORIES

by

Ph. Poisson-Quinton

ONERA, France

## INTRODUCTION TO V/STOL AIRCRAFT CONCEPTS AND CATEGORIES

Ph. Poisson-Quinton

### 1. INTRODUCTION

For fifteen years, considerable low-speed research has been directed towards V/STOL aircraft\*, i.e. machines able to take-off from and to land on a very small area, like an unprepared field. Typically, such a simple air strip is assumed to be bounded by some 50 ft obstacles, and to have lengths less than 500 ft for VTOL configurations, or less than 1000 ft for true STOL aircraft.

Much money has been spent in many countries, on wind-tunnel studies and on the development of various flight research vehicles. At least fifty different projects have reached the flight-test stage; but many of these V/STOL configurations have barely reached the exploratory flight stage, and also many have crashed. Some reasons for such poor results are well known by the aerodynamicist<sup>1</sup>.

First of all, this type of aircraft, during vertical and transition flight and also near the ground, is much more difficult to handle than aircraft in conventional flight, because of novel aerodynamic interactions. It is very difficult to predict the amount of power required to control the aircraft when hovering and during the transition flight. It is mandatory to develop sophisticated ground simulators to solve a part of this problem, preferably complemented by special experimental VTOL machines, equipped with a variable stability system in flight, such as the X-14 and the X-22 in the U.S.A.

Another reason lies in the difficulties found in predicting the flight behaviour from tests on a scaled model in a wind-tunnel. A realistic simulation of the rotor/propeller or lift-engines is difficult, and the force measurements require a very sophisticated instrumentation. Moreover, the model size must be small compared with the tunnel size, to preclude significant wall effects because of the considerable amount of energy released by the lifting devices. For this reason new large wind-tunnels, of at least 20 ft working-section and specially equipped for V/STOL tests, are being designed and built in several countries (see References 1 and 2). The so-called "full-scale tunnels", like those of Ames and Langley at NASA, or Chalais-Meudon at ONERA, are also used for semi-free flight tests on small dynamically similar V/STOL models<sup>3</sup>.

Lastly, the V/STOL aircraft safety depends much more on the engine and transmission system reliability than with conventional aircraft, as confirmed by several prototype accidents. Some of the new problems arising with V/STOL configurations are given in Figure 1. Nevertheless, flight experience gained with so many V/STOL configurations over the past fifteen years, has led to a better understanding of many specific problems. These include the importance of noise and vibration levels, ground erosion and debris ingestion during a vertical take-off and landing, needs for auto-pilot devices and instrument landing aids, minimum control power requirements as a function of the configuration and size, minimum handling qualities requirements, etc.

---

\* VTOL = Vertical take-off and landing (ADAV in French).

STOL = Short take-off and landing (ADAC in French).

Now, we have reached the beginning of a second generation of V/STOL projects designed to satisfy a vital need for new types of vehicles with a full "air mobility" and able to use very short airfields, both for military and civil purposes. These machines must take advantage of the technological progress foreseen during the next decade on gas-turbines, on structures and materials, and also on automatic control and guidance.

In the meantime, the aerodynamicist must define the best configurations for each mission, combining the vertical ability with a good cruise efficiency. Part of the difficulty is that there are too many ways of solving the problem, and that all of these seem to have at least some promise. This leaves the designer with a perplexing array of alternatives:

Should the aircraft use rotors, propellers, ducted fans, or turbo-jets?

How should the engines and lifting devices be arranged?

Should the same engines be used for the hovering mode and for forward flight, or should they be separate?

How will the aircraft be controlled during hover and transition?

These are the alternatives and arguments that will be discussed during the lecture series. As a preliminary, I must now explain some very basic elements of the V/STOL principles, and present the whole spectrum of the V/STOL field.

A typical classification of the various types of V/STOL configurations<sup>4</sup> takes account of their ability in vertical flight, and of the methods used to perform the transition to horizontal flight (Fig. 2).

We can specify four methods for hovering flight, using respectively: large rotors, free propellers, ducted fans, and jet-engines (with or without by-pass systems).

To perform the transition between hovering and cruise, four methods are available: aircraft tilting, tilting thrust, thrust vectoring, and separate propulsion.

For each item, a brief description follows later of typical experimental machines already tested in flight.

## 2. VERTICAL LIFT GENERATORS

### 2.1 Basic Relations

For every machine able to lift a given load off the ground by means of some engine thrust, it is essential to estimate the price of this vertical thrust, i.e. the power required (Fig. 3). Our reference power will be the ideal power required  $P_i$ , to generate this thrust  $T$ , by means of a jet with a uniform slipstream velocity  $V_s$ , and emerging from a given section  $S_s$ .

If the losses are negligible, the power is transferred into an axial kinetic energy:

$$P_i = \frac{1}{2} q_m V_j^2, \quad \text{with} \quad q_m = \rho S_s V_s,$$

$$\text{or} \quad P_i = \frac{1}{2} \rho S_s V_s^3 \quad (1)$$

On the other hand, the thrust  $T$  is equal to the momentum change:

$$T = q_m V_s = \rho V_s^2 S_s. \quad (2)$$

From Equations (1) and (2), we can deduce the specific thrust:

$$T/P_1 = 2/V_s . \quad (3)$$

This basic equation demonstrates a very fundamental fact, namely that from a *hovering efficiency standpoint*, it is necessary to accelerate slowly a large mass of air, as for example with a helicopter rotor ( $V_s \approx 25\text{m/sec}$ ). On the other hand, a conventional jet engine is very expensive for this purpose, because of its high jet velocity ( $V_s \approx 600\text{m/sec}$ ), while a rocket is even worse ( $V_s \approx 2,500\text{m/sec}$ ). On the graph of Fig. 3, we have plotted the mean values ( $T/P_1, V_s$ ) relative to various types of VTOL, to show that our domain of interest is very large and covers two orders of magnitude; specific thrust from 5 to 0.05kg/HP and slipstream velocity from 25 to 2500m/sec.

From Equation (2), we see also that the jet dynamic pressure is proportional to the slipstream area loading  $T/S_s$  :

$$q_s = \frac{1}{2}\rho V_s^2 = \frac{1}{2}(T/S_s) . \quad (4)$$

We shall see that many troubles near the ground, for example erosion, debris and hot gas reingestion, aerodynamic interactions on the airframe, etc, are directly functions of this slipstream dynamic pressure.

For the case of a rotor or of a *free propeller*, there is a jet contraction behind the actuator disc (Fig. 4), and the well known Froude relation shows that the slipstream velocity is twice the mean velocity through the rotor disc,  $V_s = 2V_R$ , and that  $S_s = S_R/2$ .

For a *ducted propeller* (or fan), the slipstream velocity is equal to, or less than, the fan velocity, depending on the diffuser ratio  $\sigma = S_s/S_R$ . On Figure 4, it is shown that theoretically a ducted fan has a better hovering efficiency than a free propeller, even without diffuser effect (see M. Lazareff paper).

To estimate the hovering efficiency, a *figure of merit M* is defined by the ratio of ideal power  $P_1$  to actual power  $P$  (Fig. 5), and from the previous equations. It is easy to find the relationship between the specific thrust  $T/P$  (kg/HP) and the area loading relative to the slipstream  $T/S_s$  (kg/m<sup>2</sup>) or to the disc area  $T/S_R$ ; the specific thrust decreases as the inverse of the square root of the area loading. Figure 5, plotted in logarithmic coordinates, shows that the price that has to be paid for hovering flight (i.e. the amount of horse-power for a given load lifted) increases very rapidly with the disc loading. On this graph, we have also plotted various experimental values relevant to several VTOL research aircraft, to show that the effective mean value of the figure of merit is about  $M \approx 0.75$ .

## 2.2 Lift Amplification

Various methods are available for the amplification of the thrust of a gas generator:

1. Reheating the exhaust gas to increase the exit velocity (i.e. the jet momentum) for a given mass flow. This is an expensive process, because of the high fuel consumption, and can be quite dangerous for a VTOL aircraft near the ground because of the high temperatures and velocities.
2. Using the exhaust gas as primary flux in an ejector (jet pump). This process is not very efficient and too voluminous; e.g. Lockheed XV-4A.
3. Using the gas generator to drive a second stage turbine connected to a fan or a rotor:

It is very instructive, following a Stepniewski<sup>5</sup>, to illustrate this third method with a crude scheme, to show the importance of such a by-pass system. On Figure 6, the same gas generator is used directly as a lift engine (A), or to drive a turbine connected for

example to a ducted fan (B) or to a rotor (C). With the simplified assumption given on this figure, i.e. exhaust velocity at the exit of the turbine equal to the slipstream velocity, it is easy to show that the thrust augmentation of a given by-pass system is a function of the by-pass ratio and of the resultant slipstream velocity. This thrust amplification is very large for a rotor;  $V_s \approx 35\text{m/sec}$  gives a by-pass ratio  $q_R/q_t \approx 200$ , and a resultant thrust twelve times the direct engine thrust. For a ducted fan with  $V_s \approx 140\text{m/sec}$ , we have still  $q_R/q_t \approx 13$  and  $T/T_t \approx 3.2$ ; these figures correspond roughly to those for the fan-in-wing configuration Ryan XV-5A. In these examples, the power turbine and aerodynamic efficiencies are arbitrarily taken equal to 0.85.

The next step is to look at the *fuel consumption during the hovering flight*, a fundamental criterion to estimate the relative usefulness of various VTOL configurations. For a given thermal efficiency, e.g.  $\eta_{th} = 0.25$ , and with the conventional kerosene heat value, it is easy to calculate the specific fuel consumption  $C_s = q_F/T$  as a function of the slipstream velocity. Figure 6 shows that  $C_s$  increases very rapidly with  $V_s^{(*)}$ , from  $C_s \approx 0.3$  for a ducted fan ( $V_s \approx 140\text{m/sec}$ ) to  $C_s \approx 1\text{kg/kg thrust/hr}$  for a conventional jet lift engine ( $V_s \approx 610\text{m/sec}$ ).

However, for practical application, two other important factors have to be taken into account; the weight of the overall propulsive system, and the volume occupied by this propulsive system. Unfortunately, these two factors increase with the by-pass ratio. In fact, a rocket engine is the most attractive from this point of view!

Thus, the useful efficiency of a lifting system must be judged by the ratio (vertical-thrust)/(engine weight + hover fuel), as a function of the hovering duration. The balance between propulsive system weight and the specific fuel consumption is illustrated on Figure 8. The higher  $C_s$  value for a jet VTOL is compensated by a lower engine weight, to give a better total weight (propulsive system + fuel) if the hovering time is very short. On the other hand, the helicopter configuration is the best solution when the hovering time is large, for example as for a rescue mission. Figure 9 shows another aspect of this problem for a transport/cargo VTOL aircraft, with two basic mission requirements: 8 minutes of hover and 1.5 hour of cruise regime. The partial weights for bare engines and propulsive system auxiliaries are given, along with hover and cruise fuel weights, as a percentage of aircraft gross weight, for various VTOL configurations. Here again, the hover fuel weight increases and the propulsive system weight decreases in passing from the rotor to the lift jet configurations. On this graph, it is also interesting to note another fundamental criterion of the VTOL efficiency: namely the *cruise speed*. Here the conventional helicopter configuration cannot compete with the turbo-jet VTOL solution, for which the cruise speed is about the same as a conventional subsonic jet aircraft. But we have to pay for the VTOL capability by a large reduction of the payload.

Nevertheless, it is already possible to predict a very large improvement in engine weight and volume and also in the specific fuel consumption, during the next decade, due to technological progress on materials and on internal aerodynamics. Some typical trends are illustrated in Figure 10<sup>6, 13, 19</sup>.

### 3. TRANSITION FLIGHT

The transition regime, from hovering to cruising flight, is usually the most critical for VTOL aircraft; this is defined as the speed range between hovering and a minimum speed at which the aircraft can fly on the wing lift alone, without using lift augmentation from its engines<sup>7</sup>: a tentative classification of various methods for performing transition

(\*) A "Specific impulse", given in seconds ( $I_s = 3600/C_s$ ), is generally used for the rockets; it is interesting to note that, for the best liquid rocket,  $I_s \approx 400$  sec, in comparison with  $I_s \approx 60,000$  sec for a rotor system!



with a VTOL aircraft has already been shown in Figure 2. Such methods comprise aircraft tilting, thrust tilting, thrust deflection, and dual propulsion. Moreover, there are two distinct families of VTOL, the one using the *same thrust generator* for hovering and cruising flight, and the other using *two independent thrust generators* for this purpose. The following table overleaf gives a list of all the combinations already studied. Some of these configurations are also illustrated in Figures 11-13<sup>8,9,10,12,13,15,20</sup>.

The power required during transition varies enormously with air-speed, and this represents a fundamental characteristic of VTOL aircraft. The power is greatest for the hovering and top speed conditions, dropping to a minimum at a speed between one-third and one-half the top speed (Fig.14). The transition flight corresponds to that portion of the speed range from hovering to the speed for minimum power required. As previously, the power required for hovering flight can be defined as a function of the slipstream velocity from the propulsion system (see Figure 5):

$$P_{st} = W^{3/2}/2M\sqrt{\rho S_g} .$$

The power required in forward flight (Fig.14) is the sum of the power required to overcome the induced drag, namely:

$$P_i = 2(W/b)^2/\pi\rho V_0\eta e ,$$

and that required to overcome the form and parasitic drag:

$$P_D = C_{D0}\rho S V_0^3/2\eta .$$

The induced drag can be reduced by using a wing of large aspect-ratio; but it is also important to have the spanwise lift distribution as uniform as possible during the transition regime, so as to reduce the induced power required between hovering and minimum power speed<sup>9</sup>. A good load distribution can be obtained by spreading the lift induced by the propulsive system along the span, as with a tilt wing, deflected slipstream, or jet-flap configuration. In contrast, jet lift or tilting ducted-fan configurations usually have poor load distributions, i.e. larger induced drag, and necessitates more thrust during transition (Fig.15(a)). Naturally, such VTOL configurations also tend to have poor STOL performance. The shape of the power curve over the transition regime is very important as regards flight safety and STOL operation.

Figure 15(a) gives two typical curves  $(P, V_0)$  relative to tilt-wing and tilting-duct twin-engined configurations. If the machines have barely enough power to hover with both engines operating (1.10  $P_T$  required, for example), and if one engine fails during low-speed flight, the machine must lose altitude until the speed reaches that where flight becomes possible on one engine alone. This speed is much lower for the tilt-wing configuration because of the lower induced drag. On the other hand, if the aircraft are overloaded so that they cannot take off vertically, they effectively become STOL aircraft. For take-off, the machines must run along the ground until they reach the speed at which the power required for level flight has decreased enough to become equal to the power available. Here again, the tilt-wing configuration requires a much lower take-off speed<sup>9</sup>.

#### 4. CRUISE PERFORMANCE OF VTOL CONFIGURATIONS

V/STOL aircraft, for both military and commercial use, will need good cruise performance, i.e. good aerodynamic cleanness to minimise parasitic drag, together with a good load distribution and a large aspect-ratio wing to ensure low induced drag. But this is not an easy matter for V/STOL configurations primarily designed to satisfy hovering requirements. Such poor cruise efficiency is illustrated on Figure 15(b), where we have plotted the values of specific power versus the cruise speed, for existing helicopters, low-wing loading STOL aircraft, conventional jet transports, and various other VTOL and

## A) Same Thrust Generator

## A.1) Tilt fuselage

Rotors (Helicopters, conventional or unloaded)  
 Propellers (U.S. Convair XFY1, Lockheed XFY1)  
 Ducted fans (Various "flying jeeps")  
 Jets (U.S. Ryan X13, Fr. Coleopter)

## A.2) Tilt thrust

Rotors (U.S. Bell XV.3)  
 Props (U.S. XC142 and VZ2; Can. CL-84)  
 Ducted fan (U.S. Doak VZ4 and Bell X-22)  
 Jets -

## A.3) Vectored thrust

Rotors  
 Props (U.S. Ryan VZ3 and Fairchild VZ5)  
 Ducted fans  
 Jets (U.S. Bell X14; G.B. Hawker P1127)

A.4) Vectored thrust  
augmentation

Gas gener. reheating (G.B. BS100 project)  
 Ejector system (U.S. Lockheed XV-4A)  
 Bypass System (U.S. Fan-in-Wing Ryan XV-5A)

## B) Independent Thrust Generators

## B.1) Separate functions

(lift generators for  
 hovering, cruise  
 generator for cruise)

(U.S. McDonnell XV1)  
 Rotors unloaded (U.S. Lockheed AH56A)  
 (G.B. Fairey Rotodyne)  
 " stopped (U.S. Hughes project)  
 " stowed (U.S. Lockheed project)

Props -

Ducted fans -

(G.B. Short SC-1)  
 Jets (Fr. Dassault Balzac and Mirage 3V)  
 (U.S. Lockheed XV-4B)

## B.2) Combined functions

(hovering with lift  
 generator +  
 tilting cruise  
 generator)

Jets (Germany. VJ-101C)

(hovering with lift  
 generator +  
 vectored cruise  
 generator)

(Germany. Dornier DO-31E)  
 Jets (It/G. VAK 191B)  
 (US/G. USFRG project)

STOL designs<sup>6</sup>. Here, the specific power S.P. is defined as the power available from the cruise engines (at cruise altitude and speed) divided by the gross weight times the cruise velocity:  $S.P. = P/WV_0$ . Furthermore,  $P/WV_0 = D_e V_0 / WV_0 = 1/(L/D_e)$  where  $D_e$  is the effective drag,  $L$  the lift, and  $L/D_e$  is the equivalent lift/drag ratio. On Figure 15(b) the high efficiency of conventional transports is implied by the low values of the specific power ( $L/D_e \approx 20$ ), and the poorest efficiency corresponds to the conventional helicopter ( $L/D_e \approx 4$ ) with a very limited cruise speed. The higher values of the specific power for the VTOL and STOL types are partly due to the higher levels of installed power, but also to the larger drag arising from extra volume, special devices for V/STOL performance, etc. The maximum speed of a conventional helicopter is mainly limited by aerodynamic difficulties on the rotor blades ( $C_{L_{max}}$  on the retreating blade, transonic drag rise on the advancing blade, etc.). However, the maximum aerodynamic efficiency ( $L/D_e$ ) arises before this maximum speed, and its value is very poor, as shown in Figure 16(a). Unloading the rotor by using some wing lift can give a better efficiency and, for a compound configuration at least, higher maximum speed (Fig. 16(b)).

Figure 16 also shows that the tilt wing/propeller configurations have much better cruise performance, but that their speeds are limited to about 300 knots, with an aerodynamic efficiency lower than for conventional transport aircraft. As regards jet-VTOL configurations, the cruise speeds depend essentially upon the available propulsive thrust. The conditions will vary according to the use of vectored thrust engine matching between hovering and cruise, separate cruise engine size, the absence or addition of re-heat for supersonic dash, etc. But the aircraft drag characteristics can also play a vital part, particularly as regards the Mach number limitations associated with transonic drag divergence, depending on the fuselage and nacelle cross sections, wing sweepback and thickness, parasitic drag, etc.

Nevertheless, high speed capability has already been demonstrated on several jet-VTOL configurations:

- With vectored thrust: XV5A fan-in-wing,  $M \approx 0.7$ ; P1127 with swivelling nozzles,  $M \approx 0.9$ .
- With independent thrust generators; VJ101C-X2,  $M \approx 1.4$ ; Mirage 3V,  $M \approx 2$ . Both have re-heat on the cruise engines.

Finally, another configuration, namely the tilt-rotor VTOL, seems to be able to reach quite high subsonic cruise speeds, with good hovering capability.

## 5. VTOL CONTROL SYSTEMS

Special hovering controls usually have to be provided in addition to the conventional controls for cruising flight (ailerons, rudder, and elevators), because the surfaces are completely ineffective during hovering flight unless they are immersed in the slipstream of the lift generators<sup>4</sup>. As the speed increases during transition flight, the conventional controls become more and more effective about the three axes (roll, yaw, pitch), and the special VTOL controls are progressively reduced in power by means of some mixing device for the two types of control.

During the VTOL phase, trim changes and rotations about the three axes can be achieved in a variety of ways, depending on the particular aircraft configuration; as shown on Figures 17 and 18. For example, the cyclic pitch changes on the helicopter blades are applied to move the centre-of-lift so as to produce rolling and pitching moments, the yawing moments being provided by the tail rotor. With VTOL aircraft incorporating lift units located some distance from the centre of gravity, differential variations or deflections of the thrust vectors are used for angular control about one or more axes. Furthermore, some auxiliary units located at the aircraft extremities can be employed to provide the appropriate moments; i.e. a tail rotor on helicopter for yaw and on tilt wing for

pitch; or control jets (supplied with compressor bleed air from the engines) at the wing tips and fuselage extremities for roll, pitch, and yaw (Hawker P1127, Bell X-14, Mirage 3V). In some cases, e.g. tilt wing aircraft, the ailerons used for roll in cruise also operate for yaw control during VTOL, when in the vertical propeller slipstream (Fig.19(a)). In other cases where separate thrust generators are employed, on aircraft like the DO-31E (Fig.19(b)), roll control is produced by differential throttling of the lift-engines at the wing-tips, yaw control by vectoring the engine efflux, and pitching moments by auxiliary jets at the tail.

## 6. HANDLING QUALITIES

Control, safety and handling considerations are intimately related to the performance limits of each specific configuration:-

Safety considerations for V/STOL aircraft require performance and control-path minima for the single-engine failure case. For most rotor, propeller and ducted-fan configurations, safety requirements necessitate absolute reliability of blades and transmissions, together with cross-shafting to distribute the available power after an engine failure; this is also true for STOL propeller aircraft, like the Breguet 941.

Dynamic or static instability problems exceeding the capacity of the control and stabilisation system, or of the pilot, have been the cause of many VTOL aircraft accidents; at least fifteen accidents have occurred during the last five years. Violent oscillatory instability arises with some VTOL configurations, which necessitates more complete understanding of the external aerodynamics and control dynamics in both the hovering and transition modes.

Handling qualities criteria and requirements have been studied over the past ten years by the AGARD Flight Mechanics Panel and the first recommendations given in AGARD TR-408 are currently being revised by a special FMP Committee, taking account of recent quantitative V/STOL data obtained in flight (experimental or variable stability aircraft, see Paper H by P.Yaggy, in this volume) and from ground simulators.

Handling quality requirements are generally presented as a plot of rate-damping (ratio of angular velocity damping to inertia of the aircraft, given in 1/sec) against maximum control power (i.e. control power/inertia ratio, in rad/sec<sup>2</sup>), with various boundaries for "desired" or "minimum acceptable" handling qualities. Instead of maximum control power, the control power per unit control deflection (or stick displacement), i.e. control sensitivity, is often used. Figure 20(b) gives some typical results obtained in hovering on several experimental NASA VTOL test-beds, for roll, pitch and yaw rotations. In general, pilots require much more damping and control power about the roll axis than about the other two, because they want increased aircraft response in roll to reduce the time required to correct deviations from a desired position.

Figure 20(c) gives control boundaries for the roll axis, obtained on a single-axis NASA simulator<sup>10</sup>. Here the Cooper scale rating represents a pilot opinion rating system, with numbers from 1 to 10, where a rating of 1 represents "ideal" characteristics and a rating of 10 "catastrophic" behaviour. The rating obtained from several NASA Flight Test pilots are in quite good agreement with the simulator evaluations.

Finally, Figure 20(d) shows that the maximum angular accelerations in roll obtained on several VTOL configurations are always higher than the recommended AGARD values, which prescribe that the control power can be reduced with increasing VTOL weight. In fact, the roll control must be powerful enough to serve a number of functions:-

Trimming the aircraft for aerodynamic, inertial and power plant asymmetries.

Controlling upset, i.e. maintaining attitude or position in gusty air and in ground-effect disturbances, etc.

### Manoeuvring the aircraft.

Although VTOL aircraft should if possible be made capable of being flown satisfactorily *without stability augmentation*, it seems highly desirable and sometimes mandatory to develop *auto-stabilisers* for improving the basic longitudinal and directional stability of VTOL aircraft. Such automatic stability and control devices can increase the pilot capabilities by making his job easier for the execution of specialised missions; e.g. flight in poor visibility, precise instrument approaches, passenger comfort, gun platform use, etc.

## 7. SOME INTERACTION PROBLEMS ON V/STOL AIRCRAFT

It is evident that the very high energy level developed by lift generators during hovering and transition flight *must* induce many aerodynamic and operational problems, and that their magnitude will depend on the particular VTOL aircraft configuration. Some problems are due to *induction effects* between the airframe and lift-generator slipstream *out of ground effect*; others arise when the aircraft is *in ground proximity*; moreover, the *noise problem* is always disturbing.

### 7.1 Aerodynamic Interactions out of Ground Effect

The induction effects due to very large slipstream momentum in the vicinity of the airframe can limit the flight envelope of VTOL aircraft, due to lift loss, or due to parasitic moments exceeding the available control power, or even due to the buffeting level. Figure 21(a) gives a typical example of the jet/airframe interaction arising with lift-jet VTOL aircraft (Mirage 3V family). The *loss of lift* due to suction forces on the lower side of the delta wing, induced by the 8 lift-engine efflux, increases with the transition speed. In fact, this lift loss itself is not too serious because, in the meantime, the wing aerodynamic lift can increase as the velocity squared. Of more significance, is the increasing *nose-up pitching moment* which can be difficult to trim if both the jet control and elevon power are marginal. Moreover, if sideslip (yaw angle) occurs during transition, a *rolling-moment* is developed because the lift loss is no longer the same on the port and starboard wings. Here again, this sideslip effect becomes catastrophic if the roll control power is insufficient to trim the increasing rolling moment and to *quickly stop* the induced roll oscillations.

In some other cases, such as tilt-wing configurations, a violent *buffeting* may limit the descent performance. Figure 21(b) shows that, for the original Vertol VZ-2 configuration, it was impossible to fly the aircraft in descent when a general separation of the flow on the wing upper-surface occurred; this arose because of the large angle-of-attack of the wing with insufficient propeller slipstream to preclude separation over the wing. The solution in this case was to improve the lifting capability of the wing by efficient trailing-edge flaps and to increase the wing stalling incidence by incorporating a cambered leading-edge or a slat. But even with such improvements, as later applied to the LTV XC-142A tilt wing aircraft (Fig. 22), the rate of descent is still limited by the tolerable level of *buffeting* (pilot and passenger comfort) and by *vibration* (airframe fatigue).

Many other examples of performance limitations due to poor flying qualities will be given in the following lectures for each type of VTOL aircraft.

### 7.2 Ground Interference Effects

These effects are very important for VTOL aircraft, because the slipstream or jet exhaust is directed straight downwards during vertical take-off and landing.

Aerodynamic interference of two types can arise near the ground, acting on the *thrust* of the lift generators and on the *airframe*, due to the effect of the slipstream: -

- (a) Figure 23(a) shows, for example, that the ground effect is favourable for a rotor because the slipstream fans out as the rotor approaches the ground (increasing pressure and decreasing velocity), so that there is a noticeable lift augmentation; this does not apply for a ducted propeller, when the thrust loss can induce a destabilising ground effect, as experienced in roll on the Doak 16 (Fig.23(c)).
- (b) The slipstream influence on the airframe depends upon the particular VTOL configuration, as illustrated in Fig.23(b)). The ground effect is *unfavourable* with several jet VTOL configurations, due to the induced negative pressures on the under surface of the wing. In contrast, this effect becomes *favourable* for the case where two propeller slipstreams induce positive pressures on the lower surface of the fuselage, for example. Such ground effects, both favourable and unfavourable, tend to disappear as forward speed is increased (see Figure 23(d)). Here with the STOL aircraft, the loss in lift is due to the forward flow along the ground.
- (c) Another problem, arising with the impingement of slipstreams on the ground and their reflection from the airframe surface, is that of *self-induced disturbances*. In ground effect, the aircraft motions are much greater than in still air, sometimes forcing the pilot to use full control about all three axes to maintain the aircraft attitude.

Erosion and reingestion problems<sup>11</sup> can be very significant for V/STOL aircraft hovering in ground effect. *Ground erosion* and the forces on objects in the vicinity are proportional to the outward flow of the air along the ground. As we have seen earlier, the slipstream dynamic pressure is proportional to the *disc loading*, so that erosion problems are much more severe for lift-jet VTOL configurations than for rotor or propeller types. But the ground erosion depends also on the *type of terrain* over which the aircraft is operating. Figure 24(a) gives some indication of the tolerance of various types of terrain to the dynamic pressure. *Debris ingestion* by the engine inlet is a problem for almost all the VTOL configurations; but *hot-gas reingestion* in the jet VTOL cases is more serious, because the increased inlet air temperatures cause an *engine thrust loss* near the ground; these problems are illustrated in Figure 24(b)).

### 7.3 V/STOL Noise

Naturally, aircraft engine noise represents a general problem, but tends to be much more severe for V/STOL configurations because they have very large installed power and also they often operate close to large groups of people<sup>6</sup>. Noise and ground erosion are related since reduction of the slipstream velocity will minimise both effects. Figure 25 gives a comparison of the estimated noise levels for all the VTOL aircraft family, in terms of "perceived noise" decibels. A "quiet" configuration is inevitably a machine with low thrust disc-loading (propeller deflected slipstream, tilt-rotor, or helicopter), but a method of reducing jet-VTOL noise is by *increasing the engine by-pass ratio* (fan-lift engines). To conclude, it is important to recall also that the noise below the take-off and the landing paths can be reduced by *steepening the climb-out and descent angles*, up to values about twice those in current use with conventional aircraft (Fig.25(b)).

## 8. SHORT TAKE-OFF AND LANDING AIRCRAFT

### 8.1 Aerodynamic Parameters

The ability of an STOL aircraft to operate from or into a small airfield essentially requires good low-speed performance<sup>16</sup>. Thus, we must first look at the aerodynamic parameters involved in STOL requirements for take-off and landing (Fig.26).

(a) Take-off

The ground-roll length is a function of installed thrust/weight ratio  $T/W$ , wing-loading  $W/S$ , usable wing lift coefficient  $C_{Lu}$ ; a safe take-off speed of  $1.2V_{stall}$  means  $C_{Lu} \cdot r_0 = C_{Lmax}/1.44$ .

The climb angle, i.e. the distance to clear a given obstacle height, is a function of  $T/W$  and of the lift/drag ratio  $L/D$  in the take-off configuration.

This climb capability must be available with one-engine out configurations to satisfy some given civilian or military requirements.

(b) Landing

The landing approach speed depends upon  $W/S$  and the usable lift coefficient  $C_{Lu}$ ; a safe approach speed requirement of  $1.3V_{stall}$  means  $C_{Lu} \cdot L = C_{Lmax}/1.69$ . Moreover, the air distance is also a function of the glide-slope, often fixed by the available instrument landing system (ILS).

The ground-roll is a function of the approach speed (i.e. of the approach  $C_{Lmax}$ ), but also of the efficiency of various braking devices (wheel brakes, reverse thrust from propellers or jet nozzles, spoilers, parachutes, etc), because this distance depends upon the rate of dissipation of kinetic energy at aircraft touchdown.

To cope with an abortive landing, the aircraft must be able to accelerate and climb away from the airfield; again, this depends on  $T/W$ ,  $W/S$ , and  $L/D$ .

At this point, it is interesting to bear in mind the *minimum safe approach speed* as a function of the wing loading, for a prescribed usable  $C_L$  (Fig. 27). On the same graph, we have plotted the values obtained in flight for several STOL aircraft and for light or jet-transport aircraft<sup>17</sup>, and the approximate airfield lengths required. The minimum safe speed depends also on available control at low speeds. For example, the speed at which the lateral control by conventional ailerons can be maintained in the event of an engine failure, on a twin-engined aircraft without cross-shafting, corresponds to a lift coefficient of about  $C_{Lu} \approx 2$ . A second limit exists for the longitudinal control with conventional horizontal tail and elevator system, at  $C_{Lu} \approx 5$ . Thus, the domain below the  $[C_L = 5]$  curve can be explored only by V/STOL aircraft which have special power-augmented controls. For these configurations, a large part of the aircraft weight is supported by the deflected thrust of the engines, while the aerodynamic wing-lift contribution becomes less and less important as the speed is reduced (down to zero for a vertical landing).

## 8.2 Powered Lift STOL Configurations

The STOL requirement, i.e. use of an airfield of less than 1000 ft hounded by some 50 ft obstacles, requires  $C_{Lmax}$  values much higher than those obtained on a conventional wing/flap configuration, for reasonable wing-loadings; see Figure 27. The *powered flight regime* is "that flight regime in which controlled level flight is possible below the power-off stall speed, and in which, part or all of the lift and/or control moments are derived directly from power plants" (see Paper H by P.Yaggy on "Flight Testing and V/STOL Handling Requirements" in this volume).

This power can be either:-

*associated with the aerodynamics of the wing*, to provide a much greater increase in lift than the vertical component of the thrust generator; or *independent of the wing*, so that the vertical component of the thrust generator is then used to complement the wing lift in order to support the aircraft weight.



Some examples of proven configurations for both cases are given on Figure 28:-

(a) Thrust deflected by the wing/flap system

In this case, the wing acts as a *thrust amplification device*, the circulation about the wing profile being substantially increased.

The first well-known configuration of this type is the propeller deflected slipstream scheme (Fig.32), used for example on the STOL Breguet 941, where the propeller slipstream is turned downwards by a double-slotted trailing-edge flap system (see Figure 28(a)). Such a deflection can also be achieved by using a boundary-layer control flap to preclude flow separation, using blowing for example, as on the B.L.C. Lockheed C130. Figure 29 explains clearly the successive  $C_L$  gains obtained on a conventional aircraft, by flap and aileron deflection without and with boundary-layer control, and also with the slipstream of four propellers distributed along the flap span.

The next step is to deflect the slipstream of ducted propellers, or large by-pass ratio fan-jet engines, distributed along the span (Fig.28(b)<sup>10</sup>). The  $C_L$  obtained, as a function of the momentum coefficient ( $C_\mu = T_G/q_0S$ , similar to a thrust coefficient) can be conveniently split into three parts;  $C_{L0}$  due to flap effect, the vertical component of the thrust  $C_\mu \sin \delta_f$ , and the  $C_{L\tau}$  due to circulation increase around the aerofoil section. The limiting case is well known as the *jet-flap* scheme, where the propulsive jet is distributed all along the wing span (Fig.28(d)), either from a slot ahead of a deflecting flap, or by spreading the jet exhaust from a pod-mounted engine<sup>16</sup>. The jet-flap principle has been tested in flight on the British Hunting 126 research aircraft<sup>17</sup>, and also at full-scale on the blades of the French Dorand helicopter rotor. In the latter, the blades are fixed in pitch, while the jet-flap deflection is controlled both cyclically and non-cyclically, to vary the rotor force output.

Ultimately, the jet-flap configuration can lead the way to the "*propulsive-wing*", where small fan-jet engines will be distributed inside a thick wing, so as to ensure a uniform load distribution, thus providing a good L/D during both take-off and cruise. The ADAM project, proposed by the American firm LTV, represents a first attempt towards such a configuration, with a low aspect-ratio wing of rectangular planform.

(b) Isolated vectored thrust

We have already seen that several VTOL configurations can take advantage of vectored thrust engines to direct their thrust in the optimum direction throughout the take-off run, so as to obtain the shortest STO performance. Practical examples include the P-1127 and DO-31 aircraft equipped with Bristol Pegasus lift-cruise engines, incorporating two sets of fully-deflectable double "cold" and "hot" nozzles; or the VJ-101C with tiltable lift-cruise engines.

It is interesting to illustrate (Fig.30(a)) the flexibility of such a configuration to perform various take-off distances through the range of STO to a conventional take-off<sup>19</sup>. Here, it is assumed that this lift-cruise engine has a take-off thrust/weight ratio of 1.2 to meet VTO requirements. The first case shown (with a 70° nozzle deflection) is the *rolling take-off*, a favourable VTOL technique to avoid erosion and recirculation problems near the ground. A vertical component of about 1.1W ensures clearance of a 50 ft obstacle in less than 500 ft take-off distance, when the aircraft is overloaded. A 30° nozzle deflection still gives a large vertical thrust component (60% W) to balance the aircraft weight and a strong propulsive component to accelerate up to a 800 ft take-off. In contrast, Figure 30(b) shows that a VTOL configuration with separate *fixed lift* and cruise engines does not have this flexibility, because of the fixed thrust vector ( $T/W \simeq 1.4$ ), with much reduced option for STOL performance.

With conventional aircraft, it is also possible to add *auxiliary lift-engines* equipped with some thrust deflection devices on the nozzles, to obtain very short take-off and



landing. Such a scheme will be very attractive for the next generation of STOL aircraft, incorporating some very light lift-fan jet engines now proposed for development, so as to reduce fuel consumption, noise, and efflux velocity, thereby minimising erosion, recirculation, etc, near the ground.

### 8.3 STOL Aerodynamic Limitations

The major problems comprise wing lift performance, limitations in low-speed operation, handling qualities, and stability and control characteristics at very low speed, loss of lift in ground effect. It is interesting to illustrate some of these points with results obtained in flight on several STOL aircraft. Figure 31<sup>11</sup> shows the flight  $C_L$  values versus speed, corresponding to  $C_{Lmax}$  respectively at maximum power, approach power, and idling power, for the propeller slipstream STOL Breguet 941 (slotted flaps), Lockheed C-130B (blown flaps), and for the jet transport Boeing 707 prototype equipped with blown flaps. On the same graph are plotted the usable  $C_L$  values selected by the pilots for the approach. Although far removed from maximum lift, these values are above those of  $C_{Lmax}$  at minimum power for the two slipstream configurations; on a conventional aircraft, approach speed is taken as  $1.3V_{stall}$  based on idling power, i.e. 80 knots for the Breguet 941 in comparison with the true approach speed of 60 knots achieved in flight. The jet aircraft have little direct lift due to power, i.e. small external jet-flap effect with this pod-engine configuration. But the effect is very different for propeller slipstream configurations where the  $C_{Lmax}$  increases very rapidly with the propeller thrust coefficient, as shown on Figure 32, for the Breguet 941 in its landing configuration<sup>1</sup>.

One major reason for limiting the amount of lift used on STOL configurations is to obtain a *large rate of descent* during approach, with a comfortable speed margin from the stall speed, to keep good control and to allow for gust and the flare. For the Breguet 941 (Fig.32) the descent slope is about 7 degrees during a "standard" approach with a very large safety margin (9 degrees below the stalling incidence). This descent slope can be increased by use of "propeller transparency", i.e. a zero equivalent thrust on the outboard propellers, giving larger induced drag for the same lift. Finally, it is important to recall that the Breguet 941 has cross-shafting between the four propellers, to distribute the available power along the span after an engine failure. This is *always mandatory* for the engine-out case to retain acceptable performance and handling qualities<sup>17</sup>.

To conclude this discussion of the  $C_{Lmax}$  values obtainable with high lift devices on transport aircraft, some interesting results obtained in flight on the Boeing 707 prototype are given in Figure 34 (Ref.16). On the first graph are plotted the successive *stall speeds* obtained on this experimental aircraft equipped respectively with the basic double-slotted flap ( $V_s = 104$  knots), an additional Kruger flap of the model 720 type ( $V_s \approx 95$  knots), the 727-type triple-slotted flap ( $V_s \approx 88$  knots), an additional blown-Kruger flap ( $V_s \approx 83$  knots), the experimental blown trailing-edge flap ( $V_s \approx 68$  knots). This last flap (with blowing boundary-layer control) installed on the 707 prototype is the most effective high-lift system flight-tested. For a momentum coefficient of about  $C_\mu = 0.1$  and 70 degrees flap deflection, a trimmed  $C_{Lmax}$  of about 3 is obtained, i.e. about twice the initial value.

As a final point, *ground-effect* must certainly be mentioned. This effect becomes *unfavourable* on large aspect-ratio wings when equipped with powerful high-lift devices, as on the blown flap-Boeing 707 prototype. For example, the second graph of Figure 34 shows that, when the wing is very near the ground, the maximum lift is reduced by more than 30%. Wind-tunnel predictions, obtained in the NASA Langley 17 ft tunnel equipped with a moving belt (ground velocity equals airflow velocity), are in quite good agreement with the flight results. The wind-tunnel experiments also show that ground-effect gives a drag reduction (increase of effective aspect-ratio) and a nose-down pitching moment (large change in downwash at the tail near the ground). Such adverse characteristics due to ground effect are even worse for more efficient high-lift devices, such as a jet-flap with large jet angles.

All this confirms again that Aerodynamic and Propulsion problems are intimately related for V/STOL aircraft.

## REFERENCES

1. Poisson-Quinton, Ph. *From Wind-Tunnel to Flight, the Role of the Laboratory in Aerospace Design*, 30th Wright Brothers Lecture, AIAA J. of Aircraft, May 1968.
2. Aviation Week *Special Report on V/STOL*, June 24, 1968.  
*V/STOL Push Requiring Tunnel Advances*, July 8, 1968.
3. Campbell, J.P. *Free and Semi-free Model Flight-Testing Techniques used in Low-speed Studies of Dynamic Stability and Control*, AGARDograph 76, Oct. 1963.
4. Campbell, J.P. *Vertical Take-off and Landing Aircraft*, McMillan, N.Y., 1962.
5. Stepniewski W.Z. *Some Thoughts on Optimum Wings and Vertical Thrust Generators in VTOL Aircraft*, SAE Transactions, Vol. 67, 1959.
6. Comberiate, M.B. *VTOL Propulsion*, survey paper at Gottingen AGARD meeting, AGARD A.R. No. 13, Sept. 1967.
7. Kuhn, R.E.  
McKinney, M.O. *General Performance Characteristics of V/STOL Aircraft*, Proc. of NASA/ARMY Briefing on V/STOL Aircraft Research, Dec. 1959.
8. Astronautics and Aeronautics, special issues on V/STOL *V/STOL's - Turning Promise to Reality*, Sept. 1965.  
*V/STOL, Its Day has to Come*, Sept. 1968.
9. NASA Staff *NASA Conference on V/STOL Aircraft*, NASA Proc. Langley, Nov. 1960.
10. NASA Staff *Conference on V/STOL and STOL Aircraft*, NASA SP-116, April 1966.
11. NASA Staff *Conference on Aircraft Operating Problems*, NASA SP-83, May 1965.
12. AGARD *Symposium on V/STOL Aircraft*, Paris, June 1960, AGARDograph No. 46.
13. AGARD *V/STOL Aircraft Conference*, Paris, Sept. 1964, AGARDograph No. 89.
14. AGARD *V/STOL Aircraft Bibliography*, Second supplement, 1966.
15. Ville, G.  
et al. *Recherches et réalisations américaines en matière de VTOL*, DOC-AIR-ESPACE, Nos. 94, Sept. 65 et 97, Mars 66.
16. Wimpres, J.K. *Short Take-off and Landing for the High-speed Aircraft*, Astronautics and Aeronautics, Feb. 1966.

17. Kuhn, R.E.  
Hammond, A.D.                      *Control Requirements Affecting STOLS, Astronautics and Aeronautics, May 1965.*
18. Williams, J.                      *Some British Research on the Basic Aerodynamics of Powered Lift Systems, J. of R. Aero. Soc., Vol. 64, 1960.*
19. Lucas, R.M.  
Dale, J.H.                              *Combined Lift and Propulsion, 6th ICAS Congress, Munich, Sept. 1968.*
20. Pickerell, D.J.  
Cresswell, R.A.                      *Powerplant Aspects of High-speed, Inter-city VTOL Aircraft, J. of Aircraft, Sept-Oct. 1968.*

N.B. A very interesting exercise on the *Feasibility of V/STOL Concepts for Short-haul Transport Aircraft* was asked by NASA-Ames to several U.S. Firms; a Summary of this work is given in Reference 10, and the detailed studies were recently published as NASA Contract Reports: by Ling-Temco-Vought, (CR-670, Jan.67 and CR-670(01), Dec.67), Boeing/Vertol (CR-743, May 67), and Lockheed (CR-902, Oct.67); Some typical configurations are given on Figure 35, with a Summary of the design criteria asked by NASA.



Fig. 1 V/STOL and STOL aircraft goals

**SOME V/STOL PROBLEMS:**

- HOVERING EFFICIENCY VERSUS CRUISE EFFICIENCY
- SAFETY (1 engine loss, systems reliability, etc...)
- SLIPSTREAM/AIRFRAME INTERACTIONS
- HANDLING QUALITIES during Hovering and Transition
- GROUND EFFECT (Aero-interactions, erosion, reingestion)
- NOISE during hovering and Transition
- ALL WEATHERS OPERATIONS (auto-pilot, Instrument Landing Aids)
- MULTI-MISSIONS REQUIREMENTS
- USE IN STOL MODE (Performance Gains, additional design requirements)
- DEVELOPMENT COSTS, MAINTENANCE, etc...
- PRECISE V/STOL SIMULATION (tests on Wind-Tunnel models and Training on ground simulators)

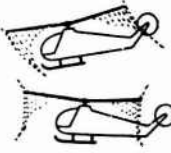
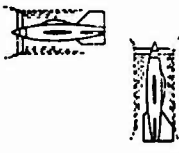
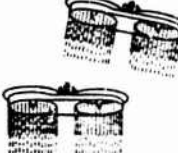
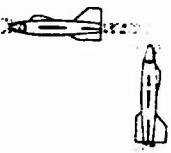
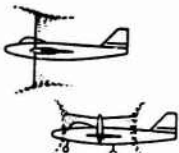
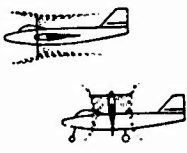
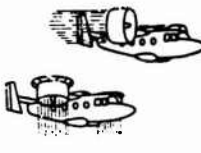
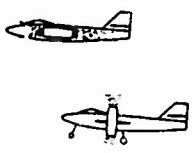
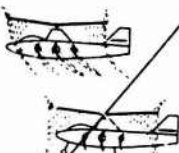
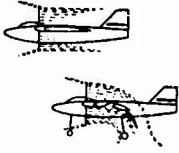
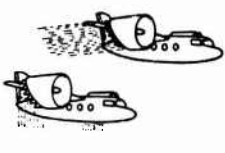
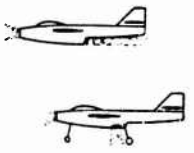
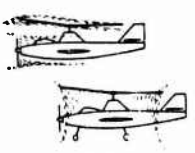
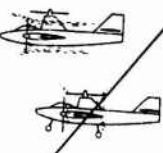
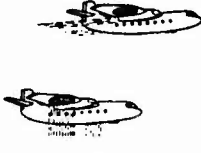
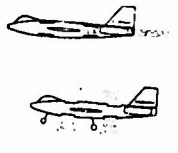
METHODS TO PERFORM THE TRANSITION	TYPES OF LIFT GENERATORS (HOVERING)			
	ROTORS	FREE PROPELLERS	DUCTED FANS	TURBO-JETS
AIRCRAFT TILTING	 <p>A 1 Hélicopter</p>	 <p>B 1 (US: Convair XFY 1, Lockheed XFY 1)</p>	 <p>C 1 (US: Flying Jeeps)</p>	 <p>D 1 (US: Ryan X 13) (F.: Cieloptère)</p>
THRUST TILTING	 <p>A 2 (US: Bell XV 3, Kaman K 16)</p>	 <p>B 2 (US: Vertol VZ-2, Hiller X 18, Vought XC 142, Curtiss X 19) (Can.: CL-84)</p>	 <p>C 2 (US: Doak VZ 4, Bell X 22) (F.: N-500)</p>	 <p>D 2 (US: Bell A.T.V.) (All.: VJ 101 C)</p>
THRUST DEFLECTION	 <p>A 3</p>	 <p>B 3 (US: Ryan VZ 3, Fairchild VZ 5) (F.: Breguet 941-STOL)</p>	 <p>C 3 (US: Adam project)</p>	 <p>D 3 (US: Bell X 14, Lockheed XV 4 A) (GB: Hawker 1127)</p>
SEPARATE PROPULSIONS	 <p>A 4 (US: McDonnell XV 1, Lockheed AH-56A) (G.B.: Rotodyne)</p>	 <p>B 4</p>	 <p>C 4 (US: Ryan XV 5-A)</p>	 <p>D 4 (G.B.: Short SC 1) (F.: Balzac, Mirage III v) (All.: Do-31E)</p>

Fig. 2 VTOL morphology, after J.Campbell (NASA)

Ideal Power:  $P_i = \frac{1}{2} q_m \cdot V_\Delta^2 = \frac{1}{2} \rho S_\Delta V_\Delta^3$  (1)

Thrust:  $T = q_m \cdot V_\Delta = \rho S_\Delta V_\Delta^2$  (2)

from (1) and (2)  $\frac{T}{P_i} = \frac{2}{V_\Delta}$  (3)

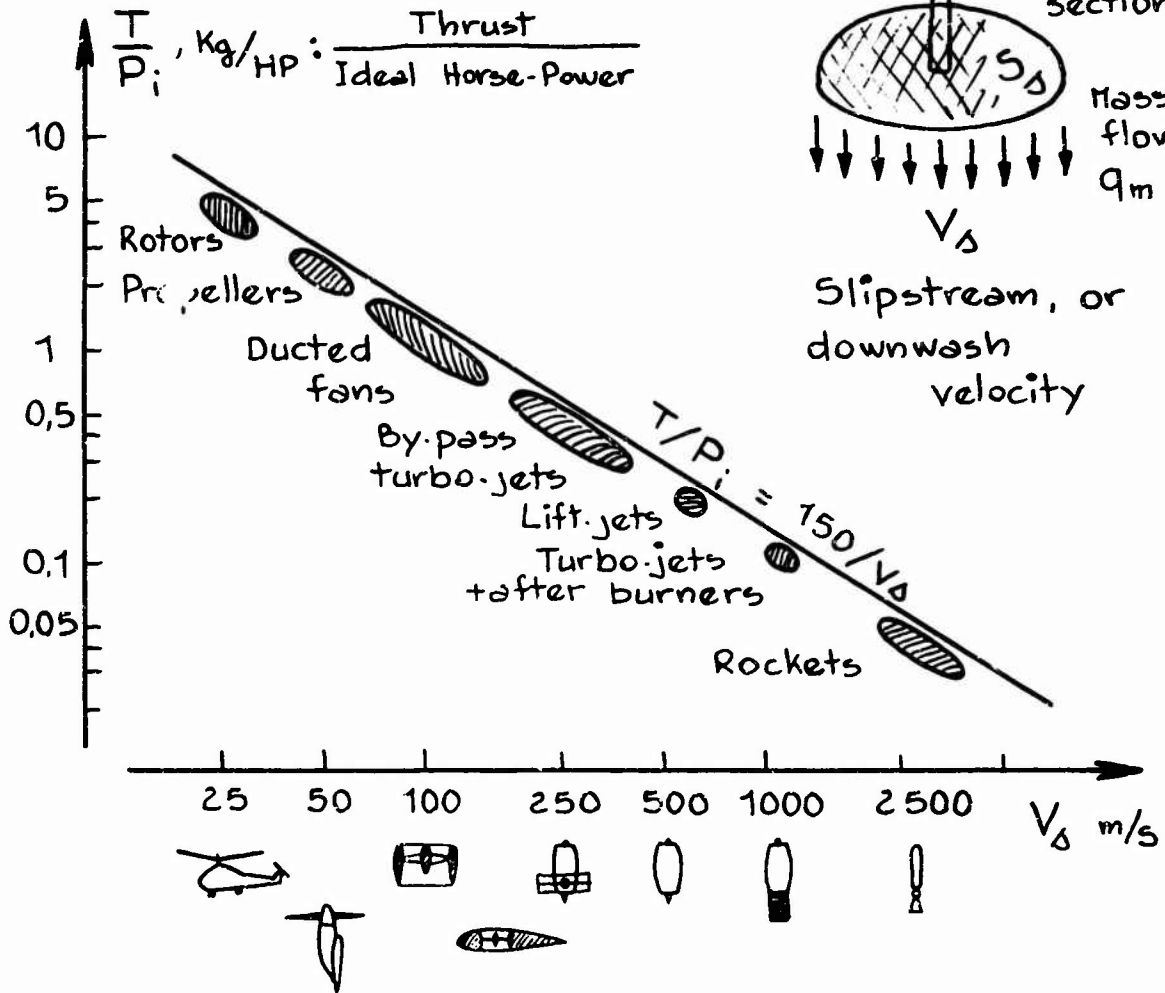
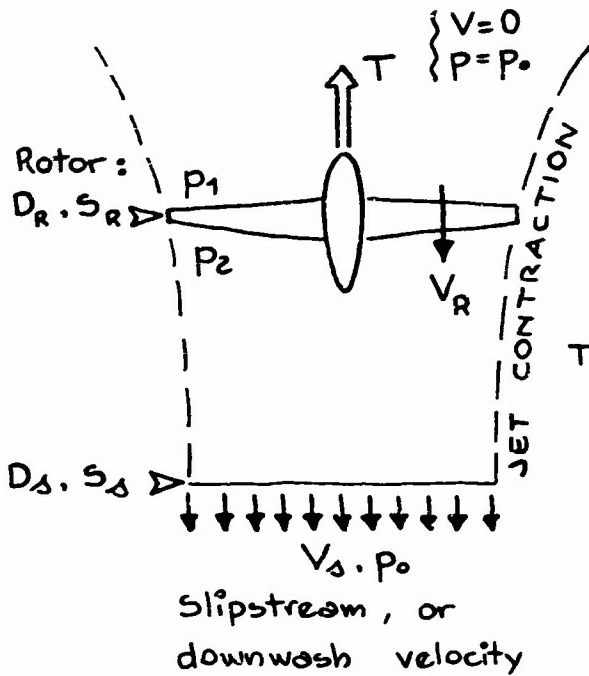


Fig.3 VTOL thrust required in hovering



1. ROTOR OR FREE PROPELLER.

from Bernoulli equations:

$$P_2 - P_1 = \rho \frac{V_\Delta^2}{2}$$

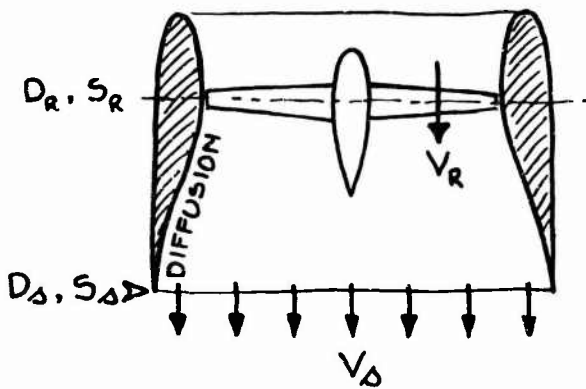
$$\text{Thrust } T = S_R (P_2 - P_1) = \rho S_R V_R V_\Delta$$

$$\downarrow$$

$$\boxed{V_\Delta = 2 V_R}$$

$$\downarrow$$

$$S_\Delta = \frac{S_R}{2}$$



2. DUCTED FAN

Diffuser ratio:

$$\sigma = \frac{S_\Delta}{S_R} \geq 1$$

(Free propeller:  $\sigma = 1/2$ )

$$V_\Delta = \frac{V_R}{\sigma}$$

a. same  $\left\{ \begin{matrix} \text{Power } W \\ \text{Thrust } T \end{matrix} \right\} \rightarrow$  Diameter

b. same  $\left\{ \begin{matrix} W \\ \text{Diameter } D_R \end{matrix} \right\} \rightarrow$  Thrust

c. same  $\left\{ \begin{matrix} T \\ D_R \end{matrix} \right\} \rightarrow$  Power

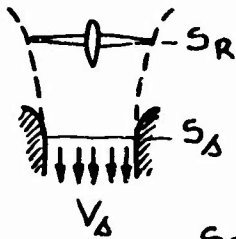
	$\sigma = 1/2$ (free propeller)	Ducted propeller $\sigma = 1$	$\sigma = 2$
D	D	0.707 D	0.5 D
T	T	1.26 T	1.59 T
W	W	0.707 W	0.5 W



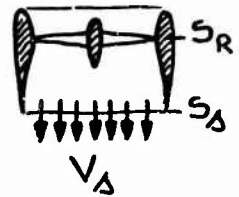
Figure 4

$$M = \frac{P_i}{P} = \frac{\text{Ideal power}}{\text{Actual power}}$$

$$\frac{T}{P_i} = \frac{2}{V_\Delta} = \frac{2\sqrt{\rho}}{\sqrt{T/S_\Delta}} \rightarrow \boxed{\frac{T}{P} = M \frac{2\sqrt{\rho}}{\sqrt{T/S_\Delta}}} = \frac{M \cdot 2\sqrt{\sigma \cdot \rho}}{\sqrt{T/S_R}}$$



$$\sigma = \frac{S_D}{S_R} \begin{cases} \text{Free propeller } \sigma = 1/2 \\ \text{Ducted propeller } \sigma \geq 1 \end{cases}$$



Specific thrust :  $\left(\frac{T}{P}\right)_{\text{kg/HP}} = M \frac{53}{\sqrt{(T/S_\Delta)_{\text{kg/m}^2}}}$  (Z=0, standard atmosphere)

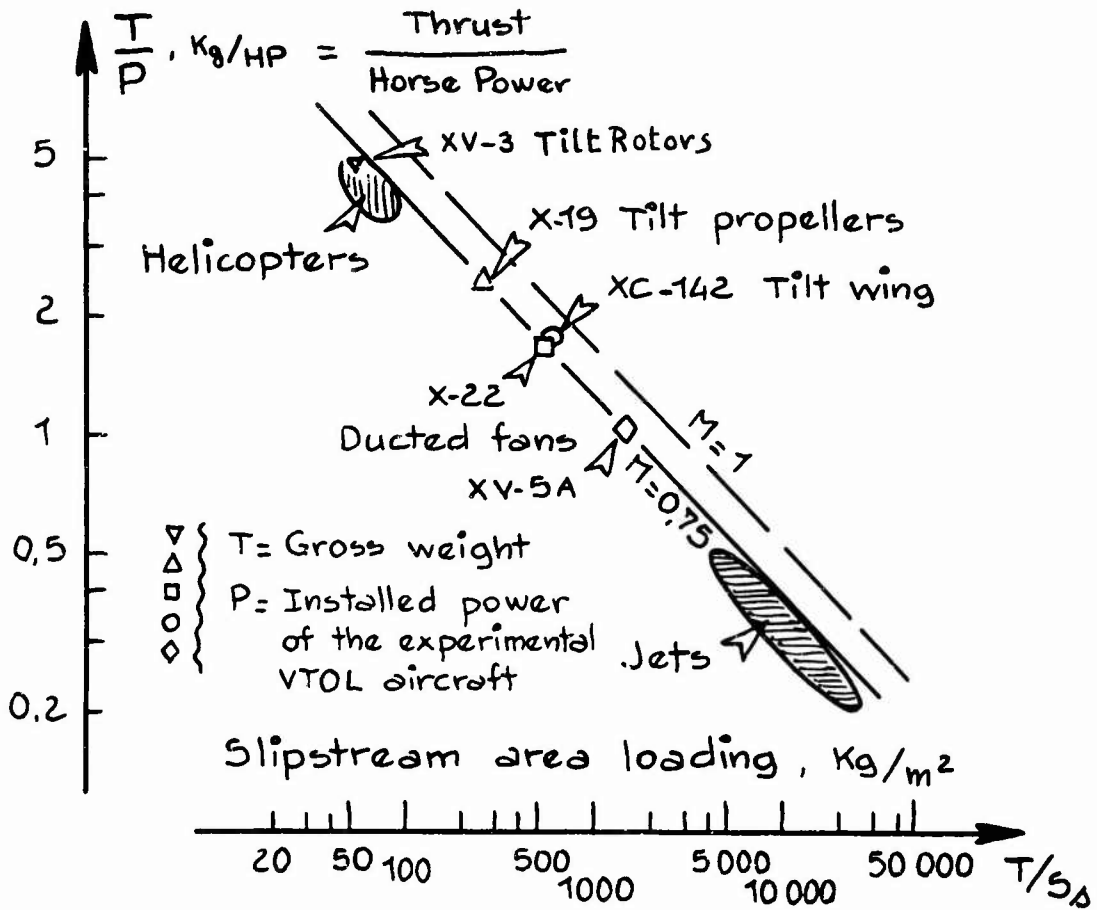
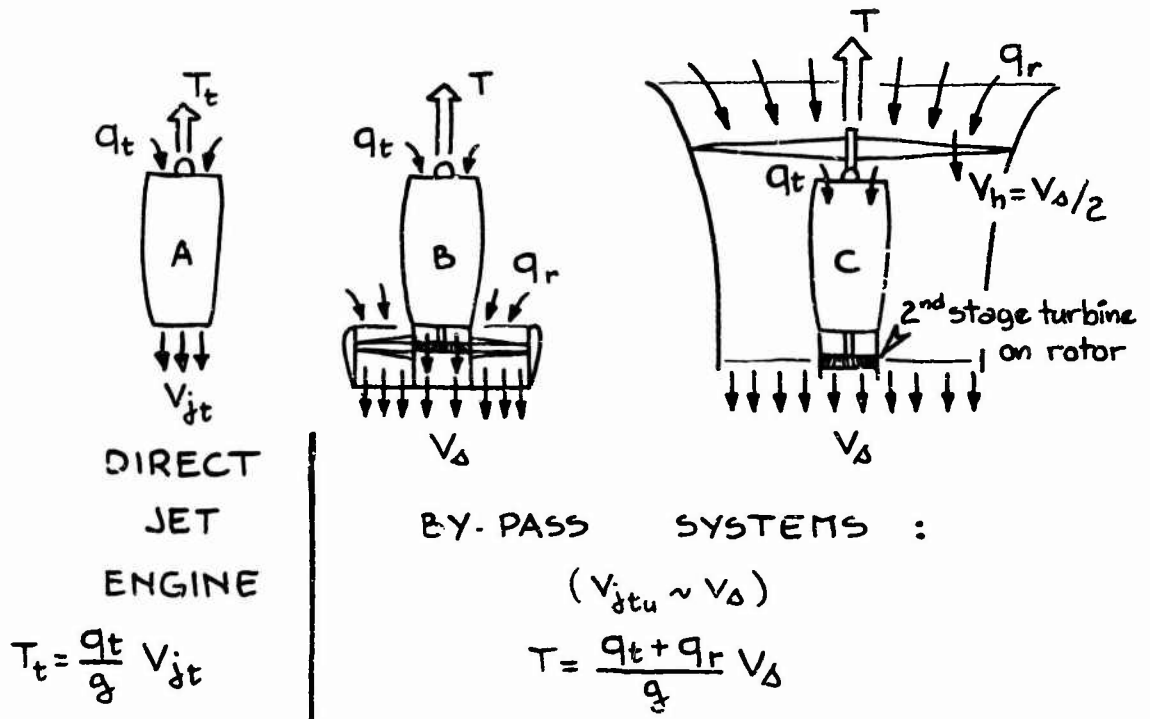


Fig. 5 Figure of merit = hovering efficiency





**THRUST AUGMENTATION**

$$\frac{T}{T_t} = \left(1 + \frac{q_r}{q_t}\right) \frac{V_\Delta}{V_{jt}}$$

Slipstream velocity  $\rightarrow V_\Delta$

$V_{jt} \sim 610 \text{ m/s}$

By-pass ratio  $\frac{q_r}{q_t} = \eta_t \cdot \eta_a \left[ \left(\frac{V_{jt}}{V_\Delta}\right)^2 - 1 \right]$

$\eta_t = \text{power turbine efficiency} \sim 0,85$

$\eta_a = \text{by-pass aerodynamic efficiency} \sim 0,85$

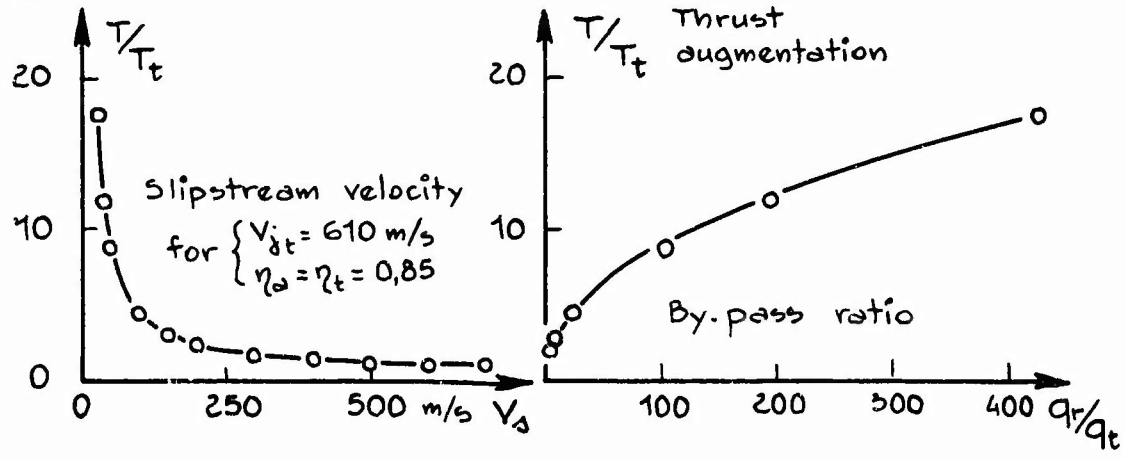


Fig.6 Thrust generators for hovering

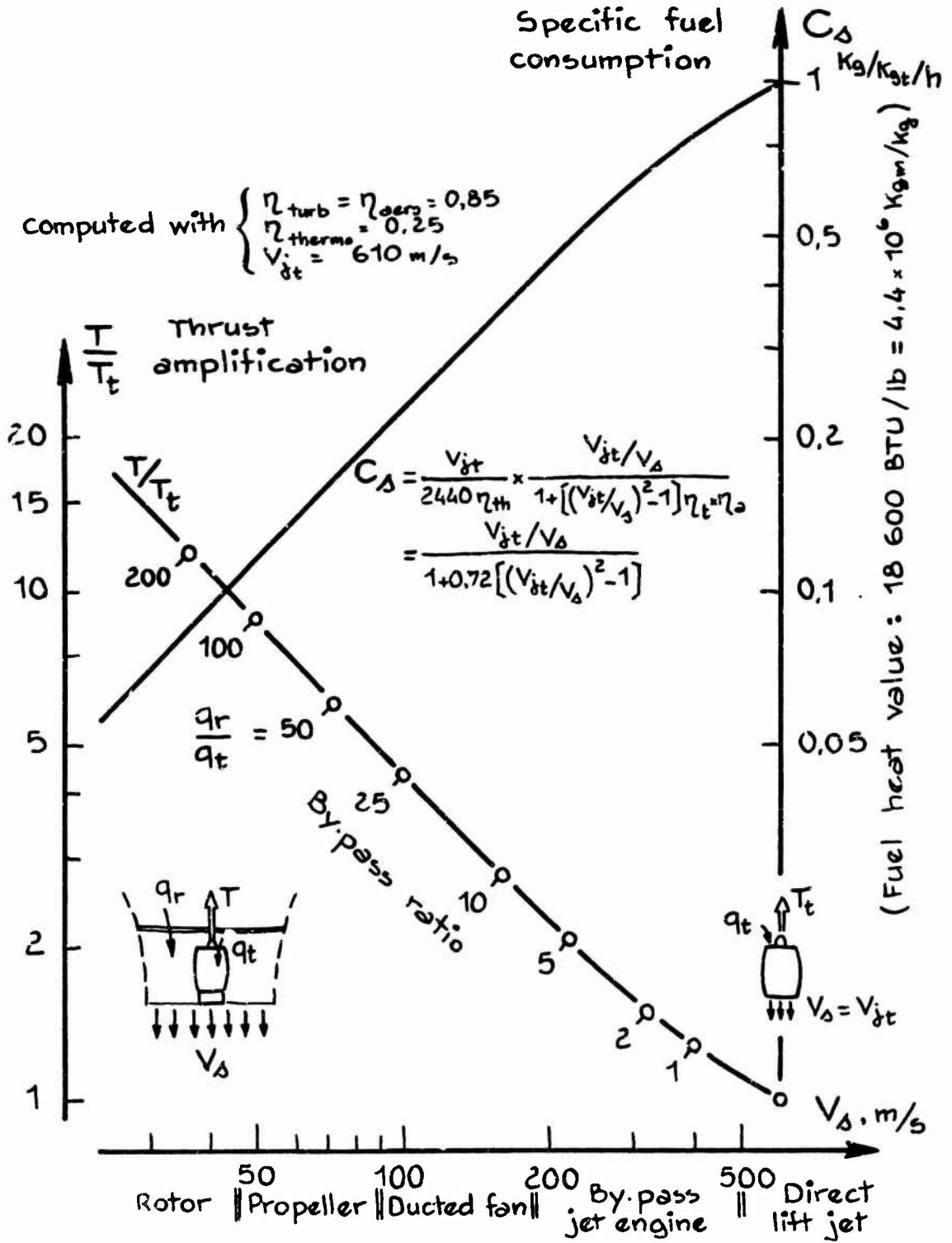


Fig. 7 Thrust generators for hovering

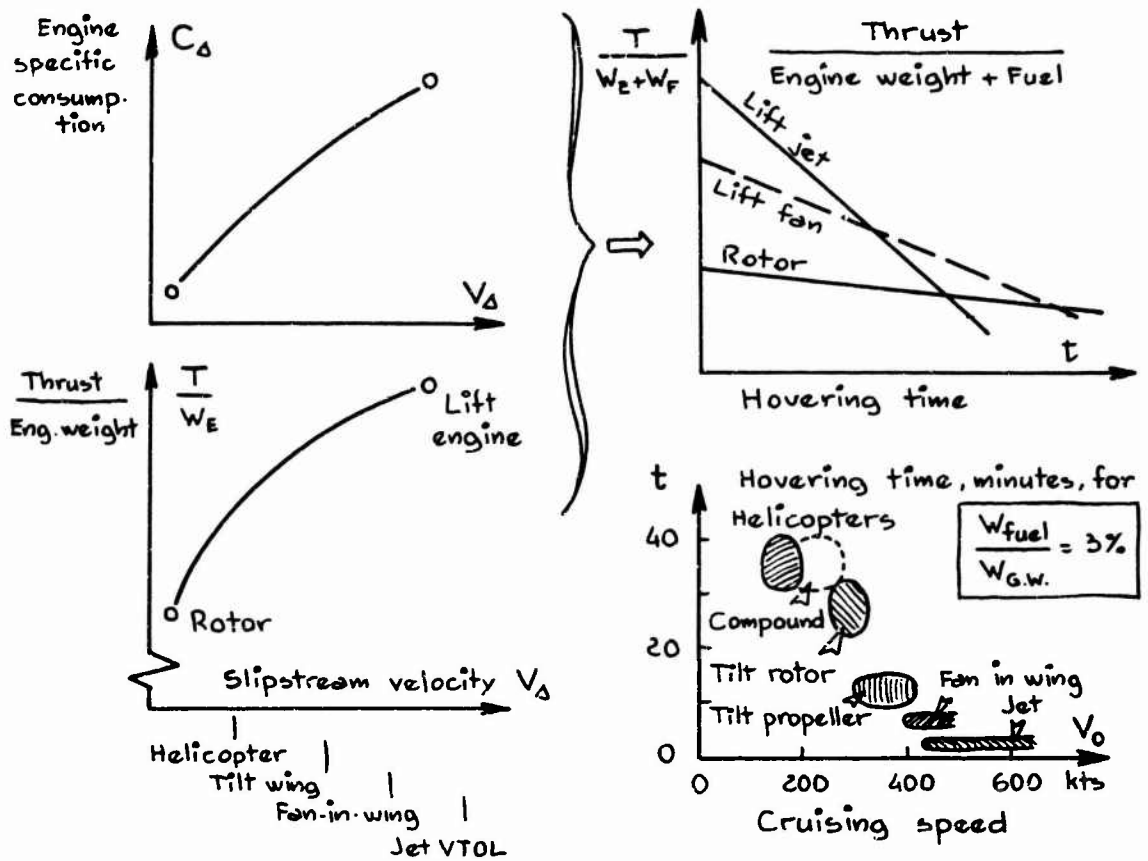


Fig. 8 Balance between engine weight and TSFC in hovering

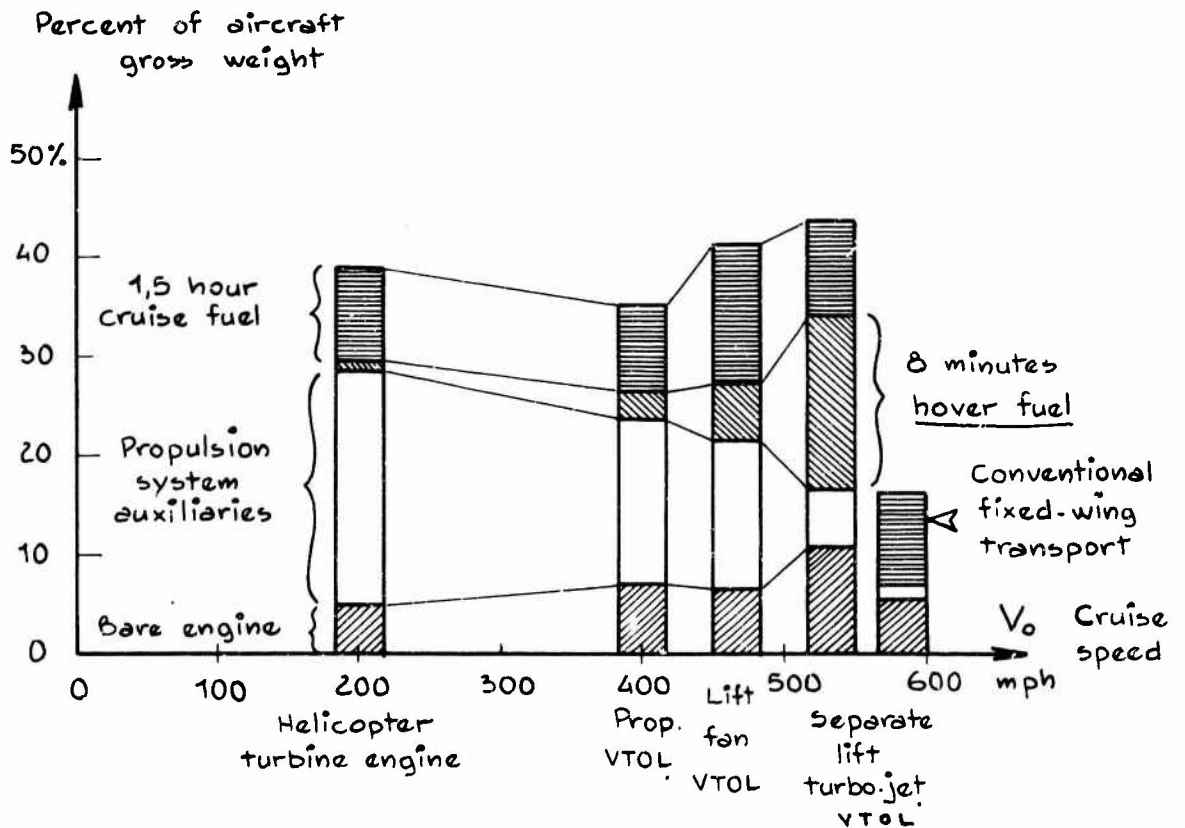
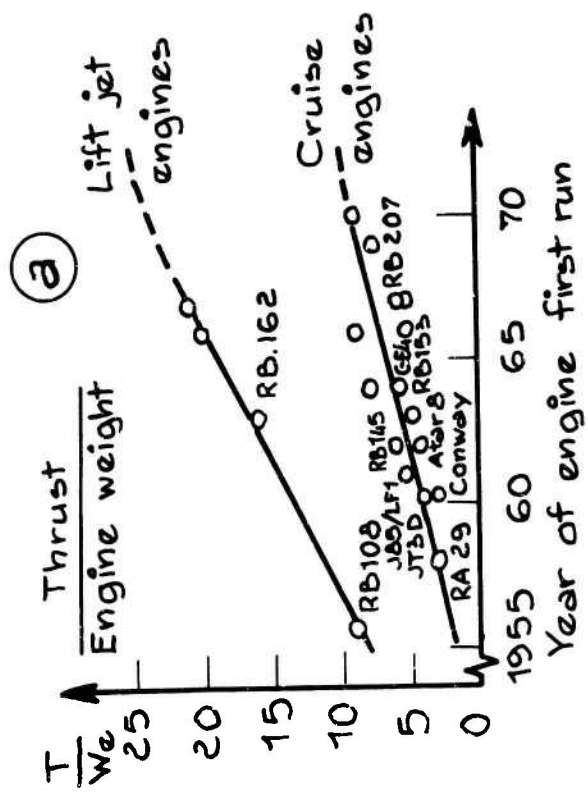
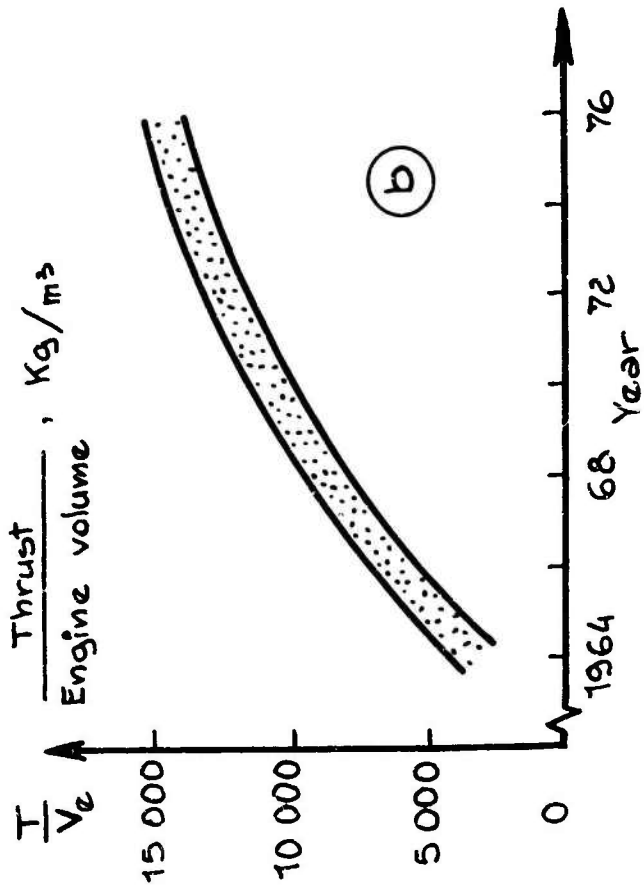


Fig. 9 VTOL aircraft weights



(a) Thrust to weight ratio  
(b) Thrust to volume ratio

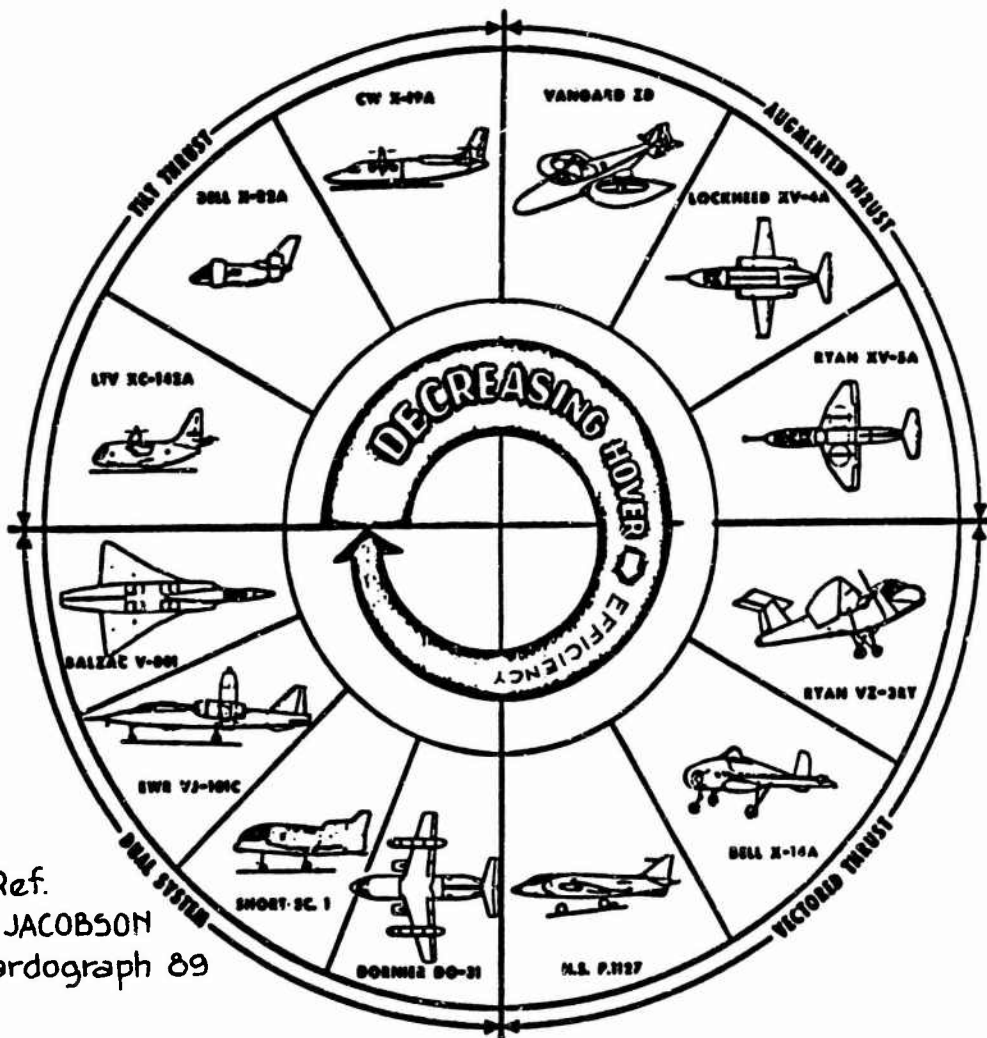
Rolls-Royce lift engines:  
 RB-108  
 RB-162.4  
 Diagrams showing engine dimensions: RB-108 (0.62m diameter, 1.67m height), RB-162.4 (0.65m diameter, 1.31m height).

(NB) Engine scaled to T = 2000 Kg (non bleed)

Fig. 10 Trends in VTOL engines

Thrust/weight	8.7/1	16/1	21/1
Installed Thrust/weight	5/1	10/1	16/1
Volume	100%	85%	27%

[Ref. 19] 1<sup>st</sup> generation 2<sup>nd</sup> g. 3<sup>rd</sup> generation



Ref.  
D.H. JACOBSON  
Agardograph 89

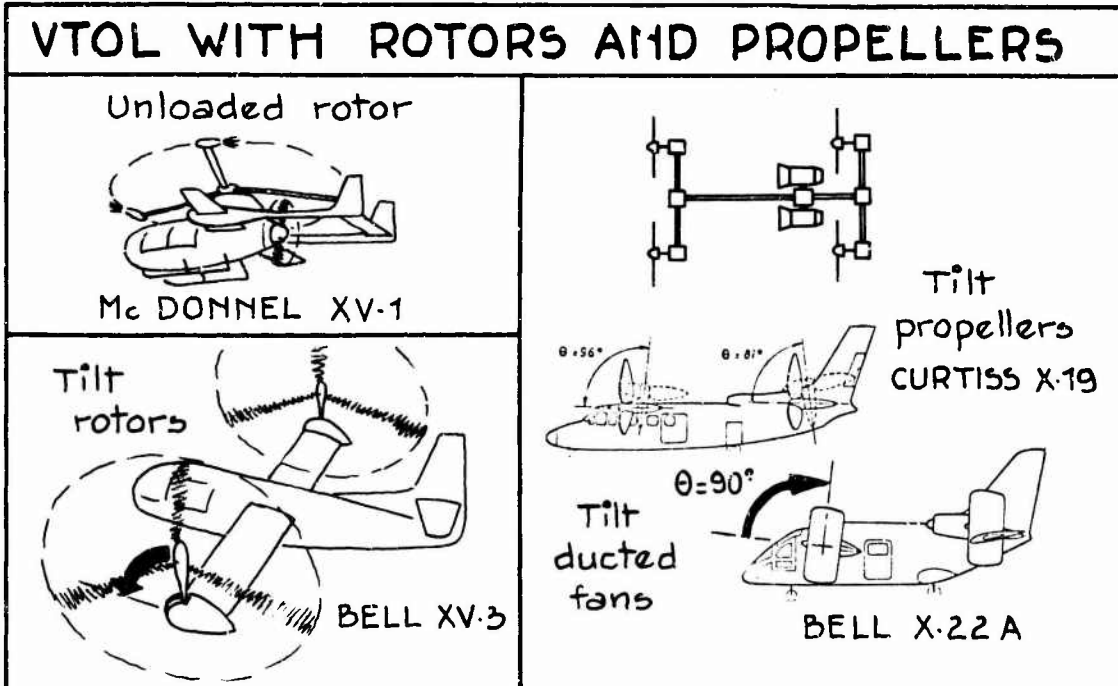


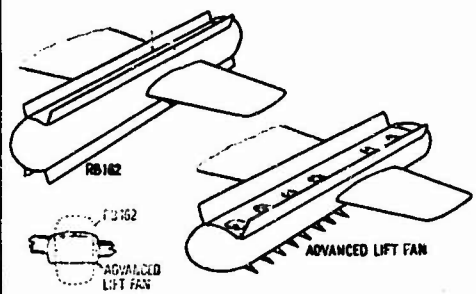
Fig. 11 V/STOL spectrum

LIFT-ENGINE DEVELOPMENT TRENDS	RB 162	ADVANCED LIFT FAN
By-pass ratio	0	12
Fuel $C_d, K_F/hr/K_T$	1.12	0.41
Thrust/Weight, $T/W$	16	17
Thrust/(Volume) <sup>2/3</sup> , $Kg/m^2$	3 400	2 500
Nozzle velocity, $V_j$ , m/s	Hot 610 Cold -	Hot 260 Cold 180
Exhaust temp., $T^\circ C$	800	110
Noise at 500ft, PNdB (2 pods = 12 lift-eng <sup>63</sup> )	135	98

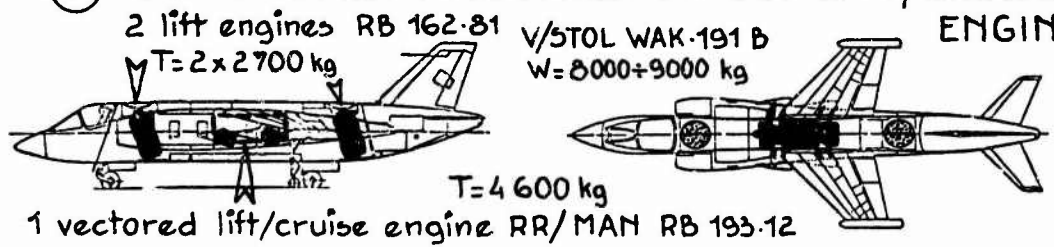
[Ref. 20]

(a) LIFT ENGINES for V/STOL aircraft

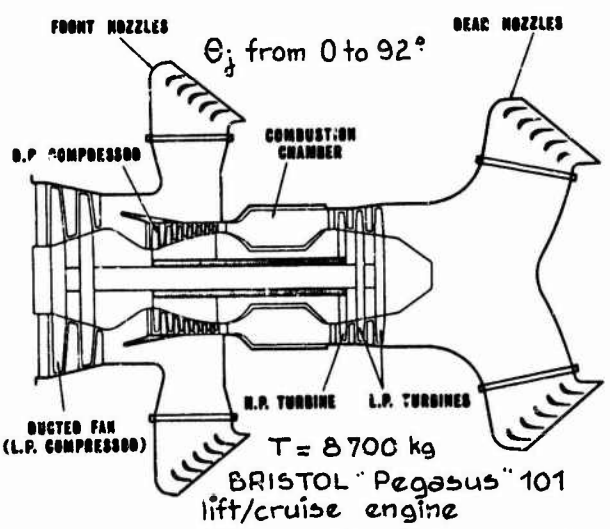
Lift-fan pod installation



(b) LIFT ENGINES + VECTORED THRUST LIFT/CRUISE ENGINE



(c) VECTORED THRUST ENGINE

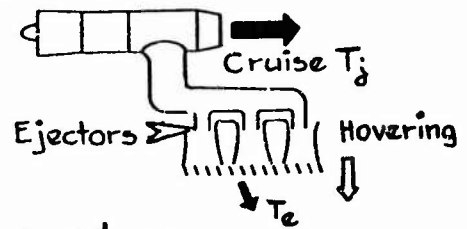


Diagrammatic cross section of a Pegasus engine

Fig. 12 Jet V/STOL configurations



2 jet-engines PW JT-12A

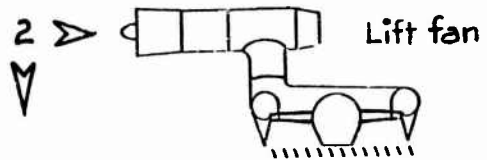
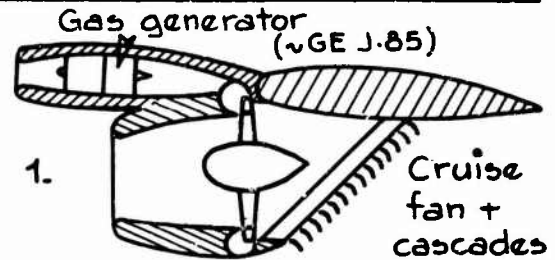


**(a) Ejector system**

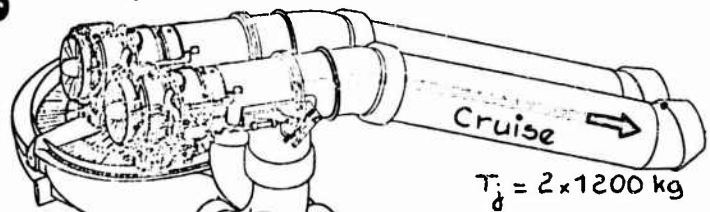
**LOCKHEED XV-4A** Thrust amplification  $T_e/T_j < 1,2$

**(b) By-pass system**

GENERAL ELECTRIC FAN WITH TIP TURBINE



2 jet-engines GE J-85-5



FAN-IN-WING VTOL AIRCRAFT

**RYAN XV-5A**

FAN-IN-WING WITH TIP-TURBINE (GE-353-5)

Pitch control fan (GE-X376)



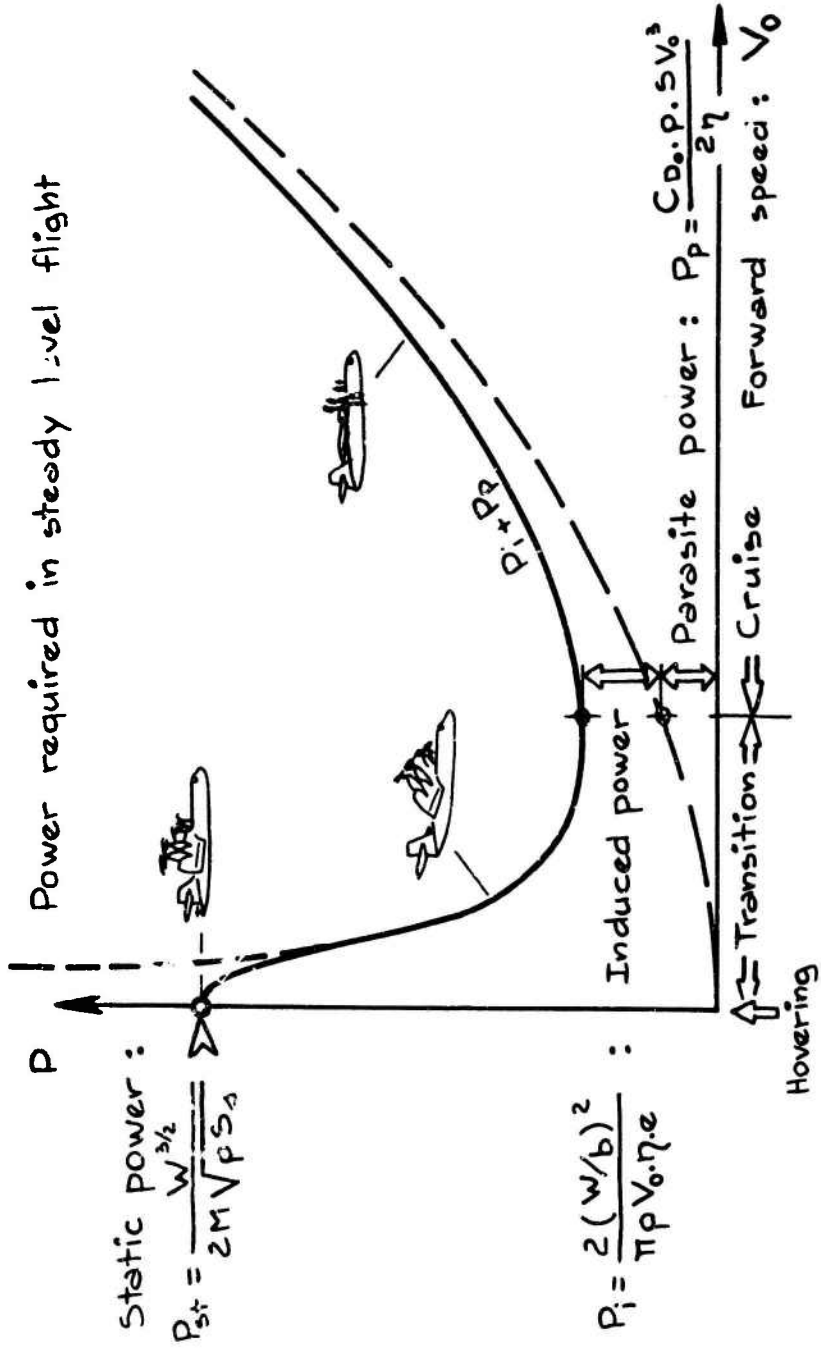
$q_c \sim 10\% q_j$

Thrust amplification  $T_F/T_j \sim 2,5$

$T_F = 2 \times 3000 \text{ kg}$   
 $\delta \sim 1.1 (V_{jF} \sim 130 \text{ m/s})$

Fig. 13 VTOL aircraft with thrust augmentation

V.T.O.L.

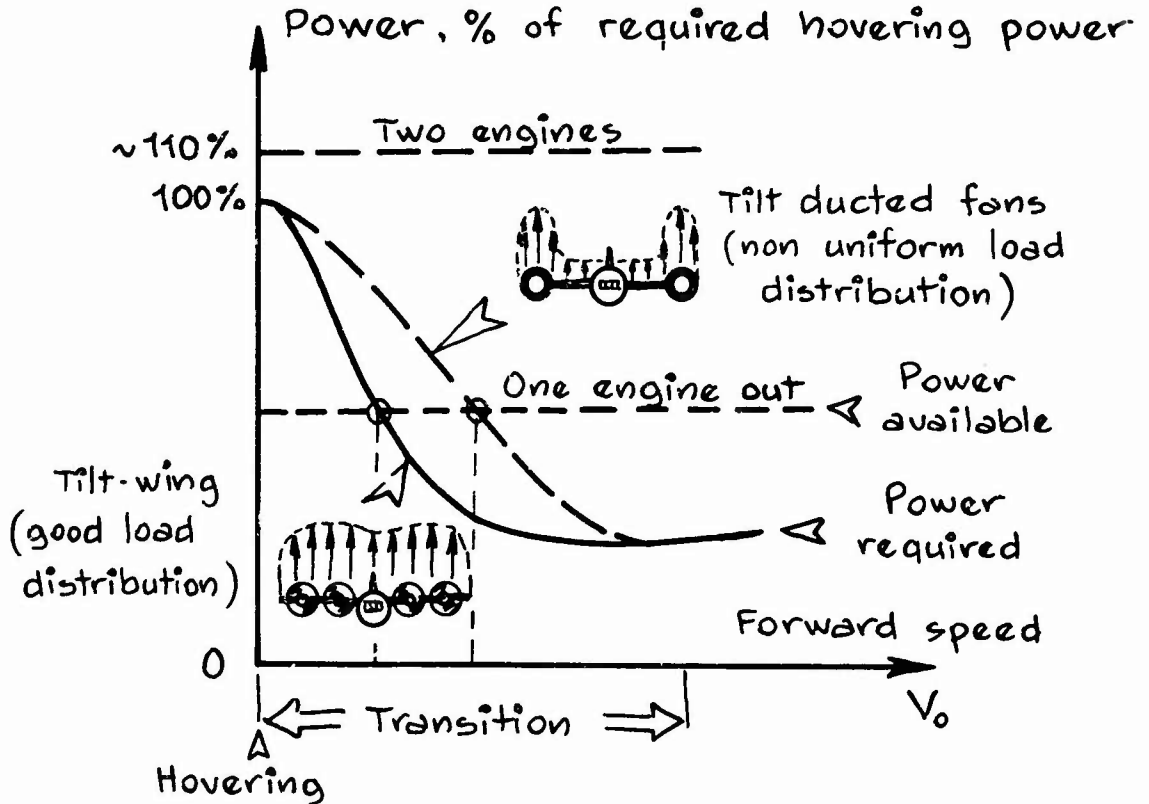


- M : Figure of Merite.
- $S_A$  : Slipstream area.
- W : Aircraft weight.
- b : Wing span.
- e : Span efficiency factor.
- $\rho$  : Mass density of air.
- S : Wing area.
- $\eta$  : Propulsive efficiency.

Figure 14



2. POWER REQUIRED DURING TRANSITION FLIGHT



b. CRUISE PERFORMANCE OF VTOL AND STOL AIRCRAFT

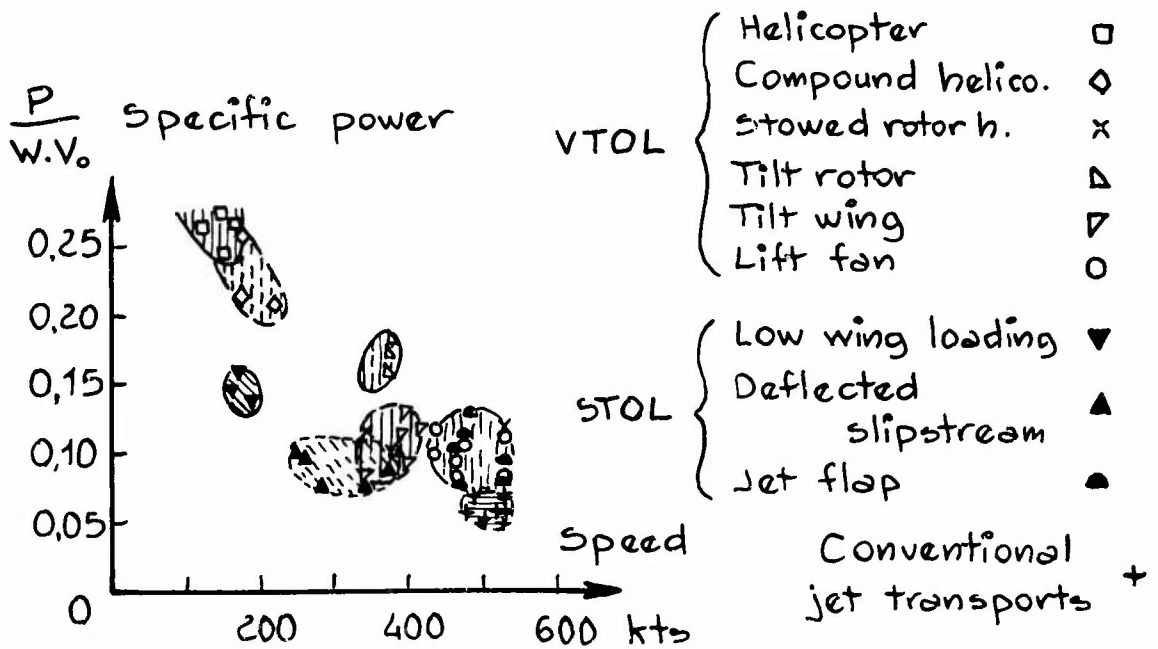
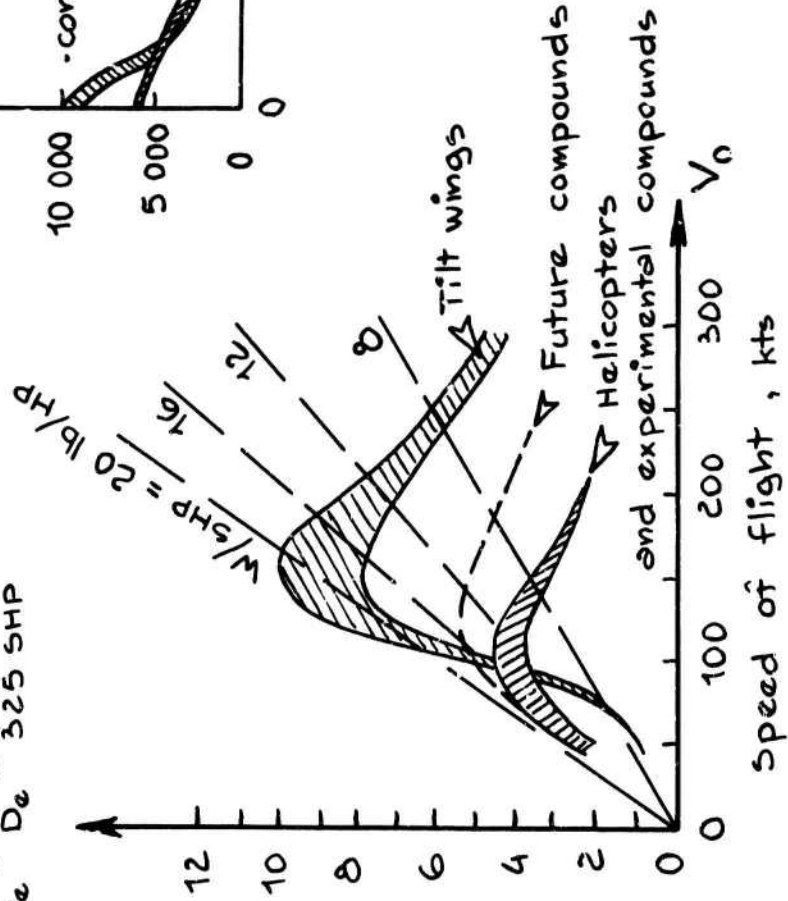


Figure 15

a. CRUISING AERODYNAMIC EFFICIENCY

Lift to equivalent drag ratio:

$$\frac{L}{D_e} = \frac{W}{D_e} = \frac{W \cdot V_0}{325 \text{ SHP}}$$



b. CRUISING SPEED AT SEA LEVEL  
Gross weight: 40 000 lbs

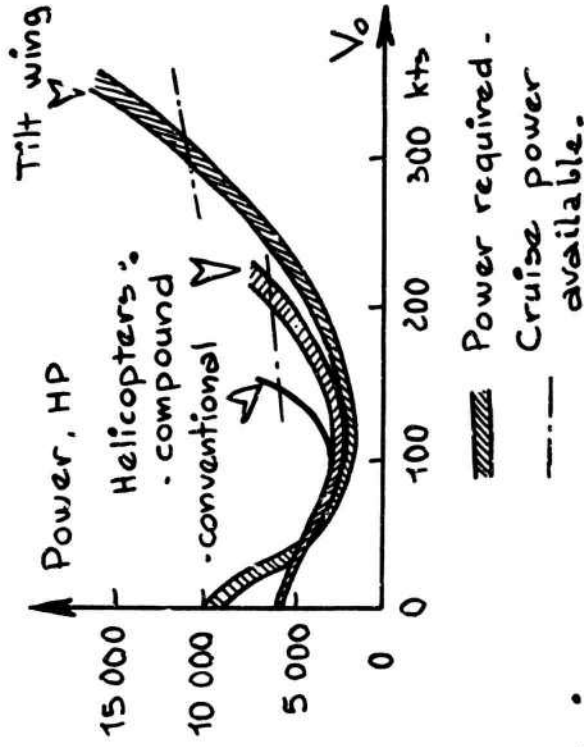


Fig. 16 Rotors and propellers VTOL performances in cruise

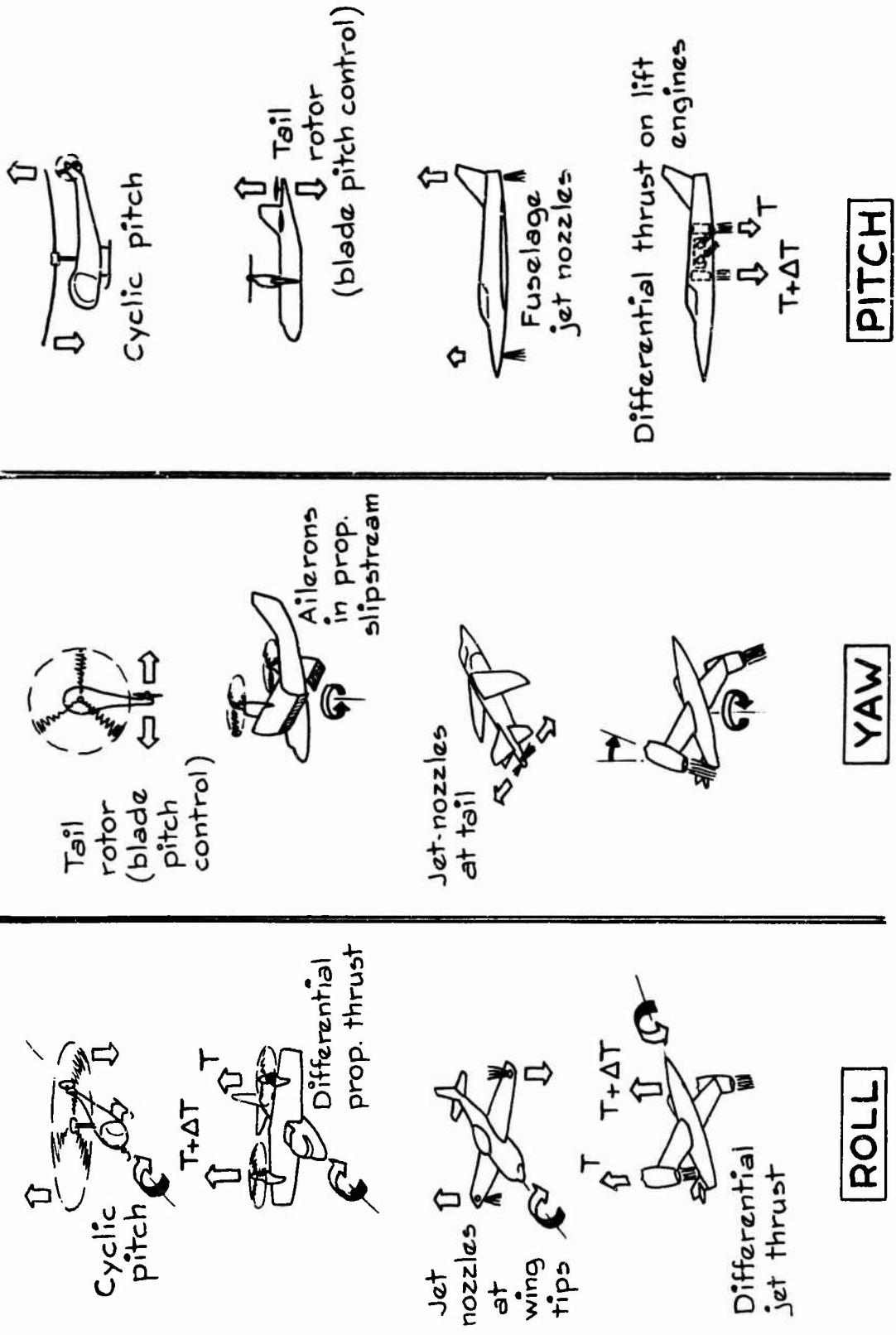


Fig. 17 Various type of controls during hovering and transition

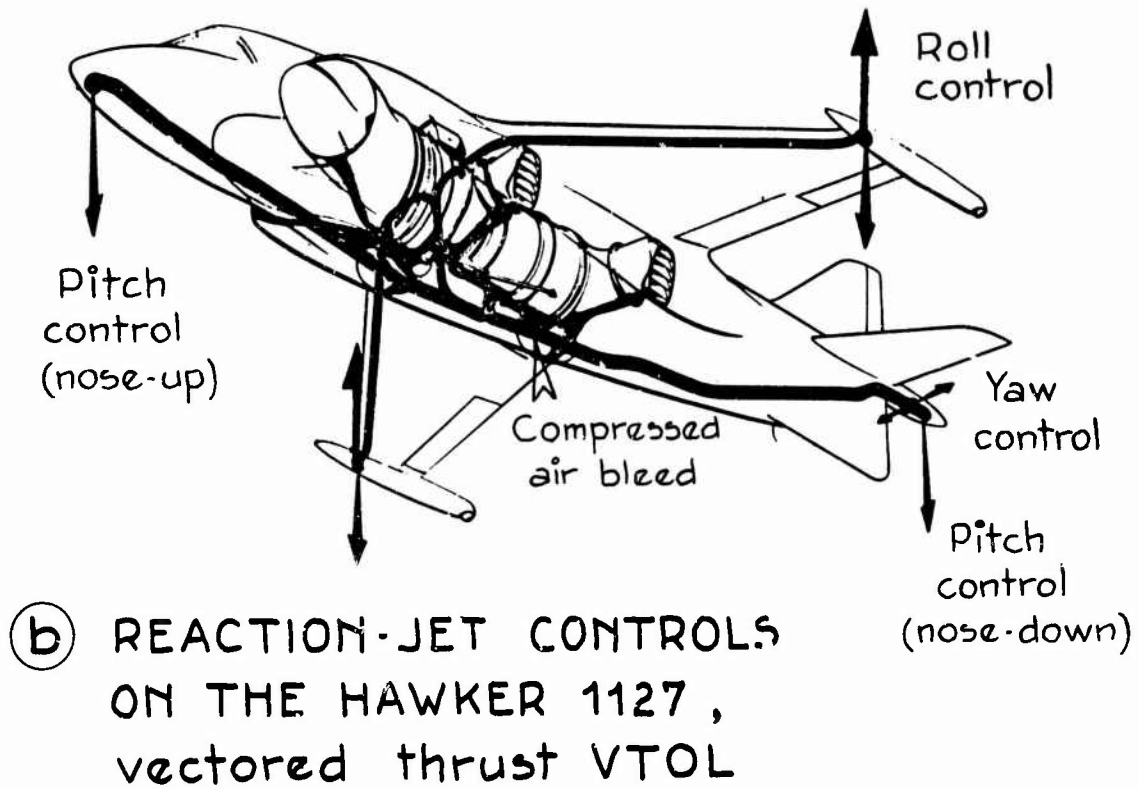
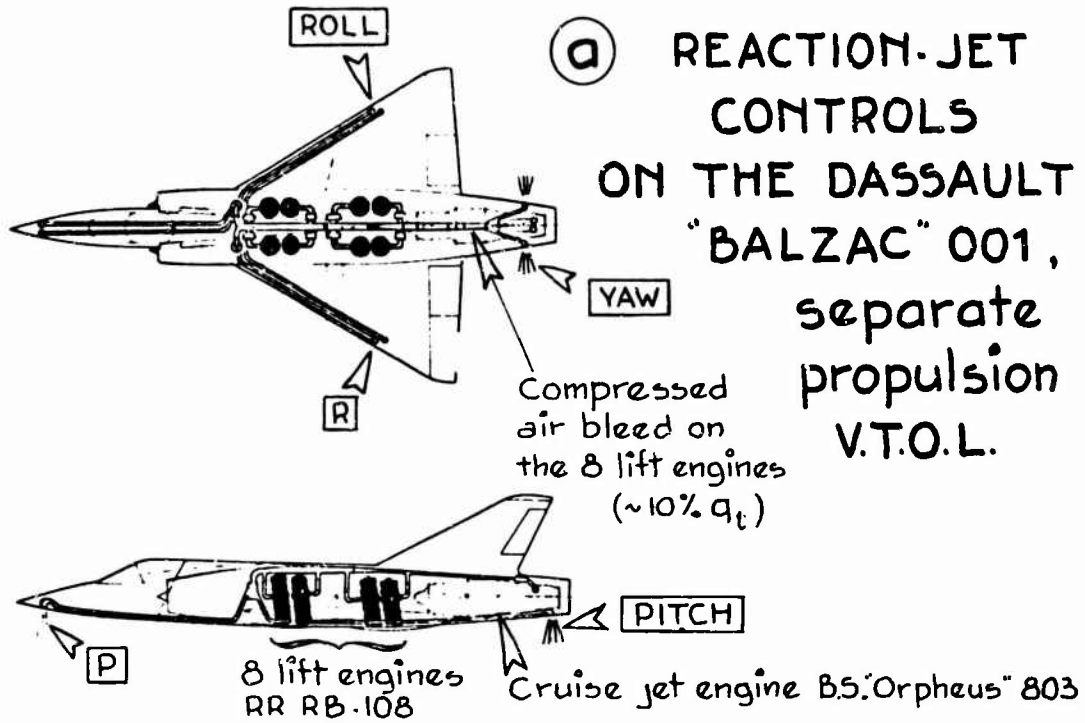
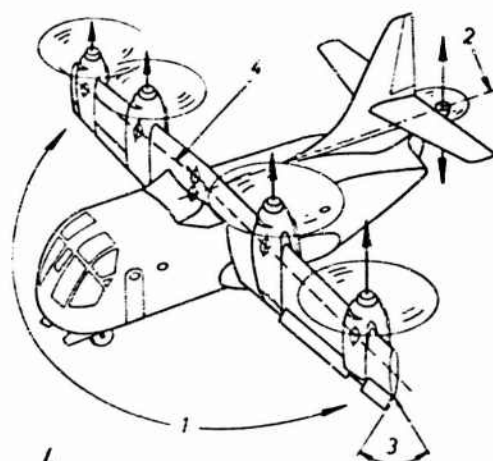


Figure 18

(a) LTV XC-142A TILT WING CONTROLS  
DURING HOVERING AND TRANSITION

CONTROLS ON:

1. ROLL: differential thrust on external propellers.
2. PITCH:  $\pm$  tail rotor thrust pitch control.
3. YAW: differential aileron deflection inside propeller slipstream.



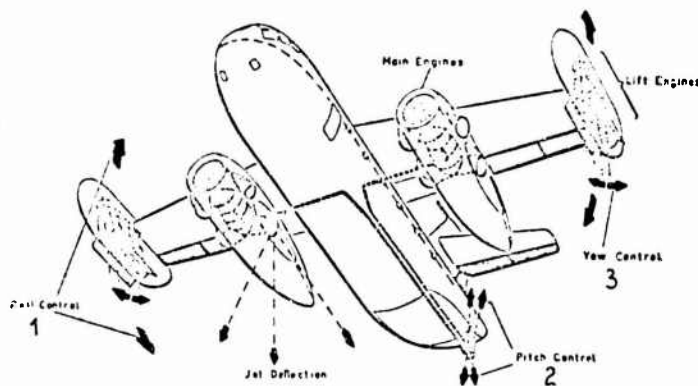
4 - Cross-shafting between the four engines and tail rotor.

VERTICAL LIFT { 4 turbo-prop. GE T64-GE1 ( $\sim 2800$  HP each)  
 $T_t/W_{T.O.} \sim 1.15$

(b) DORNIER Do-31E CONTROLS IN VTOL MODE

( $T_t/W_{T.O.} \sim 1.1$ )

1. ROLL: differential lift-engines thrust.
2. PITCH:  $\pm$  nozzle thrust at tail.
3. YAW: vanes in lift-jet exhausts.



VERTICAL LIFT { 2 BS Pegasus 5-2 (Vectored thrust  $\sim 14$  tons)  
8 RR RB 162-4D (Lift thrust  $\sim 16$  tons)

Fig. 19 VTOL controls

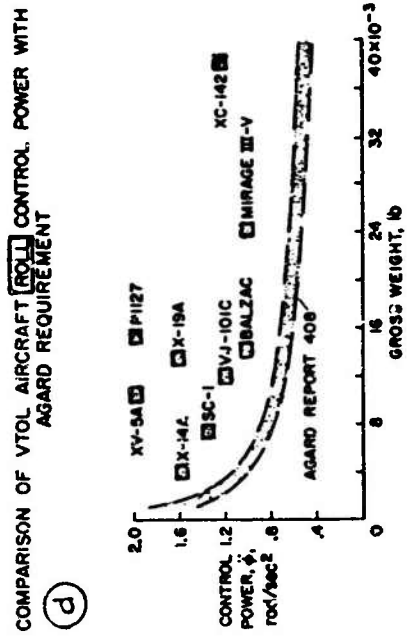
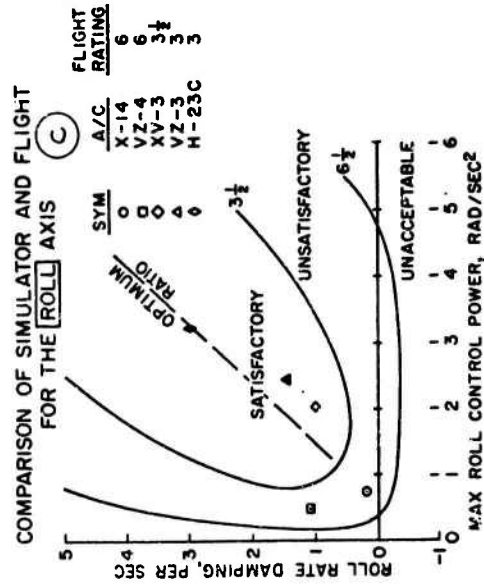
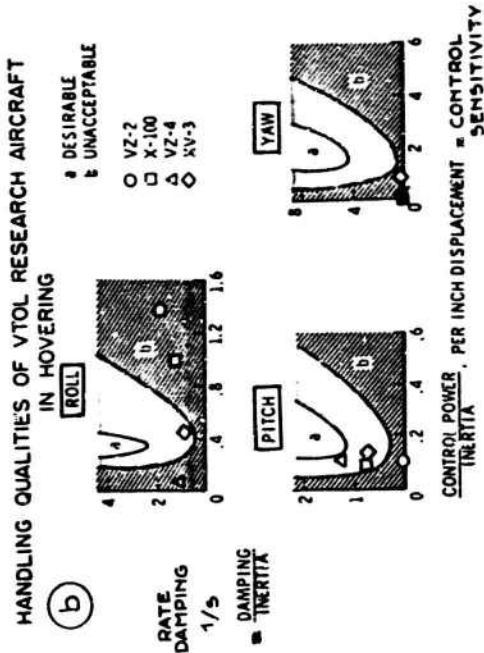
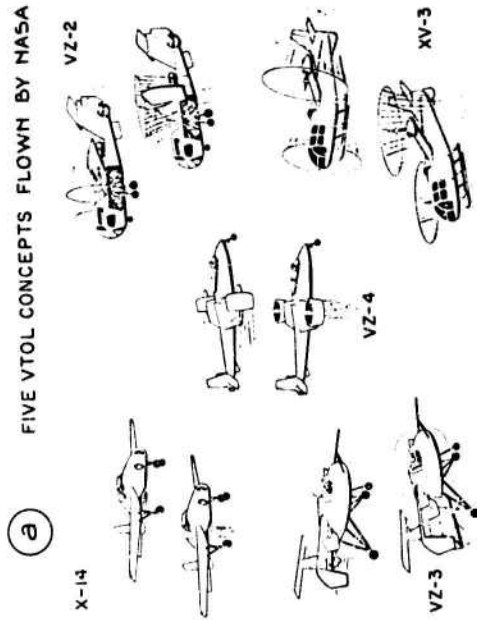


Fig. 20 Some VTOL handling criteria

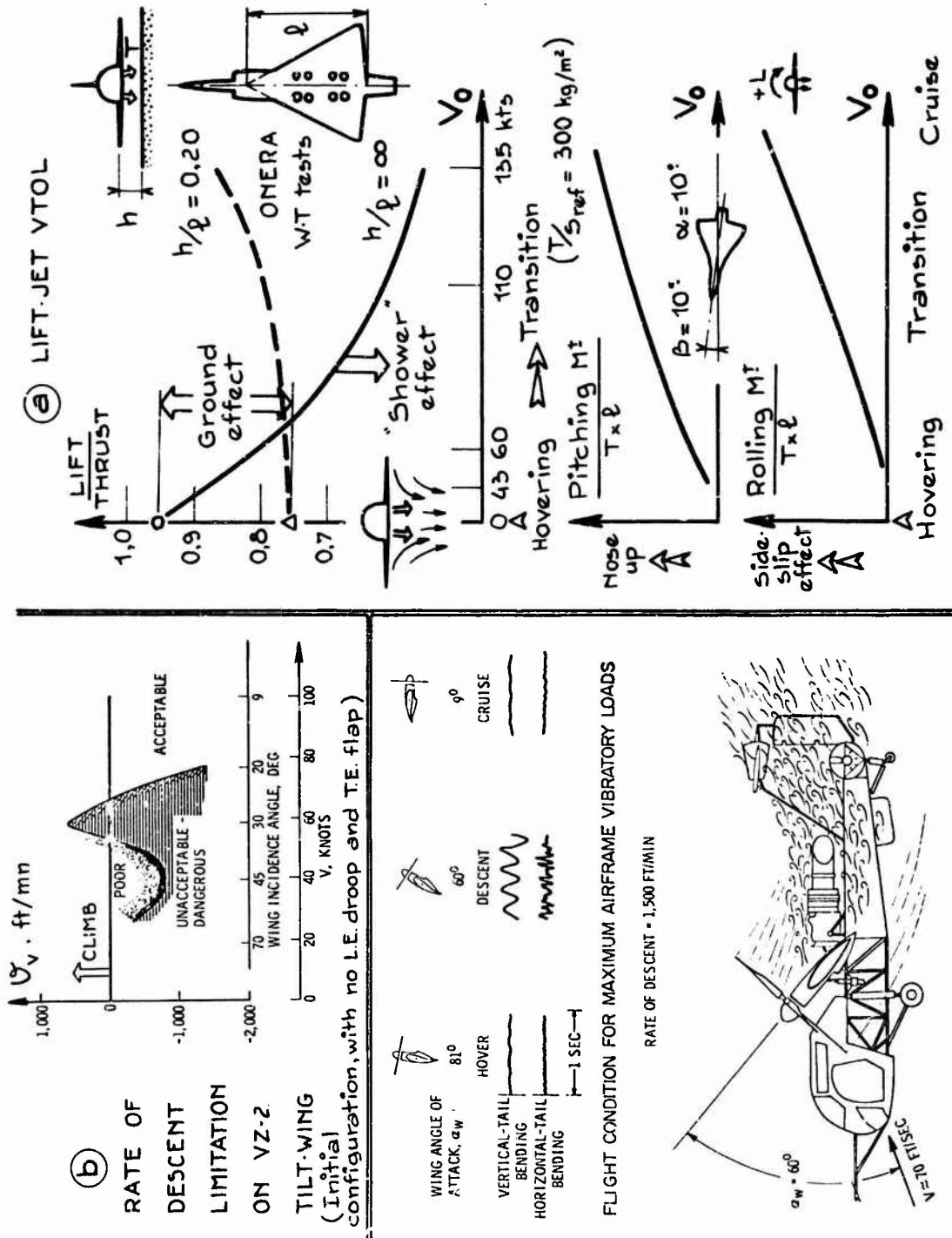
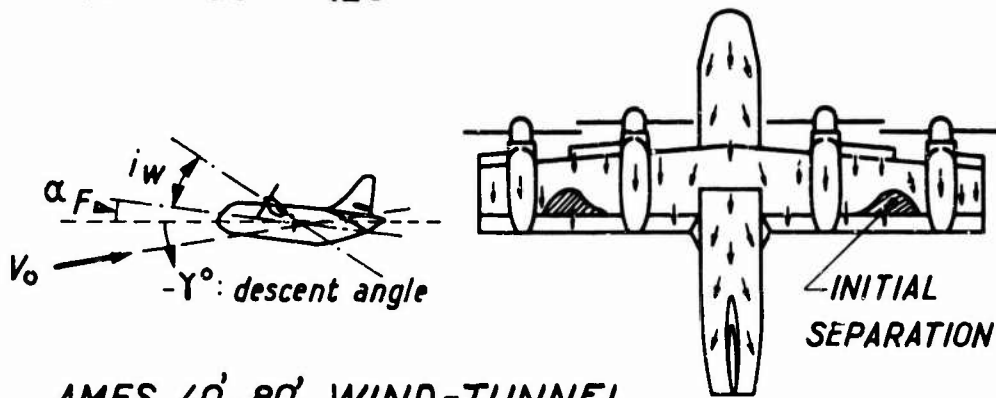
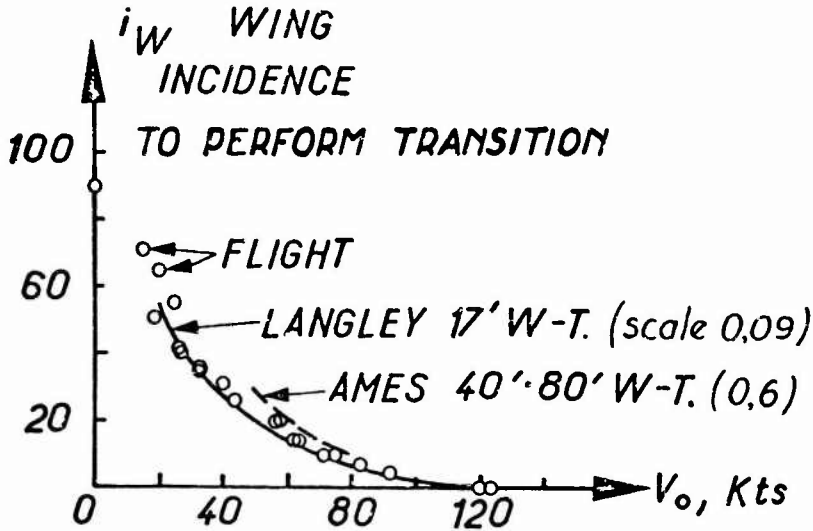


Fig. 21 Aerodynamic interactions

(a) Tilt-wing deflection



(b) AMES 40'x80' WIND-TUNNEL  
Force tests and tuft visualization, on a 0.6 Scale Model

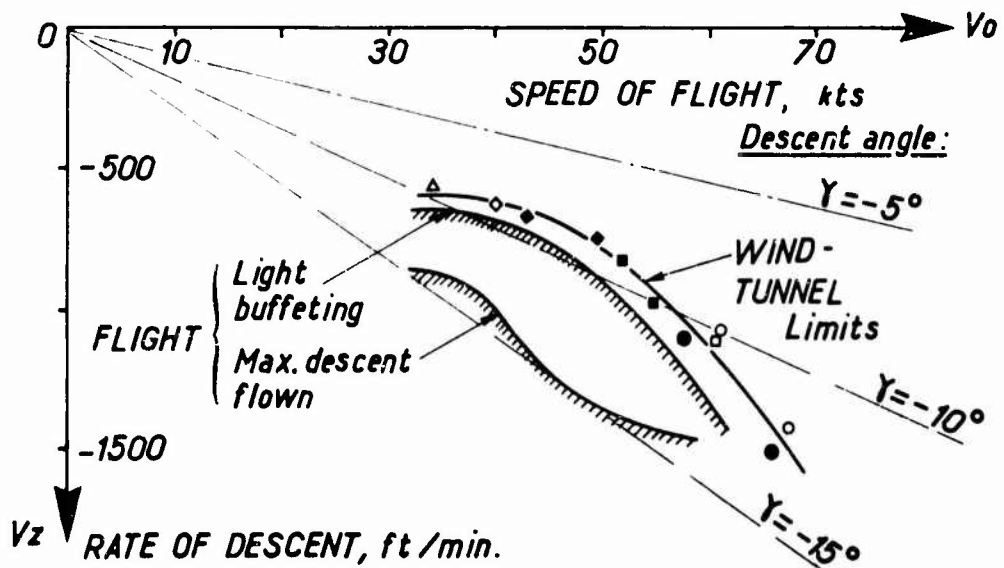
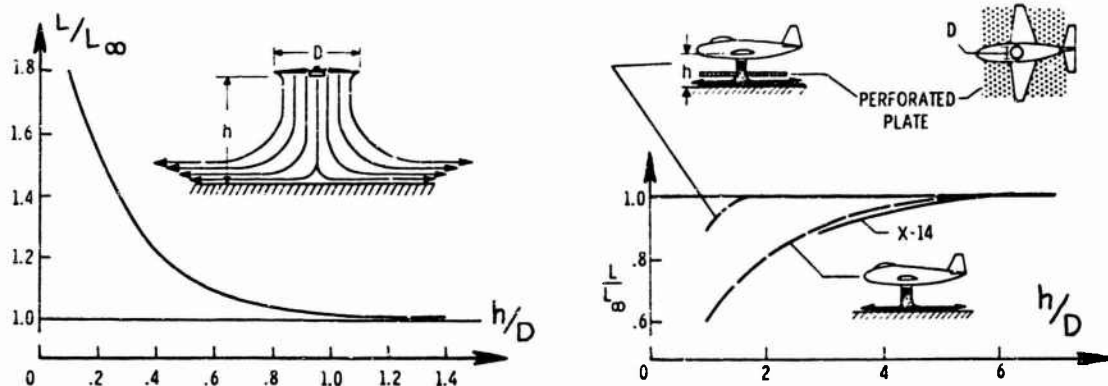
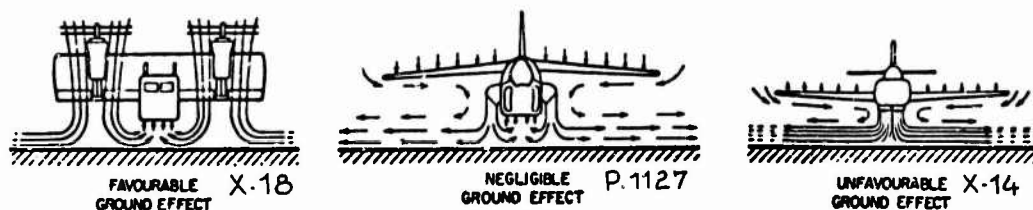


Fig. 22 XC.142A tilt-wing VTOL - Aerodynamic limitation during descent





(a) FAVOURABLE ON HELICOPTERS, and UNFAVOURABLE ON SEVERAL JET-VTOL TYPES

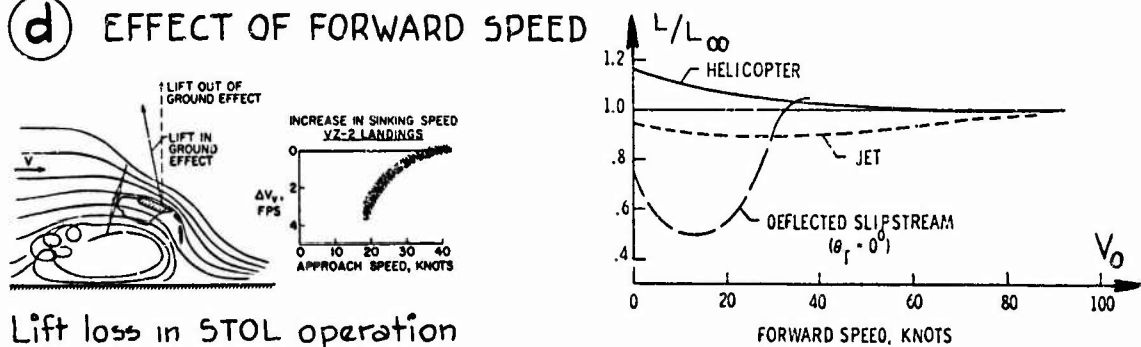


(b) SLIPSTREAM/AIRFRAME INTERFERENCE



(c) DESTABILIZING EFFECT ON ROLLING MOMENT

(d) EFFECT OF FORWARD SPEED



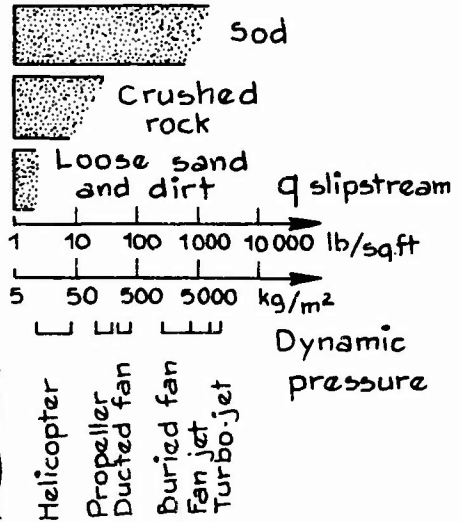
Lift loss in STOL operation

Fig.23 Ground-effect on V/STOL aircraft

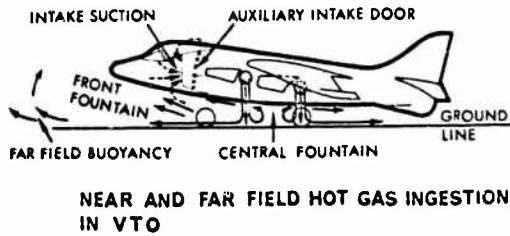
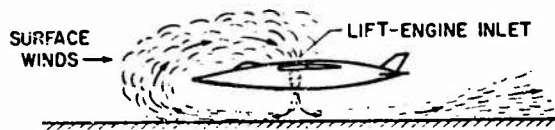
**(a) GROUND EROSION**



Resistance of various surfaces to erosion



**(b) HOT GAS INGESTION**

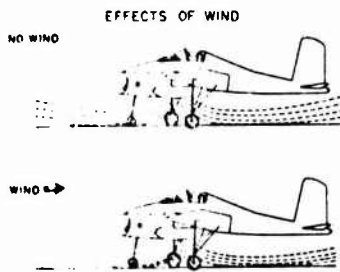


**REASONS FOR CONCERN**

- THRUST LOSS
  - TEMPERATURE RISE OF 40°F CAUSES 15% LOSS OF THRUST
- COMPRESSOR STALL
  - RAPID TEMPERATURE RISE
  - TEMPERATURE DISTRIBUTION

**CAUSES**

- BUOYANCY OF HOT EXHAUST
- SURFACE WINDS
- CONFIGURATION
  - EXHAUST AND INLET ARRANGEMENT



**EFFECT OF HEADWINDS ON REINGESTION**

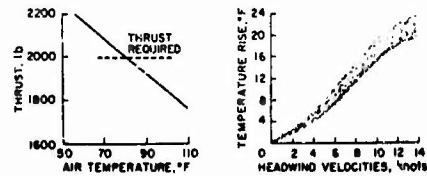
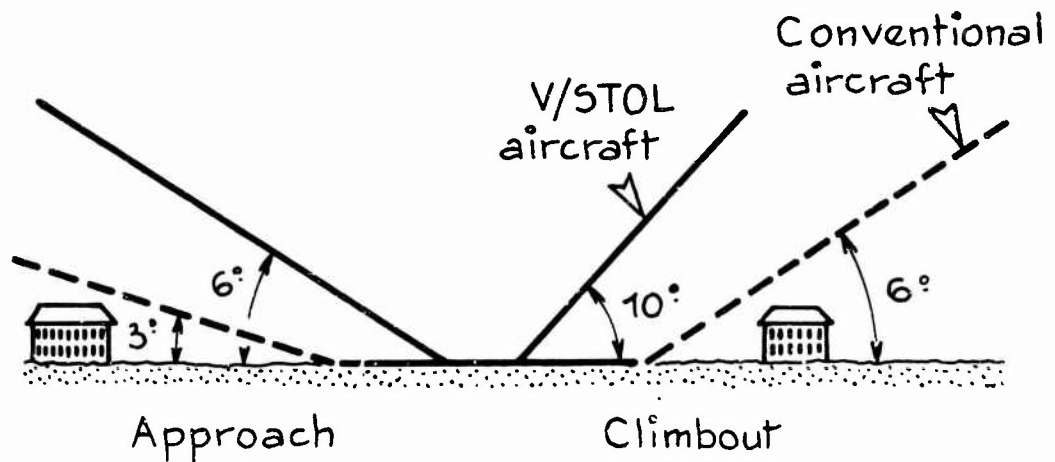
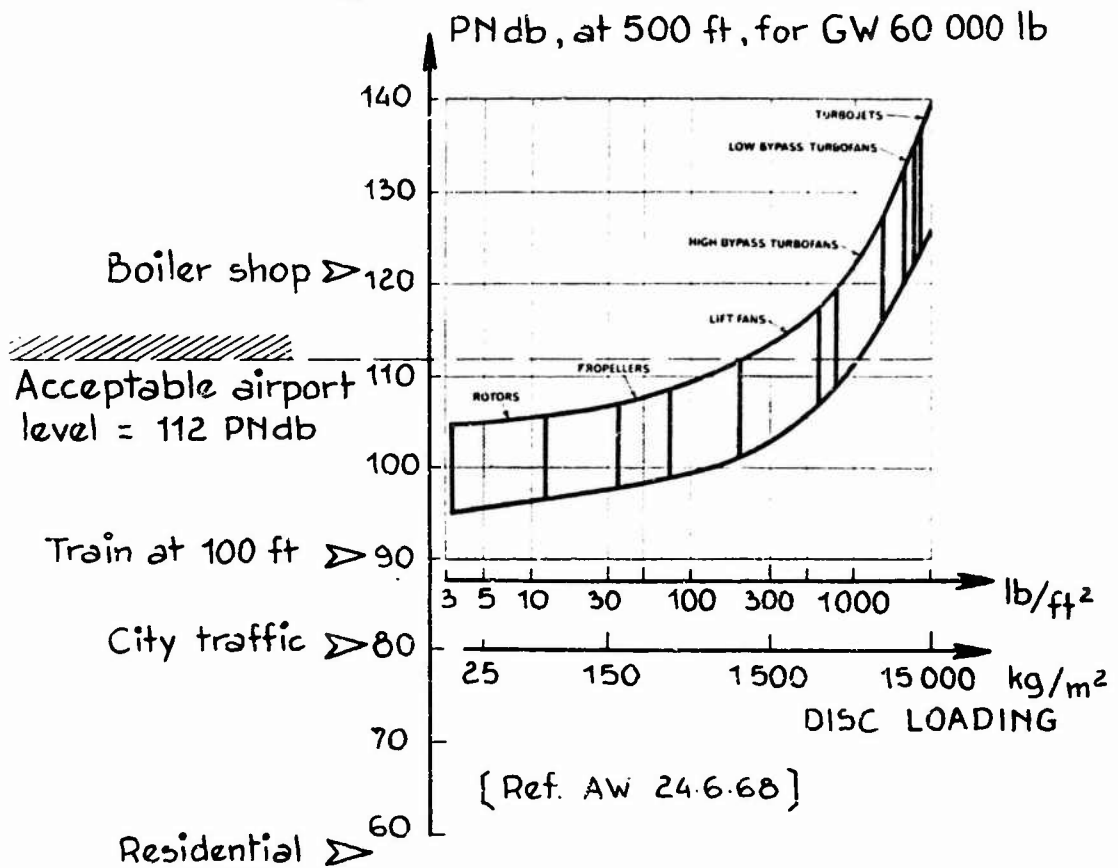


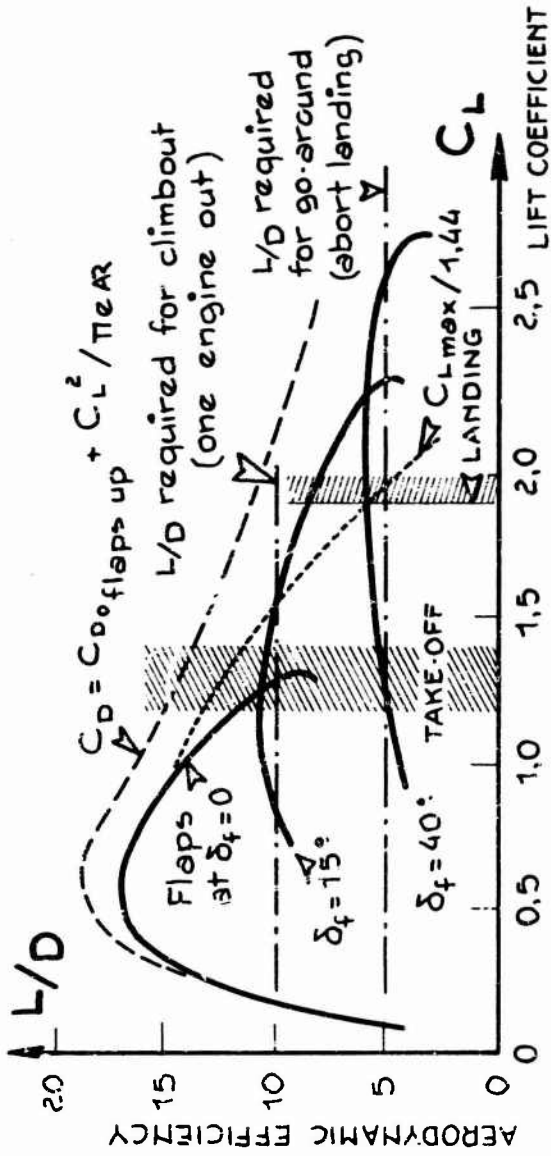
Fig. 24 Ground effect problems on V/STOL aircraft

(a) PERCEIVED NOISE LEVEL



(b) STEEPER V/STOL TRAJECTORIES MINIMIZE NOISE ON POPULATED AREA NEAR AIRPORTS

Fig. 25 V/STOL noise problem



LANDING

Approach speed and slope = f  $\left\{ \begin{matrix} C_{Lmax} \\ W/S \\ L/D \end{matrix} \right.$

Ground roll = f  $\left\{ \begin{matrix} C_{Lmax} \\ W/S \\ C_D \\ \text{Braking friction} \\ \text{Reverse thrust} \end{matrix} \right.$

APPROACH

GO AROUND

= f  $(T/W, L/D)$

FLARE

GROUND ROLL

FLARE

TAKE-OFF

Ground run = f  $\left\{ \begin{matrix} T/W \\ W/S \\ C_{LTO} \\ C_D \\ \text{Rolling friction} \end{matrix} \right.$

Climbout = f  $\left\{ \begin{matrix} T/W \\ L/D \\ \text{Low } C_{Lmax} \\ \text{High } L/D \end{matrix} \right.$

CLIMBOUT

FLARE

FLARE

35 or 50'

Fig. 26 Take-off and landing performance requirements (ref. J.K. Wimpers A/A, Feb. 1966)

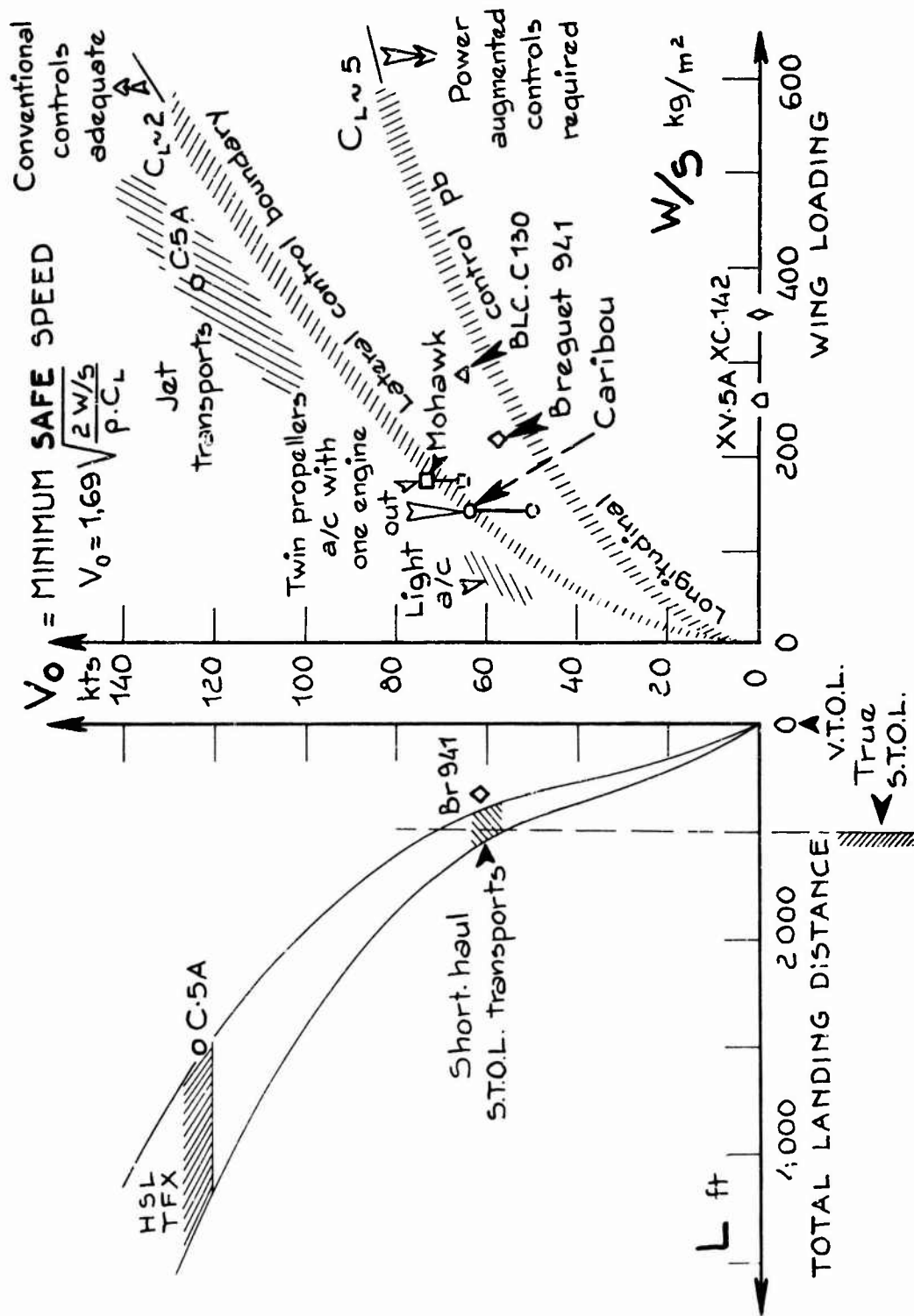


Figure 27

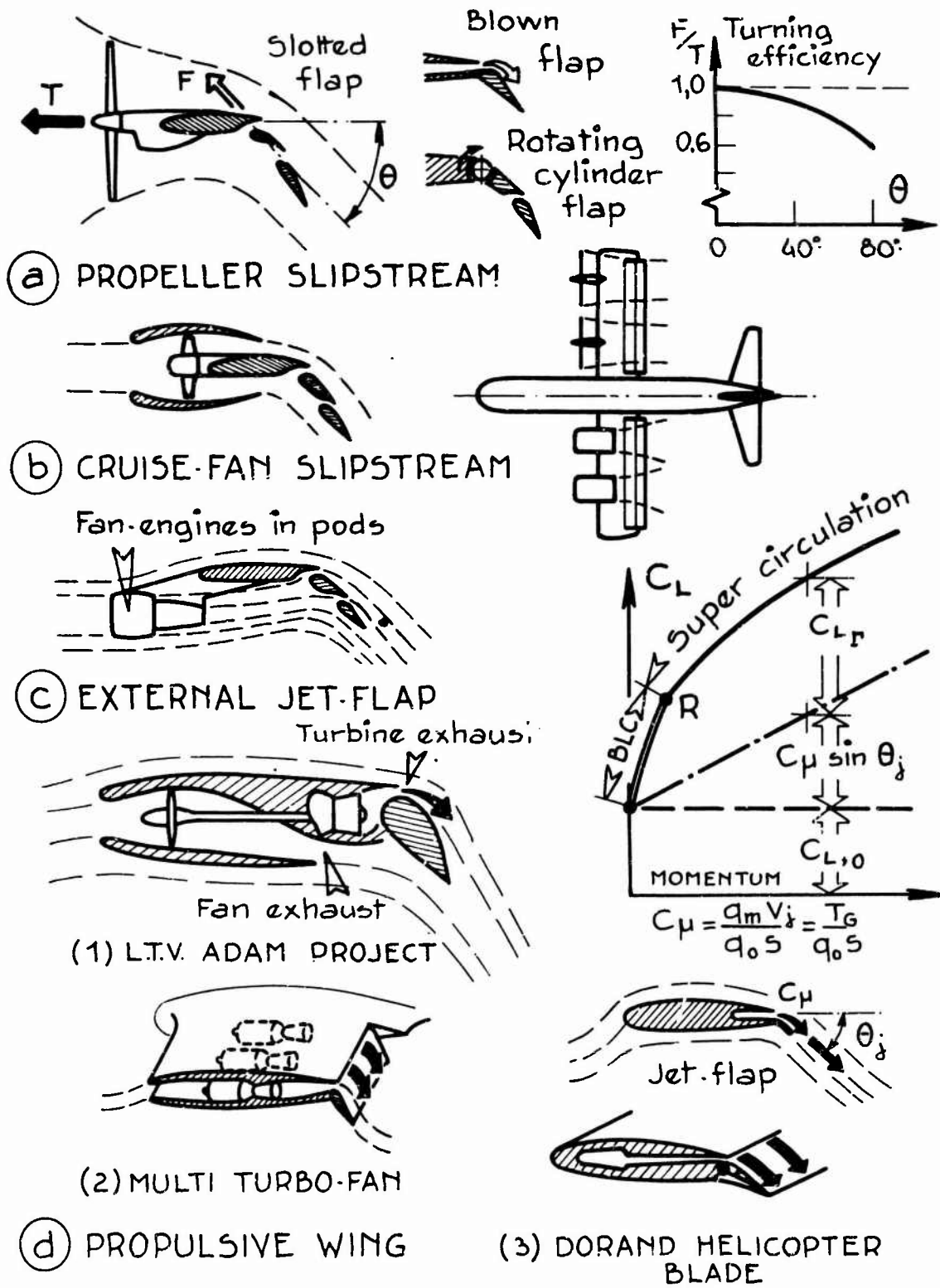


Fig. 28 Powered lift STOL systems

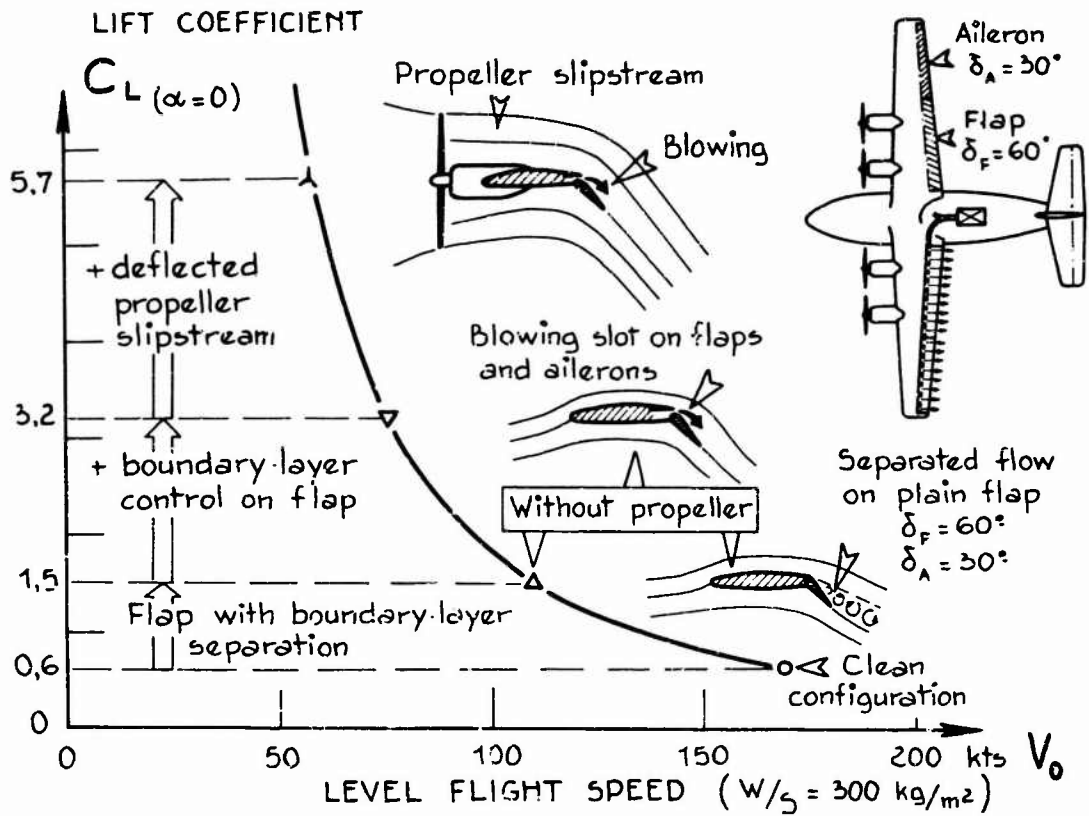


Figure 29

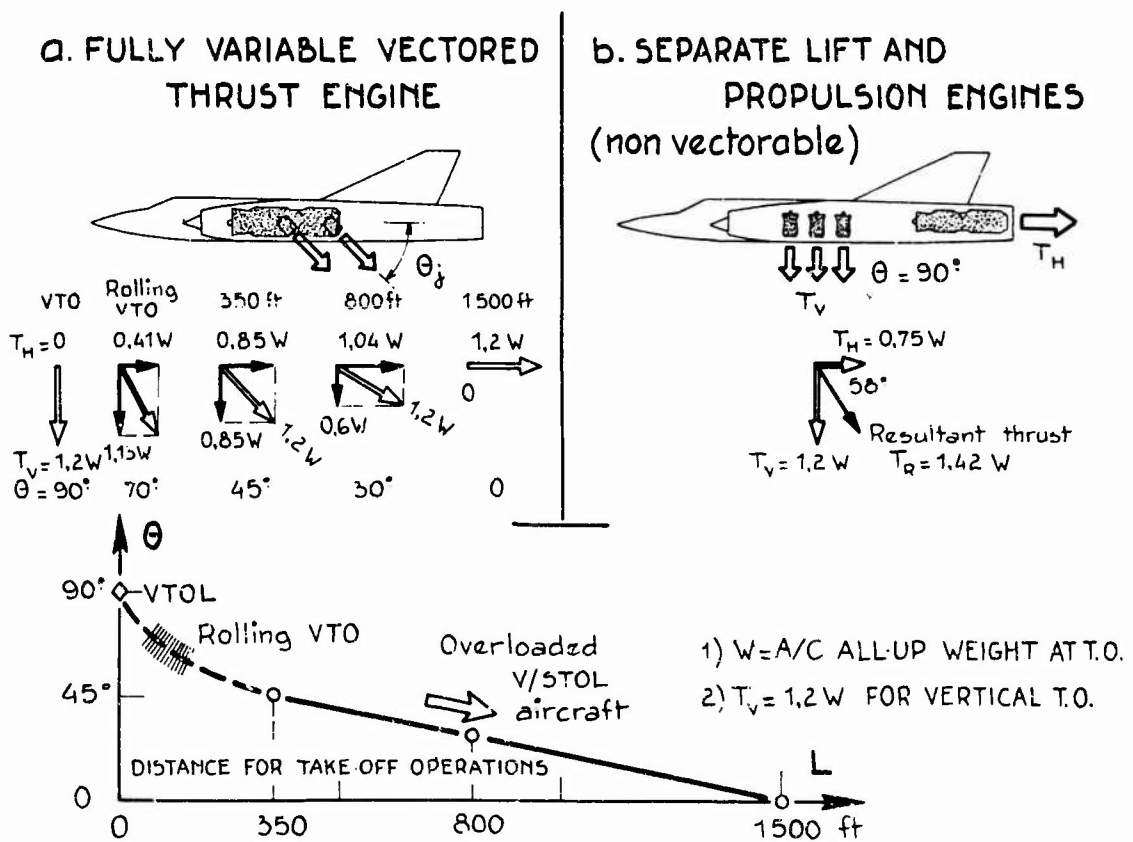


Fig. 30 Combined lift and propulsion for jet V/STOL aircraft

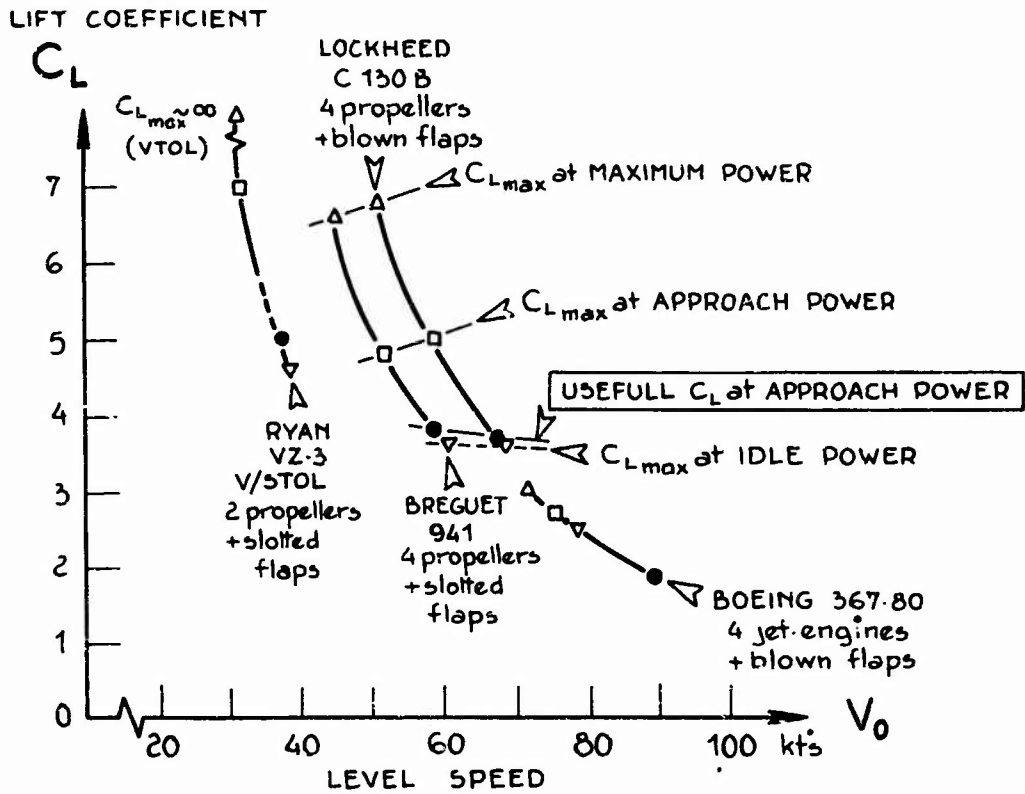


Fig. 31 Lift characteristics at various engine powers for various STOL tested in flight by NASA

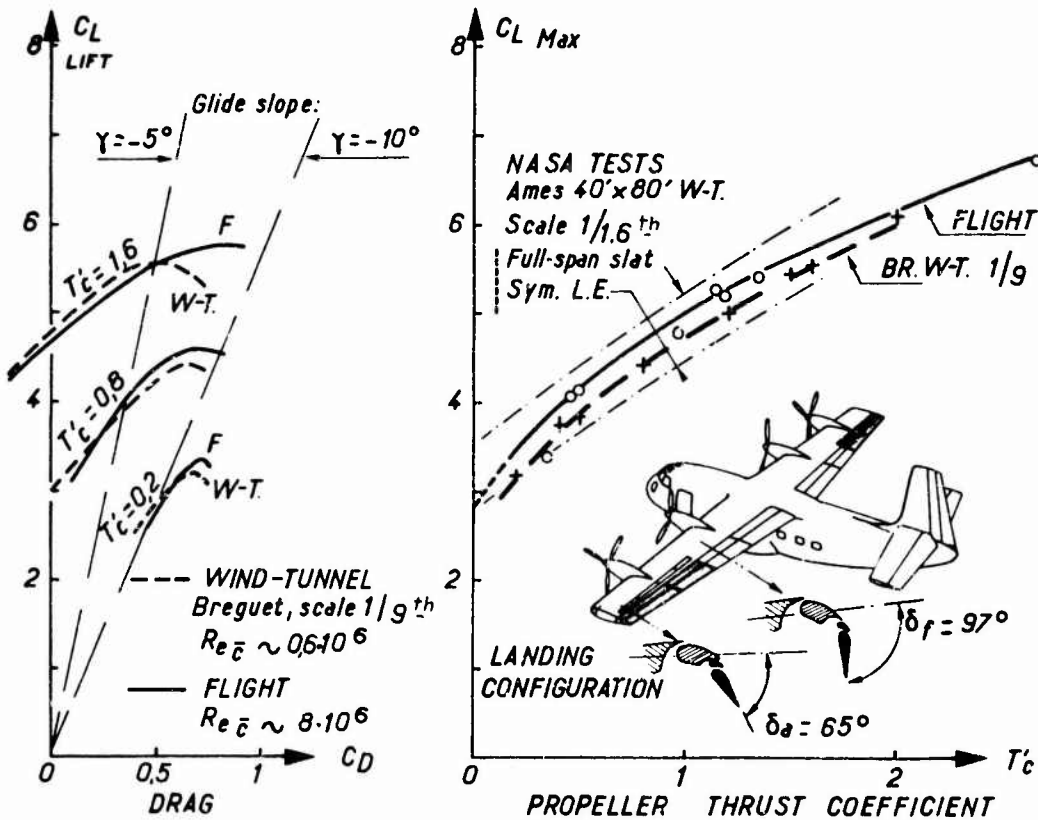
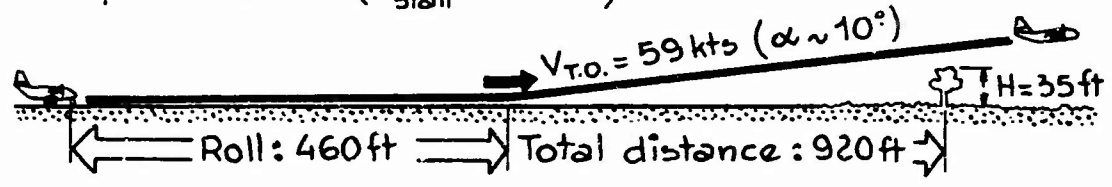


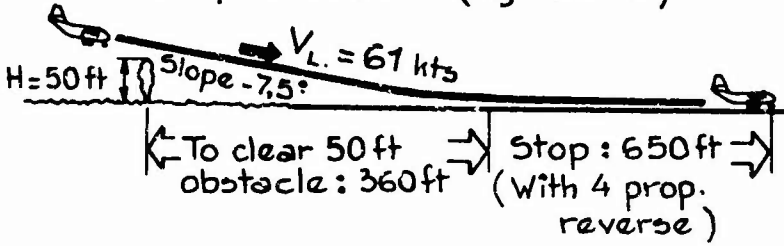
Fig. 32 Breguet 941



**a. STANDARD TAKE-OFF**  $W_{T.O.} = 17.4$  tons  
 on 4 turbines (4x1100HP)  
 Flaps :  $45^\circ/30^\circ$  ( $V_{stall} = 49$  kts)



**b. STANDARD LANDING**  $W_L = 17.4$  tons  
 on 4 turbines (4x330 HP)  
 Flaps :  $98^\circ/65^\circ$  ( $V_s = 55$  kts)



**c. CRUISE**  
 $W = 4 \times 900$  HP  
 $V_0 = 225$  kts  
 ( $Z = 10,000$  ft)

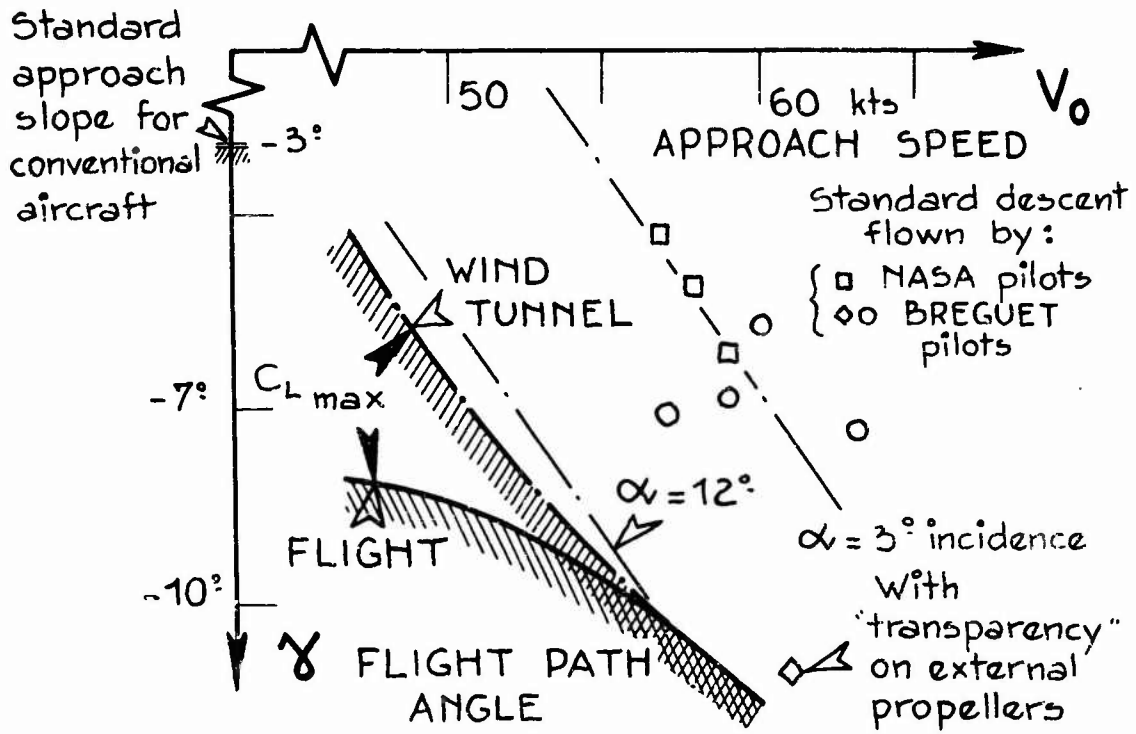
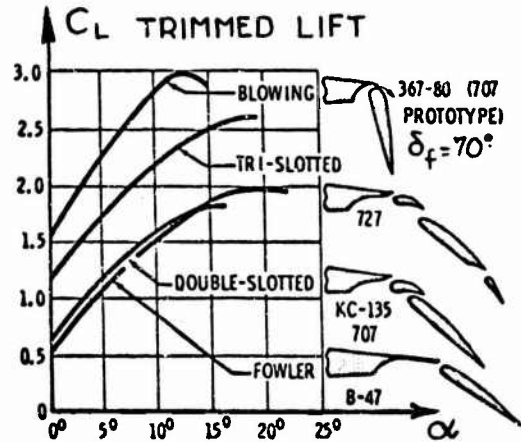
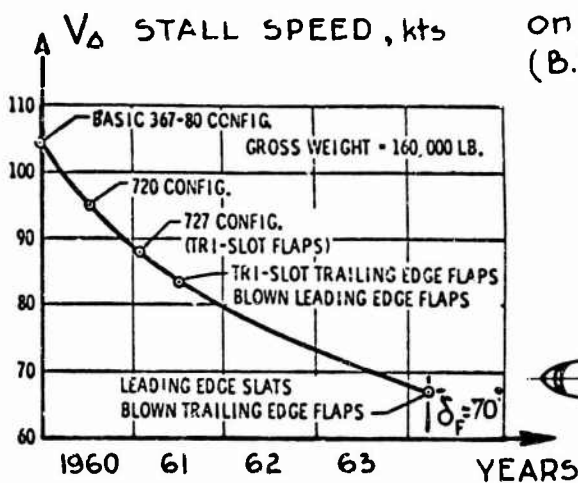


Fig. 33 STOL Breguet 941 low speed performances

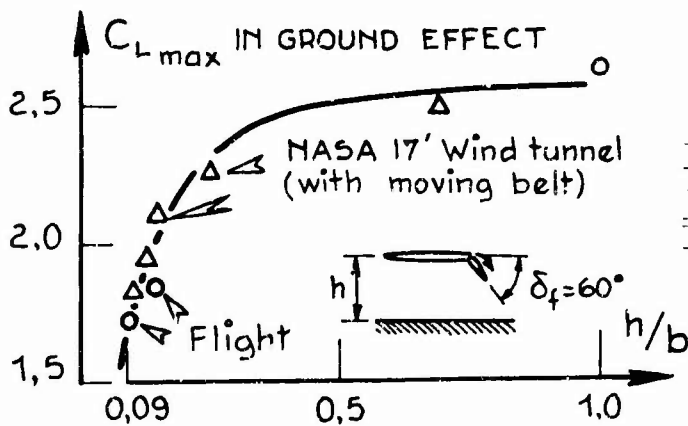
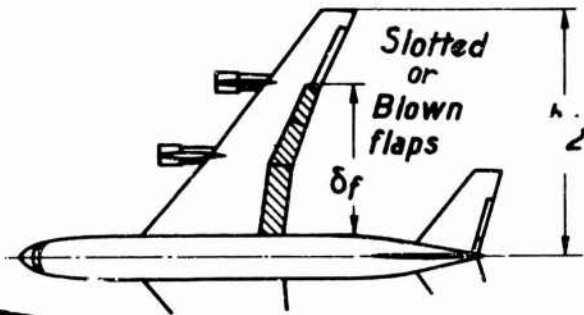
(a) HIGH LIFT DEVICES ON VARIOUS LARGE JET AIRPLANES, from Boeing flight tests.



(b) SUCCESSIVE STALL SPEED REDUCTIONS WITH HIGH LIFT DEVICES IMPROVEMENTS



on the Boeing 367-80 (B.707 prototype)



367-80 BLC INSTALLATION

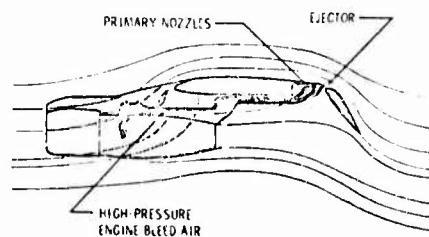


Fig. 34 Low speed capability of jet transports

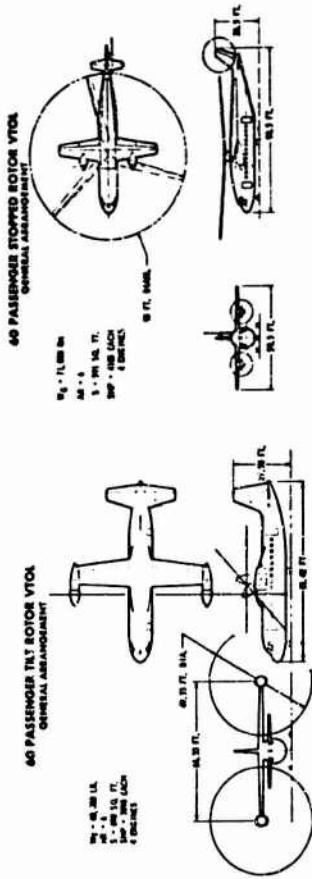
DESIGN CRITERIA FOR V/STOL STUDY

- RANGE . . . . . 500 STATUTE MILES
- PAYLOAD . . . . . 60, 90, AND 120 PASSENGERS
- FIELD LENGTH . . . . . VTOL — AS REQUIRED  
STOL — 1000 AND 2000 ft

- PROPULSION SYSTEM . . . . . AVAILABLE BY 1970
- T/W REQUIREMENTS FOR VTOL AIRCRAFT  
T/W = 1.15 (ALL ENGINES)  
T/W = 1.05 (CRITICAL ENGINE INOPERATIVE)

- CONTROL REQUIREMENTS FOR 60 PASSENGER AIRCRAFT

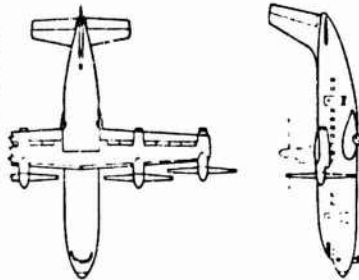
	VTOL	STOL
PITCH	.60 rad/sec <sup>2</sup>	.40 rad/sec <sup>2</sup>
ROLL	1.20	.45
YAW	.50	.20



LOCKHEED CONCEPTS

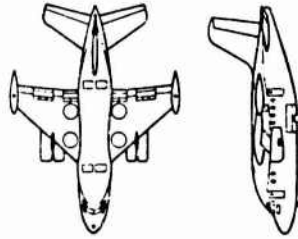
BOEING / VERTOL CONCEPTS

TILT WING VTOL



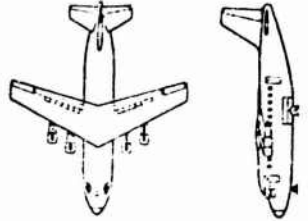
GROSS WEIGHT . . . . . 71704 LBS.  
SPAN . . . . . 79.5 FT.  
LENGTH . . . . . 79.5 FT.  
PROP. DIA. . . . . 21.1 FT.  
WING LOADING . . . . . 91 LB./SQ. FT.  
DISC LOADING . . . . . 51 LB./SQ. FT.  
ENGINES  
4 TURBO SHAFT  
6741 SHP EACH

LIFT FAN VTOL



GROSS WEIGHT . . . . . 79191 LBS.  
SPAN . . . . . 58.5 FT.  
LENGTH . . . . . 82.5 FT.  
WING LOADING . . . . . 74.6 LB./SQ. FT.  
ENGINES:  
CRUISE 4 TURBOFANS  
6960 LBS. THRUST  
LIFT:  
4 GAS GENERATORS  
DRIVING 4 TIP  
TURBINE LIFT FANS  
OF 17600 LBS. THRUST

TURBOFAN STOL



GROSS WEIGHT . . . . . 62971 LBS.  
SPAN . . . . . 68 FT.  
LENGTH . . . . . 80 FT.  
WING LOADING . . . . . 85 LB./SQ. FT.  
ENGINES  
4 BYPASS RATIO  
3 TURBOFANS  
7482 LBS. THRUST EACH

Fig. 35 NASA shorthaul V/STOL study (NASA, SP.116, April 1966)

PAPER B

PURE AND COMPOUND HELICOPTERS

by

Paul F. Yaggy

Technical Director  
US Army Aeronautical Research Laboratory  
Moffett Field, California

## NOTATION

Several symbols defined in the text are not included in the following list:

A	area
$\alpha$	angle of attack
$\alpha_0$	mean angle of attack
AR	aspect ratio
B	tip loss factor
b	number of blades
c	blade chord
$C_D$	drag coefficient
$C_L$	lift coefficient
$C_{mac}$	airfoil pitching moment coefficient about a.c.
$C_M$	pitching moment coefficient
$C_P$	pressure coefficient
$C_T$	rotor thrust coefficient
$C_Q$	rotor torque coefficient
$\delta_p$	profile drag coefficient
D/W	drag to weight ratio
f	equivalent flat plate area or frequency
g	normal acceleration factor
$\gamma$	Lock number
h	vertical translation
HP	horsepower
k	reduced frequency
$(L/D)_e$	effective lift to drag ratio
M	figure of merit or Mach number
$\mu$	advance ratio
$\Omega$	rotor angular velocity
P	power

$\phi$	$\tan^{-1} v/\Omega R$
$\psi$	blade azimuth position
q	dynamic pressure
$\rho$	air density
R	rotor radius
SFC	special fuel consumption
$\sigma$	solidity
SHP	shaft horsepower
T	thrust
$\theta$	blade geometric angle with respect to shaft
v	induced velocity
V	velocity
$V_T$	rotor tip speed
$E_{\alpha}^3$	three-dimensional aerodynamic damping parameter

*Subscripts*

c	control
cr	critical
d	divergence
e	effective
f	parasite
G	gust
ind	induced
h	hover
m	maneuver
pr	rotor profile contribution
s	separation
W & E	wing and empennage contribution
$\infty$	freestream condition

*Superscripts*

s	stall
---	-------

## PURE AND COMPOUND HELICOPTERS

Paul F. Yaggy

### 1. INTRODUCTION

#### 1.1 Role of the Helicopter - Present and Future

Historically, the concept of using air screws for vertical lift and vertical flight is very old. Starting with the Chinese top which was nothing more than a toy, progressing through Leonardo da Vinci's design in the fifteenth century, and paying tribute to the efforts of such men as Sir George Cayley and W.H. Phillips of England, Enrico Forlanini of Italy and Thomas Edison of the United States, we are led to the many attempts made at achieving vertical flight in the early twentieth century. In 1907, Paul Cornu of France constructed a machine which carried a pilot aloft. Light, fabric covered construction was utilized in the rotors and the airframe consisted merely of a single beam with a rotor shaft at either end. The machine never flew untethered. In the period from 1908 to 1929 the Berliners, father and son, spent most of their lives on the development of helicopters. In 1909 they built a two engine craft utilizing counter rotating rotors which lifted the pilot untethered. Later, they built a vehicle with side-by-side rotors and wings. This aircraft included two rather recent innovations in the form of a pair of *rigid* wooden rotors which were *tilted* from horizontal in the hover mode to vertical in the cruise mode. Other men in almost every modern nation tried to master the techniques necessary to vertical flight. These included such aeronautical greats as von Kármán, Sikorsky, Pescara, de Bothezat, and von Baumhauer. The most pivotal effort in the attempt to achieve vertical flight, however, was the work of Juan de la Cierva in developing the first truly successful rotary wing aircraft, which he called the "autogiro". The autogiro did not actually achieve truly vertical flight. It did, however, lay the groundwork by providing the knowledge and technology necessary for subsequent practical helicopter flight.

In the 1930's, rapid advances in helicopter technology were achieved through the efforts of d'Oscanio of Italy, Breguet of France, Focke and Flettner of Germany, and Sikorsky of the United States. By the end of that decade, helicopter flight had been successfully achieved. However, it was during World War II that the real impetus for helicopter development took place both in the United States and in Germany. Many helicopter designs were undertaken and several were placed in production. In the late 1940's, the general pattern of helicopter-type aircraft had been formulated to a rather complete degree and most of the current configurations had been given serious consideration by the 1950's. These included single rotors, tandem rotors, coaxial rotors, shaft driven and tip driven rotors, side-by-side rotors, and compounded rotor systems.

The helicopter has succeeded as an operational vehicle because no other aircraft, no matter how simple or inexpensive, has been able to compete with it in the performance of certain tasks. As Douglas and Schneider point out in Reference 1, the ability of the helicopter to hover and fly safely in the vertical flight regime, and then transition smoothly into the forward flight regime is a unique capability as compared with fixed wing aircraft. The decade past has seen many varied programs of research and development in the V/STOL aircraft field, all of which, with the exception of the UK P-1157 fighter, have failed to produce a type that has been committed to production. The fixed wing aircraft is generally less expensive to buy, maintain, and operate than the helicopter, but the helicopter is more cost effective for the performance of certain missions than any other

aircraft. The use of helicopters in great quantities, particularly in military missions, demonstrates that its mission effectiveness is worth the increase in cost because it can do something which no other aircraft can do with comparable efficiency.

Presently, the helicopter is used in operational procedures which take advantage of characteristics other than the ability to hover. The low downwash produced by the slowly turning large rotor has important implications in operating over environments where ingestion due to re-circulation can occur from such soil characteristics as sand and gravel. Improvements in the reliability, maintainability, and functional capability have further enhanced the desirability of the helicopter for many applications. Although many other aircraft such as the Helioplane, the Dornier 2", the Scottish Pioneer, and other STOL aircraft have been used to attempt the hovering and low speed mission requirements, these aircraft were functionally incapable of performing the variety of missions under adverse operational circumstances that the helicopter could perform. Recent innovations, many of which will be discussed during this lecture series, are capable of hover and vertical flight, but all have failed to compete satisfactorily with the helicopter for missions requiring speeds below 200 knots because of the increased complexity, higher low-speed fuel consumption, greater costs, and higher downwash velocities which result from their use. This circumstance could change in the future as the technology of VTOL aircraft advances.

The present utilization of helicopters finds many and varied uses. In the military role, we find the helicopter employed in tasks such as; light observation, light tactical transport, medium transport, armed escort, anti-submarine warfare, air-sea rescue, vertical replenishment, in-shore replenishment, and general utility. Examples of civil uses are short haul transportation, police patrol, aerial surveys, and aerial spraying for agricultural and pest control projects. These many and varied uses are represented pictorially for several American helicopters in Figure 1. It is apparent that the projected use of the helicopter extends far into the future. The helicopter configuration is by no means stabilized. The advent of new technologies, such as compounds, slowed, stopped, and trailed or retracted rotors (in addition to the conventional configurations of single rotor and tandem rotor helicopters), indicates a strong interest in the rotary wing as a continuing means of both military and civil transport. The recent commitment by the US Army for the production of an armed compound helicopter indicates the conviction that this vehicle is, at least at present, superior in its capabilities for certain missions over all other contenders. The appearance of very large heavy lift helicopters has opened an entirely new field of applications which cannot be performed competitively by any other known vehicle. It is because of the projection of future use of the helicopter in this manner that continued efforts in research are required, not only to stabilize the configuration, but to systematize and organize the technologies and produce design mathematical models which will permit the major technical advances required to realize the potential of this highly complex machine.

## 1.2 Trends in Performance and Design

Records indicate that a fourfold increase in the yearly production of helicopters in the free world has taken place within the past ten years. It will be of interest to our study at this session to examine the trends which have led to this remarkable increase in utilization. Perhaps the most significant advance is represented by the progress made in helicopter power plants. The transition from piston engines to gas turbine engines enabled a sizable increase in the overall performance of the helicopter. The trends of specific fuel consumption and specific weight of the power plants are indicated in Figure 2. Although further reductions in specific weight will be small, there is yet hope for additional reduction in specific fuel consumption. Reliability and maintainability of these power plants has increased, but has been somewhat hampered by the environment in which the engine must operate. Reingestion problems of foreign materials, as well as vibration have compromised the reliability and maintenance functions. However, it is believed that continued research will improve these characteristics. Filtering devices which can avoid pressure losses are being devised and vibration is a subject of continuing research to reduce its influence.



Another major factor in the increased use of helicopters is the trend towards increased cruise speeds. In 1947 a noted authority, Dr J.A.J. Bennett, stated that the upper limit of the speed of pure helicopters would be 150 miles per hour. This seemed optimistic at the time, since few of the existing helicopters could reach even 100 miles per hour. In 1953, when the YH-21 and XH-39 had reached this speed, many felt that further increases in speed were not to be expected. This pessimism was not shared by Prof. Rene Miller of Massachusetts Institute of Technology, who made the declaration that speeds of 170 knots would shortly be obtained. As can be seen from Figure 3, Prof. Miller's prediction was verified and ten years later the French Super Frelon attained a speed of 189 knots. This trend has been continued and recently the Lockheed XH-51A has demonstrated speeds in excess of 200 knots in the pure helicopter mode. Figure 3 also indicates the trend of compound speeds, and it is anticipated that additional increases in speed capability can be expected. Some manufacturers now project cruise speeds for pure helicopters in excess of 200 knots. As is indicated in Reference 1, from which Figure 3 has been extracted, a convenient measure of aerodynamic efficiency is given by the ratio of gross weight to flat plate area. This ratio has increased from 400 to over 1000 in the past ten years as a result of drag reduction cleanup exercises and increases in allowable gross weight. At the same time, installed power loading has been reduced from ten to six as a result of increased power available, increased design hover ceilings, and increases in gross weight with minimum increase in size.

The trend has been toward higher disc loadings, and therefore higher downwash velocities. Disc loadings doubled in the period from 1950 to the present. However, there is a decided reduction in the rate of increase in recent years. Disc loadings in excess of 15 pounds per square foot are not particularly welcome by many users, particularly in marginal terrain conditions where loose soil or water are present. Military users are much more content with disc loadings around ten pounds per square foot. However, the use of higher disc loadings has not been precluded. The aeroelasticity of the rotor system has received considerable discussion in recent times and can be a matter of misconception unless viewed carefully. The introduction of so-called "rigid" rotor systems has, to some degree, led to the belief that more rigid systems are being employed. However, it should be noted that although the mechanical hinge has been removed, equivalent flexibility has been incorporated into the hub systems. An outstanding contradiction to this fact is the Bölkow 105 rotor system, which is truly a more rigid system. The effects of additional rigidity on rotor aerodynamics is important and will be discussed in more detail later in the lecture. Much effort has been made in recent years to obtain a better understanding of the aeroelastic phenomena. Some progress has been made but considerable additional research is necessary. Since this lecture series deals primarily with aerodynamic problems, no attempt will be made to discuss in detail other items which contribute to the increased usage of the helicopter. However, a brief itemization is included. These items are: improved structural materials, simplification of rotor parts such as rotor hubs, increased power transmission efficiencies, improved safety records, reduced vibration levels, and a less than expected vulnerability factor.

### 1.3 Combinations and Permutations of Rotorcraft Design

The trends indicated in the previous section have driven the helicopter designer to consider requirements which exceed those of the conventional rotor systems with which he has been employed. The lack of understanding of many basic fluid mechanics problems in addition to those of structures and mechanics, has tempted many designers to avoid these problem areas rather than obtain their solutions. This has resulted in such concepts as compounded systems, where fixed aerodynamic surfaces are employed to unload the rotor in the high speed flight condition and forward propulsion is provided by auxiliary power plants, and in composite aircraft which employ various techniques such as tilting the rotor to become a propeller and stopping the rotor to either carry lift in its stopped condition or to be folded, in which case it is either trailed or stowed. Each of these techniques has merit and no criticism is intended, but the implication is clear that at least in some speed regimes, these techniques avoid the real issue which is to effectively solve problems that limit pure rotor applications. Some designs have sought to alleviate

some of the basic problems which are peculiar to rotary wing devices through the use of variable geometry, circulation control, and the advancing blade concept. Again, each of these has merit, but the great profusion of combinations and permutations which are appearing on the scene emphasize the fact that basic understanding is lacking and a stabilization of helicopter configurations analogous to the stabilization in fixed wing aircraft on the cantilever monoplane configuration not only has not been obtained, but is not in sight.

It cannot be clearly stated at this time whether or not it would be desirable to attempt a stabilization of configuration. It was only through continued research and much experiment that stabilization of configuration took place in fixed wing aircraft. The extreme complexity and high degree of sophistication in the problems of helicopters have discouraged intensive and sophisticated research of the problems. However, as will be discussed in this lecture, there is considerable impetus implied in present and projected roles for the helicopter to give good justification to a continued and more sophisticated research effort.

#### 1.4 General Limitations of Rotorcraft

The full listing of limitations of rotorcraft would require considerable detail. Since the intent of this section is to provide only introductory remarks, broad characterizations of these limitations will be made. This is not meant to infer that the helicopter is plagued with an undue quantity of limitations, since a full statement of limitations on any vehicle is a formidable task. When the problems of power plants and transmissions are removed from consideration in the discussion of limiting factors, those problems remaining for consideration are primarily associated with the rotor system.

Hovering performance is no longer considered to be a major problem for the helicopter. The improvement in gas turbines and lighter weight transmissions has provided the designer with a wide range of hover capability. The requirements for hovering at high altitude and the specification of hovering at 6000 feet on a 95°F day have increased the capability of the helicopter to perform adequately at zero airspeed for most mission requirements. However, to secure good hovering over a wide range of conditions usually requires a compromise of the high forward speed of the aircraft. This limitation is undesirable and research efforts should be devoted towards devising systems which can relieve this limitation.

Roughness and vibration have continually plagued the helicopter throughout its existence. Although in most regimes of operation present helicopters are smoother than their predecessors, at the more severe flight conditions encountered the vibrations can reach quite severe levels. Usually the most annoying or critical vibrations occur in the transition from hovering to forward flight, in the landing flare maneuver near the ground, and at high forward speeds. The cure for these vibration limitations is not readily apparent and will await the outcome of future research. The problem is extremely complex since it deals with dynamic coupling of the rotor and the fuselage with the initial source of excitation arising from the detailed structure of the highly complex rotor airflow. Rotor shed vorticity and trailing vortex systems in rotary wing flow are an order of magnitude more complicated than that behind an ordinary high aspect ratio wing. Individual wakes interact not only with adjacent wakes, but directly with the blades of the rotor. Thus the rotor tends to lay down its own rough road over which it must then move. The most desirable cure for these vibration problems is at the source. Considerable research is necessary to begin to understand the procedures by which this can be accomplished. In the high speed mode, the rotor system is most severely limited by a combination of stalling and compressibility phenomena. At high advance ratios and high speed, stalling of the retreating blade and high tip Mach number on the advancing blade occur as the relative wind at the airfoil of the retreating blade becomes smaller, while that at the advancing blade moves into the sonic range. At the point of stall, severe pitching moments and drag rise can occur without a drastic loss of lift, and severe loads are imposed on the control system. This has been the limiting condition. Recently it has been recognized that stall flutter can

be a limiting factor once the peak angle of attack for the airfoil is reached. This phenomenon occurs as first mode torsion of the blade, with very high root moments fed into the control system. Although very few cycles of oscillation occur before being damped out as the blade progresses to a more favorable portion of the azimuth, the stress cycles imposed can be very damaging.

The high Mach number on the advancing blade can lead to non-steady shock formation, with an accompanying increase in drag and a change in pitching moments. The Mach numbers of advancing blades often exceed 0.9 but generally this is accompanied by a rather sharp increase in power required as the Mach number exceeds 0.9 by any sizable amount. Noise radiation from the tip also increases rapidly. The shock formation on the advancing rotor blade tip is not understood at the present time. Much research effort is needed to permit progress toward a solution of this problem. In this regard, recently the whole question of the nature of the boundary layer on a rotor has come up for reexamination. Progress is being made in the comprehension of these complex boundary layer problems and meaningful relaxation of this limitation may be accomplished as a greater understanding of the boundary layer phenomena is gained.

The final limitation to be noted at this time is simply that of propulsive capability. Figure 4 shows a comparison of the conventional helicopter rotor as a propelling device with the capabilities of other current rotary wing devices. It is seen that with current technology, the pure helicopter is limited to speeds approximately 200 knots and lower. This factor of course, gives rise to the compounds and composites.

### 1.5 Recent Trends in Helicopter Research and Development

The combinations and permutations of rotorcraft design which have appeared, and the recognition of the general limitations of rotorcraft which have been mentioned in the preceding section have caused a general reconsideration on the part of many researchers of the research and development efforts which are being put forth in the rotary wing field. In his assessment of the problem in Reference 2, Prof. J.P. Jones points out the fact that the helicopter is perhaps the most advanced form of flying machine. His justification for this is that the functions of lift, propulsion, and control are completely integrated into the rotor system. Since more than enough lifting thrust to balance the pull of gravity is built in, only a slight inclination of this thrust in the required direction should be sufficient for propulsion. Similarly, the forces required to maneuver an aircraft are much less than its weight, so that control is possible merely by tilting the thrust vector rather than by distorting some "semi-rigid" portion of the structure which is well removed from the center of gravity. However, propulsion and control by slight tilting of the thrust vector implies that the plane of the rotor is almost parallel to the line of flight, and from this the many troubles associated with rotary wing aircraft begin to flow.

The inability of the inboard sections of rotating lifting surfaces to generate the same load as the outboard sections forces a non-uniform load distribution. The situation is aggravated by the need to keep the blades small in order to reduce the profile drag. The periodicity of the relative wind speed in the plane of the disc gives rise to continual fluctuations in both lift and moment. These, of course, are accommodated by a combination of hingeing the blades and cyclic variation of the rotor blade pitch angle from high values on the retreating side to low values on the advancing side. Thus, as described above, the retreating blade, which is already heavily loaded in hover, is worked at even higher lift coefficients and at a sufficiently high forward speed, stall is inevitable. On the advancing side, the incidence may even become negative while the relative wind speed approaches the speed of sound. Consequently, increases in forward speed of the helicopter can be expected to lead to flow separations with increases in power required and loss of lift on both sides of the rotor disc. And, of course, the problem of reversed flow occurs and its importance is not yet fully understood. These factors eventually lead to vibration inputs which become excessive as a result of the asymmetries introduced.

Although these factors have been recognized from the earliest days of the helicopter, they have been either considered insurmountable or generally ignored. Nevertheless, they constituted an imposing barrier to higher forward speeds of the helicopter. But then, no one considered the helicopter as much of a high speed machine because of the cumbersome and bulky body lines imposed by power plants and other components. Therefore, the helicopter was relegated in the minds of most designers to a novel machine which could accomplish certain basic vertical flight requirements, but which held little interest as an effective and productive aircraft in the air transport field. Ironically, many researchers failed to see problems worthy of their efforts in the rotary wing field, since they viewed the prospect of any real advance as being very bleak indeed. The primitive appearance of helicopters in general has not helped this situation. The extreme sophistication of the fluid mechanics problems involved have also helped to discourage logical and meaningful research on these problems. The profusion of non-linearity in the aerodynamic relationships caused many capable researchers to turn to the more direct and simple solutions of supersonic and hypersonic flight.

The most obvious solution for many of the problems apparent in the helicopter was to slow the rotor rotational speed to alleviate the advancing blade problems. This, of course, required unloading the rotor and required the addition of fixed surfaces to absorb the loss in lift. This means of resolving the problem is extremely limited in that the area of reverse flow on the retreating side of the disc is soon increased, and with it, the general asymmetry. Further, the loss in propulsive force requires the addition of an auxiliary propulsive system. Again quoting from Prof. Jones, the obvious step is then either to throw the rotor away, or stop and fold it into as small a volume as possible to stow it, or to incorporate the blades in some way into the main lifting system. This line of reasoning soon leads well beyond the helicopter concept and into the many varied forms of V/STOL aircraft which we have today, of which perhaps the ultimate is the direct jet lift V/STOL aircraft with separate lift and propulsion engines. All of these efforts have been done in the name of research and development for that is exactly what they are. However, for many modes of V/STOL flight, the most promising ideas make continuous use of the rotor. Many of these will be discussed by other lecturers during this series. Our discussion will be limited to those ideas which utilize the rotor for all regimes of flight, whether with or without auxiliary lifting surfaces, and to that concept known as the stopped and stowed rotor, which in essence throws the rotor away for a portion of the flight regime.

It is impressive that only recently have many of the rather basic problems associated with rotorcraft been undertaken by aerodynamicists. Most of these problems have been approached previously by simple engineering solutions based on rather empirical approximations derived from rather limited experimental investigations. Recently, a strong interest has been shown in the solution of these complex fluid mechanics problems by many capable aerodynamicists in many countries. Perhaps one reason for this resurgence of interest rests in the arrival of very large computers, which can render solutions for the variety of non-linear equations which arise when one attempts to construct adequate mathematical representations of the complex fluid motions in the rotary wing flow field.

The trend of helicopter research efforts is based on attacking the problems from new concepts. The adequacy of previous concepts has been recognized as insufficient to solve the many complex problems which exist. It is of interest to note that this is a complete revolution against current methods which are based upon mathematical formulations of long standing acceptance throughout the aircraft establishment, surprisingly enough without proof. These include the basic formulations of flow through the rotor based upon equations generated by Glauert, and others which are a mixture of simple momentum and lifting line theories. That is, a direct coupling is established between the momentum of the fluid flowing through the elemental area and the lift generated on the portions of the blades which occupy that elemental area. These simple relationships have ignored many of the very basic problems which are now considered to be within the grasp of formulation, or whose formulation is realized to be essential to the understanding of the problem. In short, it has been recognized that a much more complete and comprehensive understanding of

rotor flow mechanics must be acquired before the potential of rotorcraft can be realized.

It is of interest to note the various fields of endeavour which have evolved as a result of the recognition of the shortcomings in previous approaches. The application of the simple strip theory, for example, works well enough with low disc loadings in the hover mode. However, since this theory fails to consider such things as slip stream contraction and the effects of wake interaction, both in the hover mode and in the translating case where the wake has strong interaction with the rotor disc, this method is not adequate. It has been massaged in the past by introducing many empirical or semi-empirical factors, and reasonable results have been obtained for specific cases. However, the application of these methods to other design considerations is without verification and produces no confidence in the results. The effects of non-steady aerodynamics, aeroelasticity, non-steady boundary layers, non-planar wakes due to non-uniform induced velocities, wake interactions, vortex shedding and starting due to non-steady conditions, chordwise and spanwise variations of flow conditions, and the reversed flow condition existing on the retreating blade side of the disc are areas which are currently under study. All of these introduce highly non-linear sets of equations to describe the flow characteristics. They attack the problems on the basis of exact representation of the phenomena rather than on empirical correction factors. In the past, much of the blame for the failure of empirical systems has been placed on inadequate section airfoil data. It is more likely that the flow conditions in which the airfoil operates are so much different from the two dimensional case in which the airfoil data were acquired, that the use of these data is probably invalid. Thus, capable researchers are attempting to right the wrong which was begun by approaching these problems from the standpoint of two dimensional flow phenomena rather than an understanding of the complex flow which actually exists on the rotor. New theories and mathematical models are being formulated. These are being built from the sophisticated base which considers the high non-linearities of the systems. Further, it has been realized that the formulation of these models can only be successful if their adequacy is verified in experiment. Consequently, considerable effort is being devoted toward the perfection of new and unique means for measuring the flow phenomena of the rotary wing.

It is to be emphasized that efforts to date have only begun what will prove to be a highly demanding and time consuming research effort. Progress which has been made to date has resulted from a new attitude with new standards and new aims in the attack on the fluid motion problems of rotor craft. Future work will demand a closer coupling between the aerodynamicist and the aeroelastician. It must be recognized that the techniques and technology acquired from fixed wing research should be utilized to the maximum degree possible, but that an even higher degree of sophistication is necessary to accomplish the task. Further, research for its own sake will not necessarily be a valuable tool. In addition, research in the rotary wing field cannot always be directed towards a new generation of aircraft or a new speed bracket, but in many instances must be directed towards building a better foundation for current application and in some instances must be directed towards providing engineering improvement of vehicles already employed.

It will be our goal in succeeding sections to evaluate the current state of research and development in several areas pertinent to rotorcraft and its design. While no attempt will be made to provide a complete analysis, it is desired that the reader's interest will be stimulated by a presentation of current trends and future research opportunities in the field of rotorcraft.

## 2. LIFTING ROTORS IN HOVER

### 2.1 Summary of Prediction Methods for Estimating Hover Performance

The trend toward helicopters of larger size with higher installed power loadings has produced rotor designs which tend to optimize at higher disc loadings with higher

solidities operating at higher tip speeds. Thus, although it was indicated in the introductory remarks that hovering performance is no longer considered to be a major problem for the helicopter, new problem areas have arisen as a result of the inadequacies of current computational methods to predict hover performance. Further, since for every percentage point gained in static lift capability four percent is gained in payload, a continued effort to increase hover efficiencies is justified. The trend of hover figure of merit with increased disc loading and solidities is indicated in Figure 5. In this figure, the hover figure of merit ( $M$ ) is total aircraft figure of merit and not rotor figure of merit which may approach as high as 0.8. It is seen that the demands of the high performance, high speed helicopter which often times results in short, rather low aspect ratio blades and high disc loadings has a serious compromising effect on the hover figure of merit. It will be our intent in this section to review some of the various methods for calculating hover performance, and to illustrate by use of experimental evidence the degradation which occurs with increased blade loading, increased number of blades, and increased tip Mach number. The aerodynamic interference between blades and its importance to the hover performance problem will be investigated.

The most simple analysis of performance in the hover mode is attributed to Glauert, who postulated a relation between the momentum and blade element theories to derive a general expression for the velocity induced at any point on a helicopter rotor that is in hover. Derivation of this relationship can be found in many texts such as Reference 3. In this analysis, the airflow is assumed to be steady and uniform over the area of the disc and viscous effects are ignored. This method of prediction has been utilized for many years for the relatively low disc loading helicopters of previous periods with good success. It was modified to account for blade tip effects by Goldstein and Lock. The method uses standard two-dimensional airfoil data and generally any errors which result from its use have been attributed to inadequacy of the two-dimensional data. The ease with which this computational process may be accomplished has been enhanced by the digital computer. Iterative solutions using appropriate two-dimensional airfoil characteristics to account for local stall and compressibility effects can now be utilized to accomplish a "non-linear strip theory" type of computation. The non-dimensional performance charts of Reference 4 were developed in this manner.

As a need for computations of more accuracy dealing with more highly loaded discs of higher solidity was presented, it became obvious that the three-dimensional problem must be attacked. It further became evident that the rotor wake must be considered in any analysis of the three-dimensional problem. The basic vortex theory which was derived describes the wake by a series of cylindrical vortex sheets representing the radial variation of circulation. This employed an infinite number of blades. Prandtl, in Reference 5, derives an approximate correction to the vortex theory for a finite number of blades. Goldstein, in Reference 6, improved the vortex theory using a wake model consisting of a series of helicoidal surfaces of constant helix angle, one for each blade. These were assumed to move downward uniformly at the average momentum velocity, and the effects of wake contraction, viscosity, and non-uniform downwash on the wake shape were neglected. Lock, in Reference 7, further modified this method to account in an approximate fashion for the non-uniform downwash, applying Goldstein's analysis to each radial segment and assuming it operates independently within an optimum spanwise loading. The overall downwash was assumed to be uniform for each radial segment, but having a different value for each segment except where the optimum spanwise loading is actually achieved, in which case the solution is exact. The Goldstein-Lock analysis accounts for tip effects within the assumptions applied and eliminates the need for an arbitrary tip loss factor. However, the limitation of an assumption of a non-contracting wake still existed. It was not important in the development of this particular theory, since it was derived for propellers operating in axial flight.

These previous methods had imposed a restriction assuming optimum spanwise loading. This restriction was eliminated by Willmer in Reference 8 where he simplified a wake model to the form of a stack of plain vortex sheets under each blade at a given instant. The wake spacing was determined to be that resulting from an average axial momentum velocity.



A Fourier series was employed to represent the radial variation of circulation and the resulting downwash. This method provided a more accurate treatment of spanwise three-dimensional effects, but did not remove the limitation of a non-contracting wake. Further the flow near the tip was less accurately represented due to the simplification of the wake representation by planer, rather than by curved surfaces.

The increased utilization of helicopters in the 1960's has spurred additional efforts in the evolution of prediction methods for hover performance. Piziali and Duwaldt, in Reference 9, refined the wake representation by assuming it to consist of a mesh of discrete line vortices. This method did not consider wake contraction or the interaction between individual wake elements. It did eliminate the optimum spanwise loading assumption of Goldstein and Lock and improve the accuracy of Willmer's tip analysis. However, this method did not improve the estimates made by the Goldstein-Lock method, and the latter was still preferable since it was much simpler to employ in rapid performance analyses. Neither the method of Willmer nor that of Piziali and Duwaldt was conceived primarily for hover flight, but rather was designed primarily to analyze a rotor in translational flight.

Two additional methods represented in References 10 and 11 were conceived to predict the static performance of VTOL propellers. These considered the deformation of the near wake due to contraction, which had not been considered in the previous methods. It was confirmed that the inclusion of wake contraction and the resulting inflow distortion provided much improved correlation for the propellers which were analyzed. These methods require excessive computer time and have a relatively inflexible wake geometry model which make them difficult to use for studying effects of changes in rotor geometry. In Reference 12, Trenka included, in addition to wake contraction and finite blade effects, methods for accounting for wake distortion due to the presence of solid bodies such as wings and nacelles. This method calculated not only performance, but stress characteristics in the rotor. However, computer time requirements for this method are also excessive.

Thus, for routine calculation of rotor hover performance, the Goldstein-Lock analysis represents the current state-of-the-art. It has been programmed on the highspeed computer so that static performance of a specific rotor system can be calculated generally in less than 20 seconds of computer time. A review of the assumptions of this method consists of the following. Non-uniform loading and three-dimensional tip effects are calculated consistent with the assumption of a non-contracted slipstream and uniform axial wake velocity. Local blade section, Mac. number, and Reynold's number effects are included by use of appropriate two-dimensional airfoil data. Variations in blade planform, twist, tip shape, and root cutout are accounted for in addition to the number of blades. The effects of slipstream rotation are not included but this effect is considered to be small. Radial flow effects, although potentially significant in highspeed translational flight, have been demonstrated to be small at normal rotor blade loadings in hover, particularly where the airfoil sections remain unstalled. It is assumed that the rotor and its aerodynamic environment are completely symmetrical. The blade force vectors are resolved appropriately to account for coning, but wake deformation due to coning is not included since the method was originally developed for non-flapping propellers.

As a result of experimental evidence which has been gained recently, wake contraction and associated non-uniform axial velocity distributions are believed to be the major factors which contribute most to the inability of the Goldstein-Lock method to accurately predict the static thrust-power characteristics of high performance rotor systems. This evidence and the need for additional research to refine these processes will be presented in the remaining sections of this chapter.

## 2.2 Ideal Hover Performance

It is well to review, briefly, the factors affecting the hover performance and, in particular, the maximum achievable or ideal hover capability. The most simple performance analysis of a hovering rotor considers the conservation of energy and the momentum change of the air mass passing through an actuator disc. For this condition, the airflow is

assumed to be steady and uniform over the area of the disc and the viscous effects are ignored. Thus, the theoretically ideal expression for power becomes

$$HP = \frac{T^{3/2}}{550\sqrt{2\rho A}} \quad (1)$$

Generally this capability of rotors is expressed as the rotor figure of merit. It is defined by the expression

$$M = \frac{\text{minimum possible power required to hover}}{\text{actual power required to hover}} \quad (2)$$

$$= \frac{Tv}{P}$$

where  $M$  is called the rotor figure of merit,  $T$  is the thrust,  $v$  is the induced velocity through the rotor, and  $P$  is the power delivered to the rotor. This figure of merit also can be expressed independent of the induced velocity by the following expression where  $R$  is the rotor radius:

$$M = \frac{1}{\sqrt{2}} \frac{T}{P} \sqrt{\left(\frac{T}{\rho\pi R^2}\right)} \quad (3)$$

Thus the larger the figure of merit for a given rotor, the less power required to produce a given thrust or the greater the thrust per unit power. From this expression, a direct relation between disc loading and power loading may be obtained as

$$P.L. = 38M \frac{1}{\sqrt{(D.L.)}} \quad (4)$$

The ideal figure of merit,  $M = 1$ , is by definition the upper limit for any rotor since it represents a rotor with zero profile drag and with uniform induced flow. In current practice, rotors have achieved as high a figure as 0.8. Rotors with values as low as 0.5 are relatively poor. For design purposes, it is often convenient to express the figure of merit in non-dimensional terms in which case the expression becomes

$$M = 0.707 \frac{C_T^{3/2}}{C_Q} \quad (5)$$

By means of the ideal figure of merit, the upper limit to the hovering performance of any helicopter at various altitudes can be quickly estimated if the engine power and the rotor diameter are known. The use of the ideal figure of merit enables one to discount the claims of many over-enthusiastic rotor designers by showing that the combination of thrust and power claimed for their rotor is more optimistic than could be realized with an ideal rotor, and therefore could never be obtained in practice.

### 2.3 Sources of Performance Losses

The true figure of merit for any rotor is difficult to specify in that it is not a unique number, but varies with thrust coefficient and cannot easily be obtained as an analytical expression. Contrary to the assumptions in the ideal case, the airflow is not uniform over the area of the disc and the blades do have profile drag. Furthermore, wake vorticity and the three dimensional flow at the blade tips combine with other losses to produce additional power penalties. Therefore, it is not possible to consider this problem with the simplicity of the ideal case by considering merely the momentum energy relationships, but the flow at each blade element with its accompanying wake must be considered. These considerations result in a complex problem, since the flow fields



which they involve are three dimensional and often non-linear. It is possible to utilize the equation based on momentum considerations for a first order approximation to the calculation of a realistic rotor hovering performance. This is accomplished by including terms for the profile power from estimations using a typical drag polar and an average blade lift coefficient, and a term for induced power which has been arbitrarily increased to account for tip losses. The resulting expression for the torque coefficient in the non-dimensional case becomes

$$C_Q = \frac{C_T^{3/2}}{B\sqrt{2}} + \frac{\alpha\delta p}{8} \quad (6)$$

where  $B$  is the tip loss factor which is always less than 1 and usually of the order of 0.97,  $\alpha$  is the rotor solidity, and  $\delta p$  is the blade mean drag coefficient defined by an experimental drag polar as a function of the mean lift coefficient on the rotor represented by the expression

$$C_{Lm} = K(C_T/\alpha) \quad (7)$$

This expression is difficult to apply and is unsuitable for the prediction of rotor performance for design purposes.

The method of Glauert attempted to account for some of the losses by a two-dimensional approach. His analytical model of the hovering rotor equates the momentum with the two-dimensional airfoil theories to derive the inflow and resulting lift and in-plane forces at each blade element. For this purpose the rotor is divided into annuli through each of which the momentum change is equated to the blade-element lift for a given blade-element pitch. From the momentum considerations, the incremental thrust is

$$\Delta T = \rho(2\pi r \Delta r)v(2v) \quad (8)$$

where  $r$  is the blade radial station. From blade element considerations, the incremental thrust is

$$\Delta T = \frac{1}{2}\rho bc(\Omega r)^2 (C_l \cos \phi - C_d \sin \phi) \Delta r \quad (9)$$

where

$$\tan \phi = \frac{v}{\Omega R} \quad (10)$$

Integration of these equations will yield the total rotor thrust and total rotor power. The simplest application of this form makes use of linear blade-element lift curve slope and a standard two-dimensional drag polar. Derivations of these expressions can be found in References 2 and 13. With the use of a digital computer, it is possible to solve Equations 8 and 9 in an iterative manner using appropriate two-dimensional airfoil characteristics to account for local stall and compressibility effects. Tip loss is included by applying a "tip loss factor" which assumes complete loss of lift over a small percentage of the blade at the tip. This method could be labeled a non-linear strip theory and was utilized in developing the non-dimensional performance charts which are available today. This method is extremely limited in its usefulness because of the actual three-dimensional tip effects which exist and the wake non-uniformity caused by a finite number of blades.

Section 2.1 has reviewed in detail the efforts that have been made to date to account for the loss factors. In summary, these losses for the hover case can be identified as non-uniform inflow, wake contraction, interaction of wakes from preceding blades, three-dimensional tip effects, tip Mach number losses, and a finite number of blades. It has

been shown by Jenny and Olson in Reference 13 that as tip Mach number, disc loading, and the number of blades are increased, the hovering performance predicted by conventional methods becomes increasingly optimistic. These authors made a correlation of conventional methods to demonstrate the inadequacies of conventional methods of computation for hover performance utilizing calculations for an S-61 and an S-65 helicopter. Figure 6, which is extracted from Reference 13, projects the trend of optimism with increasing disc loading.

The linear analysis ignores such things as blade root cutout and spar drag, and assumes optimum spanwise loading. The non-linear analysis utilizes two-dimensional spar and blade aerodynamic data, and accounts for non-uniform downwash. The S-65 had a higher tip Mach number, higher disc loading, and 6 versus 5 blades for the S-61. It is seen that the calculation for the S-65 is considerably worse than for the S-61. It is obvious that the tip loss factor could be adjusted empirically to provide perfect correlation for either rotor; however, no systematic tip loss factor adjustment has been found which yields satisfactory correlation with available test data for a wide range of rotor systems and loadings.

It might be considered that the more sophisticated Goldstein-Lock method which makes an arbitrary tip loss factor unnecessary, would give a better correlation. Jenny and Olson found this also to be optimistic. This discrepancy was attributed to optimistic profile power estimation as a result of radial flow, root losses, and airfoil roughness.

A profile power correction factor was derived for the S-61 as a function of  $C_T/\sigma$ . This factor was then applied to the S-65 test data when it became available. Figure 7, also taken from Reference 13, shows the inadequacy of this attempt.

Jenny and Olson continued to experiment with the corrections which could be made to the Goldstein-Lock analysis and eliminated, to their satisfaction, the influence of solidity for a constant number of blades, and therefore disc loading, as an important factor in the discrepancies which they discovered. The reader is referred to Reference 13 for the derivation of this conclusion. However, they did arrive at a pronounced influence of the number of blades as a deteriorating factor in the calculation of the hover power. This is illustrated in Figure 8.

This empirical study has been considered in essence by many other investigators, and inevitably leads to the conclusion that the rotor wake is a vital consideration in the accurate evaluation of rotor hover performance. Thus, we have categorized the performance losses of the hovering rotor into two basic areas. The first is represented by the blade profile drag, and the second by the induced effects as a result of the generation of circulation vorticity on the blade elements. In particular, it has become apparent that the lack of consideration of the rotor wake contraction, and the subsequent interaction between the blade and the tip vortex are of importance. In the next section we shall consider the importance of the profile losses, and in the following section the importance of the interaction between the blades and the wakes.

#### 2.4 The Importance of Profile Losses

The effect of blade profile drag losses on the efficiency of the hovering rotor has been shown in many treatments of the subject to be of minor concern when the thrust coefficient is of a useful value. The derivation of these effects can be found in Reference 3 and a graph of the variation of the figure of merit with thrust coefficient presented on page 61 of that reference indicates that for thrust coefficients above 0.006, reductions in profile drag would produce very little in improved efficiency. This can be best appreciated by reference to Equation (6), where it can be seen readily that when the profile drag term becomes small compared to the induced terms, its influence on the overall torque requirements is also small. Thus, for practical conditions, reductions in profile drag which might be attainable produce only small increases in rotor hovering efficiency. It is obvious that this is not a fruitful area of research.

It would be well to note, however, that the effects of solidity which are to a degree coupled with profile losses are more important. Ideally the most efficient hovering rotor would be one of infinite diameter and zero rotational speed. The profile drag losses of such a rotor would, of course, be zero. Any induced losses would likewise be zero for the rotor would accelerate an infinite mass of air an infinitesimal amount to produce thrust. A practical case, of course, imposes obvious limitations. The primary factors in determining the design for minimum profile drag losses are solidity and tip speed. The choice of these two parameters is dependent upon two considerations that are somewhat interrelated. First, the rotor should operate at the mean lift coefficient closest to the stalling angle of the blade section and, second, the rotor should operate at the lowest feasible tip speed. The use of a low tip speed is equivalent to having the greatest possible solidity which for a given rotor diameter represents the greatest blade chord. These considerations are based on the fact that rotor thrust varies as the tip speed squared, whereas profile power varies as the cube of the tip speed. The obvious result of these considerations is that the thrust should be produced by a high mean lift coefficient and a low tip speed, which is tantamount to a high solidity. Practical considerations, of course, place a lower limit on rotor speed; large coning angles, and the necessity for maintaining kinetic energy in the blades for autorotation are the primary considerations. However, it may be stated as a general rule that for maximum hovering efficiency, attempts should be made to operate at the lowest tip speed and the highest mean lift coefficient attainable which, in essence, dictates a high solidity. It is emphasized that these conclusions concern the hovering rotor only and do not constitute design criteria for rotors which must operate in conditions of high forward speed. In fact, requirements for efficient and smooth operation at high speeds are in direct conflict with those for the hovering design.

## 2.5 Interaction of Blades and Wakes - Wake Contraction

The assumption of an uncontracted wake dictates the condition of a uniform vortex sheet with a radius equal to the rotor radius moving uniformly downstream with each vortex element maintaining its radial position. For this condition, little interference exists between the blade and the wake. As the number of blades increases, due to the reduced separation between blades, the proximity of the vortex sheet to the succeeding blade is closer. This will result in increased interaction and a reduction in the adequacy of the computational methods, as was illustrated in Figure 8. However, a far greater effect is realized when wake contraction is considered. Wake contraction will position the vortex generated by each blade tip much closer to the tip path plane than is assumed in the Goldstein-Lock analysis. This situation is further aggravated by coning which in a contracting wake situation increases the proximity of the vortex to the following blades. Close proximity of the tip vortex to the following blades causes severe local inflow distortion due to high rotational velocities within the vortex. These rotational velocities have been shown in Reference 14 to reach levels as high as 50% of the blade tip speed. Total strength of the vortex is related to the blade lift coefficient and the velocity distribution induced by the vortex is a function of the spanwise lift gradient at the tip. The interactions are shown pictorially in Figure 9.

The susceptibility of the blade to local inflow distortion is also a function of  $C_T/\sigma$  and the tip Mach number which together define the stall margin for a given airfoil. Further, the rotational velocity field of the induced vortex probably invalidates the use of two-dimensional blade airfoil data because of the non-uniform local velocity field. A representation of the variations which can occur in local angle of attack are shown in Figure 10. It is apparent that the methods which have been discussed are not adequate for contending with these variations. Thus, as disc loadings are raised by the use of greater numbers of blades for higher solidities, higher tip Mach numbers, and higher design  $C_T/\sigma$ , these effects will be a deterrent to be reckoned with in establishing adequacy in analytical models.

The presence of these wake contracted patterns and interferences in actual operating conditions has been demonstrated by several researchers. Pictorial evidence of the pattern

may be seen in Reference 13. In the examples shown in that reference, not only is the pattern demonstrated but it is also indicated that for at least one case the tip vortex actually passed above the succeeding blade. Other photographic evidence in this reference indicates the interaction between the tip vortex and the succeeding blade which causes a bursting of the vortex and a considerable amount of separated flow. It is obvious that none of the analytical models generated to this present time can account for such phenomena.

Tests made by several researchers have indicated a high susceptibility of the flow through the hovering rotor to small amounts of cross wind. Cross winds of five knots or less create extremely large fluctuations of local angle of attack near the blade tips where the vortex-blade interference has been observed. An example for a typical case is given in Figure 11 which was extracted from Reference 13. At the high peak values of angle of attack, stall and resultant drag divergence could be expected to occur. The values of calculated angle of attack are those considering an uncontracted wake condition. Such conditions as these would not be expected for a no-wind condition. However, a no-wind condition is rather academic and problems from lack of symmetry in the flow of a hovering rotor can be expected to occur.

The primary effects on rotor performance in hover from the interference with the tip vortex would be expected in drag divergence in the stalled areas. In one case, cited in Reference 13, a rotor performance degradation of 400 HP or about 7% of the measured total power was realized as a result of blade stall occurring due to interference, where the stall area extended only over approximately  $120^\circ$  azimuth. Induced power losses can also be expected from the severe local spanwise loading gradients caused by the vortex. Thus, the discrepancies noted earlier between actual performance and that predicted by the Goldstein-Lock analysis could be explained by interaction between the tip vortex and the succeeding blade.

A considerable quantity of supporting evidence has been acquired for the reasoning applied above. The results of one study are shown pictorially in Figure 12 where the wake contraction and interaction with the blade is clearly shown. This series of photographs also indicates a considerable difference between the downstream motion of the tip vortex and the sheet trailed from the blades. A graphical representation of the structure of the wake was presented by Gray in Reference 15. That is reproduced here as Figure 13. The results presented in Figure 13 were obtained from pictorial evidence of a study similar to that represented in Figure 12. A graphical analysis of pictorial evidence obtained during the test represented in Figure 12 resulted in the tip wake and vortex sheet coordinates presented in Figures 14 and 15. Here the decided inward movement of the tip vortex and the vortex sheet at very close proximity to the rotor are indicated. Also, the low rate at which the tip vortex moves downstream in the first  $70^\circ$  of azimuth is indicated. From these results, it is obvious that as the number of blades is increased the interaction between blades and vortex will be also increased.

Several programs for formulating these wakes have been generated and a comparison from one of these methods with the classical wake generated by a non-contracting theory, is shown in Figure 16. The extreme differences are readily apparent.

As has been mentioned earlier, the calculation of hover performance in the past has been generally acceptable. This is believed to be because of the fact that lower disc loadings have been employed and the interactive effects which have been described have not been significant because of compensating factors. In the absence of stall or drag divergence, the errors in predicted radial distributions of actual induced velocity are generally self compensating. However, as disc loading, number of blades and tip Mach number are increased, the classical wake methods will be less and less adequate.

## 2.6 Consideration of Blade Section Profiles

The establishment of the vortex blade interaction as a primary reason for performance decrement not predicted by classical theories gives rise to speculation that modification to the physical characteristics of the blade near the tip might produce significant improvements in hovering efficiency by weakening or displacing the tip vortex. Also, modification of the local airfoil shape or change in twist distribution in the area of separation could reduce the importance of the local inflow distortion caused by vortex proximity. In Reference 14, a variety of tip modification was indicated which could be used to reduce the peak rotational velocities in the vortex by as much as 80%. In an experiment conducted on the S-61 helicopter, in which the standard blade tips were replaced over the outer 6% of the radius with tapered planform tips designed to reduce the spanwise loading gradient, a power reduction of 1.5% at constant thrust was measured. This reduction was accompanied by a substantial reduction in acoustical level in the hertz range usually associated with vortex noise. Thus, a confirmation was obtained that the reduction of rotational velocity in the vortex was probably the reason for the performance gain. In a separate experiment, a drooped leading edge was placed on the blade contour on the outer 15% of the blade. The airfoil was selected to extend the two dimensional lift curve to an angle of attack approximately 2% higher than the standard blade section. Pictorial evidence indicated significantly less local stall than with the standard blades, and performance measurements confirmed a reduction in power in the order of 5% at the high thrust levels. It is evident that significant advances may be made by improvements in blade section profiles in the tip region.

## 2.7 Characteristics and Importance of Blade Boundary Layer Flow Properties

It is seen that the large distortion in inflow conditions near the tip, which are accompanied by large radial flows and severe spanwise pressure gradients, will have significant effects upon the blade boundary layer flow. Although little importance has been placed upon research in the hover mode as it pertains to boundary layer characteristics, some work is being accomplished. Those results which have been obtained to date are inconclusive and provide very little information on which to base improvements. However, it is anticipated that satisfactory solution of the problems for improvement of hovering efficiencies must take into account the boundary layer characteristics of flow on the rotor blade.

## 2.8 Areas for Further Research and Development

It has been demonstrated by researchers to date that rapid contraction of the slipstream under a hovering rotor places the vortex system so close to the rotor blades that it causes significant changes in the radial distributions of induced velocities which can result in a loss in hover performance. The magnitude of these losses increases with blade tip Mach number, number of blades, and blade operating lift coefficient. These characteristics are strongly affected by a slight amount of wind which can deform the wake in a hovering rotor to the point that the tip vortex actually passes over the following blade. It appears that the success of classical methods in predicting hover performance in the past has been largely dependent on the presence of generally compensating errors in the radial distributions of axial induced velocity. Therefore, it is apparent that rotor performance methods which take into account wake contraction are essential for design optimization of rotor geometry and through the use of such methods, significant improvement in the accuracy of purely analytical predictions can be expected. The correct axial positioning of vortex elements in the wake is as important as is the correct radial positioning. The sensitivity of rotor radial angle of attack distributions to wake geometry indicates that modifications of blade design which influence the relative blade-near wake geometry may significantly affect rotor performance.

Based on these findings, it is obvious that additional research in this area is justified. Further, it is indicated that both experimental and analytical research is required.

Research effort should be generally directed toward defining the geometry of the wake under several hovering rotor configurations through techniques of flow visualization to indicate the importance of such functions as number of blades, solidity, taper, twist, disc loading and tip Mach number. Analytical methods must be developed for predicting the true wake geometry in hover and consequently in low speed flight. These methods are currently being developed by many researchers. It is obvious that these methods must be vindicated and verified by the data which are obtained through the experimental studies.

Methods of predicting the performance of airfoils operating at a close proximity to a vortex must be extended and must be confirmed in experimental testing. References 14, 16 and 17 represent additional efforts in this direction. It should be noted that these methods are required not only for the case of the hovering rotor, but for the case of the translating rotor as will be seen in subsequent sections. This area of research probably represents one of the most demanding and important requirements in the field today.

The importance of blade tip geometry must be better understood in its effects on hover aerodynamics. Some work is being pursued in this area, but a great deal remains to be accomplished. Much information must be obtained experimentally to provide a basis for formulation of pertinent theories to represent the aerodynamics of this situation. At present, no adequate theory exists by which parametric studies of tip shape can be accomplished.

### 3. LIFTING ROTORS IN FORWARD FLIGHT

#### 3.1 Basic Thrust-Power Relationship

The problem of computing helicopter performance in forward flight is a complicated process. A combination of many variables and lengthy and complicated equations to define the rotor characteristics have made any exact performance method unattainable in the past because of the lack of capability to handle these systems of equations. It is customary to utilize a method which has been termed the NACA energy method, since it was developed and used extensively by that organization. This method involves the use of tables and charts, and it is perhaps one of the most accurate available at the present time. Its foundation rests in the equation relating the effective lift to drag ratio to the various elements which absorb power in the system. A general statement of the effective lift to drag ratio is as follows:

$$\left[ \frac{L}{D} \right]_e = \frac{WV}{325 \text{ SHP}} \quad (11)$$

where  $V$  is the flight speed in knots,  $W$  is the weight of the aircraft, and  $\text{SHP}$  represents the total shaft horsepower required by the aircraft at the speed  $V$ . For performance purposes, this equation is generally inverted and it is the drag to lift ratios which are considered. This form of equation is applicable to pure rotorcraft only and must be modified for application to the compound. For the cases where auxiliary jets are used for forward propulsion, an equivalent shaft horsepower must be utilized which is defined by the relationship

$$\text{SHP}_e = \text{SHP} + \frac{TV}{260} \quad (12)$$

where the propulsive efficiency has been assumed to be 0.8. If the pure jet augments is utilized, additional modifications must be made based on thermal efficiencies. A more detailed analysis of this problem can be found in Reference 18.

Working with the reciprocal of the lift to drag ratio and assuming that, as is the case for the level flight condition, lift equals weight, the following representation of the



energy expression is obtained:

$$\left[ \frac{D}{W} \right]_e = \left[ \frac{D}{W} \right]_f + \left[ \frac{D}{W} \right]_{ind} + \left[ \frac{D}{W} \right]_{pr} + \left[ \frac{D}{W} \right]_{W\&E}, \quad (13)$$

where the subscript *f* is that element due to parasite drag including the contribution of the hub, the subscript *ind* is the induced drag of the rotor, the subscript *pr* connotes the profile drag of the rotor, and the subscript *W&E* represents the wing and empennage including, in the case of the compound, both profile and induced drags. From this analysis, we are now able to proceed with the identification of the various sources of performance losses.

### 3.2 Sources of Performance Losses

The identification of terms within the performance equation for thrust-power relationship which was made in the preceding section allows us to consider various portions of the power requirements independently. The grouping of the losses due to parasite drag which represent those for the entire aircraft and those in the term for the wing and empennage permit us to treat these as a single subject in drag reduction. This will be accomplished in Section 5. This leaves two terms which have to do specifically with the rotary wing aerodynamics; particularly for induced drag of the rotor and the profile drag of the rotor. In short, we have come down to the very basic aerodynamics of airfoil shapes. These problems have been treated in great detail for fixed wing aircraft across very wide ranges of flight velocity; the problems can be quite well handled for the fixed wing case. Several very fine airfoil sections have been evolved to satisfy the requirements. However, for the case of the rotary wing, the problem is far more complex and it is difficult to evolve useful design procedures. The primary problem which has hampered development in this field is the extremely complex flow field in which the blade sections must operate. The non-uniform flow field created by the variation of relative speed along the span of the blade plus, the distortion of the incoming airflow which must be turned through large angles, to which must be added the wide variation of operating conditions from the advancing to the retreating blade side of the disc, create conditions which only can be represented by extremely involved and often non-linear representations in their mathematical models. As has been noted in previous sections, little work has been done in this area in the past simply because of this complexity. We shall consider some of the basic aspects of these problems in this section, and in the succeeding section which will deal with the high speed cruise problems in particular.

It can be stated in general terms that the primary source of losses in the rotor aerodynamics is associated, as it was in the case of hover, with problems of flow separation from the rotor blades as a result of stalling or with compressibility losses. As it was noted for the hover case, skin friction profile drag is not a large portion of the losses and little can be done to improve this area. Primary problems are associated with the induced drag and pressure drag losses of the rotor.

### 3.3 Importance of Airfoil Profile Characteristics

The importance placed upon the induced losses is naturally followed by the importance of the airfoil profile characteristics. The difficulties encountered in seeking out proper profile shapes to improve the rotor characteristics arise from the wide range of operating conditions in which the airfoil must operate efficiently. These range from sometimes reversed flow conditions on the retreating blade side to transonic or even supersonic requirements on the advancing blade side. Further, as has been noted earlier, the exact characteristics of the flow in which the blade section must perform are not defined and are of a highly complex three-dimensional nature. Heretofore, very simple symmetrical sections have been employed in rotors because of the ease of manufacture and because of the desire to have a minimum change in pitching moment with changes in blade loading. Yet perhaps the most important advances to be made in improving the rotary wing

efficiency are dependent upon the evolution of airfoil shapes which will operate efficiently over the wide range of required operational environment.

The introduction of fibre technology into blade fabrication has provided more freedom in the selection of the planform of the blade and in the distribution of airfoil sections. In this manner, blades with thin airfoil sections in the outboard portions of the rotor can be employed. Loss in maximum section lift coefficient, which is associated with low relative thickness of the airfoil, can be compensated for through the introduction of proper camber in the blade without materially affecting the Mach numbers at which drag divergence starts to appear. This improved tolerance of the blade tip to the resulting Mach number on the advancing side permits the use of higher tip speeds at the advance ratios which represent the stall limit, and which may be no higher than for more conventional blades. The result is that high speed capabilities are improved. Although to date these improvements are confined to the region of maximum speed, further technology may produce more advantages than are now apparent.

Perhaps one of the best assessments of the importance of airfoil profile shapes was made by Davenport and Front in Reference 19. In this paper, the authors cited two critical design quantities for rotor blade sections in modern helicopter usage. These are the drag at high Mach number and low lift, and the stall behavior at Mach numbers around 0.4. The irony of the situation is that improvement of the first generally causes deterioration of the second if the approach taken is simply thickness reduction. The authors go on to point out that airfoils can be designed to have better combinations of these properties than any previously available.

It is of interest that the NACA 0012 and 23012 sections which were designed in the early 1930's have not been superseded for helicopter applications. They are still in use in most modern rotary wing aircraft that are now in production, although they find little usage in fixed wing aircraft. The sections were evolved during the era when experimental procedures were utilized for the development of airfoil shapes and no scientific fluid dynamic basis was employed. The application of the Theodorsen technique to develop the six series airfoils was a distinct departure from current practice. From this series of airfoils came the well known bucket in the drag curve which held considerable promise for improved performance. However, for the most part, the problems of surface irregularities, dirt, and operational damage denied the benefit of the drag bucket in most practical cases.

The development of laminar flow airfoil sections, which began early in the 1940's, evolved the NACA 9-H-12 which had a cusped trailing edge that actually produced a negative loading at the rear of the airfoil to obtain the required low  $C_{m ac}$  which is essential to helicopters to minimize control loads. The difficulty with laminar flow helicopter airfoil sections to date has been that the presence of cross flow in the boundary layer is a strongly destabilizing influence on laminar boundary layers. Helicopters in translation generally have substantial cross flow in the boundary layer. Consequently, the laminar flow effects are quite frequently lost. In addition, the stall characteristics of these airfoils are usually poor because of sharp leading edges. Generally, there is a rapid deterioration in aerodynamic efficiency above lift coefficients of approximately 0.95. Although little effort has been expended in the development of airfoil sections for either fixed wing aircraft or helicopters since the late 1940's, a considerable amount of interest has been raised in this area in recent times. Work on laminar flow sections has been undertaken by Wortmann in Germany. In addition, Reference 19 reports efforts which have been made by the Boeing Vertol Company to evolve better airfoil sections. In work accomplished for high Mach number swept wing application, a striking phenomenon was uncovered. This is portrayed in Figure 17 where it is indicated that substantial amounts of supercritical flow can be tolerated near the leading edge before drag divergence is encountered. This concept was used by Percy in England and by the Boeing Company in the US to develop improved airfoil sections for transonic applications.

In Reference 19, the authors provide a good summary of logical objectives for modern effort in the improvement of airfoil sections for helicopters. These are:



- (i) Reduction of power required under the high disc loading and speed conditions possible with modern turbine power plants.
- (ii) Postponement of control load and vibration problems associated with blade stall to the highest possible rotor lift or aircraft speed.
- (iii) Maintenance of good control and vibration characteristics at speeds within the stall boundary.

These requirements imply the need for minimum airfoil drag at high and intermediate Mach numbers, maximum airfoil lift capability at moderate Mach numbers (0.3 to 0.5), and minimum  $C_{mac}$  under all conditions. Figure 18, which is extracted from Reference 19, shows typical aerodynamic environmental conditions for airfoils near the tip of a conventional helicopter flying at 160 knots.

It is important to note that the Mach number corresponding to the highest lift coefficient demanded is in the range of 0.3 to 0.4. This is often considered to be incompressible, but nearly sonic local velocities can appear at the nose for high lift coefficients implying substantial influence of Mach number on stall. Figure 19 shows how stall actually limits the lift of helicopter rotors. These curves show no noticeable break as the rotor lift passes through the stalling level. However, the blade torsion data indicate that stall makes itself felt through the onset of unacceptable alternating control loads. A comparison with a rotor having a "droop snoot" is shown for comparison. It is interesting to note that the increase in rotor lift for stall is in approximately the same proportion as the increase in static  $C_{Lmax}$  for the two airfoils.

Figure 20 summarizes the demands of the aerodynamic environment on rotor blade airfoils in terms of lift coefficients and Mach number. The three regions noted correspond to the flight regimes indicated. Region A corresponds to high gross weight hover conditions which are applicable to both conventional and compound helicopters. Region B corresponds to advancing tip conditions where drag divergence from compressibility can limit the aircraft speed. Region C corresponds to the high angle of attack region on the retreating side of the rotor disc where the effects of stall on control loads and vibration are the dominant influence. Table I, which is extracted from Reference 19, summarizes the gross geometric features of airfoil shapes and their effects on aerodynamic characteristics of interest. This table is not intended by the authors to be exhaustive, but merely to indicate relative importance. In Reference 20, the authors go into considerable detail to exemplify the improved airfoils which they have derived. It is important to note that these airfoils are derived essentially as the benefits derived from both thick and thin airfoil characteristics. In essence, the favorable surface pressure distributions are maintained while reducing airfoil thickness ratio. A summary of the stall and drag rise characteristics for several airfoil families, including those developed by the Boeing Company, is illustrated in Figure 21. It is seen that a decided advantage for the critical retreating blade conditions is realized by the Vertol airfoils, whereas the NACA six series airfoils are extremely poor and, therefore, represent no promise for helicopter applications.

From this summarization, it is implied that more speed for a given rotor blade area and power available can be obtained by the incorporation of modifications to current airfoil shapes. A comparison computed for a typical application based on these airfoil shapes is given in Figure 22. The thin tip design is a composite of airfoil shapes, the details of which are given in Reference 19. It can be seen that some advantage accrues from the use of these advanced airfoil shapes. The following trends are inferred from this figure.

- (i) The symmetrical blades have a slightly lower minimum profile power level, but are more sensitive to speed and disc loading.
- (ii) The cambered 10% thickness blades are insensitive to weight and speed at the cost of a slight penalty at low speed and weight.
- (iii) The thin tip blades are worth about seven knots at lower loading but at the higher lift they show greater speed sensitivity beyond 160 knots.

The reduction in effective rotor drag provided by the thin tip blades as compared to the NACA 0012 blades is shown in Figure 23. It is seen that a sizable advantage is gained.

In Reference 19, the authors purport that the major gains to be realized in rotor performance from airfoil design improvements have now been largely realized. This opinion is not shared by all researchers. The authors in Reference 19 do acknowledge that a break through in new technology could change this condition, but they feel that some active system must be employed. The importance of airfoil profile characteristics on helicopter performance is still an area for logical research efforts. Considerable effort is being devoted in this area at the present time.

### 3.4 Blade Boundary Layer Properties

As has been indicated in the discussion in the previous section, the boundary layer characteristics and those factors which influence them are the governing factors in selecting proper rotor geometry and in establishing rotor operational boundaries. A considerable impetus has been realized recently in research directed towards a better understanding of the boundary layer characteristics. Work recently reported in Reference 20 is directed towards a better understanding of the boundary layer in the translating case. The primary area of interest in this presentation is the influence of cross flow on the laminar boundary layer considered. It is demonstrated that the cross flow can be separated into two components; one due to rotation, and one due to the instantaneous yawing of the rotor blade relative to the direction of flight. The results reveal that the effects of rotation can be large in regions of incipient separation, but that elsewhere the boundary layer generally resembles the viscous flow over a swept wing. Also, the detailed structure of the cross flow depends upon whether the primary flow is accelerating or decelerating. The generalized inviscid solution, which is obtained in this work serves a dual purpose of determining the correct outer boundary conditions for the viscous flow and of setting the approximate orders of magnitude of the various terms in the boundary layer equations. This information provides a criteria for small cross flow and quasi-steady approximations that are mutually consistent and applicable to much of the flow field on a typical helicopter rotor. These assumptions were substantiated by experiment in Reference 21 in the case of pure rotation. Currently, data are being obtained for the forward flight condition.

The flat plate solution for the primary flow, which was obtained in Reference 20 supports generally the conclusions of Liu, Banks and Gadd, and Himmelskamp that the effects of rotation are beneficial with regard to laminar separation. The cross flow due to translation contains several components which act favorably at some azimuth positions, and unfavorably at others. Maximum benefits accrue in the quadrant  $180^\circ$  to  $270^\circ$  where retreating blade stall is commonly presumed to begin. This may be one reason that actual rotors have been observed to perform better than would be expected on the basis of steady state, two-dimensional section characteristics of the blades. This characteristic was pointed out by Harris in Reference 22.

While for unstalled conditions the details of the cross flow seem to be relatively insensitive to the magnitude and extent of the pressure gradients so that methods of analysis which rely upon local similarity assumptions should be valid and useful, flows with strong adverse pressure gradients appear to contradict these conclusions. These offer the most fruitful avenues for additional research. In retarded flows, the centrifugal pumping effect is larger and its magnitude seems to depend upon the upstream history of the boundary layer. This effect is potentially a large favorable one for the separation and stall characteristics of rotating blades, but it probably cannot be predicted accurately within the framework of small-cross flow perturbation expansions similar to the ones that were used for the flat plate.

The problem of the boundary layer characteristics is a most formidable one. The work which has been reviewed above touches only on the rudiments of the problem. When con-

sideration is given to the boundary layer problem which exists for the case of the oscillating airfoil with unsteady aerodynamics on an aeroelastic blade, the difficulties of mathematical representation are staggering. It will be essential to comprehend this problem before maximum advances in rotor technology can be realized. The degree to which this understanding must be acquired is not known at present. It is in this consideration that the illustration used earlier of research for research sake applies. Research in this area must be done in a very knowledgeable manner with a continuing evaluation to ascertain the utility of the findings.

Again quoting from J.P. Jones in Reference 2, "the task of the aerodynamicist in the general improvement of rotors is straightforward. It is merely to prevent separation; this presumably means the elimination of severe adverse gradients or perhaps one or the other of the classical methods of stimulating the boundary layer might be more effective, particularly over a range of operating conditions, but it has to be accepted that the basic knowledge does not exist. Not only do we not know whether the boundary layer is laminar or turbulent on the rotor blade, or whether it is essentially two-dimensional or irrevocably three-dimensional, but we would not know how to use the data even if we had it." Efforts are being made to obtain the boundary layer data on rotor blades in both hover and translating flight. These efforts are being carried out by the Bell Helicopter Company and by the US Army Aeronautical Research Laboratory in both individual and joint programs. It is hoped that as we acquire additional data we will know more of what to do with it. However, these considerations lead us logically to the next section.

### 3.5 Limitations of Current Theory

If we ignore for the moment that non-steady features of the flow exist and assume that we may transfer what we know of steady boundary layers on fixed airfoils to a rotating blade from instant to instant, then we have a thick airfoil working at a high lift coefficient at a fairly high subsonic Mach number and at a moderate and variable Reynolds number. Basic two-dimensional studies are not usually made under these conditions. We don't really know how transition sets in on the rotating blade or over what range of Reynolds numbers, nor do we know whether the airfoil is in the long or short bubble regime. It is possible that the approximate integral methods which have been developed for boundary layers in general can be adapted to these conditions, but this has not yet been done.

These problems noted are further compounded by such conditions as the reverse flow region, in which the trailing edge of the airfoil becomes the leading edge. Virtually nothing is known about this reverse flow region. The incidence at its edges is of the order of  $90^\circ$  but the relative wind speed is very small. What happens in this area is beyond the capabilities of current theory. The effect on the rotor lift is probably not worth considering, but the effects on blade pitching moments can be disastrous.

Current theory is completely incapable of dealing with the conditions of unsteady flow, since the rotor blade section does not perform at all like the two-dimensional airfoil section, and evidences a hysteresis effect on  $C_{L\alpha}$  which delays separation if there are rapid changes of incidence. The realms of current theory are again exceeded. The effects of rotor aeroelasticity are evidenced in the effects of torsional freedoms which permit gross changes in effective twist distribution. Stall flutter characteristics begin to enter into the picture. No adequate theory exists for handling this problem. Further, when stall is exceeded, the range of non-linear lift variation with incidence angle is encountered and the profile drag coefficient rises very rapidly. The power required to produce lift quickly becomes very large. Current theories are not capable of examining this problem. When we consider the effects of non-steady aerodynamics on the boundary layer we are faced with the ugly spectre of non-steady boundary layers which may be laminar or turbulent, and at high forward speeds the total fluctuation in the relative velocity near the blade tip is of the order of the mean velocities. The difficulties of the definition of separation in non-steady motion are then upon us.

It is obvious that the aerodynamicist is soon well beyond his basic framework of understanding when he begins to attack the problems of rotary wings from a basic fluid mechanics standpoint. It is therefore evident that considerable change must come about in the approach to these problems, which will result in new techniques from new points of view which are more commensurate with the problems. The thought of approaching the solution to these problems in the time honored traditional way of extrapolation from existing knowledge and experimental, empirical relationships is unthinkable. The amount of effort that must be expended simply is not available. New theories, which can cope with these blade sections which are being worked close to their separation boundaries at all times, must be evolved.

None of the general rules which have been applied as a framework for aeronautical research in the past will suffice in generating these new theories. The concept of flow deflected only through small angles by lifting surfaces, the efforts to reduce parasitic and skin friction drag and the thought that all fluctuating forces are the product of bad design have no application in rotor craft research. Further, rotor aerodynamics are highly non-linear, and the concept that each problem must be linearized to allow its various components to be dealt with in isolation must be abandoned. Perhaps one of the most formidable problems to be solved will be that of the testing of models and the establishment of proper scaling factors. Two-dimensional approaches obviously will not suffice. A formidable attack on scaling parameters must be made. The reader is referred to Reference 2 for a most astute and knowledgeable statement of the problems which exist. Not only must new theory be evolved, but new testing techniques as well.

### 3.6 Blade-Wake Interactions

The problems which were noted for the hover case relating to interactions between the blades and the wake flow are magnified many times when the translational case is considered. A considerable amount of effort is being expended by many researchers in many countries to better understand these problems. Most of the work to date has been accomplished through flow visualization techniques which define the vortex flow in and about the rotor. Some of these employ the introduction of smoke into the rotor flow, while others have been accomplished in water tunnels. Perhaps one of the earliest investigations of importance was that of Tararine which was presented in Reference 23. In this reference, Tararine demonstrated the distortion caused at the sides and the rear of the disc by mutual interference of successive trailing vortices. Sufficiently far downstream, the trailing vortices have all moved so that they lie almost as a vortex sheet in a curved surface. Along the edges of the disc there is, at moderately low tip speed ratios, a large upwash which keeps the trailing vortices almost in the plane of the disc. Any trailing vortex from a blade creates an upwash outside itself and consequently, as the vortices move aft relative to the disc in forward flight, those at the front create an upwash field which extends for some way over the disc until the vortex filaments are too far below to have significant influence. This sort of distortion was envisioned by Miller in Reference 24, and has been demonstrated numerically by several investigators since that time, the first of which was probably Scully in Reference 25. Ham of MIT made some instantaneous pressure measurements on a blade in the  $180^\circ$  azimuth position, and found very sharp pressure peaks which would be consistent with the presence of a vortex close to the blade. These results are reported in Reference 26. During an investigation reported in Reference 27, Simons, Pacifico, and Jones obtained pictorial evidence, through vortex flow visualization techniques, of trailing vortices passing above and impinging upon the succeeding blade. This is illustrated in Figure 24 which is extracted from Reference 27. This phenomenon has been demonstrated on several occasions by various visualization techniques. A compendium of the references covering these investigations would be very long indeed.

Perhaps the most important aspect of these investigations has been that, on occasion, vortex bursting occurs. Professor Miller of the Massachusetts Institute of Technology and his associates have probably produced more contributions to an understanding of this problem than any other group of researchers. However, the ability to handle this problem is still far from our grasp. It is obvious that when vortex bursting and annihilation

occur, some of the assumptions on which our basic vortex theory is based are invalidated. In particular, the assumption of a vortex starting and continuing to infinity is violated and we can no longer rely upon Kelvin's theorem. The exact mechanism of this breakdown has not been established, but many theories have been advanced. It is known that when a vortex breaks down, there is a rise in intensity of the pressure fluctuations on the surface below the breakdown. This matter of vortex impingement on the blade was treated in the section on the hovering rotors, and the evidence of these pressure fluctuations was shown.

It is possible that the effects of this vortex/blade interaction is not of great significance in its effects on overall lift on a translating rotor. However, its effects on power performance may be severe. Other effects also are known to be detrimental. It is obvious that because of the fluctuating pressures which occur, vibration inputs are fed into the system. Further, it is likely that high noise levels will occur. The phenomenon known as blade slap, which occurs in a rotor either at high speed or during the climbout, is probably associated with this phenomenon. A considerable amount of effort is being expended to understand the problems of noise generation in helicopters. Concerted efforts are underway in many countries to reduce the noise level and the characteristic signature of the helicopter. The most promising area of research for these purposes will be to understand more completely the phenomena of blade/vortex interaction.

Additional comments concerning this problem will be made under the high speed cruise problems discussed in Section 4. Perhaps one additional statement could be included here which refers back to material discussed in Section 3.4. The flow mechanisms which are being considered here will unquestionably have a large effect on the boundary layer flow mechanics. Currently, research programs are being undertaken which strive to simultaneously measure surface pressures, boundary layer profiles and noise emission from rotors experiencing this type of flow. It is possible that considerable advances can be made in the reduction of noise, power required, and vibratory inputs by a better understanding of the flow mechanisms associated with high speed-high power operation where vortex/blade interactions occur.

A summation of the areas of research currently being undertaken and those which are required in the area of blade/wake interactions indicates that methods must still be perfected for the basic distorted wake analysis. Both the tip vortex and the inboard vortex sheet must be included. These, of course, must be correlated with systematic flow visualization results to vindicate the theories. From these results, a coupling of the basic distorted wake program with blade response and circulation matrix programs must be accomplished, so that consistent wake geometries, blade circulations, and blade responses can be computed in an iterative procedure. In essence, this is tantamount to saying that means must be developed for predicting the airloads which operate on the blade in the forward flight mode. It is at this point that a meeting between researchers and designers is sought. It is not possible for the designer to optimize his design until he has in hand procedures which will enable him to have a comprehensive understanding not only of the overall load distribution on his rotor system, but of the detailed load distribution on the disc as well. Not only must the tip vortex characteristics be defined, but the entire characteristic of the wake behind the rotor in forward flight must be mathematically represented. It is known that this wake has the characteristics of a rolled-up vortex sheet, but it will not be possible to adequately represent this wake until such factors as the mechanics of the formation of the tip vortex and its dimensions are known, in addition to the distribution of the vorticity and circulation along the blade and the effects of such factors as Reynolds number on vortex stability and dissipation. It has not been mentioned previously, but should be strongly emphasized that the importance of knowing the rotor wake is not solely dictated by the need to establish rotor characteristics, but is required to assess the influence of this wake on wing and fuselage components immersed in it as well as the effects on the tail rotor. Not only must the effects be determined for steady state flight, but when these are in hand they must be perturbed for the effects of transient flight to permit the prediction of maneuvers, autorotative descents, and gust encounters. Currently, Dr Kurt Hohenemser of Washington University is

attempting to apply to the helicopter rotor, power spectral density techniques which have been successfully applied to fixed wings to predict gust response. This highly complex problem is representative of the type which must be attacked with highly sophisticated methods of solution, if maximum capabilities of rotary wing aircraft are to be realized.

### 3.7 Effects of Non-Uniform Downwash

Perhaps one of the most severe limitations to an understanding of the basic flow phenomena on the rotary wing imposed by previous theories was the inability of these theories to predict the non-uniform downwash. Recently, methods have been evolved which will enable this prediction, and these methods have been confirmed, at least to a first order, by rotor airload measurements in flight. Exact confirmation of these theories will await the development of instrumentation which will enable the actual measurement of effective blade section angle of attack while the rotor is in forward flight operation. Efforts are currently being made to develop this instrumentation.

Figure 25 shows a comparison of the distribution of angle of attack across the rotor disc for a representative condition of 140 knots with uniform downwash and with non-uniform downwash. It is important to note that not only are the magnitudes of the angle of attack greater and of considerably different gradient in the non-uniform than in the uniform case, but there is actually a reversal in the gradient near the tips in the area of the 270° azimuth position. The importance of these variations is evident when considered in the light of requirements for airfoil profiles and profile distribution along the blade. Tests have been performed of advanced geometry rotors incorporating section characteristics to account for the non-uniform downwash condition. These tests have indicated a decided improvement in performance.

The capability of establishing proper representations of the non-uniform downwash, and thereby the operating conditions for the rotor blades, are directly dependent upon the capability to define the wake structure which was discussed in the preceding section. The most challenging aspects of this problem will be to find analytical methods which are applicable generally, and which are not dependent specifically on particular rotor configurations or flight conditions. While it is acknowledged that considerable advance has been made in this area, the formidable aspects of the problem are well recognized by investigators. This area offers great opportunity for capable aerodynamicists who are willing to apply themselves to the rigors of this complex problem.

## 4. HIGH SPEED CRUISE PROBLEMS

### 4.1 Advancing Blade Compressibility

It must be noted at the outset of this discussion of high speed cruise problems, that the ten items to be discussed in this section are not independent with regard to the phenomena which are involved, nor with regard to the remedies which may be prescribed. For example, remedies for problems existing on the advancing blade side of the disc cannot be considered independent of problems on the retreating blade side since often times they are not compatible, even though the type of phenomena which is to be corrected is the same. Further, many of these are merely an extension of problem areas already noted into a more severe range. Each item will be dealt with in its current status, and areas for additional research and development will be noted.

As was noted in Section 3.3, one of the requirements for an airfoil suitable for utilization on helicopter rotors is that the drag at high Mach numbers and low lift coefficients must be as low as possible. This requirement is brought about by the high speed cruise case when the advancing tip Mach number approaches the transonic condition where drag divergence occurs. This phenomenon occurs, of course, because of the additive effects of the rotational speed and the forward speed. Since it is advantageous from the standpoint of the retreating blade side to maintain the rotor RPM as high as is reasonable, this problem is aggravated.



A general statement of the conditions on the advancing side of the disc is that the blade incidence and lift coefficient are small, and continue to reduce with increasing flight speed. It is possible that to maintain rotor balance, the incidence may even become negative. Because of these conditions, the onset of flow separation will have a larger proportionate change on rotor behavior than will separation effects which occur on the retreating side. It should be noted, however, that the basic problem is the same on both sides of the disc as will be discussed later for the retreating blade side; namely, to delay the onset of separation effects and drag divergence.

One of the most obvious means of dealing with the problems of separation and drag divergence on the airfoil at high Mach number is to modify the airfoil leading edge shape to such a contour as represented by the so called "droop snoot". As has been noted earlier, modifications to the leading edge are basically all that is permissible in the helicopter rotor because of the adverse changes in pitching moment resulting from trailing edge changes. The incorporation of camber into the airfoil by this means can have an adverse effect in the event that negative incidences are required, since the airfoil now becomes extremely susceptible to separation on the lower surface. An interesting point is that a loss of lift on the advancing side causes the leading edge of the disc to flap down, and so helps to maintain the propulsive force which is lost in the retreating blade stall. However, this trade-off is hardly a compensation for enduring the problems of flow separation.

For many years the rule has been not to exceed an advancing tip Mach number of 0.8, which was generally considered to be the Mach number at which drag divergence would occur and where penalties in power required would become so great as to be a limiting factor. Experience has modified this arbitrary rule, and it has been discovered that genuine benefits can be obtained from higher tip speeds through the moderation of the compressibility power losses. The ability to operate with supercritical areas on the blade without encountering drag divergence, which was illustrated in Figure 17, suggests the possibility of operating with tip Mach numbers even reaching into the supersonic range for small excursions of the azimuth without undue power requirements. This may be particularly true of compounded aircraft, as will be discussed in Section 6. Even on current aircraft, supercritical rotor blade operation is encountered regularly.

In addition to the shaping of airfoil profiles to deal with this problem, another approach has been taken which reduces the thickness of the airfoil in the tip region. This alteration produces thinner blade sections which have less severe drag divergence at higher Mach numbers, thereby lessening the adverse effects of compressibility losses. It does, however, produce a sharper leading edge which may have adverse effects on the retreating blade side particularly in the highly loaded, climb-out condition. Of course, it is obvious that a combination of leading edge treatment and reduction in blade thickness may be an optimum solution.

Some effects of composite blade geometry were shown in Section 3.3. In addition, it is interesting to consider the results of an experimental study made by the US Army-NASA-Bell team of researchers on a thin-tipped, 48 ft diameter, 21 inch chord, rotor. These results are reported in Reference 28. Comparable results were obtained in the same test program for a set of standard blades which did not include the thickness reduction near the tip. Data were obtained for the standard blades up to advancing tip Mach numbers of 0.95 and for the thin tip blades to Mach 1.025. An example of the wind tunnel data which were obtained for the thin-tipped blades is shown in Figure 26, which is extracted from Reference 28.

The symbols represent actual test points. The regularity of the data confirms the usefulness of a large scale wind tunnel in studying the problems of rotorcraft aerodynamics. The range of advance ratios encountered was generally from 0.3 to 0.4 and the range of advancing tip Mach numbers was from 0.79 to the maximum values given earlier. A comparison of the horsepower required per square foot of rotor for the two sets of blades is shown in Figure 27.

It is noted that sizable reductions in power required at the higher advancing tip Mach numbers were realized. A further benefit from the thin tip blades, which was indicated by subsequent flight tests, was that even at hover a small power reduction occurred for the thin-tip blades on a UH-1 helicopter. This finding is not in keeping with Figure 27(a), which may be accounted for by the fact that the flight tests were conducted at a higher value of  $f/bcR$ . This small hover power saving resulted in the capability for that machine of lifting one additional troop.

It is interesting to note that there are three supercritical flow states for an airfoil which must be considered in an analysis of the advancing blade problem. These are first, the critical Mach number  $M_{cr}$  which represents the free stream Mach number at which local sonic velocity is first reached on the airfoil surface; second, the drag divergence Mach number  $M_d$  which represents the free stream Mach number at which the slope of the curve of drag coefficient versus Mach number attains a value of 0.10; and third, the shock stall Mach number  $M_s$  which represents the free stream Mach number at which full separation first occurs at the rear of an airfoil. These effects for a two-dimensional airfoil are illustrated in Figure 28, which is extracted from Reference 28.

It will be noted that the drag divergence Mach number may be considered the indicator of the critical condition, after which large power increases can be expected. The shock stall Mach number is seen to be in direct correspondence with the maximum lift coefficient. For the conditions of the test reported in Reference 28 it is interesting to note the distribution of contour lines representing these values on a rotor disc within the normal flight envelope as compared to the same rotor disc operating at speeds greater than the normal flight envelope. These variations are shown in Figure 29. Within the normal flight envelope, it is seen that the area outboard of the drag divergence Mach number boundary is small and only small benefits of thinning can be expected. However, an attempt to increase high speed cruise as represented in the (b) part of Figure 29, indicates that a large portion of the disc is outboard of the drag divergence Mach number at all azimuth positions; a small portion of the disc is even above the shock stall Mach number. In this case thinning the airfoil from the 0.8 radius outboard should have significant effects on the power required. This was actually borne out by the experimental data which were obtained from this test, shown in Figure 27.

It should be noted that the calculation of such performance is virtually impossible at the present time because of the lack of adequate experimental data for the various airfoil sections being employed at the high Mach numbers. However, a word of caution is to be given at this point concerning the acquisition of two-dimensional airfoil data for application to these problems. It has been noted earlier in other sections that the flow conditions in which these airfoils are operating is not generally represented by a two-dimensional flow case. Further, as will be discussed later, the blade is operating at an unsteady airflow condition. Initiation of large programs to obtain two-dimensional airfoil data at high speeds for these conditions needs to be carefully analyzed before being undertaken to ascertain that after it is acquired, it will truly serve a useful purpose.

The development of theoretical methods to account for these cases, as was noted earlier, will be a difficult accomplishment. It has been demonstrated by many investigators that, in the low advance ratio range, fairly reasonable results can be obtained for rotor performance. Although good agreement has been obtained in these lower advance ratio ranges, it should be noted that the techniques which are employed to obtain these results become non-linear as advance ratios increase much beyond 0.5. Predictive techniques which are developed for high advance ratios will necessarily have to be vindicated by experimental tests, such as that presented in Reference 28. The availability of facilities for accomplishing this is meager and improved flight testing techniques must be developed.

It is interesting to note that, for the investigations reported in Reference 28, noise measurements were made for both sets of blades. At advancing tip Mach numbers between 0.85 and 1.025 approximately a 12 decibel reduction for each 0.1 Mach number increase was realized. (The reference decibel level is 100). These results are encouraging in that



they represent at least one technique for reducing the high level of noise and characteristic noise signature of rotor craft.

#### 4.2 Retreating Blade Stall

A consideration of the problems on the two sides of the rotor disc quickly reveals that the problem is generally the same, with emphasis on different facets. The most significant effect of compressibility at subsonic Mach numbers is for the local shock waves to cause the boundary layer to separate. Thus, it is just as desirable to have the drag divergence Mach number at the highest possible Mach number for the retreating side as it is for the advancing side. In current practice, this Mach number is between 0.3 and 0.4 on the retreating side. This is often considered to be an "incompressible" range, but nearly sonic local velocities can appear on the nose of the airfoil for a high lift coefficient, implying substantial influence of Mach number on stall.

The conditions for a classic stall of the airfoil sections are most likely to be encountered at the tip of the retreating blade at high forward speed. In these conditions, much of the blade is at extremely high incidence because of the reduced flow caused by rotor translation. The blade is not in this stalled region for very long, so the integrated effect on the total rotor lift of an abrupt separation is not very large. There is a small loss of rotor thrust due to the slight reduction in flapping angle, and this tends to maintain the conditions for stall.

It has been demonstrated on many occasions that a hysteresis effect on the maximum lift coefficient for a rotor blade gives values of maximum lift coefficient well beyond the two-dimensional maximum value. The applicability of two-dimensional airfoil data to these areas has been, and continues to be a questionable matter. It has led to a considerable amount of research which will be discussed in Section 4.8. This effect delays the onset of stall, but when stall does occur it is usually accompanied by a stall flutter phenomenon. This effect will also be discussed later in Section 4.7. It is interesting to note that since rotors are not very stiff in torsion, the occurrence of stall tends to create a twist nose-down, and so to relieve the tendency to stall. The result is a position of equilibrium almost at the stall until the conditions for stall are well exceeded over much of the blade. When the blade sections become fully stalled, then the drag divergence begins and excessive power is required to produce the lift.

It should be noted that one of the most disturbing influence of both retreating and advancing blade stall is the high load oscillations which are introduced into the control system. These loads have been a continued problem in evolving higher cruise speeds for helicopters, and the resolution is solely dependent upon the capability of new methods and techniques to prevent the stalling problem.

Here again, it should be emphasized that the problems of understanding the flow in the boundary layer are vitally important and continuing work is required to gain a better mathematical representation of the boundary layer model for the translating rotor. The ultimate approach to an understanding rests in full comprehension of the boundary layer and the influence exerted on it by the surrounding environment.

#### 4.3 Blade Twist Distribution

The effects of twist employed in helicopter rotors have been well understood for a considerable time. Ideal twist has been defined as the product of the twist at the blade tip and the ratio of the rotor radius to the radius of the blade element in question. The effects of wash out are generally favorable in the helicopter rotor for the control of tip stall and the realization of a more uniform induced velocity distribution. In the cases where twist has been employed, it has generally been as a uniform twist across the blade span. It can be seen in many references, including Reference 3, that a large portion of the advantages accrued from blade twist can be realized by the incorporation of linear twist of approximately  $12^\circ$  from root to tip of the blade. However, current research

efforts, which have demonstrated the non-uniform aspects of the induced velocity distribution, have pointed out the desirability of improving the twist distributions for conditions between flight regimes. Those areas of the rotor which are inboard of the 15% radius point are not properly accounted for in the linear twist distribution and it is well known that the optimum twist distribution varies with the flight regimes. The ideal condition would be an infinitely segmented rotor which could be infinitely controlled to provide the desired distribution at any given flight condition and which could be varied cyclically with azimuth position. Such a rotor would produce the desired uniform induced velocity distribution. .

Efforts are being made by several groups of researchers to better understand the advantages of incorporating better twist distributions into rotors and means of meeting the varying requirements of the wide range of flight conditions from hover to cruise. Harris of Vertol has made some comparisons for an infinitely segmented rotor which represents the ideal case with a conventional rotor incorporating twist, a two-segment segmented rotor and conventional lift-offset rotors at a speed of 236 knots. These comparisons are shown in Figure 30. The incorporation of such devices leads to either variable geometry blades, which will be considered in Section 4.9, or to systems which will accommodate the lift offset rotor such as, for example, the Sikorsky/Westland ABC rotor system. This discussion also leads us logically to the next section in which we shall discuss the problem of asymmetric loading.

#### 4.4 Asymmetric Loading

As forward speeds increase the unbalance on the rotor without cyclic control, asymmetric loading continues to increase. As cyclic control is fed into the rotor system, the retreating blade is drawn closer and closer to its stall margin. The inboard sections are finally subjected to reverse flow, and a down load is generated which further complicates the rotor balance problem. This asymmetric loading has led to the generation of such concepts as the lift-offset rotor in which the rotor balance is not maintained and the center of lift is allowed to shift towards the advancing side. Such an action of course, requires a balancing moment from some other component of the aircraft to prevent the aircraft upset. As mentioned in the preceding section, one concept is to utilize two contra-rotating rotors which cancel the upsetting moment at the hub. Other proposals have included the use of a wind surface on the retreating blade side of the aircraft which is sized to produce lift as a function of air speed, so as to produce a moment which will cancel the unbalance in the rotor. The primary disadvantage of such systems is that rather large oscillating moments are fed into the rotor system which must be cancelled at the hub in the case of the contra-rotating system, or which result in a large hub moment for the offset rotor utilizing an auxiliary surface. These vibratory loads will not be realized in the aircraft structure provided the proper cancellation occurs at the hub. However, the rotor parts themselves must endure rather large excursions in loading. It is probable that continued efforts will be made to provide adaptive means to offset the effects of asymmetric loading.

#### 4.5 The Effects of Solidity

Increased solidity, which is synonymous with reduction of blade loading below that required for hovering, is one of the possible means of increasing the high speed capabilities of pure helicopters. Assuming an average lift coefficient of 0.6 in hover at 6000 ft, 95°F and tip speed of about 680 ft/sec, the resulting blade loading would be about 80 lb/ft<sup>2</sup>. This is the blade loading of most current helicopters. By reducing blade loading below the above value, speed capabilities can be improved as has been demonstrated by the Super Frelon in its record flight where blade loading was about 50 lb/ft<sup>2</sup>. However, it can be seen that this method of improving high speed capabilities reduces the equivalent lift/drag ratio of the lifting system or, in terms of our previous performance equation, increases the equivalent drag/weight ratio. Overblading of helicopters may involve also some power penalty in hovering. Under some circumstances this loss may be minimized through reduction in the tip speed at hover. It should be noted however, that

an increase in rotor solidity offers the possibility of forward flight at higher altitudes where reduction in the parasite drag and improvement in specific fuel consumption of the engine may compensate for losses resulting from a lower lift/drag ratio of the rotor itself. Obviously, an increase in structural weight of the rotor system resulting from a higher solidity will remain as a penalty associated with this approach.

#### 4.6 Effects of Blade Geometry

These effects have been studied in some detail already in previous sections, but a summary of these is made for clarity. It has been ascertained that for high speed characteristics, twist and taper in both blade planform and thickness in the outboard sections can be utilized to realize performance gains. Further, it has been pointed out that the capability of varying airfoil profile geometry in the outboard sections can be of significant value in improving performance. The difficulty of manufacture of such blade geometries has prevented their usage in the past; however, the introduction of fiber technology has improved the chances for such designs. The use of all plastic blades on the Bolkow 105 is a significant step in the introduction of this technology into the production of helicopters. It is expected that, in the future, many changes will be made in blade geometry to accommodate the high speed requirements of rotorcraft.

#### 4.7 Blade Aeroelastic Effects

The helicopter rotor blade is an elastic member, and therefore tends to amplify or attenuate (depending on its natural frequency distribution) the harmonic components of the total vibratory loading. The vertical vibratory output of a single rotor blade as a function of tip speed ratio is shown in Figure 31, which, together with many of the other figures presented in this section, was abstracted from Reference 29. This figure indicates both a maximum lift condition and an 80% M loaded condition. It also indicates the region where unloading would be required. These functions of rotor unloading will be discussed in more detail in Section 6. It can be seen that as forward speed is increased, which corresponds to an increased tip speed ratio, the vibratory loading is growing very rapidly. Some of this vibratory energy is filtered out before reaching the fuselage, but it does contribute to cyclic stresses in the individual rotor blades and the associated rotating blade control system. This is also true of the vibratory loads in the plane of rotor rotation, which are indicated in Figure 32. These integrated output loads can be resolved into magnitudes of the harmonic components by power spectral density methods. The distribution of these harmonic loadings for a typical rotor blade for various tip speed ratios is indicated in Figure 33. The influence of advance ratio is plainly evident.

The amplification characteristics produced by a typical rotor blade with no internal damping on the loading distribution of a rigid articulated blade are illustrated in Figure 34. It is seen that the higher harmonic airloads are amplified disproportionately by virtue of the relatively small aerodynamic damping and negligible internal damping at these high frequencies, and represent a disproportionately large share of the cyclic stress in the rotor blade. The possibility of reducing the cyclic stresses in a rotor blade by utilizing the potential for increased gains are indicated in Figures 35 and 36. Considerable improvement is seen to be attainable.

In the foregoing, it can be seen that although the rotor is capable of providing all the required lift up to tip speed ratios of 0.73, this would be incompatible with both rotor blade stress and gross aircraft vibration levels. A practical limit to tip speed ratio of a fully loaded rotor is seen to be of the order of 0.5. With technological advances offering the possibility of reduced cyclic stress, the use of rotor isolation systems can be expected to permit pure helicopter flight at forward speeds of the order 200-220 knots. This is not only possible, but can be achieved with cyclic stress and vibration levels no worse and possibly better than today's helicopters. However, two special problems of fully loaded rotors must yet be considered in an effort to achieve this potential. These are a "flap-lag" blade motion instability in accelerated flight conditions, and rotor blade pitch-torsion "stall flutter". Figure 37 indicates that the

minimum level of damping required is virtually constant for the tip speed ratios and rotor maneuver acceleration capabilities of practical interest. Figure 38 shows that the damping required versus tip speed ratios at various practical maneuver acceleration levels in the presence of the rotor vibratory loads is increased by these loads. Typical levels of available damping for articulated, semi-rigid, or rigid rotor types can be exceeded during maneuvers within the rotor capability, and flight at the projected speeds of from 200-220 knots will require increases in the hydraulic damping normally utilized on articulated rotors for the avoidance of ground resonance. Increases in the internal plus aerodynamic damping typically available in semi-rigid or rigid rotor types must also be provided. The additional damping requirement that is foreseen is not very great, and it can be expected that this can be obtained through proper attention to hydraulic damper design or rotor blade structural damping for the various rotor types.

The problem of rotor blade pitching-torsion flutter has been examined in a qualitative way by Ham in Reference 30, and quantitatively by Ham and Young in Reference 31. Figure 39 shows the magnification of the ordinary cyclic loading versus tip speed ratio for various rotor lift to aircraft design gross weight ratios. It is seen that the nominal amount of stalling (the beginning of so-called tip stall) is associated with a greatly magnified cyclic loading which is, in fact, the result of a periodic pitching-torsion instability. This is illustrated in Figure 40 which shows that the pitch-torsion motion becomes unstable on the retreating side thus resulting in periodically unstable motion. More will be said concerning this phenomenon in Section 4.8.

The aeroelasticity of the blade also enters into the gust sensitivity. The relative sensitivity of rotor blade transient flapping increases with tip speed ratio, as is illustrated in Figure 41. At a tip speed ratio of 0.5, it is seen that the relative gust sensitivity is twice that in hover, while for tip speed ratios of 1.0 the relative gust sensitivity grows to 14 times that of the hovering rotor if the rotor is required to produce its maximum lift. Even if the rotor is completely unloaded, as will be discussed for the compound case, it is seen that at tip speed ratios of 1.0, the gust sensitivity grows to 9 times that of the hovering rotor. Gust sensitivity can be reduced, of course, by one of two fundamental approaches; either a cyclic pitch-flapping displacement feedback control system, or a cyclic pitch-flapping rate feedback control system can be utilized. These are portrayed in Figures 42 and 43 for feedback ratios of 2° per degree and ¼° per degree respectively. The rate feedback system is seen to be the more effective.

Finally, one additional problem of importance must be considered in this commentary on the effects of aeroelasticity. Large regions of reverse flow occur in the helicopter rotor disc, as has been mentioned previously. This condition can lead to classical flapping-torsion flutter and classical static torsional divergence of the rotor blades. This phenomenon is similar to the more familiar wing flutter and divergence phenomena. Figure 44 illustrates the classical flapping-torsion flutter boundary of a typical mass balance rotor blade. Increases in the blade fundamental torsion frequency ratio are required to increase this forward speed-advance ratio limit. These are so drastic that it becomes clear that only radical departures from rotor blade structural design and conventionally acceptable rotor weights will permit high speed capabilities of conventional helicopters to be increased above the projected 200-220 knot condition.

While the aeroelastic effects are not purely an aerodynamic problem, this review serves to prove the necessity for a much closer working relationship between the aerodynamicist and the aeroelastician. The outlook of the aerodynamicist who chooses to work in the field of rotor craft must be modified to include that of the aeroelastician, and even that of an environmental engineer if he is to solve the problems associated with the high speed cruise condition.

#### 4.8 Unsteady Airfoil Phenomena

The flapping-torsion problems discussed in the previous section have centered a considerable amount of interest on the occurrence of unsteady aerodynamic phenomena and

stall flutter on the retreating blade of the rotor. It is difficult to make a synoptic presentation of this subject, since it is a major part of the aerodynamic sciences. There is no intent on the part of the author to provide a complete analysis of this area of research, nor even of all the problems associated with it. A brief review of some of the efforts that are being made at present will be presented, with the hope that the reader will be stimulated to pursue the subject further in the references. It is of interest to note that one can easily find in excess of 100 references on this particular subject. However, it is only in recent times that, with the exception of work done by Halfman, reported in Reference 32, any work has been done which is of a comprehensive nature. Great quantities of data have been obtained, but the researcher was working either in such a narrow range of parameters or with such primitive equipment that his results contribute little to an understanding of the problem. More recent researchers such as Rainey, Reference 33, Ham and Young, Reference 34, Carta, Reference 35, and Liiva, Reference 36 have made significant contributions to a better understanding of the problem. Further, these astute researchers have been attacking the problem from a theoretical approach as well as the experimental approach, and have succeeded in laying the foundation for what will probably prove to be a major breakthrough in the understanding of rotor blade aerodynamics.

Halfman's early data on a pitching airfoil showed conclusively that the maximum lift experienced by an airfoil oscillating through stall can be substantially higher than the two-dimensional static value. This strongly suggests that dynamic effects are the most likely reason for the stall delay exhibited by the helicopter rotor blade. Rainey also showed that in addition to a delay of the blade stall, negative damping can occur for pitch oscillations through the stall. This negative damping is caused by the hysteresis effects occurring in the blade pitching moment-angle of attack curve, and has been shown by Ham and Young in Reference 34 and by Carta in Reference 35 in simultaneous investigations. The resulting blade and control stresses caused by stall, of course, limit the flight speed of the helicopter, often times below the speed potential for the power available.

All the researchers mentioned above have produced significant amounts of experimental data upon which to base their theoretical effort. It is difficult to compare the value of the results which have been obtained, since they emphasize different aspects of the problem. The most recent data obtained is that by Liiva, and was obtained on a two-dimensional section in the high speed wind tunnel of the Boeing Company. Perhaps the most significant aspect of these data is that they were obtained at full scale Reynolds number up to a Mach number of 0.6, which is considerably higher than most other data obtained and more nearly represent the full scale conditions. It should be noted that other researchers have obtained data on three-dimensional models. However, for those tests it is difficult to separate such phenomena as spanwise flow and elastic blade motion from the data to obtain the section angle of attack, the basic independent variable used in most theoretical rotor blade analyses.

All researchers who investigate this problem of unsteady airloads are faced with the problem of selecting the airflow motion which most closely represents the aerodynamics of the helicopter rotor blade section, and which can be executed by a practical wind tunnel model. Two basic motions occur in the rotary wing device for conditions of unsteady flow; first, motions which occur at frequencies corresponding to once-per-revolution as a result of cyclic pitch inputs, velocity variation around the disc, flapping and lead-lag motions, and second, motions at frequencies higher than once-per-revolution that are caused by elastic blade deflections. First torsional and first bending natural frequencies are of special interest, since these are the deflections that can be large. The first set of motions are important to determine the stalling behavior; the second set are of interest from the standpoint of high frequency motions which may possibly be self-sustaining elastic oscillations of one of the primary blade modes. Figure 45 portrays the general characteristics of once per revolution motion which occurs on the rotor disc. The first two are relatively simple to test independently. However, the third is rather difficult, since it requires changing the velocity of the wind tunnel at approximately 4 hertz for full-scale rotor blade sections. There is not believed to be a simple way to represent

the third type of motion. Carta's tests rely primarily on pitching motions of the airfoil section. Rainey, Ham and Liiva have investigated both pitching and plunging. A typical mechanism for investigating these phenomena in the wind tunnel is shown in Figure 46.

The results obtained by all these investigators show similar trends. For the purposes of this presentation, results from Reference 36 will be used to portray the important aspects of the unsteady airfoil phenomenon. Hysteresis loops for a modified NACA 23010 airfoil are shown in Figure 47. These loops are similar in shape to those that have been obtained for such sections as the symmetrical NACA 0012 which is in common use today. Also shown in this figure are curves representing the data obtained for static or steady conditions for the same airfoil. The frequency of 16 hertz is characteristic at model scale of the full scale once per revolution motion of a rotor blade. The response of the airfoil lift and pitching moment for  $7.3^\circ$  average angle of attack shows the characteristic elliptic shape predicted by unsteady airfoil theory as presented by Bisplinghoff, Ashley, and Halfman in Reference 37.

The area inside the trace of pitching moment indicates the work per cycle or cycle damping. This is defined as the line integral of the pitching moment as a function of angle of attack. This integral is positive for a counter-clockwise circuit. Areas enclosed by a clockwise circuit are damped negatively. For these conditions the airfoil system extracts energy from the airstream. This can lead to an increase in the amplitude of oscillation with time for an elastic system, and is precisely the condition for flutter. The range for negative damping in the hysteresis loop is indicated for the condition of an average angle of attack of  $14.92^\circ$ .

The normal force loop for this condition of  $14.92^\circ$  shows a substantial increase in the maximum normal force above the stall value for the steady airfoil. A glance at the moment trace shows that this test condition is nearly neutrally damped. It is interesting to note that moment stall occurs before lift stall. This condition has been found to exist in flight test data. The condition at an average angle of attack of  $24.6^\circ$  represents a fully separated flow condition with positive damping.

The sensitivity of these phenomena to the pitching frequency has been found by all researchers to be an important factor. An indication of this sensitivity is given in Figure 48, where a ratio of 6 to 1 in pitching frequency has been employed. It is interesting to note that the airfoil is partially stalled during the decreasing alpha portion of the cycle for the higher frequency case, even though the normal force trace shows the characteristic elliptical shape for unstalled flow. This can be confirmed by observing that the sense of the normal force trace loop is opposite to that for the average angle of attack of  $7.3^\circ$  in Figure 47. The sense of the pitching moment trace also bears out the conditions for stall, and this case is seen to be essentially negatively damped. It is also noted that the onset of stall is significantly postponed for both the normal force and pitching moment traces as the frequency is increased. The sudden stalling at the low frequency does not occur at the high frequency, and this suggests that there is an upper limit to the time rate of change of circulation on the airfoil, as has been suggested by Ham in his works. The effects of Mach number on the dynamic stalling behavior of an airfoil have been found to be similar for conditions of 0.2 and 0.4 Mach number in that both positive and negative damping areas are present in the pitching moment trace for oscillation through stall. However, for the 0.6 Mach number case, entirely different trends from those at the 0.4 Mach number case were observed. The dynamic normal force and pitching moment loops follow the static line rather closely for the 0.6 Mach number case because the reduced frequency parameter  $k$  is very low. Also the cycle damping is positive and there are no sharp breaks in the normal force and pitching moment curves for both steady and oscillatory data. This is indicated for the Mach number 0.6 case in Figure 49. The difference in behavior at the 0.6 Mach number was examined by Liiva by comparing steady and oscillatory chordwise pressure data below and above stall at Mach numbers of 0.4 and 0.6. These comparisons are shown in Figure 50. For the case of 0.4 Mach number, the loading is seen to be of the classical potential flow type before stall, with the



distribution radically altered above stall, indicating flow separation. For the 0.6 Mach number case, favorable pressure gradients exist to the 10% chordwise location due to supersonic expansion around the leading edge and separation, if any, occurs after the shock. No sudden increase in nose down pitching moment with angle of attack exists because the expansion/shock system can adjust to the changes by a slight readjustment of the leading-edge pressure and shock location.

A comparison of data for cambered and uncambered airfoils is presented in Figure 51. Although the cambered airfoil has a higher normal force capability over the whole frequency range, the general characteristics are seen to be equivalent. Further comparison for these two cases in Figure 52 show similar trends with Mach number for both airfoils at the 0.4 Mach number condition. These tests are for oscillation of 96 hertz in the model scale. The effects of amplitude of oscillation on cycle damping are shown in Figure 53 for oscillation frequency of 96 hertz. As seen, the negative damping for the  $2\frac{1}{2}^\circ$  amplitude oscillation is much larger than that for the  $5^\circ$  amplitude. This suggests, as has been indicated previously, that the rate of pitch change is a governing factor in the onset of flow separation.

A typical set of data for vertical translational tests are shown in Figure 54. The maximum normal force coefficients obtained during these tests in the plunge mode for the equivalent once-per-revolution frequency, which is 16 hertz model scale, are indicated in Figure 55. Both airfoils tested show a normal force increase over the steady value and the effect of larger Mach number is, as usual, to suppress the maximum obtainable normal force coefficient. Figure 56 compares data obtained for the vertical translatory case at Mach numbers of 0.4 and 0.6 (Theoretical damping was obtained by Theodorsen's method.) For angles well below the static stall level, damping at Mach number 0.4 remains near the theoretical value; above  $15^\circ$  angle of attack, zero or negative damping prevails. For the case of 0.6 Mach number, the loss of damping occurs at a lower angle of attack, but no large negative values were observed. These tests, made by Liiva, are apparently the first to discover negative damping in translatory motion. These tests were conducted at much larger incremental vertical displacements and at higher Mach numbers than any previous tests, and this is probably why previous researchers never measured negative damping for this case.

It can be concluded from the results obtained by the several researchers, that the effects of negative damping in pitch and plunge are strongly related to discontinuities in the static normal force and pitching moment curves. These discontinuities are caused by leading edge stall. At higher Mach numbers, where transonic effects eliminate leading edge stall, damping is reduced below the potential flow level but remains positive. The areas where negative damping occur have a profound effect upon rotor stability. In Reference 35, Carta presents a good summation of this characteristic. A summary plot indicating the two dimensional aerodynamic damping surface (extracted from Reference 35) is presented in Figure 57. This plot is a summary plot obtained from experimental results, and indicates an unstable region. The encounter of this unstable region was demonstrated by application of a stability analysis described in Reference 35 for a Sikorsky S-61F rotor. Two flight conditions were considered; one at a forward speed of 165 knots and a gross weight of 12,460 pounds, and another at 210 knots and 16,820 pounds. It was assumed that the rotor blade was capable of responding to an infinitesimal disturbance in its fundamental torsional mode at every azimuth position. The fundamental torsional frequency of the blade was 27.3 hertz and the semi-chord dimension was 0.76 ft. The reduced frequency contours and incidence contours on the rotor disc for the two cases are shown in Figure 58 and 59. The variation of aerodynamic damping for the two cases is shown in Figures 60 and 61. The occurrence of negative damping is obvious for the heavier lift case. For the conditions shown, the regions over which the negative damping extends is insufficient to excite more than  $\frac{1}{2}$  cycle of torsional motion. However, it is obvious that for other rotors and other conditions rotor instability could occur. If loading is reduced without changing inflow, a condition can be reached wherein two full cycles of torsional motion can be excited by the negative damping in the retreating blade. These results are in good agreement with work which has been done by Ham and Young.

A final consideration of the unsteady airload phenomena to be presented is drawn from recent work accomplished by Ham and Garelick at Massachusetts Institute of Technology, and is yet unpublished in its final form. Figure 62 represents cross-plotted data from a Master's Thesis by Garelick and illustrates the effect on dynamic stall angle of pitching velocity and quarter-chord heaving velocity (resulting from other than quarter-chord pitching axis locations). Note the increase in dynamic stall angle represented by the  $\alpha^{(S)}$ , and the decreasing sensitivity to heaving velocity with increasing pitching velocity. Also of interest is the fact that the maximum delay in the onset of dynamic stall occurs when the airfoil is pitching about the leading edge. These results, though qualitatively correct, are tentative since a relatively small number of experimental points are available for cross-plotting purposes.

The dependency of the peak values of lift and moment on pitching or plunging velocity has been suggested throughout the many experiments which have been conducted. A velocity parameter, which consists of the rate of change of angle of attack at the instant of stall multiplied by the chord length and divided by the free stream velocity, was suggested by Kramer in Reference 38. Figures 63 and 64 show variations of the maximum lift coefficient and maximum moment coefficient respectively as a function of this velocity parameter. Also shown are theoretical predictions based on the methods of Reference 38. The theoretical values suggest that peak lift and moment coefficients achieved during dynamic stall may approach absolute maximum values of the order 3.0 and -0.8, respectively, at high values of the velocity parameter. Both the experimental and theoretical data indicate that the maximum vortex-induced loading due to dynamic stall is relatively insensitive to pitch axis location; that is, quarter-chord heaving velocity for a given value of velocity parameter. This result is of particular importance in the helicopter application, since the instantaneous angle of attack of a helicopter blade element is determined by the instantaneous blade element pitch angle, heaving velocity, and induced downwash. The significant effect of relatively small values of heaving and/or downwash velocity on the dynamic stall angle of attack, as shown in Figure 62, therefore is of little consequence in determining the loading. The time gradient of angle of attack rather than the magnitude of the angle of attack is the primary factor, at least for the small values of quarter-chord heaving velocity corresponding to the range of pitching axis locations considered here.

The experimental results obtained by Ham and Garelick indicate that, at moderate to high pitching rates, the aerodynamic loading on a two-dimensional wing during large amplitude pitching motion is dominated by the influence of intense vorticity shed from the vicinity of the wing leading edge following the occurrence of dynamic stall at an angle of attack substantially greater than the static stall angle. In the case of oscillatory pitching motion this vortex induced aerodynamic loading generates adversely phased pitching moments that sustain the motion at certain values of reduced frequency and mean pitch angle, and the phenomena known as "stall flutter" results. Theoretical and experimental results appear to agree that the pitching axis location has little influence on the peak loading. This conclusion suggests a similar insensitivity exists with respect to quarter chord heaving velocity, at least for the low values corresponding to the range of pitch axis locations which have been considered in present studies. It should be noted that heaving velocity insensitivity corresponds to dynamic stall angle of attack insensitivity since airfoil heaving velocity influences the dynamic stall angle of attack substantially at moderate values of pitching velocity. These results tend to establish rate of change of angle of attack as the dominant factor in determining vortex induced peak lift and moment on an airfoil experiencing dynamic stall. An important conclusion resulting from the loss of leading edge suction during the shedding of leading edge vorticity is that, during the shedding period, the vortex induced pressure drag on the airfoil will be the streamwise component of the resultant force normal to the airfoil. At large angles of attack and normal forces characteristic of airfoil dynamic stall, it is evident that vortex induced drag will have large peak values.

While considerable space has been devoted to this subject, it should be emphasized again that the magnitude of this area is so great that this presentation is only cursory



in nature. It is believed that the foundations laid by the work reported in References 30 through 38 will serve as a base upon which to build a highly sophisticated knowledge of these phenomena, and that the knowledge thus gained will have a profound influence on increasing the performance and capability of rotor craft.

#### 4.9 Variable-Geometry Blades

The possibility of using variable-geometry blades to offset some of the penalties of high speed cruise has been proposed in several concepts. Two examples are: (1) the use of a two-segmented blade spanwise with the capability of varying the inboard segment pitch angle to accommodate the varying requirements of inflow at the hovering and high speed flight regimes, and (2) the possibility of varying rotor diameter and thus to realize the benefits of higher disc loading and smaller rotor diameter for the high speed case. The feasibility of these has not been demonstrated. It is likely that continued interest will be displayed in these approaches, but it is not likely that such concepts will find their way into production aircraft unless they become extremely simple and reliable mechanically and do not impose sizable weight penalties. Nevertheless, this area will continue to be researched and should be a point of interest.

#### 4.10 Circulation Control Blades

The success obtained for fixed wing aircraft utilizing blowing systems for circulation control has led to its consideration by many researchers for application to the helicopter rotor to alleviate many of the separation problems which have been discussed, and to increase the capability of the rotor to generate lift in its various operating regimes, particularly for the case of the retreating blade stall. The conventional airfoils normally used in helicopters obtain control of circulation by the normal Kutta criteria. For these conditions, circulation is modified by varying the incidence of the blade and the performance of the rotor is limited by the normal aerodynamic parameters of stalling incidence, maximum lift coefficient, critical Mach number and profile drag coefficient which have been discussed in the preceding sections. The advantages which can be realized from the employment of circulation control can be roughly categorized into six areas.

- (1) The increased maximum lift coefficient available on the blade section may be utilized to increase the advance ratio at which the retreating blade will stall.
- (2) Lift can be produced on the retreating blade in the reversed flow region which will also tend to delay retreating blade stall.
- (3) By utilizing a cyclic and collective mode of control of the blowing system, the helicopter rotor swash plate can be eliminated, and the problems of control forces be avoided.
- (4) In a more sophisticated application, the effects of variable blade twist can be acquired to even out the spanwise loading of the rotor, and thereby reduce the induced power.
- (5) The possibility exists for a sizable reduction in vibration and noise levels by maintaining a more constant load distribution on the rotor in its various flight regimes. A form of multi-cyclic control devices, coupled with advance technology sensors on the blades to determine local effective angle of attack, could be used in an adaptive manner to realize near uniform loading at all flight conditions.
- (6) The possibility of lift control without physical change of the geometric angle of attack of the blade provides for considerable simplification in mechanical systems, and the possibility of sizable reduction in vibratory input reduces the problems of instability as well as costs which accrue from maintenance and fatigue considerations.

Basically, two systems of circulation control are currently under consideration. The fundamentals of the first system are described by Cheeseman in Reference 39. This system utilizes blowing slots on the surface of the airfoil to effect the circulation control. Proponents of this system have, to date, utilized circular and elliptical blade sections in their considerations. The basic aspects of this method can be described as the control of the front and rear stagnation points on the airfoil by energizing the boundary layer. The second method employs blowing from the trailing edge of the airfoil over a flap surface which is deflected to achieve circulation control, much in the same manner as is employed on the fixed wing. The true jet flap uses the jet sheet to replace the mechanical flap of the blowing flap system. However, a practical mechanical flap system has been developed by Dorand, and its basic concepts were presented in Reference 40. This system utilizes a mechanical jet flap on the outboard 30% of the rotor. Both of these systems are being actively pursued today in England, France and the United States.

An adequate treatment of this subject would require a separate treatise. An attempt to delve into its details without an adequate treatment does detriment to its consideration and therefore only a cursory presentation will be made. A judicious assessment of the concept demands that its negative aspects be examined as well as its beneficial aspects. Perhaps the most condemning factor for the use of such systems is the relatively low efficiencies which can be realized from the pneumatic system. Efficiencies of the order of only 43% are realizable from such systems because of the losses associated with energy conversion in the compressor, and losses in the ducting as well as in the nozzles. Consequently, a sizable increase in fuel consumption will result, which cannot be offset by the weight saving which may be realized from simplified mechanical systems. It therefore rests upon proponents of these systems to demonstrate that the advantages which can be realized from the employment of such techniques in terms of reduced profile losses as a result of lower rotor solidity required, and increased capability for mission performance, justify their pursuit.

Current research in these areas involves attempts to maximize the advantages which are outlined above. For the concept of circulation control blades, efforts are being made to attain reasonable data on various airfoil sections to determine where the maximum benefits can be obtained in terms of minimum profile loss with minimum pneumatic system losses. In both England and the United States, data are being collected on sections ranging from circular to modified elliptical sections of rather low thickness ratio. Proposals have been made for blowing from both the leading and trailing edges and for cyclic control of such blowing to maximize the possibility of reducing the retreating blade stall effects and obtaining maximum airfoil section efficiencies.

The jet flap concept is being pursued actively in the United States and France by the Giravions-Dorand Corporation, NASA, the US Army, and the Ling-Temco-Vought Corporation. Currently, modifications of a 10 meter diameter rotor are being made to permit flap deflections from  $-30$  to  $+90^\circ$  to augment tests which were made for flap deflections from  $0$  to  $40^\circ$  previously in the NASA-Ames  $40 \times 80$  ft wind tunnel. The increase in flap deflection is being made to permit the generation of propulsion at higher forward speeds than were obtained previously. A theoretical study of the jet flap rotor was made by Evans and McCloud and reported in Reference 41. Comparisons of data obtained in previous tests of the 10 meter rotor with the results of this theoretical investigation indicate good agreement and further indicate potentials for lifting and forward speed capabilities of the jet flap well beyond those of rotors with conventional blade sections. This analytical investigation does not include the overall power required for a complete vehicle and hence is not conclusive regarding the applications potential. An applications study currently is underway by the Ling-Temco-Vought Corporation sponsored by the NASA and the US Army to determine potential uses for the jet flap rotor system.

The results of various studies as of the writing of this document can be summarized as somewhat confusing. Perhaps the most prominent factor in this confusion is a disparity of opinion over the losses which will be encountered in the pneumatic system. A considerable amount of effort must yet be expended in both analysis and experiment of these

systems before their true potential can be ascertained. From the aerodynamic standpoint, there are clear and definite advantages to the utilization of such a system. However, from the propulsion standpoint there are clear and definite performance losses to be considered, and a clear assessment of these losses is not available. It is interesting to note that the studies of both concepts have led to a rather obvious application in the form of a stopped rotor which can be utilized for VTOL capability in a rather conventional air frame, and then can be properly oriented or stowed for the high speed flight condition. The advantages of rotor stability, small profile, and small diameter uniquely qualify these concepts for application in such a stopped rotor system.

Although considerable controversy exists over the potential of these concepts, it is probable that research and development efforts will continue until a clear-cut picture is at hand for assessing their potential.

## 5. DRAG REDUCTION

### 5.1 Rotor Drag

It surely has been obvious to the reader in the previous sections that large portions of the discussion have a direct bearing on the levels of rotor drag. It will be our approach in this section to eliminate considerations of the hub and consider only the drag characteristics of the blades. Hub drag will be treated in Section 5.2.

Rotor drag is divided between two major sources; these are profile drag and induced drag. They are interdependent one upon the other and neither can be influenced without also influencing the other. A crude comparison of their importance may be obtained by realizing that even in the most advanced rotor systems in current production profile drag is roughly 30% of the overall rotor drag, even when operating at design conditions.

A somewhat new concept of profile drag has been obtained as a result of the work reported in Reference 20. Profile drag has generally been described as skin friction drag plus pressure drag. Skin friction drag has normally been estimated from two-dimensional airfoil characteristics. However, in Reference 20, the authors show that there is an influence of the radial flow on the level of skin friction drag. This is indicated in Figure 65, extracted from Reference 20, where the increment of skin friction drag due to radial flow is shown as the percentage of power required to overcome this additional drag referenced to that required by consideration only of the two-dimensional case. It is interesting to note that even in the hover case, roughly a 2% increase in power over the two-dimensional case is required. This is the first time that this requirement has been quantitized. It is seen that as the advance ratio increases this effect becomes of considerable importance. It is possible that through research in airfoil profiles and blade geometries this effect can be reduced. However, a sophisticated knowledge of the boundary layer and exterior flow mechanics will be required.

Those factors which affect pressure drag in the profile drag term have been discussed in some detail in the previous sections. Whenever flow separation occurs this term is very quickly increased. It is obvious that this term will always have some value since the ideal Kutta condition is never realized. Ideally, it is possible to eliminate pressure drag and have only the skin friction term in the profile drag.

The primary factors which affect profile drag are then seen to be the profile drag coefficient and the blade area. As was noted earlier, minimum profile drag is realized for infinite diameter rotors turning at very slow speeds, producing infinitesimal acceleration of large masses of air through the disc. It is therefore seen that it is desirable to minimize blade areas and use very low rotational speeds in order to minimize profile drag.

The dependence between induced and profile drag immediately comes into focus from these assumptions, since the factors mentioned dictate that the airfoil sections must then operate at their maximum possible mean lift coefficient to produce the required thrust. This means that airfoil sections are required which will produce maximum L/D at maximum lift coefficient. Since this is not practically achievable, it is then obvious that a trade off must be exercised between the profile and induced drag terms to realize the minimum drag. In essence, this is achieved at the point where the product of the total drag coefficient and the blade area is a minimum.

In consideration of the induced drag term, the ideal case is realized from momentum theory which assumes constant loading across the disc and uniform inflow velocities. For the hover case, the real world says that non-ideal conditions exist as a result of the vortex distribution across the disc. It has been discussed in the section on hover how the proximity of the vortices in the wake affects the uniformity of the flow field as a function of a finite number of blades. It is obvious that improvements in the level of induced drag will only be realized when the geometric positioning of all these vortices is identified, and proper account can be taken for them in the rotor design.

As soon as the rotor moves out of the true hover condition, either by side winds or translational motion, the load distribution on the disc becomes non-uniform and separation begins to occur because of the already highly loaded condition. As forward flight speed increases, this situation is somewhat alleviated because of the reduction in required rotor thrust, but again becomes severe at the high speed cruise condition. It has been assumed that a uniform loading with uniform induced velocity is still the ideal case for these forward flight conditions. The proof of this assumption has not yet been attained. However, the real world again tells us that we have problems with the rotor wake; this time with unsteady vortex motions which affect the load distribution and degrade performance from the ideal case. The ability to reduce induced drag in these areas also awaits the development of the wake theories which are now being pursued to exactly locate the vortex flows, so that their effect on the blades may be calculated.

It is obvious from this consideration that significant reductions in profile and induced drag to produce reductions in overall rotor drag are wholly dependent upon an understanding of the complex flow fields in and about the rotor. The fundamental aspects of pursuing this understanding are again emphasized.

## 5.2 Hub Drag

The subject of hub drag has long plagued the helicopter designer. The many rotor blade controls and aerodynamically unfavorable shapes that must be employed in order to sustain the high centrifugal loads at the blade roots result in an aerodynamic dirtiness, which results in rather high penalties. The problem is compounded by the number of blades in the rotor. For current day helicopters, the rotor hub is responsible for from 20 to 50% of the total parasite drag. It is obvious that reductions in this value will be significant in reducing the power required for any given flight speed, and thereby increasing the overall economy of the vehicle.

Significant improvements have been realized as a result of recent technologies. In particular, the so-called "rigid rotors" have produced hub designs of considerably less bulk which, although they are still not aerodynamically clean, offer less resistance to the air flow. Attempts to fair the hub to reduce the drag have not been singularly successful because of the flapping, lagging and pitching hinges, and the resulting blade motions. However, it is believed that significant advances can be made in the design of low profile hubs, and that this problem will eventually yield to substantial improvement. One concept is a completely enclosed hub which shows considerable promise. However, the intersections of the blades with the enclosing surface creates the usual juncture problems, even with the semi-rigid rotors currently being considered.

### 5.3 Airframe Drag

Very little needs to be said concerning the reduction of airframe drag, since a considerable wealth of data and design techniques are available from fixed wing technology. It is amazing that it has only been in recent times that helicopter designers have begun to design aerodynamic cleanliness into the airframes. Despite the fact that helicopter speeds were relatively low, optimum designs would have been expected to reflect better aerodynamic cleanliness. As the forward speed potential of the helicopter has increased, improvements in airframe design have been made mandatory. The ability to improve the fuselage lines has been enhanced by the introduction of the turbine engine. Reciprocating engines of radial design, with their high cooling requirements, often times dictated quite bulky airframe designs.

Many missions have dictated low speed requirements for which it is not reasonable to attempt a complete aerodynamic cleanup of the fuselage and supporting components. For example, it has been rather difficult to justify, in many cases, a retractable landing gear despite the rather severe drag penalty associated with it. When one considers a trade-off for the additional weight and maintenance requirements, the retractable gear is found to be not cost effective. It is probable that continued efforts will be made to improve the aerodynamic cleanliness of the airframe, particularly as the trend towards compounded and stopped rotor concepts increases.

The term for airframe drag is usually expressed as a non-dimensional cleanliness coefficient, defined as the equivalent drag area divided by the gross weight to the two-thirds power. A rough comparison of the significance of this factor in terms of gross weight for several types of vehicles is shown in Figure 66. Also shown on this figure are additional lines and a second scale, which illustrate the percentage of gross weight needed for fuel to overcome parasite drag for a 200 mile range mission of a high speed transport helicopter. It is seen that a beneficial size effect is evident. A comparison with the high speed fixed wing curve shown indicates the potential improvement possible.

### 5.4 Relative Importance of Drag Increments

When considering the relative importance of the drag increments, one must also consider the speed conditions or advance ratio at which the rotor is operating. Rotor profile power is a near constant value, but has a gradually increasing slope with increasing advance ratio. For a typical condition in hover, it represents 25-30% of the total power required. At the speed for minimum power, it may represent as much as 50 to 60% of the total power required, and at the maximum cruise point 30-35%. The induced drag on the rotor represents 70-75% of the total power required in the hover case. This factor rapidly reduces with increasing forward speed or advance ratio, until at the minimum power point it represents only approximately 20% of the total power and as little as 10 to 15% in the high speed cruise condition. However, as the induced power rapidly decreases with forward speed, the parasite power associated with the airframe and hub drag rapidly increases with increasing speed and advance ratio. Parasite power is nearly negligible for the hover case, increasing to 20 to 25% at the minimum power point, and is as much as 60 to 70% in the high speed cruise mode.

### 5.5 Possibility for Drag Reduction

The subject of drag reduction is akin to being against sin and for motherhood. It is something for which the aerodynamicist must always strive. However, some areas will be more fruitful in response to the research effort than others. It is likely sizable improvements can be made in the reduction of parasite drag by the development of hubs of lower profile and increased aerodynamic cleanliness, and considerable improvement can yet be made in airframe drag. However, when it comes to the consideration of the rotor drag, further improvements in this area will come only as a result of great sophistication in the knowledge of the rotor flow mechanics. As has been noted in earlier sections, the alleviation of stalling and separation on the blade surfaces will contribute towards

reduction of the rotor profile power. However, it cannot be expected that these reductions will be very large. Since it is indicated that in the area of minimum power, where most flight operations would be desired, the profile power is a very large portion of the total power required, it can be seen that reductions in induced and parasite drag will contribute in a much lower ratio to reductions in power than will reductions in profile drag. For example, reductions in parasite drag will contribute to reductions in total power at the ratio of about 4 to 1, or a 20% reduction in parasite power will produce only a 5% reduction in total power required. It is obvious that the most fruitful area for drag reduction is in the profile rotor drag, but this is also one of the most difficult areas in which to make advances.

## 6. COMPOUND AND STOPPED ROTOR HELICOPTERS

### 6.1 Promise of Compounding

The development of an aircraft with high subsonic cruising speed, which also has a capability for vertical flight, can be approached from either of two technologies which currently exist. Either, (a) the cruising efficiency of a conventional aircraft can be compromised by adding power for special flight devices and, in turn, the power to operate these devices or, (b) the vertical flight efficiency of a helicopter can be compromised by adding special devices to enable cruising flight beyond the helicopter limiting cruising speed. Utilization of the first approach results in a duration of vertical flight capability which is generally quite limited because of the poor efficiencies of this flight mode. The capabilities of these various concepts will be discussed by other lecturers during this series. The second approach maintains the vertical flight efficiency of the helicopter, and also provides the potential for cruising efficiencies comparable to those of the conventional airplane. It has been demonstrated in Section 4 that increasing horizontal speed on the lifting rotor causes the rotor to lose its capability both for generating lift and horizontal thrust. These limitations necessarily lead to the concept of compound, or as they have now been termed, composite aircraft. The term compound has been reserved for helicopters to which a fixed lifting surface and/or auxiliary power has been added. Composite aircraft includes compounds plus other vehicles employing rotary wings; e.g., tilt-rotor craft.

The ability to analyze the performance potential of various composite aircraft types is severely limited because of the lack of experience with these types, and the lack of statistical data on the weights of various components utilized. The most difficult assessment during the preliminary design of composite aircraft as a result of the lack of experience, concerns the dynamic characteristics and the consequent effects of the dynamics on the weights and performance limitations. We are beginning with a concept represented in the helicopter which is already plagued by dynamic problems. Some of the difficulties encountered are resonant vibrations, fatigue from dynamic loads, mechanical dynamic instability, aeroelastic dynamic instability, and less than desirable control dynamics. In the composite aircraft the lifting rotor, already subjected to these problems, is subjected to even more extreme conditions which tend to compound the problems.

Of all the composite aircraft considered, the most simple is no doubt the winged helicopter. No particularly new dynamic problems are encountered in the winged helicopter even though the usual dynamic problems become more severe because of increased lifting-rotor advance ratio, increased forward tilt of the rotor, reduced control power provided by the lifting rotor, and lifting rotor-fixed wing aerodynamic interference. However, if flight speeds beyond those attainable with the winged helicopter are desired, and they surely are, the lifting rotor must be relieved of its combined function as both lift and forward thrust generator. All speculations that a lifting rotor might be able to maintain satisfactory performance at high flight speeds if it is not required to provide thrust must be discarded when one remembers the problems discussed for the high-cruise speed condition in Section 4. The large lift non-uniformity with azimuth angle at the high advance ratio case, when considered from a dynamic loads point of view, makes it unfeasible



to design a lifting rotor which has both reasonable vertical flight efficiency and the capability of sustaining the entire aircraft weight at high advance ratios. Counter-rotating rotors with very rigid cantilever blades may alleviate these problems to some extent, but the transfer of the large rolling moment from one rotor to the other creates very severe dynamic load problems. Consequently, from the dynamic loads point of view it becomes obvious that the rotor must be unloaded if high speed flight range is to be extended. This poses the question of what to do with the lifting rotor in the high speed flight mode.

Dr Kurt Hobenemser of Washington University in his presentation before the 23rd Annual National Forum of the American Helicopter Society stressed the point that there seems to be four and only four alternatives for the rotor in high speed flight. These are:

- (1) The rotor can be idled at a reduced speed in an unloaded condition.
- (2) The rotor can be stopped and folded to a dynamically safe condition or stowed.
- (3) The rotor can be stopped and utilized as a fixed wing lifting surface.
- (4) The rotor axis can be tilted forward or aft  $90^\circ$  and used as a forward-thrust-generating propeller.

The fourth concept will be discussed in another session of this lecture series; we shall confine our comments to the first three. The consideration of these three indicates that all must have additional means of propulsion and a realistic assessment indicates that all, including fixed wing rotors, must have at least some additional fixed wing surface. All but the folded rotor must have high speed blade flutter suppression, and all but the idling rotor must encounter a rotor conversion. (It should be noted that these four types are in addition to the winged helicopter.)

A rather unusual observation can be made at once concerning the winged helicopter in that no aircraft based on this principle has emerged, nor is one being proposed by any designer at present. It is generally accepted that the addition of a wing alone might in some cases permit a higher speed to be achieved than with the pure helicopter, and it might permit higher gross weight and hence greater payload at the same speed. It is probable that this sort of compounding has not been done because the pure helicopter has done such a commendable job. Difficulties of matching wing and rotor lift, with the associated complications of flying controls, has not been considered worth the gain which can be realized. Therefore, we shall dismiss it from our discussion and concentrate on the fully compounded or composite aircraft.

The idling rotor type of aircraft was flight tested both by Westland as the Rotodyne, and by McDonnell as the US Army XV-1 research aircraft. These tests were made in the 1950's. For these aircraft, the rotor was autorotated during the high speed mode and propulsion and primary lift were supplied by the fixed wings. One of the main features of the XV-1 was an automatic idling speed control, which utilized changes in angle of attack of the autorotating rotor for control. The dynamic loads and vibrations at the high advance ratio with low rotor thrust were acceptable and transition from full rotor speed to idling rotor speed, or vice versa, was performed in level autorotational flight within one minute without excessive resonance. The limiting factor on the maximum speed of this type of aircraft is the dynamics created by the retreating blade flutter. This phenomenon has been discussed in Section 4 and is associated with the reversed flow region which occurs on the retreating blade side. Effectively the blade center of gravity is changed from the 25% chord for the forward blade flow condition to the 75% chord for the reverse flow condition. The prevention of blade flutter under these conditions is very difficult. Subharmonic, unstable blade flapping was also encountered at high rotor advance ratio.

This class of vehicle has been the subject of an exploratory development program by the US Army in recent years. Vehicles investigated in this program were the prototype of the UH-1 series to which was added a 64 square foot wing and 1840 pounds of additional thrust,

the UH-2 helicopter to which was added 186 square feet of wing area and 2500 pounds of additional thrust, the XH-51A helicopter with a wing area of 70 square feet and auxiliary thrust of 2500 pounds, the Piaseki Model 16-H aircraft which utilized a shrouded propeller for thrust and anti-torque and has a wing area of 86 square feet and the SH-3A helicopter with added wing area of 170 square feet and auxiliary thrust of 5800 pounds. A description of this program can be found in Reference 42. These compounds have shown an increased capability above that of the pure helicopter, as represented in Figure 3. The gains are seen to be on the order of 10 to 15% in maximum attainable speed. The limitations of these devices will be discussed in the next section. Detailed discussions of the promise of compounding are found in References 29, 42, 43 and 44. In these references, a considerable disparity of opinion exists, but the overall conclusion which can be drawn is that magnitude increases in speed capability are not considered to be possible and only increases of the order shown in Figure 3 can reasonably be expected. Further conclusions concerning the application of these devices in the lower speed ranges will be drawn in the next section.

## 6.2 Limitations of Compounding

We have examined in Section 4 the limitations to rotor stability and dynamics for the case of the pure helicopter. It is readily comprehended that unloading and/or slowing the rotor rotational speed does not cure these problems, but may delay their severity to higher advance ratios and forward speeds. It will be recalled that as forward speed is increased and, more specifically, as the helicopter tip speed ratio increases there is a continuous decrease in the maximum thrust capability of the helicopter rotor. This first arises because of the requirement to balance the asymmetric loading on the rotor, and is then further compromised as the advancing rotor blade tip Mach number approaches unity. When the Mach number becomes critical, it is necessary to slow the rotor rotational speed to avoid the excessive power losses resulting from increases in airfoil profile drag for those sections in the high transonic or supersonic flow regimes. Figure 67 indicates the variation of normal acceleration capability of the rotor as a function of tip speed ratio. This rotor, which was designed to hover at 6000 ft on a 95°F day, shows a normal acceleration capability decreasing from a maximum of 2.67 at sea level on a standard day, to unity at a tip speed ratio of 0.73 and an advancing tip Mach number of 0.95. This tip Mach number is considered to be a probable practical limit at present. At smaller advancing tip Mach numbers, this maximum acceleration capability is correspondingly less. From this assessment, it is obvious that to maintain maneuver capability auxiliary lift must be provided at a tip speed ratio of 0.73, and that at the tip speed ratios exceeding unity a wing would be required capable of supporting at least 50% of the aircraft gross weight and much more perhaps, depending upon factors to be discussed.

Considering this limitation on the lift or gross weight capability of conventional rotors, it is now necessary to return to Section 4 for further consideration of the vibration and cyclic stress in the rotor blades as they are affected by lift or gross weight ratio and tip speed ratio. It must be borne in mind that a practical compromise must be obtained between the potential aerodynamic efficiencies and the limitations of crew, passenger, cargo and structure to withstand vibratory loads. One consideration which must be examined is the effect of the rotor vibrations on the power required in the high speed mode. Power associated with the lift and drag must always be greater than that expended for the mean lift and mean drag forces, since the average power is the power associated with each of the oscillatory loadings. Thus a rotor producing constant lift will progressively require a greater portion of the power for lift to be expended on the oscillatory loading. This is also true of power expended to balance the drag of the rotor and fuselage, since this is associated in a growing proportion with a periodic variation of the rotor blade drag forces. Observation based on experience indicates that vibration and cyclic stress trends tend in forward flight to follow the power required curve, and this has been supported by energy conservation principles.

If we return again to Figures 31 and 32 and examine the areas where unloading is required for the rotor represented there, it is obvious that these vertical outputs can be restricted by the unloading of the rotor. There is, however, a practical limit to tip



speed ratio even for the unloaded case; the considerations of rotor instability will begin to limit reductions in RPM because of the increasing reverse flow area on the re-treating side. These effects were covered in Section 4 and were demonstrated in Figures 37 through 40. Generally, since the rotor power reduces quickly with moderate reductions in RPM, the gains to be obtained from lowering RPM more than about 25% are slight. It is questionable whether greater reductions are advisable in view of the resulting difficult dynamic problems. In Figures 40 to 42 the relative gust sensitivity was shown not only for the lifting rotor, but for the unloaded rotor. These problems, as they are associated with the flap-torsion flutter boundary, are seen to be only slightly delayed by unloading the rotor. As was noted in Section 4, increases in the fundamental torsion frequency ratio are required to increase the forward speed-advance ratio limits shown in Figure 44, and this is a formidable task.

A composite presentation of the various limitations to rotor operation at tip speed consistent with compound helicopter operations is shown in Figure 68. Reduction in the rotor tip speed to avoid the tip Mach number limitation causes the rotor to encounter various blade resonances at different combinations of forward speed and tip speed ratio. Thus, excluded regions of operation are imposed by normal cyclic stress and vibration limits. It is seen that Mach number limits, flutter limits, and blade resonance limits limit the practical combinations of rotor tip speed ratio and forward speed very severely. It would appear from these considerations that a practical maximum forward speed limit for a compound helicopter with an unloaded rotor would be about 250 knots.

It would appear that the optimum, compatible design conditions for a maximum speed compound helicopter objective are a tip speed ratio of about 0.73 and an advancing tip Mach number of about 0.92. Four or six blades would be utilized to avoid the third and fifth blade harmonic resonances.

### 6.3 Comparison of Compounds with Other VTOL Aircraft

It appears rather doubtful that the conventional unloaded-rotor compound helicopter would be competitive with the pure helicopter. At a speed of 200 knots the compound helicopter projected above would have relatively good flying qualities and modest vibration levels, but it would be much more complex than a pure helicopter and its lift-drag ratio would still be poor by fixed wing standards. Its payload to weight empty ratio would be lower than the projected 200 knot pure helicopter. At the maximum speed of 250 knots, the lift to drag ratio of the unloaded rotor compound is very poor because of the aeroelastic necessity of maintaining full rotor speed while producing virtually no lift.

It is interesting to compare the compound and the helicopter with other types of VTOL vehicles for the high speed mission on the basis of the drag to weight ratio which was presented as Equation (13) in Section 3.1. Figure 69 shows a comparison of equivalent flat plate area loading as a function of gross weight for helicopters and turbo prop transports. Also shown is the rotary wing goal set by two Sikorsky engineers in 1963. The equivalent flat plate area presented here is determined by the total aircraft drag, with the exceptions noted in the figure title, divided by the drag of one square foot of flat plate area. It will be noted that ratios of from 5:1 to 8:1 exist between the turbo-prop transport aircraft and current production helicopters. Even if the rotary wing goal were reached, factors of 2 or 3 to 1 still exist. The curve which indicates projected and specially cleaned up helicopters represents essentially what can be done by reduction in parasite drag; the improvement is small.

A comparison of the equivalent lift-drag ratios for rotary and tilt wing aircraft is shown in Figure 70. This comparison indicates that factors of as much as 2 to 1 exist between the best helicopter capability and the tilt wing aircraft in terms of equivalent lift-drag ratio. Since it was indicated that little can be accomplished for increases in equivalent lift-drag ratio by parasite drag reduction, it is well to consider what is the source of the difference in equivalent lift-drag ratio. This is most easily accomplished by examining the equivalent lift-drag ratio of the lifting system alone. A comparison is

shown in Figure 71 for the rotors of pure helicopters, the rotor and wings of compound helicopters and the wing alone for the tilt wing system. It is seen that ratios of from 2½ to 3:1 and more at the higher speeds above 240 knots exist. This is directly attributable to the rotor profile drag and the necessity to keep the rotor operating at its higher RPM for dynamic reasons. This assessment of the compound helicopter, although it is pessimistic, is believed to be essentially correct and places definite limitations upon its use. For those areas where it is deemed to be applicable from a mission standpoint, it is likely that its cost effectiveness will be lower than for other types of vehicles. Nevertheless, this vehicle has found its way into the inventory of the US Army in the form of the AH-56 Cheyenne which is currently in production. The projected use of this aircraft is as a gun ship escort for other rotor craft, and therefore it is required that it maintain the hover and low speed efficiencies of the helicopter with the addition of the requirements of agility at cruise speeds. It is perhaps in this area of agility that the compound helicopter makes its greatest contribution. Agility implies the ability to quickly perform various maneuvers throughout the range of operational speeds. Included is the ability to execute tight turns up to 360°, either at a sustained speed or with deceleration, with the smallest radius and in the shortest time. The ability to accelerate and decelerate about all axes and climb or descend at the steepest possible angles also represent aspects of agility. Further, it is important that transition maneuvers be performed in a continuous manner with minimum restrictions resulting from aircraft attitudes, air turbulence and so forth. For combat aircraft such as the AH-56, this requirement of agility is obviously important. It is less important for transport vehicles and other lower performance types. Transition maneuvers should be able to be interrupted at will, but also should be accomplished in a minimum time.

Agility at or near the hovering condition depends chiefly upon the ability to develop thrust in excess of gross weight, which is normally rated as the number of g's. For all aircraft with rotors and without power restriction, the vertical g capability can be represented by Equation (14).

$$ng_v = \left( \frac{\rho_m}{\rho_h} \right) \left( \frac{\bar{c}_{lm}}{\bar{c}_{lh}} \right) \left( \frac{v_{tm}}{v_{th}} \right)^2 \quad (14)$$

where the term on the left of the equation represents the number of vertical g's, the first term on the right represents the ratio of densities at the maneuver and at the hover conditions, the second term represents the ratio of average lift coefficient at the two conditions and the third term represents the square of the tip speed ratio for the two conditions. This equation indicates that both the rotor and propeller type aircraft can achieve the same level of vertical acceleration. However, the vertical rate of climb for the aircraft with a higher disc loading will tend to be greater when operating at lower altitudes and temperatures than those of the design hovering conditions. This is brought about by the fact that the relative excess power at altitudes and temperatures lower than the design conditions is proportional to the shaft horsepower to weight ratio required for the design hovering.

For the case of forward flight, radius of turn depends on the level of normal accelerations that can be developed. For the compound helicopter it becomes

$$ng_f = \left( \frac{T_R}{W} \right)_m + gC_{Lm}W_w \quad (15)$$

where the first term on the right of the equation is the ratio of thrust developed by the rotor in maneuver to the aircraft gross weight and the second term is the product of the gravity term, the wing lift coefficient in maneuver, and the nominal loading which is derived considering only the wing area. At low speeds and low advance ratios, the rotor thrust is the main source of normal acceleration, while at medium speeds and moderate tip speed ratios the rotor thrust may also represent a large fraction of the total values of normal acceleration. However, at higher speeds and higher advance ratios as the rotor is

unloaded, the fixed wing is the primary source of normal acceleration capability. Figure 72 shows the  $g$  capability, assuming no power limit, as a function of speed for plain wings and wings equipped with flaps. A variable scale at the left of the graph permits evaluation of the importance of wing loading. It is pointed out in Reference 29 that the nominal wing loading may be somewhat dependent on disc loading because of autorotational requirements. Thus, wing loadings from 55 to 110 lb/ft<sup>2</sup> may be expected in the compound aircraft. The contribution of the rotor to the normal acceleration ability could be enhanced by over-blading, but this will obviously be detrimental to the equivalent lift-drag ratio of the lifting system.

An example of normal  $g$  capability in steady turn with power limitations for a compound helicopter and for a comparable tilt wing with half the wing loading of the compound is shown in Figure 72. In Figure 73, general relationships between the radius of turn and speed of flight for various normal acceleration levels as well as time required for a 360° turn are shown. Comparative curves for the compound and the tilt wing are shown on this plot. A clear limitation of the compound in the 200 knot range is indicated. It is seen that the compound can be superior to the pure helicopter as an escort vehicle in the frame of reference speeds for a helicopter, but fixed wing aircraft are clearly superior at all speeds.

#### 6.4 Case for Stopping and Stowing Rotors

The case for stopping and stowing the rotors now becomes very clear. The two stopped rotor configurations to be considered were noted earlier as rotors which are stopped and utilized as lifting surfaces and rotors which are stopped and folded in a trailed position, or are stowed. The advantages of these concepts is immediately evident, since all of the benefits of reduction in rotor profile power and increased agility can be realized. Thus the stopped, folded, and/or stowed rotor concept represents to the designer proponent a direct means of removing the forward flight limitations of the slowed rotor compound helicopter. To him it represents the best part of two worlds; but it does not come without some of the sin associated with both. Some studies have indicated that the stopped rotor configuration could exhibit empty to gross weight fractions 10% higher than conventional helicopters with attendant compromises in range-payload characteristics that affix gross weight. It yet remains to be demonstrated that these possibilities claimed can be attained. Since this type of design is completely beyond any current experience, the ability to evaluate the weight components of such vehicles is much in question as was mentioned earlier.

It is well known from wind tunnel tests which were conducted in the 1950's, that stopping and starting of properly designed lifting rotors is feasible at considerable relative wind velocities. It does remain to be demonstrated however, what the effects of such a procedure will be on the aircraft dynamics when executed in flight, and in particular, in a turbulent atmosphere. It may be possible that certain atmospheric turbulence conditions exist beyond which rotor conversion may be too risky. It may be necessary, therefore, to impose the requirements of idling at high speed on the ability to stop and fold.

Currently, primary interest in this area is devoted to the Lockheed XH-51 rotor, modified to accommodate the stopping and stowing sequence. Wind tunnel tests of this rotor have been performed which have demonstrated the general feasibility of the stopping and folding sequence. However, to date tests have not been performed in what could be considered a routine manner across the speed spectrum corresponding to the transition range because of problems in sensing and providing adequate control requirements to the rotor. This work is being continued under sponsorship of the US Army, and it is believed that a successful conclusion will be obtained. Additional tests are planned which will demonstrate not only the control capabilities, but also the sensitivity to gusts and the coupling of rotor dynamic loads with airframe modes. This concept was a leading contender in a recent competition by the United States Army for a composite aircraft. A discussion of the problems associated with this concept will be made in the next section.

The fixed wing rotor accentuates the problem of reversed flow flutter since, when it is stopped for high speed flight, the blade which is in the retreating half of the disc will be experiencing reversed flow at the full flight velocity rather than at the reduced velocity experienced when the rotor is rotating. Proponents of this concept declare that the rotor stopping process can be accomplished without the necessity for fixed wings to provide auxiliary lift during the rotor conversion process. If no auxiliary lifting surface is supplied, the starting and stopping process becomes analogous to changing the wing sweep on a variable sweep aircraft except that one wing is sweeping forward while the other is sweeping aft. In this concept, the rotor usually has a large inner portion which carries the majority of the lift in the stopped mode. If this large hub area is to be considered in lieu of an auxiliary fixed surface, the problem then becomes to transfer during the conversion most of the aircraft lift to the disc and to unload the stubby rotary wings by appropriate periodic pitch variations. Structural and control dynamics associated with this process are very complex, and, of course, compounded by an order of magnitude when gust sensitivity is considered.

This concept of the fixed-wing stopped rotor has come under consideration from many sources. It has taken many forms, the most popular of which are probably the one proposed by the Hughes Aircraft Company, and others where a high solidity inner portion of the rotor serves as the primary lifting surface when the rotor is stopped. Other concepts, such as single bladed and two bladed systems stopped with the axis perpendicular or parallel to the oncoming airstream, have been proposed. The problems associated with these systems will be discussed in the next section.

#### 6.5 Problems of Stowing Rotors

Since the tests of the Lockheed rotor have been the primary effort in this field for stopped, folded, and stowed rotors, it will be used as an example for this discussion. The problems of enclosing the rotor for the stowed condition inside the aerodynamic envelope of the vehicle will not be considered since they are not aerodynamic in nature, but are solely mechanical. There is no question that stowing can be accomplished, and the effects of stowing on the aerodynamics of the vehicle are no greater than for the retraction of a landing gear. However, the volume required and the structural problems, including weight, can be severe penalties.

The Lockheed 33 ft diameter stopped rotor, which has been tested extensively in the NASA-Ames 40 x 80 ft wind tunnel, was designed for conversion speeds of 120 knots. This is a lower speed than will be required for conversion of an actual vehicle in flight, but it is considered that the data which have been obtained are applicable to the higher conversion speeds since the primary variable will be increased strength in the rotor to take the additional steady and vibratory loads associated with the higher speed.

The rotor has been tested on three separate occasions in the wind tunnel and a synopsis of the investigations, together with a fourth investigation of blade divergence on HU-1 blades, is as follows:

#### *Stopped Rotor Studies at Arc*

- Design studies - V/STOL transports
- Experimental investigations -
  - Lockheed 33 ft diameter stopped rotor tests
    1. Aero vane + rotor shaft driven gyro, rotor not powered.
    2. Aero vane + rotor shaft driven gyro, rotor powered.
    3. No vane, independent gyro drive, rotor powered.
  - Blade divergence study
    - Non-rotating tests using HU-1 blades with pressure instrumentation.

The tests for blade divergence will be discussed later. The next chart indicates the objectives of the first test. The results range from good to bad and definitely indicated a lack of definition of the state-of-the-art. A considerable amount of information was gained from this test which enabled refinements of the design to be made.

*Objectives of First Test of Lockheed Stopped Rotor*

- Determine blade divergence limits
- Study blade folding procedure
- Determine lift and drag characteristics
- Study rotor start and stop process

These tests were performed with the control system portrayed in Figure 74. This control system is a special proprietary development of the Lockheed Company and is represented here only in schematic form. This gyro control system was coupled with an aerodynamic vane which was programmed to assume authority when the rotor speed became so low that the gyro was ineffective. The gyro was turning at a 1:1 ratio with the rotor. It was the intention that the gust vane would sense the local flow conditions and adjust the blade pitch accordingly. The authority of the vane with rotor RPM is shown in Figure 75. It is seen that the gyro is completely ineffective at 40% of design RPM and the aerovane authority was the sole source of control.

A typical example of the determination of blade divergence speed is shown in Figure 76. The solid line represents measured data. An extrapolation of this line through the point of intersection with the horizontal axis represents the divergence speed, or the speed at which the flapwise bending moment approaches infinity. This method was employed throughout the test to determine the blade divergence speeds.

The objectives of the second test are as follows:

*Objectives of Second Test of Lockheed Stopped Rotor*

- Study characteristics of improved aerodynamic vane + gyro control system with powered rotor
- Demonstrate capability of rotor control system to trim out rotor loads due to 30 fps vertical gust during start-stop process

Whereas the first set of tests were made with an autorotative rotor, the rotor was now powered and an improved aerodynamic vane was installed. Further, it was sought to demonstrate the capability of the rotor control system to encounter 30 ft per second vertical gust during the start-stop process. The investigation regarding the gust was accomplished by a steady state approach whereby an equivalent angle was determined representing the 30 ft per second gust at various flight speeds. The equivalent gust angle as a function of flight speed is presented in Figure 77. This process is not a conclusive demonstration, since the dynamics under such a scheme are not representative of those which would actually be encountered during the transient condition. It will be necessary to demonstrate resistance to gusts in the transient condition for conclusive evidence of this capability. The results which were obtained during this series of tests for gust sensitivity are shown in Figure 78. It is seen that the test objectives were not realized and that the design rotor speed was not achieved, nor did the control system follow the design schedule. The tests had to be halted because of the rotor loads which were encountered, and because of malfunctions in the control system.

*Objectives of Third Test of Lockheed Stopped Rotor*

- Determine control gyro stability limits
- Demonstrate starts and stops with revised rotor control system
- Determine optimum cyclic pitch schedule to alleviate rotor loads as a function of  $V_{\infty}$ ,  $\dot{\Omega}$  and  $\alpha$
- Study effects of operating rotor near a highly loaded wing

For these tests, several design changes were made to the rotor control system and a separately driven high speed gyro system was incorporated. The aerodynamic gust vane was removed from the system and the design provided for the high speed gyro to maintain control for all rotor speeds. The high speed gyro control system concept is shown in Figure 79. It is seen that the system now incorporates spring restraint for the gyro at low rotor speeds for additional stability. Results obtained for the high speed gyro stability study were extremely limited because of a mechanical failure of the rotor drive system. Much of the tests were performed with the swash plate fixed to determine optimum cyclic pitch scheduling. The results which were obtained indicated the trends shown in Figure 80 for the gyro stability boundary.

The summary of the conclusions based on this series of tests is as follows:

*Conclusions based on Stopped Rotor Studies*

- Determination and implementation of optimum control system to alleviate gust loads is major problem
  1. Trade between control moments and vibration
  2. More experimental and theoretical work required
- High drag of hub indicates retraction of rotor into fuselage required
- Provision of bumpers or latches to prevent blade damage when folded required
- Blade divergence with rotor stopped is predictable

Based on the test results and these conclusions, analysis of the problem has been made and a consideration of those areas which may be fruitful for further research has been accomplished. The suggestions for further study, which follow, are believed to be a proper approach to continued research of the problem.

The fourth set of tests, which were made by Cornell Aero Labs for the US Army, used a set of UH-1 blades in a special hub. The rotor was stopped at all times and the primary test variable was the azimuth position of the blades. The flight speed and shaft angle were fixed and the blade pitch angle varied, and the stability boundaries for blade divergence were determined from stress records. The general conclusions from these tests are reported in Reference 46. It was found that a form of stall flutter was encountered in the azimuth range from 225 to 300 degrees. This was not a single degree of freedom torsion motion, but was modulated by the low frequency beam bending mode. Further, the blade pitch angle at which instability was encountered was influenced by the large beamwise bending deflections. Thus, stall flutter can be limiting for stopped rotors in the azimuth range from 225 to 300 degrees, and is a function of blade bending stiffness. The

stability boundaries obtained for the test rotor are shown in Figure 81 for several shaft angles (positive shaft angle is in the conventional sense of wing angle of attack). The open symbols are for a dynamic pressure of 28.95 lb/ft<sup>2</sup>. A few points for a dynamic pressure of 43.7 lb/ft<sup>2</sup> are shown which demonstrate the strong  $q$  dependence of the boundaries.

#### *Suggestions for Further Study*

- For gyro-controlled hingeless rotor
  - Establish control system stability boundaries as a function of  $\alpha$ ,  $V$ ,  $\Omega$ ,  $\theta_c$ ,  $N_G$  and  $I_G$
  - Establish optimum cyclic pitch schedule as a function of  $\alpha$ ,  $V$ ,  $\Omega$ ,  $\theta_c$
  - Establish transient response of rotor to disturbances in  $\alpha$  or  $\theta_c$
  - Determine optimum means of introducing restraint to gyro after stability boundary is passed
- For other stopped rotor systems
  - Analyze existing experimental results and generalize where possible to other systems
  - For flapping rotors must devise means of locking out flapping

It was discovered by analysis of the data that a dependence existed between blade pitch and shaft angle. This dependence is shown in Figure 82, wherein the boundaries of Figure 81 are now found to merge essentially into a single curve. The criticality of the range of effective blade angle in the azimuth range from 225° to 260° is now very evident, as is the  $q$  effect.

A further analysis of this concept, which presents additional data and a general assessment of potential application for these vehicles in terms of short haul transports, is presented in Reference 45. The summary of conclusions from that paper indicate that stowage is considered nearly unavoidable if reasonable economies are to be obtained, since the drag of the folded rotor approaches approximately 7 square feet equivalent drag area. In addition, the blades tended to interfere with each other in the folded position and a stabilizing device must be provided. Significant aeroelastic effects of the stopped rotor blades were encountered and extrapolation of these results indicated an aeroelastic divergence speed of about 200 knots for the blades which were tested. Since both negative and positive automatic blade cyclic feathering must be provided to alleviate gust loads, a rotor shaft angle of near zero will be required for the start and stop process. Large shaft moments were encountered during starts and stops, even at zero degrees of rotor shaft angle of attack. These required large amounts of cyclic feathering, even for the unloaded rotor at zero degrees angle of attack. Large, third harmonic components were measured in the oscillatory shaft moments, which would result in vibration transmitted to the fuselage during the start-stop process. The authors finally conclude that additional research must be accomplished to determine the cyclic feathering motion as a function of air speed, angle of attack, and rotor rotation speed. From this research, information concerning blade loads, shaft moments, control capabilities and vibration levels corresponding to the optimum cyclic feathering schedule would be obtained. After this basic research has been accomplished, the feasibility of starting and stopping a rotor in gusty air can then be assessed. In essence, the programs which are planned will be directed towards the accomplishment of these tasks.



Only paper studies and a limited amount of experimental work have been accomplished on the class of rotors wherein the stopped rotor becomes the major fixed lifting surface of the vehicle. While no problems other than those anticipated from the previous discussion have been encountered, it has been ascertained such devices are essentially neither good hovering devices nor good fixed wing devices, but are compromised in both areas. One particular problem peculiar to this device is that of a varying center of pressure as the rotor is started or stopped. Tests made at the NASA-Langley Research Center have shown that this problem can be handled in a reasonable manner. However, the primary source of concern for this concept, other than the poor efficiencies, is the same as for the stopped stowed rotor; i.e. control of the rotor during the stop-start cycle.

### 6.6 Penalties of Stopped Rotor Systems

A brief assessment of the penalties for stopping the rotor is very easy to make when one excludes the problems which have already been discussed. If it is assumed that these problems can be satisfactorily solved, then there remains only the inherent penalties for which there is no remedy. For the case of the stopped and stowed rotor, the primary penalties are in weight and the duplicity of equipment which must be maintained and serviced. A stopped and stowed rotor can be likened in a rather crude analogy to a landing gear, since it is there primarily to enable a particular type of take off and landing. During all other modes of flight it becomes a weight penalty and a high-cost maintenance item. It is for this reason Cheeseman and others advocate the circulation controlled rotors which are of high blade cross-sectional inertia and can be stowed exterior to the aircraft envelope if necessary. Further, these rotors are of low solidity and take less stowing volume and have relatively simple hub designs which may possibly result in reduced weight. However, no matter how the cheese is sliced, the penalty remains and must be accepted if the capabilities of the vehicle are desired.

For the stopped-rotor/fixed-wing concept, the primary penalties are those already suggested in reduced efficiency of both the hover and the high-speed flight mission. Proponents of this vehicle claim that the high speed compromise can be reasonably overcome. However, any effort made to improve the characteristics of the high speed flight case inevitably appear to be detrimental to the hover mode. These penalties are also inescapable and must be accepted if the vehicle is to be employed. It is probable that the compromise accepted would be one which has reduced efficiency in hover at the expense of high speed efficiency, and attempts will be made to keep the hover duration to a minimum.

### REFERENCES

1. Douglas, L.L.  
Schneider, J.J.                    *The Helicopter Comes of Age, Review of Present and Future Roles of Rotary Wing Aircraft.* Paper presented at the International Congress of Subsonic Aerodynamics, New York Academy of Sciences, April, 1967.
2. Jones, J.P.                        *Rotor Aerodynamics - Retrospect and Prospect.* AGARD Advisory Report 13, Sept. 1967.
3. Gessow, A.  
Myers, G.C.                        *Aerodynamics of the Helicopter.* The Macmillan Company, New York, 1952.
4. Tanner, W.H.                     *Charts for Estimating Rotary Wing Performance in Hover and at High Forward Speeds.* NASA CR-114, 1964.
5. Durand, W.F.                     *Aerodynamic Theory, Vol. IV.* Berlin, Julius Springer, 1934.



6. Goldstein, S. *On the Vortex Theory of Screw Propellers.* Proceedings, Royal Society of London, Vol. A123, No.A792, 1929.
7. Lock, C.N.H. *The Application of Goldstein's Theory to the Practical Design of Airscrews.* British ARC R&M No.1377, 1931.
8. Willmer, M.A.P. *The Loading of Helicopter Rotor Blades in Forward Flight.* RAE Report Naval 2-N-76935 No.8, April, 1959.
9. Piziali, R.  
Duwaldt, F. *Computation of Rotary Wing Harmonic Airloads and Comparison with Experimental Results.* Proceedings of AHS Forum, May, 1962.
10. Erickson, J.C.  
Ordway, D.E. *A Theory for Static Propeller Performance.* CAL/USAAVLABS Symposium Proceedings, Vol.I, June, 1966.
11. Erickson, J.C. Jr.,  
et al. *A Theory for VTOL Propeller Operation in a Static Condition.* US Army Aviation Materials Laboratories, TR-65-69, Oct. 1965, AD 623527.
12. Trenka, A.R. *Prediction of the Performance and Stress Characteristics of VTOL Propellers.* CAL/USAAVLABS Symposium Proceedings, Vol.I, June, 1966.
13. Jenny, D.S.  
et al. *A Reassessment of Rotor Hovering Performance Prediction Methods.* AHS Forum, May, 1967.
14. McCormick, B.N.  
et al. *Tip Vortex Core Thickening for Application to Helicopter Rotor Noise Reduction.* USAAVLABS TR 66-1, Sept. 1966.
15. Gray, R.B. *An Aerodynamic Analysis of a Single Bladed Rotor in Hovering and Low Speed Forward Flight as Determined from the Smoke Studies of the Vorticity Distribution in the Wake.* Princeton Aeronautical Engineering Department Report No.356, Sept. 1956.
16. Jones, J.P. *An Extended Lifting Line Theory for the Loads on a Rotor Blade in the Vicinity of a Vortex.* MIT Aeroelastic and Structures Laboratory Report TR-123-3, December, 1965.
17. Kfoury, D.J. *A Routine Method for the Calculation of Aerodynamic Loads on a Wing in the Vicinity of Infinite Vortices.* MIT Aeroelastic and Structures Laboratory Report TR-133-2, May, 1966.
18. Stepniewski, W.Z. *Remarks on High Speed and Payload Capability of Rotary Wing Aircraft.* AGARD Conference Proceedings No.7, January, 1966.
19. Davenport, F.J.  
Front, J.V. *Airfoil Sections for Rotor Blades - A Reconsideration.* AHS Forum, May, 1966.
20. McCroskey, W.J.  
Yaggy, P.F. *Laminar Boundary Layers on Helicopter Rotors in Forward Flight.* AIAA Paper No.68-70, January, 1968.
21. Tanner, W.H.  
Yaggy, P.F. *Experimental Boundary Layer Study on Hovering Rotors.* J. Am. Helicopter Soc. II, 22, 1966.
22. Harris, F.D. *Preliminary Study of Radial Flow Effects on Rotor Blades.* J. Am. Helicopter Soc., II, 1, 1966.

23. Tararine, S. *Experimental and Theoretical Study of Local Induced Velocities Over a Rotor Disc.* Proceedings CAL/TRECOM Symposium, Vol.I, June, 1963.
24. Miller, R.H. *Unsteady Airloads on Helicopter Rotor Blades.* Fourth Cierva Memorial Lecture to the Royal Aeronautical Society, October 1963, Journal R. Ae. Soc.68, 640, April, 1964.
25. Scully, M. *MIT Bachelor's Thesis, 1964.* Paper presented at the Symposium on the Noise and Loading Actions on Helicopters, V/STOL Aircraft and Ground Effect Machines, University of Southampton, England, September, 1965.
26. Ham, N.D. *An Experimental Investigation of the Effect of a Non-Rigid Wake on Rotor Blade Airloads in Transition Flight.* Proceedings CAL/TRECOM Symposium Vol.I, June, 1963.
27. Simons, I.A.  
et al. *The Movement Structure, and Breakdown of Trailing Vortices from a Rotor Blade.* CAL/USAAVLABS Symposium Proceedings, Vol.I, June, 1966.
28. Tanner, W.H.  
et al. *The Helicopter Rotor at High Mach Numbers.* AHS Forum, May, 1967.
29. Stepniewski, W.Z.  
Young, M.I. *Helicopters and Propeller-Type VTOL Aircraft in the Light of Technologies.* SAE National Aeronautics Meeting, April, 1965.
30. Ham, N.D. *An Experimental Investigation of Stall Flutter.* J. Am. Helicopter Soc., January, 1962.
31. Young, M.I. *A Theory of Rotor Blade Motion Stability in Powered Flight.* J. Am. Helicopter Soc., Vol.9, No.3, July, 1964.
32. Halfman, R.C.  
et al. *Evaluation of High-Angle-of-Attack Aerodynamic-Derivative Data and Stall Flutter Prediction Techniques.* NACA TN-2533, November, 1951.
33. Rainey, G.A. *Measurement of Aerodynamic Forces for Various Mean Angles of Attack on an Airfoil Oscillating in Pitch and on Two Finite-Span Wings Oscillating in Bending with Emphasis on Damping in the Stall.* NACA TN-3643, May, 1956.
34. Ham, N.D.  
Young, M.I. *Torsional Oscillations of Helicopter Blades Due to Stall.* J. of Aircraft, Vol.3, No.3, May-June, 1966.
35. Carta, F.O.  
Ham, N.D. *An Analysis of the Stall Flutter Instability of Helicopter Rotor Blades.* AHS Forum, No.130, May, 1967.
36. Liiva, J. *Unsteady Aerodynamic and Stall Effects on Helicopter Rotor Blade Airfoil Sections.* AIAA Paper No.68-58, January, 1968.
37. Bisplinghoff, R.L.  
et al. *Aeroelasticity.* Addison Wesley Publishing Co., Inc., Reading, Massachusetts, 1955.
38. Kramer, M. *Increase in the Maximum Lift of an Airplane Due to a Sudden Increase in its Effective Angle of Attack Resulting from a Gust.* NACA TM-678, 1932.

39. Cheeseman, I.C. *The Application of Circulation Control by Blowing to Helicopter Rotors.* J. of the Royal Aero. Soc. Vol.71, No.679. July, 1967.
40. Dorand, R. *The Application of the Jet Flap to Helicopter Rotor Control.* J. of the Helicopter Assoc. of G.B., Vol.13, December, 1959.
41. Evans, W.T.  
McCloud, J.L. III *An Analytical Investigation of a Helicopter Rotor Driven and Controlled by a Jet Flap.* NASA TN D-3028, September, 1965.
42. Connor, A.B. *The Promise of Compounding.* AGARD Conference Proceedings, No.7, January, 1966.
43. Drees, J.M.  
Lynn, R.R. *The Promise of Compounding.* AGARD Conference Proceedings, No.7, January, 1966.
44. Davies, D.M.  
Hislop, G.S. *The Compound Helicopter.* AGARD Conference Proceedings, No.7, January, 1966.
45. Deckert, W.H.  
McCloud, J.L. III *Considerations of the Stopped Rotor V/STOL Concept.* J. American Helicopter Soc., Vol.13, No.1, January, 1968.
46. White, R.P., Jr. *Instabilities Associated with a Rotor Blade Stopped in Flight.* AHS Forum, May, 1968.

TABLE I  
Airfoil Geometry and Aerodynamic Summary

Geometric Feature		Aerodynamic Characteristics					
		$C_{Lmax}$	$C_{Dmin}$	$\Delta C_{Dlift}$	$M_{DD}$ $C_{L=0}$	$C_{mac}$	
Thickness	Thick (>12%)	Fair	Fair	Good	Poor	No effect	
	Moderate (9-12%)	Good	Good	Good	Fair	No effect	
	Thin (<9%)	Depends on camber, i.e.	Good	Depends on camber, i.e.	Good	No effect	
Leading Edge	Blunt	Good	No effect	Good	No effect	No effect	
	Sharp	Poor	No effect	Poor	No effect	No effect	
Camber	None	Fair to poor	Good	Fair	Good	Good	
	Uniform loading	Fair	Minute penalty	Fair to good	Fair	Unacceptable	
	Trailing edge	Best	Unacceptable	Good	Unacceptable	Unacceptable	
	Leading edge	Good	Slight penalty	Good	Fair	Fair (can be corrected to good)	

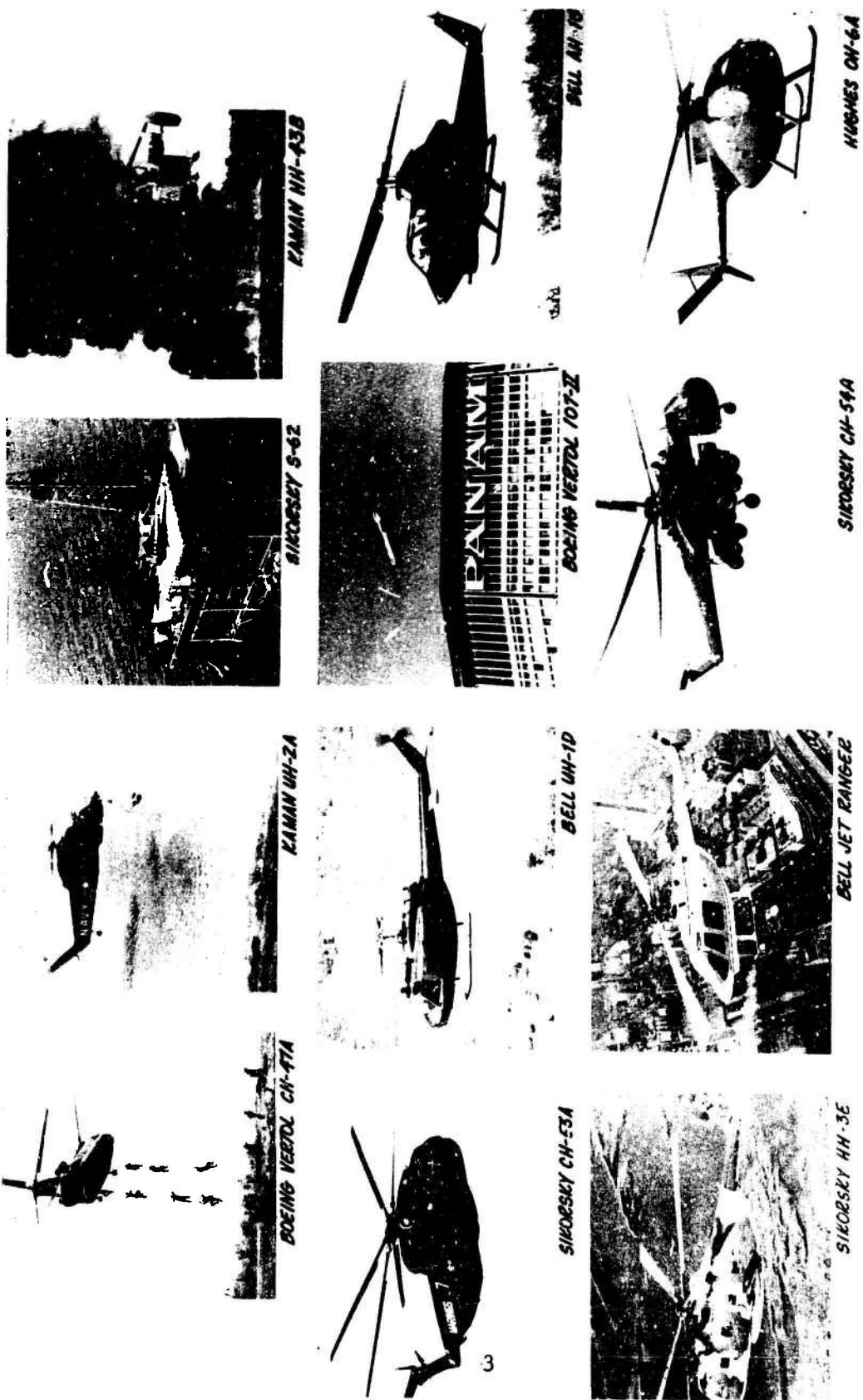


Figure 1

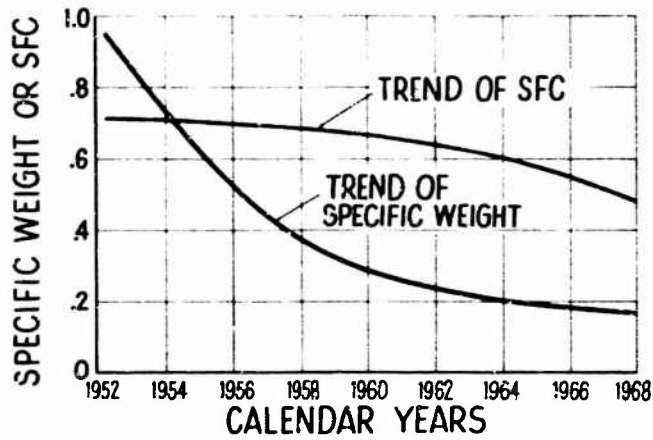


Fig. 2 Progress in helicopter power plants

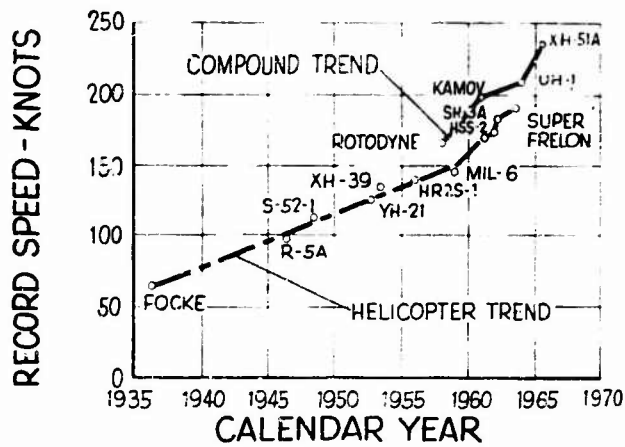


Fig. 3 Helicopter speed records

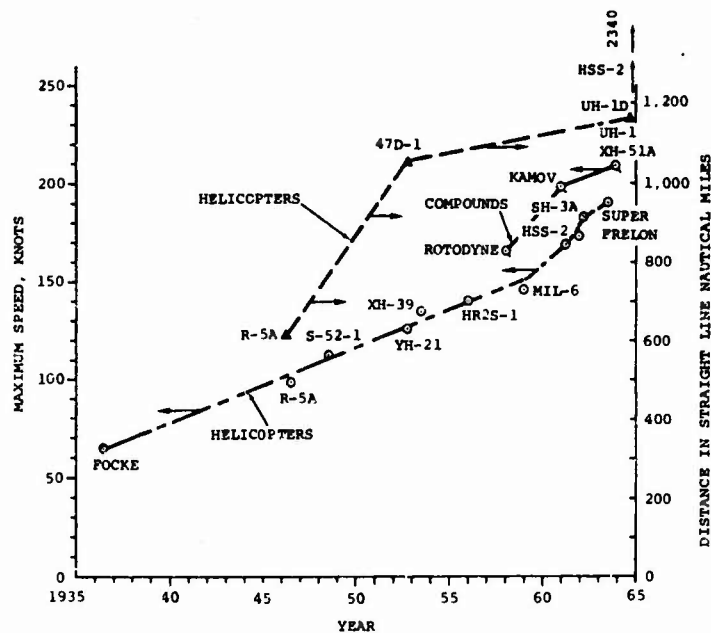


Fig. 4 Maximum speed and straight-line distance records of pure and compound helicopters versus years

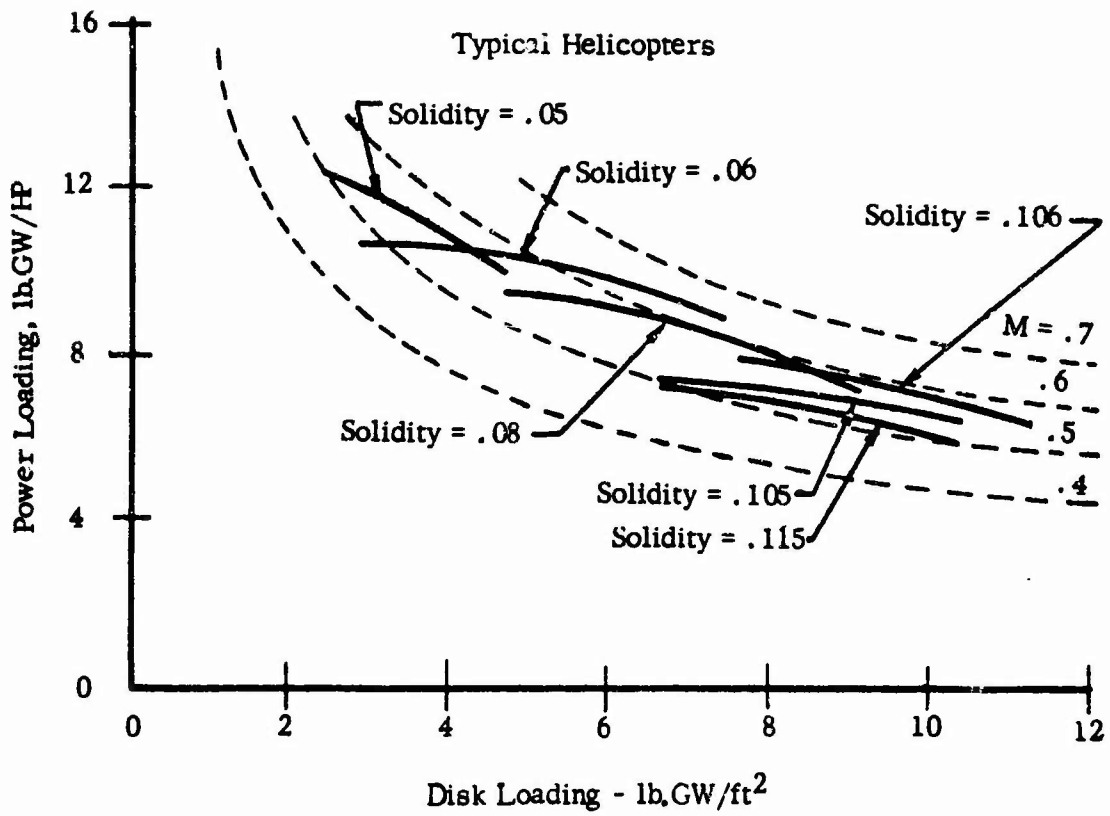


Fig. 5 Power loading versus disk loading

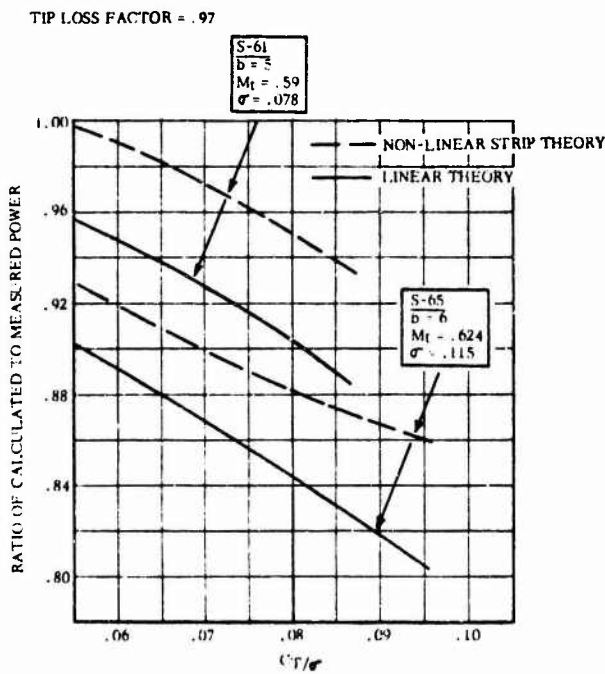


Figure 6

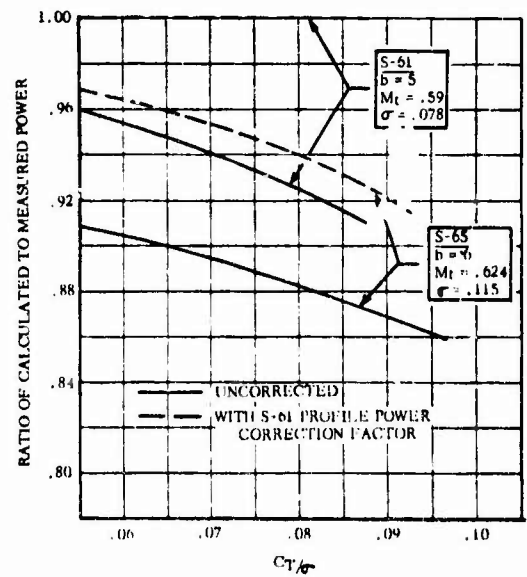


Figure 7

GOLDSTEIN-LOCK  
UNCORRECTED

S-65 MAIN ROTOR  
 $M_t = .624$

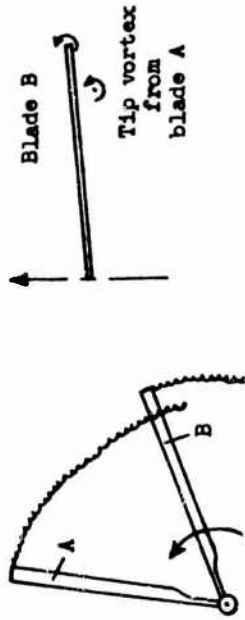
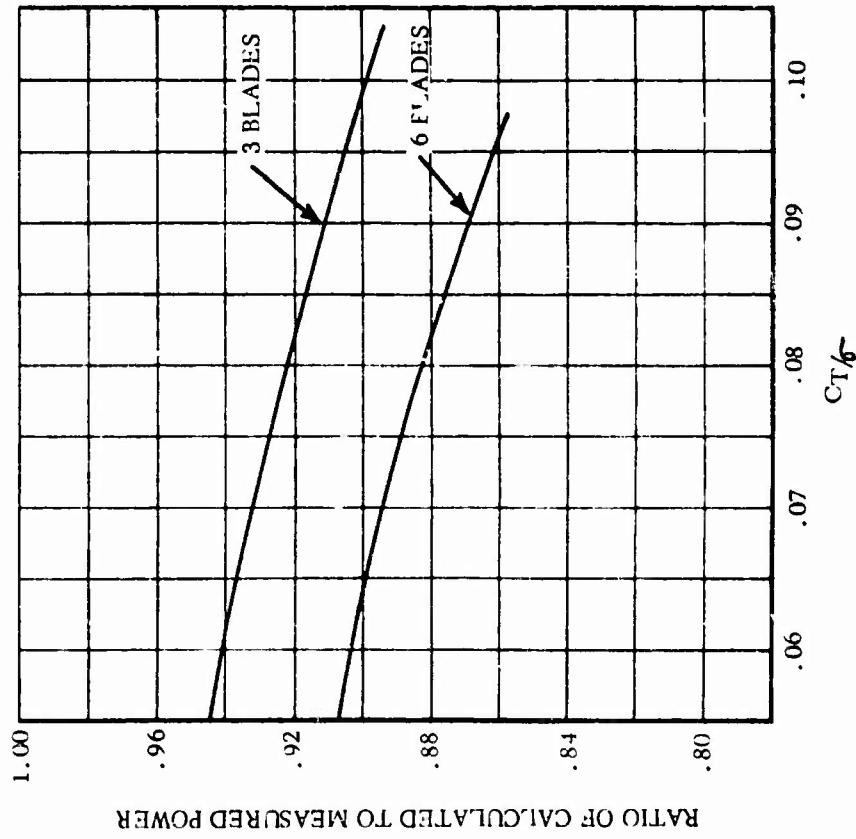


Figure 9

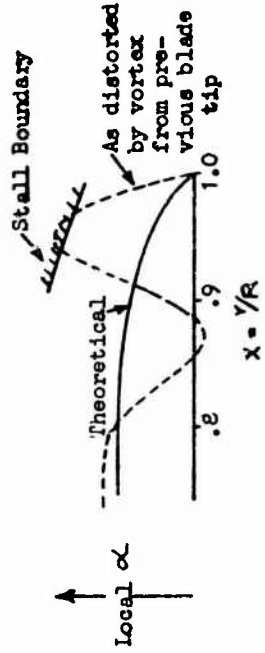
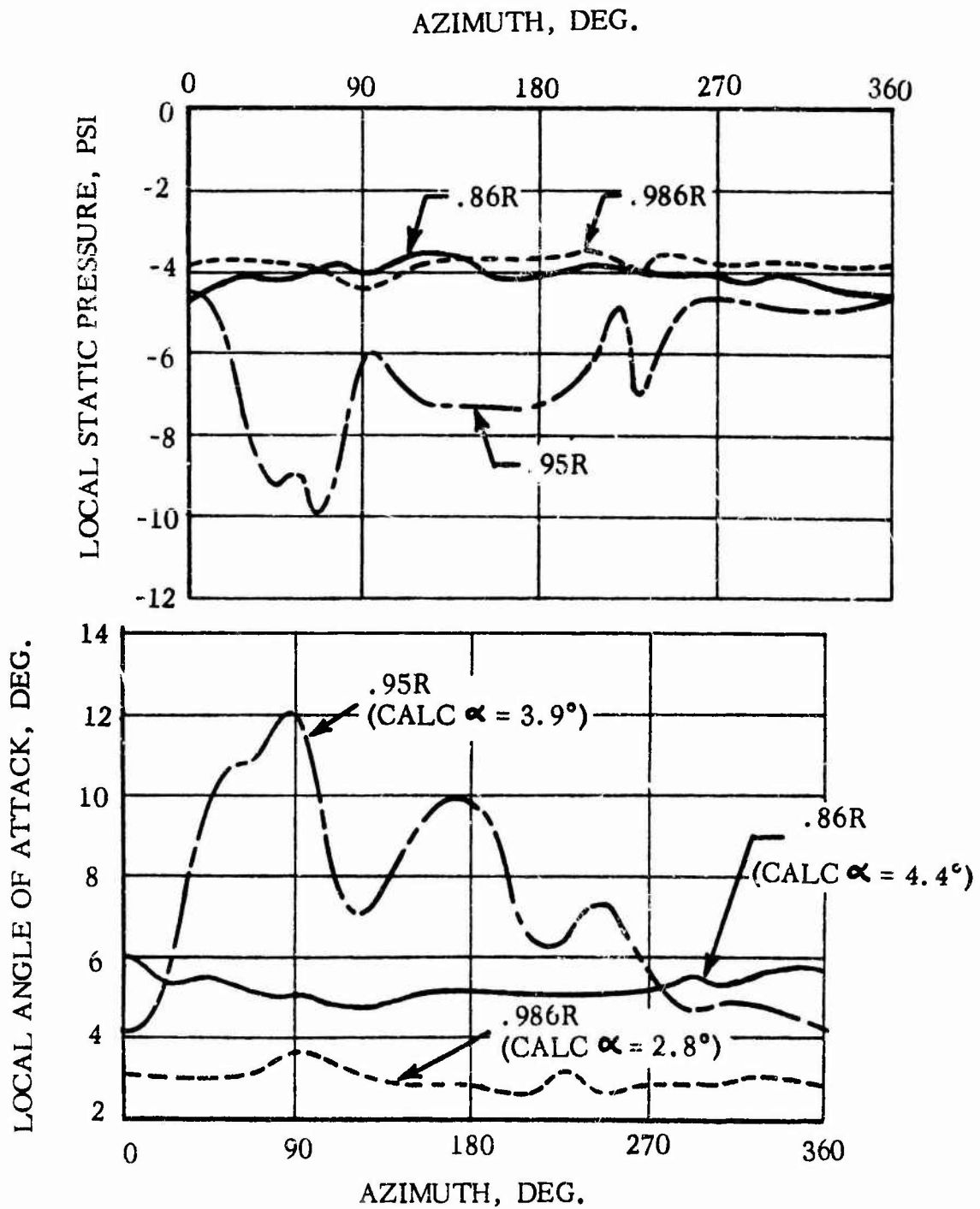


Figure 10

Fig. 8 Number of blades effect





BLADE PRESSURE MEASUREMENTS

Fig.11 10% upper surface chord station

$$\theta_{75} = 12^\circ, \quad C_{\frac{T}{\sigma}} = .097, \quad \text{RPM} = 1400$$

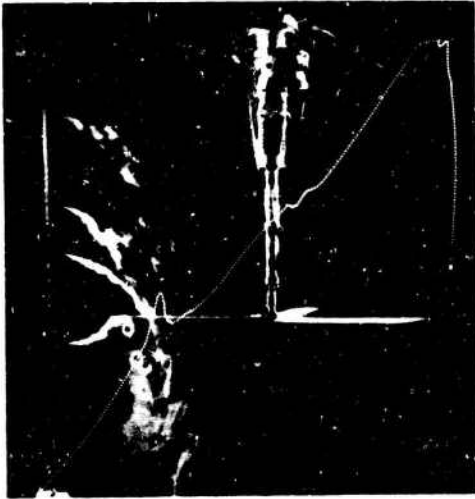
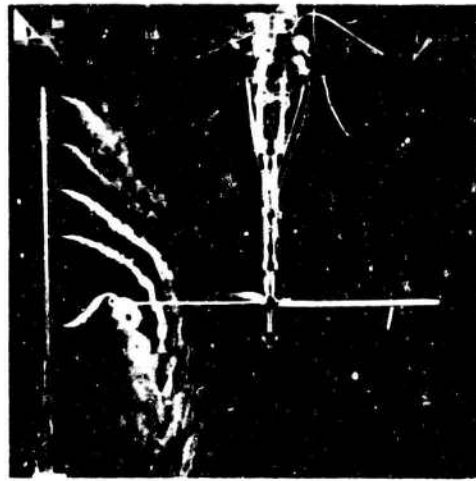
 $\psi \approx 10^\circ$  $\psi \approx 40^\circ$  $\psi \approx 90^\circ$  $\psi \approx 110^\circ$ 

Fig. 12 Wake geometry photos

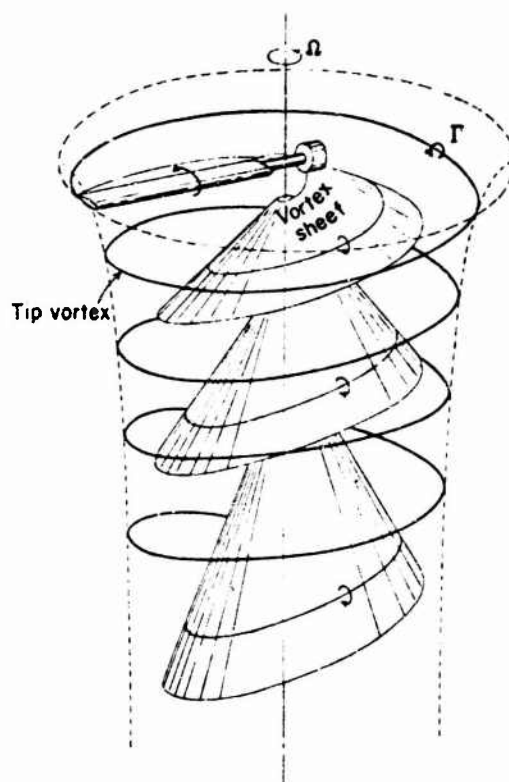


Fig. 13 Structure of wake from one blade

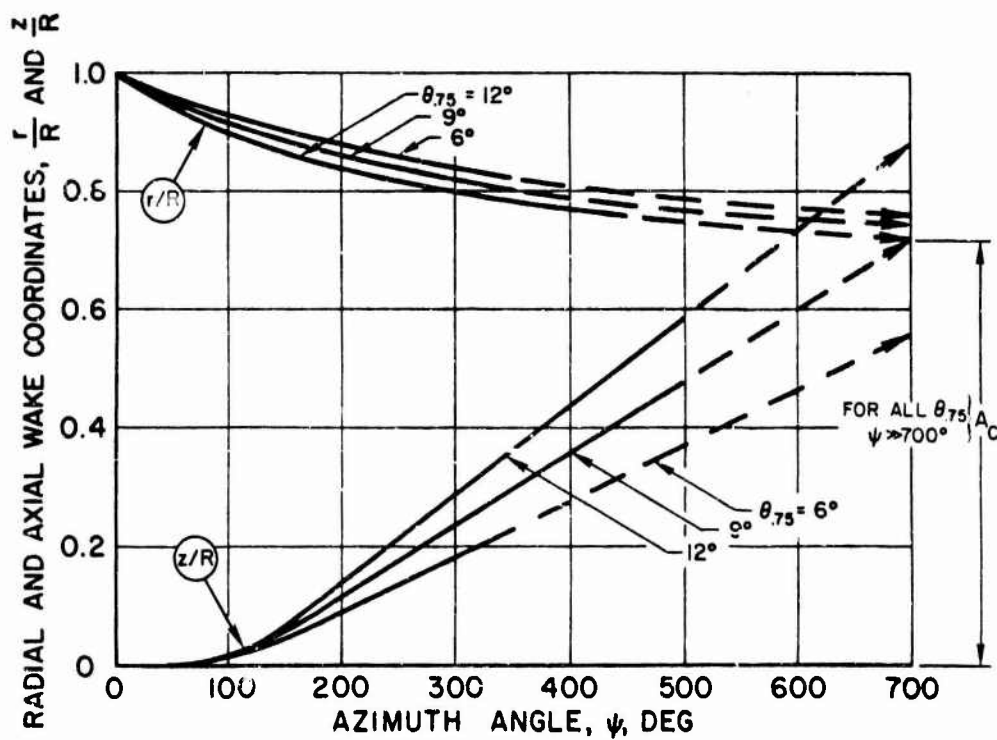


Fig. 14 Model rotor tip wake coordinates

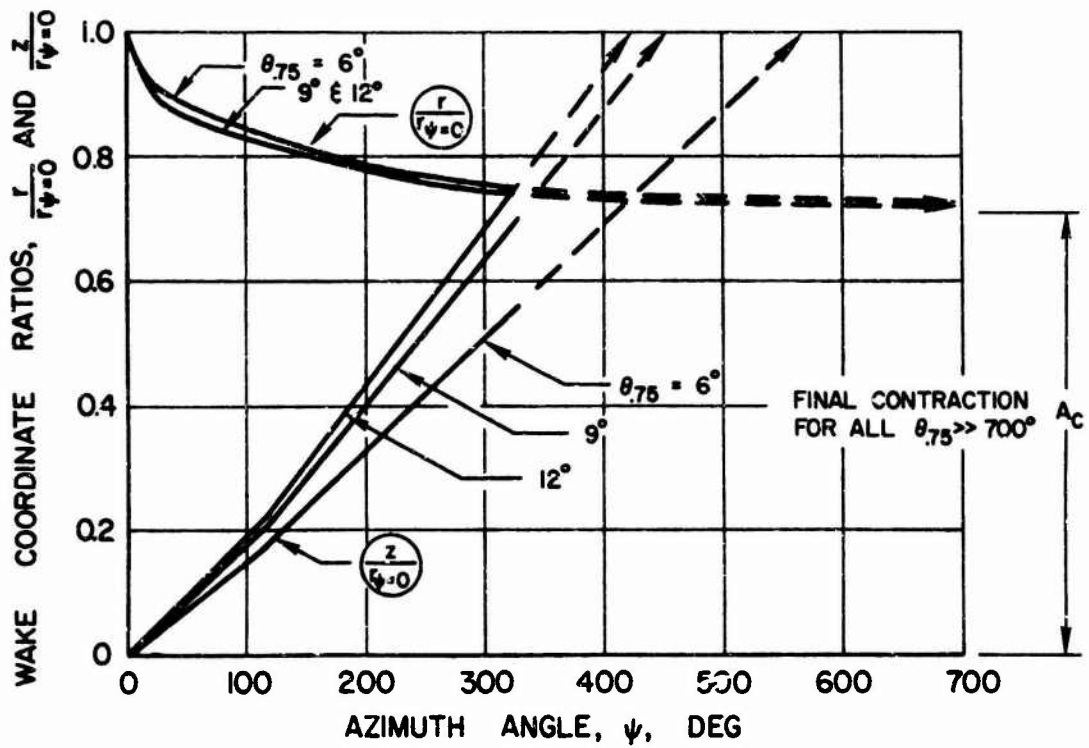


Fig.15 Model rotor inboard vortex sheet coordinates

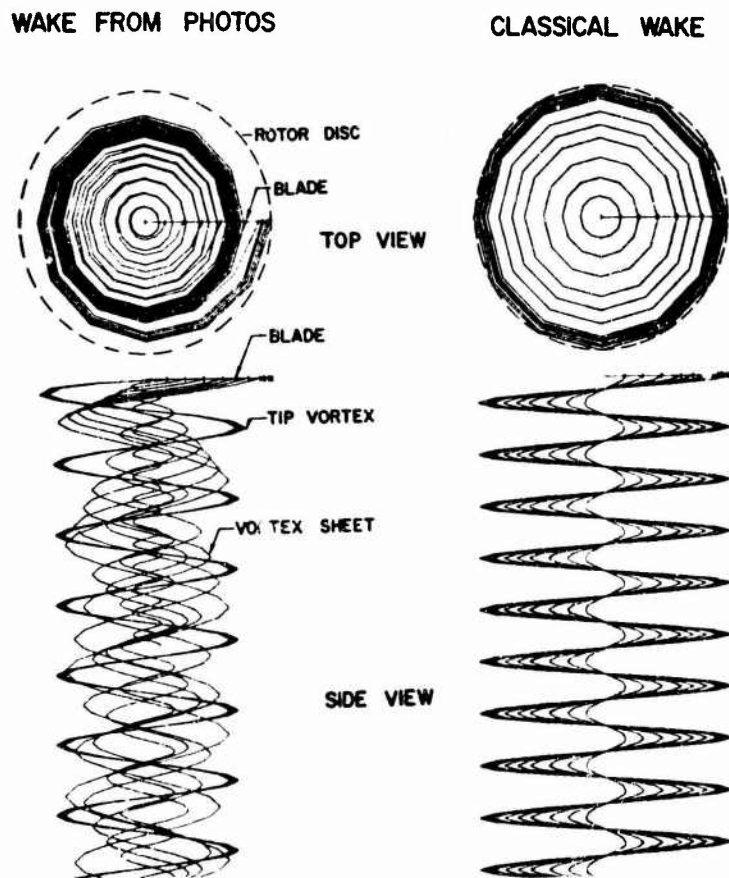


Fig.16 Computer wake trajectories for one blade

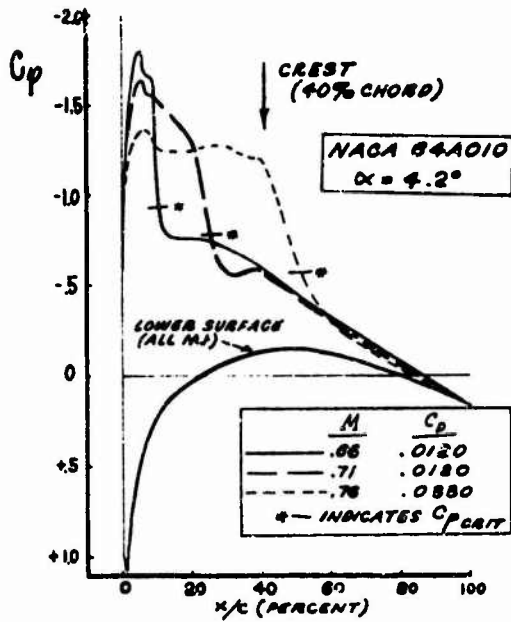


Fig. 17 Pressure distribution at drag rise, showing "crest-line" effect

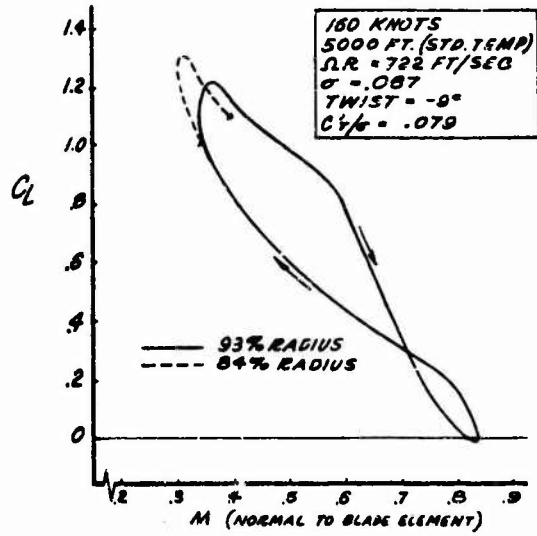


Fig. 18 Rotor blade airfoil working environment in forward flight (conventional helicopter)

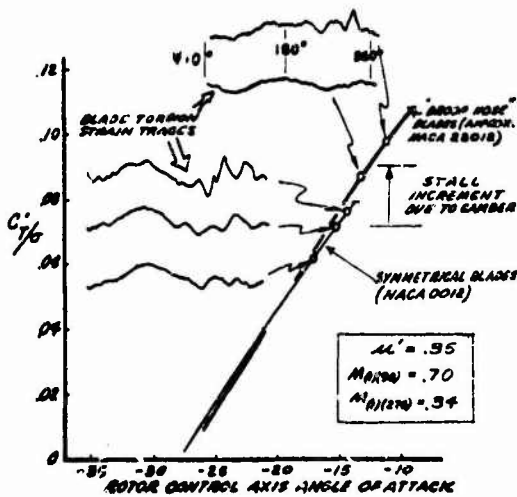


Fig. 19 Rotor blade stall as affected by airfoil camber. 3-inch chord model rotor blades

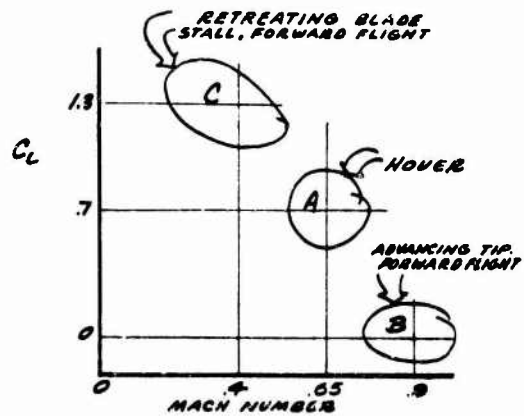


Fig. 20 The three critical areas of blade element environment

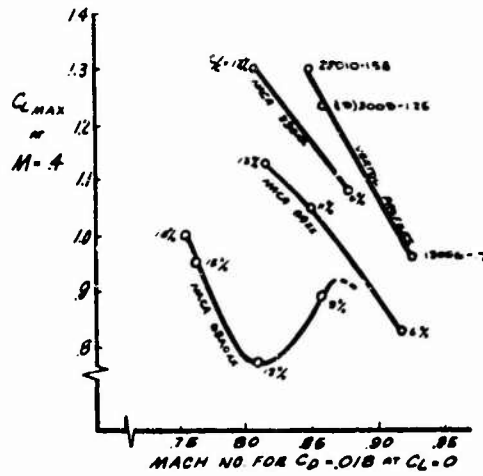


Fig. 21 Summary of stall and drag rise characteristics for several airfoil families

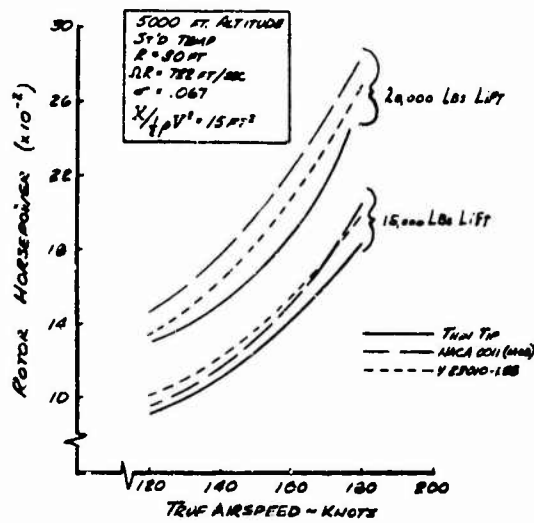


Fig. 22 Effect of airfoil section on rotor performance

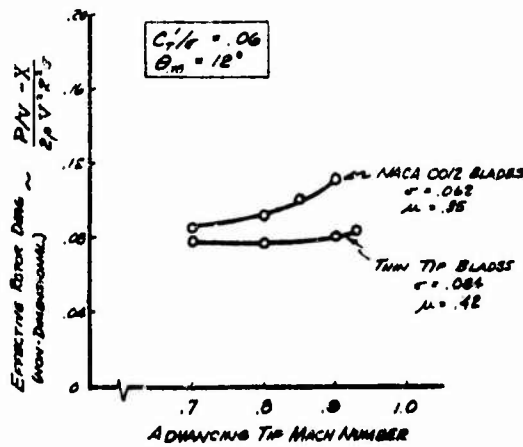


Fig. 23 Rotor performance comparison, experimental data (Sources: NACA 0012 blades, University of Maryland Wind Tunnel Test No. 413; thin tip blades UMWT 456. Both unpublished)

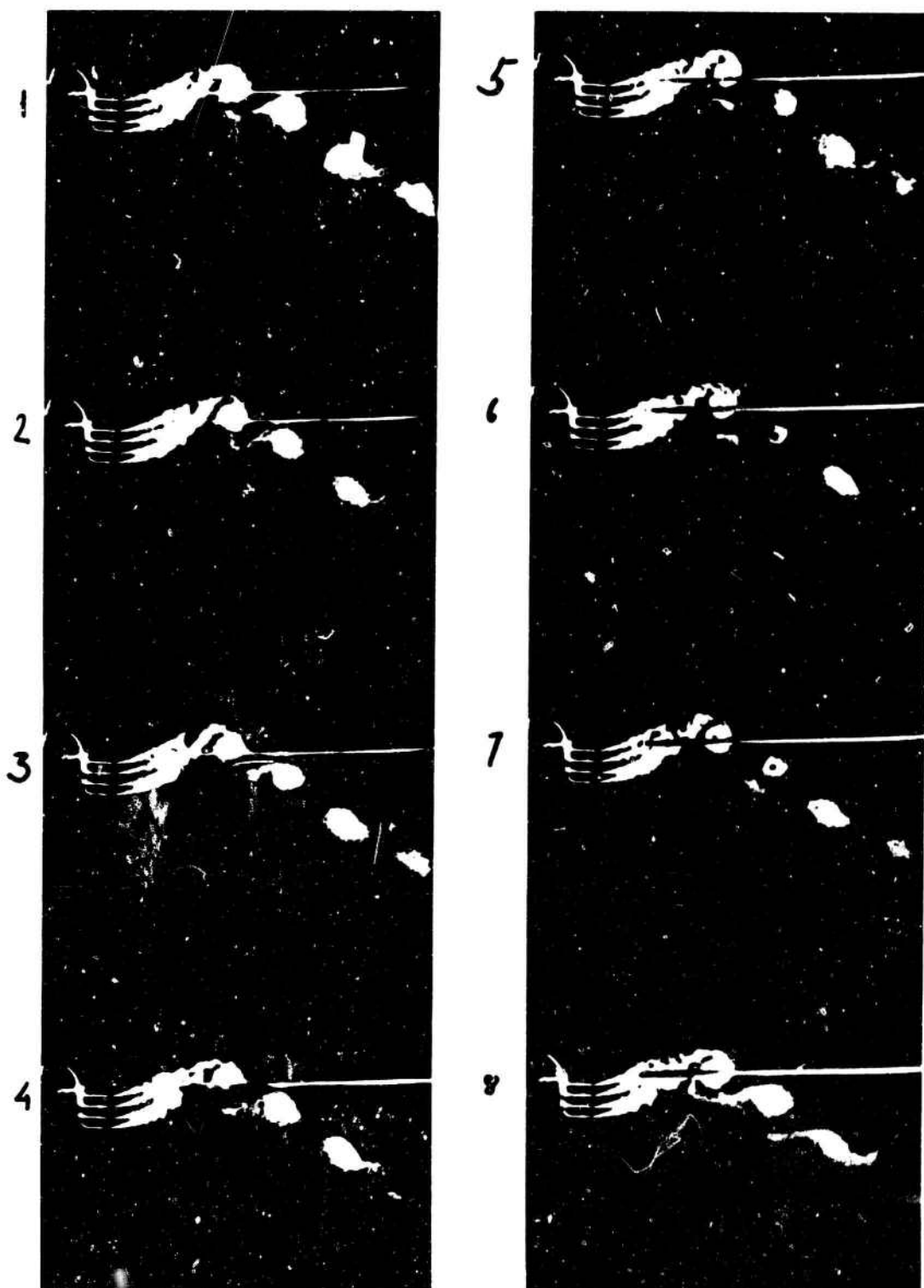


Fig. 24 Trailing vortices near disc leading edge

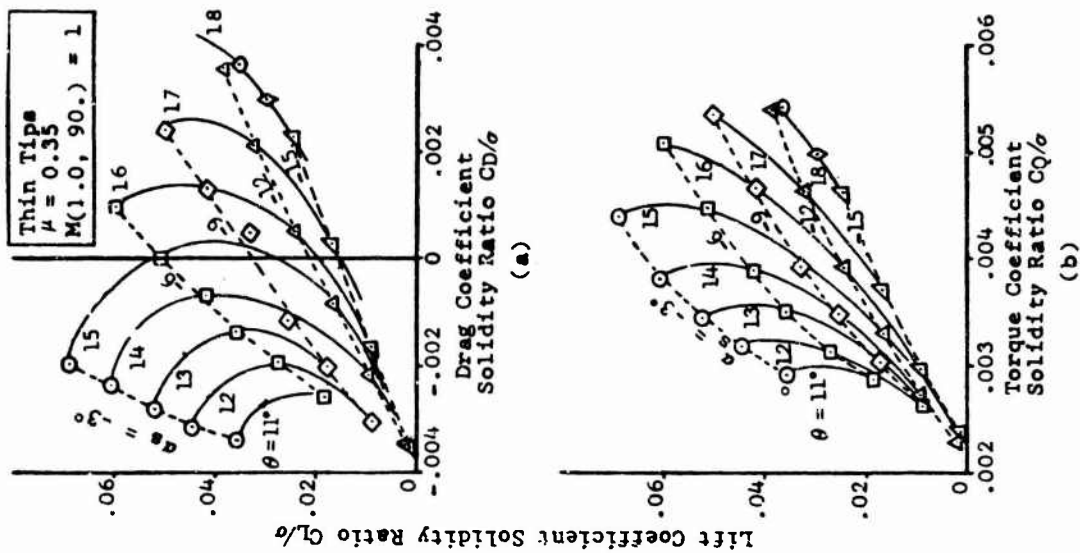


Fig. 26 Example of wind tunnel data

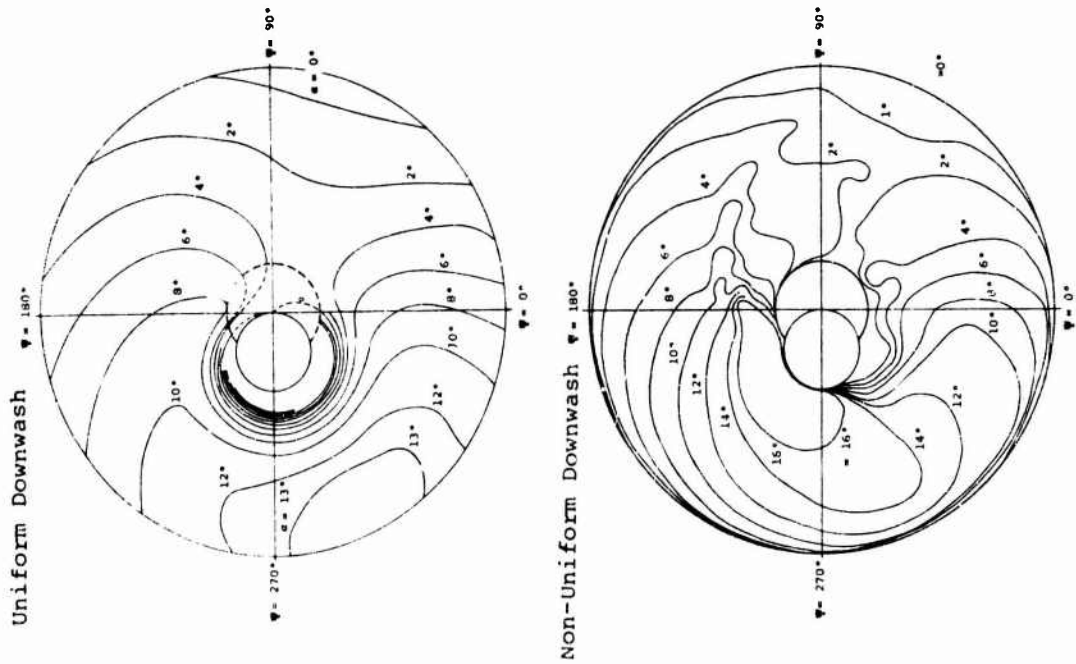


Fig. 25 Typical angle-of-attack distribution at 140 knots



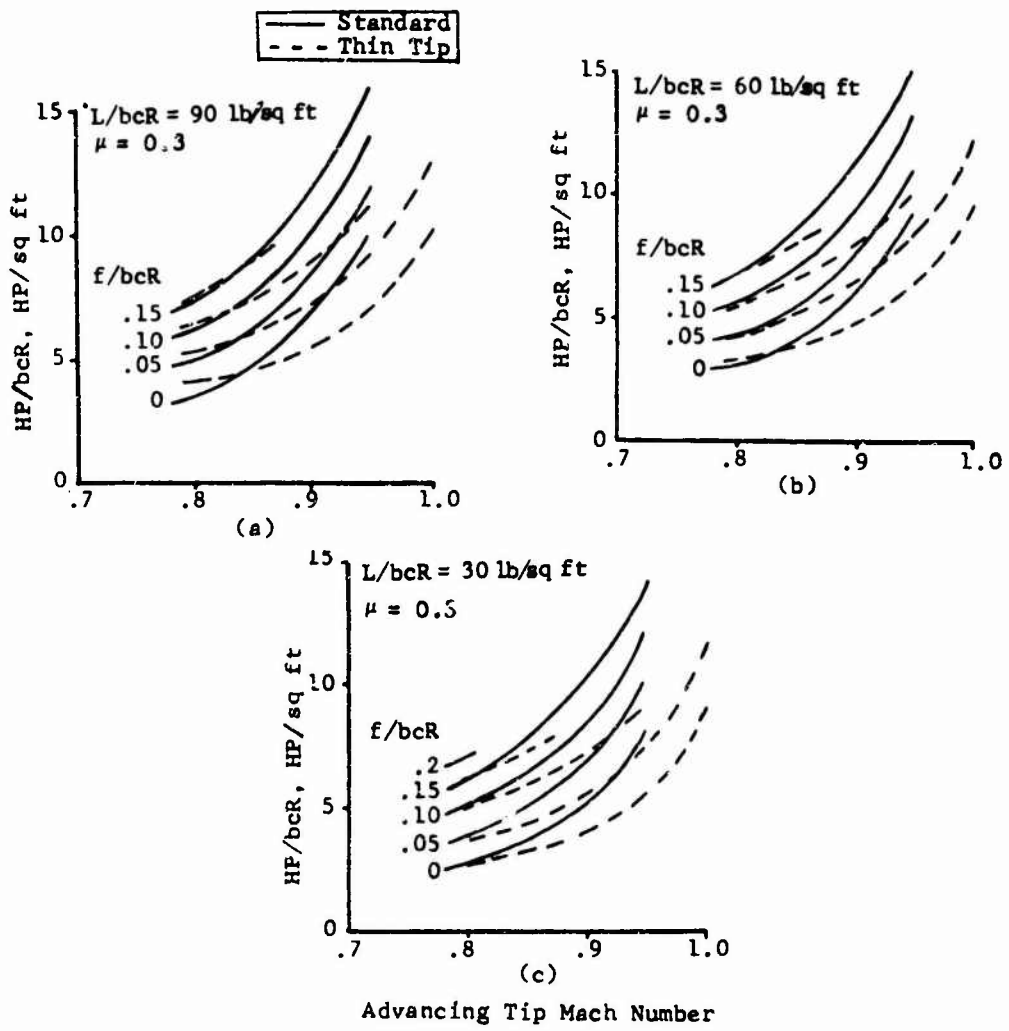


Fig. 27 Performance comparison of standard and thin-tip rotors

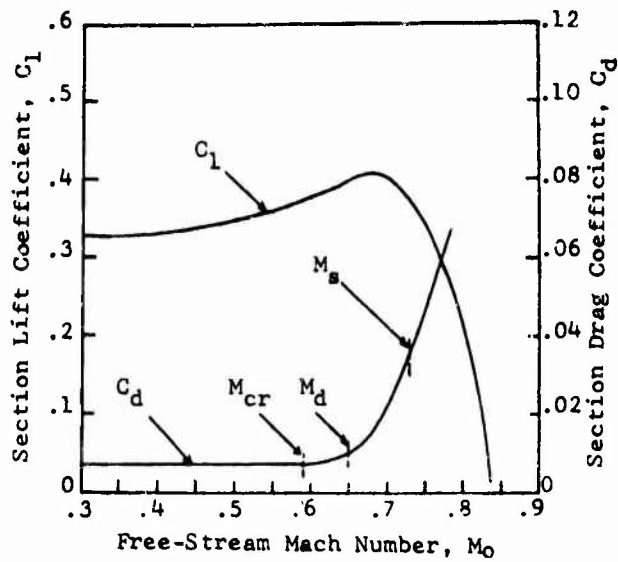
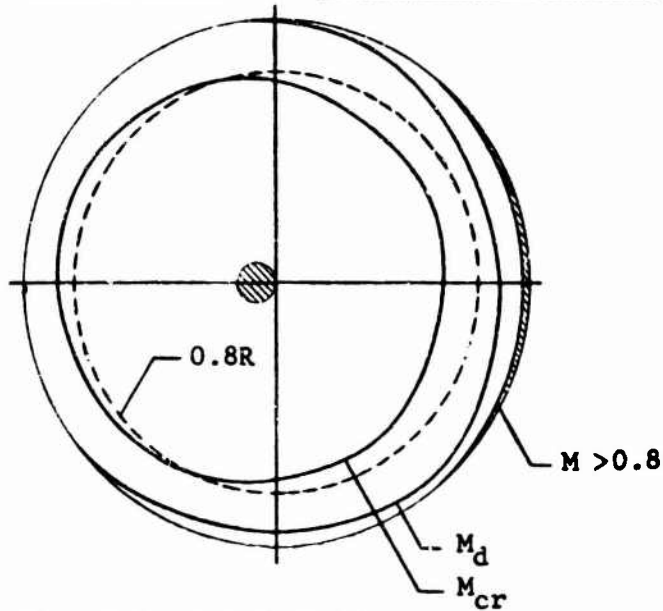


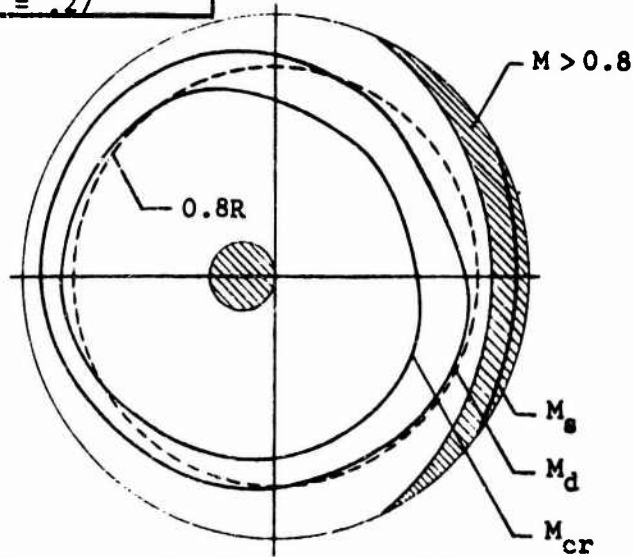
Fig. 28 Section characteristics with Mach number

$M(1.0, 90.) = .83$ $\mu = .17$	$L/bcR = 94 \text{ lb/sq ft}$ $E/bcR = .23$
------------------------------------	--



a) Within Normal Flight Envelope

$M(1.0, 90.) = .92$ $\mu = .27$
------------------------------------



b) Higher Speeds Than Normal Flight Envelope

Fig. 29 UH-1D rotor disc area affected by supercritical flow

V = 236 KTS.

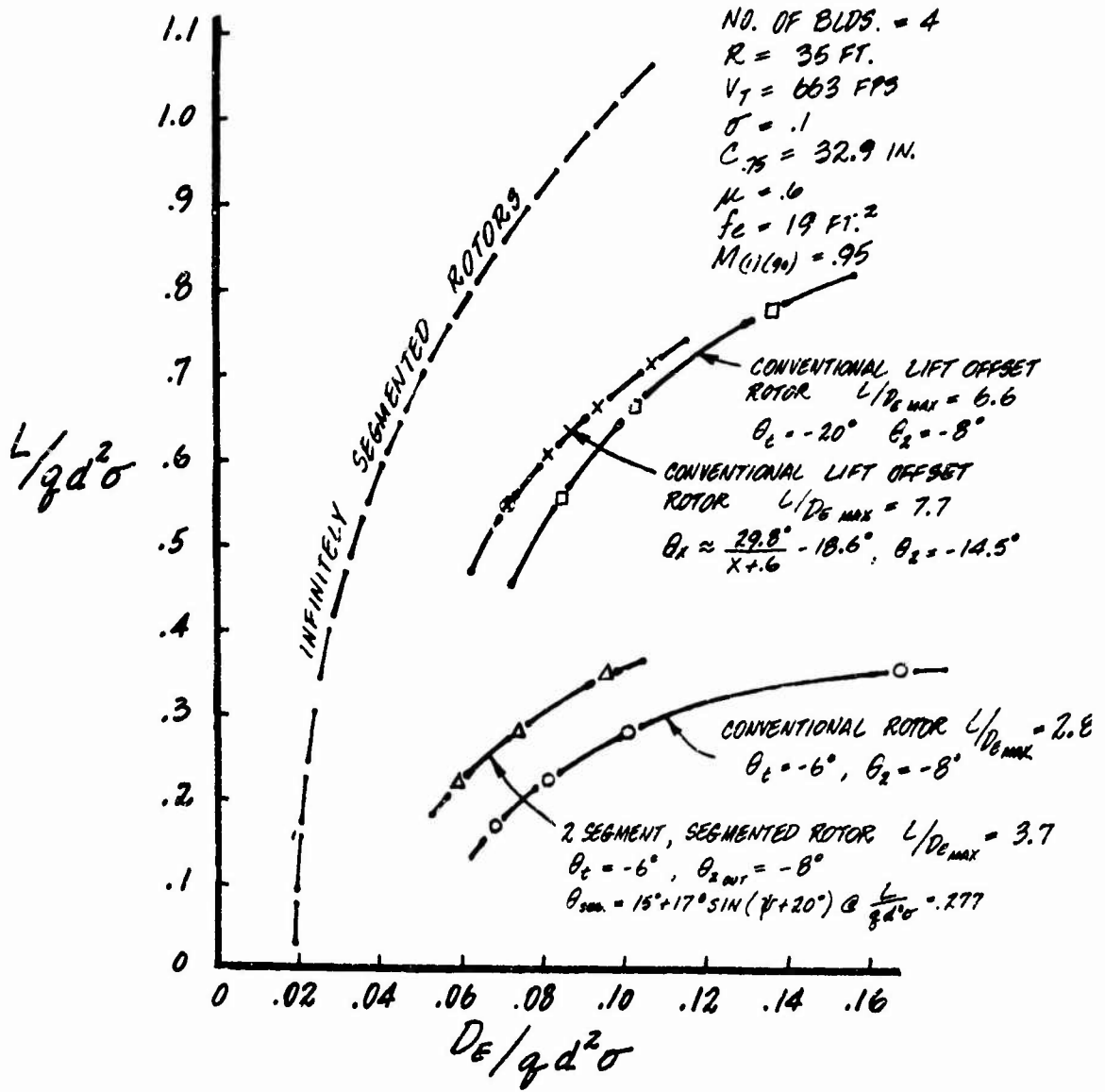


Figure 30

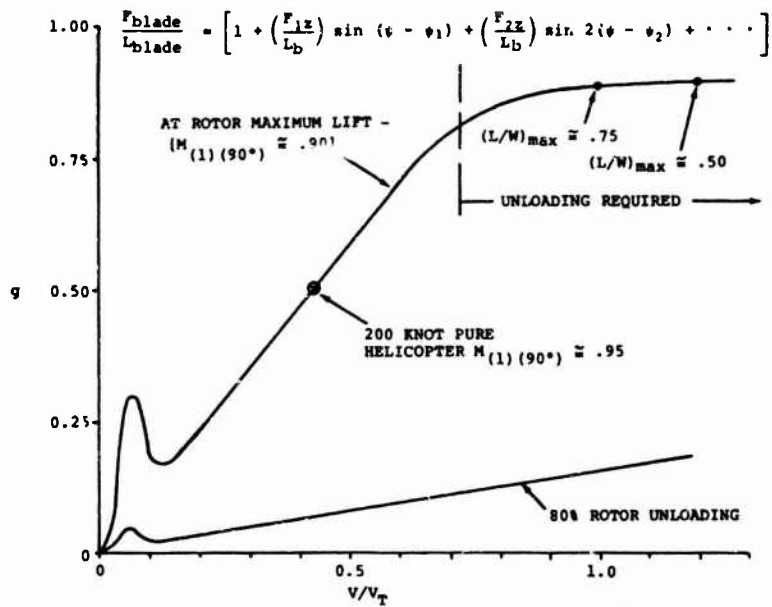


Fig.31 Rotor blade relative vibratory vertical output for rigid articulated blade

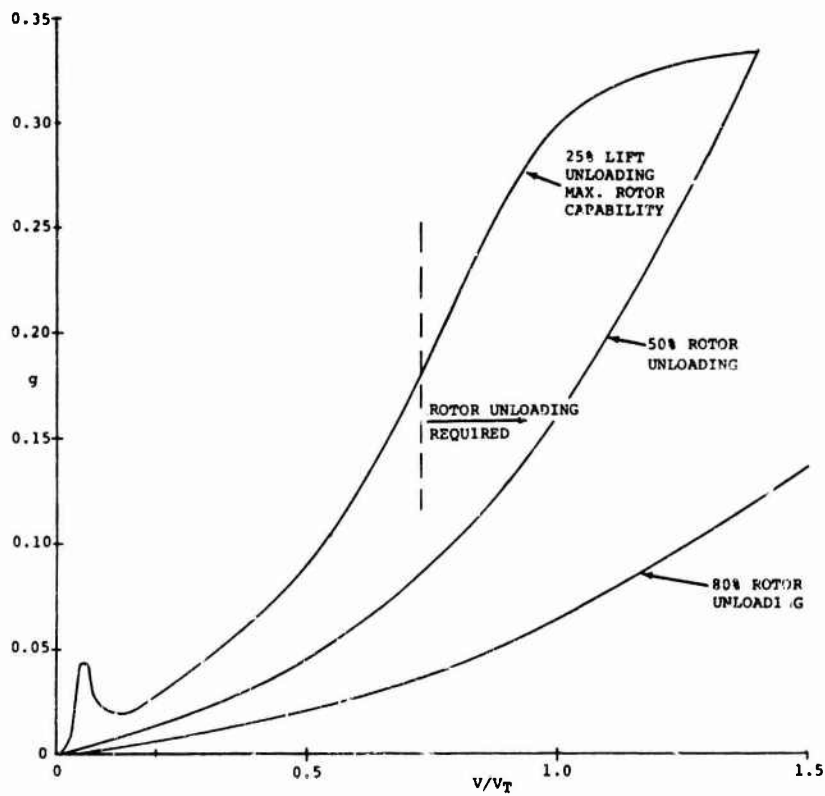


Fig.32 Rotor blade relative vibratory in-plane output for rigid articulated blade

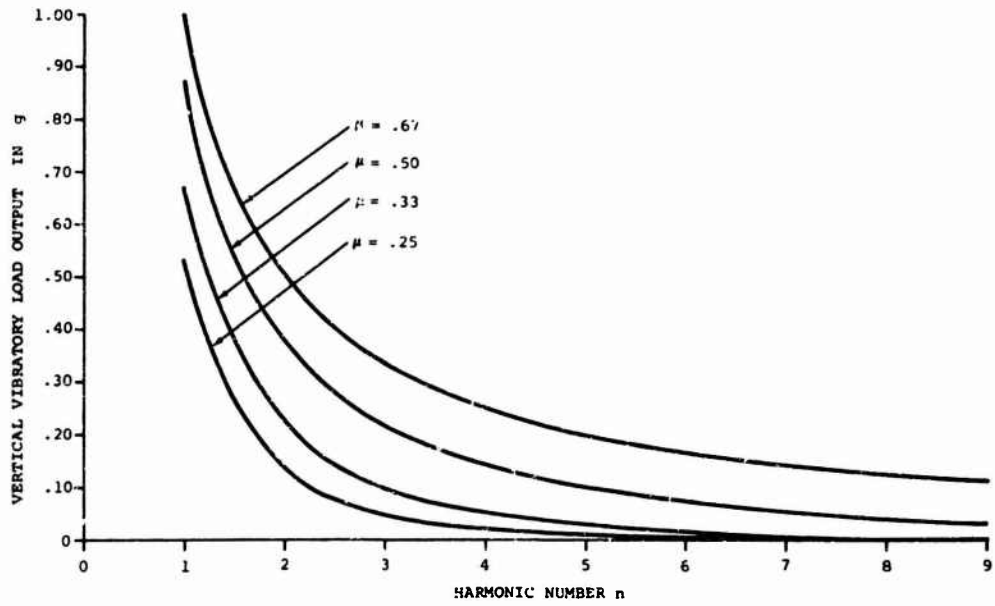


Fig. 33 Vertical vibratory load output versus harmonic number for rigid articulated blade at various tip-speed ratios

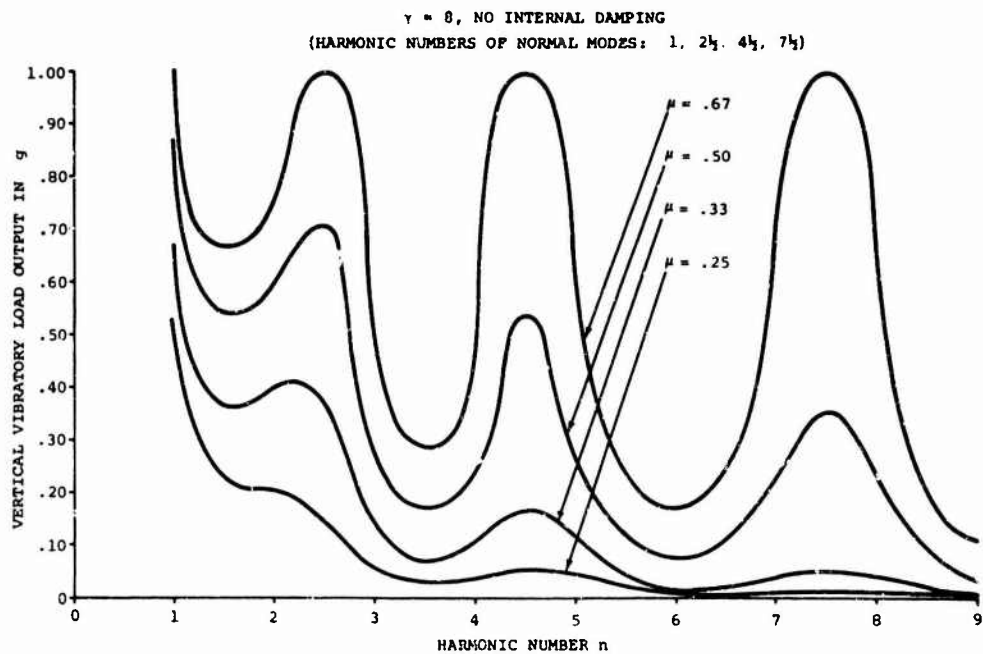


Fig. 34 Typical elastic blade vertical vibratory load output versus harmonic number for various tip-speed ratios

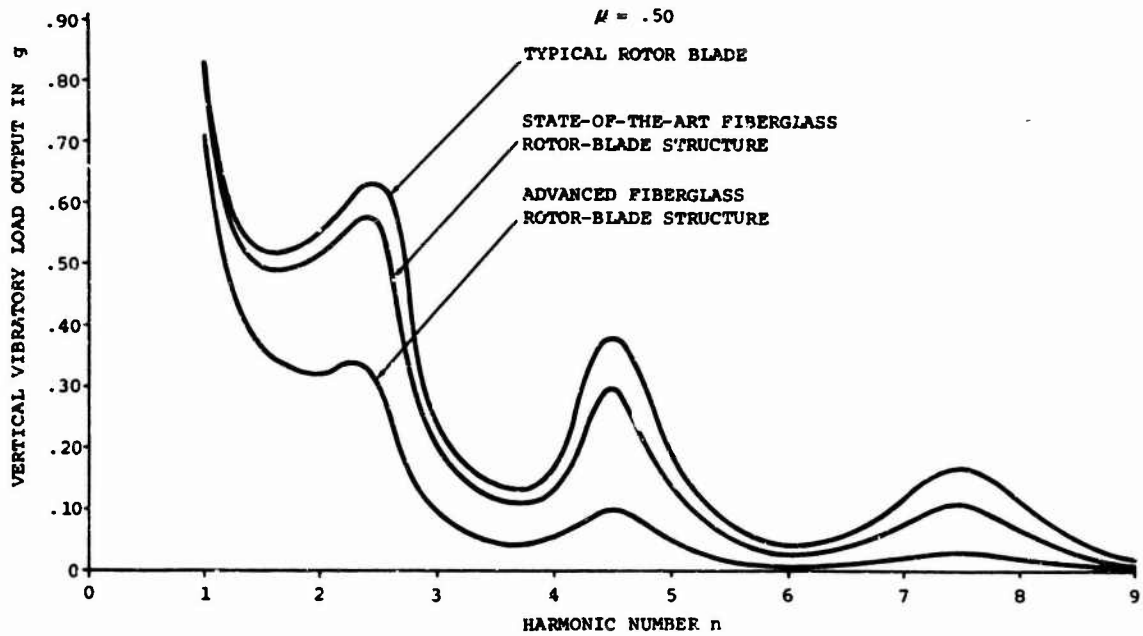


Fig.35 Influence of internal damping on typical elastic blade vertical vibratory load output

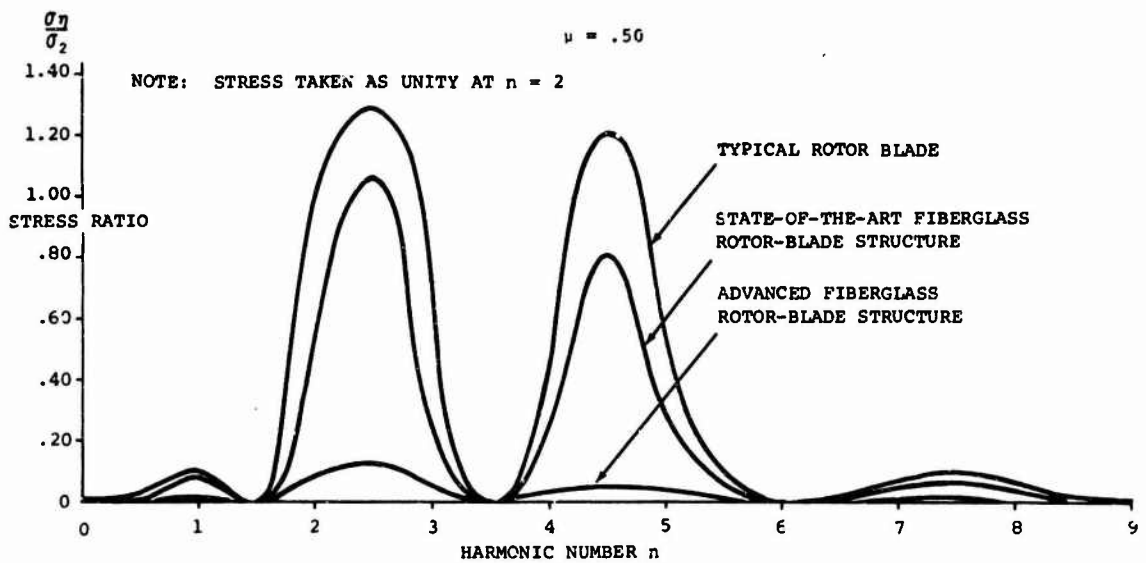


Fig.36 Influence of internal damping on frequency distribution of blade cyclic stress

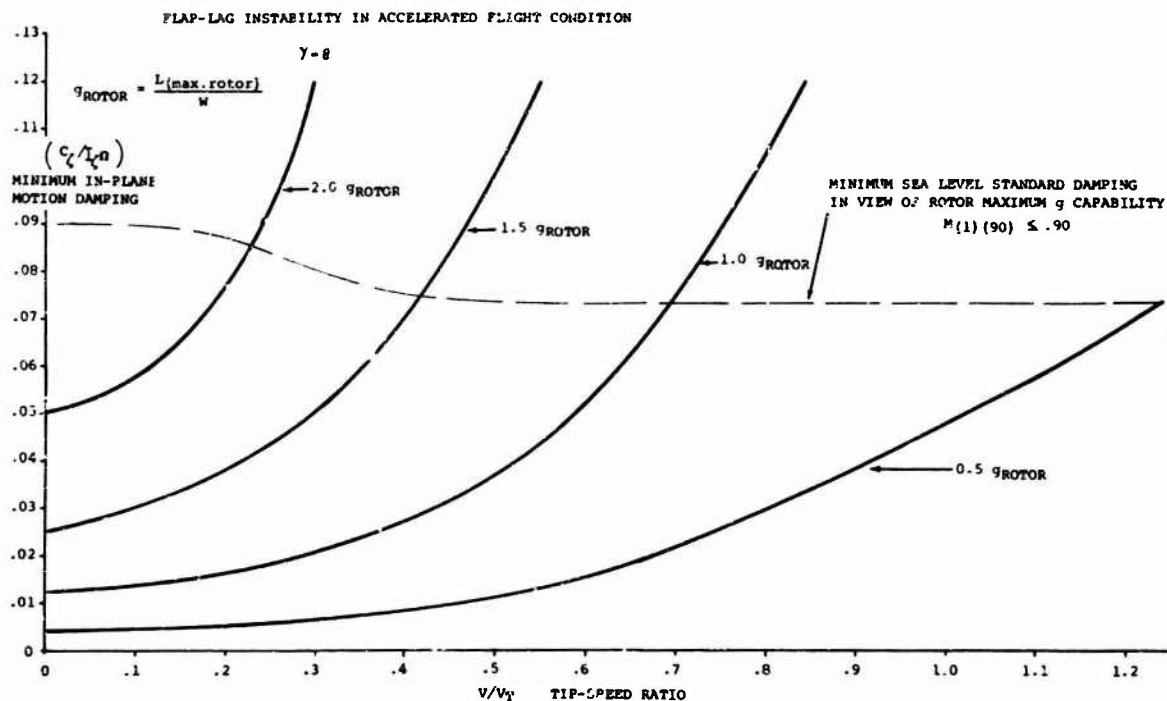


Fig. 37 Minimum in-plane motion damping required versus tip-speed ratio for several rotor g levels

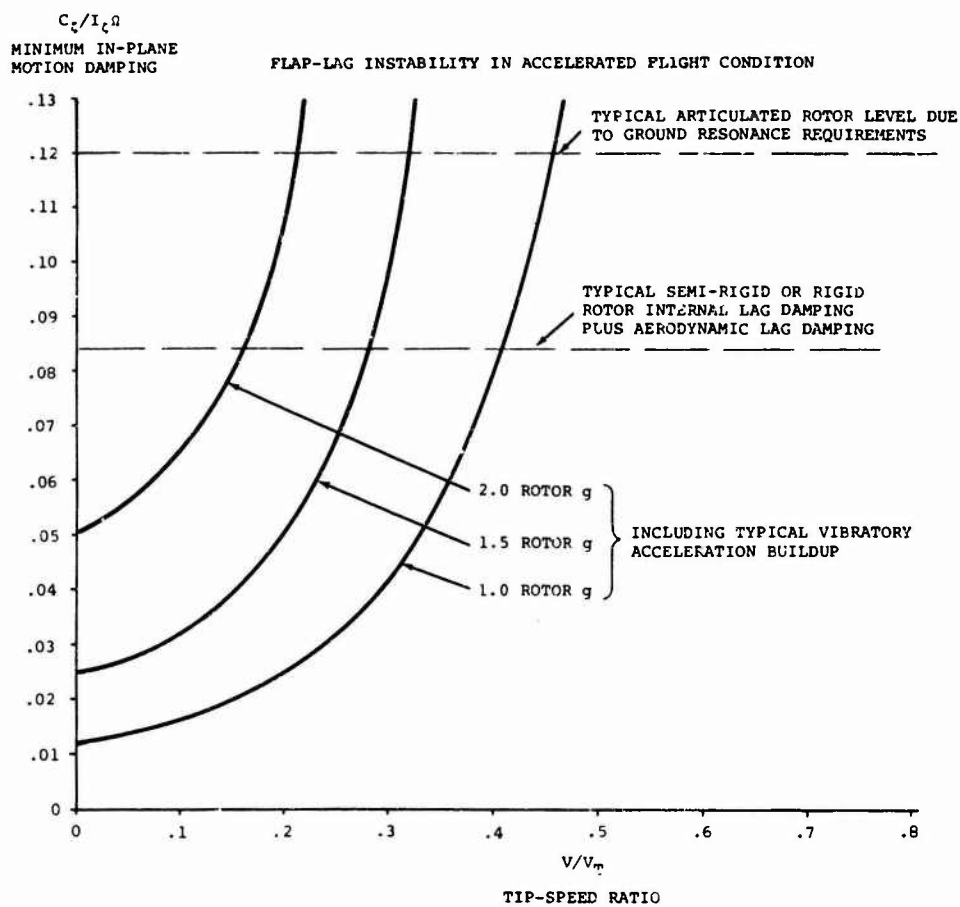


Fig. 38 Minimum in-plane motion damping required versus tip-speed ratio in presence of rotor vibratory loads

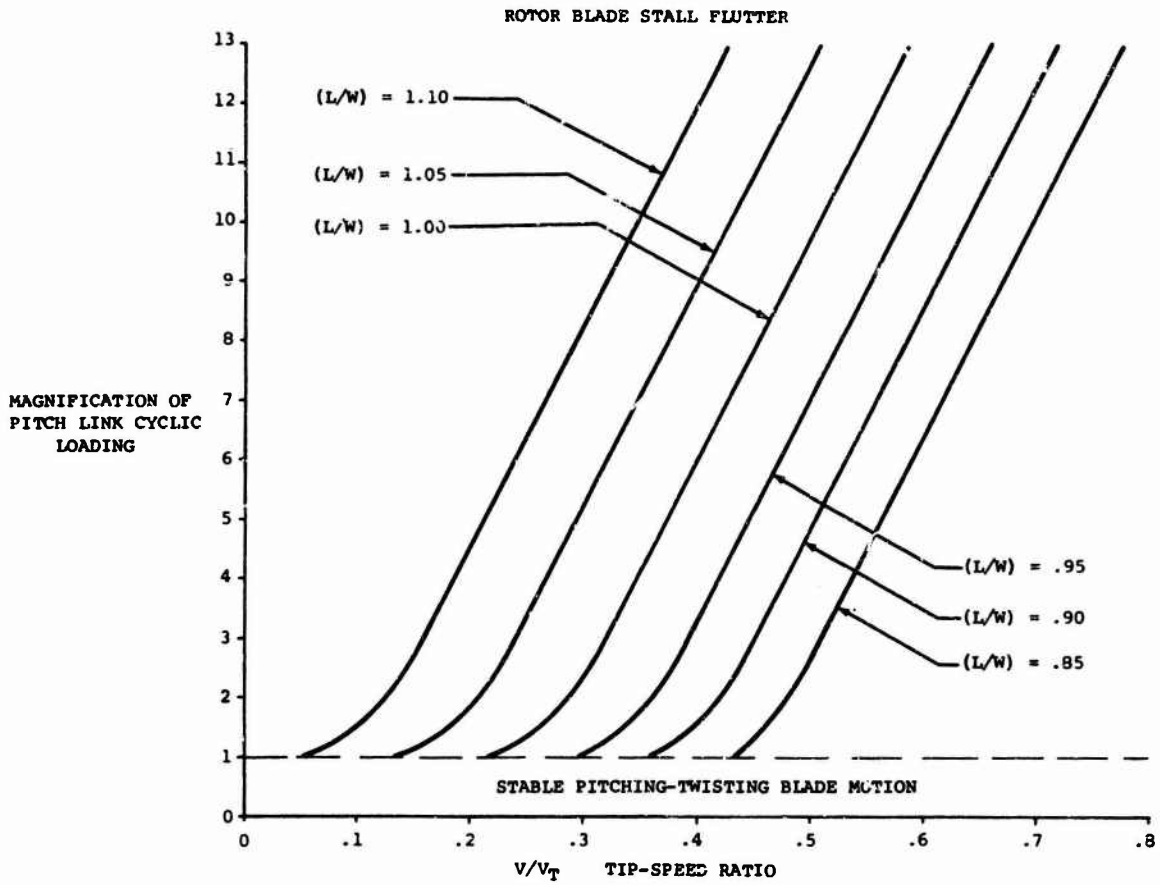


Fig. 39 Magnification of pitch link cyclic loading at various rotor lift to design gross weight ratios

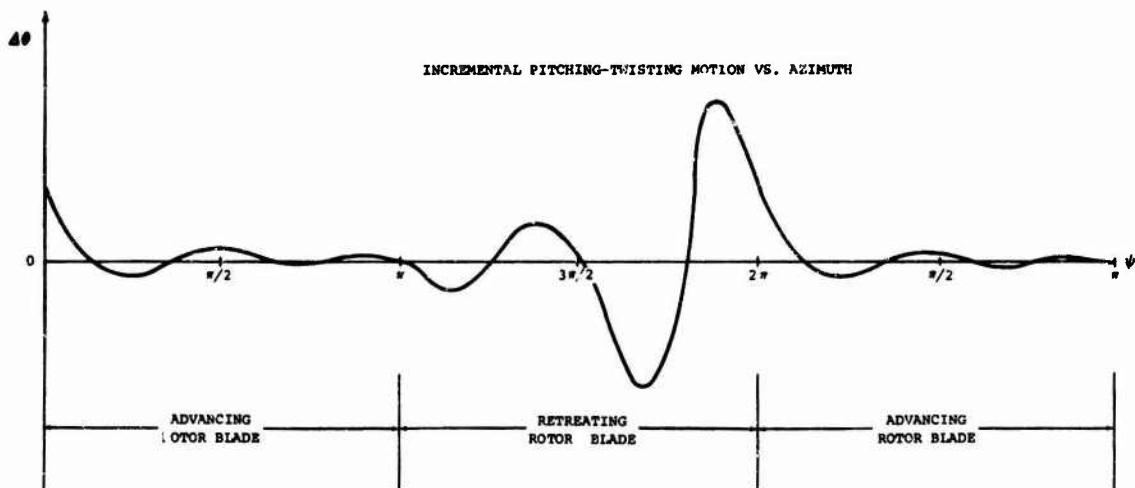


Fig. 40 "Stall Flutter": Typical rotor blade periodic pitching-torsion instability



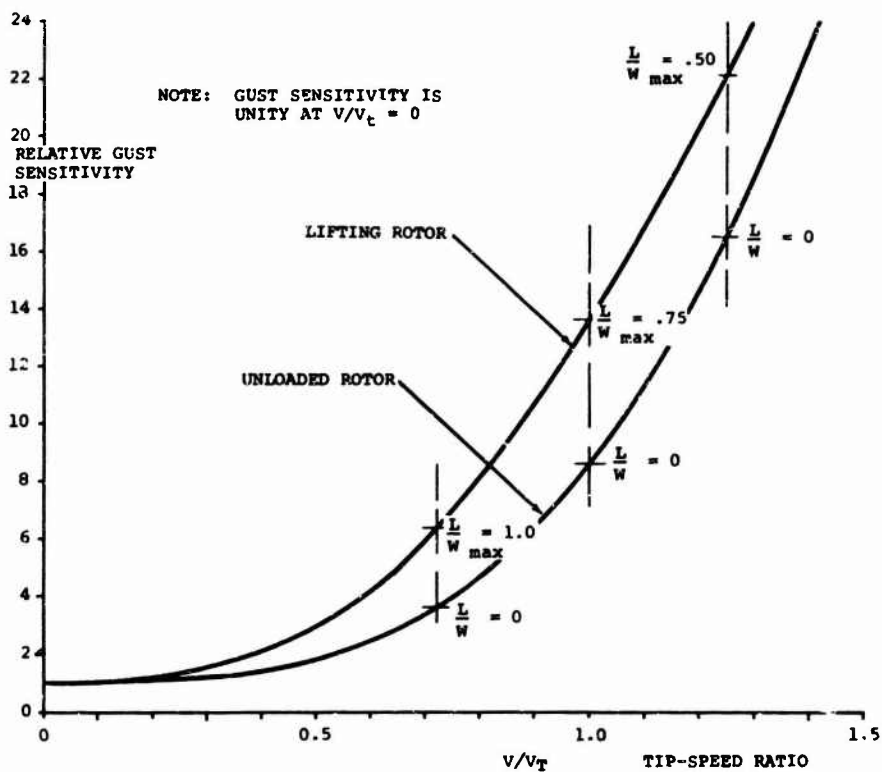


Fig.41 Rotor blade transient flapping: relative gust sensitivity versus tip speed ratio

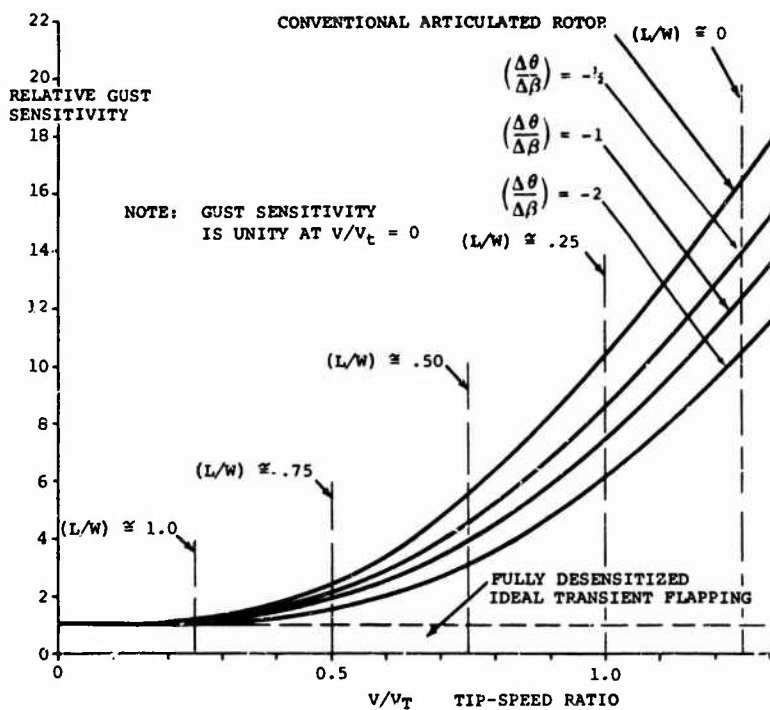


Fig.42 Rotor blade transient flapping: relative gust sensitivity with cyclic pitch-flapping displacement feedback control

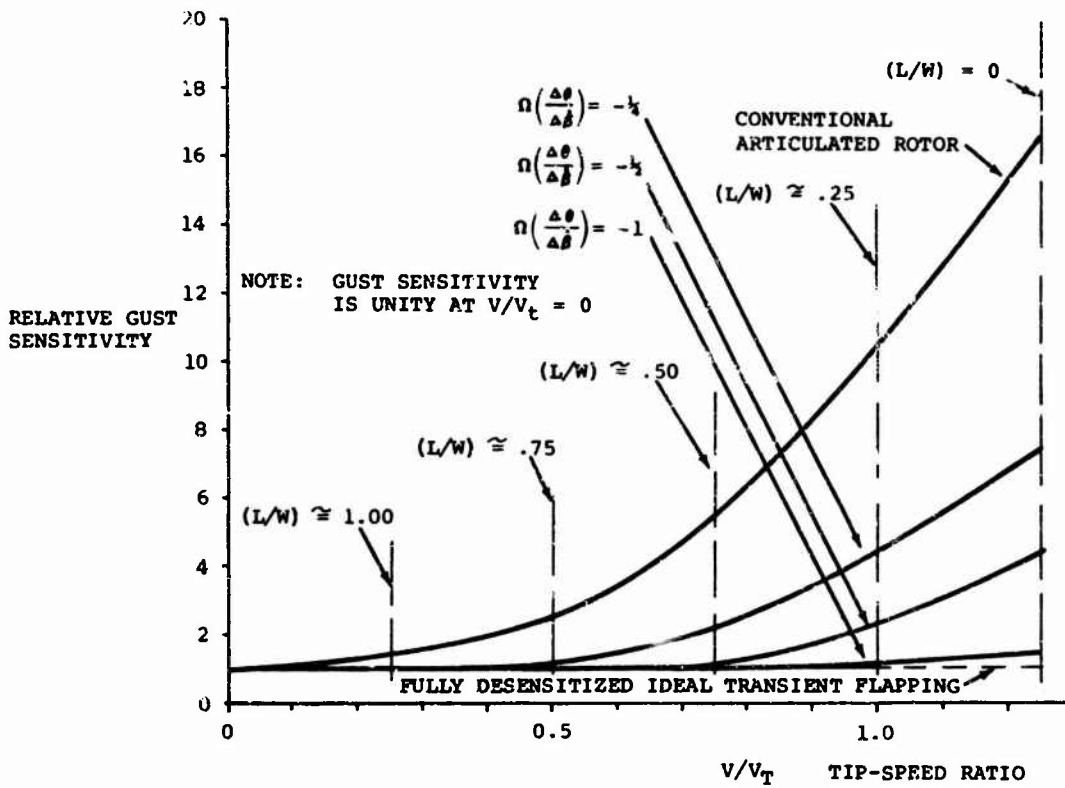


Fig. 43 Rotor blade transient flapping: relative gust sensitivity with cyclic pitch-flapping rate feedback control

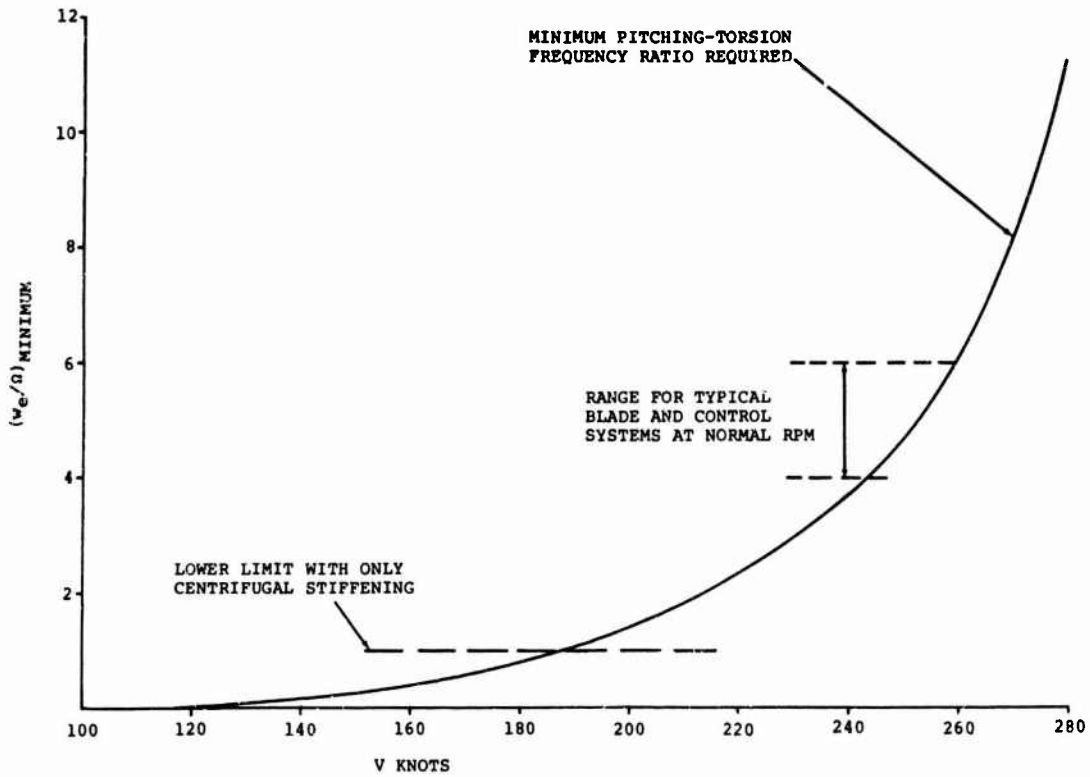


Fig. 44 Reversed flow flapping-torsion flutter boundary for a typical rotor blade

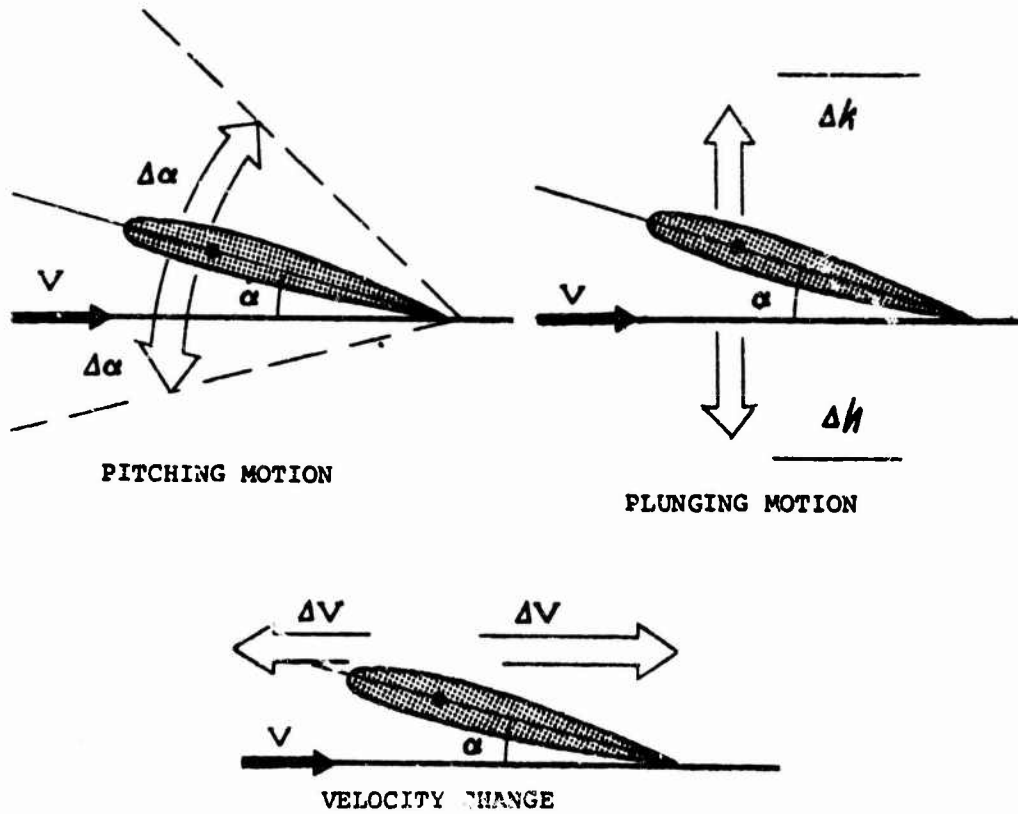


Fig. 45 Helicopter blade motions

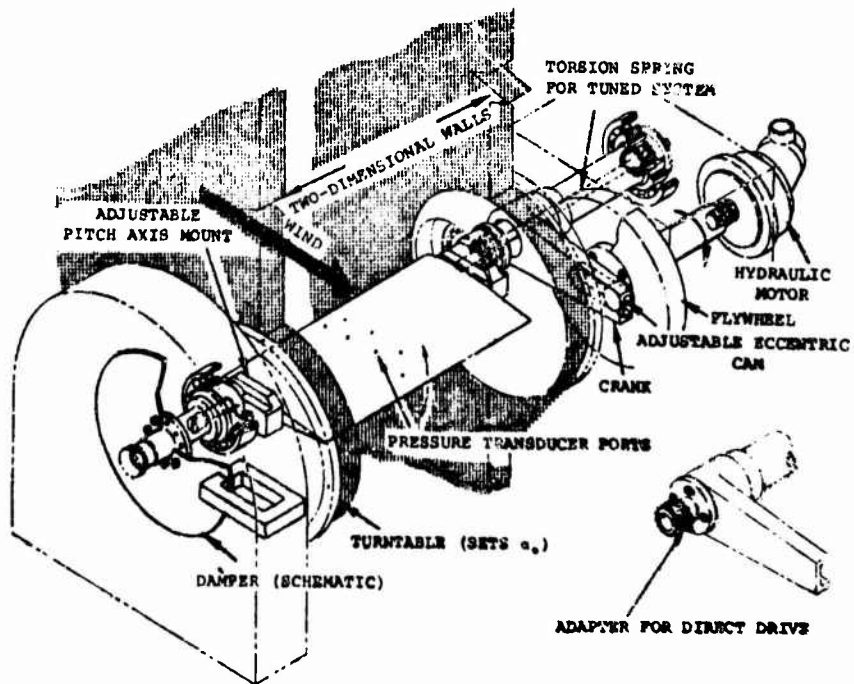


Fig. 46 Pitch oscillating mechanism

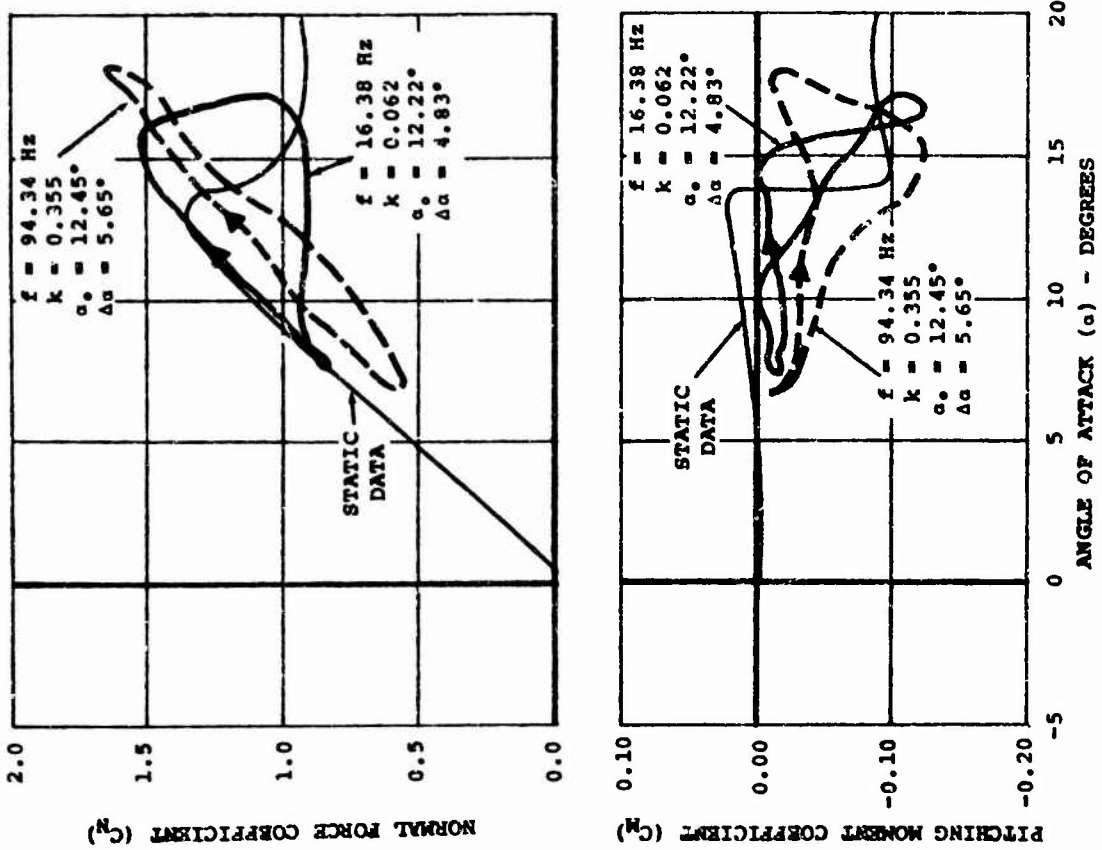


Fig. 48 Effect of frequency

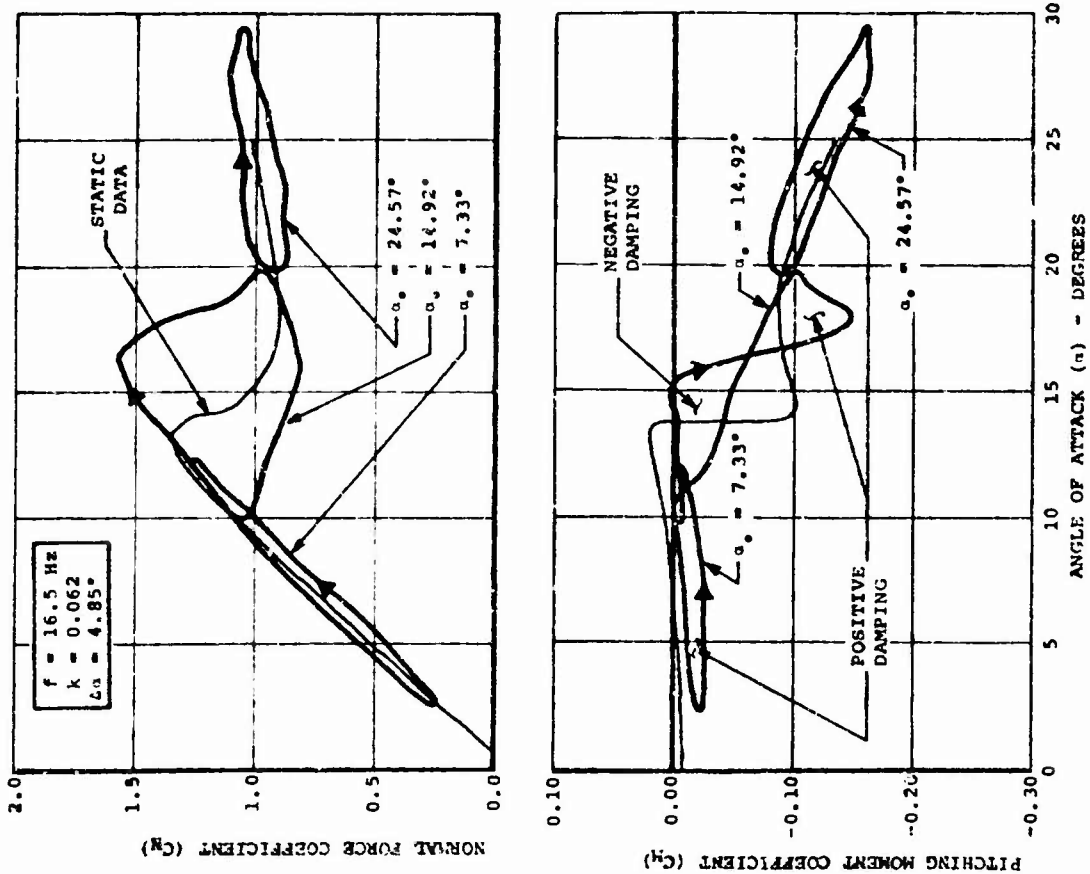


Fig. 47 Typical pitch oscillation data

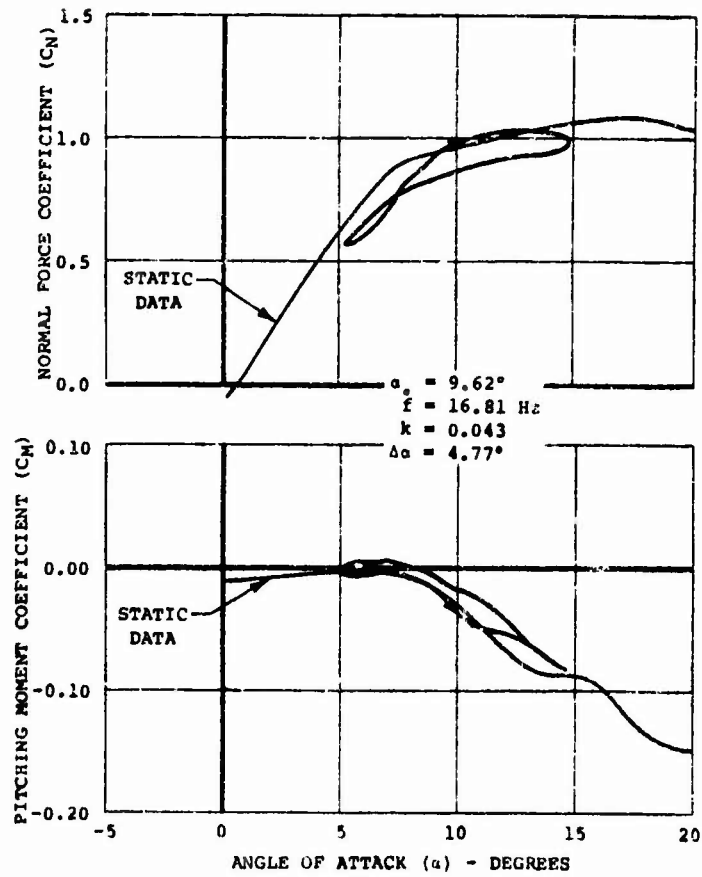
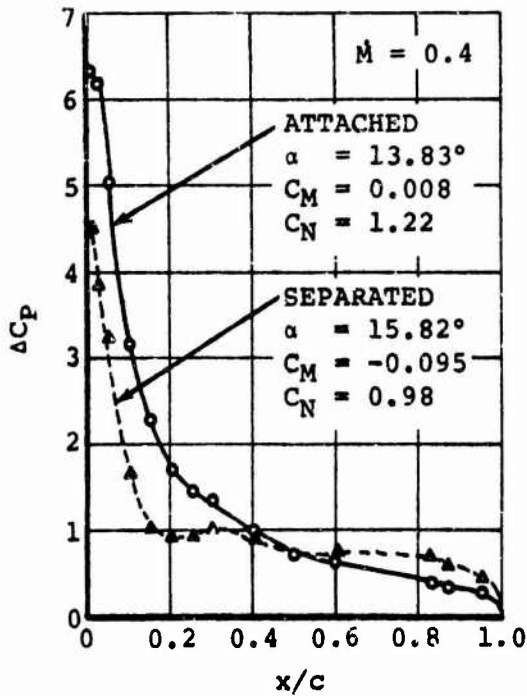


Fig.49 Effect of Mach number



NOTE: VERTOL 23010-1.58 AIRFOIL

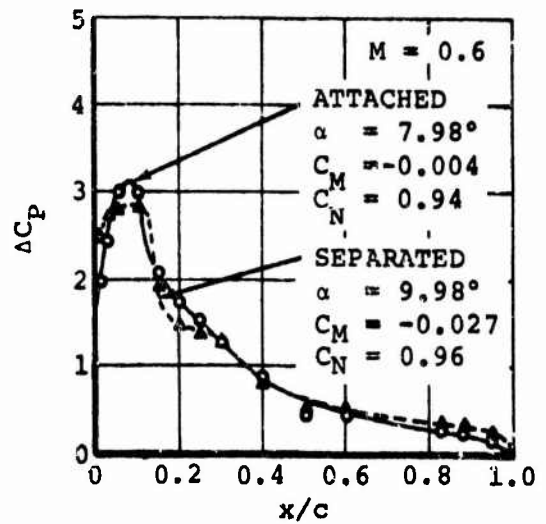


Fig.50 Effect of Mach number on the loading distributions

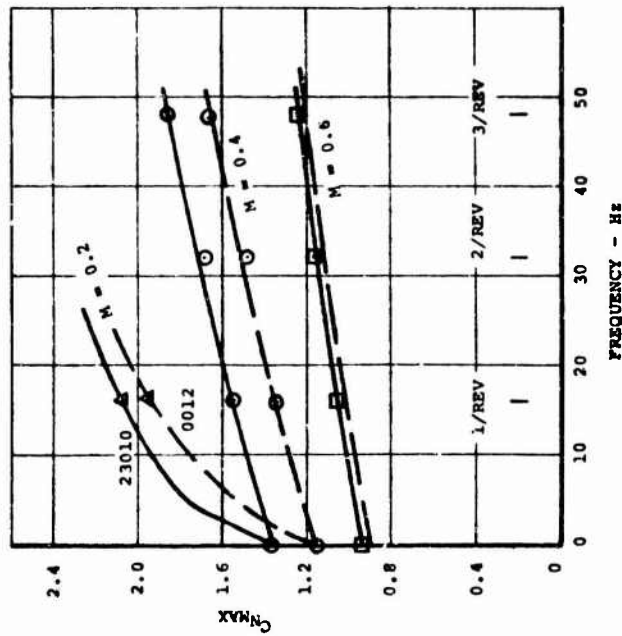


Fig. 51 Summary of  $C_{nmax}$  for pitching

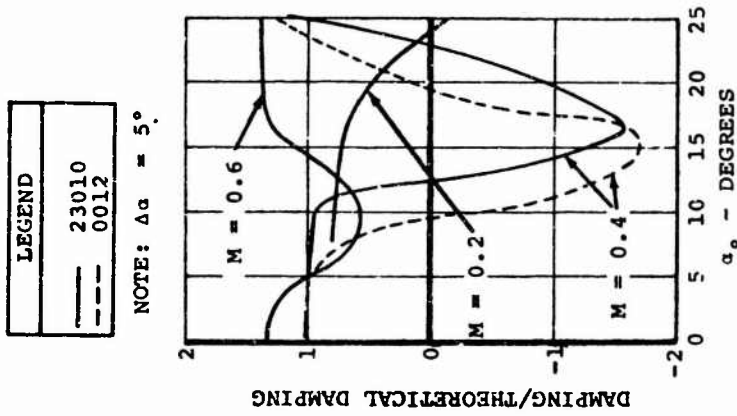
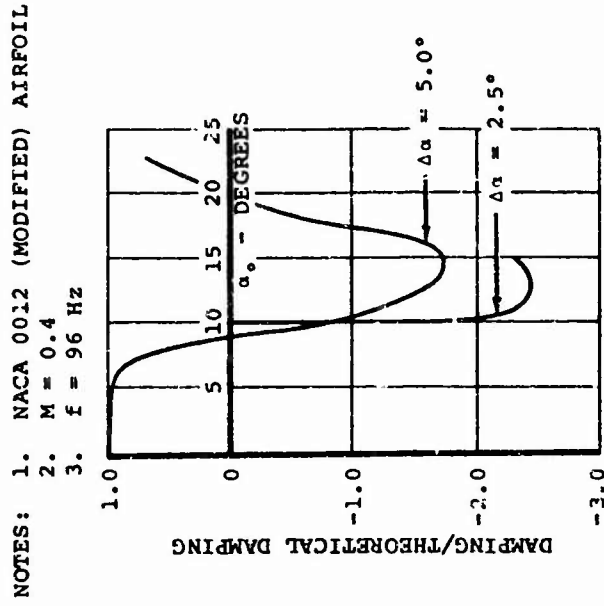


Fig. 52 Summary of pitch damping



NOTES: 1. NACA 0012 (MODIFIED) AIRFOIL  
 2.  $M = 0.4$   
 3.  $f = 96$  Hz

Fig. 53 Effect of oscillation amplitude

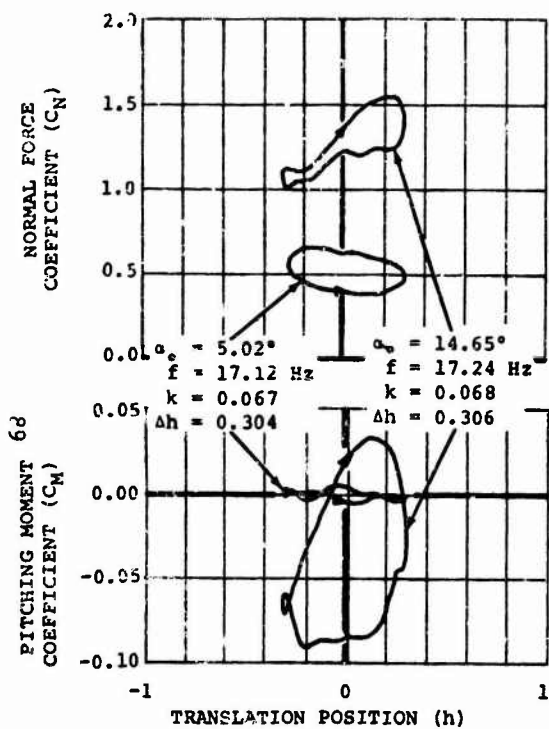


Fig. 54 Typical vertical translation data

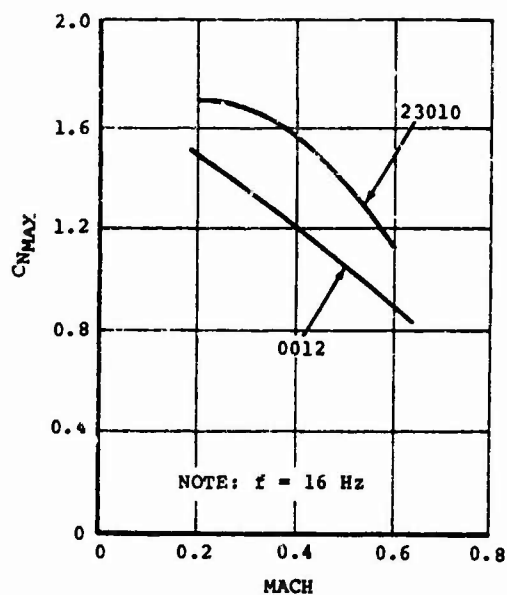


Fig. 55 Summary of  $C_{Nmax}$  in plunge

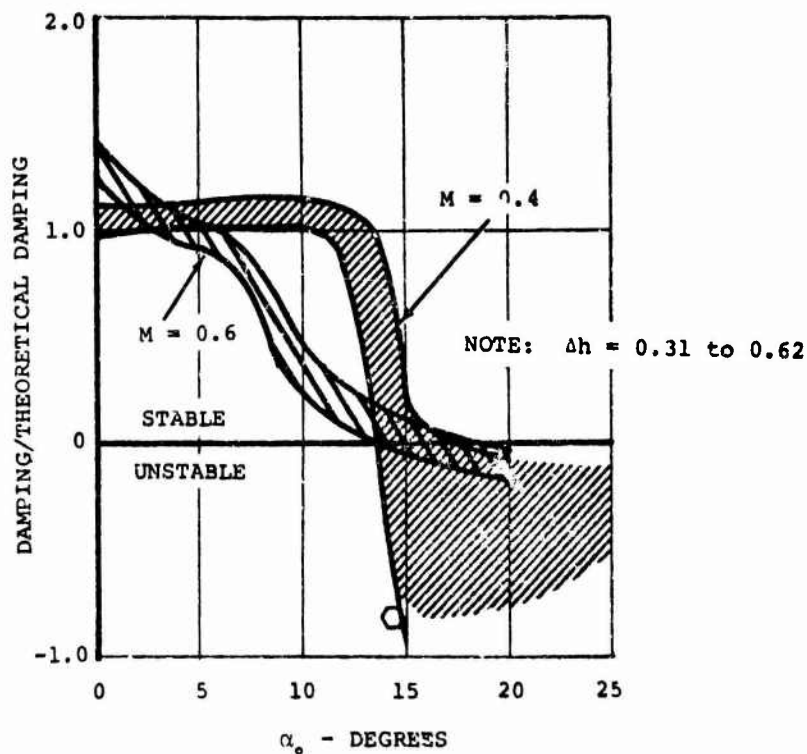


Fig. 56 Summary of damping data in vertical translation

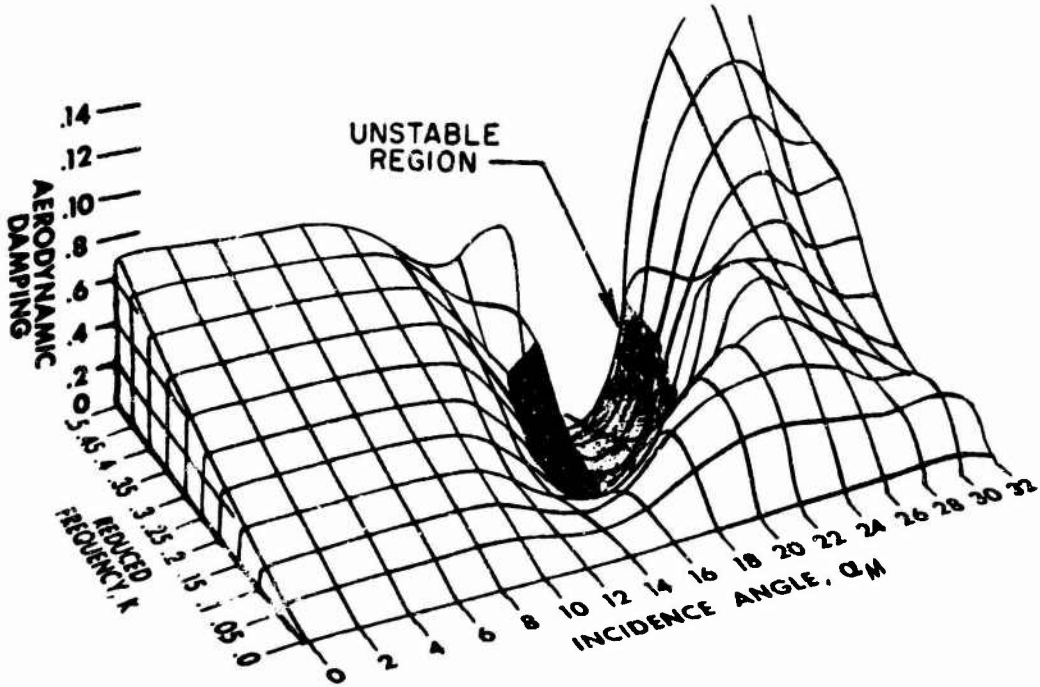


Fig. 57 Two-dimensional aerodynamic damping surface

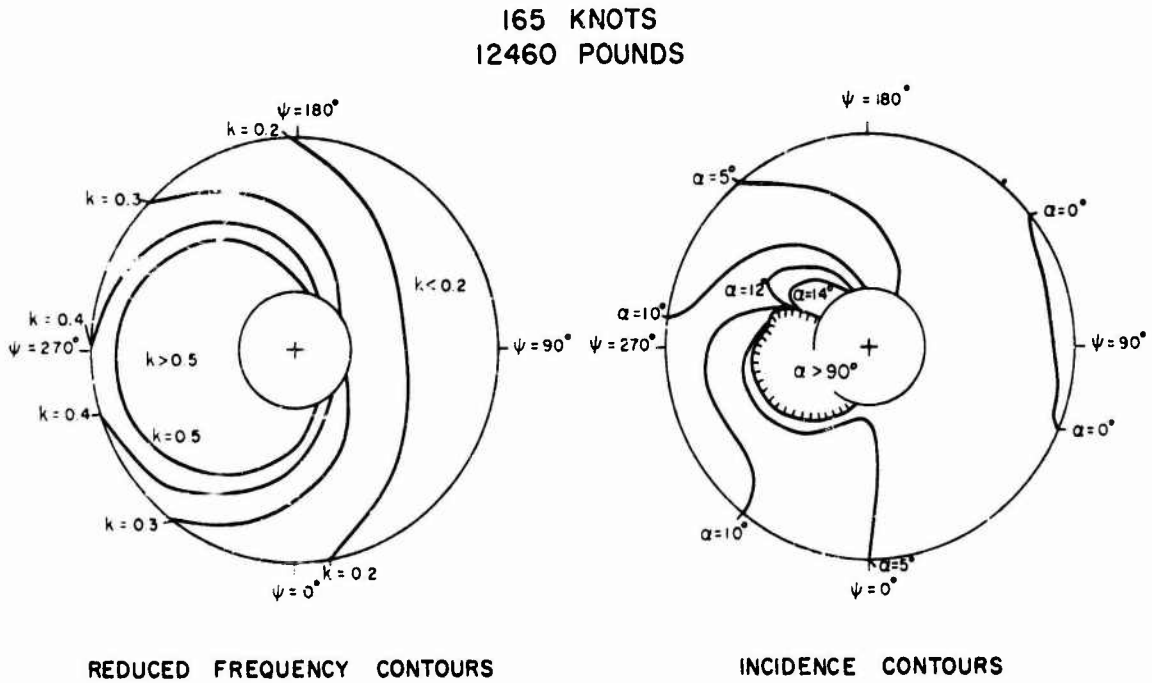
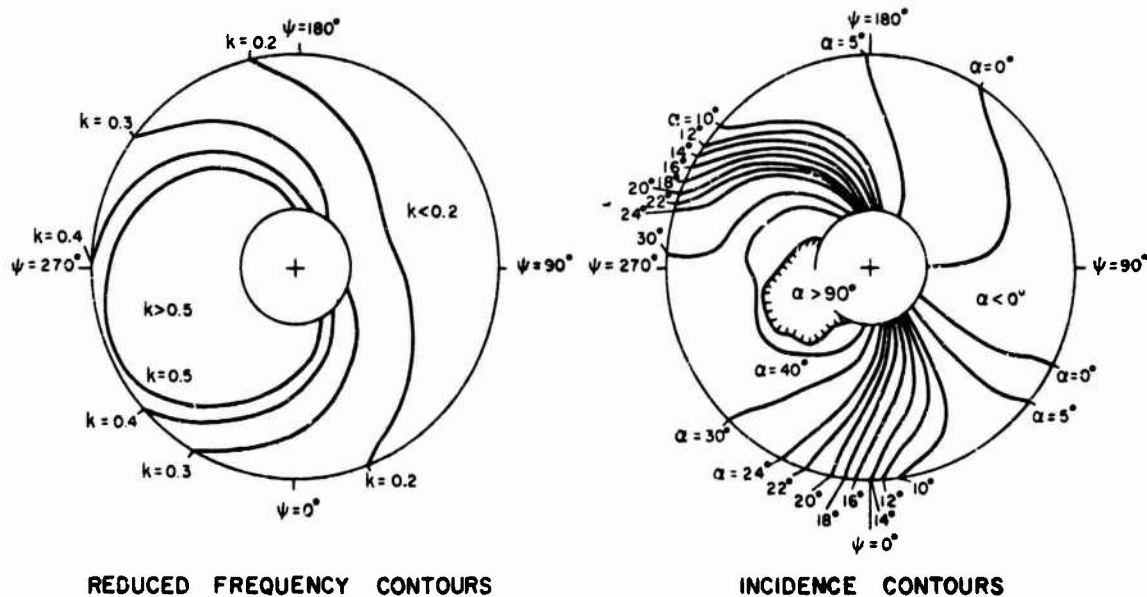


Fig. 58 Polar plots of reduced frequency contours and incidence contours for S-61F rotor



210 KNOTS  
16280 POUNDS



REDUCED FREQUENCY CONTOURS

INCIDENCE CONTOURS

Fig. 59 Polar plots of reduced frequency contours and incidence contours for S-61F rotor

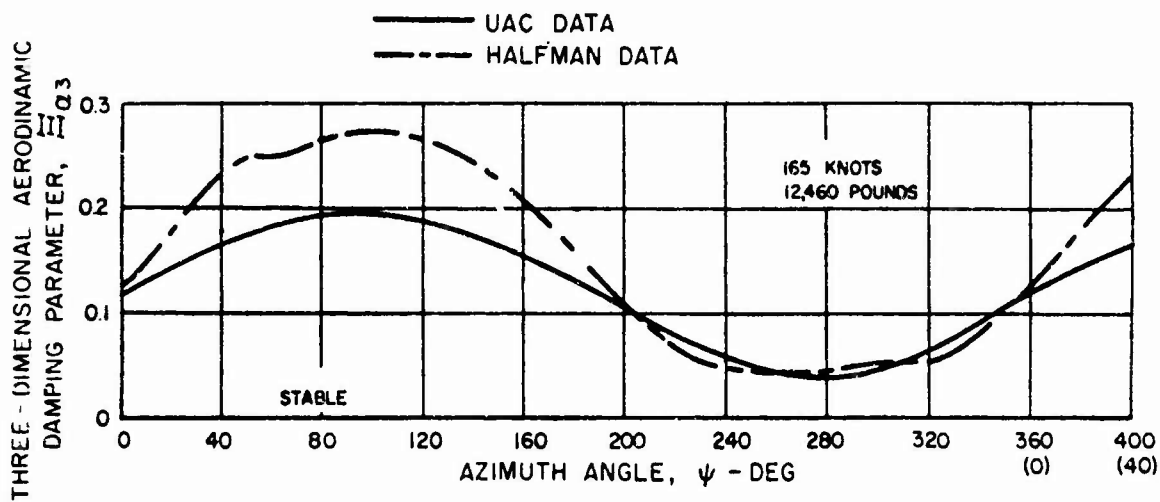


Fig. 60 Variation of aerodynamic damping with azimuth for a lightly loaded S-61F rotor blade

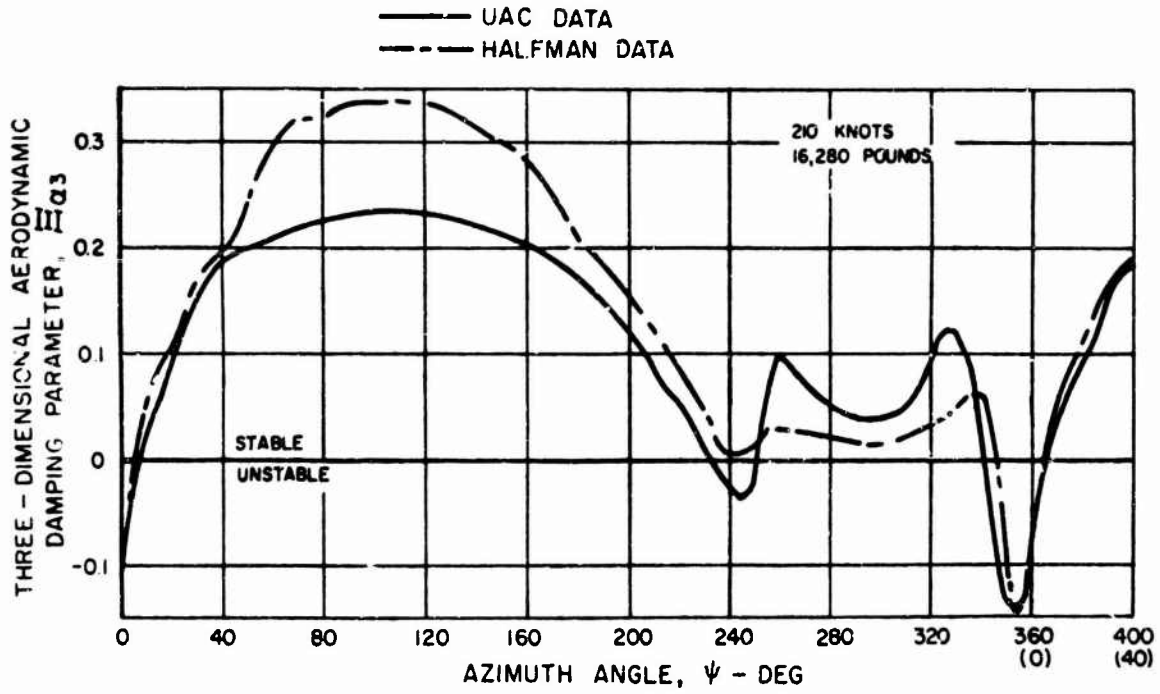


Fig. 61 Variation of aerodynamic damping with azimuth for a heavily loaded S-61F rotor blade

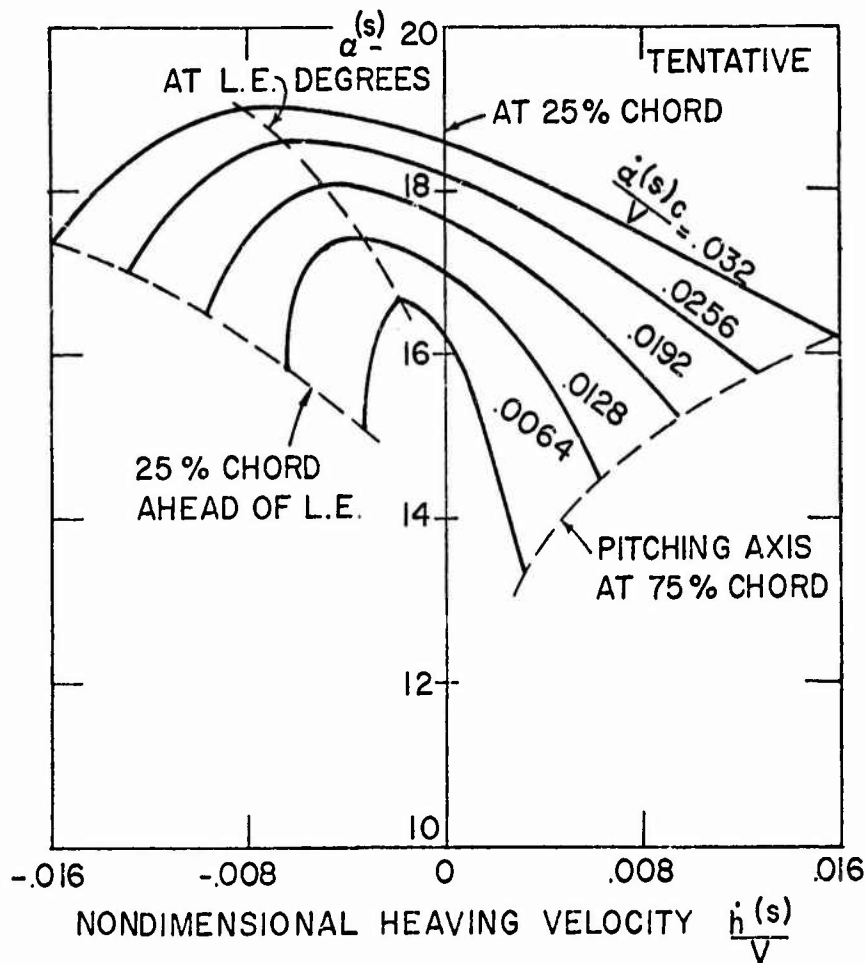


Fig. 62 Effect of pitching and heaving velocity on dynamic stall angle of attack

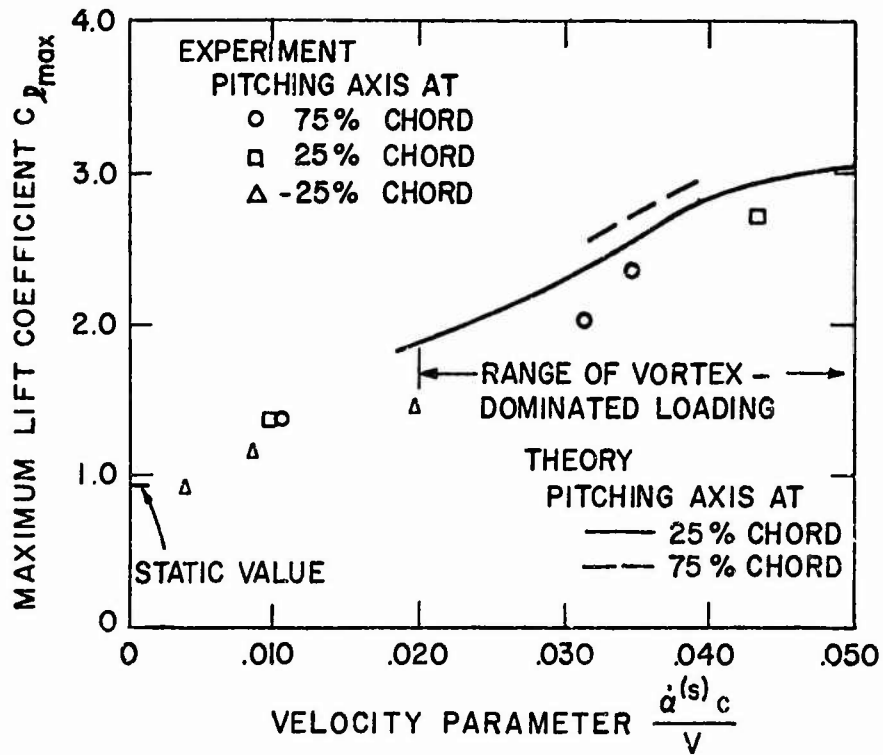


Fig. 63 Maximum lift coefficient versus velocity parameter

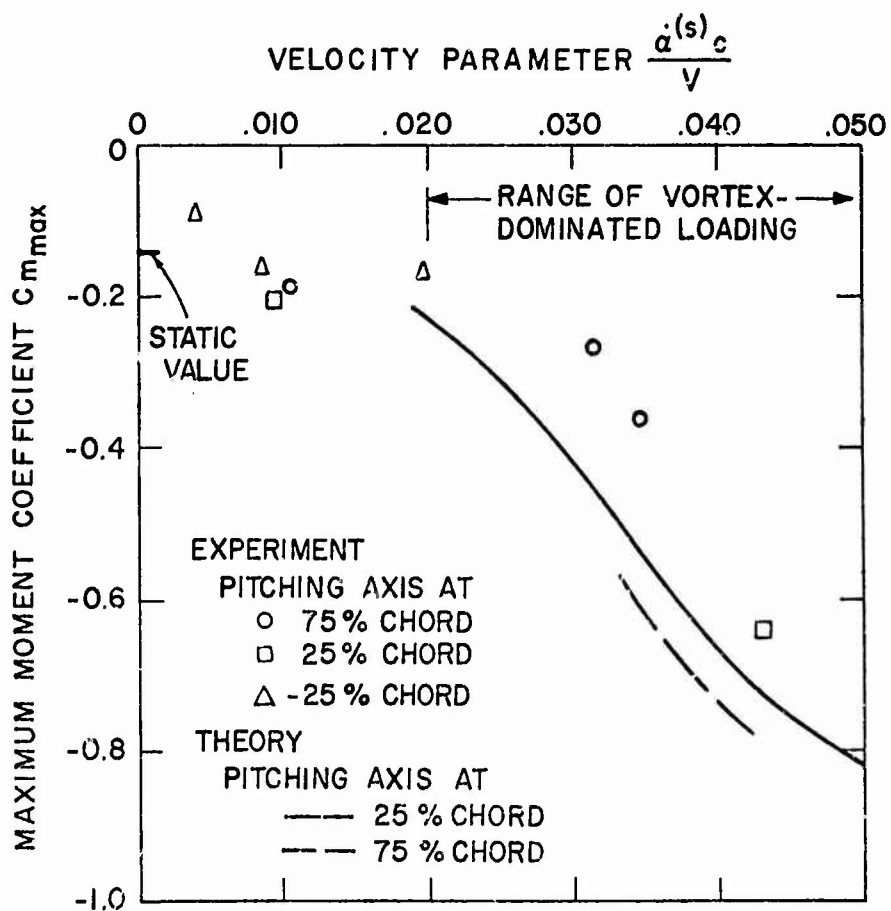


Fig. 64 Maximum moment coefficient versus velocity parameter

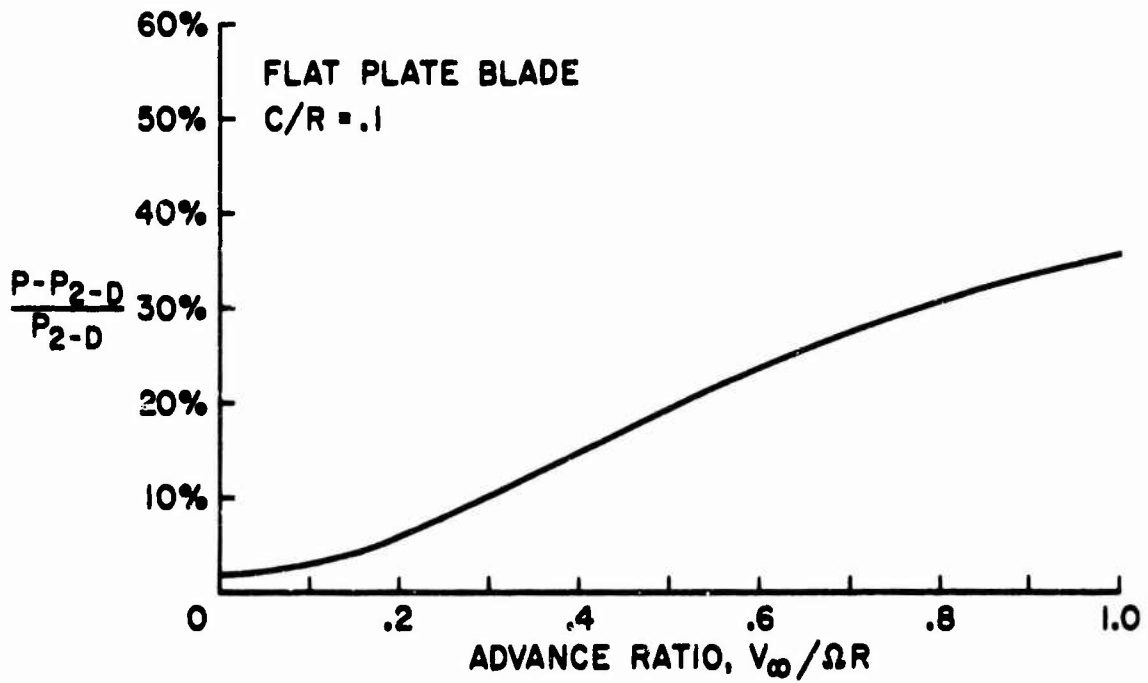


Fig.65 Effect of three-dimensional flow on power required to overcome skin friction drag

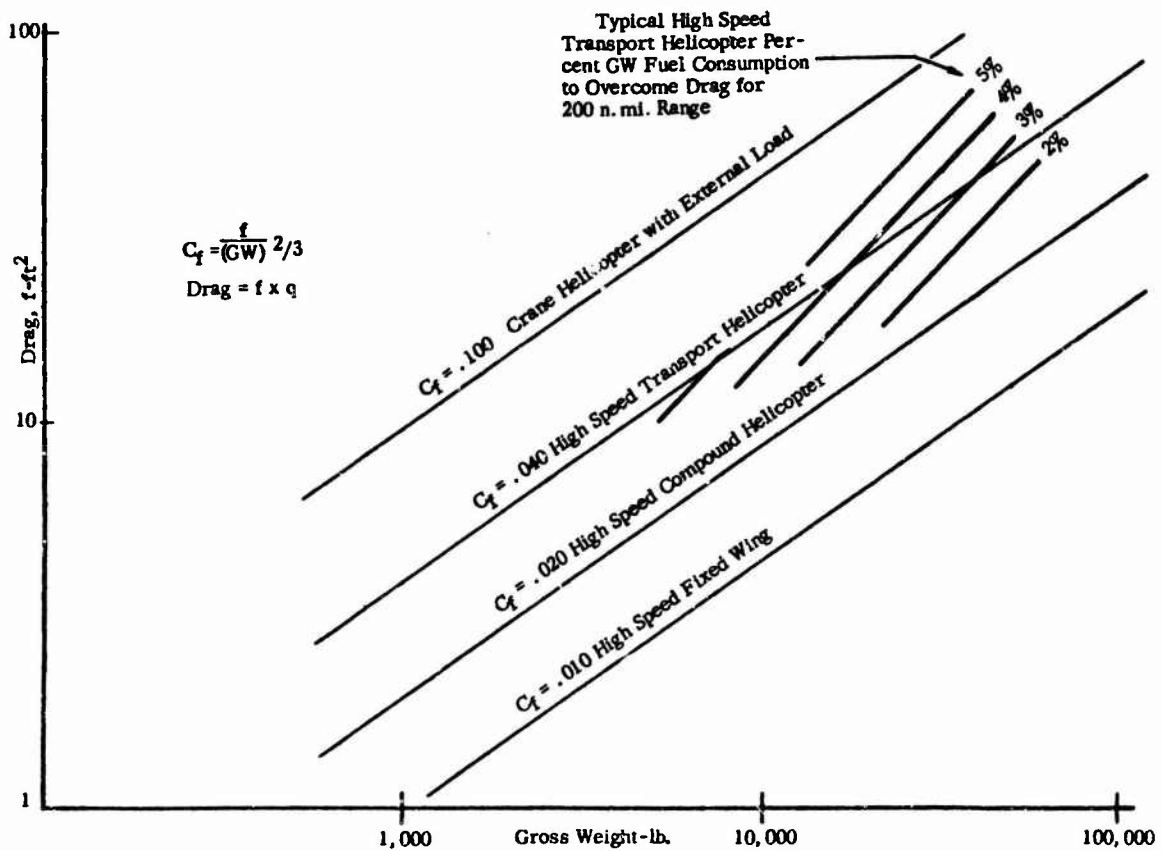


Fig.66 Parasite drag versus gross weight

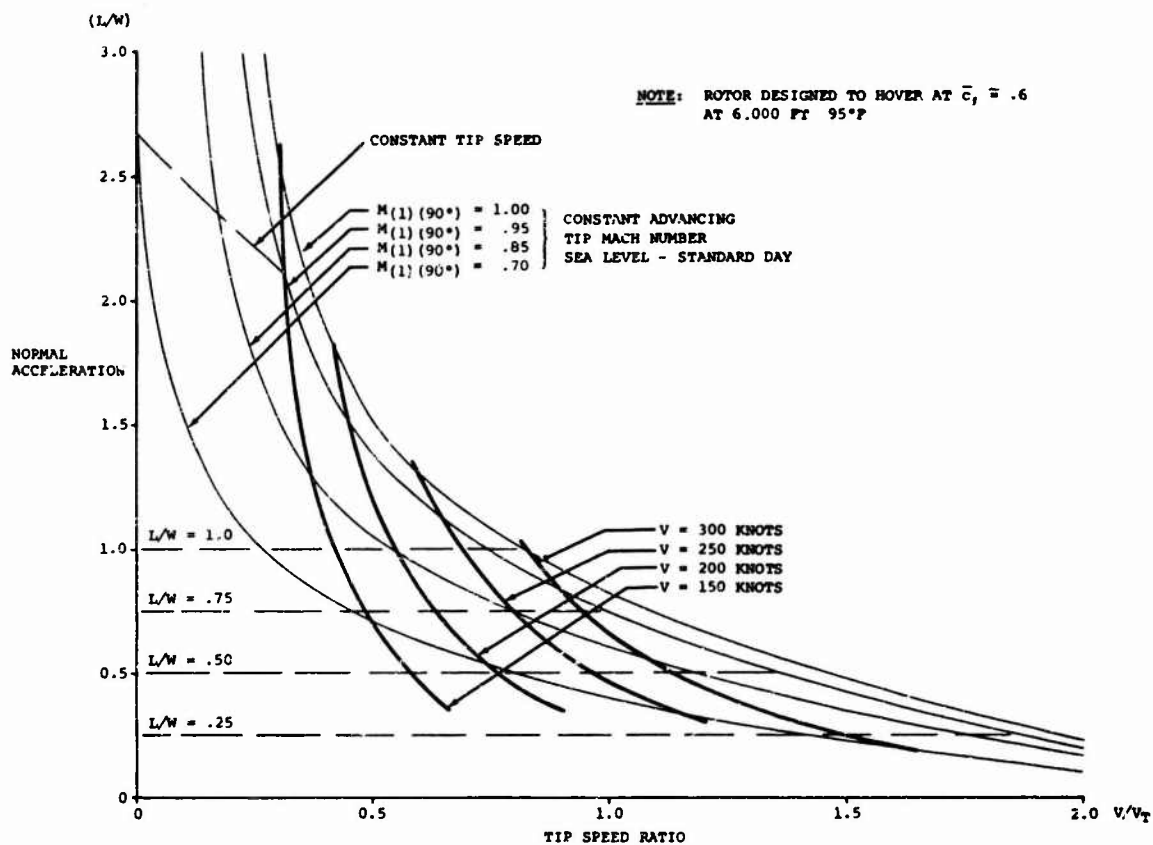


Fig. 67 Maximum rotor normal-acceleration capability versus tip speed ratio

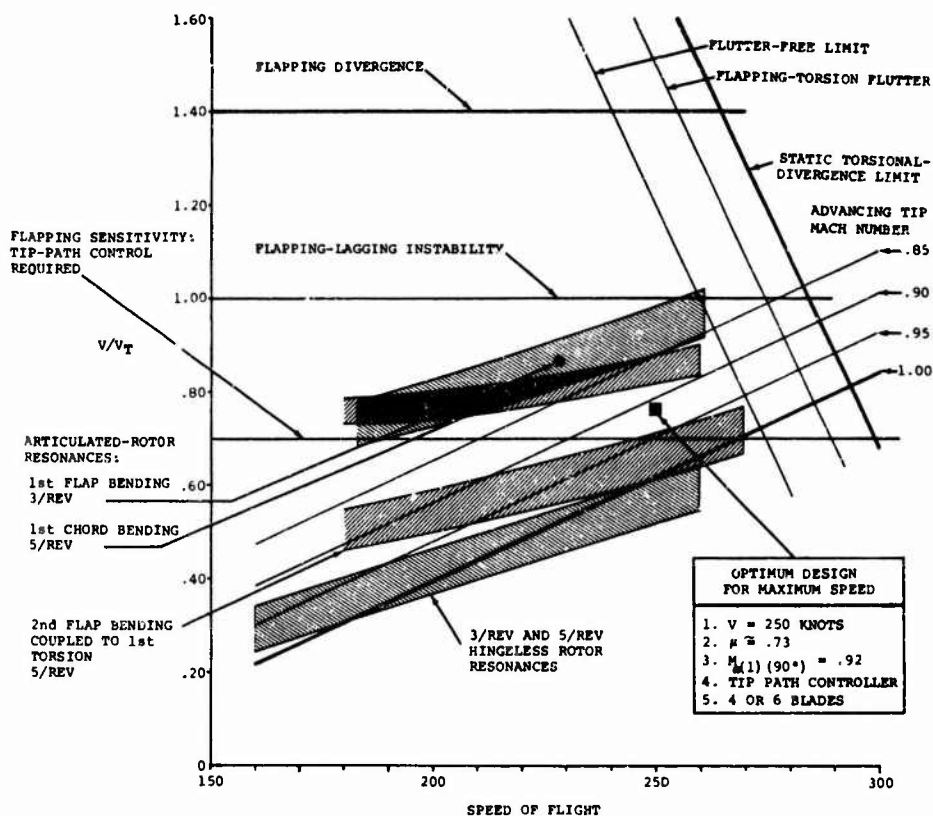


Fig. 68 Unloaded-rotor operating limits

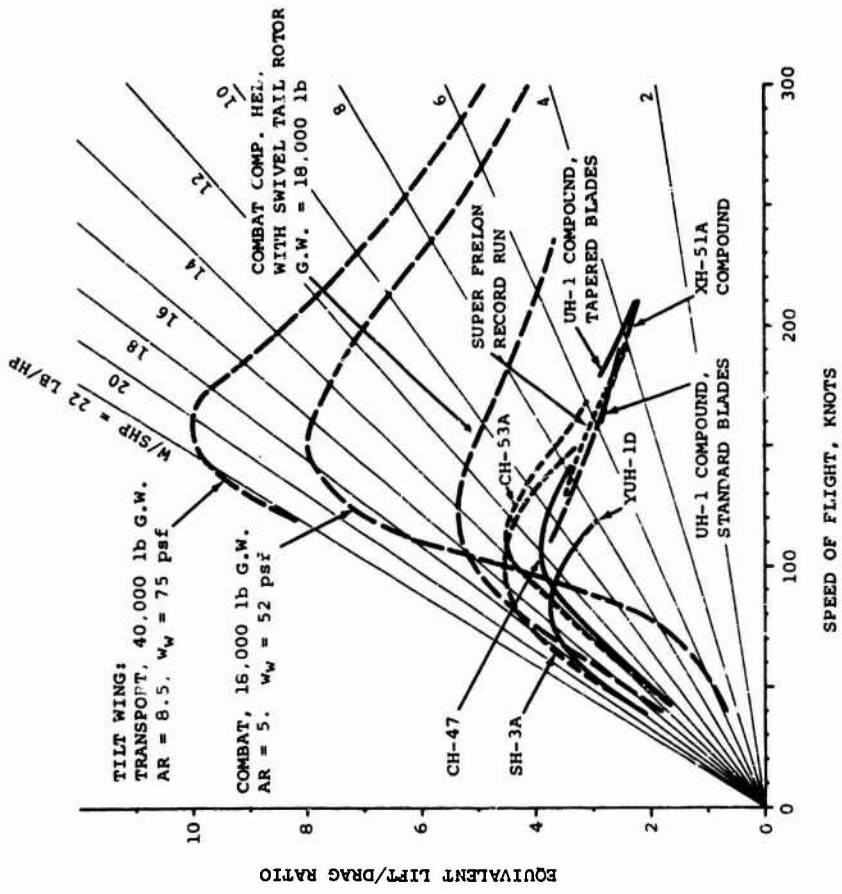


Fig. 70 Equivalent lift-to-drag ratios of rotary and tilt wing aircraft

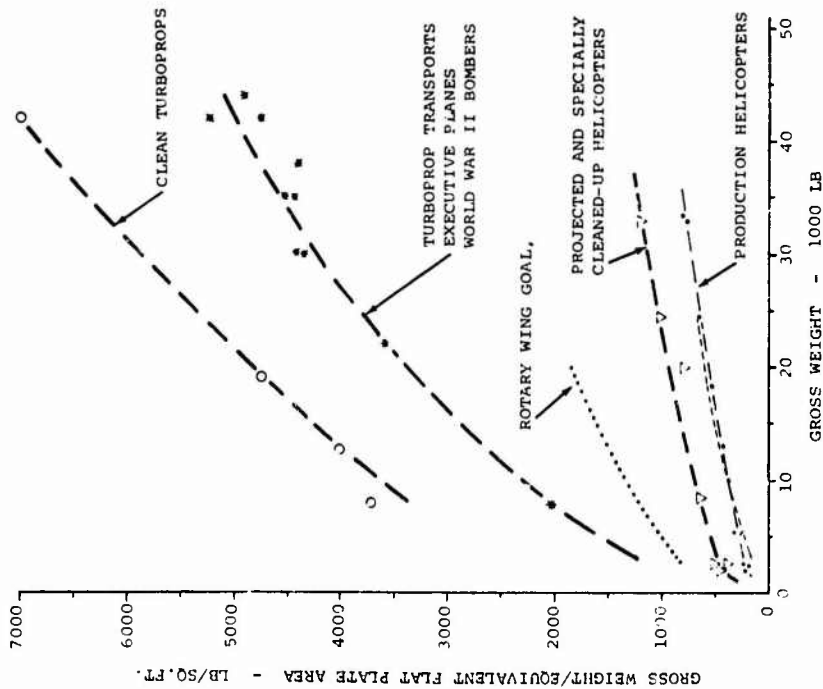


Fig. 69 Trends with gross weight of equivalent flat plate area loading of helicopters (hubs included) and fixed wing aircraft (profile drag of wings and empennages excluded)

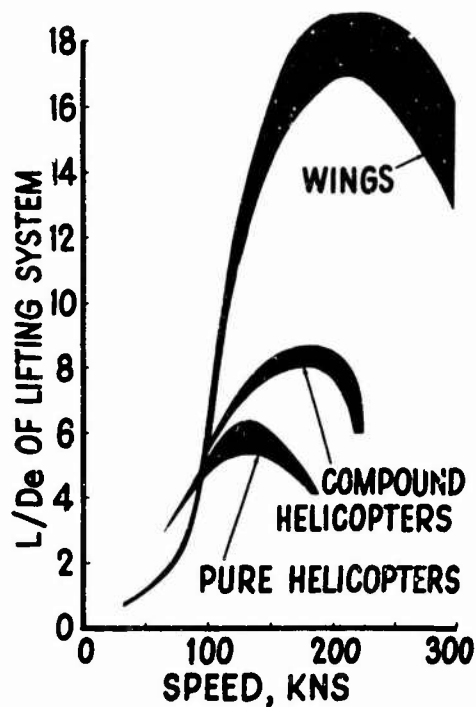


Fig. 71  $L/D_e$  of lifting system versus speed at S.L.

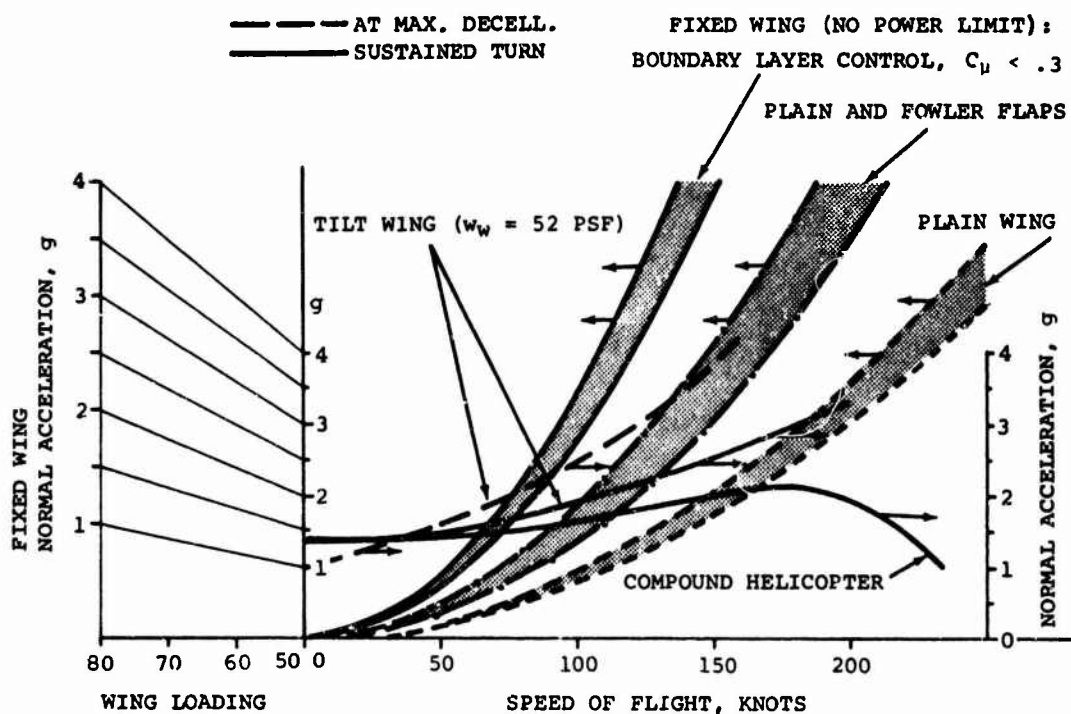


Fig. 72 Normal acceleration capabilities of fixed wing versus speed and examples of normal acceleration for tilt wing and compound helicopter

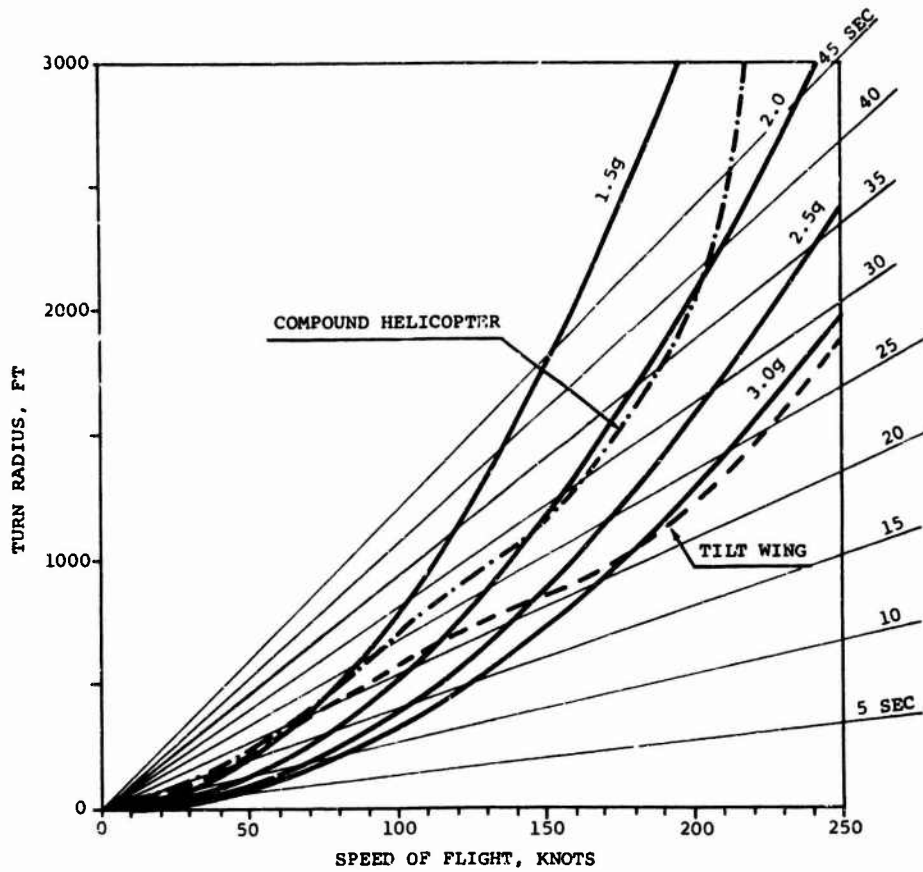


Fig. 73 Radius and time of 360° sustained turn at various normal acceleration levels versus speed of flight

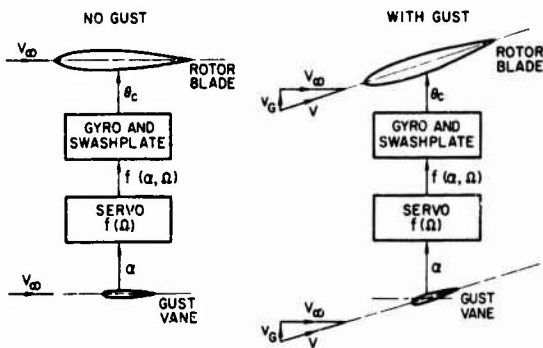


Fig. 74 Aerodynamic vane and gyro control system

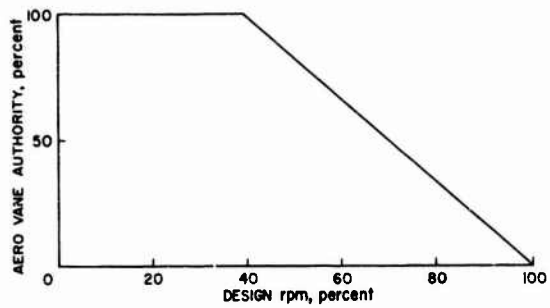


Fig. 75 Schedule for aero vane control system authority



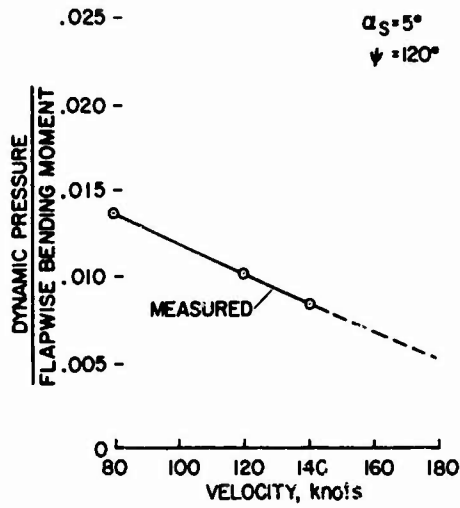


Fig. 76 Typical determination of blade divergence speed

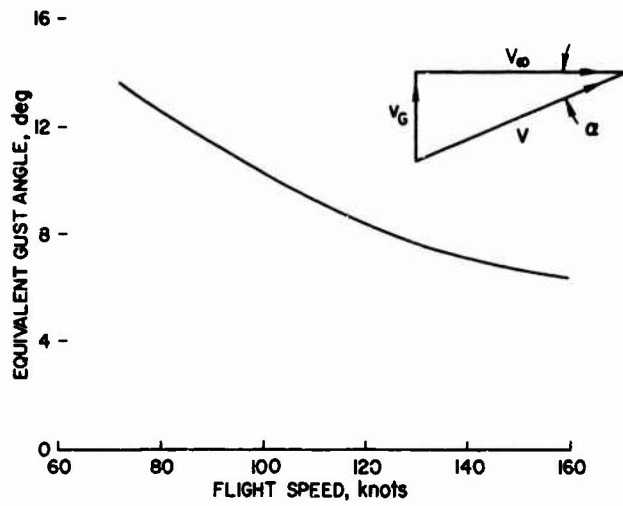


Fig. 77 Equivalent angle of attack due to a 30ft per second gust

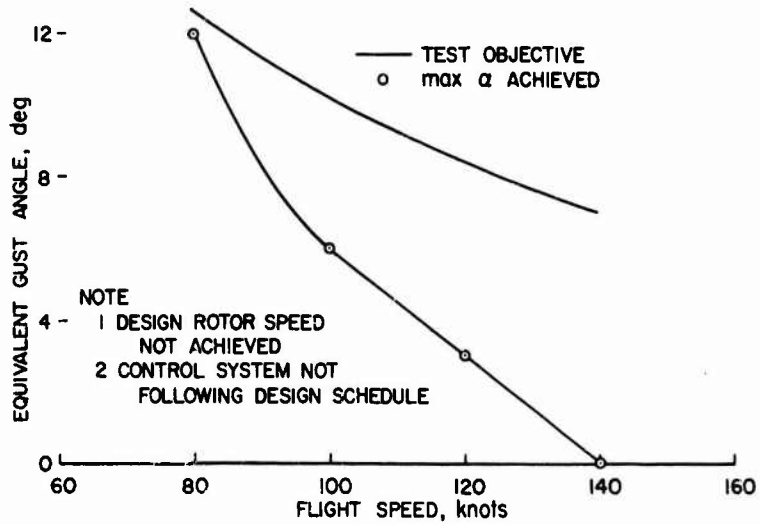


Fig. 78 Rotor start and stops conducted during second tests of Lockheed rotor

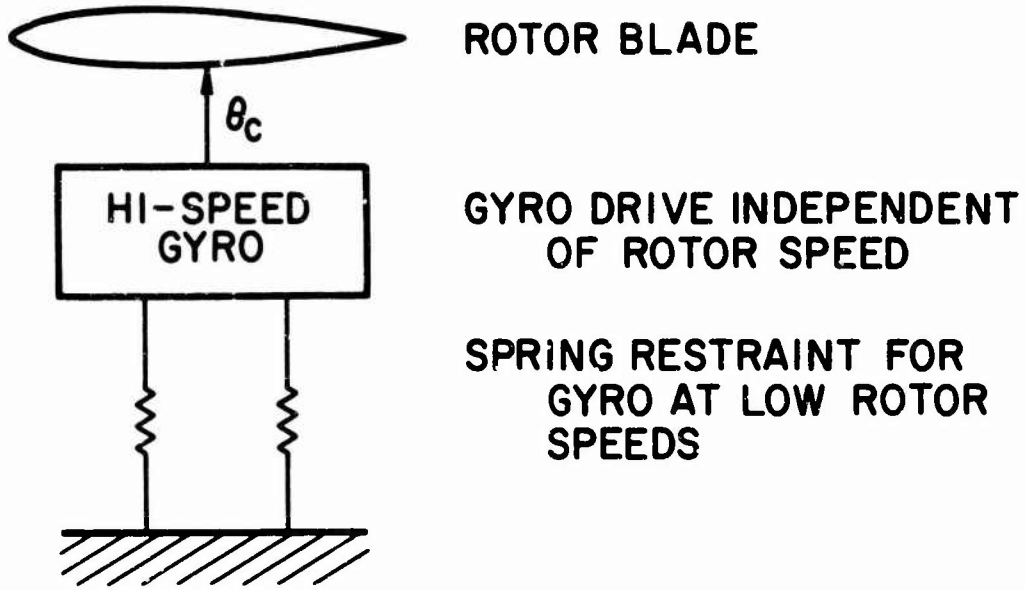


Fig. 79 High-speed gyro control system concept

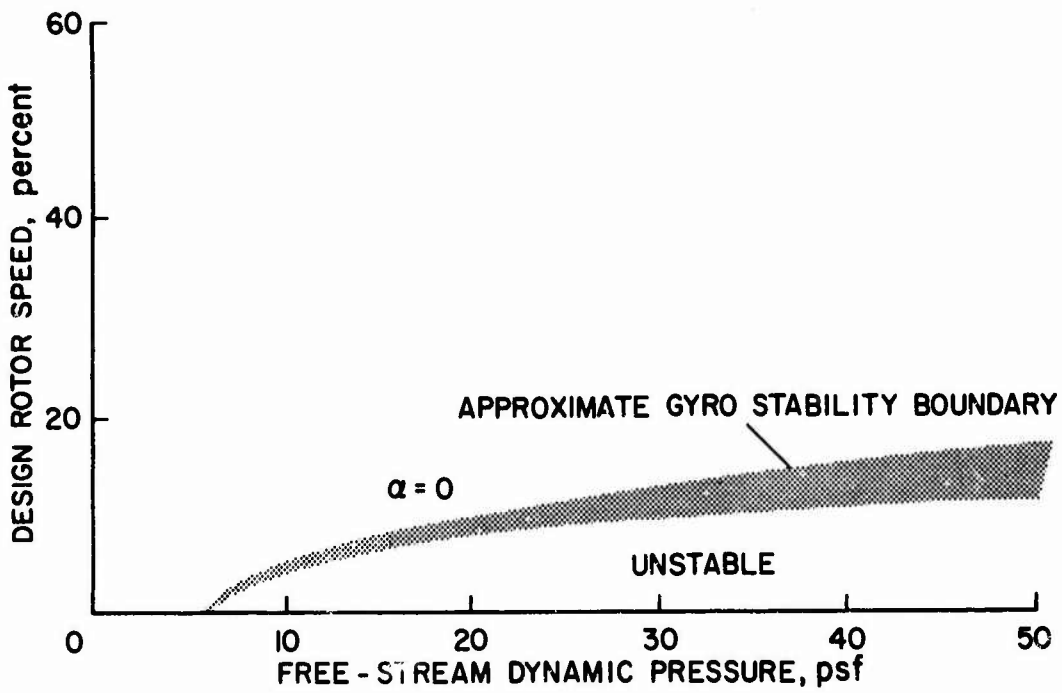


Fig. 80 Results of high-speed gyro stability study

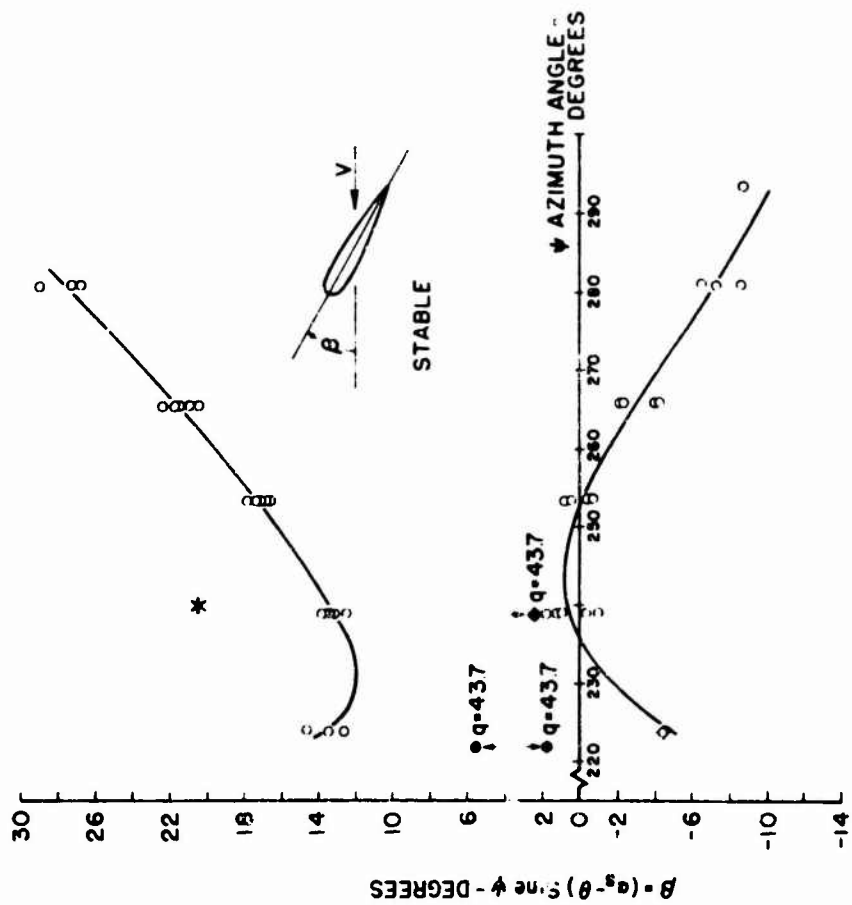


Fig. 82 Composite stability boundaries

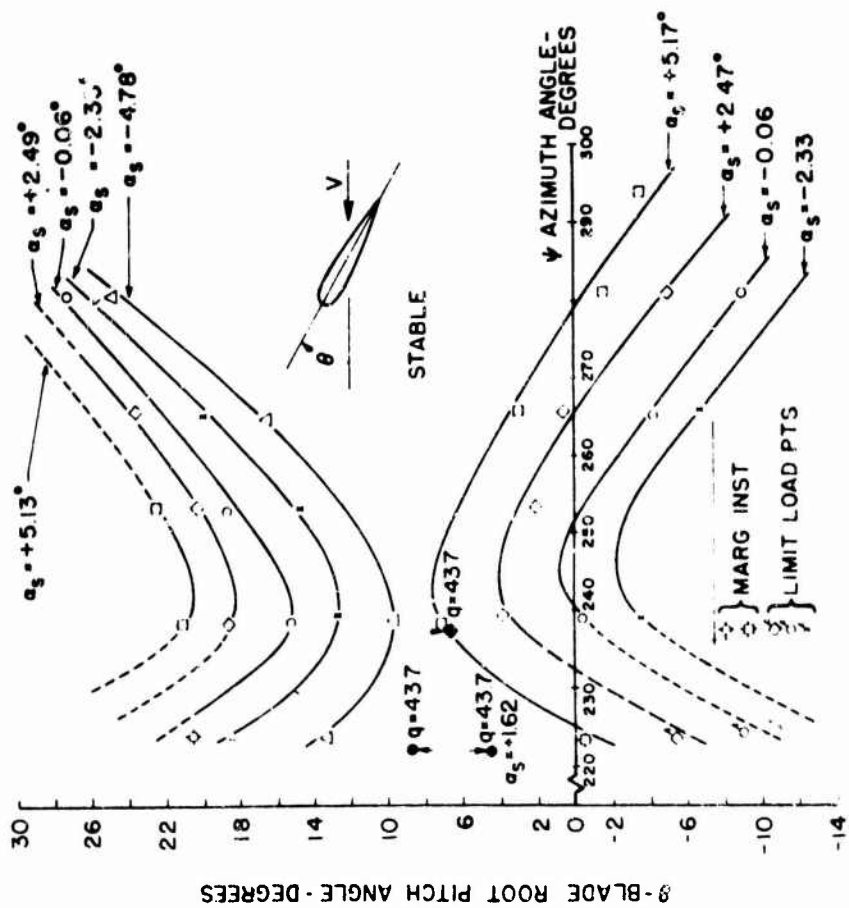


Fig. 81 Stability boundaries

PAPER C

BASIC AERODYNAMICS OF CONVERTIBLE  
ROTOR/PROPELLER AIRCRAFT

IN 4 CHAPTERS

by

W.Z. Stepniewski

The Boeing Company  
Vertol Division

## PREFACE

These lecture notes were prepared with the intent to permit the reader to go somewhat beyond the material that can actually be presented during the short time allocated for the class sessions. The subjects discussed here were selected and presented in such a way as to help the reader to better understand the aerodynamic aspects of design and operation of V/STOL configurations belonging to the Convertible Rotor/Propeller family of aircraft.

Because of that emphasis on understanding, physical aspects of the discussed aerodynamic phenomena were strongly underlined, while mathematical presentation tended toward an illustration of the relative importance of various parameters, rather than giving more rigorous methods for the determination of the actual quantities. However, wherever available, those more rigorous methods are referenced in the text.

The whole subject matter is broken down into four chapters: Chapter I very briefly reviews basic concepts of Convertible Rotor Propeller Aircraft; Chapter II discusses hovering and vertical climb phenomena; Chapter III deals with some problems of forward flight which appear to be of particular importance to the considered family of aircraft, and finally, in Chapter IV, some aspects of operation in the STOL mode of the considered VTOL aircraft are discussed.

With reference to the adjective "Preliminary" appearing on the preprint of this paper, the reader must realize that they were prepared on a few weeks' notice, mostly from the material that was immediately available under the form of my various already existing scribbles, works of my colleagues from the company, some inputs of my friends from NASA Langley and Ames and reports and books that happened to be in my private library.

In that race against the deadline, I got able assistance from my associates to all of whom I wish to express my sincere gratitude. In particular, I wish to thank Mr C.Kalmbach for his help in numerical computations and checking the formulae. To Mr Craig Smith for his help in editing the text, arranging for artists' drawings, etc. However, my special thanks are due to Mrs Wanda Metz, my secretary, who somehow was able to decipher my hastily scribbled notes, transfer them into a typed text, type all formulae and properly arrange the text, formulae and figures into a presentable whole. Finally, I wish to express my indebtedness to Mr R.W.Tharrington, General Manager, and Mr L.L.Douglas, Assistant General Manager, New Products, of the Vertol Division of The Boeing Company for permission to take an active part in the VKI-AGARD lecture series, and company support for my participation and the preparation of these notes.

W.Z.Stepniewski

## CHAPTER I

INTRODUCTION TO BASIC CONCEPTS OF  
CONVERTIBLE ROTOR/PROPELLER AIRCRAFT

## 1.1 WHY CONVERTIBLE ROTOR/PROPELLER AIRCRAFT?

Because of a relatively high specific impulse of airscrews (rotors and propellers) under static conditions (Figure 1-1), it may be expected that aircraft incorporating vertical thrust generators of this type will tend to find an application to the missions stressing requirements for long periods of hovering and near-hovering flight. Furthermore, relatively low downwash velocities associated with rotors and propellers (abscissa in Figure 1-1) will make those aircraft especially suitable for operations from unprepared sites and under all other conditions where high downwash velocities cannot be tolerated. Finally, it appears that (at least at present and in the near future) noise (at the same static thrust) of both rotors and propellers can be kept at a considerably lower level than that of the thrust generators based on the jet principle.

Thus, acoustic characteristics favor airscrew type vertical thrust generators for such military missions as ASW, etc., and civilian operations close to the population centers (Figure 1-2 from Reference 1-1).

It is a truism that as far as hovering and near-hovering regimes of flight are concerned, the helicopter represents the most efficient configuration, both aerodynamically and operationally.

However, in forward flight, overall efficiency of the helicopter is poor by comparison with that of fixed-wing aircraft. For aircraft equipped with powerplants delivering their power through a shaft, lift or gross weight to the equivalent drag ratio may serve as a convenient yardstick to measure that efficiency. Understanding that lift ( $L$ ) is the total lift equal to the aircraft gross weight ( $W$ ) in steady state level flight at speed ( $V$ ) in knots, lift or gross weight to the equivalent drag ( $D_e$ ) ratio for the whole aircraft can be expressed as follows:

$$L/D_e \equiv W/D_e = \frac{WV}{325 \text{ SHP}}, \quad (1-1)$$

where SHP represents the total power delivered by the engine or engines at the speed of flight  $V$  and at gross weight  $W$  (pounds).

By analogy, lift or gross weight to equivalent drag ratio of the lifting system alone may be written as

$$(L/D_e)_{LS} \equiv (W/D_e)_{LS} = \frac{WV}{325(\text{SHP} - \text{SHP}_f)}, \quad (1-2)$$

where  $\text{SHP}_f$  is the shaft horsepower required to overcome the parasite drag; i.e., that of non-lifting components (fuselage, nacelles, etc.) of the aircraft. Figure 1-3, comparing  $(L/D_e)_{LS}$  of the rotary-wing type with those of the fixed-wing type aircraft, explains why there is a continuous search for configurations where, in cruise and high speed flight, weight of the aircraft will be either entirely or at least partially supported by a fixed wing.

Of many possible configurations using an airscrew for vertical thrust in hover and near-hover regimes while relying on a fixed wing for high speed forward flight, attention will be concentrated on aerodynamic problems of convertible rotor/propeller aircraft. They may be defined as configurations where through a conversion process, the airscrew(s) changes its (their) role from a vertical thrust generator to that of a forward propulsor. This conversion from one role to another can be accomplished either through actual rotation of the airscrew axis from vertical to horizontal, or through rotation of the airscrew slipstream, while the axis of the airscrew itself remains approximately horizontal.

## 1.2 POSSIBLE CONFIGURATIONS

### 1.2.1 Deflected Slipstream

Deflected slipstream is considered first as the phenomena of the propeller slipstream deflection by a wing will also appear to some degree in other configurations as well. In the deflected slipstream, the aircraft propeller slipstream is rotated through large angles (up to about  $90^\circ$ ) so that its momentum flux can point vertically down while the axis of the thrust generator remains inclined at a small angle (from  $0^\circ$  to about  $15^\circ$  or  $20^\circ$ ) to the horizontal. Transition from hover to forward flight is accomplished through rotation of the slipstream with reference to the airframe which also may be accompanied by the rotation in pitch of the aircraft as a whole. In this way, momentum flux direction gradually changes from the lift supporting position in hover to that of forward propulsion in forward flight.

For the airscrew type configurations, it appears that because of the ground clearance problems, higher disc loading thrust generators will be used, thus qualifying them as propellers rather than rotors. The slipstream deflection itself is usually performed by a wing equipped with lift-increasing devices (Figure 1-4).

In order to get some idea regarding the magnitude of the wing lift coefficients and the wing chord to propeller diameter ratio ( $k_c = c/D$ ) as may be required for a given slipstream rotation angle ( $\theta$ ), the following simple considerations (based on the momentum concept) are performed.

Using notations from Figure 1-4a and assuming no profile drag losses in the total momentum flow in the slipstream, it becomes apparent that the resultant force ( $F$ ) acting on the aircraft will be equal to the static thrust ( $T$ ) of the free propeller which, according to the simple momentum theory, can be expressed as

$$F = T = 2\pi R^2 \rho v^2, \quad (1-3)$$

where  $v$  is the induced velocity at the disc and  $\rho$  is the air density.

The lift component ( $L$ ) of  $F$  in the direction normal to the propeller axis will be

$$L = 2\pi R^2 \rho v^2 \sin \theta, \quad (1-4)$$

where  $\theta$  is the slipstream rotation angle. Dividing equation (1-4) by (1-3), one obtains

$$\sin \theta = L/F. \quad (1-5)$$

But the component,  $L$ , perpendicular to the propeller axis, can also be expressed in terms of an aerodynamic force (lift) coefficient of the slipstream submerged wing portion ( $C_{L_s}$ ) and the area ( $S_s$ ) of the slipstream-covered portion of the wing:

$$L = \frac{1}{2} (\rho V_s^2 S_s C_{L_s}). \quad (1-6)$$

Substituting into equation (1-5) expressions for  $L$  and  $F$  as given by equations (1-3) and (1-6), the following is obtained:

$$\sin \theta = (V_s^2 S_s / 4\pi R^2 v^2) C_{L_s} . \quad (1-7)$$

Before reaching the wing, the propeller slipstream may be somewhere between complete contraction ( $V_s = 2v$ ) and no contraction at all ( $V_s = v$ ).

calling that ratio  $k_s = V_s/v$  and defining the chord in terms of the propeller diameter:  $c = k_c 2R$ , equation (1-7) may be rewritten as

$$\sin \theta = (k_s^{3/2} k_c / \pi) C_{L_s} \quad (1-7a)$$

or, the lift coefficient required to deflect the slipstream through an angle  $\theta$  will be

$$C_{L_s} = \pi \sin \theta / k_c k_s^{3/2} . \quad (1-8)$$

It can be seen from equation (1-8) that for  $k_c = \frac{1}{2}$  it would be necessary to develop  $C_{L_s} = 2\pi$  if contraction of the slipstream would not occur ( $k_s = 1.0$ ) before it reaches the wing. In contrast, should the slipstream completely contract before reaching the wing ( $k_s = 2.0$ ), then only  $C_{L_s} \approx 2.2$  would be required.

Similar momentum considerations in the axial direction would show that for a  $90^\circ$  deflection, axial force (induced drag) aerodynamic coefficients in the axial direction of the same value as the  $C_{L_s}$  would be required. This would indicate that the total aerodynamic force coefficient of the slipstream submerged portion of the wing should be  $\sqrt{2}$  times higher than the lift coefficient itself.

The above considerations should give a better understanding of practical difficulties of achieving large slipstream deflection angles and still maintain  $k_c$  values desirable from the overall design point of view. Figure 1-5 (taken from Reference 1-2) illustrates this point by showing recovery factors,  $L_s/T$  versus angle of slipstream deflection.

Hovering control of the deflected slipstream configurations may be achieved through the following means: *height above the ground* through variation of the collective pitch of propellers, *rotation in pitch* through auxiliary thrust generators in the fuselage (tail rotors, fans or jet nozzles most probably located in the tail area). However, as in other configurations discussed later, pitching moments can also be obtained through monocyclic control of the propellers capable of developing large hub moments; i.e., having either "rigid" blades, or sufficiently large off-set of the flapping hinges. Control in roll can be obtained (with laterally disposed propellers) through differential collective pitch, which, in turn, would also vary differentially the vertical thrust components developed by the two halves of the wing. It may be supplemented (as in the case of the VZ-3RY) by slot-lip spoilers (Reference 1-3). Control in yaw can be obtained through special thrusting devices (from tail rotors to jet nozzles). In principle, it may also be achieved by producing on both wing halves opposite horizontal components of the thrust vector (most likely through a differential deflection of flaps). However, due to partial flow separation in the trailing edge portion of the wing, that may occur at large slipstream turning angles, effectiveness of this type of yaw control is rather doubtful.

The most important problem area of the deflected slipstream configuration is the previously discussed aspect of an effective turning of the propeller slipstream through large angles. Since a complete  $90^\circ$  deflection is difficult to achieve, deflected slipstream aircraft designed for hovering operations must usually compensate that deficiency through hovering in the "nose-up" position. Another problem area is also connected with hovering (especially close to the ground) and consists of aircraft "skittishness" and difficulties of precise control. To these problems, H.L. Turner and F.J. Drinkwater add (Reference 1-3): "Changes in power and flap configurations required for flight over the design speed range produce moment variations and wing stall which constitute basic aerodynamic problems in the design of a V/STOL vehicle based on the deflected slipstream concept."



### 1.2.2 Tilt Wing

The tilt wing represents a configuration wherein axis of the airscrew (usually of the propeller type) both in hovering and horizontal flight remains either parallel or makes a small angle (a few degrees) with the zero lift chord of the wing (Figure 1-6). During the intermediate wing tilt angles, this relationship between the propeller axis and wing chord may lag behind the wing in order to reduce angle of attack of the wing with reference to the resultant slipstream.

Control in hovering can be accomplished in several ways: *vertical translation* - through collective pitch of propellers; *pitch control* - as required for both C.G. trim and angular acceleration, can be obtained through special force generators located in the tail. This represents a widely accepted solution.

However, the same goal can be accomplished through the use of cyclic control of the rotor about a single axis (monocyclic) by varying the blade pitch angle ( $\theta$ ) with the azimuth angle ( $\psi$ ) according to the following first harmonic input:

$$\theta_{\psi} = \theta_0 + \theta_m \cos \psi \quad (1-9)$$

where  $\theta_m$  is the maximum blade pitch cyclic control displacement.

In the case of propeller blades articulated about the flapping axis, these control inputs will incline the propeller disc and thus, the thrust vector which, in turn, might provide a displacement of the thrust axis with reference to the C.G. (Figure 1-7), thus providing the necessary pitching moment. However, it must be remembered that the new slipstream direction will generate lift force on the wing which, depending on the relative position of the wing center of pressure and aircraft center of gravity may reduce the pitching moment acting on the aircraft. Large flaps deflecting in the proper direction may alleviate those unfavorable propeller-wing interference effects (Figure 1-7).

For "rigid" blades, application of the monocyclic inputs would not produce any tilt of the thrust vector, but would generate a pure pitching moment. For blades with root attachment characteristics included between complete articulation with no offset of the flapping hinge and infinite rigidity, there will be a mixture of hub pitching moments and thrust vector inclinations.

Other possible pitch control in hovering and near-hovering can be accomplished through variation of aerodynamic pitching moment on the wing through a deflection of flaps. But this normally would generate rather weak moments not sufficient to provide, by itself, the necessary angular acceleration for the aircraft as a whole.

However, forces and moments resulting from the wing flap deflection still can be used as a source of longitudinal control in the Geared Flap Control System proposed by Gary Churchill of Boeing, Vertol Div. This system is based on utilizing the wing flap as an aerodynamic servomechanism (as a servo tab) to control the wing incidence relative to the fuselage (Figure 1-8).\*

The wing hinge pivot is located between the thrust axis and wing chord planes to favor a normal downward flap deflection at all times. A forward control input by the pilot causes an increase in flap deflection, creating a diving moment about the wing pivot, and initiating the wing motion. A moment unbalance exists until the wing displacement is sufficient to neutralize the moment due to flap through the follow-up linkage. The wing displacement results, then, in both pitching and axial accelerations of the aircraft due to the shifting the aircraft center of gravity forward and applying an axial force above the C.G.

---

\*U.S. Patent 3,029,043, "Free Floating Wing Structure and Control System for Convertible Aircraft." Issued to G.B.Churchill, April 10, 1962.

The system is analogous, longitudinally, to a single rotor helicopter in control concept. The entire tilting system (wing, propellers, engines, etc.) represents the rotor, which simply produces a resultant force. An input of control (flap deflection) is equivalent to a cyclic pitch input, and causes the resultant vector to rotate about the wing hinge (rotor flapping response). Wing motion ceases when the steady state equivalent flapping (wing incidence change) cancels the equivalent cyclic input (initial flap deflection).

Control in roll of the tilt wing is most naturally accomplished through differential thrust variation of the laterally disposed propellers.

Force and/or moment inputs required for *yaw control* can be obtained either from special rotors, ducted fans, or nozzles usually located in the tail area, or through a differential deflection of aerodynamic surfaces (usually flap-ailerons of the wing) submerged in the propeller slipstream.

Differential inclination of the thrust vector (through differential longitudinal cyclic for articulated blades, or differential deflection of nacelles with reference to the wing for rigid blades) could also be a source of the yaw moment. But this should be accompanied by a proper deflection of aerodynamic surfaces to eliminate, or reduce, wing forces opposite to the intended yaw components (see Figure 1-7).

Aerodynamic problem areas particular to the tilt-wing configuration can be identified as follows: (1) partial power descent and high deceleration conversion from forward flight, (2) propeller aerodynamic efficiency, both in hover and cruise, (3) detrimental ground effects at some wing settings at landing with forward speed and (4) vertical gust sensitivity at high speeds. This latter problem may be of special importance for the high aspect ratio configurations (four propellers) with relatively low wing loadings.

The problem of high propeller efficiency in all regimes of flight is, obviously, common to all configurations using the same airscrew as a vertical thruster in hover and a forward propulsor in high speed flight.

### 1.2.3 Tilting Rotor/Propeller

In this configuration, rotors or propellers (usually located at the wing tips) tilt through the conversion cycle, while the wing remains fixed with reference to the fuselage (Figure 1-9). This approach permits (from the aerodynamic, but not necessarily the structural point of view) more freedom in the independent selection of the disc and wing loadings than in the case of the tilt wing, but it encounters new problems which will be mentioned later.

As to the *control of the tilting rotor in hovering*, it shows many analogies with the tilt wing: Control in pitch can be achieved through tail rotors, monocyclic inputs, etc. Roll control also appears to be most naturally solved through differential monitoring of the rotor thrusts. Yaw control in the absence of straightening-vane effect of the wing would favor the application of differential cyclic.

Regarding main aerodynamic problem areas, it appears that they may be traced to two sources: (1) fixed horizontal position of the wing, producing considerable downloads, both in hovering and in conversion, and (2) aerodynamic characteristics (efficiency, sensitivity to horizontal gusts, etc.) and aeroelastic instability of the rotors at high forward speeds, especially when low hovering disc loadings are used.

Those low disc loadings requiring large diameter rotors may also lead to a reduction of takeoff performance from their potential values. This would result from the inability (because of the ground clearance of the rotors) to lower the rotor axis to the position assuring maximum acceleration on the ground (see Chapter 4). On the positive side, however, low disc loadings ( $W \leq 12$  fps) may assure autorotational landing capabilities in case of complete power failure. By contrast, it appears that propeller-type airscrews (as for instance,

in tilt wings) would probably not show any autorotational benefits within practical limits of vertical descent velocities. Figure 1-10, reproduced from Reference 1-4 and based on full-scale wind tunnel tests of a Vertol 76 propeller by P.F. Yaggy and K.W. Mort (Ref. 1-5) seems to indicate that at least within the investigated blade pitch angles, no additional thrust is developed in a vertical, or near vertical, descent, and power required per pound of thrust at a given blade pitch angle remains practically the same as under static conditions.

#### 1.2.4 Tilting Rotor with Foldable or Feathered Blades

The tilting rotor with foldable or feathered blades represents a concept where an attempt is made to avoid the previously mentioned rotor problems in high speed flight, as well as to eliminate the Mach number limitations of the airscrews. In this concept, after conversion to the forward flight configuration, rotor is stopped, blades feathered and possibly left in that position for the high speed flight regime. However, due to the additional drag and aeroelastic problems associated with this solution, it appears more advantageous after stopping and feathering the blades to have them folded either behind or along the nacelles (Fig. 1-11). The high speed forward propulsion is provided by turbofans or, less likely, propellers of a smaller diameter. Control aspects and aerodynamic problems in hover, rolling takeoffs, and transition are obviously very similar to those of the "classical" tilting rotor.

### 1.3 POWER MATCH

All the configurations considered in the preceding section offer (at least in principle) an opportunity for the so-called power match. This means that the shaft horsepower installed resulting from hovering requirements (at a specified altitude and temperature) can be made equal, or at least close, to that needed at maximum speed in forward flight at some operational altitude.

In the first approximation, installed power ( $SHP_{ins}$ ) per pound of design gross weight ( $W$ ) can be defined on the basis of the hovering requirements as follows:

$$(SHP_{ins}/W)_h = \frac{k_{e_x}^{3/2}}{550 \eta_{tr} \eta_A \lambda_{THh}} \sqrt{\left(\frac{w}{2\rho_h}\right)}, \quad (1-10)$$

where  $k_{e_x}$  is the ratio of the maximum airscrew thrust to the gross weight,  $\eta_{tr}$  is the mechanical transmission efficiency,  $\eta_A$  is the aerodynamic efficiency (figure of merit) in hovering\*,  $\lambda_{THh}$  is the powerplant lapse rate corresponding to the ambient hovering conditions,  $w$  is the nominal disc loading and  $\rho_h$  is the air density corresponding to the ambient conditions in hover.

On the other hand, the installed shaft horsepower per pound of gross weight resulting from a speed of flight  $V$  (knots) at an altitude  $H$  (feet), i.e., at an air density  $\rho_f$ , is

$$(SHP_{ins}/W)_f = \frac{V}{325 \eta_{tr} \eta_{pr} \lambda_{THf}} \left[ 1.43 \rho_f V^2 \left( \frac{1}{w_f} + \frac{C_{Do eq}}{w_w} \right) + \frac{w_w}{1.43 \rho_f V^2 \pi (AR)_e} \right], \quad (1-11)$$

where new symbols are:  $\eta_{pr}$  - propulsive efficiency of rotor/propeller at speed  $V$ ;  $w_f$  - equivalent flat plate area ( $f$ ) loading ( $w_f \equiv W/f$ );  $C_{Do eq}$  - equivalent (i.e. based on the wing area) profile drag coefficient of the wing and empennage;  $w_w$  - wing loading and  $(AR)_e$  - effective aspect ratio of the wing.

\* See Section 2-1.

By equating Equations (1-10) and (1-11), a relationship tying together hovering and forward flight requirements is obtained. This, at least in principle, should permit an indication of hovering disc loading (for required  $H_h$  and  $T_h$ ) that is best (power-wise) suited for a given  $V_{max}$  at a given altitude ( $H_f$ ). Magnitude of some design parameters appearing in Equations (1-10) and (1-11) can be rather closely guessed for a given category of aircraft (say, military, or civilian transport of a given class).

For instance, anticipating the gross weight class of the aircraft and its type of fuselage (military with rear loading versus short-haul civilian aircraft) the  $w_f$  values can be approximated (see Figure 1-12). The same goes for the equivalent profile drag: since area of the empennage usually amounts to 25-35% of the wing area and practical  $C_{Do} \approx 0.01$ ,  $C_{Do eq} \approx 0.013$  would probably represent an acceptable first order approximation. Transmission and propulsive efficiencies as well as aerodynamic efficiency in hover should also be contained within rather narrow limits\* ( $\eta_{tr} < 0.95$ ;  $0.72 < \eta_{pr} < 0.82$  and  $0.7 < \eta_A < 0.8$ ).

However, the remaining two parameters in Equation (1-11), namely, the wing loading and wing aspect ratio can, in principle, be varied within large limits. If there were no such constraints as the restrictions regarding propeller diameter to wing chord ratio, then the effective aspect ratio could be assumed within limits generally accepted in the design practice of the considered category of aircraft (say transports), and the wing loading could be optimized for the maximum wing L/D at the selected operational conditions of flying speed and altitude:

$$w_{w opt} = q_f \sqrt{C_{Do eq} \pi (AR)_e} \quad (1-12)$$

where  $q_f$  is the flight velocity dynamic pressure in forward flight. Figure 1-13 permits to get at a glance a feeling regarding those optimum wing loading values for various forward speeds and altitudes. In spite of the fact that many VTOL missions require operations at low altitudes, ferry and other long-range considerations would probably push the selection of unrestricted wing loadings toward optima indicated for 20,000 ft cruise altitudes, or even higher.

Figure 1-14 permits assessment of maximum flying speed values at S/L std., corresponding to a power match resulting from hovering requirements, either at S/L Std., or at 3000 95°F. It was assumed in this case that, at every speed of flight, the wing loading is optimized by Equation (1-12) for the 20,000 ft altitude.

It should be remembered, however, that in such configurations as the deflected slipstream and the tilt wing, a need for the propeller slipstream rotation by the wing may impose a minimum acceptable limit for a ratio between the wing chord and propeller diameter. This constraint would eliminate the (aerodynamic) freedom of selecting the wing aspect ratio and using optimum wing loading for a given altitude and speed of flight.

In order to give some idea regarding the relationship between the disc and wing loadings with constraints, it is assumed that the width of the fuselage and distance of the inboard propeller tips to the fuselage is constant. This means that the central portion of the wing span ( $b_c$ ) also remains constant. On the other hand, the external part of the wing span varies with propeller diameter ( $D$ ), number of propellers ( $n$ ) and the mutual propeller-wing arrangement, reflected through a coefficient  $k_b$ . The whole wing span ( $b$ ) can now be expressed as:

$$b = b_c + k_b n D \quad (1-13)$$

---

\* A more detailed discussion of the  $\eta_A$  values will be in Section 2.1 and of the  $\eta_{pr}$  magnitudes in Section 3.1

With a coefficient  $k_c = \bar{c}/D$ , the relationship between the disc and wing loading can be expressed as:

$$w_w = w \frac{1}{k_c \left[ b_c \sqrt{\left( \frac{4w}{\pi \pi R} \right)^2 + \frac{4k_b}{\pi}} \right]} \quad (1-14)$$

As an example of the above relationship, a four-propeller tilt-wing configuration similar to that shown in Figure 1-6 is considered with  $b_c = 12$  ft,  $k_c = 0.5$ , and  $k_b = 0.85$ . Assuming 3 values of the gross weight (50,000, 75,000 and 100,000 pounds),  $w_w = f(w)$  was computed and is shown in Figure 1-15. It can be seen from Figure 1-15 that for the selected geometric constraints, the  $w_w = f(w)$  relationship is rather insensitive to the gross weight values that may be encountered within a given gross weight class (in this case, from 50,000 to 100,000 pounds). Thus by selecting wing loadings versus disc loadings as given by the 75,000 pounds curve and substituting those  $w_w$  and aspect ratio  $((AR)_e = e(b/\bar{c}))$  values into the power match equations (Equations 1-10 and 1-11), maximum speed at sea level is found for various disc loading values. Thus, the obtained  $V_{max} = f(w)$  is compared with the  $V_{max} = f(w)$  for the non-constrained (optimum) wing loadings. It can be seen from Figure 1-16 that some penalties in the high speed capabilities may be expected for those configurations where geometric constraints would force a deviation from the optimum wing-loading values. Figure 1-16 indicates that in the considered case of a 4-propeller configuration with  $k_c = 0.5$  and  $k_b = 0.85$ , those penalties amount to about 50 knots. With  $k_c > 0.5$  they would be still higher.

In all the above examples, the power match was considered under the assumption of using, in forward flight, all the installed power resulting from the hovering requirements. This, obviously, led to the indication of the maximum forward flight speed capabilities. However, the power match may be investigated according to some different rules expressed, for instance, as a requirement for a high speed cruise when only a given percentage (say, 80%) of the installed (or takeoff) power is used. Introduction of a proper factor into Equation (1-11) would permit computation of the new relationship between the disc loading and the corresponding "matched" forward speed (this time for a high speed cruise).

#### REFERENCES TO CHAPTER I

- 1-1. Fry, B.L. *Assessment of Commercial VTOL Aircraft with Rotor or Propeller Lift System* presented at the AIAA Commercial Aircraft Design & Operation Meeting, June 12-14, 1967.
- 1-2. Kirby, R.H. *Aerodynamic Characteristics of Propeller-Driven VTOL Aircraft*, Proceedings of NASA Conference on V/STOL Aircraft, Langley Field, Va., Nov. 17-18, 1960.
- 1-3. Turner, H.L. *Some Flight Characteristics of a Deflected Slipstream V/STOL Aircraft*, NASA TN D-1891, 1963.  
Drinkwater III, F.J.
- 1-4. Stepniewski, W.Z. *The Subsonic VTOL and GTOL in Perspective*, Aerospace Engineering, Vol.21, No.4, Apr. 1962.
- 1-5. Yaggy, P.F. *Wind-Tunnel Tests of Two VTOL Propellers in Descent*, NASA TN D-1766, 1963.  
Mort, K.W.

## RECOMMENDED READING

- 1-a. - AGARD Proceedings of VTOL/STOL Meeting, Paris, June 28-30, 1960.
- 1-b. Campbell, J. *Vertical Take-Off and Landing Aircraft*. The MacMillan Company, New York, 1962.
- 1-c. McCormick, B.W., Jr *Aerodynamics of V/STOL Flight*, Academic Press, 1967.
- 1-d. - *NASA Conference on V/STOL Aircraft*, Langley Field, Va., November 17-18, 1960.
- 1-e. - *NASA Conference on V/STOL and STOL Aircraft*, Ames Res. Ctr., Moffett Field, Calif., April 4-5, 1966.
- 1-f. - New York Academy of Sciences, *Proceedings of the International Congress of Subsonic Aeronautics*, New York, N.Y. April 3-6, 1967 (to be published in 1968).
- 1-g. Strand, T.  
et al. *Unified Performance Theory for V/STOL Aircraft in Equilibrium Level Flight*.

## CHAPTER II

## HOVERING AND VERTICAL FLIGHT

## 2.1 BASIC THRUST-POWER RELATIONSHIPS IN HOVER

In order to clearly represent the relative importance of the parameters which are significant from the design point of view as, for instance, disc loading ( $w$ ), blade loading ( $w_b$ ), tip speed ( $V_t$ ), airfoil characteristics ( $c_l$  and  $c_{do}$ ), etc., the combined momentum-blade element theory will be used in the interpretation of the hovering and vertical flight phenomena.

Shaft horsepower required per pound of thrust of an airscrew can be expressed (see, for instance, p.143, Reference 2-1) as:

$$(\text{SHP}/T)_h = \frac{1}{550\eta_{tr}} \left( k_i \sqrt{\left( \frac{w}{2\rho_h} \right)} + \frac{1}{8T} \sigma \pi R^2 \rho_h \bar{c}_{do} V_t^3 \right), \quad (2-1)$$

where new symbols appearing in Equation (2-1) are:  $k_i$  - the induced power coefficient expressing the ratio of actual induced power (taking into consideration non-uniform downwash distribution and tip losses) to the ideal one;  $\sigma$  - propeller or rotor solidity ratio; and  $\bar{c}_{do}$  - average profile drag coefficient of the blade.

It should be noted that  $\sigma \pi R^2$  appearing in Equation (2-1) is the blade area ( $S_b$ ) while  $T/\sigma \pi R^2 = T/S_b = w_b$  will be the blade area loading.

Remembering that average lift coefficient in hovering is defined as

$$\bar{c}_{lh} = \frac{6T}{\sigma \pi R^2 \rho_h V_t^2} = \frac{3w_b}{\rho_h V_t^2}, \quad (2-2)$$

Equation (2-1) can be rewritten as follows:

$$(\text{SHP}/T)_h = \frac{1}{550\eta_{tr}} \left( k_i \sqrt{\left( \frac{w}{2\rho_h} \right)} + \frac{3}{4} \frac{\bar{c}_{do}}{\bar{c}_{lh}} V_t \right). \quad (2-3)$$

Equation (2-3) clearly indicates that reduction of the induced power per pound of thrust (first term in the brackets) will depend on the uniformity of the induced velocity through the disc, and decrease of the blade tip losses as reflected by the diminishing  $k_i$  values. It also will decrease with the decreasing disc loading and increasing air density.

As to the profile power contribution to the total power required per pound of thrust, it can be seen that it decreases proportionally to the  $\bar{c}_{do}/\bar{c}_{lh}$  ratio or, in other words, it improves with the increasing average lift to the corresponding average profile drag coefficients ratio in hover. It can be seen that a low tip speed  $V_t$  is also beneficial. However, one must remember that a low tip speed would lead to large total blade area for a given thrust value; since, (see Equation(2-2))

$$S_b = \frac{6T}{\bar{c}_{lh} \rho_h v_t^2} \quad (2-4)$$

or, in more general terms, blade area required per pound of thrust is

$$S_b/T = \frac{6}{\bar{c}_{lh} v_t^2 \rho_h} \quad (2-4a)$$

It will be seen later that reduction of the total blade area required for a given thrust level is quite important.

From Equation (2-2) it is easy to express blade loading in terms of the average lift coefficient in hover, air density and tip speed. Figure 2-1 is shown as an example of blade loadings that may be encountered in practice.

It is obvious now that minimization of the  $S_b$  and  $S_b/T$  and maximization of  $w_b$  require maximization of the product of the average lift coefficient and the corresponding tip speed squared. Since tip speed is synonymous with Mach number at which blade sections operate, it is clear hence, that in order to make Equations (2-4) and (2-4a) a minimum, such airfoil sections are required that would permit operation at the combination of high section lift coefficients and high Mach numbers with as low as possible increase in the  $C_{do}$  values.

However, in practical designs, external noise requirements may favor a compromise at lower tip speeds (see Section 2-6).

In order to have a better feel regarding the influence of various design parameters on the aerodynamic efficiency (figure of merit in hover), the ideal rotor power required per pound of static thrust ( $P_{id}/T = \sqrt{w/2\rho_h}$ ) is divided by the expression in brackets of Equation (2-1), leading to

$$\eta_A = \frac{1}{k_1 + \frac{3}{4} \left( \frac{\bar{c}_{doh}}{\bar{c}_{lh}} \right) \frac{v_t}{\sqrt{w/2\rho_h}}} \quad (2-5)$$

Remembering that the ideal induced velocity under static conditions (hover) is:  $v_{id} = \sqrt{w/2\rho_h}$ , it is possible to give Equation (2-5) still another interpretation:

$$\eta_A = \frac{1}{k_1 + \frac{3}{4} \left( \frac{\bar{c}_{doh}}{\bar{c}_{lh}} \right) \left( \frac{v_t}{v_{id}} \right)} \quad (2-5a)$$

Both of the above equations indicate that low values of the induced power factor ( $k_1$ ) are always important as well as the high ratios of average lift to mean profile drag coefficients. It is, however, interesting to notice how the relative significance of the profile power term varies with the ratio of tip speed to the ideal induced velocity (increases for lightly-loaded airscrews). It appears, hence, that reduction of the profile drag coefficients through such means as BLC would greater contribute to the figure of merit improvement of lightly-loaded rotors than propellers. Study of Figure 2-2 may be quite instructive in that respect. The upper graph of this figure permits a rapid estimation of the  $v_t/v_{id}$  values, while the lower graph should give an idea regarding the order of magnitude of the aerodynamic efficiencies that may be expected under static conditions for those  $v_t/v_{id}$  ratios.



Figure 2-3 presents  $\eta_A$  directly versus disc loading for one assumed tip speed  $V_t = 800$  ft/sec and one value of the average lift to the average profile drag ratios ( $\bar{c}_{lh}/\bar{c}_{do} = 60$ ) and  $k_i = 1.07$ . In the above presentation the induced power coefficient was assumed constant  $k_i = 1.07$ , probably approximating quite well the aerodynamic efficiency levels of lightly-loaded airscrews (i.e., rotors)  $w < 12$  lb/ft<sup>2</sup>. However, they may be too optimistic for more highly loaded airscrews of the propeller type. More rapid increase of actual induced power than its ideal value (higher  $k_i$  factor) is chiefly responsible for this. One of the contributing factors to the  $k_i$  increase is the increasing importance of the slipstream rotation. It is shown in Reference 2-1 (p.127) that the induced power loss due to the slipstream rotation can be approximately expressed as:

$$(\Delta P_{ind})_{rot} \approx 1.36 P_{ind} (v/V_t)^2 \quad (2-6)$$

For  $v/V_t$  ratios typical of helicopter rotors, this contribution expressed by Equation (2-6) amounts to about 0.35%, but for disc loadings of 40 lb/ft<sup>2</sup>, it may grow to about 2.5%. Furthermore, induced power increase associated with tip losses will also be more significant for low aspect ratio blades encountered in the VTOL propellers than in the slender helicopter blades. Also because of the compromise in the twist distribution that may be dictated by the forward flight requirements (see Section 3-1), actual downwash distribution may deviate from the uniform one. For all the above reasons, it will probably be difficult to obtain for the propeller-type static thrust generators  $\eta_A > 0.8$ .

With reference to the problem of minimizing the  $k_i$  values, the combined momentum-blade element theory may provide some guidance by permitting to discuss the influence of such factors as airfoil characteristics, blade planform, twist distribution, etc. More refined computational methods (see, for instance, Reference 2-1, pp.112-125, and Reference 2-2, pp.73-113) based on the combined blade element and momentum theories would permit to obtain a better definition of the  $\eta_A$  values or to establish a direct relationship between static thrust and power required of rotors and propellers. It should be remembered, however, that the combined blade element momentum theory fails in describing phenomena occurring at the blade tips and roots and their influence on the flow conditions at intermediate blade stations as well as to indicate the influence of the number of blades. Theories based on vorticity distribution at the blade itself and in the wake are more promising in that respect.

## 2.2 APPLICATION OF VORTEX THEORY TO STATIC STATE AND AXIAL MOTION OF ROTORS AND PROPELLERS

Beginnings of the application of the vortex theory to performance analysis of a free airscrew (rotor or propeller) under static conditions, or in translatory flight, may be traced to the classical Goldstein's paper of 1929 (Ref.2-3). Propeller aspects of that approach were further developed by Lock, Theodorsen and others (Refs.2-4 and 2-5), while M.Knight and R.Hefner were probably the first to apply vortex theory to the analysis of the static thrust of a rotor far from the ground (Ref.2-6). Later, using a mirror deflection concept, Knight extended that analysis to the ground effects on the thrust and induced power relationships of a rotor operating under those conditions.

It should be noted, however, that the above approach was based on linearized theory, assuming a constant circulation along the blade, so that vortices are shed only at the tip. Furthermore, it was assumed that the thus shed vorticity forms a cylindrical wake moving at a speed equal to the average downwash velocity while vortex density ( $d\Gamma/dh$ ) along the wake itself is constant and its value is determined by the thrust alone.

H.Heyson of NASA (Ref.2-7) has shown by thrust and power measurements as well as by flow visualization that for rotor-propellers operating in ground effect, differences between the predicted and measured values of thrust and power as well as between the actual flow patterns and those predicted by this simplified theory are quite great. It became

obvious that the source of these differences can be traced to the lack of reflection in the mathematical model of such important physical facts as: (a) contraction of the wake, and (b) proper vorticity distribution within the wake itself.

Looking closer at the wake contraction and the resulting from this fact of acceleration of the flow that carries with it vorticity left behind by the airscrew, one must realize that the importance of this problem is not the same for a rotor-propeller at a high speed of translation (for example, in cruise) and the same rotor or propeller in hover.

From the simple momentum theory, it is easy to show that at an axial translation with speed  $V$ , the induced velocity (at the disc)  $v_v$  will be

$$v_v = \frac{1}{2} V[-1 + \sqrt{1 + w_v/q_v}] \quad (2-7)$$

where  $w_v$  is the disc loading corresponding to the velocity  $V$  and  $q_v$  is the dynamic pressure of forward flight ( $q_v = \frac{1}{2} \rho V^2$ ). In the fully developed wake (in  $\infty$ ),  $v_{v\infty} = 2v_v$  and the ratio of the cross-section of the slipstream for downstream ( $A_{S\infty}$ ) to that at the disc ( $A_{S0}$ ) will be:

$$A_{S\infty}/A_{S0} = [1 + \frac{1}{2}(-1 + \sqrt{1 + w_v/q_v})] / [1 + (-1 + \sqrt{1 + w_v/q_v})] \quad (2-8)$$

It is obvious from Equation (2-8) that in cruise when the speed of flight  $V$  and the corresponding  $q_v$  are high, and rotor or propeller disc loading corresponding to that speed amounts to a fraction of that in hover ( $w_v = w_0/(L/D)_v$  where  $(L/D)_v$  is the aircraft lift to drag ratio at speed  $V$ ), the ratio expressed by Equation (2-8) is close to 1.0\*. This means that under those conditions, assumptions of a cylindrical wake is justified by physical phenomena. By the same token, at slow axial translations of the propeller or rotor ( $A_{S\infty} \approx 1/2$ ), or in hover ( $A_{S\infty}/A_{S0} = 1/2$ ) physical facts of the accelerated flow in the wake as it moves away from the disc should be reflected in the mathematical model.

As to the vorticity distribution in the wake, the advent of high-speed computers made it possible to better represent the physical reality through a sufficiently large number of discrete vortex filaments leaving the blade along its span as well as at the tip. Figure 2-4 (reproduced from Reference 2-8) is shown as a typical example of the representation of the vorticity in the wake through discrete vortex filaments\*\*.

Once, with the help of a system of discrete vortex filaments, the physically correct model of vorticity distribution in the whole wake is established, the velocity induced at any point of space can be computed through the Biot-Savart law. This law states that at any point  $P$ , increment of velocity ( $dV_p$ ) induced by a vortex filament of strength  $\Gamma$  and  $ds$  length can be expressed as follows:

$$dV_p = \frac{\Gamma}{4\pi R^3} r \, ds \quad (2-9)$$

This induced velocity increment  $dV_p$  will be perpendicular to the plane passing through point  $P$  and vortex filament  $ds$ . (For other definitions, see Figure 2-5).

Establishment of a proper computer program would permit summing up the influences of all vortex filaments representing the whole wake and thus computing both magnitude and direction of the induced flow at point  $P$ . Repeating the same procedure for a sufficient number of points in the disc area, downwash velocity distribution can be obtained, thus permitting computation of both the total thrust and the corresponding induced power.

\* For instance, for  $V = 340$  ft/sec and  $w_v = 5$  lb/ft<sup>2</sup> ( $w_0 \approx 50$  lb/ft<sup>2</sup>):  $A_{S\infty}/A_{S0} \approx 0.992$ .

\*\* In this particular case, for a helicopter rotor in forward flight.

This new opportunity offered by the computers regarding the possibilities of obtaining numerical results from a more realistic representation of the wake, produced a large number of papers and studies referring to the application of vortex theory to both rotors and propellers in various regimes of flight. Of more recent U.S. contributions to this domain, the works of Loewy, Miller, and the Cornell Aeronautical Laboratory (References 2-9 to 2-13) should be mentioned. There are indications that in the Soviet block a similar approach is also used (References 2-14 and 2-15).

As an illustration of the vortex theory approach to the analysis of rotor/propeller performance under static conditions and in axial translation, a method developed by F.J. Davenport of Boeing, Vertol Division, under the name of "An Explicit Vortex Influence Technique", is briefly outlined.

This method and the resulting computer program (for the IBM 360) permits to predict, both in hover and in axial flight, thrust produced, power required and radial distribution of aerodynamic loading on a rotor or propeller blade of arbitrary planform, twist and radial variation of airfoil characteristics. With respect to the latter point, it should be noted that in the actual computer program, inputs of airfoil lift and drag characteristics are provided in tabular form (at 10 blade stations). This permits to consider in performance calculations, any peculiarity that may exist due to the airfoil shape as well as its operating conditions (Mach and Reynolds numbers, etc.)<sup>\*</sup>.

As to the computational model of the airscrew, the considered method states that: Each blade is treated as a rotating lifting line, trailing a vortex wake which is mathematically approximated by a finite number of concentrated vortex filaments. One of such filaments leaving the blade from an element located at a station located at radius  $r(o)$  is shown in Figure 2-6.

Since the actual airscrew wake consists of vorticity sheets, the number of discrete vortices representing this sheet should be sufficiently large to assure a correct representation of the physical phenomena. On the basis of a comparative study, it was decided to use 13 vortices and 12 control points as a good comparison between computer time and accuracy requirements. Furthermore, since trailed vorticity is concentrated toward the tips, the number of vortex filaments per unit of blade length is increased close to the tip.

As to the velocity distribution at the disc, it may be expected that its overall shape and actual downwash values are determined chiefly by the far wake. By contrast, the flow at the tip and the cut-out areas is influenced by the near wake.

Structure of the wake itself reflects the vortex law requiring that vortex filaments must travel at the same velocity as flow in the wake which, in turn, is a sum of the axial speed of the airscrew ( $V$ ) and the three components of flow induced by the vortex filaments themselves. In hovering, obviously, the flow in the wake is only due to the induced effects and thus mutual interdependence between the vortex structure and the flow phenomena induced by them becomes of prime importance. To resolve this problem, the method proposed by Davenport uses the momentum theory to establish a reference or 'normal' vortex structure from which the influence coefficients will be computed. Deviations of the loading from that corresponding to the nominal structure will change the vortex structure. The influence coefficients must then be used with adjustment factors to reflect this new vortex structure.

---

<sup>\*</sup> At present, two-dimensional (non-rotating) data are used. But it is recognized that special flow conditions existing at the rotating blade may alter sectional aerodynamic characteristics.

As to the variation of the slipstream velocity with its distance  $x$  (Fig. 2-6) downstream from the disc, the classical approximation of Glauert (Reference 2-16, p. 367) was used. This finally led to the approximate formula

$$v_x/v_\infty = \frac{1}{2}[2 - (1-AP)e^{-Nx/R}] \quad (2-9)$$

where the "slipstream acceleration factor"  $AP$  is about 0.19 and falls asymptotically to zero as  $v$  increases.

The slipstream model based on the above relationship worked quite well for low disc loadings, but gave too optimistic results for propellers as used in the tilt-wing configurations. Assuming that the general form of Equation (2-9) is correct, values of the so-called contraction rate parameter  $N$  were selected to match theoretical results against experimental data. In this way a curve of "correct" values of  $N$  versus airscrew thrust coefficient values ( $C_T = T/A\rho V_t^2$ ) was obtained. Thus, the established relationship of  $N = f(C_T)$  was used in the computer program.

With these corrections, the performance predictions based on the above described method show an excellent agreement with tests for both a helicopter rotor and a tilt-wing propeller (see Figures 2-7 and 2-8). It should be noted, however, that because of the semi-empirical determination of the  $N$  coefficient, the present basis of the whole method extends only to  $C_T < 0.025$ .

### 2.3 DOWNLOAD AND SKITTISHNESS

It is easy to show that in the fully developed wake of an airscrew under static conditions (slipstream velocity  $V_s = 2v$ ), the dynamic pressure ( $q_s$ ) is equal to the airscrew disc loading

$$q_s = \frac{1}{2} \rho (2v)^2 = 2\rho \left( \sqrt{\frac{w}{2\rho}} \right)^2 = w.$$

This obviously means that aircraft components characterized by high drag coefficients, when exposed to the downflow, may substantially contribute to the decrease of the net vertical thrust available in hovering. This download problem becomes especially serious for the tilting propeller and rotor configurations. Here, relative value of download on the wing (ratio of vertical drag  $D_v$  to total thrust  $T$ ) can be expressed as

$$D_v/T = \left( \frac{S_s}{S_w} \right) C_{Dv} \frac{w}{w_w} \quad (2-10)$$

where  $S_s/S_w$  is the fraction of the total wing area submerged into the fully developed airscrew slipstream, and  $C_{Dv}$  is the vertical drag coefficient of the wing. It can be seen that for, say,  $S_s/S_w \approx 0.75$  and  $C_{Dv} \approx 1.3$ , the download on the wing may roughly be equal to the ratio of the disc to wing loadings. It is easy to see that for the tilting rotor-propeller configurations, even with low disc loadings ( $w \approx 12 \text{ lb/ft}^2$ ) and rather high wing loadings ( $w_w \approx 100 \text{ lb/ft}^2$ ), thrust losses due to the download could become prohibitive unless a proper action to alleviate this situation is undertaken. This is usually done through a reduction of the wing area in the slipstream through large (close to  $90^\circ$ ) down deflections of flaps and ailerons combined with an attack on the vertical drag coefficient by providing a better flow (see Figure 2-9).

The problem of skittishness and resulting control difficulties in hovering close to the ground is related to that of the download. Conditions leading to high downloads will result in the appearance of strong Karman type vortices separating at relatively low frequency. Because of their strength and frequency, their disturbing effects on the aircraft will be large. By the same token, reduction of the total download (less energy

in the vortices) as well as flow modifications resulting in weaker vortices of higher frequency should decrease the disturbing effects of the downwash on the aircraft.

## 2.4 GROUND EFFECT

Ground effect from the performance point of view can manifest itself in the variation of the thrust-power relationship of the rotor or propeller and development of either positive (lifting) or negative (suck-down) forces on the airframe.

Proximity of the ground improves airscrew performance (see, for instance, pp.148-150, Reference 2-1) by increasing thrust at a constant power, or reducing power required for a given thrust. Figure 2-10 (based on Figure 4, p.149, Reference 2-1) gives some idea regarding those improvements. It indicates, at the same time, that for the tilt-wing configuration where usually  $h/D > 1.0$ , and the average lift coefficient in hovering will probably be  $0.4 \leq \bar{c}_{lh} \leq 0.6$ , no noticeable gains in the propeller performance should be expected from ground effect. However, for the tilt-rotor types where  $h/D$  could be as low as  $h/D \approx 0.4$  (with the same ranges of values of  $\bar{c}_{lh}$ ), some performance improvements in ground effect may be noticed (see Figure 2-10).

Ground effects on the airframe (either positive or negative) depend on the flow patterns which, in turn, may depend to a large extent on the mutual positions and shapes of various components of the airframe. Such aspects as cross-section of the fuselage, presence or absence of auxiliary structures (sponsons, etc.) may be important (see Figure 2-11 for possible flow patterns for a 2-propeller tilt-wing in hover close to the ground).

For this reason, it is still difficult to present more general conclusions and almost every design should be individually tested in that respect. For instance, NASA, Langley Studies (Ref.2-17) indicated that for a two-propeller tilt-wing aircraft with a wide flat (at the bottom) fuselage, some positive effect close to the ground was noticed due to the build-up of pressure under the fuselage (see Figure 2-12, taken from Reference 2-17). However, this build-up of pressure under the fuselage may also contribute to some undesirable effects. Since that captured "pressure bubble" must not be stable, its either random or periodic release may lead to skittishness. Additional information about flow patterns along the ground and above can be found in References 2-18 and 2-19.

## 2.5 VERTICAL RATE OF CLIMB

Concepts of the momentum theory become quite useful in establishing working formulae for computation of the vertical rate of climb. It can be shown (Ref. 2-1) that for an ideal airscrew, the vertical rate of climb ( $V_{cid}$ ) can be expressed as the difference between the rate of total flow through the disc ( $U$ ) and the induced velocity ( $v$ ):

$$V_{cid} = U - v. \quad (2-11)$$

The above equation (true for the ideal airscrew-type VTOL) can be worked out into a practical procedure for computing rate of climb ( $V_c$ ) of a real aircraft when its gross weight  $W$  and SHP delivered by the engine(s) are known. This will be done through a substitution for a real aircraft, an ideal one, which will have a vertical rate of climb equal to that of the real machine. The reasoning leading to this substitution can be represented as follows:

Rotor or propeller power ( $P_R$ ) available at the rotor should be found by multiplying the SHP available by the transmission efficiency  $\eta_t$ .

The ideal airscrew-type aircraft in vertical ascent uses the rotor (or propeller) power exclusively for covering induced losses (induced power) and work against gravity. Hence, the power available for these two functions ( $P_{id}$ ) should be computed. This is easily

obtained by subtracting from the rotor or propeller power available ( $P_{R\ av}$ ) the power required to overcome the profile drag ( $P_{pr}$ ):

$$P_{id} = P_{R\ av} - P_{pr} . \quad (2-12)$$

The rate of flow ( $U$ ) for the ideal VTOL is (see page 57, Reference 2-1)

$$U = \frac{550 P_{id}}{W} , \quad (2-13)$$

where  $W$  is the gross weight of the aircraft.

The induced velocity in vertical ascent for the ideal airscrew is (see page 57, Reference 2-1)

$$v_{id} = \frac{W}{2A\rho U} , \quad (2-14)$$

where  $A$  is the total rotor (or propeller) disc area of the aircraft.

The numerator and denominator of the above relationship can be multiplied by the downwash velocity in hovering ( $v_{hov}$ ) without changing the validity of the equation

$$v_{id} = \frac{W}{2A\rho v_{hov}} \frac{v_{hov}}{U} . \quad (2-15)$$

But  $W/2A\rho v_{hov}$  is simply the downwash in hovering ( $v_{hov}$ ), hence Equation (2-15) can be rewritten as

$$v_{id} = \frac{v_{hov}^2}{U} \quad (2-16)$$

and the rate of climb (in ft/sec) for the ideal VTOL can be represented as

$$v_{c\ id} = \frac{550 P_{id}}{W} - \frac{v_{hov}^2}{U} \quad (2-17)$$

or, in ft/min,

$$v_{c\ id} = \frac{550 P_{id}}{W} - \frac{v_{hov}^2}{U} . \quad (2-17a)$$

With the proper interpretation of the physical meaning of the symbol  $v_{hov}$  in Equation (2-17), it can readily be applied to the real aircraft also. It is only necessary to substitute for  $v_{hov}$  the equivalent induced velocity which may be obtained by a proper interpretation of the relationship between the induced power and downwash in hovering. It has been shown (page 45, Reference 2-1) that

$$P_{in} = \frac{Wv_{hov}}{550} ;$$

hence

$$v_{hov} = \frac{550 P_{in}}{W} , \quad (2-18)$$

where  $P_{in}$  is the actual induced power in hover. For the ideal VTOL, the  $v_{hov}$  computed from Equation (2-18) represents the mean equivalent downwash velocity through the disc. In actual computations of vertical rate of climb, advantage should be taken of the known relationship between the (real) induced power in hover and gross weight. From this relationship,  $P_{in}$ , corresponding to the weight  $W$ , can be found and  $v_{hov}$  computed from Equation (2-18). By the same token, when values of the induced power coefficient  $k_i$  (see page 161) are known, or estimated, Equation (2-18) can be written as follows:

$$v_{hov} = k_i v_i \quad (2-18a)$$

Having  $v_{hov}$ , it is easy to calculate the vertical rate of climb  $V_c$  from Equation (2-17a) which, in ft/min, will be

$$V_c = \frac{33000}{W} \left( P_{id_{av}} - \frac{P_{ind}^2}{P_{id}} \right) \quad (2-19)$$

Remembering that maximum rotor/propeller horsepower available at ambient conditions of altitude  $H$  and temperature  $T$  is  $SHP_{av} = SHP_{INS} \eta_{tr} \lambda_{TH}$  and remembering the expression for the profile power per pound of gross weight (see page 168) Equation (2-19) can be rewritten as

$$V_c = 60 \left[ 550 \left( \frac{SHP_{INS}}{W} \right) \eta_{tr} \lambda_{HT} - \frac{3}{4} \frac{V_t}{(\bar{c}_{lh} / \bar{c}_{doh})} + \frac{k_i^2 (W/2\rho)}{550 \left( \frac{SHP_{INS}}{W} \right) \eta_{tr} \lambda_{HT} - \frac{3}{4} \frac{V_t}{(\bar{c}_{lh} / \bar{c}_{doh})}} \right] \quad (2-20)$$

The above equation, giving vertical rate of climb in ft/min, permits to ascertain the importance of various design-wise significant parameters, as well as to perform actual calculations of the vertical rate of climb at various gross weights and a given altitude and ambient temperature (Fig. 2-13). Conversely, it also permits to calculate the vertical rate of climb at a constant gross weight and varying altitude, thus determining the practical hovering ceiling at a constant gross weight (Fig. 2-14).

Since, away from the hovering ceiling conditions, VTOL aircraft may exhibit high rates of vertical climb, a significant vertical drag may be developed. Whenever such a situation exists, power associated with that vertical drag should be estimated, and in the determination of the ideal power for climb in Equation (2-12), subtracted, in addition to the profile power term.

## 2.6 NOISE OF ROTOR/PROPELLERS IN HOVER

Noise aspects in and near hovering regimes of flight are especially important from the operational viewpoint of the civilian VTOL aircraft (see for instance pp. 5C-53 of Reference 2-20) chiefly because of the human reaction. In military operations, noise is related to the problem of minimizing detection. In this latter respect, noise aspects in forward flight are probably more important. However, in spite of much research (as exemplified by References 2-21 to 2-30), many phenomena of noise generation and especially the relationship between noise signature and its acceptability to the human ear is not fully understood as yet. For this reason, it is necessary to use such methods as synthesis of the flight noise signature and subsequent investigation of subjective responses of a large group of people (see for instance, Reference 2-31). With reference to rotors and propellers, there are numerous methods (see appropriate references in the 2-21 to 2-30

group) for predicting their sound pressure levels as well as frequencies of the noise spectrum. These methods usually predict sound levels and frequencies associated with vortex noise and rotational noise.

However, of particular significance because of its annoyance for the human ear (civilian applications) and a low decay of its intensity with distance (military aspect) is the banging noise. This noise manifests itself quite distinctively on such low RPM airscrews as helicopter rotors, but according to H. Sternfeld of Boeing, Vertol Division, it may exist somewhat "masked" because of its frequency in the higher RPM propeller-type airscrews as well. Sternfeld defines the bang as an acoustical noise from the rotor or propeller system, which occurs at rotor passage period and is characterized objectively by high rates of pressure rise (spiked wave forms), and subjectively by an annoying sharp quality.

It appears that there are special conditions that contribute to the rotor/propeller bang (and thus should be avoided for a satisfactory external noise level). These conditions are: (1) combination of high blade loading and high tip speed which (especially for rotors) can produce, even in hover, a recirculation of the vortex through the airscrew disc; (2) high resultant velocity of the advancing tip (as it may occur during transition with a partial tilt of the airscrew) which may result in high pressure fluctuations due to compressibility effects, and (3) multi-rotor/propeller configurations when the tip vortex shed from one rotor or propeller is intersected by a blade from the other one.

Figures 2-15 and 2-16, reproduced from Reference 2-23, will illustrate the above statements.

Further insight into generation of the banging can be gained through the following considerations outlined by Sternfeld.

Leverton and Taylor of the University of Southampton show that the sound pressure level (SPL) of a rotor intersecting a vortex is proportional to the following parameters:

$$\text{SPL} \sim V^4 L^2 l^2 \quad (2-21)$$

where  $V$  is the velocity of intersection,  $L$  is the blade span loading and  $l$  is the length of the intersection.

In the case of a blade intersecting a vortex generated by its own rotor or propeller, it may be assumed that the length of intersection is constant, and thus it may be anticipated that lines defined by constant values of the  $V_t^2 L$  product will separate regions of acceptable and unacceptable (say, because of subjective reactions) combinations of tip speeds ( $V_t$ ) and blade span loading. Figure 2-17 is an example of regions of acceptability of the bang noise of a single rotor propeller, established on the basis of subjective reaction to noise produced by a helicopter rotor under static conditions. It should be noted that in this approach, blade span loading rather than blade loading per se (as in Figure 2-15) is considered as a significant parameter. Figure 2-18 is another example of a combination of different parameters (this time resultant Mach number at the advancing tip and blade thickness ratio) affecting the acceptable noise level. Although Figure 2-18 refers to the helicopter rotor in forward flight, nevertheless, it is shown here to call attention to the importance of airfoil thickness ratio in combination with the resultant Mach number.

The whole brief discussion of the external noise problem outlined in this section, should emphasize that quite often operational requirements may force upon the designer a deviation from some parameter values appearing favorable from the pure aerodynamic or structural (e.g. weight) point of view. Both tip speed and blade loading are good examples in that respect.



## 2.7 MONOCYCLIC CONTROL OF RIGID ROTOR/PROPELLER

It was indicated in Chapter I that monocyclic rotor/propeller control may find an application in hovering and low speed control of aircraft incorporating articulated as well as "rigid" blades. Principles of the cyclic control in general, or monocyclic in particular, with respect to articulated blades are well known (see for instance, References 2-1, 2-2 and 2-32) because of the long history of their application to the helicopter rotor. Attention here will, hence, be called to the monocyclic control of "rigid" rotors/propellers only. One of the early proofs of basic feasibility of this concept as a source of pitching control and trimming moments was furnished by the NASA, Ames tests of the Vertol 76 (VZ-2) rigidized propeller (Ref. 2-33). Consequent test results published (Ref. 3-34) and unpublished, with models of various scales (up to 5 ft diameter) performed by Boeing, Vertol Div. further confirmed the initial findings.

In order to get a better insight into functioning of the monocyclic control, the combined momentum-blade element theory will be used to explain its principles.

The elementary moment about the  $y$ - $y$  axis ( $dM_{x\psi}$ ) developed by thrust element  $dT_{x\psi}$  located on the disc of radius  $R$  by the coordinates  $(x, \psi)$  can be written (see Figure 2-19) as

$$dM_{x\psi} = dT_{x\psi} R_x \cos \psi. \quad (2-22)$$

Using notations from Figure 2-19, thrust  $dT_{x\psi}$  developed by an element (of area  $dS = R^2 dx d\psi$ ) located on the disc by the coordinates  $(x, \psi)$  can be expressed according to the momentum theory as

$$dT_{x\psi} = 2\rho R^2 v_{x\psi}^2 x dx d\psi, \quad (2-23)$$

where  $v_{x\psi}$  is the induced velocity at the considered element. The same elementary thrust can also be expressed using notions of the blade element theory.

For an airscrew with  $b$  blades and known blade chord  $c_x$  at the station  $x$ , the thrust value "credited" to the considered element of the disc would be

$$dT_{x\psi} = (d\psi/2\pi) \frac{1}{2} \rho (xV_t)^2 b c_x R c_{l_{x\psi}} dx \quad (2-24)$$

where  $c_{l_{x\psi}}$  is the blade section lift coefficient existing at the disc coordinates  $x, \psi$ . Assuming for simplicity that the blade is of constant chord ( $c_x = \text{const} = c$ ),  $b c R = \sigma \pi R^2$  where  $\sigma$  is the rotor/propeller solidity. But blade section lift coefficient can be expressed in terms of the lift curve slope,  $a$ ; local geometric blade pitch angle,  $\theta_{x\psi}$ ; and the induced flow angle which, within validity of the small angles assumption, is  $v_{x\psi}/xV_t$ :

$$c_{l_{x\psi}} = a [\theta_{x\psi} - (v_{x\psi}/xV_t)].$$

Equation (2-24) can be rewritten now as

$$dT_{x\psi} = \frac{1}{4} \rho R^2 (xV_t)^2 \sigma a [\theta_{x\psi} - (v_{x\psi}/xV_t)] dx d\psi. \quad (2-24a)$$

Equating right sides of Equations (2-23) and (2-24a), a quadratic equation in  $v_{x\psi}$  is obtained that permits to find values of the induced velocity at any point  $(x, \psi)$  of the airscrew disc when geometry of the rotor/propeller, its tip speed and control inputs, needed to define the  $\theta_{x\psi}$  values, are known.

$$v_{x\psi} = V_t \left[ -\frac{1}{16} \sigma a + \sqrt{\left\{ \left( \frac{1}{16} \sigma a \right)^2 + \frac{1}{8} \sigma a x \theta_{x\psi} \right\}} \right]. \quad (2-25)$$

As to the  $v_{x\psi}$  value, it can easily be determined for a nominal blade pitch angle at the root ( $\theta_0$ ), total blade twist value  $\theta_t$  (usually negative) and its distribution along the blade  $\theta_t f(x)$  and, finally, control inputs  $\theta_{c\psi}$ :

$$\theta_{x\psi} = \theta_0 + \theta_t f(x) + \theta_{c\psi}.$$

When monocyclic for pitch control is used and  $\theta_m$  is the control input (half amplitude);  $\theta_{c\psi} = \theta_m \cos \psi$  and Equation (2-25) can now be rewritten as

$$v_{x\psi} = v_t - \left[ \frac{1}{16} \sigma a + \sqrt{\left( \frac{1}{16} \sigma a \right)^2 + \frac{1}{8} \sigma a x (\theta_0 + \theta_t f(x) + \theta_m \cos \psi)} \right]. \quad (2-25a)$$

Equation (2-25a) substituted into Equation (2-23) permits now to calculate the elementary thrust ( $dT_{x\psi}$ ) or local disc loading ( $dT/R^2 x dx d\psi$ ) at any point ( $x, \psi$ ) of the rotor/propeller disc. Total thrust developed by the rotor/propeller under these circumstances will be

$$T = 2\rho R^2 \int_{x_1}^{x_t} \int_0^{2\pi} v_{x\psi}^2 x dx d\psi, \quad (2-26)$$

where  $x_1$  is the inboard station where the blade begins and  $x_t$  is the tip station up to which the integration is carried (usually  $x_t \approx 0.97$ ).

The induced power ( $P_{ind}$ , in ft lb/sec) corresponding to that thrust  $T$  will be:

$$P_{ind} = 2\rho R^2 \int_{x_1}^{x_t} \int_0^{2\pi} v_{x\psi}^3 x^2 dx d\psi. \quad (2-27)$$

while total moment (in ft-lb) about the  $y$ - $y$  axis can be obtained by substituting into Equation (2-22), Equation (2-23) with  $v_{x\psi}$  expressed by Equation (2-25a) and integrating over the whole disc:

$$M = 2\rho R^3 \int_{x_1}^{x_t} \int_0^{2\pi} v_{x\psi}^2 x^2 \cos \psi dx d\psi. \quad (2-28)$$

In order to have a better feel regarding the effectiveness of the monocyclic, it is often desirable to know what offset ( $m$ ) of the total thrust (expressed as a fraction or percentage of the rotor/propeller radius) is equivalent to the pitching moment produced by a given monocyclic control input: since  $M = mRT$ ,

$$m = M/RT. \quad (2-29)$$

A graph showing  $m = f(\theta_m)$  can be prepared and the  $dm/d\theta_m$  slope obtained by substituting into Equation (2-29), Equations (2-26) and (2-28) and computing values corresponding to selected monocyclic inputs  $\theta_m$ .

As to the computational procedures required to obtain values of thrust, moment and induced power (Equations (2-26), (2-27) and (2-28)) numerical, or even graphical methods of integration will probably be more suitable for the actual practice than an attempt to find a close form solution of the indicated integrals.

In order to get a better insight into the anatomy of monocyclic, it may be advisable to examine thrust, induced power and moment associated with a ring of  $Rx$  radius and  $\Delta R = R\Delta x$  width. Because of application of the monocyclic (say,  $\theta_m$ ; i.e. pitch down), induced velocity in the  $3\pi/2$  to  $\pi/2$  azimuth sector (Fig.2-19) will be higher than that corresponding to the  $\theta_m = 0$  value. On the other hand, it will be lower in the  $\pi/2$  to  $3\pi/2$  sector. The character of that velocity variation will be as in Figure 2-10.

For given  $\theta_0$  and  $\theta_m$  values, it probably can be approximated by the relationship

$$v_{x\psi} = v_x(1 + k \cos \psi), \quad (2-30)$$

where  $v_x$  is the induced velocity at the  $x$  station for a given  $\theta_0$  and  $\theta_m = 0$ , and  $k$  is a proper coefficient.

To improve the approximation of velocity distribution with  $\psi$ , two values of  $k$  may be selected, say  $k_1$  for the  $\pi/2$  to  $3\pi/2$ , and  $k_2$  for  $3\pi/2$  to  $\pi/2$  sectors. Using Equation (2-26) and selecting  $R\Delta x$  small enough that downwash velocity variation with  $x$  can be neglected, total thrust developed by the considered ring becomes

$$\Delta T_{x\psi} = 4R^2x\rho v_x^2 \left[ \int_0^{\pi/2} (1 + k_1 \cos \psi)^2 d\psi + \int_{\pi/2}^{\pi} (1 + k_2 \cos \psi)^2 d\psi \right]. \quad (2-31)$$

Performing the integration indicated in Equation (2-31) and dividing the result by  $4\pi R^2x\rho v_x^2$  (i.e. by the thrust for  $\theta_m = 0$ ), the ratio of thrust developed by the considered ring with monocyclic to that without it is obtained:

$$\Delta T_{x\psi}/\Delta T_x = 1 + \frac{1}{4}(k_1^2 + k_2^2) - \frac{2}{\pi}(k_2 - k_1). \quad (2-32)$$

Through a similar process, the ratio of induced powers can be obtained:

$$\Delta P_{ind_{x\psi}}/\Delta P_{ind_x} = 1 - \frac{3}{\pi}(k_2 - k_1) + \frac{3}{4}(k_1^2 + k_2^2) - \frac{2}{3\pi}(k_2^3 - k_1^3), \quad (2-33)$$

while shift of the thrust vector ( $\Delta T_{x\psi}$ ) expressed as a fraction ( $m_x$ ) of the rotor propeller radius ( $R$ ) becomes

$$m_x = \frac{x(2k_1 + 2k_2 + k_1^2 + k_2^2)}{4 \left[ 1 + \frac{1}{4}(k_1^2 + k_2^2) - \frac{2}{\pi}(k_2 - k_1) \right]}. \quad (2-34)$$

For example, for the case shown in Figure 2-20; representing  $v_{x\psi} = f(\psi)$  at  $x = 0.8$  for a propeller with disc loading of  $w = 40 \text{ lb/ft}^2$ ,  $V_t = 800 \text{ ft/sec}$ ,  $\theta_t = -20^\circ$ , and  $\sigma = 0.28$ ; for  $\theta_m = 8^\circ$ :  $\Delta T_{x\psi}/\Delta T_x \approx 1.075$ ,  $\Delta P_{ind_{x\psi}} \approx 1.3$  and  $m_x \approx 0.5$ . It can be

seen from the above example that application of  $8^\circ$  of cyclic produced, at the radius  $r = 0.8R$  a large shift in the thrust vector accompanied by some increase in the thrust produced by the considered ring and rather considerable increase in the induced power. Dividing the whole disc into a number of rings, examining thrust, induced power and thrust vector shift associated with the application of the monocyclic and summing up the results, it is possible to quickly obtain a rough idea about the changes of those values for the propeller as a whole.

It should be indicated at the end of these considerations that the whole problem of the monocyclic control can also be approached through the vortex theory; for instance, as outlined by R.H.Miller and discussed in Reference 2-34.

Finally, it should be noted that monocyclic inputs may introduce a rapid periodic variation of the blade section angle of attack. This oscillatory movement of the blades will obviously introduce special aspects of unsteady aerodynamics. The whole field of unsteady aerodynamics that owes its initial development to the flutter phenomena now gets new attention because of its importance to the rotary wing aircraft. From the steadily growing number of theoretical and experimental research studies, for example, the works of J.Liiva and F.Davenport (Refs. 2-35 and 2-36) typify current efforts in that domain.

#### REFERENCES TO CHAPTER II

- 2-1. Stepniewski, W.Z. *Introduction to Helicopter Aerodynamics*, Rotorcraft Publishing Committee, Morton, Pa. 1958.
- 2-2. McCormick, B.W., Jr *Aerodynamics of V/STOL Flight*, Academic Press, New York, London, 1967.
- 2-3. Goldstein, S. *On the Vortex Theory of Screw Propellers*, Royal Society Proceedings, (a) Vol.123, 1929.
- 2-4. Lock, C.N.H. *Application of Goldstein's Airscrew Theory to Design*, ARC R & M 1377, 1930.
- 2-5. Theodorsen, T. *The Theory of Propellers, Parts I, II, III and IV*, NACA Reports Nos. 775, 776, 777 and 778.
- 2-6. Knight, M.  
Hefner, R.A. *Static Thrust Analysis of the Lifting Airscrew*, NACA TN 626, 1937.
- 2-7. Heyson, H.H. *An Evaluation of Linearized Vortex Theory as Applied to Single and Multiple Rotors Hovering In and Out of Ground Effect*, NASA TN D-43, Sept. 1959.
- 2-8. Daughaday, H.  
Piziali, R.A. *An Improved Computational Model for Predicting the Unsteady Aerodynamic Loads of Rotor Blades*, Journal of the AHS, Vol.II, No.4, Oct. 1966.
- 2-9. Loewy, R.G. *A Two-Dimensional Approach to the Unsteady Aerodynamics of Rotary Wings*, IAS, Vol.24, No.2, Feb. 1957.
- 2-10. Miller, R.H. *Rotor Blade Harmonic Air Loading*, AIAA Journal, Vol.2, No.7, July, 1964.
- 2-11. Brady, W.G.  
Crimi, P. *Representation of Propeller Wakes by Systems of Finite Core Vortices*, Cornell Aeronautical Laboratory Report No.BB-1665-S-2, Feb. 1965.
- 2-12. DuWaldt, F.A. *Representation of Propeller Wakes by Systems of Finite Core Vortices*, Cornell Aeronautical Laboratory Report No.BB-1665-3, Nov. 1966.
- 2-13. Crimi, P. *Theoretical Prediction of the Flow in the Wake of a Helicopter Rotor, Part I - Development of Theory and Results of Computations and Part II - Formulation and Application of the Rotor-Wake-Flow Computer Program*, Cornell Aeronautical Laboratory Report Nos. BB-1994-S-1 and BB-1994-S-2, respectively, Sept. 1965.

- 2-14. Van Shi-Tsun. *The Aerodynamic Characteristics of a Loaded Helicopter Rotor from a Three-Dimensional Vortex System*, *Aviatsionnaya Tekhnika* No.1, 1961, pp.3-12, Trans. 1013 RAE, Nov. 1962.
- 2-15. Lepikkin, A.M. *Vortex Theory of a Lifting Airscrew and Mutual Influence of Airscrews*, *Izvestia Akademii Nauk of USSR*, No.5, 1963.
- 2-16. Durand, W.F. *Aerodynamic Theory*, Vol.IV, Div. L, Durand Reprinting Committee, Cal Tech., 1943.
- 2-17. Schade, R.O. *Ground Interference Effects*, NASA TN D-727, April 1961.
- 2-18. Newsom, W.A., Jr *Effect of Ground Proximity on the Aerodynamic Characteristics of a Four-Engine Vertical-Take-Off-and-Landing Transport-Airplane Model with Tilting Wing and Propellers*, NACA TN 4124, Oct. 1957.
- 2-19. Newsom, W.A.  
Tosti, L.P. *Slipstream Flow Around Several Tilt-Wing VTOL Aircraft Models Operating Near the Ground*, NASA TN D-1382, 1962.
- 2-20. Staff of Langley  
Research Center *A Preliminary Study of V/STOL Transport Aircraft and Bibliography of NASA Research in the VTOL-STOL Field*, NASA TN D-624, Jan. 1961.
- 2-21. Hubbard, Harvey H.  
Maglieri, Domenic J. *Noise Characteristics of Helicopter Rotors at Tip Speeds up to 900 Feet per Second*, *Jour. Acous. Soc. of America*, Vol.32, No.9, Sept. 1960, pp.1105-1107.
- 2-22. Hubbard, Harvey H. *Propeller-Noise Charts for Transport Airplanes*, NACA TN 2968, 1953.
- 2-23. Maglieri, D.J.  
et al. *Noise Considerations in the Design and Operation of V/STOL Aircraft*, NASA TN
- 2-24. ARP 865 *Definitions and Procedures for Computing the Perceived Noise Level of Aircraft Noise*, Society of Automotive Engineers Aerospace Recommended Practice, Oct. 1964.
- 2-25. Beranek, L.L. *Noise Reduction*, McGraw-Hill Book Co., Inc., New York, 1960.
- 2-26. Lawson, M.V. *Basic Mechanisms of Noise Generation by Helicopters, V/STOL Aircraft, and Ground Effect Machines*, Wyle Laboratories, Research Staff Report No.WR 65-9, May, 1965.
- 2-27. Schlegel, R.  
et al. *Helicopter Rotor Noise Generation and Propagation*, USAAVLABS Technical Report 66-4, Oct. 1966.
- 2-28. Loewy, R.G.  
Sutton, L.R. *A Theory for Predicting the Rotational Noise of Lifting Rotors in Forward Flight, including a Comparison with Experiment*, *Journal of Sound and Vibration*, Vol.4, No.3, Nov. 1966.
- 2-29. Hargest, T.J. *VTOL Aircraft Noise*, AGARD Conference Proceedings No.22, Gottingen, Germany, Sept. 1967.
- 2-30. Kenyon, G.C. *Noise Considerations for V/STOL Transports*, AIAA Paper No. 68-194, Feb. 1968.

- 2-31. Hinterkeuser, E.G.  
Sternfeld, H., Jr      *Subjective Response to Synthesized Flight Noise Signatures of Several Types of V/STOL Aircraft*, Boeing, Vertol Div. Document D8-0907A, prepared under contract to NASA.
- 2-32. Gessow, A.  
Myers, G.C.              *Aerodynamics of the Helicopter*, The MacMillan Company, New York, 1952.
- 2-33. Wort, K.W.  
Yaggy, P.F.              *Aerodynamic Characteristics of a Full-Scale Propeller with both Rigid & Flapping Blades and with Cyclic Pitch Control*, NASA TN D-1774, May 1963.
- 2-34. Fay, C.B.            *Recent Development in Simplifying & Improving the Tilt-Wing Design*, Proceedings of the Twentieth Annual Forum of AHS, May, 1964.
- 2-35. Liiva, J.             *Unsteady Aerodynamic and Stall Effects on Helicopter Rotor Blade Airfoil Sections*, Paper No.68-58, presented at the 6th Aerospace Sciences Meeting of the American Inst. of Aeronautics and Astronautics, Jan. 1968.
- 2-36. Liiva, J.  
et al.                      *Two-Dimensional Tests of Airfoils Oscillating Near Stall, Vol.I, Summary and Evaluation of Results*, Boeing Document D8-0678-1, Oct. 1967.

## CHAPTER III

## SOME PROBLEMS OF FORWARD FLIGHT

## 3.1 PROPULSIVE EFFICIENCY OF ROTOR-PROPELLER

With the exception of the tilting rotor with folding blades (Fig.1-11), in all other concepts of rotor-propeller convertible aircraft, the same airscrew is used in hovering for vertical thrust generation and, later, as a source of propelling thrust in cruise and high speed flight. As a result of this double role, there is a special category of problems resulting from large differences in thrust required and inflow conditions in hover and in forward flight. Various aspects of aerodynamic efficiency at static conditions ( $\eta_A$ ) were discussed in Section 2.1. Here, attention will be focused on propulsive efficiency ( $\eta_{pr}$ ) through the whole spectrum of forward flight. As in the case of hovering, the combined momentum-blade element theory is selected as a guide to a better understanding of the forward flight problems.

In order to facilitate considerations of propulsive efficiency, it is broken down into that based purely on the momentum considerations (Froude's efficiency) and that resulting from the presence of the profile drag. In order to have a better feel on whether, in the considerations of the profile drag effects, induced velocities may be neglected, the order of magnitude of induced velocities that may be encountered in practice will be indicated.

The ideal (uniform) induced velocity in forward flight (see Equation (2-7)) can be expressed as

$$v = \frac{1}{2}V(-1 + \sqrt{1 + w_f/q_f}) , \quad (3-1)$$

where  $w_f$  is the propeller disc loading in forward flight and  $q_f$  is the dynamic pressure of forward flight ( $q_f = (1/2)\rho V^2$ ). It should be noticed that at any given speed,  $V$ ,

$$w_f = \frac{w_h}{(L/D)_v} ,$$

where  $w_h$  is propeller disc loading in hovering and  $(L/D)_v$  is the lift/drag ratio of aircraft at speed  $V$ .

Since for VTOL configurations at speeds higher than 100 knots,  $w_f/w_q \ll 1.0$ , it may be assumed that

$$-1 + \sqrt{1 + w_f/q_f} \simeq \frac{1}{2} \frac{w_f}{q_f} ,$$

and hence

$$v = \frac{1}{4}V \frac{w_f}{q_f} = \frac{1}{4}V \frac{w_h}{(L/D)_v q_f} , \quad (3-2)$$

or

$$v = \frac{1}{2} [w_h / \rho (L/D)_v V] , \quad (3-2a)$$

while the ratio of average induced velocity to forward speed becomes

$$\nu \equiv \frac{v}{V} = \frac{1}{4} \frac{w_h}{(L/D)_V q_f} \quad (3-3)$$

Froude's propulsive efficiency (based on the ideal induced velocity),  $\eta_{FR} = 1/(1 + v/V) = 1/(1 + \nu)$  becomes

$$\eta_{FR} = \frac{1}{1 + \frac{1}{4} \frac{w_h}{(L/D)_V q_t \mu_f^2}} \quad (3-4)$$

or

$$\eta_{FR} = \frac{1}{1 + \frac{1}{4} \frac{w_h}{(L/D)_V q_f}} \quad (3-4a)$$

where  $q_t$  is the dynamic pressure based on propeller tip speed and  $\mu_f = V/V_t$  is the ratio of forward speed to tip speed.

Equation (3-2a) indicates that at sufficiently high forward speeds ( $w_f \ll q_f$ ), it may be assumed that at a given  $V$  value, the average induced velocity is proportional to the disc loading in hovering and inversely proportional to the lift to drag ratio value at this speed  $V$ .

In order to have some idea of the lift to drag ratio which may be incurred in aircraft V/STOL transports, Figure 3-1a was prepared, while Figure 3-1b shows induced velocities that may correspond to the assumed  $L/D$  envelope of Figure 3-1a and 3 disc loadings in hover. A glance at Figure 3-1b would indicate that for the speed range of 100 to 400 knots, the induced velocities are quite low by comparison with those of forward flight and thus may be neglected in the construction of velocity diagrams at various blade stations (Fig.3-2).

The ideal induced velocity values shown in Figure 3-1b show that Froude efficiency ( $\eta_{FR}$ ) based on them will be quite high in cruise and at high-speed flight even for propellers having high disc loadings in hovering. For instance, at  $V > 200$  knots,  $\eta_{FR}$  will approach, or exceed, the 99% value even for  $w_h = 60 \text{ lb/ft}^2$ .

It should be remembered, however, that in actual practice, the induced power efficiency may be lower (by several percent) than its ideal Froude value. This will be due to the fact that section lift coefficients of various blade stations will be very low, since they will be of the same order of magnitude as the average lift coefficient in forward flight ( $\bar{c}_{lf}$ ), whose value can be expressed as

$$\bar{c}_{lf} \approx [\bar{c}_{lh}/(L/D)_V] (V_{th}/V_{tf})^2.$$

It is apparent, hence, that even small deviations from the station pitch values  $[\theta_x = \theta_0 + \theta_t f(x)]$ , required for a uniform induced velocity distribution, may result in large non-uniformities or even in negative induced velocities, thus leading to lower induced efficiencies than those indicated by their ideal Froude values.

The non-Froude propulsive efficiency, i.e. that resulting from the presence of profile drag can be studied by calling attention to its values ( $\eta_x$ ) at various blade stations ( $x \equiv r/R$ ).



Thrust coefficient  $C_{Tx}$  at a blade station  $x$  can be determined from relationships resulting from the combined momentum and blade element theories.

Since, at cruise and at high speeds (regimes of flight of interest)  $v \ll V$ ,  $v$  can be neglected in determining resultant speed at station  $x$  (see Figure 3-2).

Under those assumptions, equations expressing elementary thrust  $dT$  according to the momentum and blade element theories can be written as one equation relating blade characteristics and induced velocity:

$$2\pi\rho R dx (V + v)2v = \frac{1}{2} \rho [V^2 + (V_t x)^2] C_{Tx} \sigma \pi R^2 dx \quad (3-5)$$

Denoting  $\mu_f \equiv V/V_t$ , and remembering that  $\nu \equiv v/V$  and simplifying, Equation (3-5) yields

$$C_{Tx} = \frac{8\mu_f^2(\nu + \nu^2)}{\sigma(\mu_f^2 + x^2)} \quad (3-6)$$

Since  $\nu$  is small, it may be assumed that  $\nu^2 \simeq 0$ , and Equation (3-6) can be still further simplified to

$$C_{Tx} = \frac{8\mu_f^2\nu}{\sigma(\mu_f^2 + x^2)} \quad (3-6a)$$

Solidity  $\sigma$  can be expressed as a ratio of the hovering disc loading ( $w_h$ ) to the blade loading also in hover  $\sigma \equiv w_h/w_{bh}$  and Equation (3-6a) can be rewritten again as

$$C_{Tx} = \frac{8\mu_f^2\nu}{(w_h/w_{bh})(\mu_f^2 + x^2)} \quad (3-6b)$$

This latter expression can still be modified by expressing  $\nu$  according to Equation (3-3) and remembering that dynamic pressure in forward speed is  $q_f = q_t \mu_f^2$ , where  $q_t$  is the dynamic pressure at the propeller tip at a given  $V_t$ :

$$C_{Tx} = \frac{2w_{bh}}{(\mu_f^2 + x^2)(L/D)_v q_t} \quad (3-6c)$$

Equation (3-6c) represents a suitable form for expressing thrust coefficient at station  $x$  in terms of significant design parameters (forward speed/tip speed ratio:  $\mu_f$ ; blade loading in hovering:  $w_{bh}$ ; aircraft lift/drag ratio:  $L/D$ ; and blade tip dynamic pressure:  $q_t$ , at a given tip speed  $V_t$ ).

Lift coefficient at station  $x$  can be expressed in terms of  $C_{Tx}$  and propeller blade profile drag coefficient  $c_{do}$ . It can be seen from Figure 3-2 that:

$$C_{lx} = \left( C_{Tx} + c_{do} \frac{\mu_f}{\sqrt{(\mu_f^2 + x^2)}} \right) \frac{\sqrt{(\mu_f^2 + x^2)}}{x} \quad (3-7)$$

Substituting for  $C_{Tx}$  its value from Equation (3-6c), Equation (3-7) becomes

$$C_{lx} = \frac{2w_{bh}}{\sqrt{(\mu_f^2 + x^2)}(L/D)q_t x} + c_{do} \frac{\mu_f}{x} \quad (3-7a)$$

Propulsive Efficiency at station  $x$ , disregarding induced velocity (Froude efficiency), can be determined using notations from Figure 3-2, as follows;

$$\eta_x = \frac{VdT_x}{xV_t dD_{Qx}} = \frac{\mu_f C_{Tx}}{x C_{DQx}} \quad (3-8)$$

But, from Figure 3-2, it can be determined that

$$C_{DQx} = c_{do} \frac{x}{\sqrt{(\mu_f^2 + x^2)}} + \left( \frac{\mu_f}{x} C_{Tx} + c_{do} \frac{\mu_f}{\sqrt{(\mu_f^2 + x^2)}} \right) \quad (3-9)$$

Substituting Equations (3-9) and (3-6c) into (3-8), and simplifying, one obtains

$$\eta_x = \frac{1}{1 + \frac{c_{do}(L/D)_v q_t}{2\mu_f w_{bh}} (\mu_f^2 + x^2)^{3/2}} \quad (3-10)$$

Remembering that the dynamic pressure corresponding to the blade tip speed ( $q_t$ ) can also be expressed in terms of the flight dynamic pressure ( $q_f$ ) and forward velocity to the tip speed ratio ( $\mu_f = V/V_t$ );  $q_t = q_f/\mu_f^2$ , Equation (3-10) can be rewritten as follows:

$$\eta_x = \frac{1}{1 + \frac{c_{do}(L/D)_v q_f}{2w_{bh}} (1 + x^2/\mu_f^2)^{3/2}} \quad (3-10a)$$

Equations (3-10) and (3-10a) permit interpreting the importance of various significant design parameters for the non-Froude propulsive efficiency at a given blade station.

The non-Froude propulsive efficiency ( $\eta_{nF}$ ) for the whole blade and hence, for the whole airscrew will be:

$$\eta_{nF} = \int_{x_0}^{1.0} \frac{2\pi R_x}{\pi R^2 (1 - x_0^2)} \eta_x R dx = \frac{2}{(1 - x_0^2)} \int_{x_0}^{1.0} \eta_x x dx \quad (3-11)$$

where  $x_0$  is the blade inboard station.

It can be shown that  $\eta_x$  at  $x = 0.75$  approximates quite well  $\eta_{nF}$ . Finally, corrections due to Froude's efficiency can be included, giving the overall, but still idealized\*, propeller propulsive efficiency as:

$$\eta_{pr} = \eta_{0.75} \eta_{nF} = \frac{1}{1 + \frac{c_{do}(L/D)_v q_f}{2w_{bh}} \left(1 + \frac{0.75^2}{\mu_f^2}\right)^{3/2}} \frac{1}{1 + \frac{1}{4} \frac{w_h}{(L/D)_v q_f}} \quad (3-12)$$

Looking at the first term of Equation (3-12), it becomes clear that, in order to obtain the highest possible efficiency at a given speed, it means at a known  $L/D$ , and  $q_f$ , profile coefficient should be kept as low as possible, while blade loading in hovering should be made as high as possible (small blade area).

---

\* It includes the ideal Froude and not true induced power efficiency.

This shows that various means (from airfoil shapes to active BLC) offering high blade section lift coefficients in hover (and the resulting high  $w_{bh}$  values) and low profile drag coefficients at  $c_{lx}$  values expected in cruise, should be considered regarding their possibilities of improving the forward flight propulsive efficiency of rotor/propellers.

It should also be noted that an effective increase in the blade loading in forward flight can be achieved through variable diameter (reduced for forward flight) rotor/propellers. An additional advantage of this arrangement would be operation in forward flight at higher section lift coefficients, thus making the blade less sensitive to the deviation of the blade pitch distribution from their ideal values (improved actual Froude efficiency).

As to the tip speed in forward flight, it is clear that it should be kept as low as practical in order to reduce the  $x^2/\mu_t^2$  values. However, in determining the practical lower limit design penalties that may be associated with a high tip speed reduction (ex. need for a gear shift arrangement) should be considered. On the aerodynamic side, it should be checked whether  $c_l$ 's will not increase beyond limits leading to higher  $c_{do}$  values.

Figure 3-3 was prepared with the intent to indicate the trends regarding the influence of tip speed and profile power coefficient values on the non-Froude propulsive efficiencies. Because of the assumed high (probably beyond present state of the art) blade loading values ( $w_b = 165 \text{ lb/ft}^2$ ) and some simplifying assumptions, this figure should be regarded as an illustration of trends only.

Blade twist distribution represents another area where it is difficult to satisfy both hovering and forward speed requirements for rotor/propellers with fixed geometry blades, or without aerodynamic means equivalent to the variable geometry blades.

In order to find first the section lift distribution and then pitch angle distribution required to provide a uniform induced velocity through the disc both in forward flight and in hover, Equation (3-5) is rewritten in terms of  $c_{lx}$ . From Figure 3-2 one will find that  $C_{Tx} = c_{lx} V_t x / (V^2 + (V_t x)^2)$  and thus (considering Equation (3-5)) the  $c_{lx}$  value required to produce a uniform induced velocity\*  $v$  at a speed of flight  $V$  will be:

$$c_{lx} = 8(V + v)^2 / \sigma V_t \sqrt{V^2 + (V_t x)^2} . \quad (3-13)$$

In hovering, when  $V = 0$ , Equation (3-13) becomes

$$(c_{lx})_h = 8v_h^2 / \sigma V_t^2 x . \quad (3-14)$$

Since  $v_h^2 = w_h / 2\rho$ , or  $v_h^2 = \sigma w_{bh} / 2\rho$ , Equation (3-14) can be written as

$$(c_{lx})_h = 4w_{bh} / \rho V_t^2 x . \quad (3-14a)$$

It can be seen from Figure 3-2\*\* that total pitch angle ( $\theta_x$ ) at station  $x$  can be expressed in the case of forward flight as

$$\theta_x = \text{tg}^{-1}[(V + v)/V_t x] + \alpha_x . \quad (3-15)$$

where  $\alpha_x$  is the blade section angle of attack at station  $x$ .

Knowing the section lift coefficient value required to produce a uniform induced velocity and lift curve slope ( $a$ ) of the considered airfoil, Equation (3-15) becomes

\* Velocity  $v$  can be calculated from Equation (3-1).

\*\* In Figure 3-2, the induced velocity component ( $v$ ) is neglected.

$$c_{lx} = \text{tg}^{-1}[(V + v)/V_{cx}] + c_{lx}/a. \quad (3-15a)$$

Substituting into Equation (3-15a), for the case of forward flight, the  $c_{lx}$  values as given by Equation (3-13) and for hovering from Equation (3-14a), the section pitch distribution required in various regimes of flight and hence, the necessary built-in twist distribution can be obtained (Fig. 3-4).

Figure 3-5 clearly indicates that blade twist requirements for an optimum induced velocity distribution in hover and in high speed forward flight are quite different. This points out once more the difficulty of obtaining, in all regimes of flight, (from hover to  $V_{\max}$ ), the aerodynamic ( $\eta_A$ ) and propulsive ( $\eta_{pr}$ ) efficiencies that are possible for an airscrew optimized for a single flight condition.

Discussion presented in this section, together with that given in 2.1 may be quite helpful in the "first cut" phase of the rotor/propeller design. Once an approximate geometry of a rotor/propeller on that basis has been established, more refined methods, as, for instance, that outlined in Section 2.2 should be used.

### 3.2 AEROELASTIC INSTABILITIES

Problems of aeroelastic instabilities of rotors and large propellers in the propeller mode of operation attract more and more attention as witnessed by the constantly growing number of studies and publications on that subject (see as examples, Refs. 3-1 to 3-4). Of the many possible modes of instability, the backward whirling (Fig. 3-6) identified by W. Reed of NASA in conjunction with the Electra accidents (Ref. 3-1) is highly divergent.

Edenborough in Reference 3-4 indicates that destabilizing moment has the average value:

$$M_H = I_b(\dot{\phi}_x + \dot{a}_1)Vh/\bar{R}^2, \quad (3-16)$$

where  $I_b$  is the blade flapping inertia (slugs ft<sup>2</sup>),  $\dot{\phi}_x$  is the pylon rate (rad/sec),  $\dot{a}_1$  is the rotor longitudinal flapping rate (rad/sec),  $V$  is the speed of flight (ft/sec),  $h$  is the pylon mast length (ft) and  $\bar{R} \equiv 3R/4$  is the effective rotor radius.

Looking at Equation (3-16) from the point of view of aerodynamic parameters only, one finds that tendency toward instability will increase with the speed of flight. It also will be influenced by the flapping rate ( $\dot{a}_1$ ), but it should be remembered at this point that since the  $M_H$  values are proportioned to the expression in the brackets, hence, both magnitude and phase of the two variables ( $\dot{\phi}$  and  $\dot{a}_1$ ) are important.

M. Young and R. Lytwyn showed (Ref. 3-2) that optimum conditions for stability exist when the rotational natural frequency of the blade is  $1.1 < \omega_\beta/\Omega < 1.2$  where  $\omega_\beta$  is the rotating blade natural undamped frequency and  $\Omega$  is the rotor/propeller angular velocity (rad/sec). The above frequency limits seem to indicate that rotor/propellers with hingeless (non-articulated) blades probably can achieve the necessary stability without special stabilizing devices. However, it is stated in Reference 3-4 that simple mechanical means are available to provide rotor-pylon stability of a teetering rotor.

In addition to the rotor-pylon instability with all its structural integrity aspects, there are other aeroelastic instability phenomena which, although not potentially as destructive as the backward whirl, nevertheless may be of significance because of their influence on flying characteristics and control requirements of aircraft. Those phenomena, first noticed in conjunction with flight tests of the XV-3 tilting rotor aircraft (Ref. 3-5), are more likely to appear in the aircraft with large, lightly-loaded rotors and thus should be investigated both analytically and experimentally through such means as free flight tests of dynamically similar models.

### 3.3 ROTOR/PROPELLER DOWNWASH AT VARIOUS TILT ANGLES

With the exception of the deflected slipstream, in all other convertible rotor/propeller configurations the rotor/propeller axis is tilted from its approximately vertical position in hover to a roughly horizontal one in the high speed flight. An even approximate knowledge of the downwash developed by an airscrew throughout its tilt angle from  $i_T = 90^\circ$  (Fig.3-7) to  $0^\circ$  (horizontal) should contribute to a better understanding of the flow patterns and, hence, of the forces developed by aerodynamic surfaces submerged into those flows.

Formula for the fully developed downwash velocity ( $V_d = 2v$ ) in the propeller slipstream at a speed of flight  $V_f$  and at a rotor/propeller thrust inclination  $i_T$  can be developed from the following relationship (Ref.3-6)

$$550(\text{RHP} - P_{\text{pr}}) = T\left(\frac{1}{2} V_d + V_f \cos i_T\right), \quad (3-17)$$

where RHP is the power available at the rotor/propeller and  $P_{\text{pr}}$  is the rotor propeller profile power.

Using Glauert's theory of (unshrouded) airscrews, thrust  $T$  can be expressed in terms of the fully developed downwash and forward velocities:

$$T = \pi R^2 \rho \sqrt{\left(V_f^2 + \frac{1}{4} V_d^2 + V_f V_d \cos i_T\right)} V_d \quad (3-18)$$

Substituting Equation (3-17) into Equation (3-18), the following equation in  $V_d$  is obtained:

$$V_d \left(\frac{1}{2} V_d + V_f \cos i_T\right) \sqrt{\left(V_f^2 + \frac{1}{4} V_d^2 + V_f V_d \cos i_T\right)} = \frac{550(\text{RHP} - P_{\text{pr}})}{N\pi R^2 \rho}, \quad (3-19)$$

where the as yet undefined symbol  $N$  is the number of rotors or propellers.

Because of the high degree of Equation (3-19), finding a solution for every combination of the parameters  $V_f$ ,  $i_T$  and  $(\text{RHP} - P_{\text{pr}})/N\pi R^2 \rho$  may be inconvenient. A graph shown in Figure 3-8 may be quite helpful for a rapid estimation of the approximate downwash velocity for selected values of  $V_f$  and  $i_T$  and any effective power loading of the propeller discs divided by air density (right side of Equation (3-19)). This figure gives at least some qualitative idea about the influence of the above-mentioned parameters on the average downwash velocity in the fully developed slipstream.

Velocity of the rotor/propeller slipstream can now be added (vectorially) to that resulting from the translation of the aircraft itself (Fig.3-7) thus giving some notion regarding angle of attack and flow speed around aerodynamic surfaces submerged in the slipstream. As an illustrative example of this cursory analysis, a case of a two-propeller tilt wing will be considered.

### 3.4 EXAMPLE OF A TWO-PROPELLER TILT WING IN CONVERSION

It will be assumed for simplicity that the propeller thrust inclination ( $i_T$ ) is identical with the wing incidence (Fig.3-7).

Using notations of Figure 3-7, the resultant velocity,  $V_r$ , at the lifting line of the wing portion submerged in the slipstream can be expressed as

$$V_r = V_d \sqrt{\left[\left(\frac{V_f}{V_d}\right)^2 + 1 + 2\left(\frac{V_f}{V_d}\right) \cos(i_T - \delta)\right]}, \quad (3-20)$$

where  $\delta$  is the deflection of the free-stream ( $-V_f$ ) velocity vector due to the lift on the wing as a whole:

$$\delta = 57.3(C_{L_w}/\pi AR_w) .$$

Angle of attack of the slipstream-covered portion of the wing ( $\alpha_s$ ) becomes

$$\alpha_s = \text{tg}^{-1} \frac{(V_f/V_d) \sin(i_T - \delta)}{1 + (V_f/V_d) \cos(i_T - \delta)} . \quad (3-21)$$

Angle of attack of the part of the wing not covered by the slipstream is defined as  $\alpha_w$  and under the previously made assumption that the propeller thrust line coincides with the wing chord, it is identical with the thrust tilt angles:

$$\alpha_w = i_T .$$

Radius ( $R_s$ ) of the slipstream tube at the wing lifting line can be found from the continuity considerations as

$$R_s = R \sqrt{\left[ \frac{(V_f/V_d) \cos i_T + \frac{1}{2}}{(V_f/V_d) \cos i_T + 1} \right]} , \quad (3-22)$$

while total cross-sectional area ( $A_s$ ) of the slipstream of two propellers is

$$A_s = 2\pi R^2 \frac{(V_f/V_d) \cos i_T + \frac{1}{2}}{(V_f/V_d) \cos i_T + 1} . \quad (3-23)$$

Aspect ratio of the slipstream-covered part of the wing ( $AR_s$ ) is

$$AR_s = 4R_s^2/\frac{1}{2}S_s . \quad (3-24)$$

where  $S_s$  is the wing area covered by the slipstream of two propellers. For a constant wing chord ( $c$ ), Equation (3-24) becomes

$$AR_s = 2R_s/c . \quad (3-24a)$$

Using the momentum interpretation of lift generation by a wing (Ref.3-7), aerodynamic forces associated with the stream tube affected by the wing as a whole, but with the exclusion of the parts influenced by the propeller slipstream (see Figure 3-9) can be expressed as follows:

Lift ( $L_w$ ):

$$L_w = 2(C_{L_w}/\pi AR_w)V_f \rho [(\pi b^2/4) - A_s \cos \gamma] \quad (3-25)$$

Induced drag ( $D_{i_w}$ ):

$$D_{i_w} = L_w(C_{L_w}/\pi AR_w) \quad (3-26)$$

Profile drag ( $D_{o_w}$ ):

$$D_{o_w} = \frac{1}{2}[\rho V_f^2 C_{d_{o_w}}(S_w - S_s)] , \quad (3-27)$$

where  $S_s$  is the wing area covered by the slipstream.

In Equations (3-25) to (3-27), values of aerodynamic coefficients ( $C_{L_w}$ ) and ( $C_{d_{o_w}}$ ) are obtained for a given wing angle of attack ( $\alpha_w$ ) which, in horizontal flight, is identical with the tilt angle ( $i_T$ ), from a graph as in Figure 3-10 where the above

coefficients are shown through 0-90° angle of attack range\*.

Problems of lift produced by the propeller slipstream-covered portion of the wing have been investigated both experimentally and theoretically. References 3-7 to 3-9 may be given as examples of work performed in that domain, while the bibliography in References 3-8 and 3-9 would permit the interested reader to further enlarge his studies of this subject. However, in the present cursory considerations, the momentum approach will be used again with respect to lift ( $L_s$ ) generated by the slipstream-covered part of the wing in order to gain some insight into the phenomena of interaction between the propellers and the wing.

It can be seen from Figures 3-7 and 3-9 that the propeller-slipstream generated lift can be expressed as

$$L_s = 2A_s V_r \rho (V_r \alpha_{i_s}) , \quad (3-28)$$

where  $\alpha_{i_s}$  is the induced angle.

As a matter of convenience this induced angle can be expressed in terms of the lift coefficient ( $C_{L_s}$ ) of the slipstream-covered wing portion and the equivalent aspect ratio ( $AR_{e_s}$ ):

$$\alpha_{i_s} = C_{L_s} / \pi AR_{e_s} \quad (3-29)$$

and lift of the slipstream-covered portion of the wing becomes

$$L_s = 2A_s \frac{C_{L_s}}{\pi AR_{e_s}} V_r^2 \rho . \quad (3-30)$$

The induced drag ( $D_{i_s}$ ) is

$$D_{i_s} = L_s (C_{L_s} / \pi AR_{e_s}) \quad (3-31)$$

and the profile drag ( $D_{o_s}$ ) is

$$D_{o_s} = \frac{1}{2} (V_r^2 C_{d_{o_s}} S_s) . \quad (3-32)$$

In order to determine values of the lift coefficient ( $C_{L_s}$ ), it is necessary to know angle of attack ( $\alpha_s$ ) of the slipstream-covered wing portion and its effective aspect ratio. Having those two values, lift coefficient can be read from a graph as in Figure 3-10, as well as the corresponding profile drag coefficient.

As to the equivalent aspect ratio, a relationship between it and the geometric aspect ratio of the slipstream-covered portion [ $AR_s = 4R_s^2 / (\frac{1}{2} S_s)$ ] is selected under such mathematical form that at zero flight speed the equivalent aspect ratio is identical with the geometric one. On the other hand, when  $V_r \rightarrow V_f \cos \gamma$ , the  $AR_{e_s} \rightarrow AR_w$ . In the intermediate cases, the equivalent aspect ratio should be rather close to  $AR_s$  with a rapid transition toward  $AR_w$  when  $V_r$  approaches  $V_f \cos \gamma$ . With this general aim (and no particular physical justification) the following relationship was selected:

$$AR_{e_s} = AR_s + (AR_w - AR_s) (V_f \cos \gamma / V_r)^2 (AR_w - AR_s) \quad (3-33)$$

Having developed all the procedures necessary to establish forces acting on the propeller-wing assembly, actual calculations of the power required and the wing tilt angle in horizontal forward flight can be performed.

---

\* For  $C_L$ 's corresponding to angles of attack higher than that at  $C_{L_{max}}$ ,  $C_{d_0}$  values are obviously read from left branch of the  $C_{d_0}$  versus  $C_L$  curve.

For the particular case of a steady state horizontal flight, all vertical as well as horizontal, components of forces acting on the aircraft are in equilibrium.

$$\left. \begin{aligned} \Sigma F_y &= 0 \\ \Sigma F_x &= 0 \end{aligned} \right\} \quad (3-34)$$

Using notations of Figure 3-7, this condition can be expressed as:

$$\left. \begin{aligned} L_w + T \sin i_T + L_s \cos \gamma - (D_{i_s} + D_{o_s}) \sin \gamma - W &= 0 \\ T \cos i_T - [D_{i_w} + D_{o_w} + L_s \sin \gamma + (D_{i_s} + D_{o_s}) \cos \gamma] &= 0 \end{aligned} \right\} \quad (3-35)$$

Actual calculations can be performed through an iteration process which, under its simplest form, can be reduced to an interpolation between two values. In the latter case, the actual procedure can be as follows:

1. At a selected wing tilt ( $i_T$ ) assume 2 values of rotor horsepower and calculate the RHP- $P_{pr}$  values.
2. From a graph, as in Figure 3-8, obtain rotor-propeller downwash velocities for the 2 selected forward velocities.
3. By procedures outlined in the preceding pages, calculate the thrust and all forces acting on the wing. Calculate parasite drag.
4. Using Equation (3-35), compute  $\Sigma F_y$  and  $\Sigma F_x$  for the assumed cases of RPH and flight speed.
5. Plot  $\Sigma F_y$  and  $\Sigma F_x$  versus forward speed and interpolate the results in order to obtain both forward velocity and power corresponding to the assumed thrust tilt (wing incidence) angle  $i_T$ .

Figure 3-11 is given as an example of a comparison of predicted (by the above method) and flight test measured values of  $i_T = f(V)$  and  $SHP = f(V)$  for the VZ-2 (Vertol 76) flight research tilt-wing aircraft.

Approaches, similar to that described in this section, can be used for the power-speed relationship analysis of the tilt wing with a separate schedule of tilt for the propeller axis and the wing, as well as for the tilt-rotor or tilt-propeller configurations.

### 3.5 DISCUSSION OF THE FLIGHT ENVELOPE ASPECTS

#### (a) General Remarks

Of all configurations belonging to the convertible rotor/propeller aircraft family, the largest wind tunnel and flight research test material has been assembled for the tilt wing. Efforts of members of the NASA, Langley, like J. Campbell, R. Kuhn, M. McKinney and their associates provided the aerodynamic data, while J. Reeder and other NASA pilots built up the flight research experience. Efforts of other US and Canadian research institutions and industry of those two countries have also been quite considerable.

Experimental aerodynamics and flight research experience related to the tilt rotor, or propeller and deflected slipstream VTOL configurations is somewhat less abundant, but still represents a wealth of data accumulated through full-scale wind tunnel and flight research tests by the NASA, Ames group, AF Flight Research Center at Edwards AFB, and industry.

Complete bibliography of all NASA, other US research organizations and the industry reports on the subject of aerodynamics and flight research of convertible rotor/propeller



aircraft is too large to be given here in extenso. The reader is directed, hence, to publications like References 3-11 to 3-13.

Outside of the American Continent, Great Britain has conducted some wind-tunnel tests and associated theoretical studies of the airscrew type V/STOL configurations as reported, for instance, by J. Williams in References 3-14 and 3-14a.

Considerable experience, based on both wind-tunnel tests and flight research, has been assembled in France for the pure STOL configuration in conjunction with the development of the Breguet 940 and 941 aircraft (see, for instance, Ref. 3-15).

Ph. Poisson-Quinton has shown (Ref. 3-16) that properly interpreted wind-tunnel tests should result in a satisfactory correlation with flight of the airscrew-type V/STOL aircraft as well as other flight vehicles. In view of all this, it appears that considerations of the flight envelope aspects, based on that broad background of wind-tunnel tests and flight test experience, should properly indicate possibilities and problems of the considered VTOL configurations.

(b) *Power-Speed Relationship in Steady Horizontal Flight*

NASA experience, as reported by McKinney, et al, in Reference 3-17, indicates that in the transition range when power needed for parasite drag is still low, power required versus flying speed relationship of convertible rotor/propeller aircraft can be well approximated by the classical expression for induced power:

$$\text{SHP} \simeq \text{SHP}_{\text{ind}} = \frac{(W/b)^2}{550 \eta_{\text{pr}} \eta_{\text{tr}} \rho (\pi/2) V e} \quad (3-36)$$

where the new symbols are:  $W/b$  - wing span loading, and  $e$  - wing span efficiency factor.

Figure 3-12 shows that, indeed, the experimental data confirm the approximation of power required by Equation (3-36) to speeds from a range of about 120 down to 30 or 40 knots. From this latter region to  $V = 0$ , the power required makes a gradual transition to that required in hover. It should be emphasized, however, that the approximation by Equation (3-36) is valid only under the condition that there is no, or very little, stalling and no negative load on the wing.

Configurations of the tilt-wing type are susceptible to the wing stall problems (which will be discussed later), while those of the tilt rotor with fixed-wing type encounter, at low speeds, negative wing-rotor slipstream interference. It may be expected, hence, that in the low speed region, negative load on the wing and (usually) a higher span loading will lead, in general, to a less favorable character of the power drop-off with speed for the tilt-rotor configurations than for a (properly designed) tilt wing. However, even tilt-wing configurations having a high span loading in combination with a low wing chord to rotor/propeller diameter ratio ( $c/2R \ll 0.5$ ) will exhibit a similar unfavorable power versus speed relationship as a tilt rotor in the transition from hover to forward flight (see the low speed part of the power versus speed graph shown in Figure 3-13; reproduced from Ref. 3-17).

It becomes clear from the consideration of Sections 3.3 and 3.4, as well as the present discussion, that avoidance of stall and negative wing loads during transition is a necessary condition for a favorable shape (rapid drop-off) of the power versus speed curve in this regime. This leads to a requirement that at all transitional speeds, the flow resulting from the rotor-propeller downwash and translational speed of the aircraft should make, with the wing, an angle lower than that corresponding to stall. In the tilting airscrew configurations, rotor propeller thrust still provides a considerable part of the lift force at the intermediate transitional speeds. It is obvious, hence, that the greater the share of the wing in generating the lift at any of the transitional speeds, the lower

the tilt angle (with respect to the flight path) of the airscrew axis that would be required. This would create more favorable conditions for avoidance of the wing stall. This problem of the highest possible share of the wing in the lift generation can be interpreted in the manner similar to the discussion of deflected slipstream in Section 1.2, which indicated that the higher the slipstream-turning ability of the wing, the lower (at a given speed) may be the tilt angle of the airscrew axis.

Both interpretations point out that in such configurations as the tilt-wing, effective lift-increasing devices and a large wing chord to rotor/propeller diameter ratio (wing area in the slipstream) are beneficial\*. Since lift and thus, the slipstream turning angle are proportional to the product of the lift coefficient and slipstream submerged wing area, it is obvious that one factor can be played against the other: more efficient lift-increasing devices would permit reduction of the  $c/2R$  ratios. Figure 3-14, reproduced from Reference 3-17, illustrates gains resulting from lift-increasing devices.

(c) *Climb and Descent*

Problems of the wing stall in the tilt-wing configuration become less severe in climb. By contrast, tilting rotors with fixed wings may find the problems of negative wing loads and associated stall more severe, especially at the lower transitional speeds. Figure 3-15, also reproduced from Reference 3-17, explains, through simple velocity diagrams, how in climb, because of a higher thrust and consequently a higher downwash velocity, the wing angle of attack is reduced from that in level flight at the same speed of flight.

In descent, due to a reduced rotor/propeller thrust and the resulting lower downwash velocity plus variation in the flight-path speed direction, wing angle of attack is increased. It is obvious, hence, that effective lift-increasing devices and proper  $c/2R$  values are even more critical for descent than level transition, or steady state level flight at intermediate wing tilts. Wing stall and the resulting buffeting and degradation of controls is usually the limiting factor in establishing rate of descents and flight path slopes of the tilt-wing. Figure 3-16 shows improvements obtained in the rate of descent in the case of the VZ-2 (Vertol 76) through various lift-increasing devices and some increase of the  $c/2R$  ratio in transition due to the kinematics of the Fowler flap.

Wing fences, direction of propeller rotation, and position of the propeller thrust axis with respect to the wing chord also contribute to the improvement of descent characteristics of the tilt-wing. Gains due to these factors were reported in Reference 3-18 and reconfirmed (Ref.3-19) by NASA, Langley wind tunnel tests (see Figures 3-17 and 3-18, reproduced from Reference 3-19).

An increase in drag (through devices not reducing the wing lift) could also contribute to the improvement of rate of descent versus speed envelope, by necessitating a higher thrust and thus, generating a higher velocity propeller slipstream.

(d) *Interpretation of Flight Boundaries through Non-Dimensional Coefficients*

Wind tunnel test results of V/STOL aircraft are usually presented under the form of various non-dimensional coefficients. Since inputs represented by those coefficients are used to determine flight boundaries, some definitions of the non-dimensional coefficients are briefly reviewed.

Non-dimensional aerodynamic force (lift and drag) coefficients of V/STOL aircraft are obtained, as in the case of conventional aircraft, by dividing the force by the two reference quantities: some dynamic pressure ( $q$ ), and some area. This dynamic pressure can be selected, for instance, as that corresponding to the free stream velocity, while the

---

\* See References 3-23 and 3-25.

wing area may represent the other quantity. This will, obviously, result in conventional lift and drag coefficients.

$$\left. \begin{aligned} C_L &= \frac{\text{Lift}}{q_0 S_w} \\ C_D &= \frac{\text{Drag}}{q_0 S_w} \end{aligned} \right\} \quad (3-37)$$

where  $q_0$  is free stream dynamic pressure and  $S_w$  is wing area.

Many aspects of the flight boundaries as, for instance, those of descent with forward speed or any other problem associated with forward flight away from the hovering and near-hovering conditions can be investigated with the help of the conventional (Eq. (3-37)) aerodynamic coefficients. Figures 3-19 and 3-20 (taken from References 3-20 and 3-21, respectively) are shown as examples of this approach to an STOL (Fig.3-20) and a tilt-wing (Fig.3-21) aircraft.

In the aerodynamic force coefficients based on the freestream dynamic pressure, some surface other than the wing may be used. For instance, wing span squared was proposed by G.Schairer in Reference 3-22. However, all approaches based on the free-stream dynamic pressure have this drawback: all of the coefficients grow very rapidly at near-hovering speeds and become infinite in hover.

For this reason, coefficients based on a sum of the free-stream dynamic pressure  $q_0$  and variously defined dynamic pressure in the rotor-propeller slipstream become more useful in dealing with the whole flight envelope from hover to high speed flight. For instance, NASA uses as a reference, dynamic pressure ( $q_s$ ), defined as:

$$q_s = q_0 + w \quad (3-38)$$

where  $w$  is the disc loading of the rotor propeller.

The same philosophy of using either free-stream dynamic pressure ( $q_0$ ), or that accounting for the slipstream as well ( $q_s$ ) can be used in defining moment, thrust and power coefficients.

The intent of this brief discussion was to call the reader's attention to various philosophies in defining non-dimensional coefficients which he may encounter in wind tunnel test reports as, for instance, References 3-23 to 3-28.

### 3.6 AGILITY

Because of restricted takeoff and landing sites, agility should be an important characteristic of all V/STOL aircraft, but especially of the military ones (both transports and combat types).

In a broad sense, agility reflects an ability to quickly perform various maneuvers throughout the range of operational speeds. This obviously includes an ability to execute tight turns (up to  $360^\circ$ ), either at a sustained speed or with deceleration, in order to perform this maneuver with the smallest average radius and in the shortest possible time.

Ability to accelerate and decelerate along all axes, to climb or to descent at the steepest angles, also represent some aspects of agility. Furthermore, since all the considered aircraft concepts go through a conversion from the low to high speed regime of flight, and vice versa, it is important that this transition maneuver can be performed in a continuous manner with minimum restrictions resulting from aircraft attitude, air turbulence, etc. This requirement is obviously of special importance to the combat aircraft. Furthermore, it would be desirable that the pilot could interrupt conversion or reconversion

and be able to fly the aircraft at those intermediate stages with an acceptable degree of maneuverability.

In hovering and near-hovering, agility will depend chiefly on the ability to develop thrust in excess of gross weight, or in other words, on the number of g's that can be obtained  $[(ng)_v]$ . For all aircraft of the airscrew type (with no power restriction), vertical g capability related to the gross weight defined by hovering under design conditions becomes

$$ng_v = \left(\frac{\rho_m}{\rho_h}\right) \left(\frac{\bar{c}_{l_m}}{c_{l_h}}\right) \left(\frac{v_{t_m}}{v_{t_h}}\right)^2, \quad (3-39)$$

where symbols with a subscript h refer to the design hovering altitude and air density, while those with the subscript m refer to the maneuver conditions.

Equation (3-39) indicates that, in principle, both the rotor and the propeller-type aircraft can achieve the same level of vertical acceleration. However, as far as vertical rate of climb is concerned, aircraft with a higher disc loading will tend to have a higher vertical rate of climb when operating at lower altitudes and temperatures than those of the design hovering conditions. This results from a larger excess of relative power  $(SHP/W)$  over that required for hovering (see Section 2.5). Relative excess power per pound of gross weight at an altitude H, and ambient temperature T,  $(SHP/W)_{exHT}$  will be:

$$\left(\frac{SHP}{W}\right)_{exHT} = \left(\frac{SHP}{W}\right)_h \left[ \frac{\lambda_{HT}}{\lambda_h} - \sqrt{\left(\frac{\rho_h}{\rho_{HT}}\right)} \right] \quad (3-40)$$

where  $(SHP/W)_h$  is the power per pound at the design hovering conditions and  $\lambda$  is the engine power lapse rate with altitude and temperature. Since the second term of equation (3-40) can be considered as the same for all turboshaft powered aircraft, it becomes clear that the relative excess power at altitudes and temperatures lower than the design conditions is proportional to the  $SHP/W$  required for the design hovering.

Radius of turn in forward flight depends on the level of normal accelerations (number of g's:  $ng_f$ ) that can be developed.

For the tilt-rotor types flying in the helicopter configuration, it becomes

$$ng_f = \left(\frac{T_R}{W}\right)_m + qC_{L_m}/w_w, \quad (3-41)$$

where  $(T_R/W)_m$  is the ratio of thrust developed by the rotor ( $T_R$ ) in maneuver to the aircraft gross weight ( $W$ ).  $C_{L_m}$  is the wing lift coefficient in maneuver and  $w_w$  is the nominal wing loading ( $w_w = W/S_w$ ).

At low speeds, rotor thrust is the main source of normal acceleration. For V/STOL aircraft solely relying on fixed wings as a source of lift in forward flight (e.g. after a complete conversion to the high speed configurations), their g capability obviously depends only on the lift coefficient which can be developed in pull-outs and maintained during the turn. Figure 3-21 shows the g capability (no power limit) versus speed for plain wings, wings equipped with mechanical flaps (from simple slotted to Fowler type) and those with moderate BLC.

A variable scale at the left of the graph permits evaluation of the importance of wing loading. For instance, it can be seen from Figure 3-21 that at 100 knots, a fixed wing equipped with an effective mechanical flap can pull about 2g when wing loading is  $w_w = 50 \text{ lb/ft}^2$ , but only about 1.2 g at  $w_w = 80 \text{ lb/ft}^2$ . In order to maintain the

2g normal acceleration level at 100 knots, and  $w_w = 80 \text{ lb/ft}^2$  ELC would be required.

General relationships between radius of turn (in ft) and speed of flight for various normal acceleration levels (in g's) as well as time required (seconds) for a  $360^\circ$  turn is shown in Figure 3-22. Problems of agility in transport operations are also discussed by J.Reeder in Reference 3-11.

The agility level of the tilt wing and tilt rotor in and near hovering should be governed by Equations 3-39 and 3-40. In the completely converted stage, it will be as that of fixed wing aircraft. Of particular interest, however, are intermediate stages with the rotor/propeller axis partially tilted. For the tilt wing in this stage, an interplay between lift developed by the wing as a whole, thrust of the propellers and lift over the wing portion submerged in the slipstream (see Figure 3.23) results in an ability to develop relatively high normal and horizontal accelerations. Figure 3-24 gives a typical example (based on wind tunnel tests) of normal and tangential g's that can be developed at various ratios of actual shaft horsepower to that required in unaccelerated horizontal flight ( $g_n = 1, g_h = 0$ ). It can be seen from Figure 3-24 that at a given power level, normal g's can be developed by increasing wing-propeller incidence with reference to the flight path. However, this maneuver will also generate tangential deceleration. Development of normal acceleration without introducing tangential acceleration (as this is required in a sustained turn) is accompanied by an increase of shaft horsepower above that required for an unaccelerated flight. It should be emphasized at this point that because the tilt wing shows a fast drop-off of power required with forward speed, large excess power (high  $\text{SHP}/\text{SHP}_{g=1}$ ) becomes available to develop normal plus tangential g's for either decelerated or sustained turns.

Figure 3-25 is shown as an illustration of ratios of shaft horsepower available to that required in a steady state horizontal flight at sea level, standard.

#### REFERENCES TO CHAPTER III

- 3-1. Reed, W.H., III *Propeller-Rotor Whirl Flutter: A State-of-the-Art Review*, Proceedings of the Symposium on the Noise and Loading Actions on Helicopter and V/STOL Aircraft, University of Southampton, England, August, 1965.
- 3-2. Young, M.I.  
Lytwyn, R.T. *The Influence of Blade Flapping Restraint on Dynamic Stability of Low Disc Loading Propeller-Rotors*, Proceedings of the 23rd Annual National Forum of the American Helicopter Society, Washington, D.C., May, 1967.
- 3-3. Hall, W.E., Jr. *Prop-Rotor Stability at High Advance Ratios*, Journal of American Helicopter Society, Vol. II, No.2, April, 1966.
- 3-4. Edenborough, H.K. *Investigation of Tilt-Rotor VTOL Aircraft Rotor-Pylon Stability*, Journal of Aircraft, Vol.5, No.6, March-April, 1968.
- 3-5. Quigley, H.C.  
Koenig, D.G. *The Effect of Blade Flapping on the Dynamic Stability of a Tilting-Rotor Convertiplane*, NASA Conference on V/STOL Aircraft, November, 1960.
- 3-6. Stepniewski, W.Z. *Introduction to Helicopter Aerodynamics*, Rotorcraft Publishing Committee, Morton, Pa., 1958.

- 3-7. Kuhn, Richard E. *Semi-empirical Procedure for Estimating Lift and Drag Characteristics of Propeller-Wing-Flap Configurations for Vertical- and Short-Take-Off-and-Landing Airplanes*, NASA Memo 1-16-59L, 1959.
- 3-8. Vidal, R. J.  
et al. *The Aerodynamic Appraisal of STOL/VTOL Configurations*, IAS Paper 60-37, January, 1960.
- 3-9. Strand, T.  
et al. *Unified Performance Theory for V/STOL Aircraft in Equilibrium Flight*, Air Vehicle Corporation, LaJolla, Calif., Report No. 350, May, 1966.
- 3-10. Ribner, H.S.  
Ellis, N.D. *Computer Study of a Wing in the Slipstream*, AIAA Preprint 66-466, 1966.
- 3-11. Staff of Langley  
Research Center *A Preliminary Study of V/STOL Transport Aircraft and Bibliography of NASA Research in the VTOL-STOL Field*, NASA TN D-624, January, 1961.
- 3-12. NASA *Vertical Lift Aircraft, Bibliography, No. 492, Part I from 1962 to April 1964.*
- 3-13. Bock, G.H.G.  
et al. *VTOL/STOL Aircraft Bibliography 2*, AGARD, June, 1963.
- 3-14. Williams, J. *Some British Research on the Basic Aerodynamics of Powered Lift Systems*, Journal of the RAeS, Vol. 64, July, 1960.
- 3-14a. Williams, J. *Recent Basic Research on V/STOL Aerodynamics at R. F. E.*, Zeitschrift fur Flugwissenschaften, 14, Heft 6, 1961.
- 3-15.
- 3-16. Poisson-Quinton, Ph. *Comparison of Flight & Wind-Tunnel Tests*, AIAA Wright Brothers Lecture, 1967.
- 3-17. McKinney, M.O.  
et al. *Aerodynamic Factors to be Considered in the Design of Tilt-Wing V/STOL Airplanes*, Annals of the New York Academy of Sciences, Vol. 107, Art. 1, March, 1963.
- 3-18. Fry, B.L. *Low-Speed Aerodynamic Flight Boundaries and Control Aspects of Tilt-Wing Aircraft*, Proceedings of the 21st National Forum of AHS, May, 1965.
- 3-19. Hassell, J.L., Jr  
Kirby, R.H. *Descent Capability of Two-Propeller Tilt-Wing Configuration*, Proceedings of NASA Conference on V/STOL and STOL Aircraft, April, 1966.
- 3-20. Deckert, W.H.  
et al. *A Summary of Recent Large-Scale Research on High-Lift Devices*, Proceedings of NASA Conference on V/STOL and STOL Aircraft, April, 1966.
- 3-21. Fay, B.C. *Recent Development in Simplifying and Improving the Tilt Wing Design*, Proceedings of the 20th Annual National Forum of AHS, May, 1964.
- 3-22. Schairer, G.S. *Looking Ahead at V/STOL*, Proceedings of IAS-RAeS Meeting in London, September, 1961.

- 3-23. Taylor, R. T. *Wind-Tunnel Investigation of Effect of Ratio of Wing Chord to Propeller Diameter with Addition of Slats on the Aerodynamic Characteristics of Tilt-Wing VTOL Configurations in the Transition Speed Range, NASA, TN D-17, September, 1959.*
- 3-24. Fink, M. P.  
et al. *Aerodynamic Data on Large Semispan Tilting Wing with 0.6-Diameter Chord, Single Slotted Flap, and Single Propeller Rotating Up at Tip, NASA TN D-1586, October, 1964.*
- 3-25. Spreemann, K. P. *Investigation of a Semispan Tilting-Propeller Configuration and Effects of Wing Chord to Propeller Diameter on Several Small-Chord Tilting-Wing Configurations, NASA TN D-1815, July, 1963.*
- 3-26. Weiberg, J. A.  
Giulianetti, D. J. *Large Scale Wind-Tunnel Tests of an Airplane Model with an Unswept Tilt Wing of Aspect Ratio 5.5 and with Various Stall Control Devices, NASA TN D-2133, February, 1964.*
- 3-27. Fink, M. P.  
et al. *Aerodynamic Data on a Large Semispan Tilting Wing with 0.6-Diameter Chord, Fowler Flap, and Single Propeller Rotating up at Tip, NASA TN D-2180, February, 1964.*
- 3-28. Fink, M. P.  
et al. *Aerodynamic Data on Large Semispan Tilting Wing with 0.6-Diameter Chord, Single-Slotted Flap, and Single Propeller Rotating Down at Tip, NASA TN D-2412, August, 1964.*

## CHAPTER IV

## TAKEOFF AND LANDING WITH GROUND RUN

## 4.1 SIMPLIFIED CONSIDERATIONS OF TAKEOFF AND LANDING

When any VTOL aircraft is overloaded beyond its vertical takeoff capacity, i.e., when

$$T_{\max V}/W < 1.0 \quad (4-1)$$

(where  $T_{\max V}$  is the maximum vertical component of the available thrust) it still may show operational advantages through its STOL capabilities.

In order to better understand the basic factors influencing takeoff and landing distances, a very rudimentary analysis of these operations will be made first, while a discussion of takeoff optimization will be given later as an example of a more refined approach to those problems.

The most simplified takeoff scheme over an obstacle of a height  $h$  may be represented as a ground run of length  $l_{gr}$  (see Figure 4-1a) until the unstick (takeoff) speed  $V_u > V_{\min}$  is reached. This is assumed to be immediately followed by a steady climb up to the height of the obstacle. Total takeoff distance will obviously be  $l_{gr}$  plus the horizontal projection  $l_{cp}$  of the climb path:

$$l = l_{gr} + l_{cp} \quad (4-2)$$

Denoting average net thrust (propulsive thrust minus ground friction and aerodynamic drag) during the ground run as  $\bar{T}_n$ , energy consideration at the end of run  $l_{gr}$  will result in the following equation:

$$\frac{1}{2} \frac{W}{g} V_u^2 = \bar{T}_n l_{gr} \quad (4-3)$$

where  $W$  is the aircraft gross weight.

Equation (4-3) can be rewritten as follows:

$$l_{gr} = \frac{1}{2g} \frac{V_u^2}{(\bar{T}_n/W)} \quad (4-3a)$$

Simple geometric considerations (see Figure 4-1a) will show that the climb path projection will be

$$l_{cp} = h / (1 / (T_{nc}/W)^2 - 1) \quad (4-4)$$

where  $T_{nc}$  is the net thrust (propulsive thrust minus aircraft drag) in climb.

The approximate expression for the total takeoff distance now becomes

$$l_{to} = \left( \frac{1}{2g} \right) V_u^2 / (\bar{T}_n/W) + h / [1 / (T_{nc}/W)^2 - 1] \quad (4-5)$$



Equation (4-5) clearly indicates the importance of the speed  $V_u$  (appearing to the second power) at which the pilot actually unsticks the aircraft from the ground. VTOL aircraft overloaded (within practical limits of 25-35% of the normal gross weight) beyond their hovering capacity usually are still capable of quite low minimum flying speeds. In addition, they possess hovering type controls that remain effective at the low flying speeds. In addition, powerplant interconnects reduce danger of asymmetric thrust in case of engine failure. In view of all this, it may be expected that pilots, flying VTOL aircraft in the STOL mode will be more willing to unstick the aircraft at speeds close to the potential  $V_{min}$ , if this becomes necessary to optimize the takeoff distance. NASA, Ames research team discusses, in Reference 4-1, operational problems resulting from the lack of interconnect in conventional STOL aircraft (for general discussion of STOL operation, see Reference 4-2).

Equation (4-5) also shows the importance of the net thrust to gross weight ratios, both in the ground run and in climb. Since the net thrust to gross weight ratios are closely related to the available thrust to gross weight ratios, VTOL aircraft will show an advantage in this respect, even in STOL operations. Thrust available to gross weight ratios will still probably be  $T/W > 0.75$ .

In landing, the most simplified (no flare) scheme of this maneuver can be presented as in Figure 4-1b. It can be seen from this figure that ground projection ( $l_{dp}$ ) of the descent path (from the obstacle to the touchdown point) will be (under small angle assumption):

$$l_{dp} = h(W/D_{nd}) \quad (4-6)$$

where  $D_{nd}$  is the net drag of the aircraft in descent.

$l_{dp}$  can also be expressed in terms of the rate of descent ( $V_d$ ):

$$l_{dp} = h \sqrt{(V_l/V_d)^2 - 1} \quad (4-7)$$

where  $V_l$  is the landing speed (along the flight path).

Assuming that energy associated with rate of descent is instantaneously absorbed at the touchdown point, while aircraft speed along the ground remains approximately the same as along the descent flight path, ground distance ( $l_{grp}$ ) required to bring the aircraft to a stop can be found, by analogy, with Equations (4-3) and (4-3a), as

$$l_{grp} = \frac{1}{2g} V_l^2 / (\bar{F}_b/W) \quad (4-8)$$

where  $\bar{F}_b/W$  is the ratio of the average braking force (reversed thrust, plus ground friction, plus aerodynamic drag) to the aircraft weight ratio.

Total approximate landing distance will obviously be:

$$l_l = h \sqrt{(V_l/V_d)^2 - 1} + \frac{1}{2g} V_l^2 / (\bar{F}_b/W) \quad (4-9)$$

It can be seen from Equation (4-9) that, as in the case of takeoff, landing speed is the most important parameter. Inclination of the landing flight path (as expressed by the  $V_l/V_d$  ratio) and the ratio of the average braking force to the aircraft weight are other important parameters.

The prime importance of the landing speed is reflected in Figure 4-2 (reproduced from Reference 4-3) showing field length requirements versus landing speed.

VTOL aircraft operating in the STOL mode will again show, in landing, a double advantage regarding their practical landing speeds: first, potentially those speeds are low,

and secondly, because of the speed-independent controls and thrust symmetry in case of an engine failure, pilots will not be reluctant to take full advantage of those potentially low landing speeds (see References 4-1 and 4-2).

Descent flight path problems of the convertible rotor/propeller aircraft have already been discussed in Section 3-5. It should be pointed out here that, because of the energy-absorbing limitations of the landing gear, it may be necessary to deviate from the aerodynamically possible steepest descent angle in order to reduce the  $V_d$  values at touchdown as long as no aerodynamic or power flares are assumed.

In such configurations as the tilt-wing and deflected slipstream, reversed thrust can probably be used to its full level capability. This may amount to 60-70% of the static thrust value. Tilt rotors, because of the ground clearance limitations, will probably not be able to take full advantage of the negative thrust as a braking force.

#### 4.2 EFFECTS OF GROUND PROXIMITY

It should be remembered, however, that in addition to all the advantages of operating VTOL convertible rotor/propeller aircraft in the STOL mode, there are problems, also. They manifest themselves chiefly in landing of such configurations as the tilt wing and the deflected slipstream. Most of those problems have their source in the characteristic type of flow developing in ground proximity as shown in Figure 4-3 (reproduced from Reference 4-4). This forward flow of the part of the propeller slipstream occurs close to the ground at some combination of forward speed and wing position (tilt wing) and/or flap deflection (both tilt wing and deflected slipstream). The aerodynamic effect of the type of flow shown in Figure 4-3 may be drop-off of lift and an associated increase in the rate of descent (Fig. 4-3). It may also cause disturbances (sometimes difficult to control) both in yaw and roll.

The whole subject of the ground proximity effects on control and aerodynamic characteristics is more thoroughly discussed by K.W. Goodson in References 4-5 and 4-5a. For instance, Figure 4-4 (reproduced from Ref. 4-5a) shows yaw acceleration experienced in flight by a four-propeller tilt-wing aircraft. It can be seen from that figure that disturbances anticipated between  $30^\circ$  and  $80^\circ$  of wing incidence, and flight speeds between 30 to 12 knots, may be of the same order of magnitude as angular acceleration available through hovering controls. At speeds higher than 30 knots, no disturbance was encountered as the slipstream was not projected ahead of the aircraft.

Figure 4-5, also from Reference 4-5a, shows wind tunnel tests of the same aircraft in a 1:11 scale. Results of these wind tunnel tests are compared in Figure 4-6 with those obtained in flight.

From the operational point of view, the above-discussed forward flow may contribute to the damage of propellers and engines by debris picked up from the unprepared landing and takeoff sites (Ref. 4-6).

Some information regarding ground proximity aspects of deflected slipstream aircraft can be found in Reference 4-7.

#### 4.3 STATEMENT OF THE SHORTEST TAKEOFF TECHNIQUE PROBLEM\*

Problems of determining a technique leading to the shortest takeoff distance over a given obstacle (e.g. 50 ft) for a given VTOL airscrew-type aircraft operating in the STOL mode can be stated in the following way:

---

\* Presentation of this problem closely follows considerations of Reference 4-8.

With the engines developing constant power (maximum permissible for takeoff) and knowing at each speed along the flight path the whole possible range of magnitudes and positions (relative to the flight path) of a vector representing the resultant aerodynamic force acting on the aircraft, find the functional relationship between the position of that vector and speed along the flight path that would minimize ground projection of the total flight path between the takeoff point and the prescribed altitude above the ground (50 ft) (Fig. 4-7).

This can be phrased as a mathematical requirement of determining a control function (say  $i_T = f(V)$ ) that would minimize a functional representing the sum of two definite integrals - one giving the run on the ground ( $l_{gr}$ ) and another one expressing horizontal projection of the climb path ( $l_{cp}$ ) up to the prescribed altitude ( $h$ ):

$$l \equiv l_{gr} + l_{cp} = \int_0^{v_{gr}} f(v)dv + \int_0^h f(h)dh = \min . \quad (4-10)$$

However, before the problem stated by Equation (4-10) can be attacked, a few basic relationships should be discussed.

#### 4.4 REPRESENTATION OF AERODYNAMIC FORCES

The most important aerodynamic forces that act on the aircraft during the considered takeoff maneuver are propeller thrust ( $T$ ), total wing and body lift ( $L$ ) (within and outside the slipstream), and total drag ( $D$ ). All these forces can be summed up into one resultant aerodynamic force ( $F$ ). It may be anticipated from discussion in Section 3-5 that, for the airscrew-type configurations most suitable for STOL operation (the tilt-wing and deflected slipstream), the character of variation of that resultant aerodynamic force  $F$  with the wing inclination and/or flap deflection while both engine power and speed along the flight path remain constant will be as in Figure 4-8: Under static conditions it may be assumed that for the tilt-wing force  $F_{V=0} = T_0$  (where  $T_0$  is the total static thrust of propellers) and remains practically constant throughout all wing incidences. By contrast, for the deflected slipstream, some drop-off in the  $F_{V=0}$  values below that of  $T_0$  can be expected with the increasing upward inclination of the  $F_{V=0}$  force (Fig. 4-8)\*.

In forward motion at a constant speed, the character of variation of the resultant aerodynamic force ( $F_{V>0}$ ) with its inclination (caused by the wing incidence and/or flap deflections) to the motion (flight) path will probably be quite similar for the two considered configurations: When pointing along the flight (motion) path, the  $F_{V>0}$  value will be lower than under static conditions, and the lowest for the whole force polar at a given speed and power. With the increasing inclination to the flight path, the  $F_{V>0}$  force will increase in the manner shown in Figure 4-8.

The vector representing that resultant aerodynamic force can be conveniently defined by its normal ( $F_n$ ) and parallel ( $F_p$ ) components with respect to the flight path. Furthermore, the values of these components can be related to the aircraft gross weight ( $W$ ) in the following manner:

$$f_n \equiv F_n/W ; \quad f_p \equiv F_p/W \quad \text{and} \quad f \equiv F/W . \quad (4-11)$$

Typical variations of the non-dimensionalized forces acting on a tilt-wing aircraft at various flight path\*\* speeds are shown in Figure 4-9\*\*\*.

\* For the tilt-rotor configuration, there also will be a drop-off (download on the wing) at the higher  $F$  angles, while low angles are of an academic interest only because of the ground clearance problems.

\*\* The expression 'flight path' also refers to the ground run.

\*\*\* Aircraft characteristics are assumed as in Table I, p.205.

Under static conditions the resultant aerodynamic force is lower than the gross weight, ( $F_0 < W$ ) i.e.  $f_0 < 1.0$  and remains constant through the available tilt angles.

Furthermore, it is assumed here that the maximum resultant aerodynamic force acting on the aircraft at rest is equal to the total static thrust of the propellers ( $T_0$ ):  $t_0 = T_0/W = F_0/W$ . However, as the speed along the flight path increases, the maximum possible thrust component along the flight path ( $f_p$ ) decreases, while the maximum possible value of the normal component  $f_n$  increases. When the resultant vector  $\bar{F} = \bar{f}_p + \bar{f}_n > 1.0$ , the aircraft can be airborne (Fig.4-9).

For actual takeoff calculations, inputs of  $f_p = f(f_n)$  at various speeds along the flight path can be obtained from wind tunnel tests of suitable models, or determined analytically. However, in order to facilitate general discussion of the take-off problems, an expression analogous to the induced drag relationship is suggested for  $f_p = f(f_n)$ :

$$f_p = f_{p \max} - k_3 f_n^2, \quad (4-12)$$

and consequently

$$f_n = \sqrt{(f_{p \max} - f_p/k_3)}. \quad (4-13)$$

It is assumed that  $f_p$  at  $f_n = 0$  represents the maximum value ( $f_{p \max}$ ) of  $f_p$  that can be obtained at a given flight speed. The decrease with speed of that  $f_{p \max}$  component can be approximated by the following expression (derived from the momentum theory considerations):

$$f_{p \max} = t_0 [1 - k_1 (V/v_{i0})] \quad (4-14)$$

where  $v_{i0}$  is the rotor-propeller induced velocity under static conditions and  $k_1 = 0.3$  (see Figure 4.10).

By contrast with the  $f_{p \max} = f(V)$  trend, values of  $f_n$  at  $f_p = 0$  (which will be called  $f_{n0}$ ) increase with the flight path speed (Fig.4-9); that increase can be represented as follows:

$$f_{n0} = t_0 [1 + k_2 (V/v_{i0})] \quad (4-15)$$

The  $k_3$  coefficient can now be expressed in terms of  $k_1$ ,  $k_2$ ,  $(V/v_{i0})$ , and  $t_0$  from the condition that Equation (4-12) should be satisfied for the point  $(0, f_{n0})$  with  $(f_{p \max})$  given by Equation (4-14) and  $(f_{n0})$  by Equation (4-15):

$$k_3 = \frac{1}{(t_0)} \frac{1 - k_1 (V/v_{i0})}{[1 + k_2 (V/v_{i0})]^2} \quad (4-16)$$

Equations ((4-12) and (4-13)) can now be rewritten as follows:

$$f_p = t_0 \left(1 - k_1 \frac{V}{v_{i0}}\right) \left[1 - \frac{f_n^2}{t_0^2} \frac{1}{[1 + k_2 (V/v_{i0})]^2}\right] \quad (4-17)$$

and

$$f_n = [1 + k_2 (V/v_{i0})] \sqrt{\left[ \left\{ t_0 - \frac{f_p}{1 - k_1 (V/v_{i0})} \right\} t_0 \right]} \quad (4-18)$$

Knowing the takeoff shaft horsepower of the aircraft ( $SHP_{T0}$ ), the nominal disc loading of the rotor/propellers ( $w \equiv W/A$ , where  $A$  is the total rotor/propeller disc area), and the power loading of the aircraft at takeoff ( $W/SHP_{T0}$ ), the following expressions for  $v_{i0}$  and  $t_0$  can be developed from the simple momentum theory:

$$v_{i_0} = \left[ \frac{275\eta_{tr}\eta_A}{\rho} \frac{w}{W/SHP_{T0}} \right]^{1/3} \quad (4-19)$$

and

$$t_0 = \frac{2\rho}{w} \left[ \frac{275\eta_{tr}\eta_A}{\rho} \frac{w}{W/SHP_{T0}} \right]^{2/3} \quad (4-20)$$

where  $\eta_{tr}$  = transmission efficiency  
 $\eta_A$  = aerodynamic efficiency (figure of merit) in hover,  
and  $\rho$  = air density at takeoff.

#### 4.5 OPTIMIZATION OF GROUND RUN

Acceleration during the ground run can be expressed as follows:

$$\dot{V}_x \equiv \dot{V}_{gr} = g[f_p - (1 - f_n)\mu] \quad (4-21)$$

where  $\mu$  is the ground friction coefficient.

The final value of the ground speed ( $V_u$ ) at which it will be most advantageous to unstick the aircraft is not known as yet. However, it is evident that, regardless of its magnitude, the ground distance covered in the process of attaining this speed will be the shortest when the ground acceleration (Eq.(4-21)) becomes a maximum. This occurs when

$$f_{n \text{ opt}} = \frac{\mu}{2k_3} \quad (4-22)$$

Then the maximum ground acceleration (at any ground speed  $V_{gr}$ , or rather,  $V_{gr}/v_{i_0}$ , as reflected in the  $k_3$  values) will be

$$\dot{V}_{gr \text{ max}} = g f_{p \text{ max}} - \mu + \frac{1}{4k_3} \mu^2 \quad (4-23)$$

Equation (4-23) clearly indicates that the higher the ground friction coefficient the higher should be the vertical component of the resultant force. In order to realize this maximum on-the-ground-acceleration in practice, the wing and flap position of the tilt wing, flap deflection of the deflected slipstream and rotor inclination of the tilt-rotor configurations should follow a schedule with ground speed that will assure that the relationship of Equation (4-22) is fulfilled.

Figure 4-11 shows the optimum angle of inclination ( $\theta_F$ ) of the resultant aerodynamic force (see Figure 4-8) versus  $v_1/V$  for two values of the ground friction coefficient ( $\mu = 0.05$  and  $\mu = 0.25$ ) and the assumed values of  $k_1 = 0.3$  (rather typical for all rotor-propellers; see Figure 4-10) and  $k_2 = 0.46$ . This latter value was established for a particular tilt-wing aircraft, but still may be considered as representative of other configurations as well.

In order to give a better idea regarding optimum  $\theta_F$  values that may be required at actual speeds (expressed in ft/sec and not as the  $V/v_{i_0}$  ratios) during ground runs, two auxiliary scales were added in Figure 4-11. One, marked Tilt Wing, refers to an aircraft of that configuration with the assumed characteristics as in Table I. The other scale, marked, Tilt Rotor, shows actual speeds for a tilt rotor aircraft with the assumed characteristics as in Table II.

$(\theta_F)_{gr} = f(V/v_{i_0})$ , shown in Figure 4-11, represents, in a mathematical sense, a control function which optimizes the first term (regardless of its upper limit of integration)

of the functional given by Equation (4-10). From the point of view of operational technique, Figure 4-11 shows how wing tilt and/or wing flaps for the tilt wing, rotor tilt and/or wing flaps for the tilt rotor, and flaps for the deflected slipstream, should vary with the speed of ground run in order to provide an optimum inclination of the resultant aerodynamic force. This, in turn, would assure a maximum acceleration on the ground.

A glance at Figure 4-11 will indicate that for the low values of ground friction coefficients ( $\mu = 0.05$ ), rather low  $\theta_F$  values ranging from  $\theta_F \approx 1.5^\circ$  to  $\theta_F \approx 11^\circ$  may be required for maximum ground acceleration. Realization of those low  $\theta_F$  values may not be difficult for the tilt-wing and deflected slipstream configurations, but due to the ground clearance problems of the tilt-rotor types, the latter may not achieve their maximum, aerodynamically possible, acceleration in the ground run. By contrast, for the higher ground friction coefficients ( $\mu = 0.25$ ) even the initial  $\theta_F$  values will be higher (for  $V = 0$ ,  $\theta_F \approx 7^\circ$ ) growing rapidly to  $\theta_F \approx 47^\circ$  for the  $V/V_{10}$  ratio of 1.4, corresponding to about 120 ft/sec for the assumed tilt wing and only 60 lb/ft<sup>2</sup> for the assumed tilt rotor.

In actual design practice, it will not always be possible to provide a rapidly changing aircraft geometry (wing and rotor tilt, flap deflection, etc.) with the ground run speed as may be required for maximum acceleration. Some compromise fixed geometry may be selected instead. Nevertheless, the above considerations should be helpful by indicating, on one hand, the trend while on the other, it would permit an estimation as to how ground accelerations resulting from the fixed, compromised geometry would compare with the optimum possibilities.

#### 4.6 SEARCH FOR AN OPTIMUM CLIMB TECHNIQUE

It will be assumed for simplicity that in achieving a ground unstick speed  $V_u$  at which climb is possible (i.e. when the  $f_n$  values can be made greater than one) (see Figure 4-9), the wing, rotor, flaps, etc., are rotated instantaneously to a proper position assuring that  $f_n > 1.0$ .

Vertical acceleration  $\overset{\circ}{V}_y \equiv \overset{\circ}{V}_{c_p}$  at any point along the climb path will now be (see Figure 4-7):

$$\overset{\circ}{V}_y = g[f_n(V_x/V_p) + f_p(V_y/V_p) - (V_y/V_p)^2 - 1] , \quad (4-24)$$

and horizontal acceleration ( $\overset{\circ}{V}_x \equiv \overset{\circ}{V}_{c_{l_{gr}}}$ ):

$$\overset{\circ}{V}_x = g[f_p(V_x/V_p) - f_n(V_y/V_p) - (V_y/V_p)(V_x/V_p)] , \quad (4-25)$$

$$V_p = \sqrt{(V_x^2 + V_y^2)} \quad \text{while} \quad V_x = V_u + \int_{t_u}^{t_0} \overset{\circ}{V}_x dt \quad \text{and} \quad V_y = \int_{t_u}^{t_0} \overset{\circ}{V}_y dt , \quad (4-26)$$

where  $t_u$  is the time of the unstick.

As to the actual execution of the climb maneuver to the obstacle height, several techniques are possible; two of these will be considered.

In the constant speed technique, it is assumed that the unstick velocity ( $V_u$ ), once achieved, is maintained constant until the obstacle height is reached. This obviously means that all forces along the flight path must be balanced all the time, hence (see Figure 4-9).

$$f_p = V_y/V_p . \quad (4-27)$$

Equation (4-27) indicates that for the initial moment of the unstick maneuver, when  $V_y = 0$ ,  $f_p$  should also be  $f_p = 0$ , and thus the initial vertical acceleration is governed by the  $f_{n0}$  value corresponding to the assumed unstick speed ( $V_u$ ) and becomes

$$\overset{\circ}{V}_{y0} = g(f_{n0} - 1). \quad (4-28)$$

As the aircraft starts to climb with  $V_p = V_u$  and Equation (4-27) remains valid Equation (4-29) becomes as follows:

$$\overset{\circ}{V}_y = g f_n \sqrt{[1 - (V_y/V_u)]^2 - 1}. \quad (4-29)$$

Remembering that  $f_n = \sqrt{[f_{p \max} - f_p]/k_3}$  while  $f_p = V_y/V_u$ , the following expression for  $V_y$  at time  $t$  (time interval from the unstick time  $t_u$  to  $t$ ) is obtained:

$$V_y = g \int_{t_u}^t \{ \sqrt{[f_{p \max} - (V_y/V_u)] [1 - (V_y/V_u)^2]/k_3} - 1 \} dt, \quad (4-30)$$

while at the same time  $t$ , the horizontal components of the flight path speed will be (for  $V_p = V_u$ ),

$$V_x = \sqrt{(V_u^2 - V_y^2)} \quad (4-31)$$

Equations (4-30) and (4-31) enable the computation of first  $V_y = f(t)$  and  $V_x = f(t)$ , and then  $y = f(t)$  and  $x_{cp} = f(t)$ . The latter two relationships permit the solution of  $l_{cp}$  corresponding to the selected obstacle height.

A plot of  $l_{cp} = f(V_u)$  can now be drawn (see Figure 4-12). Adding to  $l_{cp} = f(V_u)$ , optimum  $l_{gr} = f(V_u)$ , the total takeoff distance over a given obstacle versus the unstick speed is obtained as  $l = f(V_u)$ . From this graph it is easy to obtain the value of the optimum takeoff distance as well as the optimum unstick speed.

Another takeoff technique can be based on higher initial vertical accelerations, but accompanied by a decreasing flight-path velocity ( $V_p$ ) from its unstick value. This decrease in  $V_p$  should be limited by the requirement that, at the obstacle height, the aircraft should either be able to climb steadily at a given angle  $\phi = \sin^{-1}(f_p/f)$  at  $f = 1.0$  (see Figure 4-9), or at least be able to maintain a steady horizontal flight (i.e. at a speed  $V_p$  corresponding to  $f_{n0} = 1.0$ , Figure 4-9).

In this takeoff technique, it is assumed that upon reaching an unstick velocity ( $V_u$ ) the wing and flaps are brought instantaneously to such an attitude with reference to the flight path that the vertical component  $f_n$  assumes its maximum permissible  $f_n$  values corresponding to the  $f_p/f_n = -0.2$  ratio (Fig. 4-9).

It is evident that an infinite number of paths can be selected between the initial (unstick) pairs of the  $f_n$  and  $f_p$  values and those representing the minimum flight requirements of climb or horizontal flight (Fig. 4-9). Selection of the best possible path obviously represents one element of the  $l_{cp}$  optimization. However, in the present case, only two types of paths are investigated; one path is taken as a straight line from  $f_{n \max}$  at a given  $V_u$  to the  $f_n = 1.0$ ,  $f_p = 0$  point. In Figure 4-9, this point corresponds to a flight speed  $V_p \approx 40$  ft/sec. In the second approach, a path along the  $f_p/f_n = 0.2$  line is considered down to  $V_p \approx 50$  ft/sec where it is assumed that the wing and flap position is instantaneously adjusted to the position corresponding to  $f_n = 1.0$  and  $f_p = 0$ ; i.e. to that of steady horizontal flight.

Starting with Equations (4-24) and (4-25) to compute  $\overset{\circ}{V}_y = f(t)$  and  $\overset{\circ}{V}_x = f(t)$ ,  $V_y = f(t)$ ,  $V_x = f(t)$ , and finally  $x_{cl} = f(t)$  and  $y = f(t)$  were determined for various  $V_u$  values and the two types of the  $f_n, f_p$  paths. The  $f_p/f_n = -0.2$  path appeared very slightly more advantageous, hence the  $l_{cp} = f(V_u)$  curve corresponding to the latter case

is plotted in Figure 4-12, and is combined with the  $l_{gr\ opt} = f(V_u)$  graph to obtain the  $l = f(V_u)$  curve.

A glance at Figure 4-12 will indicate that the takeoff technique permitting the speed of flight to decrease during climb to the obstacle height should be more advantageous than that of maintaining a constant flight speed equal to its unstick value. As to the unstick velocity itself, it appears that slightly higher  $V_u$  values are more favorable for takeoffs with decreasing flight path speeds.

It should be noted, however, that in the climb portion of the considered takeoff problem, no single control function was obtained that, in combination with that expressed by the graph in Figure 4-11, would minimize the functional given by Equation (4-10) or, in other words, provide a complete schedule of  $\theta_F$  versus  $V$  that would lead to the shortest takeoff distance. Nevertheless, an analysis outlined in the preceding sections should suffice for indicating at least a direction for the shortest takeoff technique.

As to a different mathematical treatment of the shortest takeoff problem, Reference 4-8 suggests that since the equations describing the physical phenomenon of the takeoff are ordinary differential equations, one may use as the optimization technique either calculus of variations or Pontryagin's maximum principle. The second technique has the advantage over the first one in that, by means of suitable transformations, the problem can be reduced to a linear Hamilton-Jacobi system.

#### REFERENCES TO CHAPTER IV

- |  |  |
|--|--|
| 4-1. Feistal, T.W.<br>et al.             | <i>Results of a Brief Flight Investigation of a Coin-Type STOL Aircraft</i> , NASA Conference on V/STOL and STOL Aircraft, April, 1966. NASA SP-116.   |
| 4-2. Innis, R.C.<br>Quigley, J.C.        | <i>A Flight Examination of Operating Problems of V/STOL Aircraft in STOL-Type Landing and Approach</i> , NASA TN D-862, June 1961.   |
| 4-3. Staff of Langley<br>Research Center | <i>A Preliminary Study of V/STOL Transport Aircraft and Bibliography of NASA Research in the VTOL-STOL Field</i> , NASA TN D-624, January, 1961.   |
| 4-4. Kuhn, R.E.                          | <i>Technological Gaps in V/STOL Development</i> , Presented at the University of Tennessee Space Institute Short Course "Modern Developments in Low Speed Aerodynamics with Application to VTOL", Tallahassee, Tennessee, September-October, 1967. |
| 4-5a. Goodson, K.W.                      | <i>Comparison of Wind-Tunnel and Flight Results on a Four-Propeller Tilt-Wing Configuration</i> , NASA Conference on V/STOL and STOL Aircraft, April, 1966. NASA SP-116.   |
| 4-5b. Goodson, K.W.                      | <i>Effect of Ground Proximity on the Longitudinal, Lateral, and Control Aerodynamic Characteristics of a Tilt-Wing Four-Propeller V/STOL Model</i> , NASA TN D-4237, December, 1967.   |
| 4-6. Pegg, R.J.                          | <i>Damage Incurred on a Tilt-Wing Multi-propeller VTOL/STOL Aircraft Operating over a Level, Gravel-Covered Surface</i> , NASA TN D-535, December, 1960.   |



- 4-7. Kuhn, R.E.  
Grunwald, K.J. *Lateral Stability and Control Characteristics of a Four-Propeller Deflected-Slipstream VTOL Model including the Effect of Ground Proximity, NASA TN D-444, January, 1961.*
- 4-8. van Krzywoblocki, M.Z.  
Stepniewski, W.Z. *Application of Optimization Techniques to the Design and Operation of V/STOL Aircraft, Proceedings of the International Congress on Subsonic Aeronautics, in New York, April, 1967, New York Academy of Sciences (now in publication).*

**TABLE I**  
**Assumed Characteristics of Tilt Wing**

<i>Item</i>	<i>Value</i>
Takeoff Conditions	H = 0, Standard
Disc Loading in Hover, lb/ft <sup>2</sup>	w <sub>h</sub> = 36
Power Loading in Hover, lb/shp	W <sub>h</sub> /SHP = 4.8
Efficiencies	η <sub>A</sub> = 0.8; η <sub>tr</sub> = 0.94
Overload for Running Takeoff, 25%	T <sub>0</sub> /W = 0.8
Ideal Induced Velocity at T <sub>0</sub> , ft/sec	v <sub>i0</sub> = 87

**TABLE II**  
**Assumed Characteristics of Tilt Rotor**

<i>Item</i>	<i>Value</i>
Takeoff Conditions	H = 0, Standard
Disc Loading in Hover, lb/ft <sup>2</sup>	w <sub>h</sub> = 10
Power Loading in Hover, lb/shp	W <sub>h</sub> /SHP = 8.4
Efficiencies	η <sub>A</sub> = 0.76; η <sub>tr</sub> = 0.94
Overload for Running Takeoff, 25%	T <sub>0</sub> /W = 0.8
Ideal Induced Velocity at T <sub>0</sub> , ft/sec	v <sub>i0</sub> = 46

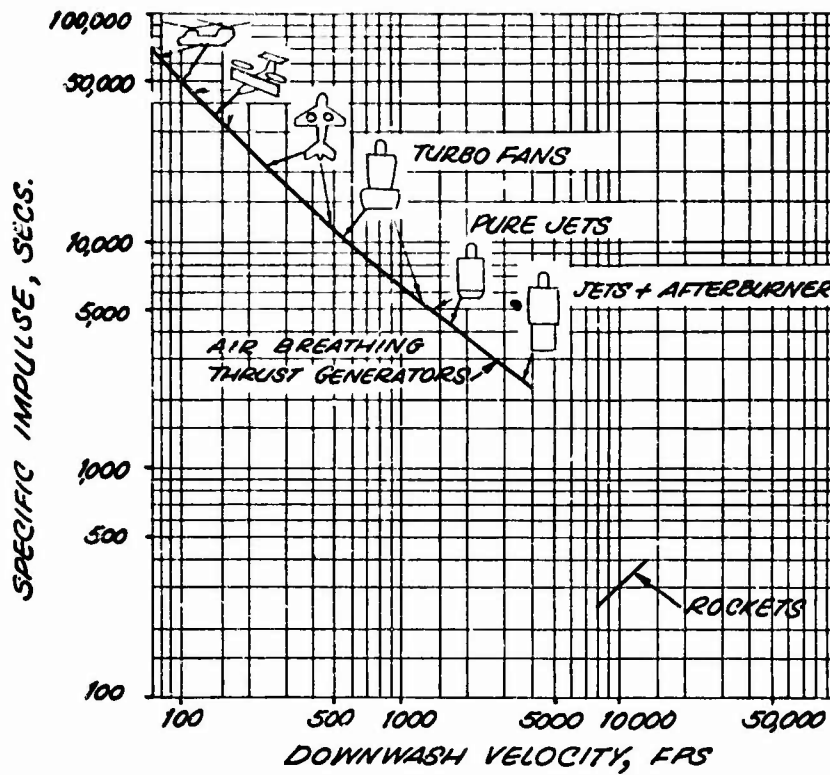


Fig. 1-1 Specific impulse of various thrust generators versus downwash velocity (equivalent velocity for rockets)

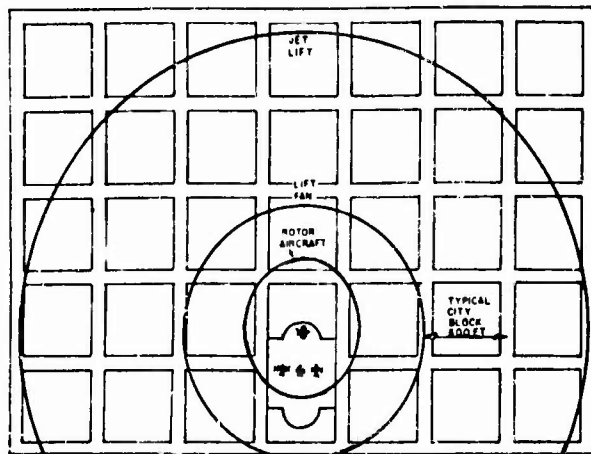


Fig. 1-2 112 PNdB contours for typical VTOL short-haul transports on takeoff; 1980 technology

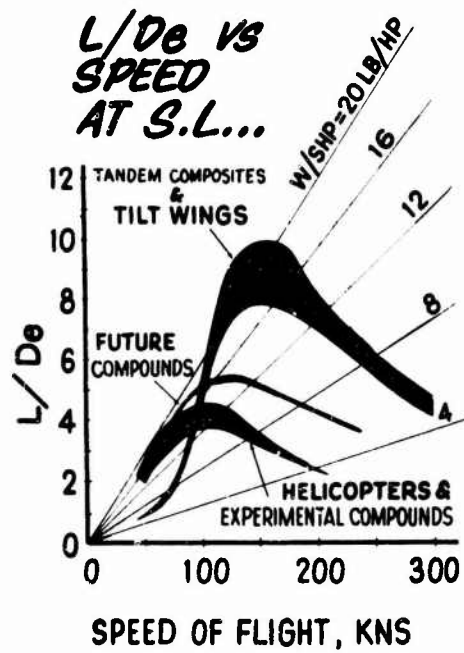


Fig. 1-3 Gross weight (lift) to equivalent drag ratios versus speed of flight

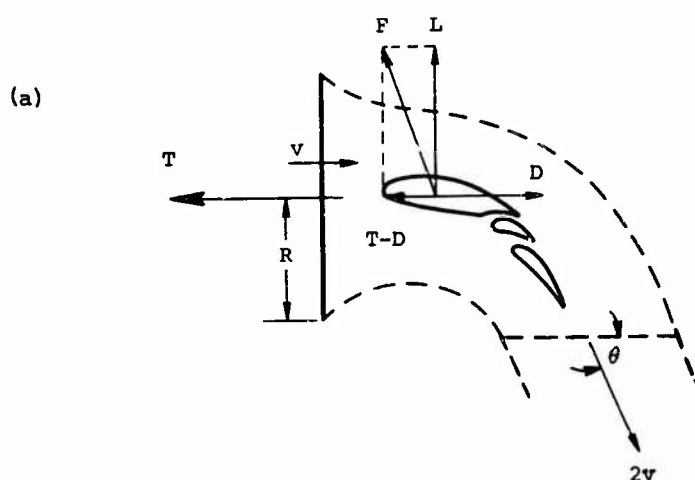
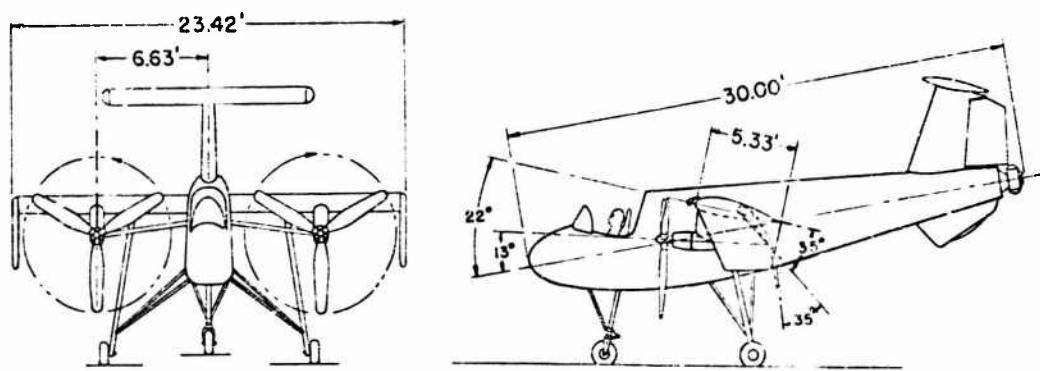


Fig.1-4 Ryan VZ-3RY flight research aircraft, and schematic of slipstream deflection

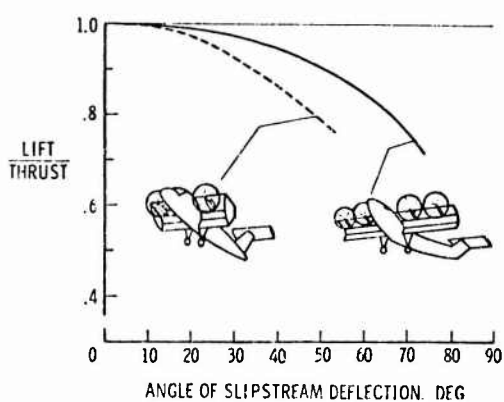


Fig.1-5 Hovering effectiveness of deflected-slipstream configurations



Fig.1-6 An artist's conception of the tilt-wing short-haul VTOL transport

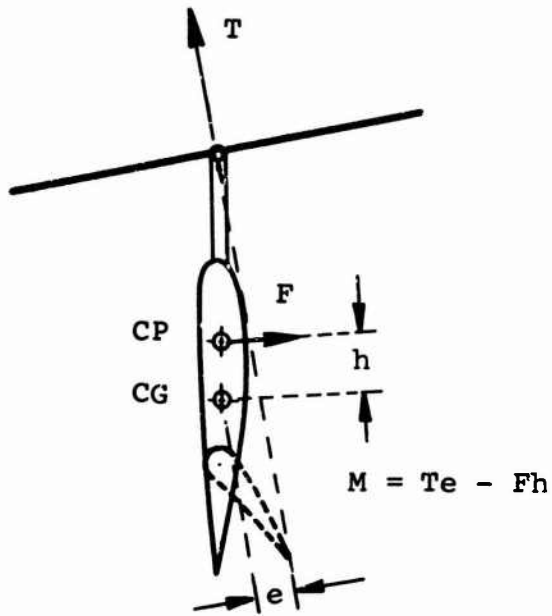


Fig.1-7 Application of monocyclic to tilt-wing with flapping rotor/propeller

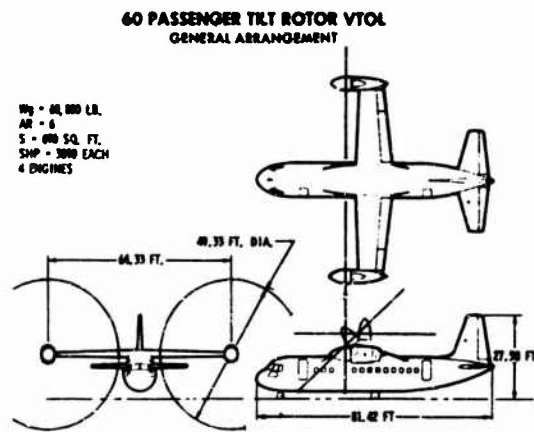


Fig.1-9 Three-view drawing of tilt-rotor short-haul VTOL transport

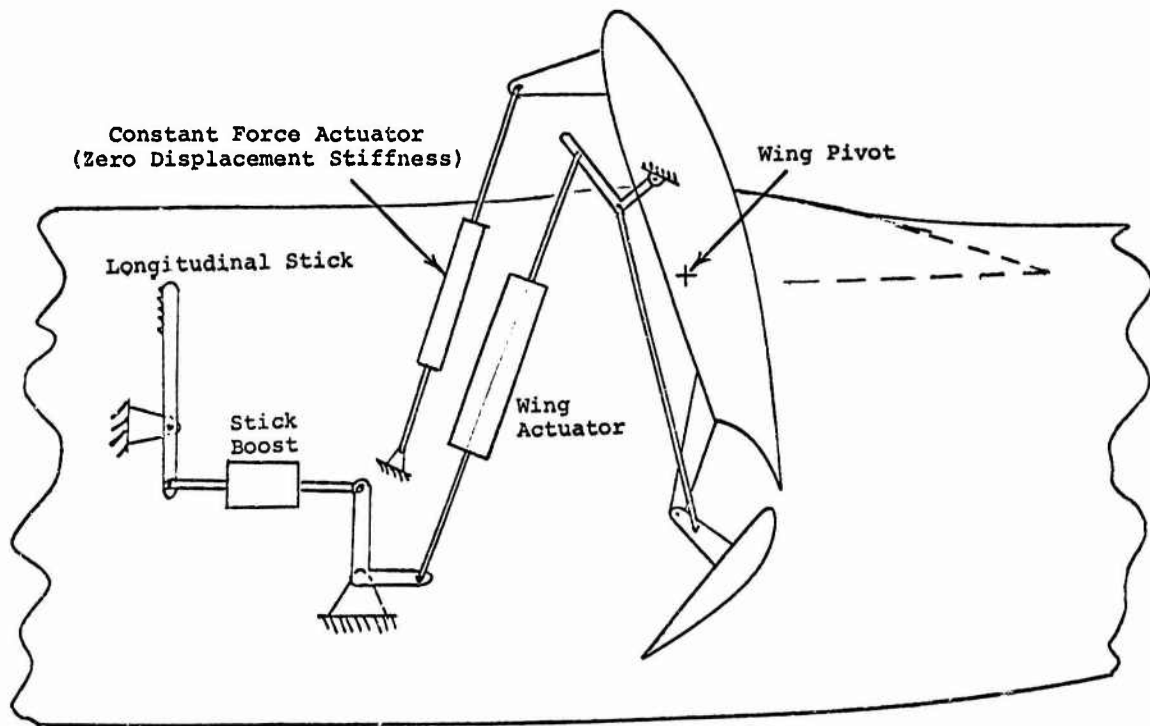


Fig.1-8 Schematic drawing of geared flap system

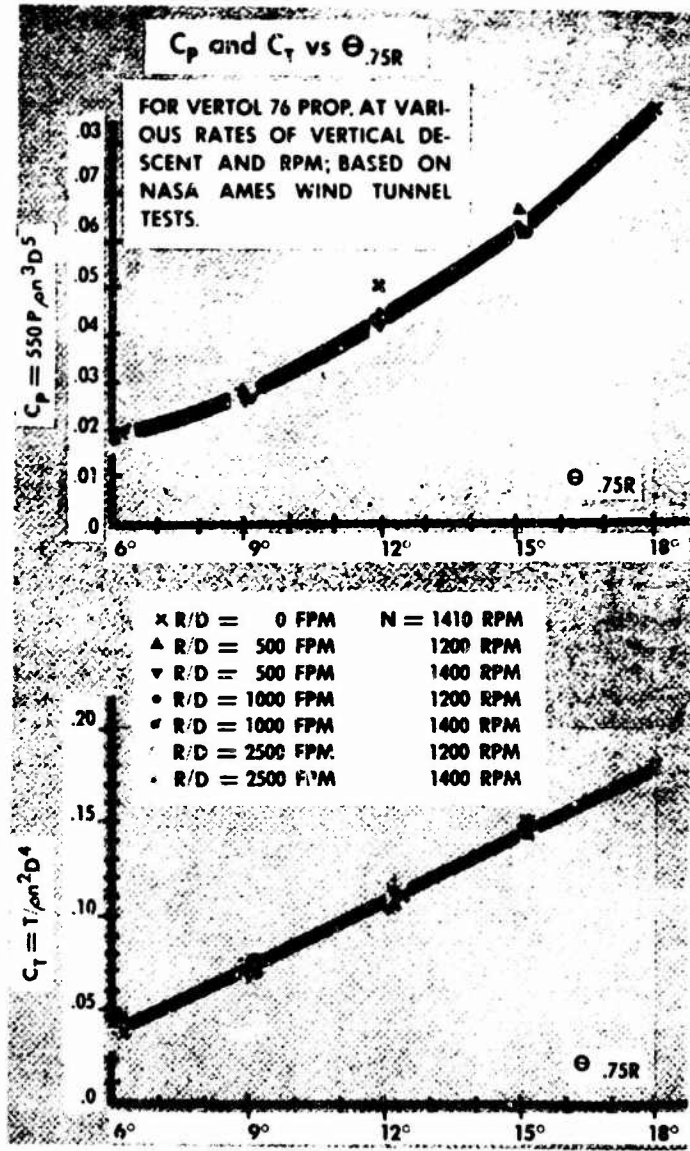


Fig. 1-10 Thrust and power coefficients of a VTOL propeller in vertical descent

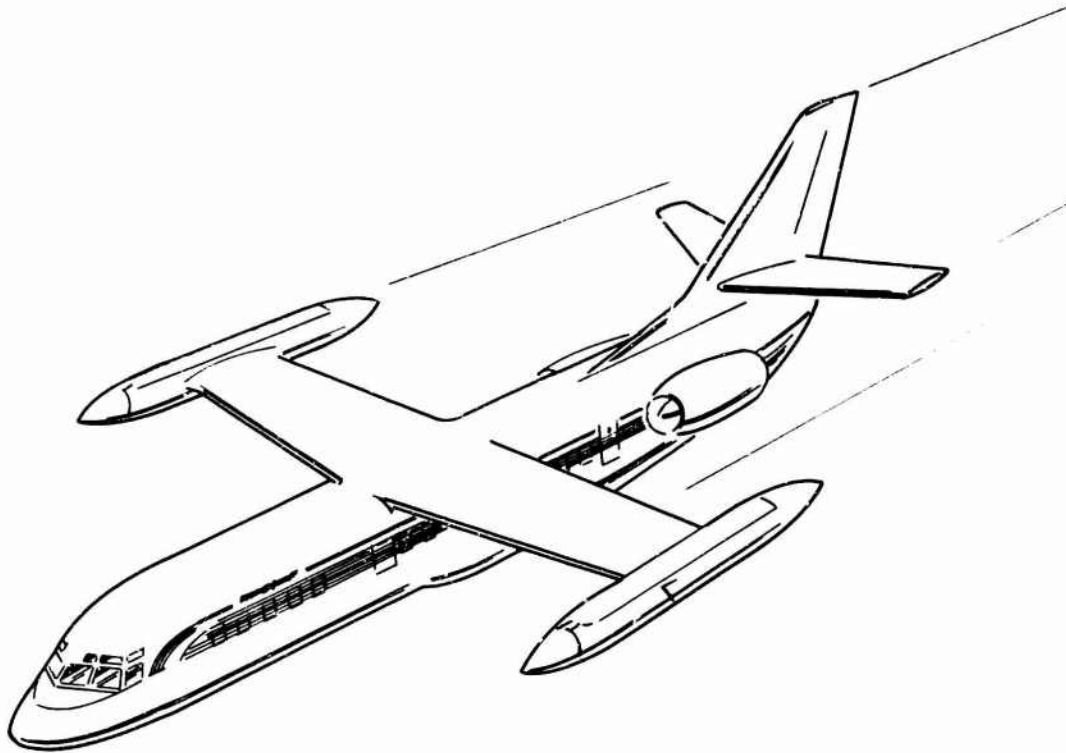


Fig.1-11 An example of a short-haul transport based on the concept of tilting rotor with foldable blades

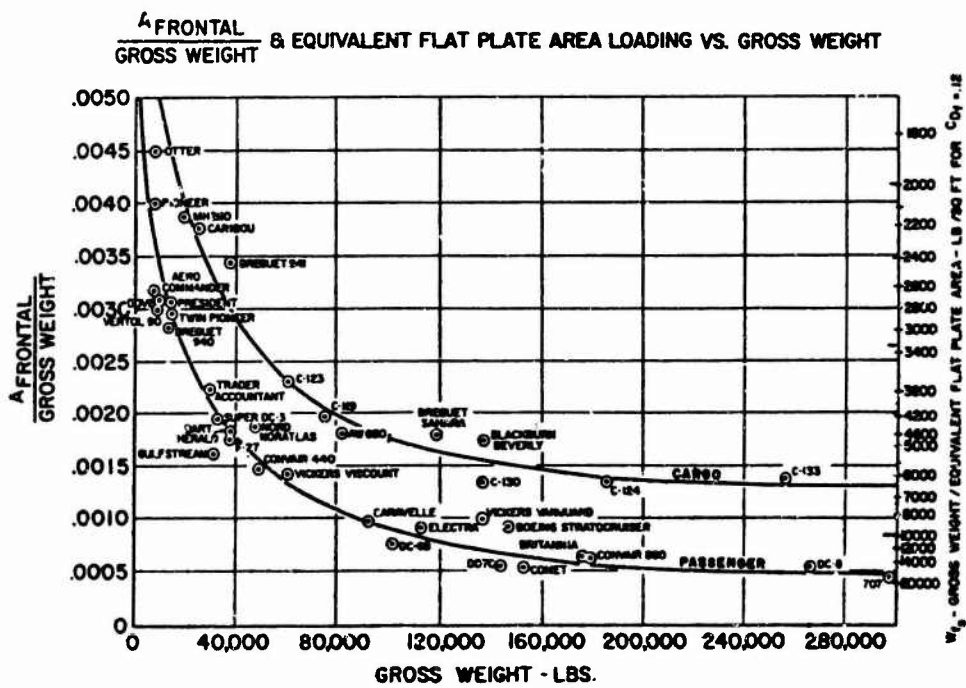


Fig.1-12 Statistical chart

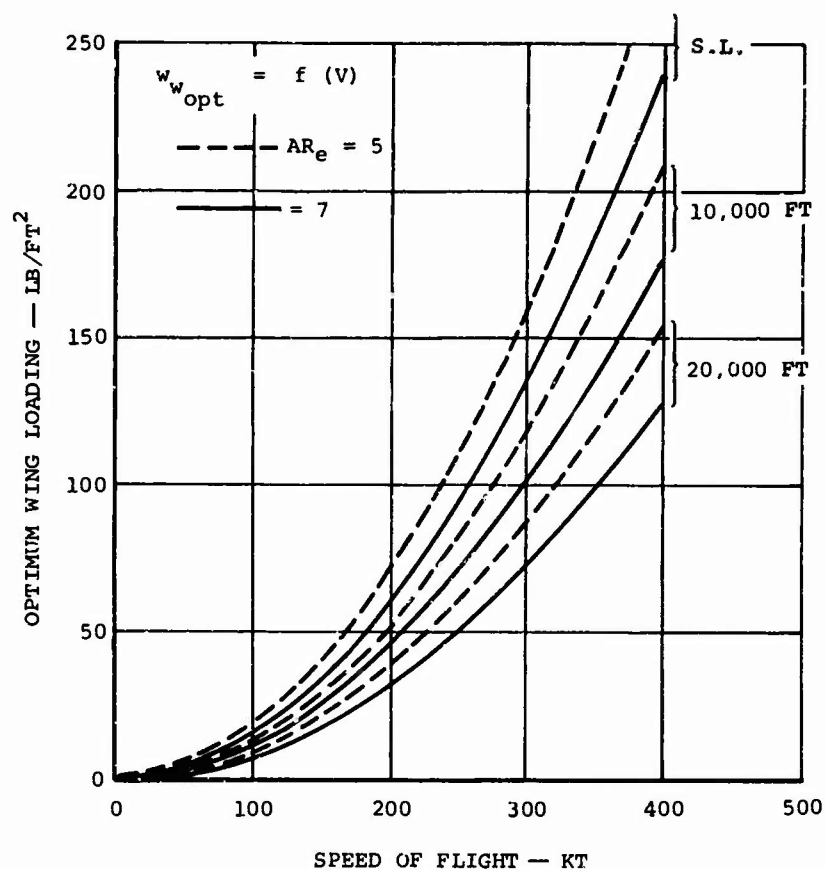
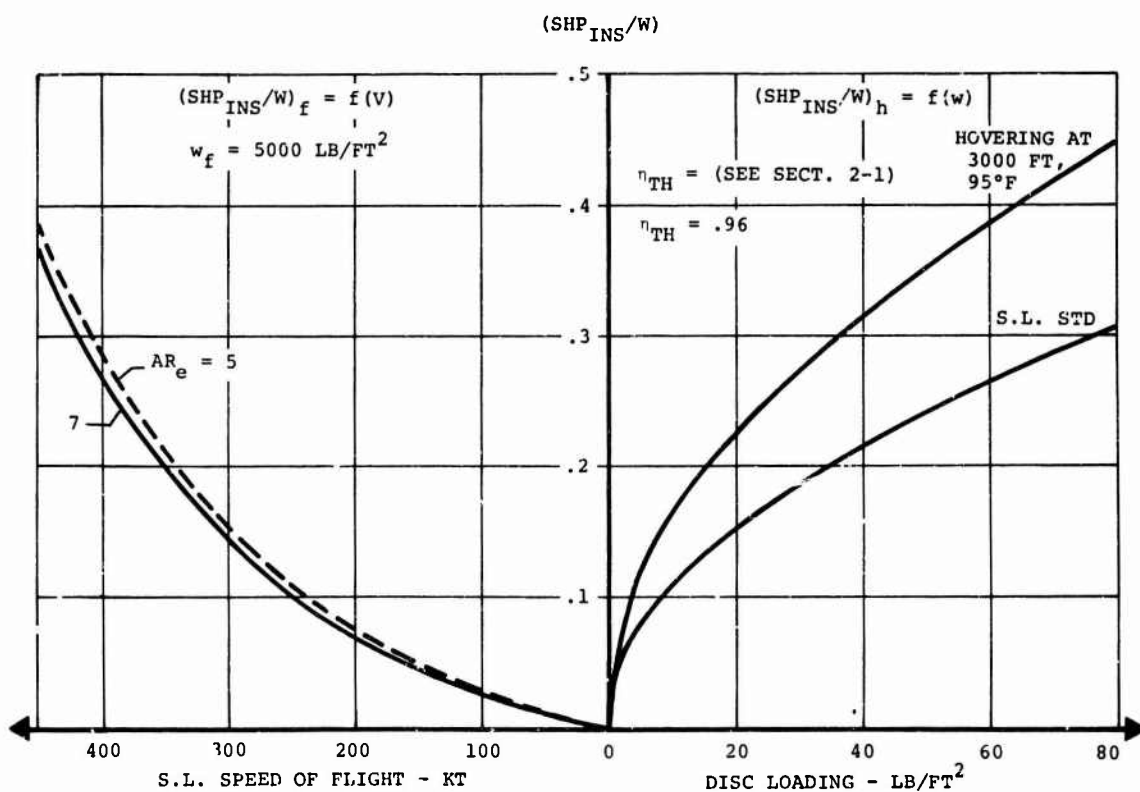


Fig.1-13 Optimum wing loading versus speed of flight

Fig.1-14 Example of power match with  $w_w$  optimized for 20,000 ft



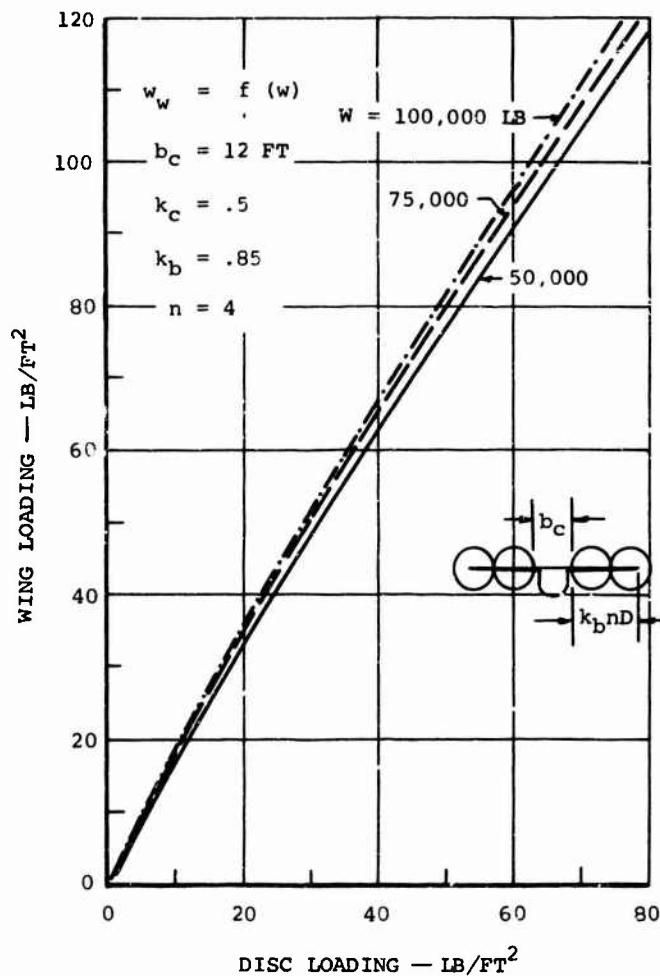


Fig.1-15 Example of wing loading versus disc loading with geometric constraints

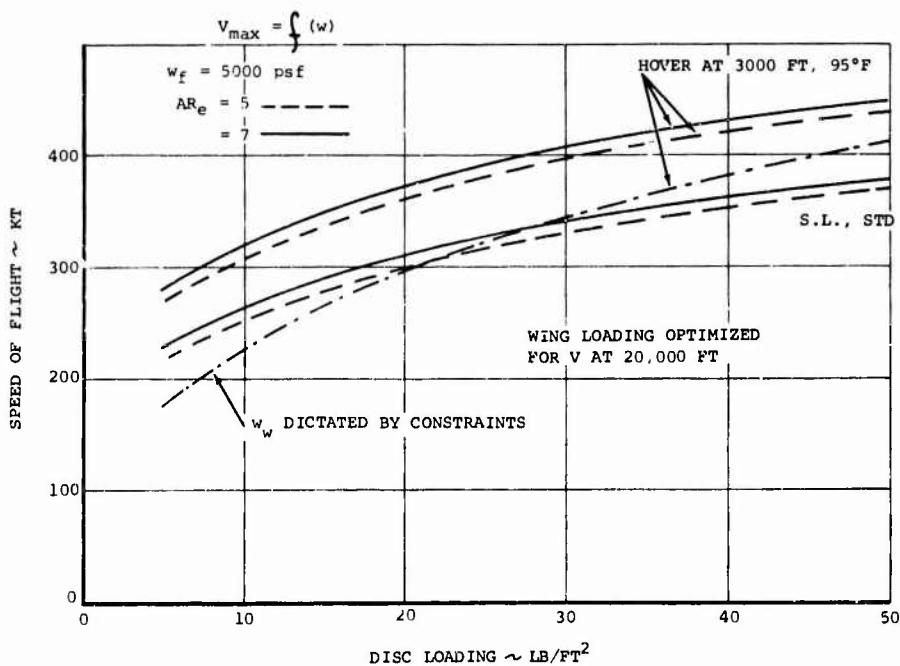


Fig.1-16 High speed capabilities at S.L. versus disc loading

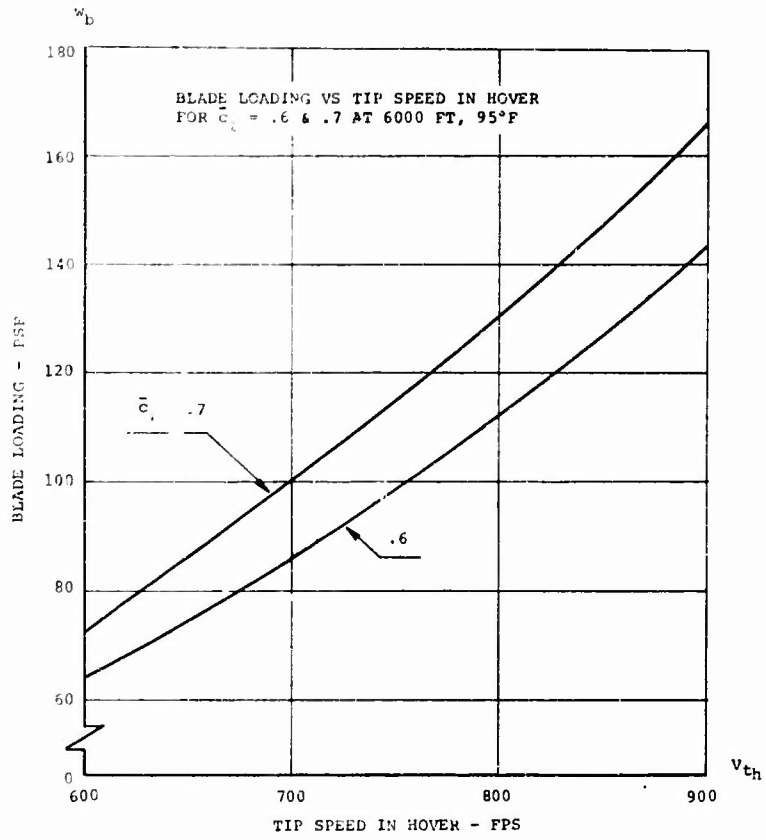


Fig.2-1 Example of the practical range of blade loadings

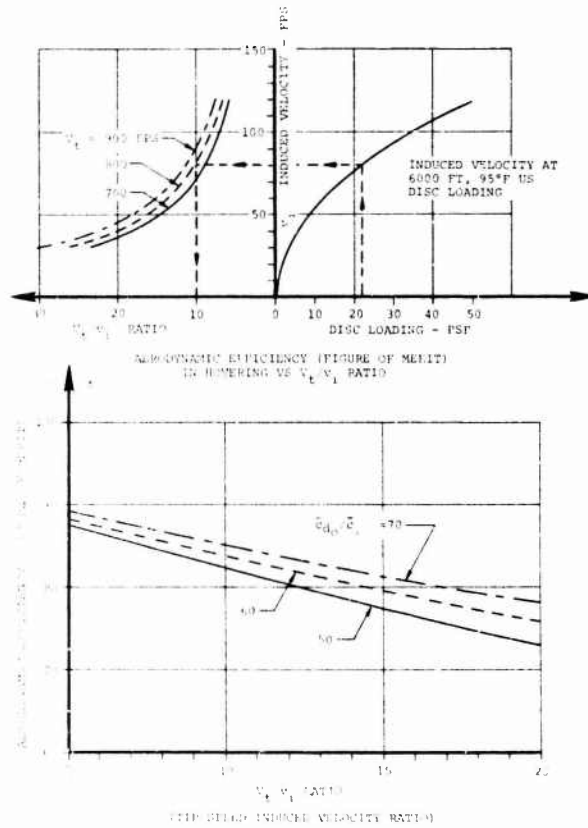


Fig.2-2 Ideal induced velocity to tip speed ratios and aerodynamic efficiencies.

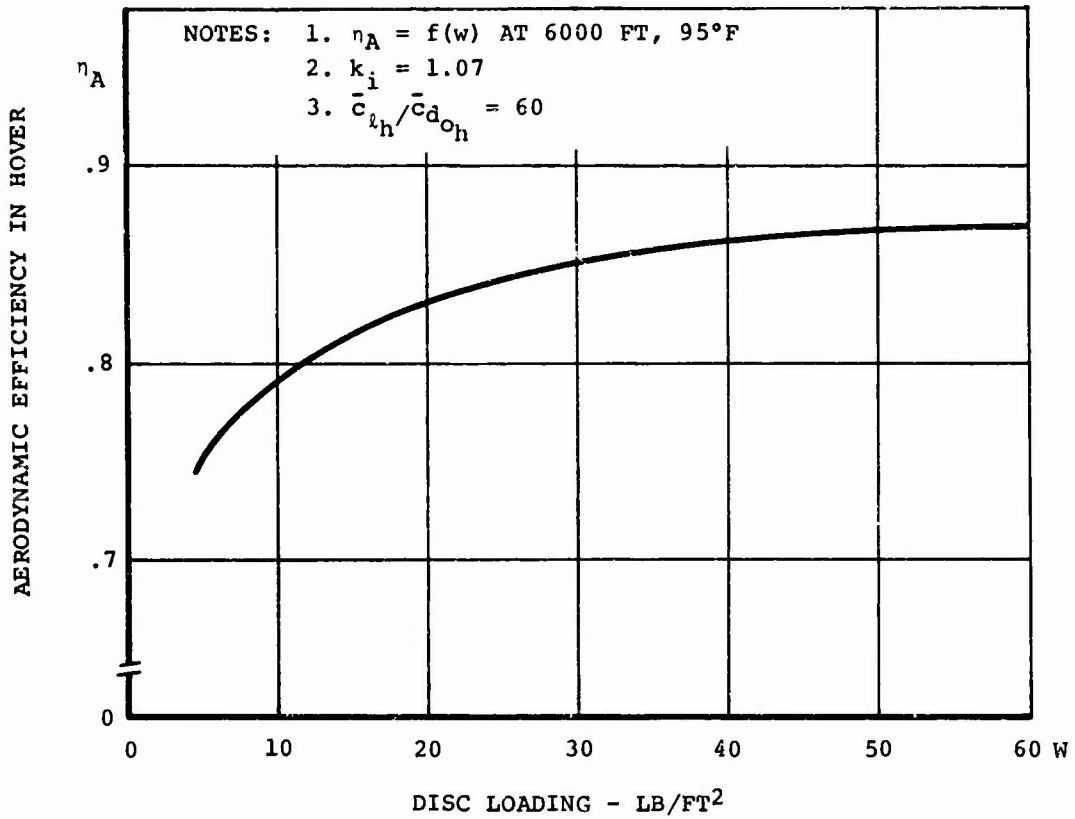


Fig. 2-3 Trends in aerodynamic efficiency (figure of merit) in hover that would exist if  $k_i$  and  $\bar{c}_{l_h} / \bar{c}_{d_{0h}}$  were constant

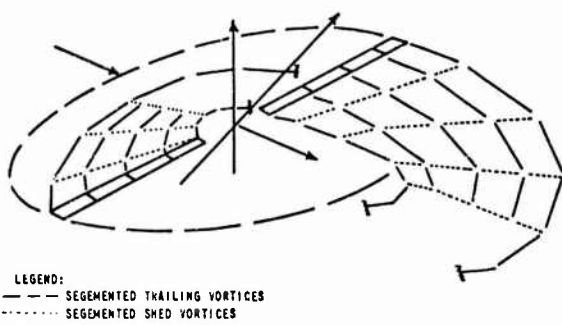


Fig. 2-4 Typical mathematical model based on discrete vortex wake representation

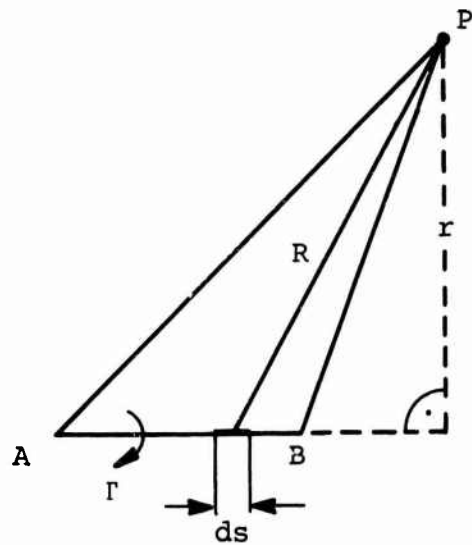


Fig. 2-5 Induced velocity at point P

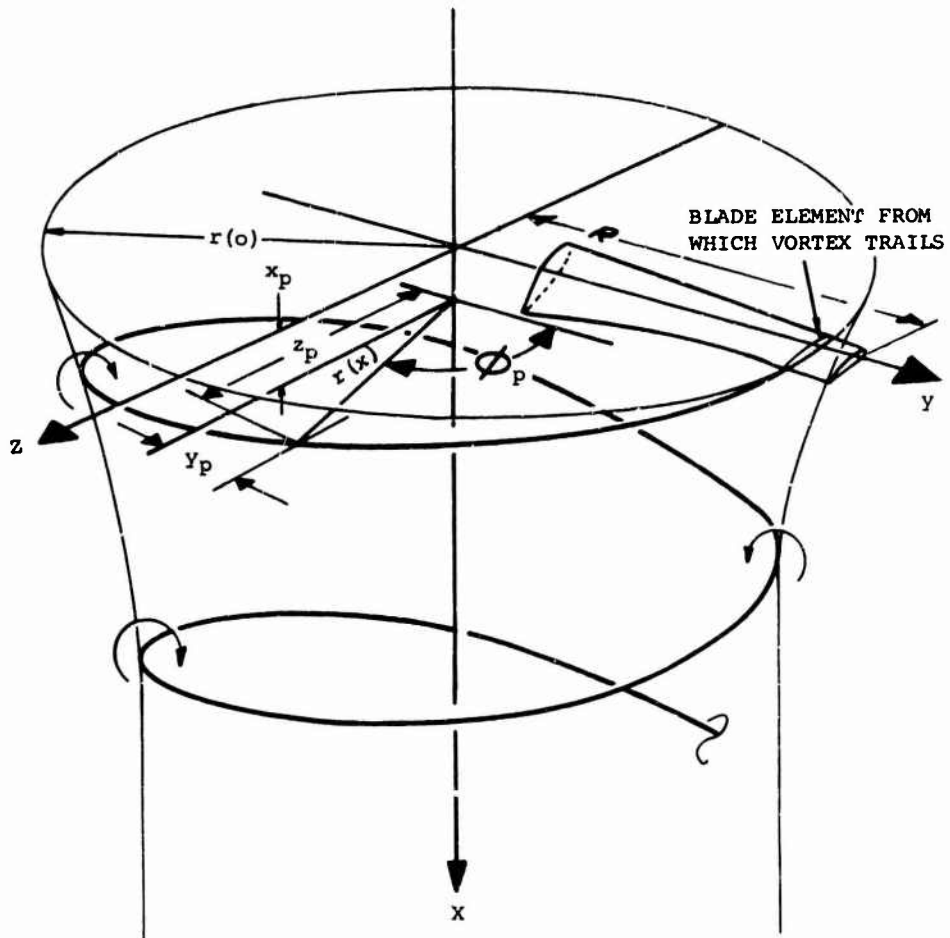


Fig.2-6 Typical geometry of a single vortex filament

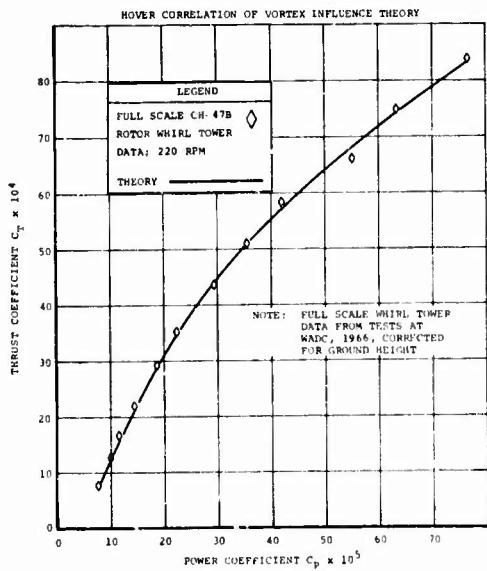


Fig.2-7 Comparison of tested and predicted static performance of a helicopter rotor

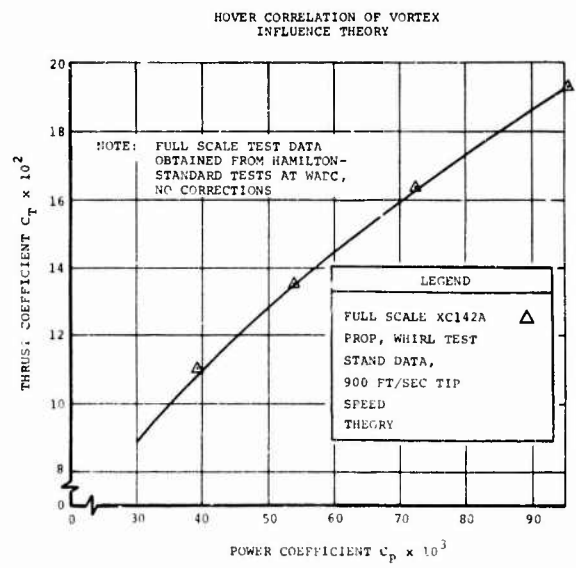


Fig.2-8 Comparison of tested and predicted static performance of a tilt-wing propeller

# DOWNWASH FLOW PATTERNS

PLAIN WING

WITH SPECIAL DEVICES

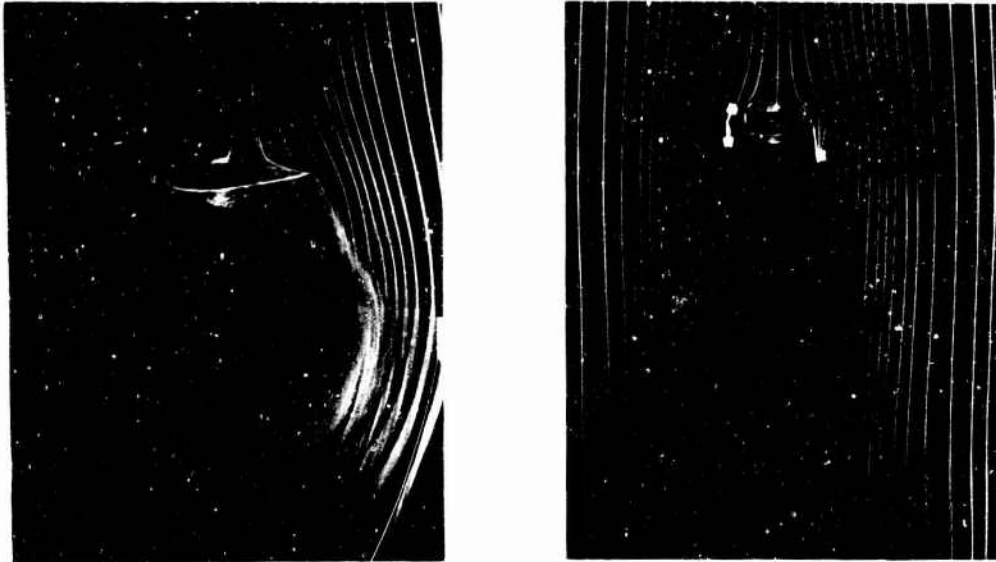


Fig.2-9 Two-Dimensional smoke studies of the rotor downwash submerged wing

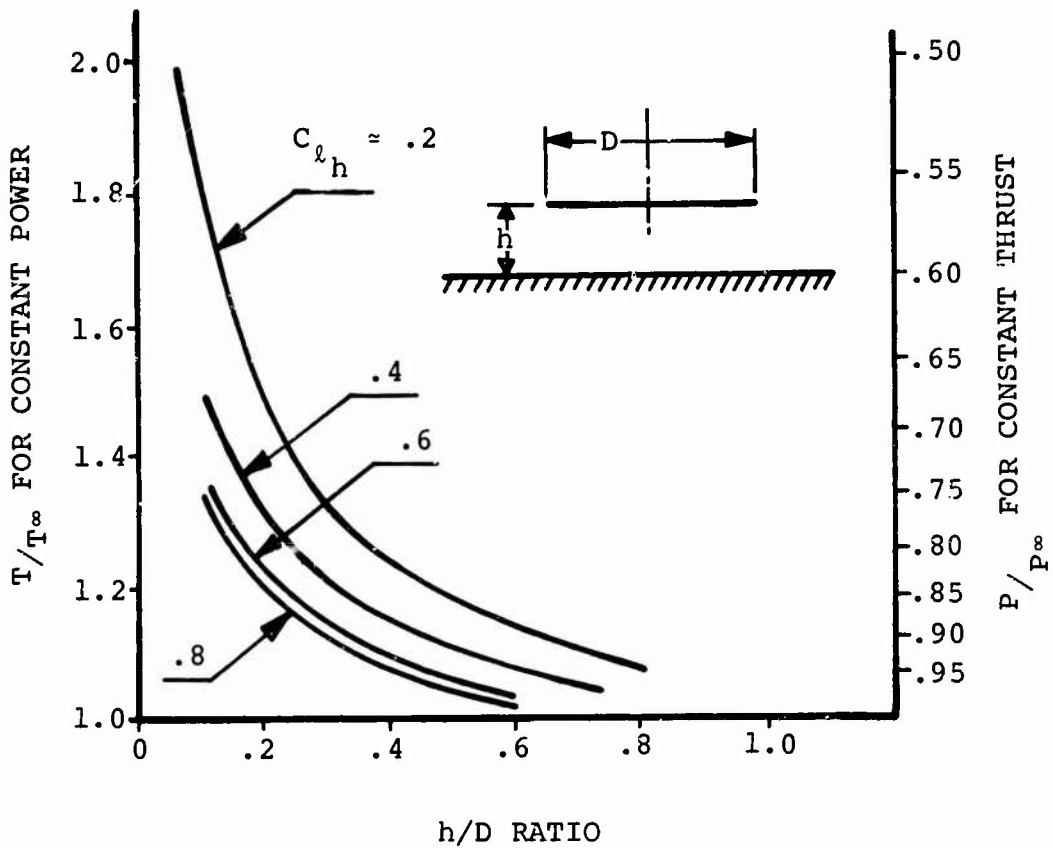
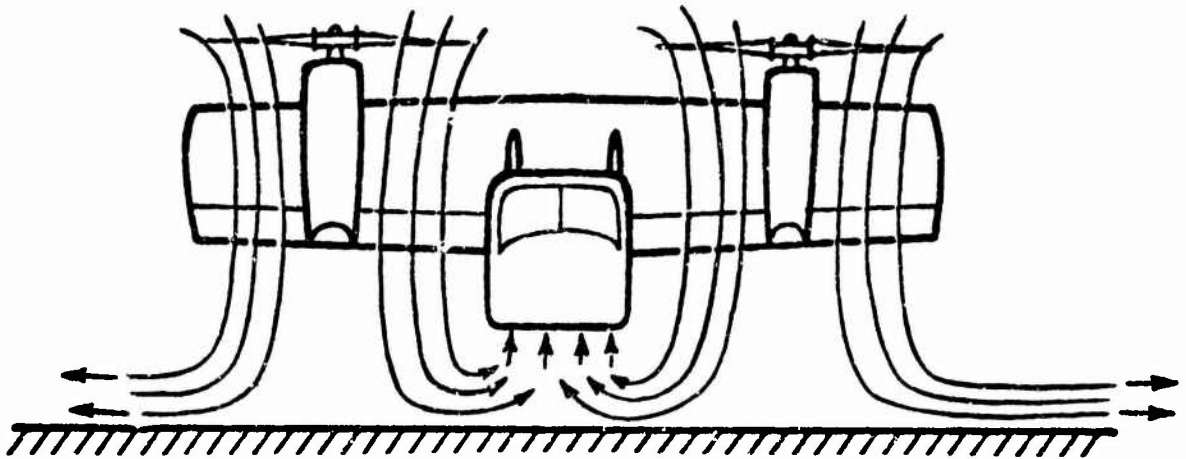


Fig.2-10 Static thrust augmentation, or reduction of power required due to ground effect



## MULTIPLE SLIPSTREAMS

Fig.2-11 Flow patterns for a two-propeller tilt-wing in hover close to the ground

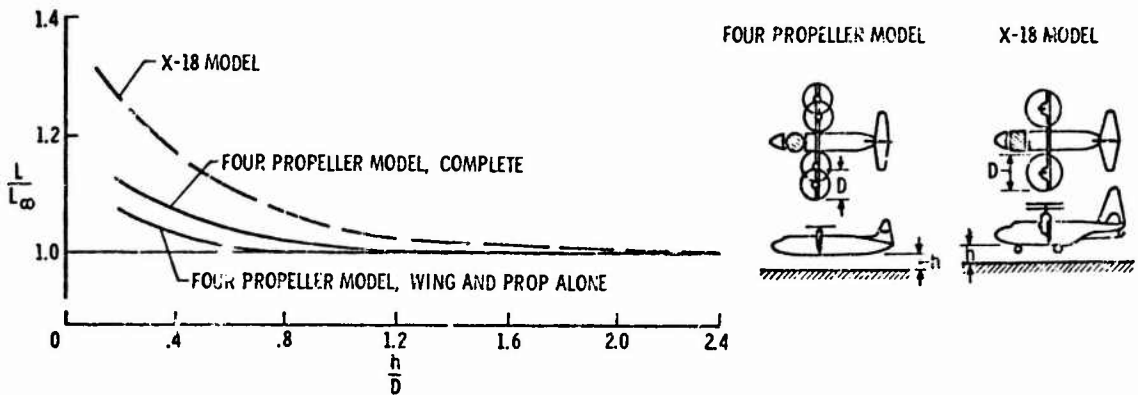


Fig.2-12 Effect of the ground on two tilt-wing configurations

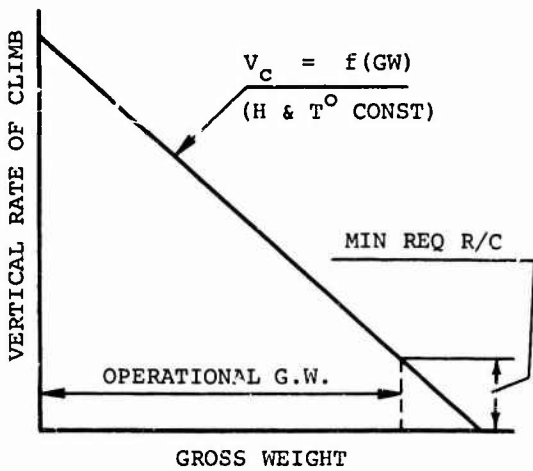


Fig.2-13 Determination of operational gross weight by vertical climb requirements

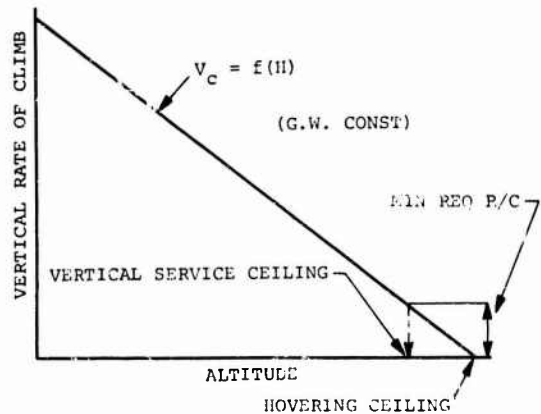


Fig.2-14 Determination of vertical service and hovering ceiling

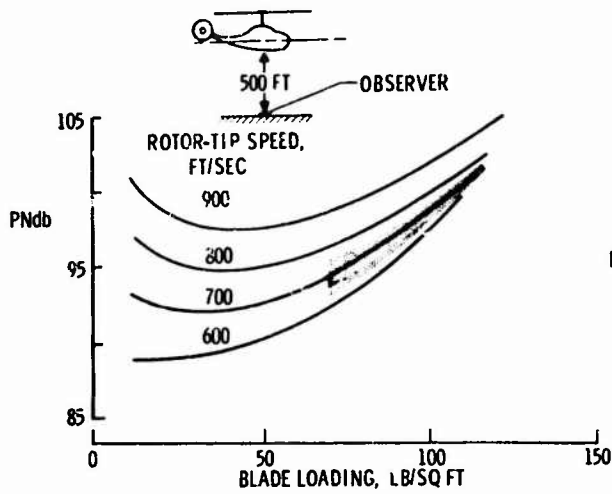


Fig. 2-15 Influence of tip speed and blade loading on noise level of helicopter

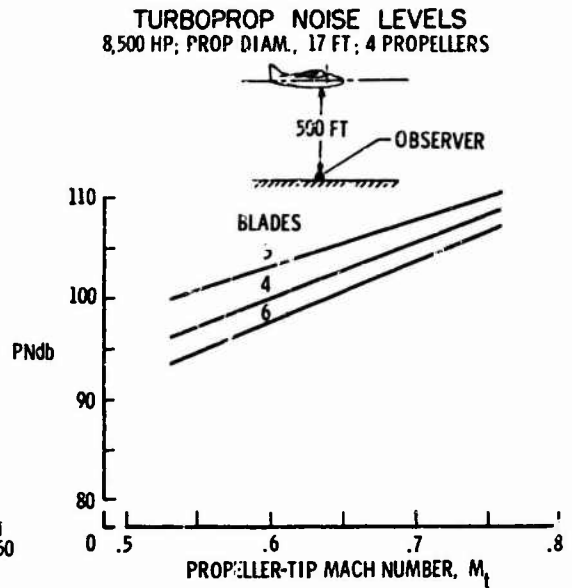


Fig. 2-16 Example of the influence of propeller tip Mach number and number of blades on noise level of turboprop

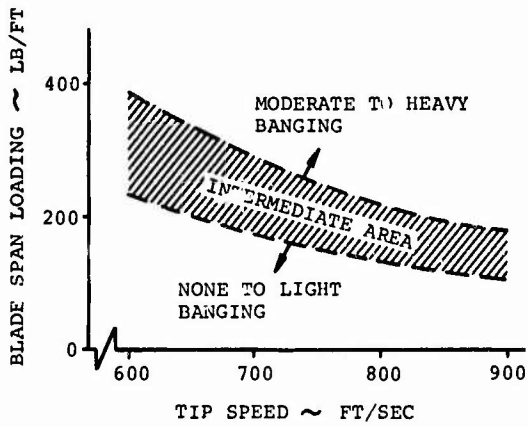


Fig. 2-17 Single rotor bang criteria

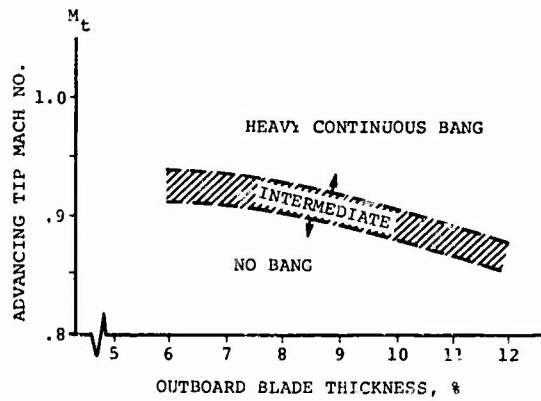


Fig. 2-18 Bang criteria for helicopter rotor in highspeed flight

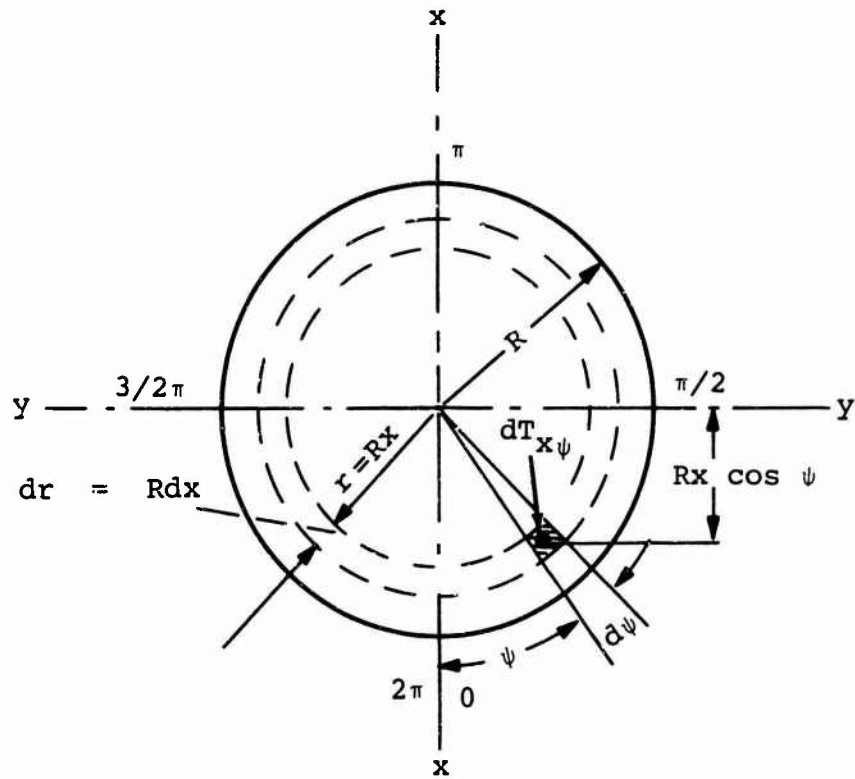


Fig.2-19 Elementary pitching moment

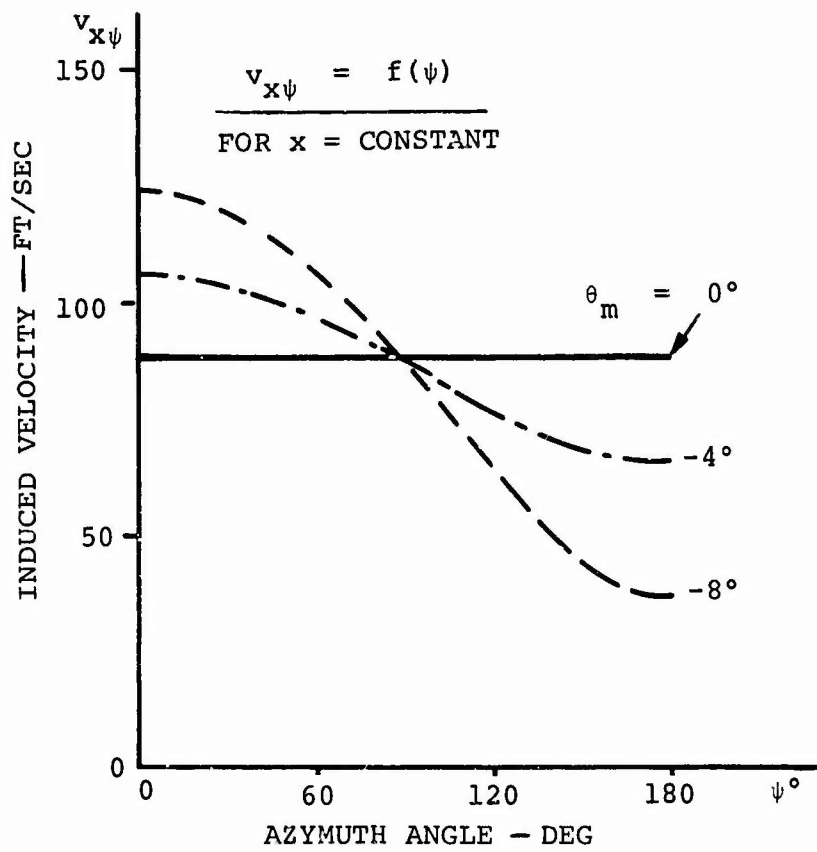


Fig.2-20 Typical variation of induced velocity with azimuth, at constant radius, when monocyclic is applied



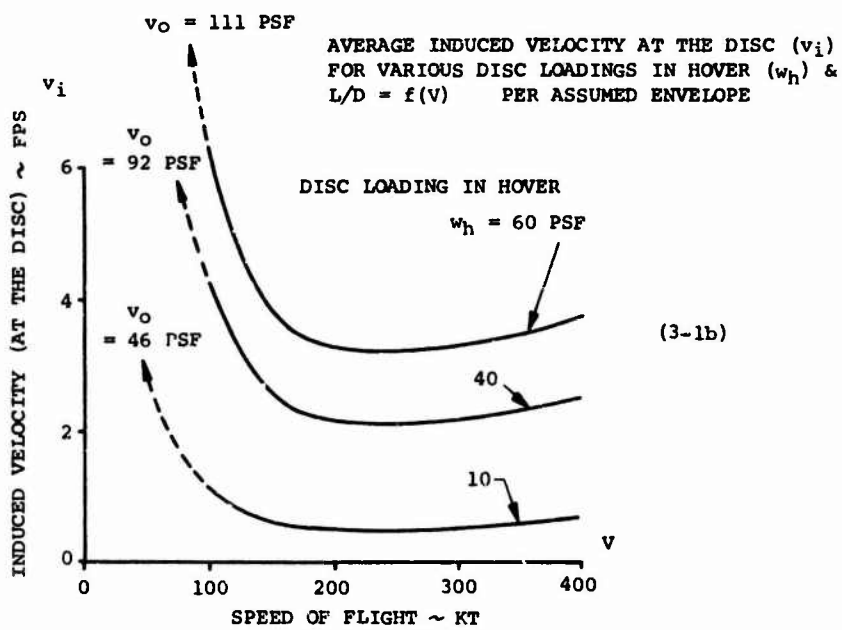
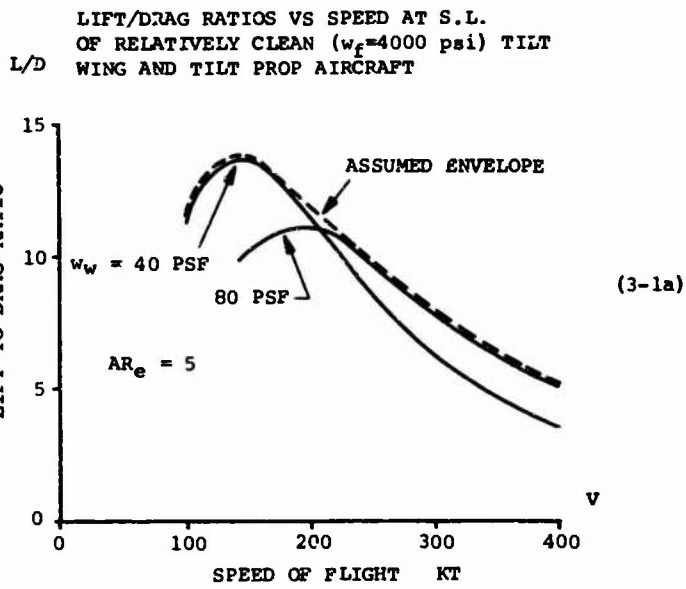


Fig.3-1 Examples of lift to drag ratios and induced velocities in forward flight

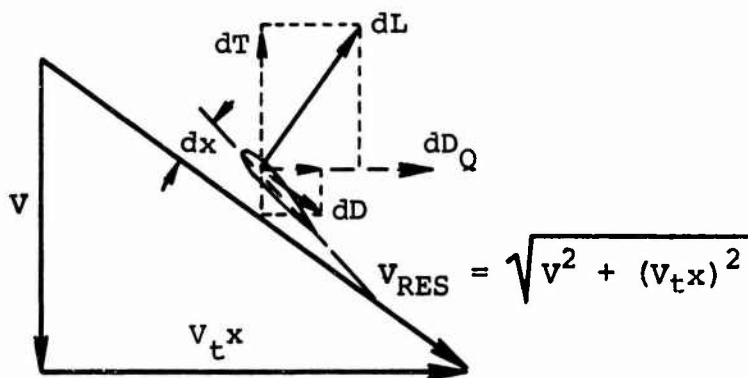


Fig.3-2 Speed and force diagram at a blade station (x)

POSSIBLE PROPULSIVE EFFICIENCIES  
VS SPEED

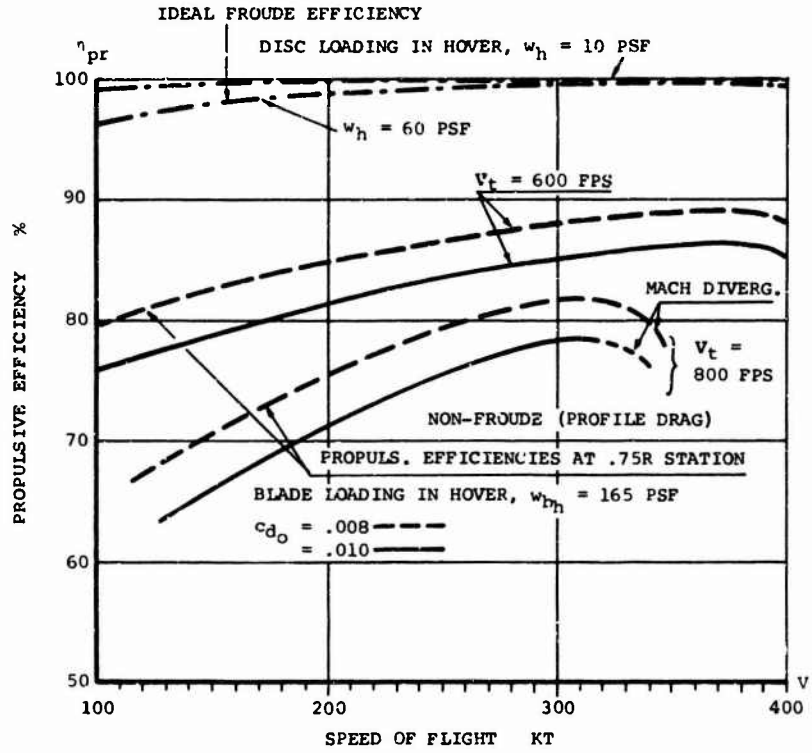


Fig.3-3 Trends in the ideal Froude and non-Froude propulsive efficiencies

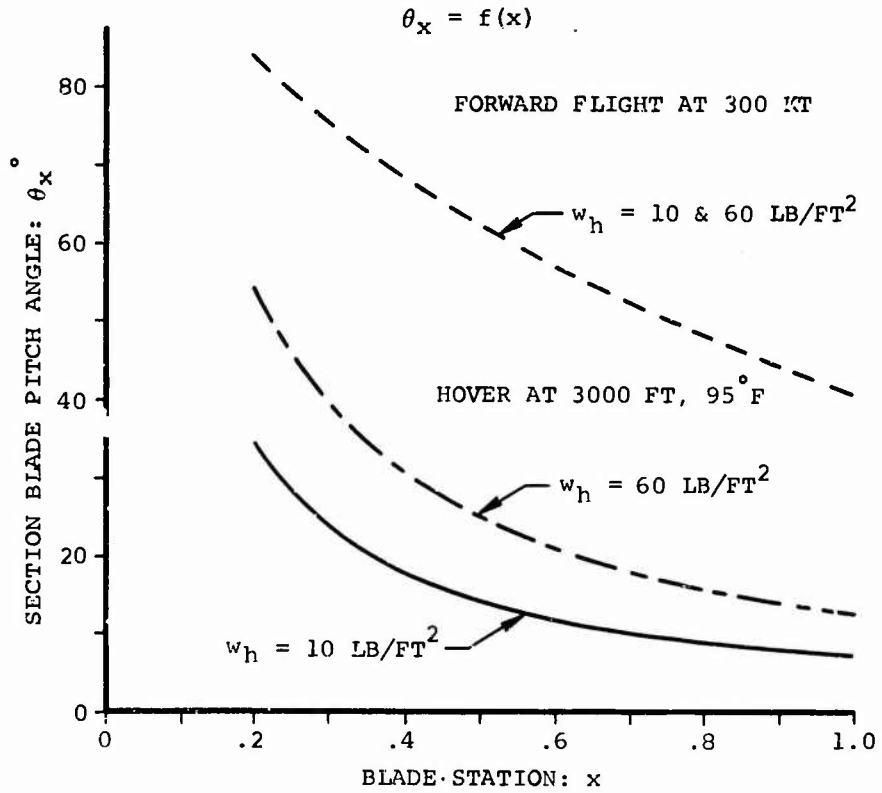


Fig.3-4 Examples of section pitch distribution required in hover and in forward flight for uniform induced velocity

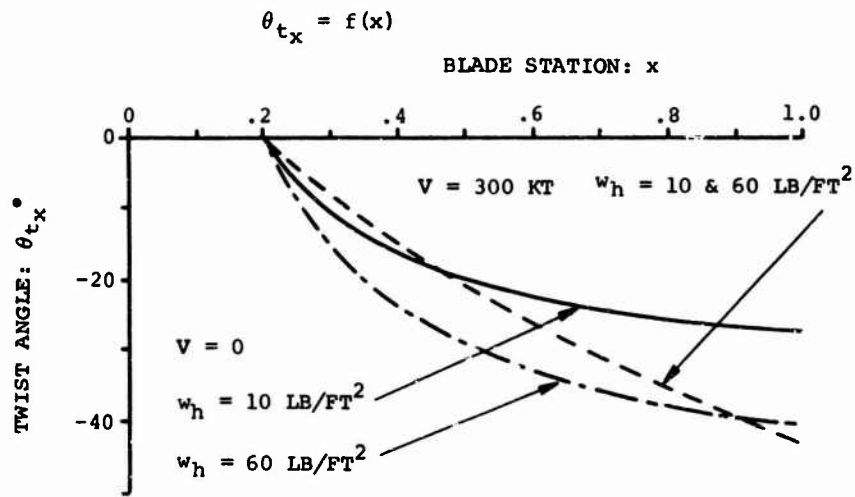


Fig.3-5 Twist distribution (from  $x = 0.2$  to  $x = 1.0$ ) resulting from Figure 3-4

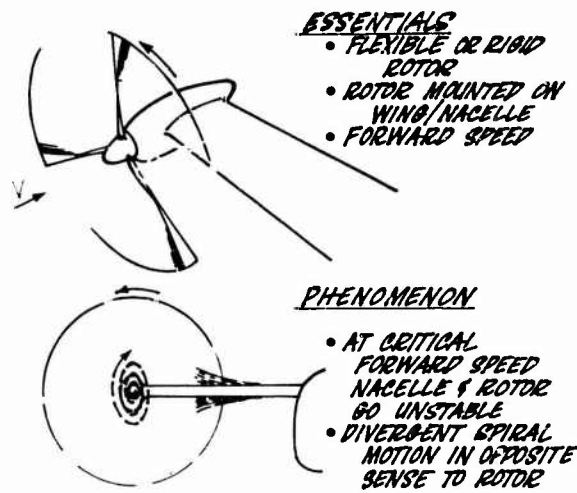


Fig.3-6 Backward whirling

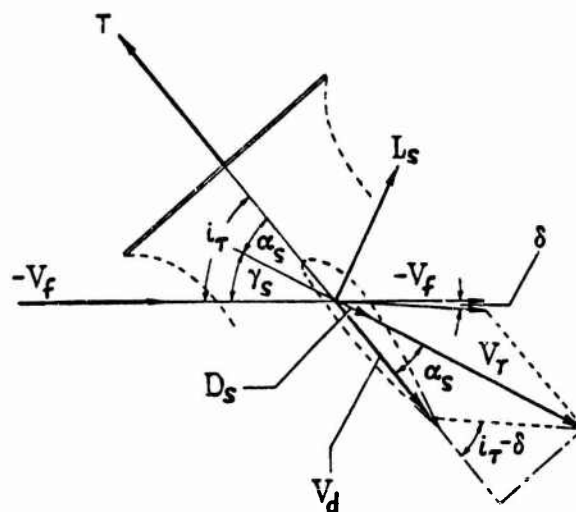


Fig.3-7 Flow and force diagram in the propeller slipstream

DOWNWASH VELOCITIES AT VARIOUS FORWARD SPEEDS & THRUST INCLINATIONS

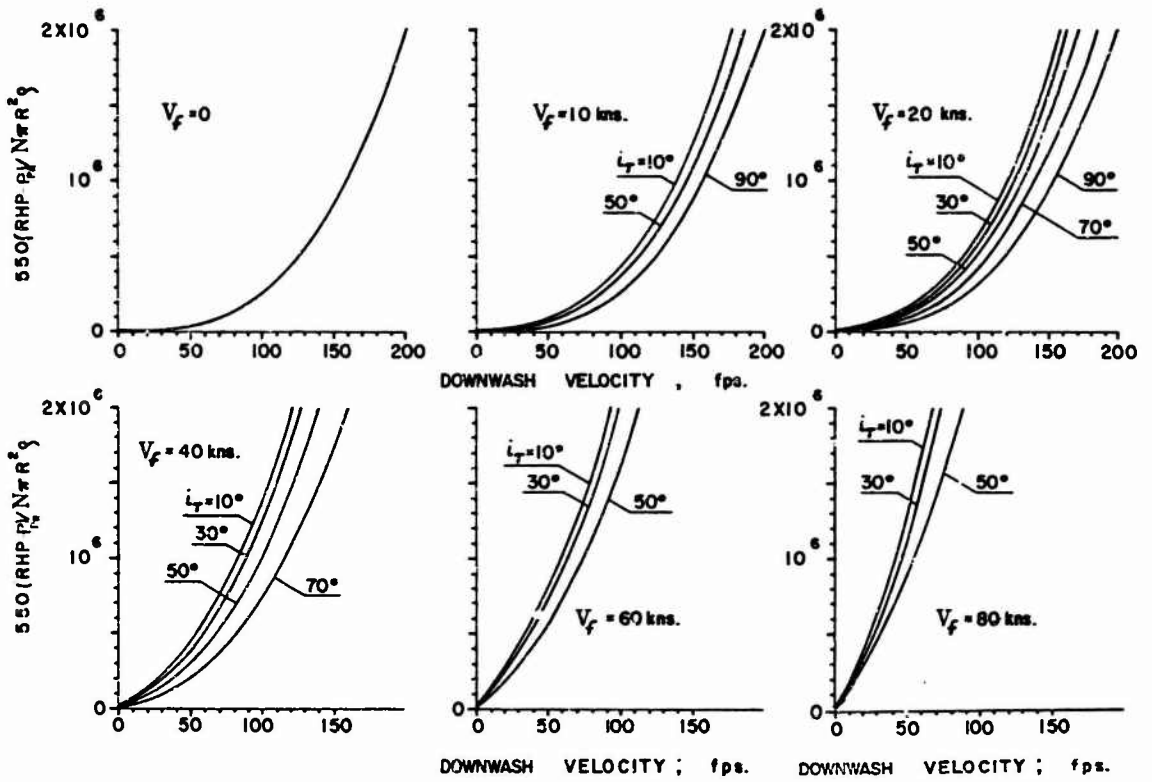


Fig.3-8 Graph for estimating fully developed downwash velocity

SCHEME OF AIR TUBES AFFECTED BY WING ( $\pi b^2/4$ ) AND PROLLER SLIPSTREAM

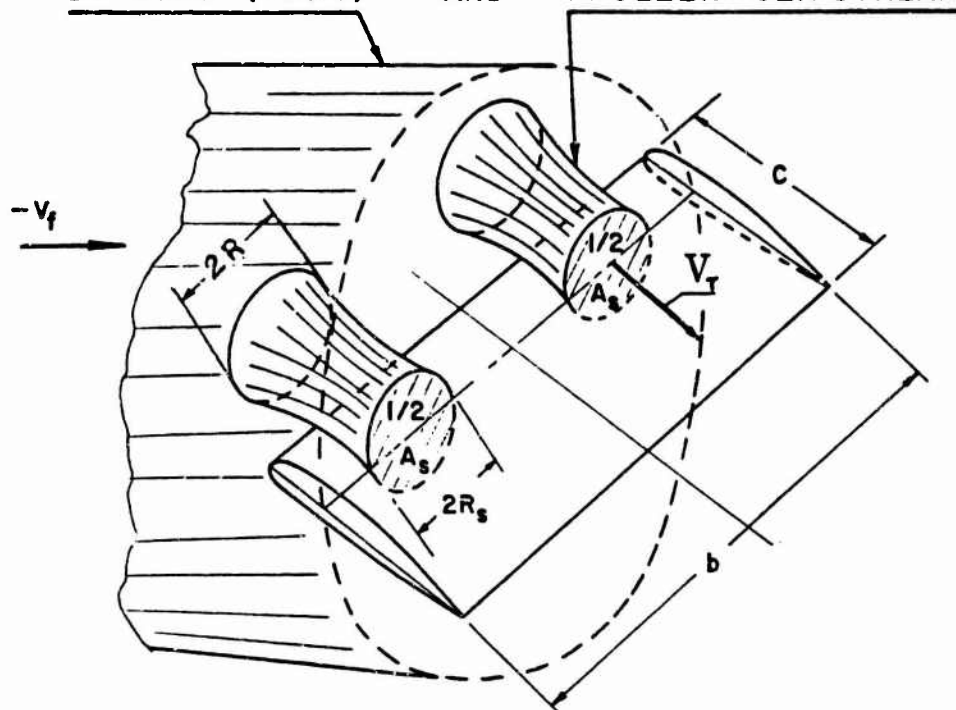


Fig.3-9 Interaction of the propeller and wing affected stream tubes

ASSUMED CHARACTERISTICS OF NACA — 4415  
AIRFOIL SECTION THROUGH 90°

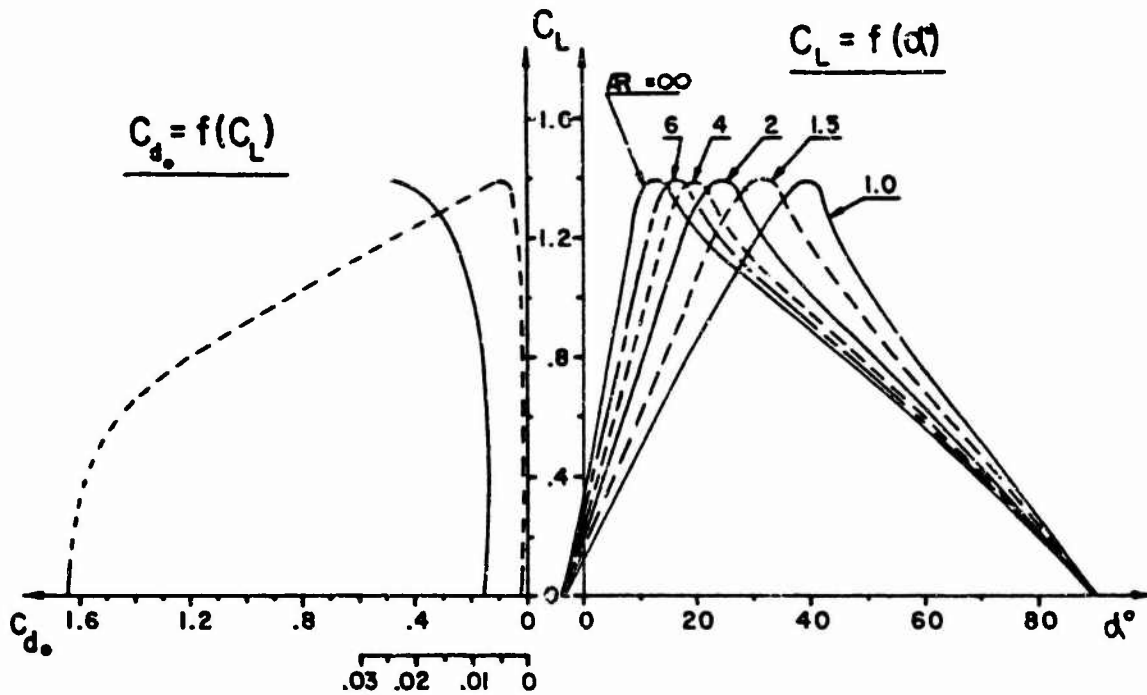


Fig.3-10 Example of airfoil characteristics through 90°

ROTOR HORSEPOWER & WING ANGLE OF INCIDENCE  
vs. SPEED IN HORIZONTAL FLIGHT AT S/L

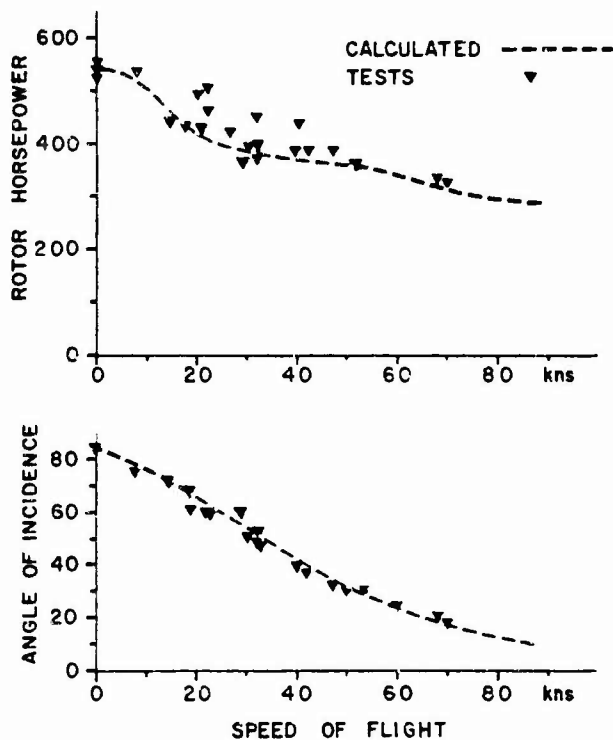


Fig.3-11 Comparison of flight test results with predictions for the VZ-2

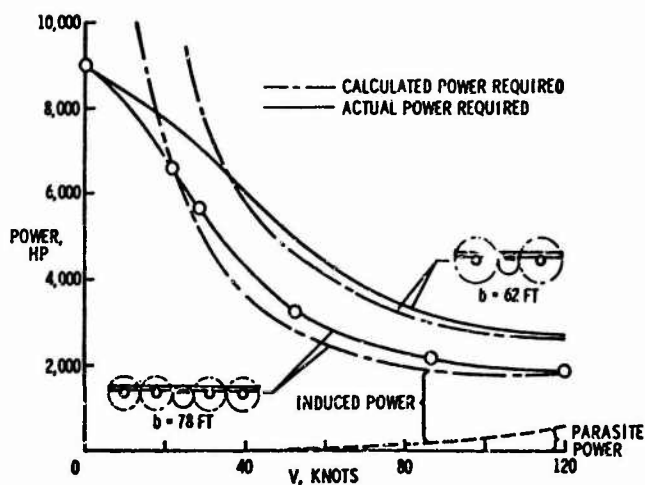


Fig. 3-12 Comparison of actual with induced power versus speed relationships

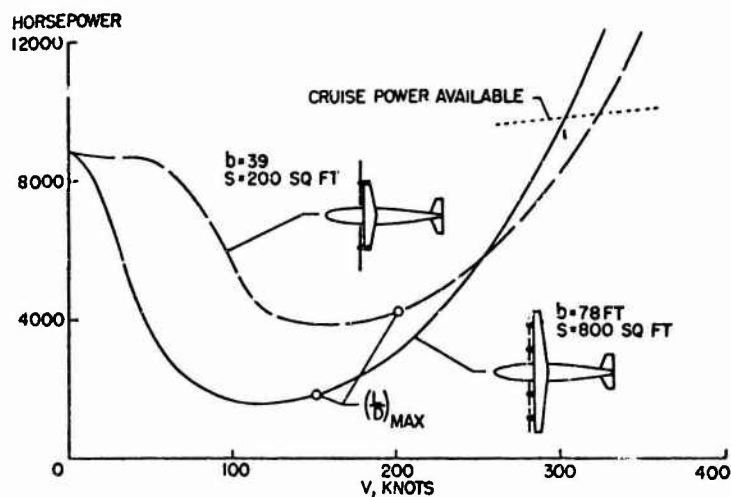


Fig. 3-13 Example of effect of wing span and wing chord to rotor/propeller diameter ratio on power versus speed ( $W = 40,000$  lb)

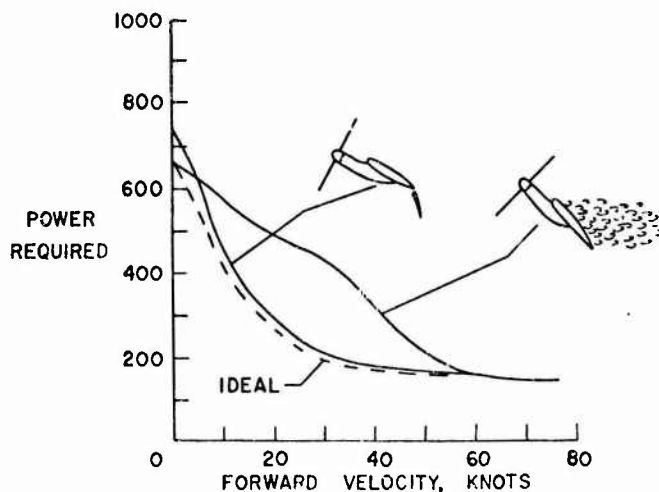


Fig. 3-14 Example of improvements in the transitional power versus speed relationships through lift-increasing devices

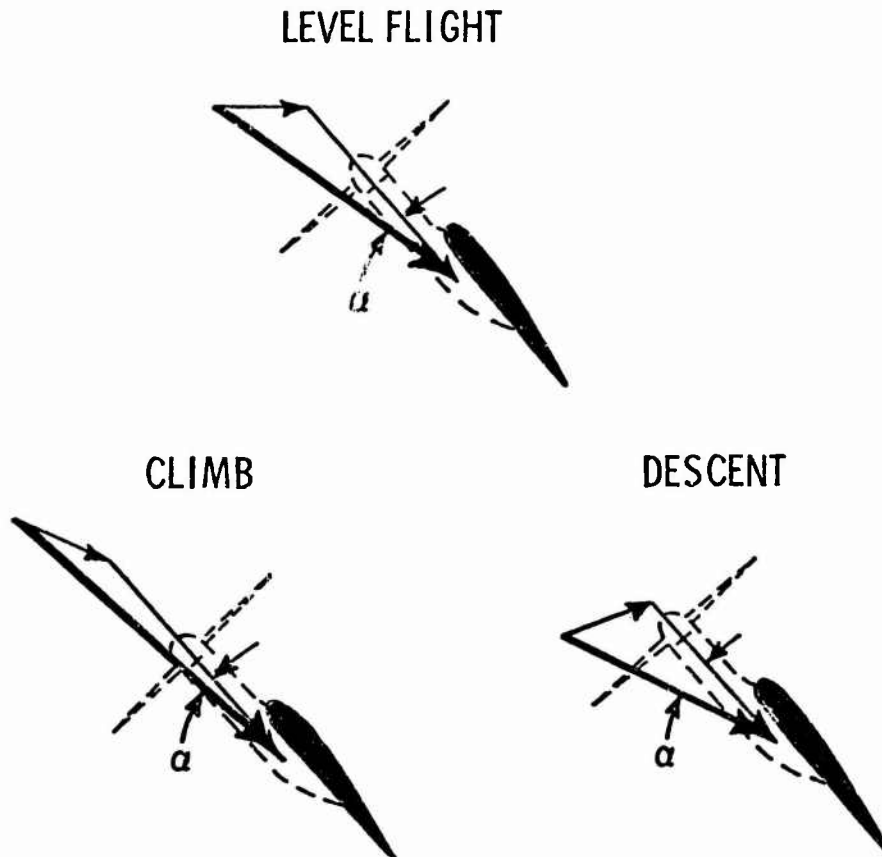


Fig.3-15 Wing angle of attack in three regimes of flight at a transitional speed

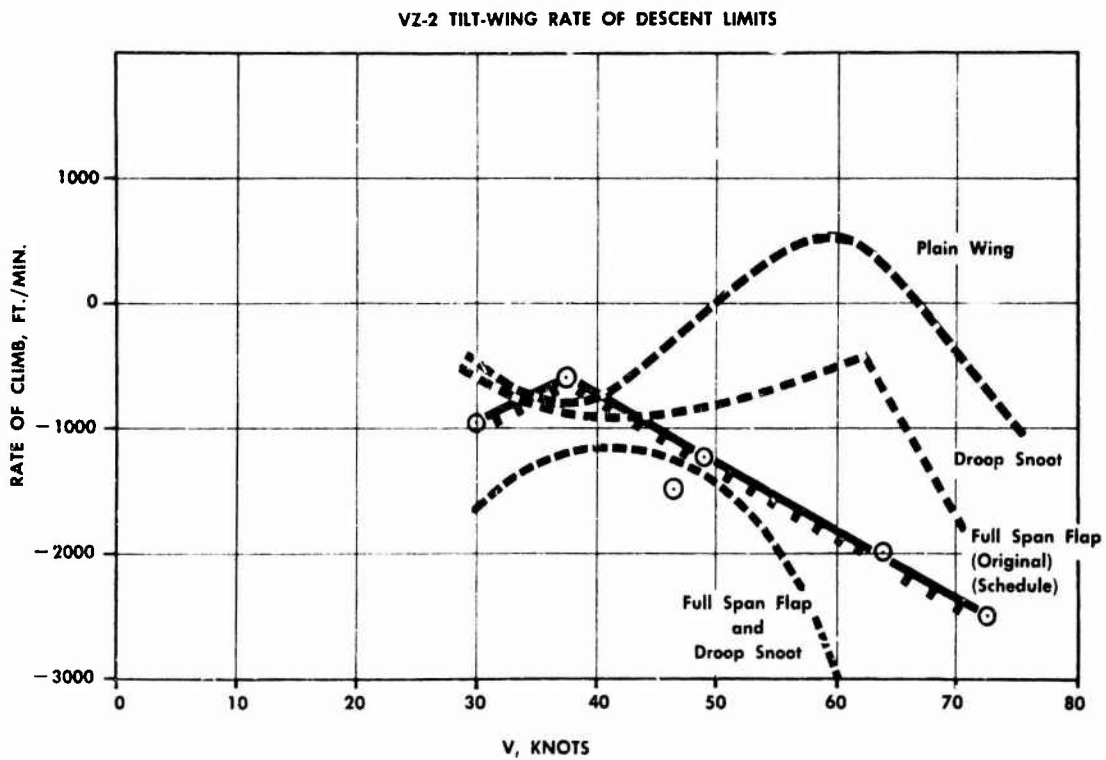


Fig.3-16 Flight test results showing rate of descent improvements in the VZ<sup>2</sup>

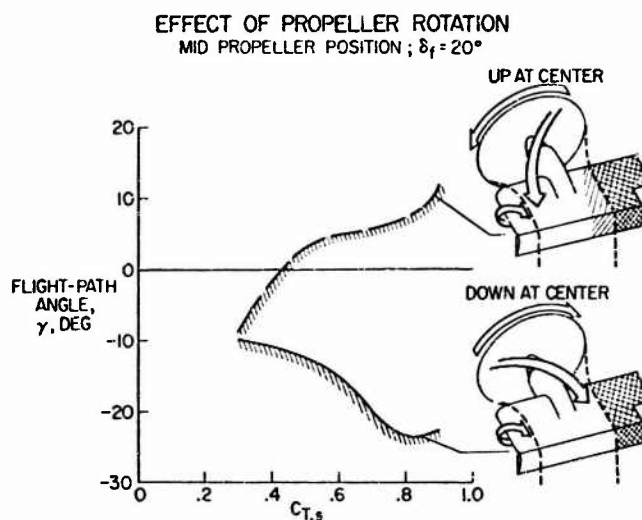
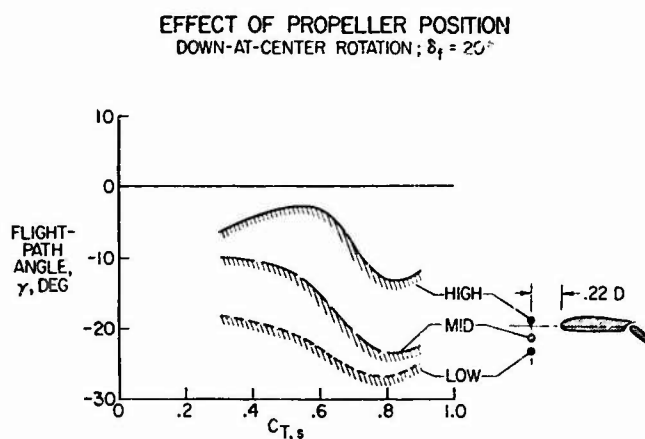
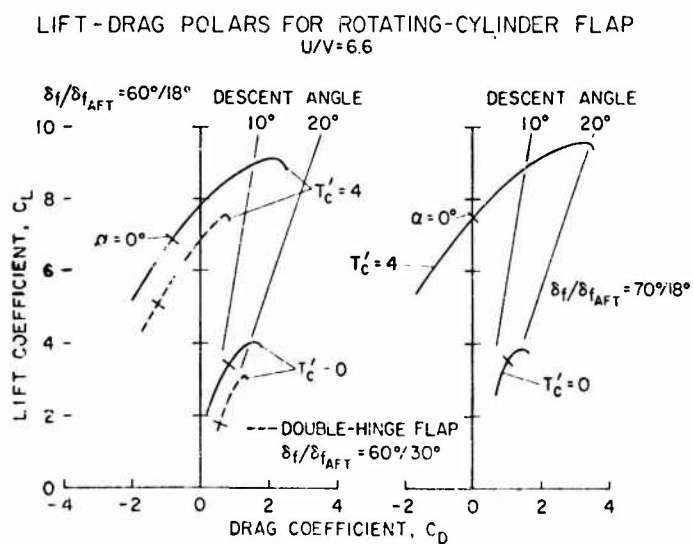
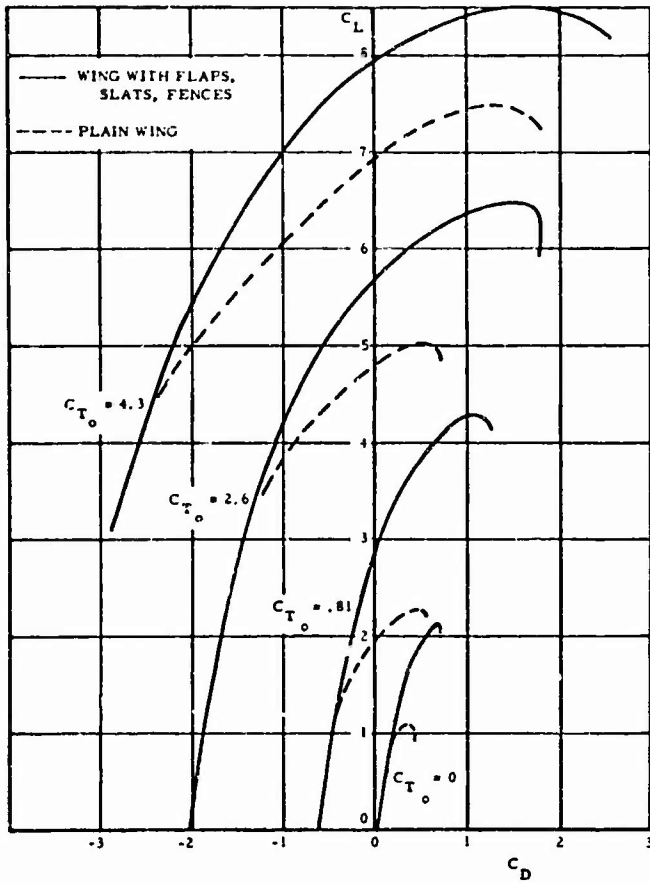
Fig.3-17 Effect of propeller rotation on flight path angle  $\gamma$ Fig.3-18 Effect of propeller position on flight path angle  $\gamma$ 

Fig.3-19 Lift-drag polars of STOL expressed in conventional aerodynamic coefficients





EFFECT OF HIGH LIFT DEVICES ON TILT WING MODEL WIND TUNNEL DATA

Fig.3-20 Lift-drag polars of a tilt wing in terms of  $C_L$  and  $C_D$

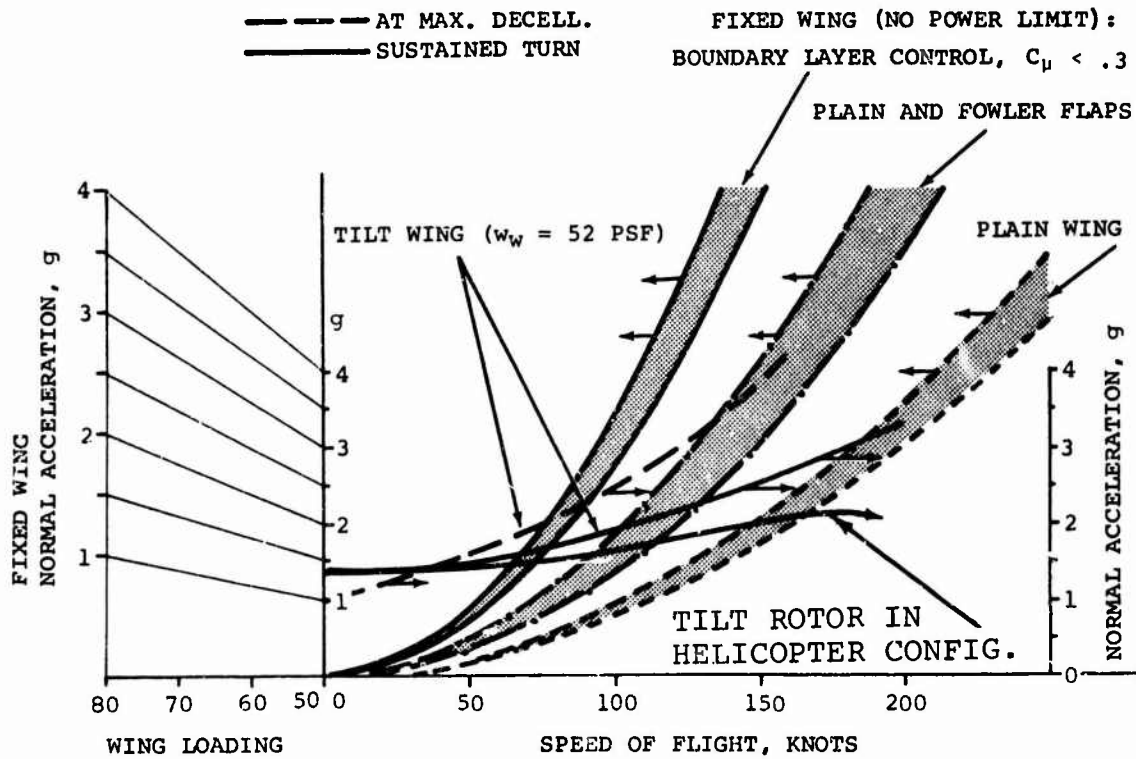


Fig.3-21 Normal acceleration capabilities of fixed wing versus speed and examples of normal acceleration for tilt wing and tilt rotor in helicopter configuration

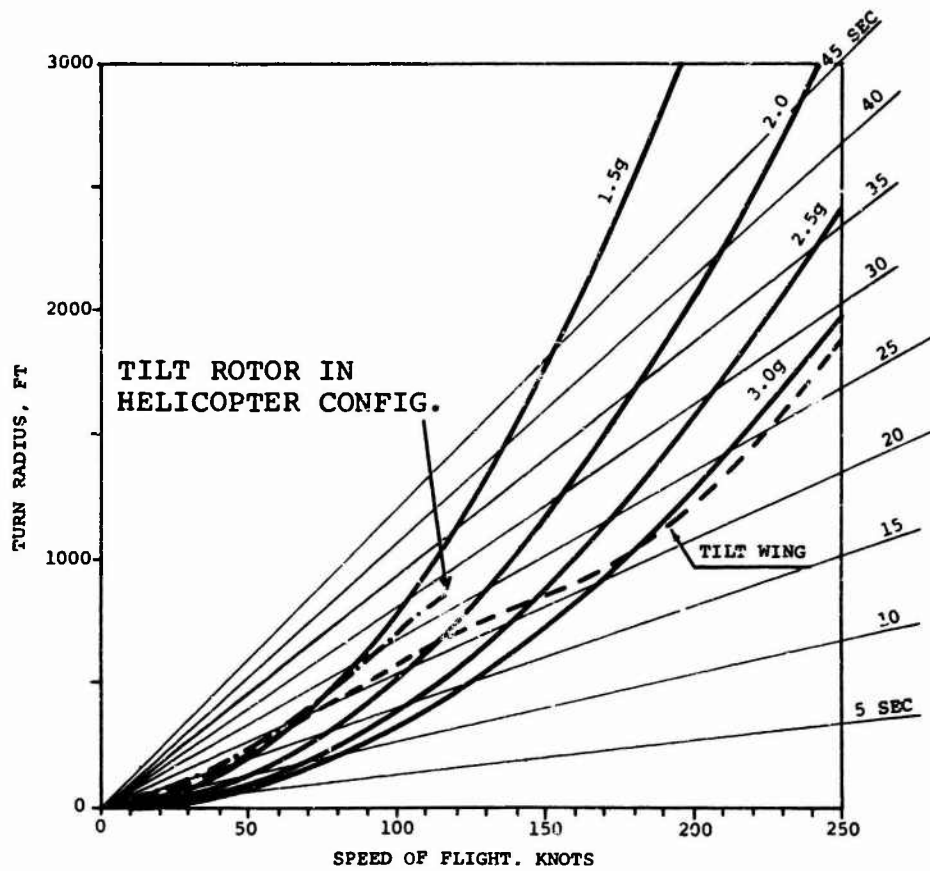


Fig.3-22 Radius and time of 360° sustained turn at various normal acceleration levels ve speed of flight

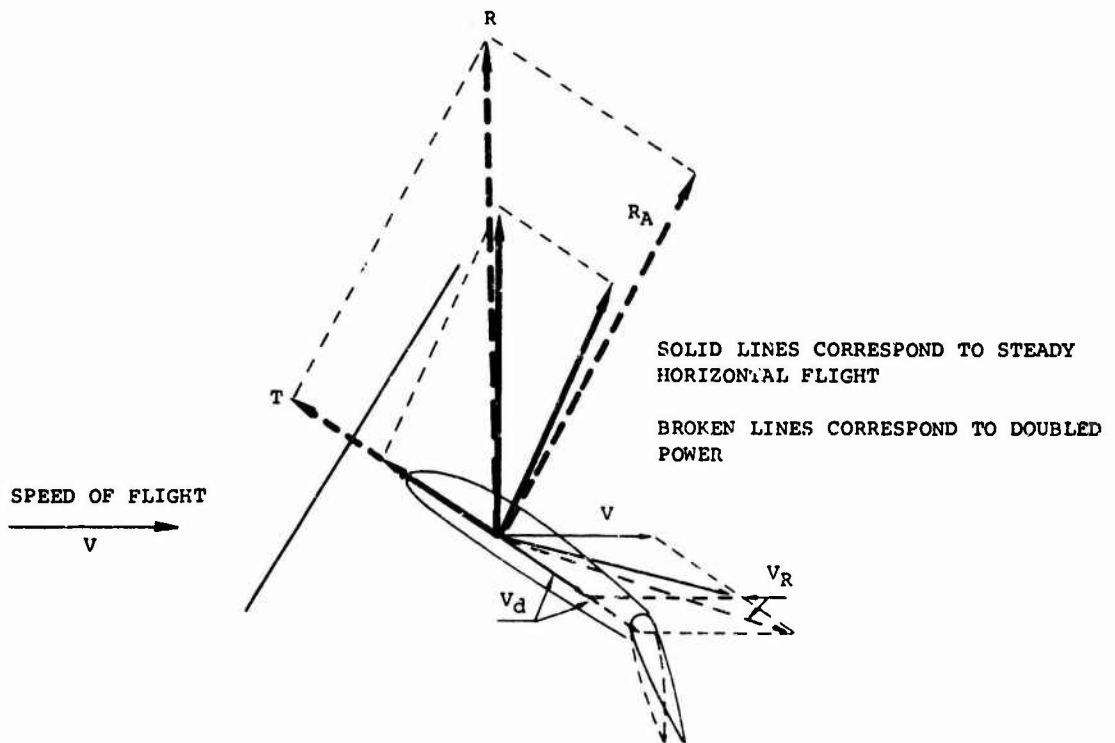


Fig.3-23 Schematic representation of flow and forces when power required for steady horizontal flight is doubled

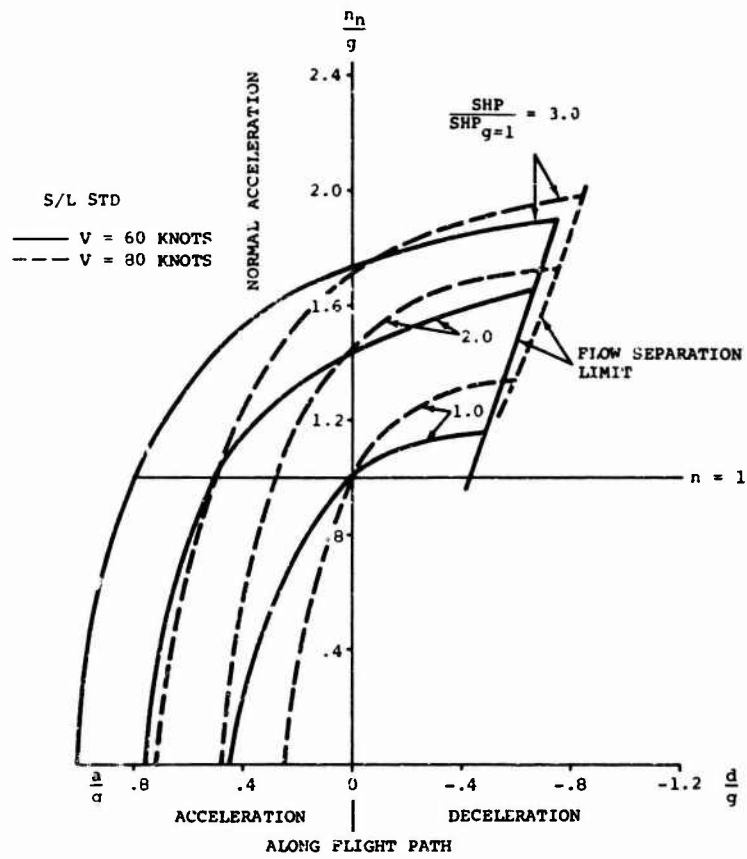


Fig.3-24 Example of acceleration capabilities of a tilt wing

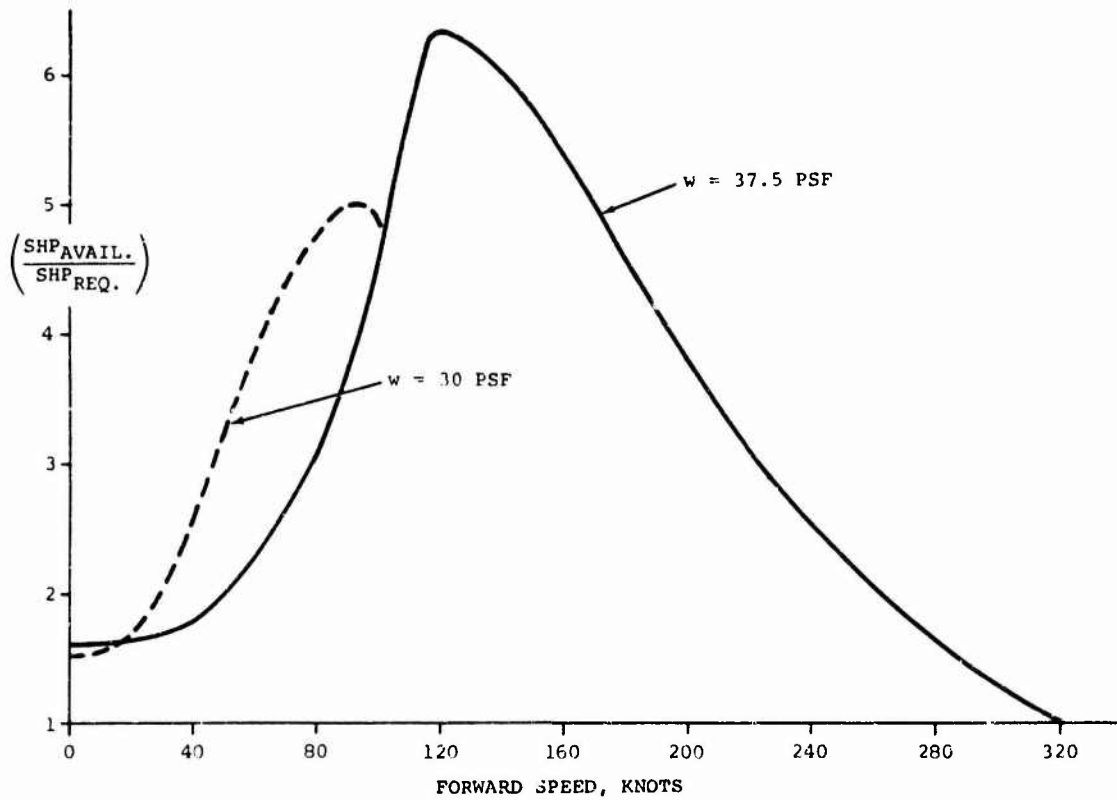


Fig.3-25 Example of the ratio of power available to required in steady level flight at sea level standard

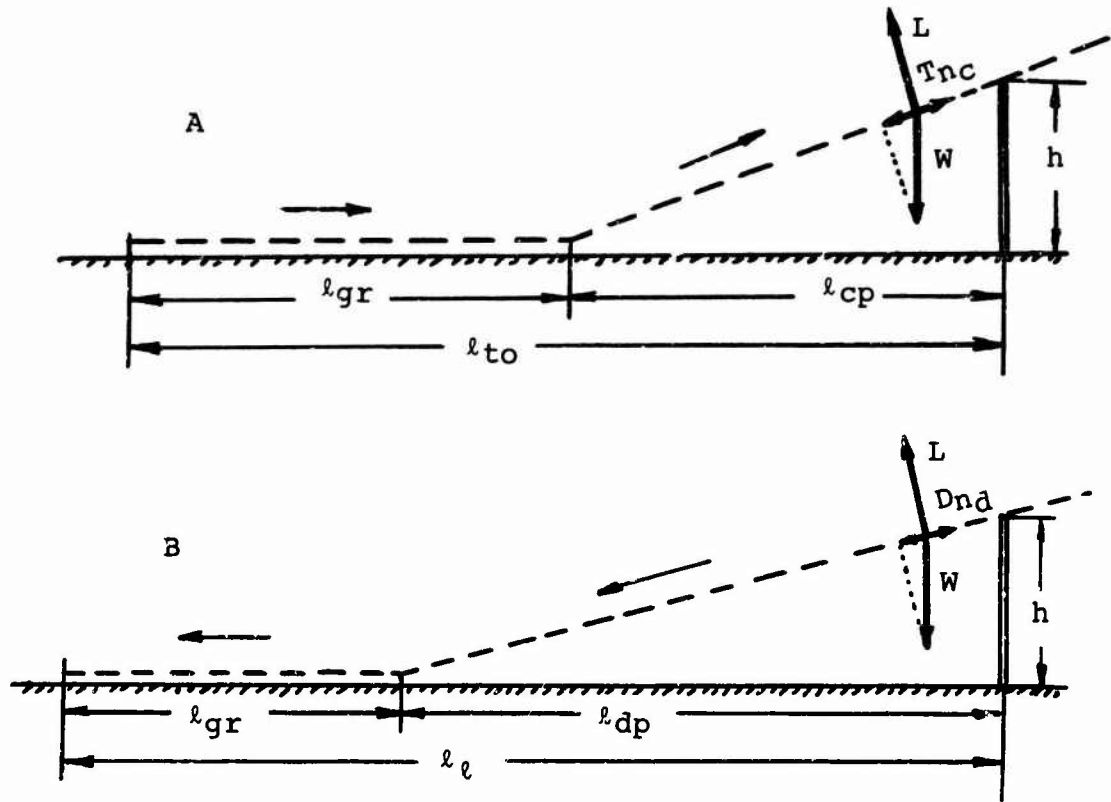


Fig. 4-1 Simplified scheme of takeoff (A) and landing (B)

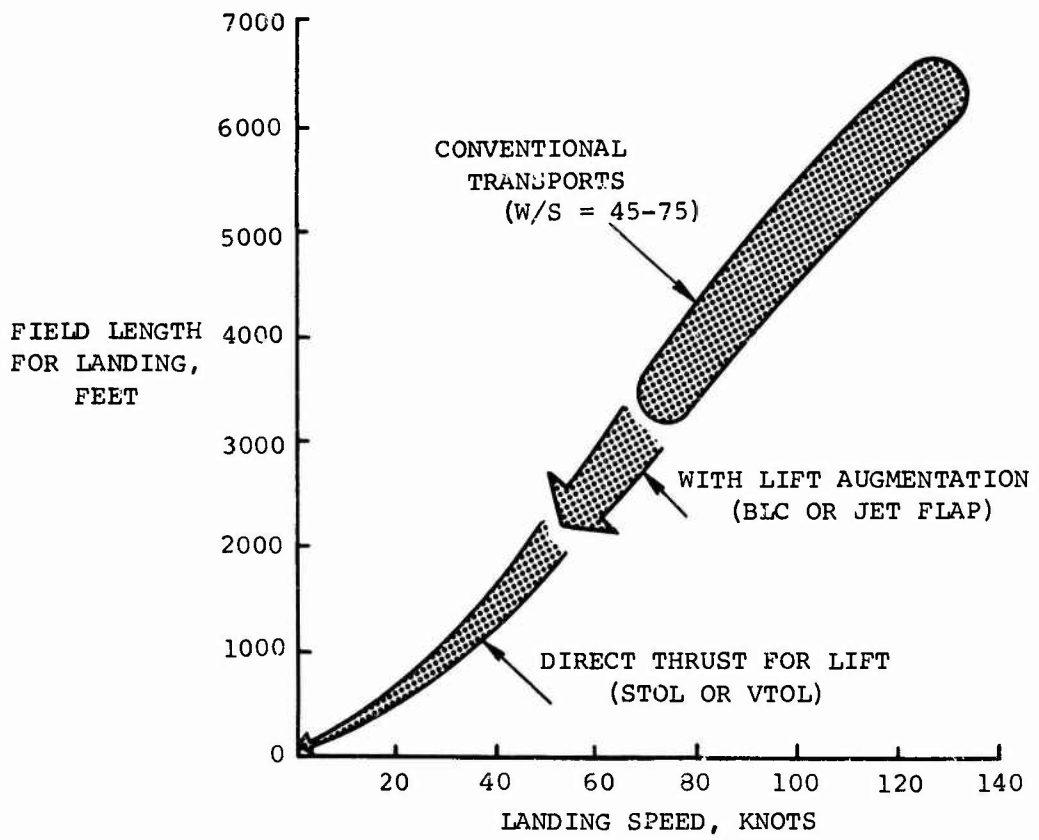


Fig. 4-2 Field length for landing

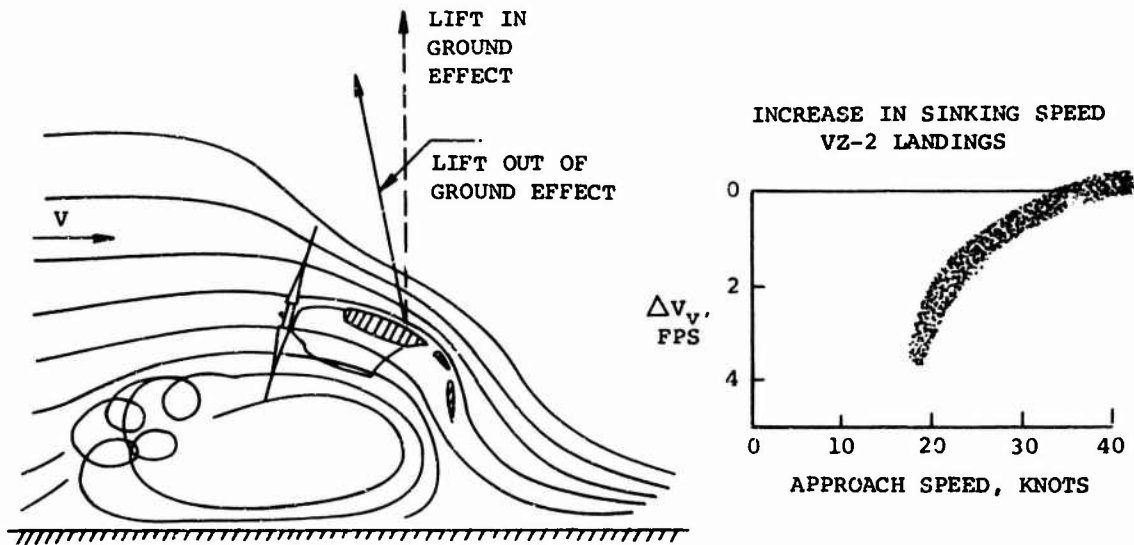


Fig.4-3 Scheme of slipstream recirculation and some of the effects: decrease in lift and increase in sinking speed

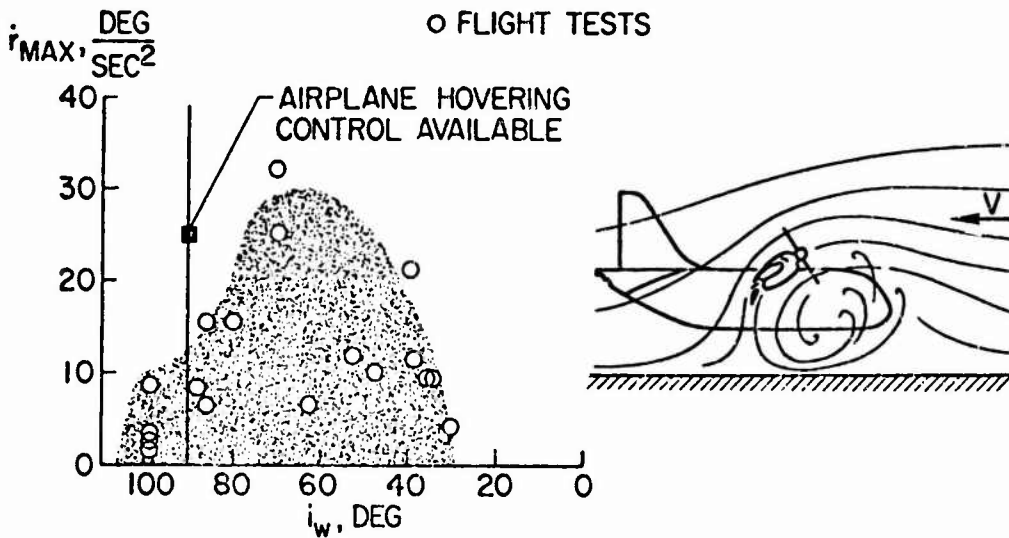


Fig.4-4 Effect of ground proximity on yaw acceleration

VARIATION OF RECIRCULATION HEIGHT.  
WITH RATIO OF DISK LOADING TO DYNAMIC PRESSURE  
 $\delta_f = 60^\circ$

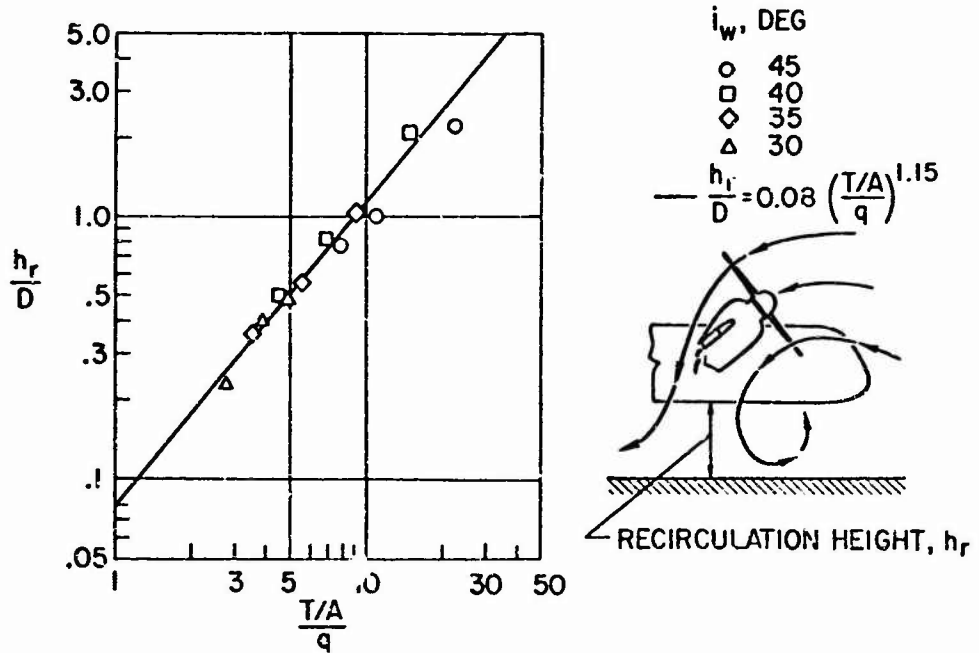


Fig. 4-5 Wind tunnel tests with the moving ground plane belt

HEIGHT AT WHICH DISTURBANCE IS ENCOUNTERED  
VARIABLE  $i_w$

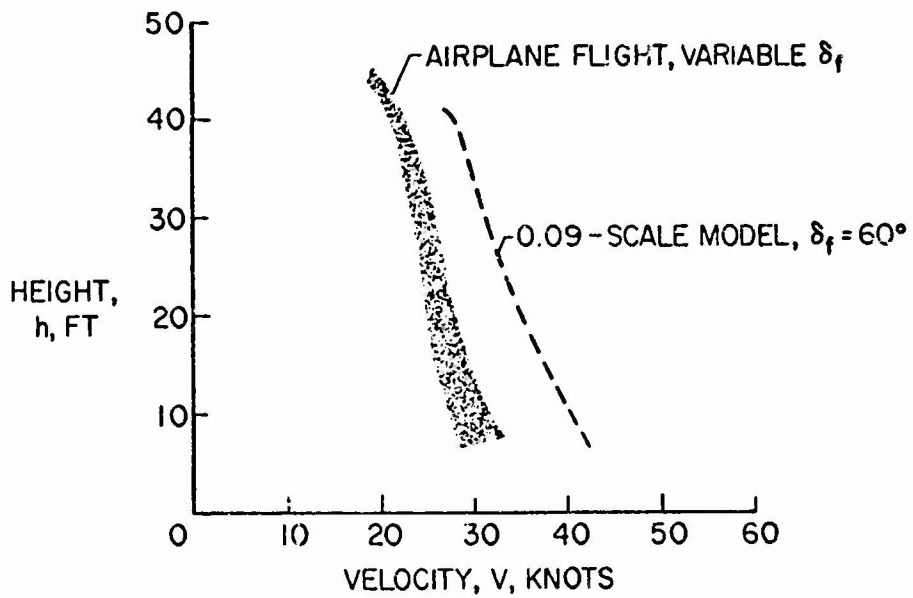


Fig. 4-6 Comparison of wind tunnel and flight test results

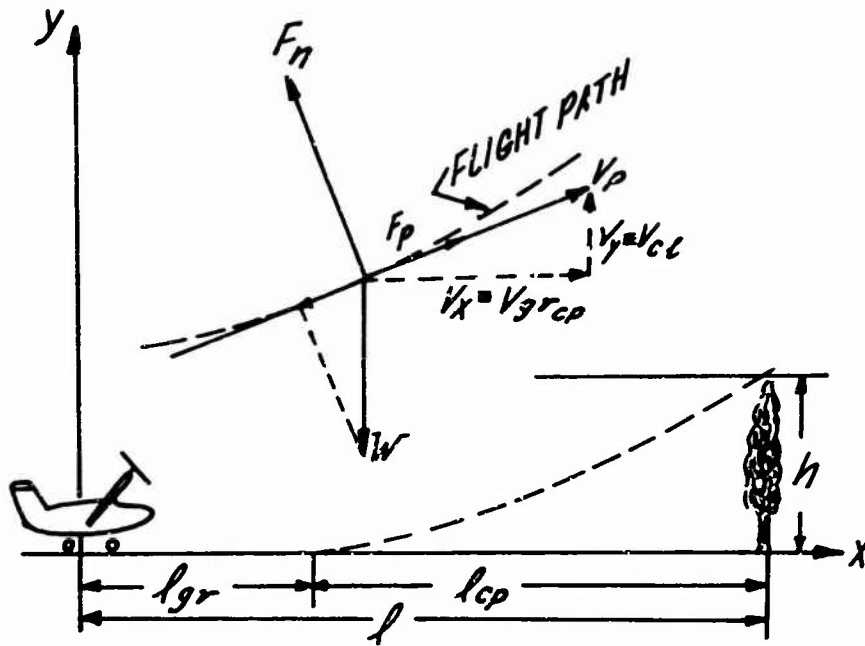


Fig.4-7 Takeoff of a tilt-wing aircraft at  $T < W$

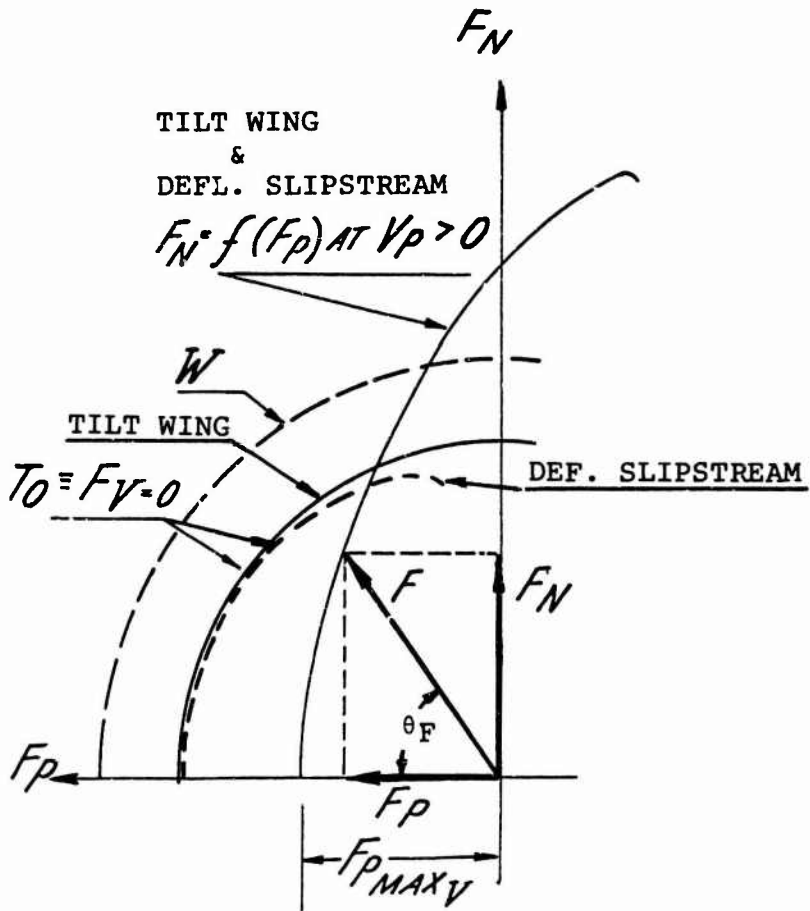


Fig.4-8 Character of resultant aerodynamic force at constant power at rest and in forward motion

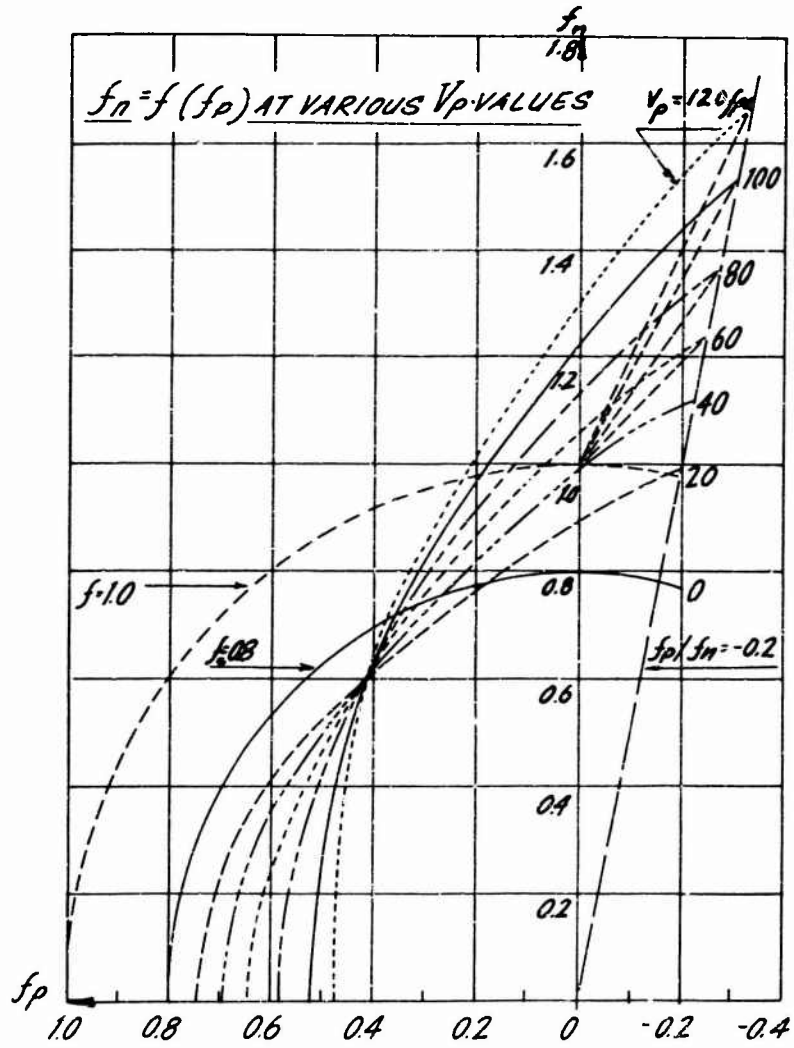


Fig.4-9 Ratios of resultant aerodynamic force at constant power

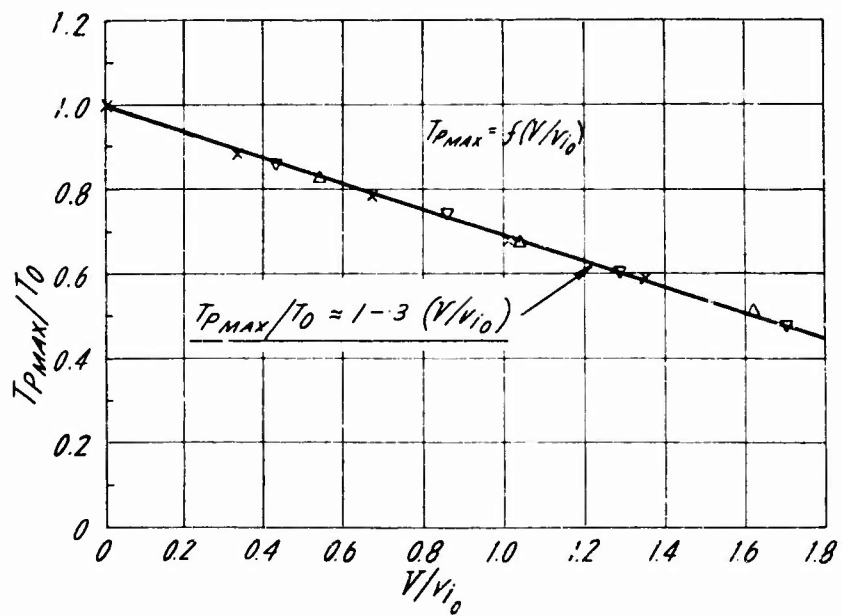


Fig.4-10 Decrease of relative axial thrust with the  $v/v_{10}$  ratio



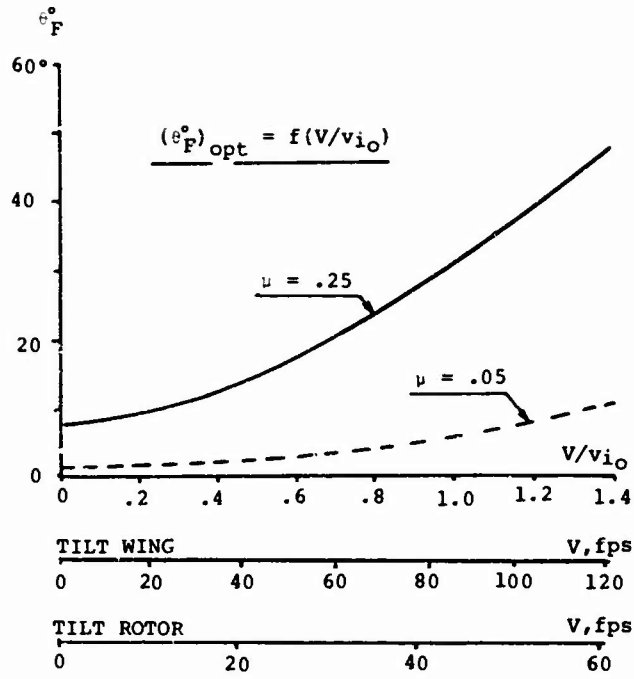


Fig. 4-11 Optimum inclination of the resultant aerodynamic force, for maximum acceleration during ground run

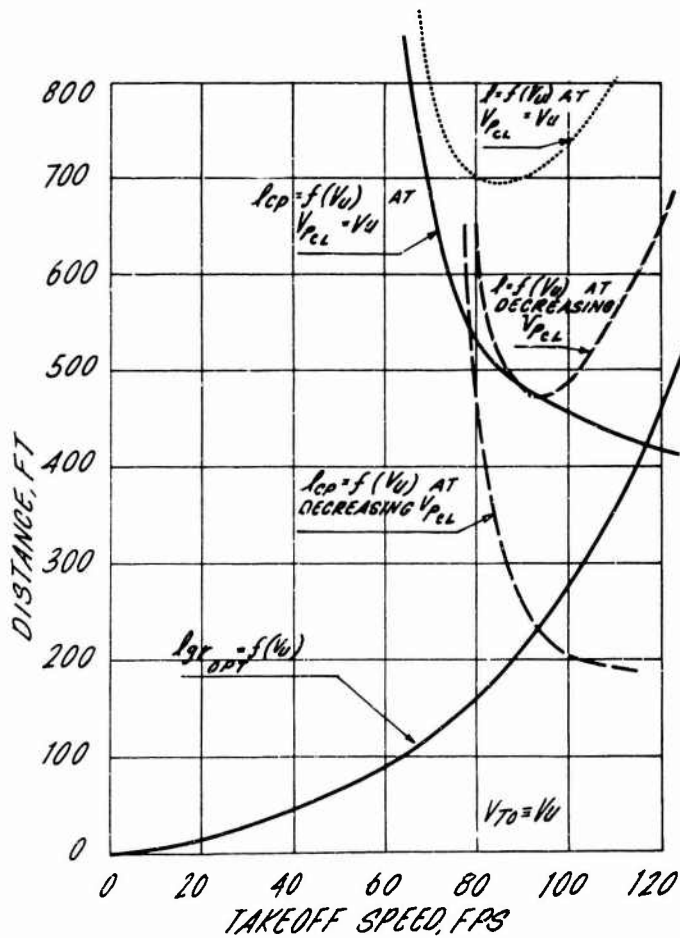


Fig. 4-12 Takeoff distance versus unstick speed

**PAPER D**

**AERODYNAMICS OF SHROUDED PROPELLERS**

by

**M. Lazareff**

**Nord-Aviation, France**

## FOREWORD

The shrouded propeller is a lifting and propulsive device which has led to design and prototype developments in the last ten years.

A successful outcome would require a time period of at least ten more years, which is not too much for an entirely new system: a shrouded propeller is not merely a free propeller with a shroud around it.

The interest raised by this system is explained by its capability to insure:

- a hovering flight with a fuel consumption and noise levels very much less than in the case of a turbojet,
- a forward subsonic flight higher than with a free propeller.

It is not possible to cover the subject matter in a few pages and everything is not yet known.

Therefore I shall not go into details, but I shall try to point out the main points necessary to build up a sound basis.

I shall afterwards emphasize the principles which result from a few ideal assumptions on the nature of the flow. The results obtained with those none too realistic assumptions are nevertheless very useful to refer to with experimental results and also to know beforehand the maximum performance which cannot be exceeded.

Before entering the lecture matter itself, here is a picture which sums up the main points very briefly. If you remember this picture well you can forget everything I am going to say after (Fig.1).

## AERODYNAMICS OF SHROUDED PROPELLERS

M. Lazareff

### 1. GENERAL PRINCIPLES\*

#### 1.1 General Features

Figure 2 shows the mean relative dimensions of the shroud:

$$\text{Length } l : 0.3D_1 < l < 0.5D_1$$

$$\text{Thickness } \Delta R_1 : 0.1R_1 < \Delta R_1 < 0.3R_1 .$$

Generally this shroud is not rotating with the propeller blades; it is connected to the hub by means of streamlined supports which may operate as guide vanes.

The number of blades is variable as for the value of *disk loading*, a relevant parameter we will be mentioning again.

In order to obtain the full potential performance, the gap between the blades and the shroud should be kept very small. Numerous experiments on models as well as at full scale have shown that the gap referred to the radius  $R_1$  should be at any rate less than 0.5%.

This condition requires:

- either a very accurate and stiff mounting of the shroud on the hub, which is heavy,
- or the use of soft material at the tip of the blades or on the corresponding region of the shroud.

The hub can contain the engine. It can also only contain a bevel shaft when the engines are located elsewhere. It can finally consist of a shaft only, the motion being then produced by a peripheric turbine.

The shrouded propeller can be placed in the wing or the fuselage of the aircraft, the shroud being then part of the airframe.

Figure 3 is a photograph of a model. The diameter of the propeller is 16 inches.

Figure 4 is a photograph of the experimental aircraft N.500 which is powered and controlled by two tilting shrouded propellers.

Figure 5 is an artist concept of this same aircraft.

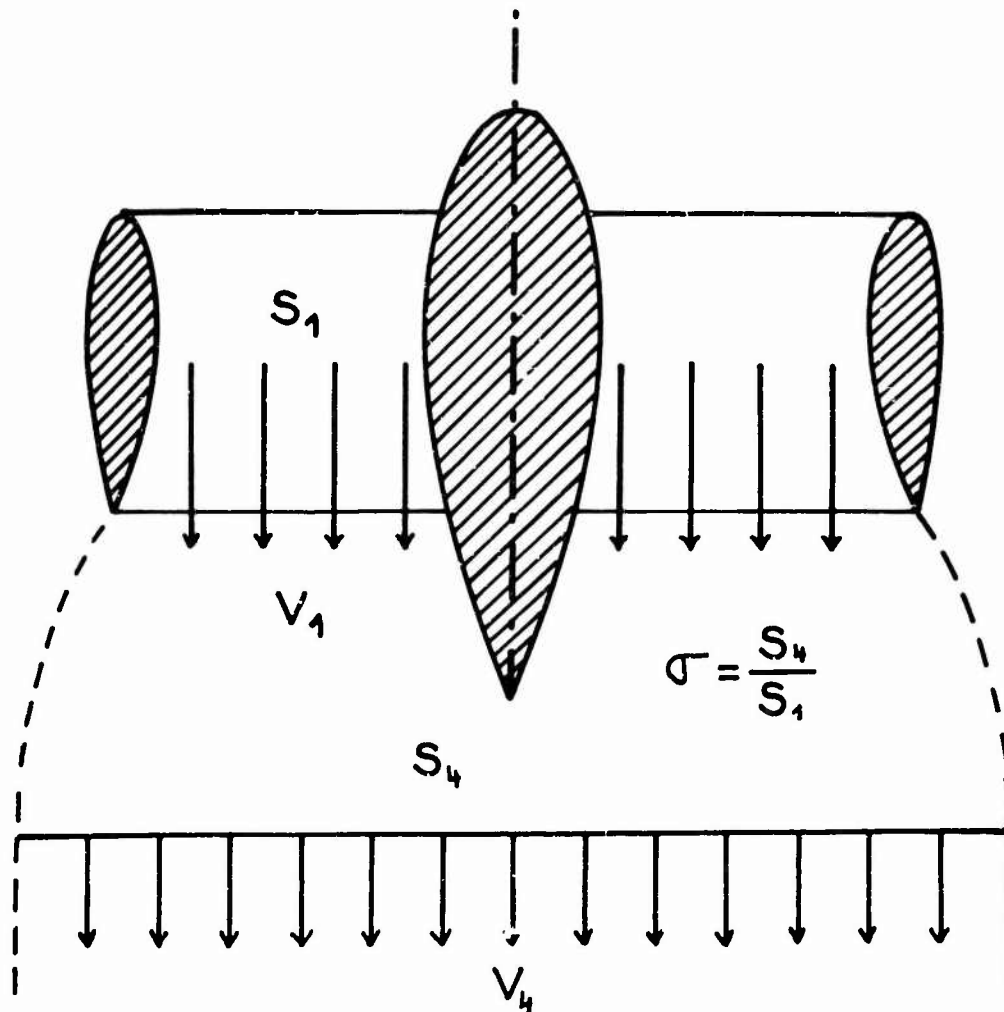
---

\*Note: The international SI system of units has been used throughout. Force : 1 daN  $\simeq$  1 kg.  
Power : 1 kW  $\simeq$  1.34 h.p.

### 1.2 Aerodynamic Principles in Static Conditions

In this paragraph the assumptions are:

- non-viscous flow;
- velocity is uniform and parallel to the axis (no rotation) at Station 4.



Under these conditions the whole of the mechanical power  $W$  on the shaft is found again in the final kinetic energy of the mass flow  $m$  at Station 4 where ambient pressure  $P_0$  has been reached:

$$W = \frac{1}{2}mV_4^2 = \frac{\rho}{2}V_4^3S_4. \quad (1)$$

Taking into account the constant mass flow condition

$$m = \rho V_1 S_1 = \rho V_4 S_4,$$

and the momentum Equation for the thrust  $T$ ,

$$T = mV_4,$$

one obtains the following relationships where  $\sigma$  represents the diffusion parameter that is to say the area ratio:

$$\sigma = \frac{S_4}{S_1}$$

$$V_u = \left[ \frac{2W}{\rho S_u} \right]^{1/3} = \left[ \frac{2W}{\rho \sigma S_1} \right]^{1/3} = \left[ \frac{T}{\rho \sigma S_1} \right]^{1/2} = \frac{2}{T/W} \quad (2)$$

$$T = mV_u = \frac{2W}{V_u} = [\rho \sigma S_1]^{1/3} [2W]^{2/3} \quad (3)$$

$$\frac{T}{S_1} = [\rho \sigma]^{1/3} \left[ 2 \frac{W}{S_1} \right]^{2/3} \quad (4)$$

$$\frac{T}{W} = [2\rho \sigma]^{1/3} \left[ \frac{2}{W/S_1} \right]^{1/3} = [2\rho \sigma]^{1/3} \left[ \frac{2}{T/S_1} \right]^{1/2} \quad (5)$$

$$m = [\rho \sigma S_1]^{2/3} [2W]^{1/3} . \quad (6)$$

Let us see first the simple and rather general case without diffusion ( $\sigma = 1$ ).

Equation (5) shows that the specific thrust  $T/W$  (thrust per unit power) increases as the power disk loading  $W/S_1$  decreases.

If we consider a constant power  $W$  this means that in order to increase the static thrust one has to increase the size of the machine. It follows that in the case  $\sigma = 1$  a large specific static thrust will mean a weight and drag penalty in forward flight.

The equations which have provided this result are general and the above conclusion is valid for all types of thrust systems which are compared in Figure 6 in terms of disk loading. It may be seen that the shrouded propeller fills in a substantial void between the free propeller and the by-pass turbojet engine (the cold part of which is in fact a shrouded propeller).

Let us assume now that thanks to appropriate devices, such as boundary layer control on the walls of the diffuser, we have achieved a value

$$\sigma > 1 .$$

The equations above show that the value of the thrust as a function of power is determined by the fluid cross section  $S_u$  (at least with the assumption of ideal flow which is made here). Consequently the achievement of  $\sigma > 1$  enables to lower the weight and drag penalty due to the shroud.

Using the momentum theorem between sections: 0 and 1, 1 and 2, 2 and 4 we obtain the components  $T_0$ ,  $T_1$ ,  $T_2$  of the total thrust  $T$  which are respectively applied to:

the air intake ( $T_0$ )

the blades ( $T_1$ )

the diffuser ( $T_2$ ) .

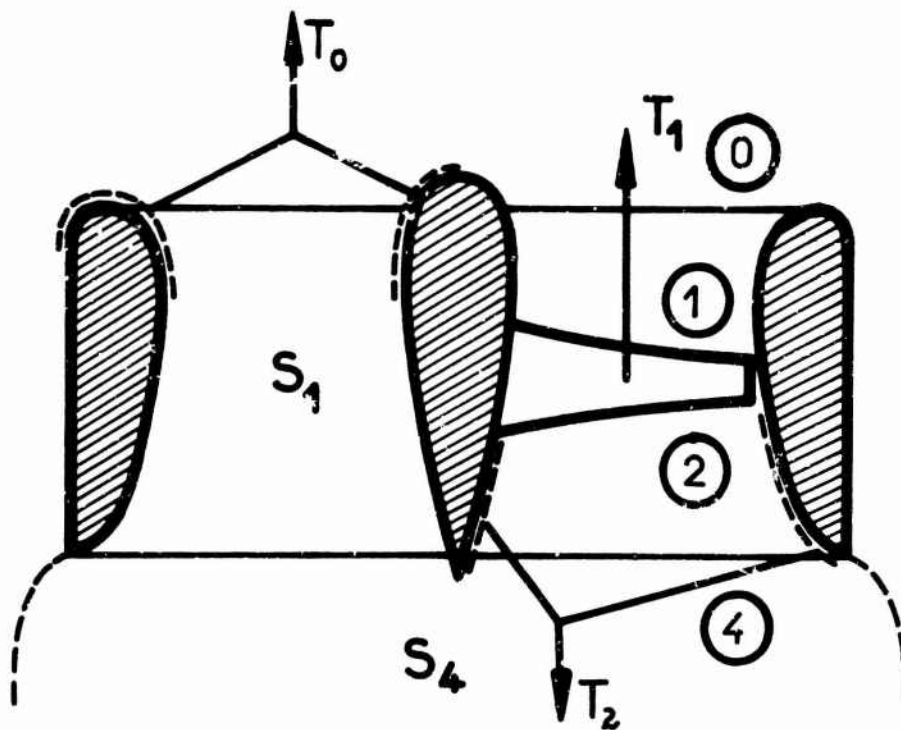
Referring those partial thrusts to the total thrust  $T$ , one obtains the following equations:

$$\frac{T_0}{T} = \frac{\sigma}{2} \quad (7)$$

$$\frac{T_1}{T} = \frac{1}{2\sigma} \quad (8)$$

$$\frac{T_2}{T} = - \frac{[\sigma - 1]^2}{2\sigma} . \quad (9)$$

These equations are plotted in Figure 7.



It should be noted that the contribution  $T_2$  of the diffuser alone is always negative, but its overall effect is favorable thanks to the additional thrust produced on the intake.

One also notices that the thrust  $T_1$  of the blades themselves quickly decreases with the diffusion parameter  $\sigma$ , making the mechanical design of those blades easier.

## 2. THEORETICAL AND EXPERIMENTAL PERFORMANCES

### 2.1 Static (or hovering)

#### 2.1.1 Theoretical Performance

The above equations enable to build up the following table of theoretical performance. The value of the axial Mach number  $M_1$  in front of the blades is also indicated.

	$\sigma = 0.5$		$\sigma = 1$		$\sigma = 1.4$		$\sigma = 1.8$	
	$M_1$	T/W daN/kW	$M_1$	T/W	$M_1$	T/W	$M_1$	T/W
200	0.07	3.57	0.11 <sup>4</sup>	5.2	0.14 <sup>5</sup>	6.0	0.17 <sup>6</sup>	6.8
500	0.11 <sup>3</sup>	2.25	0.18	3.3	0.23	3.8	0.28	4.3
1000	0.20	1.69	0.28	2.3	0.33	2.7	0.39	3.1
1500	0.25	1.41	0.35	1.9	0.42	2.2	0.50	2.5
2000	0.29	1.17	0.41	1.6	0.51	1.9	0.62	2.2
2500	0.33	1.03	0.48	1.4	0.60	1.7	0.80	1.9
3000	0.37	0.94	0.54	1.3	0.70	1.5	choked	

It is worthwhile to make the following comments about the above figures.

- (a) It can be noted once again that, for a fixed value of  $\sigma$ , the evolution of the disk loading  $T/S_1$  and that of the specific thrust  $T/W$  are opposite: this means that for a required total thrust the economy of power is to be paid for by an increase of size  $S_1$ .
- (b) For a given disk loading  $T/S_1$  the specific thrust increases with  $\sigma$ .
- (c) The comparison with the free ideal propeller is immediate since in this case, according to the Froude pattern, the value of  $\sigma$  is  $\sigma = 0.5$ , which is one of the configurations accounted for in the Table. Besides one must remember that the free propeller can only usefully absorb a moderate power per square meter: the figure  $T/S_1 = 200 \text{ daN/m}^2$  is an average value which can hardly be doubled.

Here is a comparison which is obtained from the above table.

We assume that we require a thrust of 2000 daN. We can for example use a free propeller of 10 square meters (diameter  $\sim 3.600 \text{ m}$ ) with a shaft power:

$$W = \frac{2000}{3.57} = 560 \text{ kW}.$$

This solution can be compared to two other solutions using shrouded propellers with  $\sigma = 1.4$ : the first one (A) has the same diameter, the second one (B) is supposed to have the same shaftpower (and therefore a different diameter).

	Free propeller	Shrouded propeller $\sigma = 1.4$	
		A	B
Thrust daN	2000	2000	2000
Diameter m	3.60	3.60	2.05
Power kW	560	330	560

### 2.1.2 Experimental Performance

There are two general causes for losses in the experimental performance compared to the theoretical one mentioned above:

- (a) If there are no guide vanes one part of the shaftpower is absorbed by the kinetic energy of rotation and therefore does not contribute to the thrust. This loss is the more important one as the applied torque is greater; therefore it increases with the disk-loading and decreases when the r.p.m. increases at constant power (by resetting the pitch of the blades).
- (b) The action of viscosity on the blades and all the surfaces of the shroud. Viscosity leads to friction forces and adverse pressure forces; the latter become very important in case of flow separation, for instance if the angle of the diffuser is too large.

Accurate tests enable the measurement of these effects and to separate them.

We shall only use here a total qualification coefficient which is well known as "Figure of Merit". Its definition is:

$$M'_1 = \frac{\text{theoretical shaftpower}}{\text{experimental shaftpower}},$$



the theoretical value being calculated for a thrust equal to the experimental one, assuming a shrouded propeller of the same diameter, without diffusion ( $\sigma = 1$ ).

Referring to the equations of Section 1, one finds the expression of  $M'_1$  as a function of the experimental value of the thrust  $T$  and of the power  $W$ .

$$M'_1 = \frac{T^{3/2}}{2\sqrt{(\rho S_1)W}}$$

where  $\rho$  is the specific mass of air.

In theory this expression becomes:

$$M'_1 = \sqrt{\sigma}$$

and therefore for an ideal shrouded propeller without diffusion

$$M'_1 = 1,$$

and for an ideal free propeller

$$M'_1 = \sqrt{0.5} = 0.707.$$

It must be noted also that according to the general expression of  $M'_1$  one has for an identical power:

$$\frac{\text{experimental thrust}}{\text{theoretical thrust}} = [M'_1]^{2/3}.$$

Let us now consider the actual experimental values of  $M'_1$  which are presented in the following table:

Type of propeller	Test conditions	$M'_1$	Thrust
			Thrust of free propeller (diameter and power identical)
Free propeller	Full scale	0.52	1
Shrouded propeller without diffusion ( $\sigma = 1$ )	Model	0.88	1.42
	Full scale	0.7 - 0.8	1.22 - 1.33
Shrouded propeller with diffusion	Model (Sté. Bertin)	1.17	1.72

It is worth noting that the last result is the best ever obtained. To the best of our knowledge the American values have not reached the figure of 0.9.

In order to understand completely the aerodynamic results one must take into account the weight of the shroud. This factor makes clear the importance of the disk loading. It is obvious that the weight of the shroud is but a small part of the gross thrust if

the disk loading is of the order of 1000 daN per square meter. But this weight can represent a large part of the thrust for a low disk loading of 100 daN/m<sup>2</sup>. In fact it is not altogether correct to build up a balance by a mere subtraction of the weight of the shroud because this shroud also plays the part of a wing surface in cruise flight. Nevertheless in order to get some idea of weight influence in hovering conditions one can admit that it is of the order of 50 daN per square meter of cross section  $S_1$ , for average full scale dimensions. Consequently a shrouded propeller with a very low disk loading of 50 daN/m<sup>2</sup> provides no net thrust at all.

We shall see later on that taking into account the drag of the shroud in level flight also leads to large disk loadings, very much larger than for free propellers.

Lastly, in order to appreciate the figures quoted in the table, it is worth comparing the increases of thrust to the pay-load: for instance a figure of merit of 1.17 instead of 0.88 would increase an initial pay-load of 20% by at least 60%.

## 2.2 Level Flight Without Compressibility Effects

### 2.2.1 Theoretical Performance

We consider first the ideal case without viscous effects and assuming no rotation of the flow about the axis.

Taking into account the kinetic energy of the relative upstream flow of velocity  $V_0$ , the conservation of the mechanical power  $W$  is expressed by:

$$W = \frac{1}{2}mV_u^2 - \frac{1}{2}mV_0^2. \quad (10)$$

The condition of constant mass flow

$$m = \rho V_0 S_0 = \rho V_1 S_1 = \rho V_u S_u$$

leads to the following formula

$$V_0 = \sqrt{\left[\frac{V_1}{\sigma}\right]^2 - \frac{2}{\rho V_1} \frac{W}{S_1}} = \sqrt{V_u^2 - \frac{2}{\rho V_u} \frac{W}{S_u}}, \quad (11)$$

which becomes identical to the static Equation (2) if  $V_0 = 0$ .

If the diffusion  $\sigma$  is known this formula determines completely the theoretical performance. Usually the following parameters are given:

- The mechanical power  $W$
- The propeller disk area  $S_1$
- The specific mass of air  $\rho$
- The speed of flight  $V_0$ .

Equation (11) enables to calculate the axial velocity  $V_1$  and consequently the final exit velocity  $V_u = V_1/\sigma$ . The total theoretical thrust  $T_x$  is then derived by means of the momentum equation:

$$T_x = m[V_u - V_0] = \rho V_u S_u [V_u - V_0]. \quad (12)$$

Figure 8 is a numerical example of the last formulae. It must be noted that the specific thrust is larger for low power disk loadings, as in hovering. But the rate of decrease with speed is more rapid.

The performance in level flight is usually qualified by means of the propulsive efficiency  $\eta$  defined by:

$$T_x = \frac{\eta W}{V_0} \quad (13)$$

or

$$\eta = \frac{T_x V_0}{W}, \quad (13')$$

where  $W$  is the actual power and  $T_x V_0$  is the minimum ideal power related to the thrust  $T_x$ .

Combining the power equation

$$W = \frac{1}{2} m [v_u^2 - v_0^2] \quad (14)$$

and the thrust equation

$$T = m [v_u - v_0], \quad (15)$$

yields the following expression of the ideal propulsive efficiency:

$$\eta = \frac{2}{1 + \frac{v_u}{v_0}}. \quad (16)$$

Although viscous effects are absent this efficiency is always below unity, and is equal to zero in the static case. This comes from the fact that the minimum ideal reference power  $T_x V_0$  in Equation (13') is implicitly associated with an exit velocity  $v_u$  equal to the forward speed  $v_0$ , which occurs for a zero disk loading.

Combining Equation (16) with the Froude formula for the free propeller and Equation (11) for the shrouded propeller provides the expressions of efficiency  $\eta$  as functions of forward speed  $v_0$  and power disk loading  $W/S_1$ :

Free propeller

$$\frac{1 - \eta}{\eta^3} = \frac{1}{2\rho v_0^3} \frac{W}{S_1}. \quad (17)$$

Shrouded propeller

$$\frac{4 - 3\eta}{\eta^3} - \frac{1}{\eta} = \frac{4}{\rho\sigma v_0^3} \frac{W}{S_1}. \quad (18)$$

It can be shown that if  $\eta_1$  is the efficiency of the blades themselves

$$\eta_1 = \left[ \frac{T_1 v_1}{W} \right]$$

this equation becomes:

$$\frac{[4\eta_1 - 3\eta]^2}{\eta^3} - \frac{1}{\eta} = \frac{4}{\rho\sigma v_0^3} \frac{W}{S_1}. \quad (18')$$

Figure 9 represents this relationship.

The following remark has to be made: the slope of these curves is large at low speeds on the left, and very low at the higher speeds. Now it may be seen from the equation above that the diffusion  $\sigma$  plays the same role as  $V_0^{1/3}$ . Consequently an increase of the diffusion  $\sigma$  will produce a beneficial effect at low speed (large slopes). On the contrary, at high speed a variation of  $\sigma$  has no noticeable effect on the efficiency  $\eta$ . This is favorable because, as we shall see later, compressibility problems on the blade tips may be avoided by reduction of the exit cross section.

### 2.2.2 Experimental Performance

The losses which appear in a real flow arise from three sources:

- (a) Viscous effects on the rotating blades;
- (b) Rotation of the jet if no guide vanes are installed;
- (c) Viscous effects on the shroud and all fixed parts of the engine.

Items (a) and (b) are included in the blade efficiency  $\eta_1$  defined with the axial velocity  $V_1$  and the thrust of the blades  $T_1$

$$T_1 = \frac{\eta_1 W}{V_1} \quad (19)$$

For very good designs the value  $\eta_1 = 0.88$  is valid.

Item (c) can be estimated in the following manner:

Let  $S_{mi}$  and  $S_{me}$  be the internal and external wetted areas of the fixed parts and

$$S_m = S_{mi} + S_{me} .$$

Let  $C_f$  be the average *equivalent* friction coefficient (including the pressure drag).

The drag of the shroud is:

$$R_x = \frac{\rho}{2} C_f [S_{mi} V_1^2 + S_{me} V_0^2]$$

$$R_x \simeq \frac{\rho}{2} \frac{S_m}{S_1} C_f [V_1^2 + V_0^2] \quad (20)$$

and the corresponding power loss:

$$\Delta W = R_x V_0 .$$

Using for the internal flow the equation mentioned earlier,

$$\eta = \frac{2}{1 + \frac{V_1}{V_0}} = \frac{2}{1 + \frac{1}{\sigma} \frac{V_1}{V_0}} ,$$

we obtain the loss of efficiency equivalent to the loss of power

$$\Delta \eta = \frac{\frac{\rho}{4} \frac{S_m}{S_1} C_f V_0^3 \left[ 1 + \sigma^2 \left( \frac{2}{\eta} - 1 \right)^2 \right]}{W/S_1} \quad (21)$$

and consequently the net efficiency:

$$\eta_{\text{net}} = \eta - \Delta\eta, \quad (22)$$

where  $\eta$  is to be calculated by Equation (18').

The following numerical values of the relevant parameters are obtained from experimental data:

(a) In high speed forward flight the value of  $\sigma$  is generally  $\sigma \leq 1$ . We assume  $\sigma = 1$ .

(b) For an average shroud

$$\frac{S_m}{S_1} \approx 4.$$

(c) Numerous tests show that the equivalent friction coefficient is approximately three times as large as the turbulent friction coefficient on a flat plate. In the examples below we assume:

$$C_f = 3 \times 0.033 \approx 0.10.$$

This large experimental value is accounted for by the following factors:

(a) The well matched shrouds have a relative thickness of the order of 25% and consequently bear substantial high velocity regions where the drag is increased.

(b) This same relative thickness is responsible for a rather large pressure drag.

Figure (10) is a graph of Equation (22) established with the realistic numerical assumptions indicated above.

The difference with the dragless efficiency of Figure (9) is obvious: we have now to face an uneasy compromise between low and high speed: as seen before, the low disk loadings remain favourable at low speeds when the shroud drag is negligible. But as the speed is increased the drag becomes a predominant factor for the low disk loadings and the net efficiency drops rapidly. On the other hand one has to keep in mind that the low disk loadings are also handicapped in hover by the weight of the shroud.

Therefore our conclusion will be that the domain of interest of the shrouded propeller is shifted to the relatively high disk loadings for which the weight and the drag of the shroud are not an important portion of the gross thrust.

Nevertheless it is interesting to compare the shrouded and the free propeller for equal disk loadings, although they should be different in practice. Figure (11) is an example for a power disk loading of  $200 \text{ kW/m}^2$ . The improvement provided by the shroud and the diffusion at low speeds is associated with a visible loss at high speeds, especially with diffusion  $\sigma$  because of the larger internal speeds induced by the diffusion.

## 2.3 Transition

### 2.3.1 Theoretical Results

In a non viscous flow the inside impact pressure is preserved whatever the angle of attack of the shroud. Therefore the following equation is still valid for the forward speed and the exit velocity  $V_u$ .

$$V_0 = \sqrt{\left( V_u^2 - \frac{2}{\rho V_u} \frac{W}{S_u} \right)}.$$

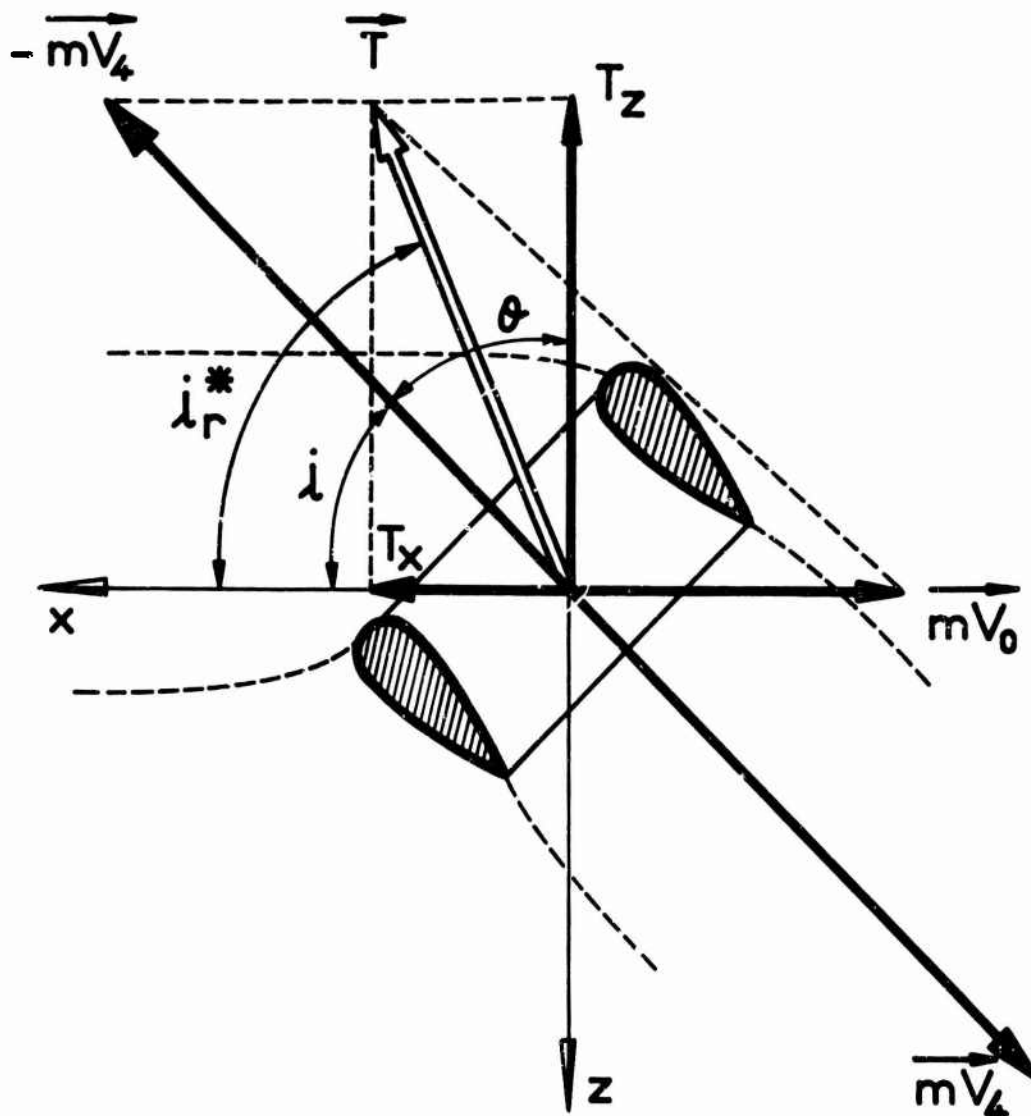
The resulting force  $\vec{T}$  is obtained by the momentum theorem and consequently its components:

$$T_x = mV_u \cos i - mV_0 = \rho V_u S_u [V \cos i - V_0] \quad (23)$$

$$T_z = -mV_u \sin i = -\rho V_u^2 S_u \sin i \quad (24)$$

$$T = \rho V_u S_u \sqrt{(V_0^2 + V_u^2 - 2V_0 V_u \cos i)} . \quad (24')$$

It must be noted that in this scheme the assumed exit flow direction is the same as the axis of the propeller. In practice the jet has a curvature due to the action of the outside flow. This effect is ignored here. On the other hand the diffusion  $\sigma$  is assumed to be a known quantity, although it is in fact a complicated function of speed  $V_0$  and angle of attack.



It is often useful to express the results in terms of the dimensionless coefficients which are used with free propellers.

Advance ratio:

$$\gamma_0 = \frac{V_0}{nD_1} .$$

Power coefficient:

$$\chi = \frac{W}{\rho n^3 D_1^5} .$$

Force and momentum coefficients:

$$\tau = \frac{T}{\rho n^2 D_1^4}$$

$$\tau_0 = \frac{\rho V_0^2 S_0}{\rho n^2 D_1^4}$$

$$\tau_u = \frac{\rho V_u^2 S_u}{\rho n^2 D_1^4} .$$

A simple but not pleasant calculation provides the equations:

$$\frac{1}{(\pi\sigma)^2} \tau_u^3 - \frac{\gamma_0^2}{2\pi\sigma} \tau_u^2 + \frac{\gamma_0^4}{16} \tau_u - \frac{\chi^2}{\pi\sigma} = 0 \quad (25)$$

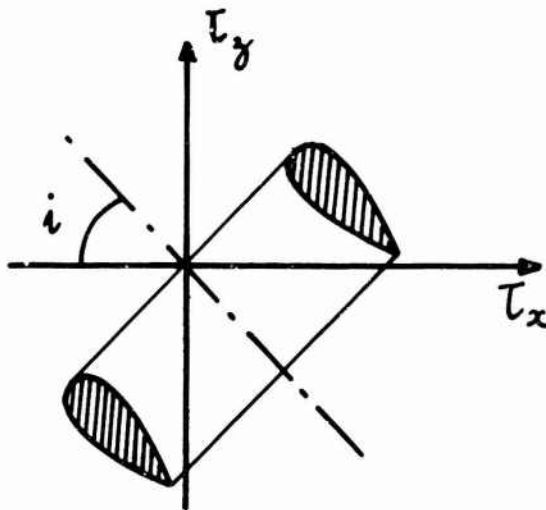
$$\frac{1}{(\pi\sigma)^2} \tau_0^3 - \frac{\gamma_0^4}{16} \tau_0 - \frac{\gamma_0^3 \chi}{8} = 0 , \quad (26)$$

which can be solved for the unknowns  $\tau_u$  and  $\tau_0$  as functions of advance ratio  $\gamma_0$ , power coefficient  $\chi$  and diffusion  $\sigma$ . The larger root only is valid.

For each set of the given parameters  $\gamma_0$ ,  $\chi$ ,  $\sigma$  a polar can then be drawn using the relationships:

$$\tau_y = \tau_u \sin i$$

$$\tau_x = -[\tau_u \cos i - \tau_0]$$



The above equations show that these polars are circles with each centre at the point  $\tau_x = \tau_0$  and with a radius equal to  $\tau_u$ .

An example of the influence of the parameters on these polars is given in Figure (12).

For practical use the calculation can be at first restrained to the points of level flight at constant forward speed, where:

$$\tau_u \cos i = \tau_0 ,$$

or

$$V_u \cos i = V_0 .$$

and the total weight  $P$  being equal to the vertical force

$$P = mV_u \sin i .$$

The use of the power equation provides the necessary power

$$\frac{W}{P} = \frac{(A-1) \sqrt{A} \rho \sigma V_c^3}{2P/S_1} . \quad (27)$$

where

$$A = \frac{1}{2} \left[ 1 + \sqrt{1 + \left[ \frac{2}{\rho \sigma V_0^2 S_1} P \right]^2} \right] . \quad (28)$$

Figure (13) is a typical graph of the specific power  $W/P$  for the value  $\sigma = 1$ . This power decreases with forward speed  $V_0$  and increases with disk loading  $P/S_1$ .

In practice, when the drag related to the actual flow conditions is taken into account, the necessary power has a minimum at a certain speed, and then increases the more rapidly the lower the disk loading (large shroud = large drag). Therefore the actual curves of required power relative to low disk loading overtake, at a certain speed, the curves representing higher disk loadings. Figure (14) is an example of calculated power curves with drag effect included. It may be seen that the advantage of low disk loadings vanishes rapidly with forward speed.

### 2.3.2 Experimental Results

The only complete and correct qualification of experimental results is a comparison of the test polars to the corresponding theoretical ones calculated for the same values of the coefficients of advance ratio  $\gamma_0$ , power  $\lambda$  and diffusion  $\sigma$  if the latter is known; if not the theoretical polars can be established with the reference value  $\sigma = 1$ .

The differences between the experimental and theoretical polars are due to the following factors:

- (a) Viscosity (losses).
- (b) Experimental gain of lift provided by the external lift of the shroud which is not included in the theoretical polars.
- (c) Experimental gains due to a diffusion  $\sigma > 1$  which appear in the case when the theoretical reference polar has been calculated with  $\sigma = 1$ .

Figure (15) is an example of comparison between tests and theory. The experimental results are taken from NASA - TN-D 995. The calculated polars are obtained by means of the above equations with equal value of  $\gamma_0$  and  $\lambda$  and with  $\sigma = 1$ . It may be seen that the differences are generally moderate. Of course they could become larger if the shroud or the blades were subject to separation of the flow. Inversely, if the shroud is equipped with additional lifting elements which provide extra lift with a good lift/drag ratio, the experimental polar may be higher than the theoretical one.



### 3. FLOW SEPARATION ON THE SHROUD

#### 3.1 Qualitative Survey - Typical Diagrams

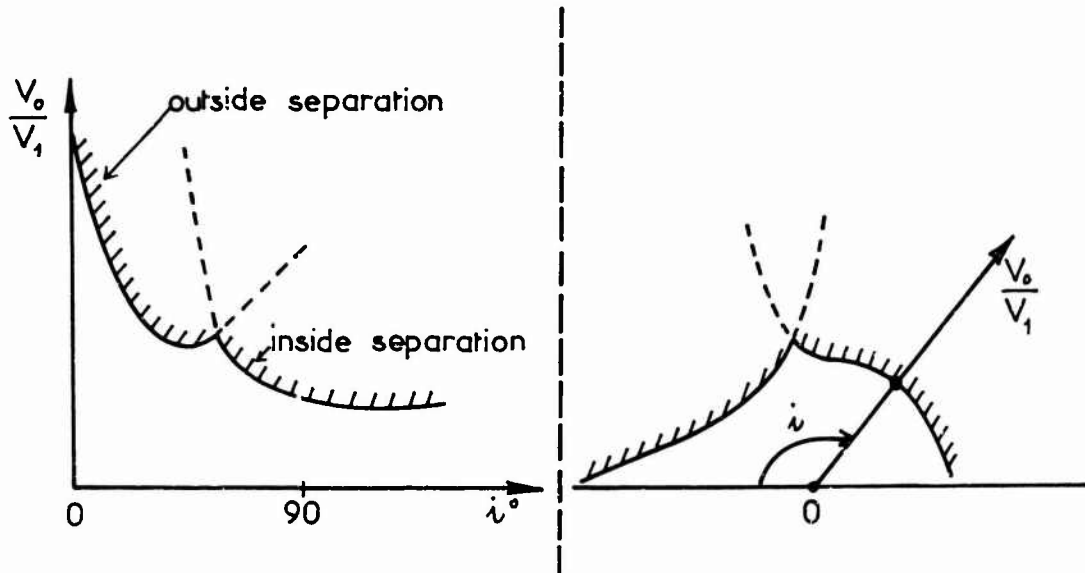
It is obvious that the flow over the shroud is chiefly determined by the two following dimensionless parameters:

$$\begin{aligned} \text{Angle of attack} & \quad i \\ \text{Intake flow coefficient} & \quad \frac{V_0}{V_1} \end{aligned}$$

Intuition and experiments agree on the following flow patterns: at low speed (large angles of attack) the stagnation line is well on the outside surface of the shroud. Therefore the risk of separation is greater on the front and inside of the shroud.

At high speed the stagnation line is shifted towards the inside and the risk of separation is then on the aft outside lip.

The plotting of the separation limits can be made in both coordinate systems.



Although the polar system on the right is more suggestive, we shall use the left one where the plot is easier.

These separation limits depend essentially on the shape of the profiles. Several typical cases may be drawn without any experimental result.

At last it is obvious that a perfectly thin cylinder enjoys only one operation point free of separation

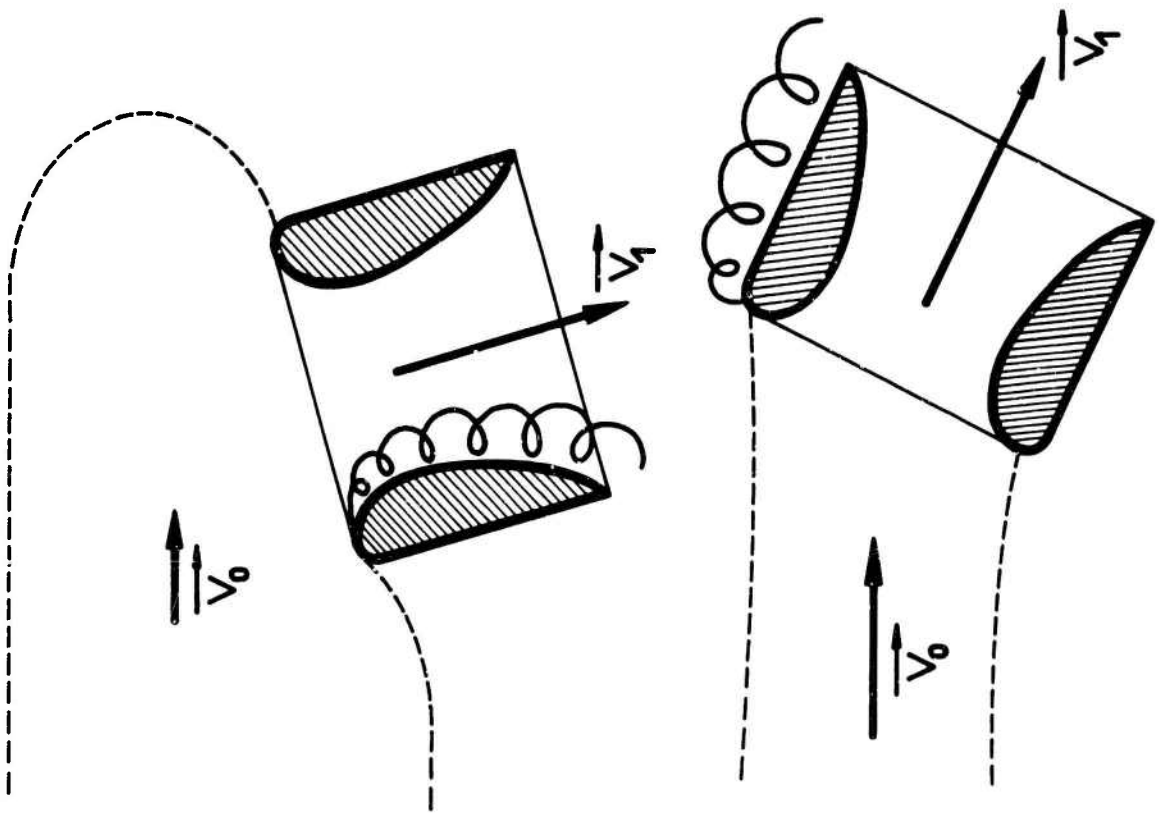
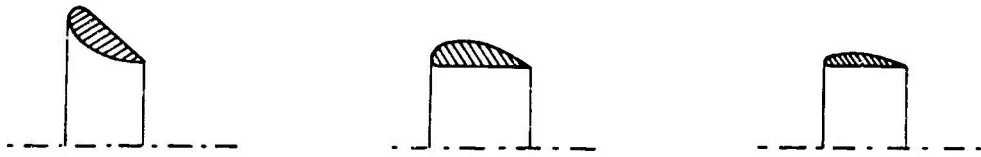
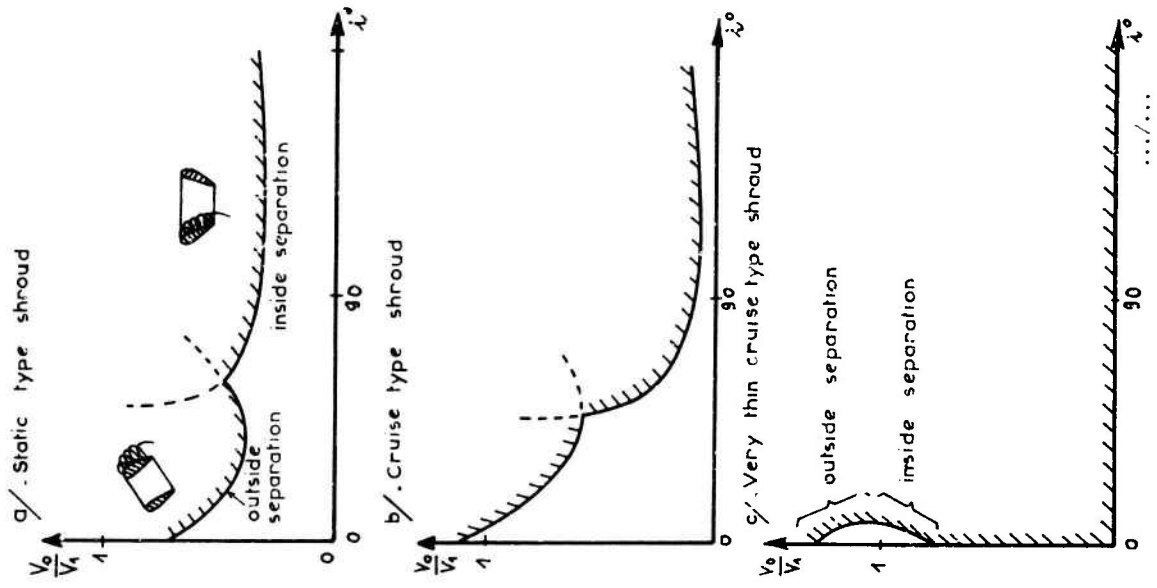
$$i = 0 \quad \frac{V_0}{V_1} = 1.$$

#### 3.2 Influence of the diffusion - Experimental results

It has to be remembered that in level flight at constant speed and zero drag the following equation is valid:

$$\frac{V_0}{V_u} = \cos i \quad \text{or} \quad \frac{V_0}{V_1} = \frac{\cos i}{\sigma}.$$

Once the experimental limit of separation for a given shroud has been drawn in the diagram  $V_0/V_1(i)$ , this limit can be easily compared to the points representing level flight at constant speed; one can notice the favorable part played by the diffusion  $\sigma$  by increasing the margin relative to the separation limit.



As an illustration the experimental limits of separation obtained on three different shrouds have been plotted in Figure (16), as well as the points representing the level flight at constant speed for three assumed values of the diffusion  $\sigma$  :

$$\sigma = 1; 2; 2.5 .$$

One can see the difficulty of ensuring good flow conditions throughout, but also the favorable part played by the diffusion  $\sigma$  .

Recent studies are tending toward a non symmetrical shape of shroud which produces more favorable boundaries.

#### 4. PITCHING MOMENT

##### 4.1 General

The pitching moment is a serious problem of the shrouded propeller. Generally this pitching moment is very important and its maximum value is difficult to forecast accurately for the full scale conditions.

Theoretical attempts to predict the pitching moment do not often provide correct values. This is due to the fact that the maximum value of the moment depends to a large extent on the separation conditions which are very sensitive to local modifications of shape, not taken into account at all by simple theories.

Therefore we shall limit ourselves to a mere qualitative physical scheme which helps the understanding of experimental results and the forecast of the main trends.

##### 4.2 Physical Qualitative Representation of The Pitching Moment

Generally speaking the pitching moment about a given axis is the resultant of all the local pressure (and friction) actions.

Qualitative application of the momentum theorem leads to a simple representation of the extreme cases as function of two relevant parameters:

- Quality of the shroud the forward part of which is or is not able to sustain the low pressures of the flow there;
- Length of the shroud.

The exit diffusion, which has also an effect on the pitching moment, will be mentioned at the end of the next paragraph.

Figure (17) requires some comment. The centre of the moments is in the intake plane. If this centre is moved forward or rearward the resultant moment is obviously changed.

##### 4.3 Experimental Results

For comparison all the results are given about a point on the axis and in the intake plane.

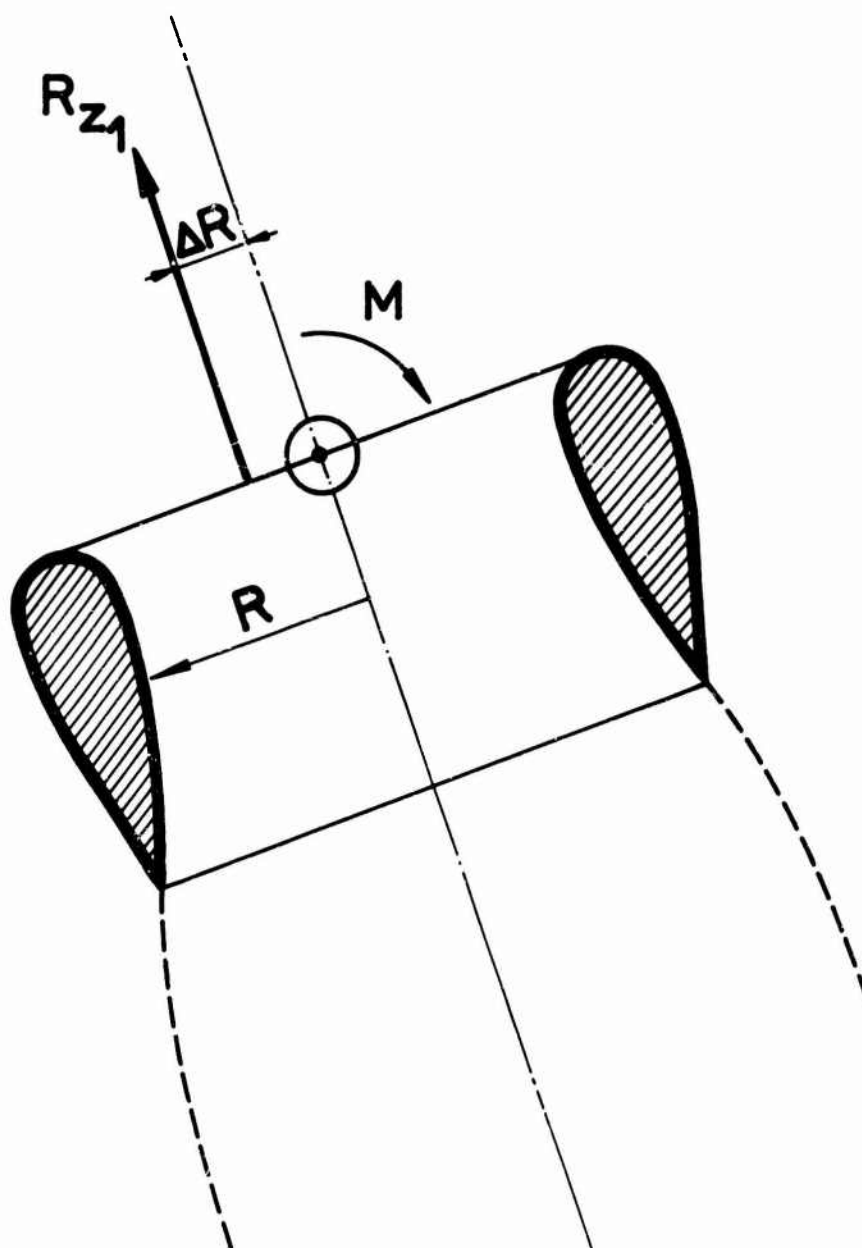
The moment coefficient is defined as:

$$C_m = \frac{M}{\frac{\rho}{2} V_1^2 S_1 D_1} .$$

The reference dynamic pressure is based on the internal speed  $V_1$  , which avoids the infinite value of  $C_m$  in the static case.

The results are generally given as function of the speed coefficient  $V_c/V_1$  and angle of attack: it can be assumed that the propeller itself is not a very important parameter once the internal speed  $V_1$  is specified.

The chosen representation has the drawback of hiding the absolute value of the moment which is often considerable. In order to avoid this difficulty one can also use the following representation which is much more suggestive.



Fictitiously the totality of the moment is supposed to be due to the moment of the force  $R_{z1}$  parallel to the axis. Thus the moment is qualified by the distance  $\Delta R$  referred to the radius  $R_1$ .

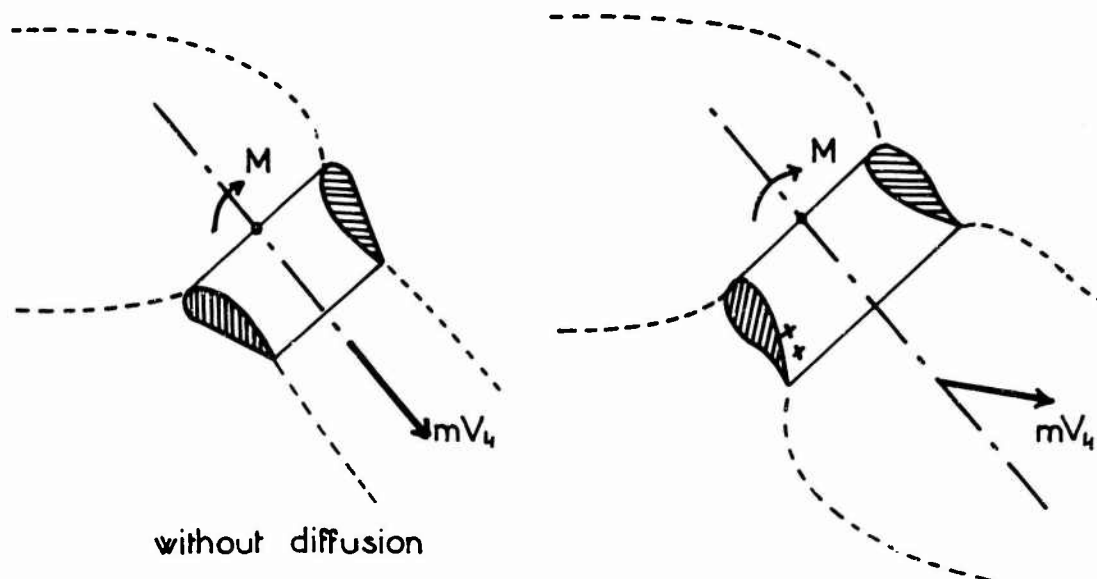
It is worth noticing that at low speed the distance  $\Delta R$  which qualifies the moment is the lever arm of a force practically equal to the weight of the aircraft, or at any rate the weight divided by the number of rotors.

Figure (18) is an example, for a  $90^\circ$  incidence, of the drastic influence of the shape of the shroud which leads to more or less premature separation.

Figure (19) gives the results obtained on a shroud which was absolutely free from separation in the domain covered by the figure. Both of the representations mentioned above are presented.

If the curve representing level flight at constant speed was drawn on this graph, one could see that the maximum moment occurs at an angle of attack comprised between  $60^\circ$  and  $70^\circ$ . The relative fictitious lever arm is then of the order  $1/5 R_1$  (for the centre which has been assumed here).

Other tests, not published here, have shown that the diffusion increases the pitching nose up moment at fixed values of incidence and speed ratio  $V_0/V_1$ . This effect is explained by the curvature of the outgoing jet under the influence of the general flow: the reduced velocity by the diffusion is equivalent to a reduced "stiffness".



## 5. EFFECT OF THE EXIT CROSS SECTION AT HIGH SPEED

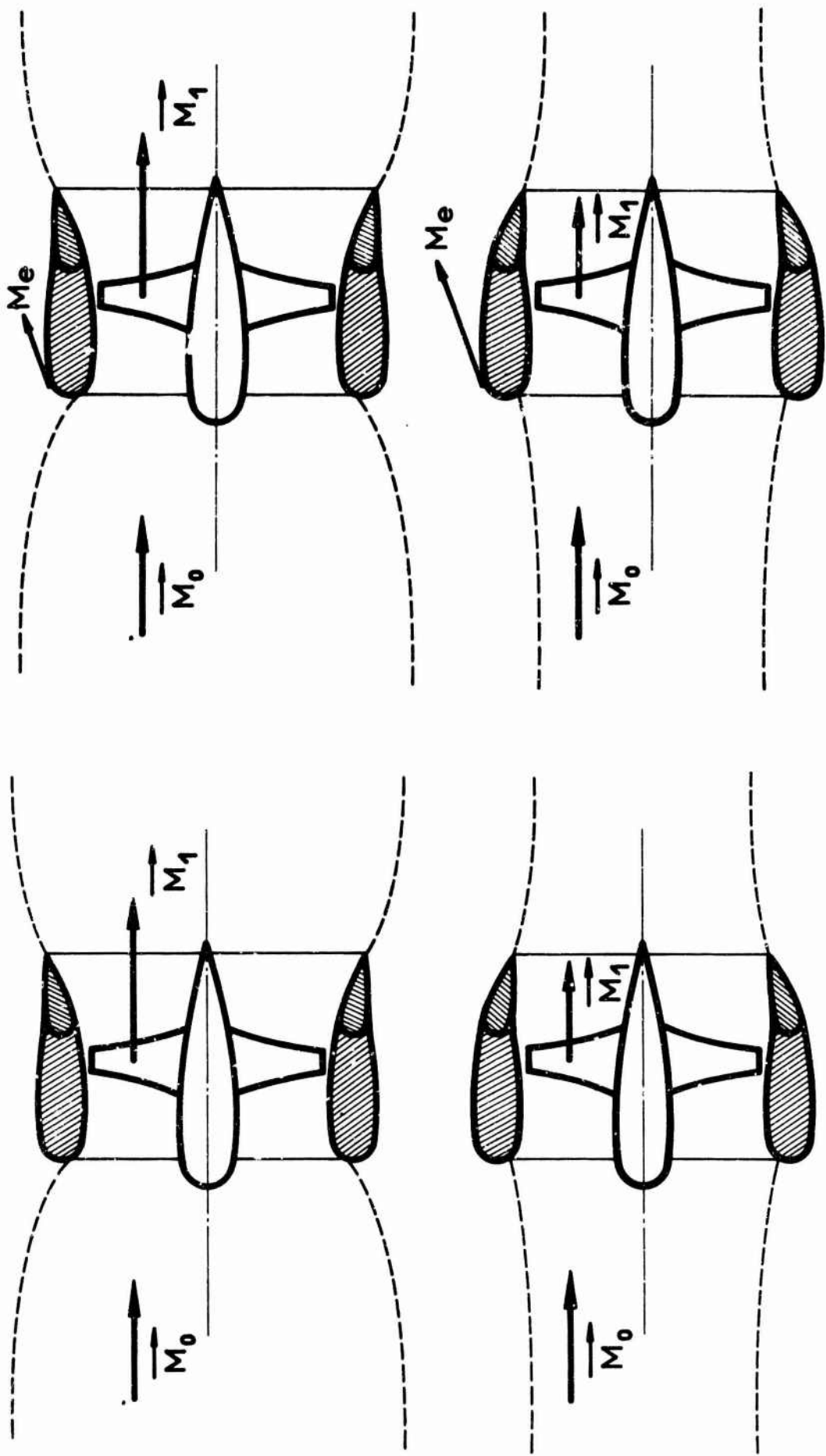
### 5.1 General

We have seen in the paragraph dealing with performance that the increase of diffusion  $\sigma$  in relatively fast forward flight does not provide a large increase of thrust. We have seen also that this moderate theoretical increase becomes a loss when the drag effects are considered.

On the other hand a reduction of the cross section of the jet in high speed flight is quite favourable: it is obvious that compressibility problems appear at first at the tip of the blades. It is also obvious that a reduction of the exit cross section will decrease the internal speed  $V_1$  and therefore the resultant Mach number at the tips.

Because of this possibility of aerodynamic protection of the propeller by the rear part of the shroud, the shrouded propeller is able to work at higher Mach numbers than the free propeller.

It is fair to say that the reduction of internal Mach number  $M_1$  does not go without an increase of the external Mach numbers  $M_0$  on the profile of the shroud. Nevertheless it is easier to design the profile of the shroud for compressibility effects than the rotating blades.



### 5.2 Forward Flight in The Compressible Domain

The isentropic efficiency of the propeller is defined by the ratio:

$$\eta_i = \frac{\text{Isentropic temperature increase}}{\text{Actual temperature increase}}$$

For equal values of total pressure ratios across the propeller.

Apart from this efficiency, it is assumed that there are no losses nor rotation of flow and that the flow is uniform in the control cross sections 0, 1, 2, 4.

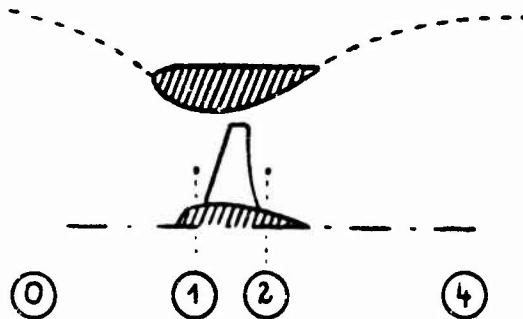
At low speed the efficiency  $\eta_i$  is identical to the efficiency  $\eta_1$  already used above:

$$\eta_i = \frac{T_1 V_0}{W}$$

The following relationships have been established by using the classical equations of compressible one dimensional flow.

$$f(M) = \frac{M}{\left[1 + \frac{\gamma-1}{2} M^2\right]^{\frac{\gamma+1}{2(\gamma-1)}}$$

$$f(M_2) = \sigma f(M_1)$$

$$\frac{S_2}{S_1} = \frac{f(M_1)}{f(M_2)}$$


Ratio of total temperatures

$$\frac{\theta_{t_2}}{\theta_{t_1}} = \sigma^2 \frac{M_1^2 \left[1 + \frac{\gamma-1}{2} M_1^2\right]}{f^2(M_2) \left[1 + \frac{\gamma-1}{2} M_0^2\right]^{\frac{2\gamma}{\gamma-1}}}$$

Power disk loading

$$\frac{W}{S_1} = \gamma C_p \frac{P_0 \theta_0}{q_0} f(M_1) \left(1 + \frac{\gamma-1}{2} M_0^2\right)^{\frac{\gamma-1}{2(\gamma-1)}} \left[ \frac{\sigma^2 M_1^2 \left(1 + \frac{\gamma-1}{2} M_1^2\right)}{f^2(M_2) \left(1 + \frac{\gamma-1}{2} M_0^2\right)^{\frac{2\gamma}{\gamma-1}}} - 1 \right]$$

Efficiency

$$\eta_i = \frac{\frac{\gamma-1}{2} (M_1^2 - M_0^2) \theta_0}{\left(1 + \frac{\gamma-1}{2} M_0^2\right) \left(\frac{\theta_{t_2}}{\theta_{t_1}} - 1\right)}$$

$$\eta_i = \frac{\gamma - 1}{2} \frac{M_4^2 - M_0^2}{\left(1 + \frac{\gamma - 1}{2} M_0^2\right) \left[ \frac{\left(1 + \frac{\gamma - 1}{2} M_4^2\right) \sigma^2 M_4^2}{\rho^2(M_4) \left(1 + \frac{\gamma - 1}{2} M_0^2\right)^{\frac{2\gamma}{\gamma - 1}} - 1} \dots / \dots \right]}$$

Disk loading

$$\frac{T}{S_1} = \gamma P_0 \left[ \sigma M_4^2 - M_0^2 \frac{f(M_4)}{f(M_0)} \right]$$

Air intake loading

$$\frac{T_0}{S_1} = P_0 \left[ \left( \frac{1 + \frac{\gamma - 1}{2} M_0^2}{1 + \frac{\gamma - 1}{2} M_1^2} \right)^{\frac{\gamma}{\gamma - 1}} \left( 1 + \gamma M_1^2 \right) - 1 - \gamma M_0^2 \frac{f(M_4)}{f(M_0)} \right]$$

Propeller loading

$$\frac{T_1}{S_1} = P_0 \left[ \left( 1 + \gamma M_2^2 \right) \left( \frac{1 + \frac{\gamma - 1}{2} M_4^2}{1 + \frac{\gamma - 1}{2} M_2^2} \right)^{\frac{\gamma}{\gamma - 1}} - \left( 1 + \gamma M_1^2 \right) \left( \frac{1 + \frac{\gamma - 1}{2} M_0^2}{1 + \frac{\gamma - 1}{2} M_1^2} \right)^{\frac{\gamma}{\gamma - 1}} \right]$$

Diffuser loading

$$\frac{T_2}{S_1} = P_0 \left[ 1 + \gamma \sigma M_4^2 - \left( \frac{1 + \frac{\gamma - 1}{2} M_4^2}{1 + \frac{\gamma - 1}{2} M_2^2} \right)^{\frac{\gamma}{\gamma - 1}} \left( 1 + \gamma M_2^2 \right) \right]$$

Ratio of total pressures

$$\frac{P_{t_2}}{P_{t_1}} = \left[ \frac{1 + \frac{\gamma - 1}{2} M_4^2}{1 + \frac{\gamma - 1}{2} M_0^2} \right]^{\frac{\gamma}{\gamma - 1}}$$

#### Important Note

In the ideal case when  $\eta_i = 1$  it can be shown that the specific thrust  $T/W$  as a function of power disk loading  $W/S_1$  is exactly the same as in incompressible flow. The compressible equations indicated have to be used only when the correct velocities or Mach numbers are needed.

This remarkable result can be explained in the following way: the modification of the state equation of the gas ( $P/\rho = RT$  instead of  $\rho = \text{constant}$  in the incompressible case)



does not influence the two major conditions which exist for  $\eta_i = 1$ :

- (a) The flow is isentropic upstream and downstream of the actuator;
- (b) Downstream, the flow has resumed its initial state:

Static pressure  $P_0$   
 Specific mass  $\rho_0$   
 Static temperature  $\theta_0$ .

Therefore the transformation is isentropic and closed and the result does not depend on the intermediate states.

The performance is plotted in Figures 20 to 25 for the efficiency value  $\eta_i = 0.8$ .

The main interest of these graphs lies in the values of the internal Mach number  $M_1$  and in the two limits:

- Sonic conditions  $M_1 = 1$  in the cross Section  $S_1$ .
- Sonic conditions  $M_u = 1$  in the cross section  $S_u$ .

In practice the latter boundary is well beyond the range for shrouded propellers. But the first one can be dangerously approached or even reached when the three following parameters are combined having relatively large values:

Power disk loading  $W/S_1$   
 Flight Mach number  $M_0$   
 Diffusion  $\sigma > 1$ .

The next comparative example shows the unfavorable effect of the diffusion in high speed flight

$$\text{We assume } \left\{ \begin{array}{l} M_0 = 0.4 \\ \frac{W}{S_1} = 1000 \text{ kW/m}^2 \\ \eta_i = 0.8 \end{array} \right.$$

The graphs just discussed lead to the following comparison as function of the assumed value of  $\sigma$

$\sigma$	$\frac{T}{W}$ daN/kW	$M_1$
0.0	0.54	0.39
1.4	0.56	<u>1.00</u>

It is obvious that the slight increase in specific thrust due to an increase of  $\sigma$  is absolutely without interest because of the drastic simultaneous increase of the Mach number  $M_1$  in front of the propeller: the design of the blades is definitely impossible when  $M_1 = 1$ .

Whatever the value of the flight Mach number  $M_0$ , the internal Mach number  $M_1$  can be kept at a reasonable value by reducing the exit cross section ( $\sigma < 1$ ). Furthermore the law of exit section versus Mach number  $M_0$  can be matched for a constant pitch propeller.

## 6. GROUND EFFECT

Ground proximity results in two different effects:

- The first one purely static, is a modification of the thrust as a function of height above the ground.
- The second one arises at constant height as time dependant disturbances affecting all the components.

In the following paragraphs we shall limit ourselves to the effect of ground proximity on vertical thrust in hover.

### 6.1 Static Influence of Ground Proximity

The influence on the vertical thrust is qualified by the value at each height of the so called amplification coefficient

$$A = \frac{T}{T_0} = \frac{\text{Thrust in ground effect}}{\text{Thrust out of ground effect}},$$

the two forces involved being compared at constant power.

The *power* needs to be carefully defined:

- (a) In a theoretical ground effect study this expression can only mean the kinetic energy of the jet when it has resumed the ambient pressure  $P_0$ .
- (b) In an experimental study this expression can mean two different energies.
  - Either the kinetic energy as defined in (a). But this quantity can be obtained only through a tiresome exploration and it has but a doubtful practical meaning because this energy is not equal to the shaftpower.
  - Or the mechanical shaftpower. But in this case the effect of the ground on the internal flow and therefore on the propeller efficiency cannot be ignored and generally a constant shaftpower test performed at various heights is *not* a constant kinetic energy test. Therefore a comparison with theory requires a calculation of this energy through the estimated propeller efficiencies as function of the heights tested.

On the other hand the configuration must be divided into two groups:

- (a) The shrouded propeller is isolated.
- (b) The shrouded propeller is part of an aircraft which bears interaction forces from the outgoing jet.

#### 6.1.1 Isolated Shrouded Propeller

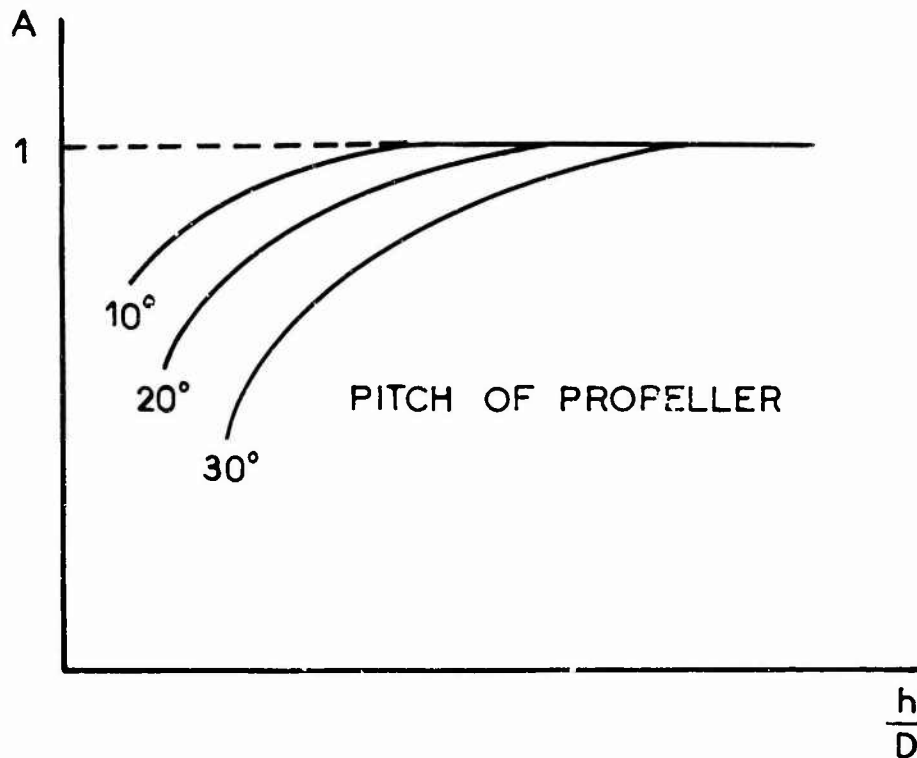
Theoretical methods only deal with rather simplified configurations: no viscosity and a two dimensional flow pattern without diffusion. All the results obtained with these assumptions agree with the curve of amplification coefficient  $A$  given in Figure 27. There is a minimum equal to 0.95 at a height of approximately one diameter. In other words the loss is 5%. When the height is decreased, the factor  $A$  increases asymptotically. This increase has but a mere theoretical value: it is explained by the fact that the theoretical power which is needed to maintain a constant pressure in a tank with an aperture tends to zero when the leakage mass flow tends to zero.

The experimental curves are roughly similar to the theoretical ones for a height exceeding one diameter approximately, which is the range of practical use. At lower

heights parameter A keeps decreasing, unless the configuration is of the "ground effect machine" type which has nothing to do with an isolated propeller.

The same figure gives three examples of ground effects obtained experimentally for isolated shrouded propellers.

Theory and experiments show that a progressive decrease of blade pitch with decreasing height contributes to maintain a constant thrust for a fixed power. The shape of the curves of parameter A is given on the following figure.



This shape is obvious if one remembers that the approach of ground is equivalent to a progressive reduction of the exit cross section which decreases the internal speed and therefore increases the angle of attack of the blades.

But decreasing the pitch is not a suitable remedy in practice because in order to keep a constant shaftpower it would be necessary to increase substantially the r.p.m. This is not permitted on the basis of either engine or compressibility considerations:

#### 6.1.2 Shrouded Propeller with Air-Frame

Very often the outgoing jet after its impact on the ground, hits the adjacent wing or fuselage and produces on these parts pressures which increase or decrease the thrust of the rotors.

Figure 28 gives two examples of beneficial interaction.

Nevertheless, even when this interaction is favourable, the individual losses of the rotors alone have to be taken into account as they maintain responsible for the roll instability in ground effect.

#### 6.2 Unsteady Interaction with the Ground

Full scale as well as model tests show that the proximity of the ground is the cause of fluctuation of all the components of force and moment. This behavior can already be observed on an isolated rotor. Local measurements in the jet confirm this instability.

The precise physical cause of this unsteadiness has not been found. It seems that the origin lies in the unsteady location of the jet stagnation point on the ground.

Several tests on different models have demonstrated that this unsteadiness decays very slowly with increasing height: at a distance of 20 diameters the amplitudes are still of the order of one half of their value at a height of one diameter. The pseudo-period of the fluctuations was about 10 seconds in our experiments. Figure 29 is an example of the amplitudes of thrust obtained full scale and on a model.

This unsteadiness makes the task of the pilot very difficult, even when auto-dampers have been provided. The matching of the characteristics of the dampers, or of a more sophisticated auto-pilot has to take into account the ground effect fluctuations in the first place.

## 7. DESIGN PROBLEMS

Several types of installations have been designed, and many have already been experimented upon.

The two main groups are:

- Nearby shrouded propellers

(Doak, Bell X 22) .

- Integrated shrouded propellers or lift fans.

(Ryan XV5a) .

In the latter case the propellers are used at low speed only, mainly as lift devices.

Regarding the mechanics of flight, two concepts are possible. Both have first to take into account the very large pitching moment in transition flight. Only the first concept has been tested in flight.

*First Concept.* The number of rotors is at least 3 (Doak) or 4 (Bell X 22), so that the equilibrium and the pitching movements of the whole aircraft can be obtained by differential thrust between the fore and aft rotors. The angular position of each forward rotor is controlled by servo-jacks. This configuration has the advantage of ensuring effective pitching moments, but requires long and heavy gears and driving shafts and very powerful jacks.

*Second Concept.* The number of rotors is reduced to two (NORD 500). Their tilt axis is located vertically above the centre of gravity. Mechanically speaking each rotor is free to rotate about its axis, the position and movements in pitch being obtained by a flap working as a tab in the jet of each rotor. The rest of the aircraft "hangs" as a pendulum on the axis of the two rotors and takes the natural pitch angle under the influence of gravity, inertial forces and aerodynamic forces. This is approximately the behaviour of a helicopter fuselage.

This solution has been applied in the case of the NORD 500. In this case preliminary stability studies have demonstrated that each rotor should be provided with a rotation damper.

The advantages of this configuration are:

- Short driving shafts.
- No rear rotor.
- The equilibrium and control moments to be provided to the flaps are relatively small, the active forces being provided by the propeller jets, that is to say by the engines.

One can think of various combinations of the two main configurations mentioned above. For instance each rotor can be provided with a flap and a servo-jack each being respectively responsible for the equilibrium and the manoeuvres.

## 8. WEIGHT OPTIMISATION

The number of prototypes with shrouded propellers is not sufficient to allow an accurate extension to operational aircraft.

But a method of optimisation can be proposed now. This method intends to provide information on the relative importance of the various parameters in their possible range of variation.

Whatever the values retained for each of these parameters the method emphasises the outstanding importance of disk-loading.

### 8.1 Basic Equations

The algebraic equations are given hereafter. They must express the following conditions:

- In the static case, the thrust is equal to the maximum weight increased by the margin needed for manoeuvres, hot weather, safety in case of engine failure.
- The thrust in cruise condition is equal to the total drag.
- The ratio of the power required in cruise to the maximum static power is equal to the available ratio on the type of engine considered.
- The total mass at take-off is the sum of all the partial masses: airframe, engines, gears, payload, fuel for the mission.

The equations will show that if the cruise speed is fixed, the total mass is not a minimum as a rule. Inversely if a minimum mass is demanded, the cruise speed results from the equations.

Here are the notations and the values used as an example for the relevant parameters. These values can be changed as required without questioning either the method or the trend of the results.

$m$	maximum mass at take-off
$m_p$	mass of airframe
$m_m$	mass of motorisation
$m_r$	mass of the rotors
$C_u$	payload
$C'_{s0}$	specific consumption in the static case
$C_s$	specific consumption in cruise
$t$	time of hovering
$k$	maximum static thrust/maximum weight
$\rho_0$	specific mass of the air at take-off

$p$	specific mass of the air in cruise
$M'_i$	figure of merit in the static case
$X$	total range
$V$	cruise speed
$C_x$	drag coefficient referred to the cross section of the fuselage $S_M$
$\frac{C_U}{S_M}$	$\frac{\text{payload}}{\text{cross section of the fuselage}}$

The latter parameter is of particular importance for the static thrust required is related to the weight only and the thrust required in cruise is mainly related to the drag, that is to say to the cross section  $S_M$ .

$$\gamma = \frac{W}{W_0} = \frac{\text{power required in cruise (drag)}}{\text{maximum static power}}$$

$$\gamma_m = \frac{\text{power available in cruise (engine)}}{\text{maximum static power}}$$

$$\gamma^* = \frac{\gamma}{\gamma_m} \quad \text{in all cases one must have } \gamma^* \leq 1$$

for good matching:  $\gamma^* = 1$

$$\eta \quad \text{propulsive efficiency in cruise: one curve per power disk loading } \frac{W}{S_1}$$

Mass equation

$$m = \frac{m_p}{m} m + \frac{m_r}{S_1} S_1 + \frac{m_M}{W_0} W_0 + C_{s_0} t W_0 + \frac{C_x X}{V} W + C_U$$

Total mass	Airframe	Rotors	Motorisation	Consumption in the static case	Consumption in cruise	Payload
------------	----------	--------	--------------	--------------------------------	-----------------------	---------

Static power required

$$W_0 = \frac{1}{2} k^{3/2} g^{3/2} m \sqrt{\left( \frac{1}{\rho_0 M_1'^2} \frac{m}{S_1} \right)}$$

Power required in cruise

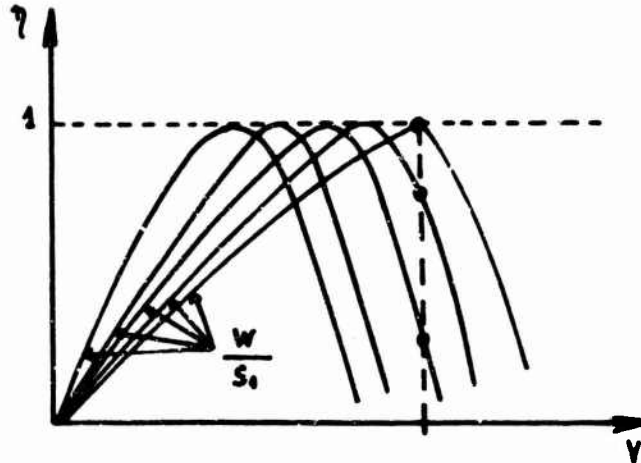
$$W = \frac{1}{\eta} \frac{\rho}{2} C_x S_M V^3$$

Propulsive efficiency in cruise  $\eta$

Curves of Figure 10.

These curves show the *net* propulsive efficiency, which means that the drag of the shroud is already included.

It must be noted that for each value of the speed  $V$  there is a choice between a set of values of  $\eta$  depending on the power disk-loading parameter  $W/S_1$ : for large values of the disk loading the cruise efficiency is nearly the best but the low speed and static performance is poor and inversely. It is obvious that the best compromise for both flight conditions will be obtained for a disk loading value such that the related efficiency curve has its maximum on the left of the cruise speed (otherwise there would be a penalty both in the static and cruise configuration in comparison with the curve which has its maximum at the cruise speed).



The calculation must in practice be performed for the whole set of suitable disk loading values at each speed.

The main equation is presented below:

Feeding the two power equations (static and cruise) into the mass relationship where the unknown is  $m/S_M$ :

$$\left[ \frac{m}{S_M} \right]^{3/2} - \left( 1 - \frac{m_p}{m} \right) \frac{M'_1 \sqrt{\rho_0}}{\frac{1}{2} \left( \frac{m_m}{W_0} + C'_{s0} t \right) (\text{kg})^{3/2}} - \sqrt{\left( \frac{S_1}{S_M} \right) \left[ \frac{m}{S_M} \right]} +$$

$$+ \frac{M'_1 \sqrt{\rho_0}}{\frac{1}{2} \left( \frac{m_m}{W_0} + C'_{s0} t \right) (\text{kg})^{3/2}} \sqrt{\left( \frac{S_1}{S_M} \right) \left[ \frac{m_e S_1}{S_1 S_M} + C_s X \frac{\rho}{2} C_x \frac{V^2}{\eta} + \frac{C_u}{S_M} \right]} = \dots$$

A particular value of speed  $V$  being chosen, this equation must be solved for a set of values of the cruise efficiency  $\eta$ , that is to say for the corresponding values of the assumed power disk-loading parameter  $W/S_1$ .

As an example, this process has been performed with the following numerical values of the relevant parameters:

$$C_x = 0.2$$

$$\frac{C_u}{S_M} = 500 \text{ kg/m}^2$$

$$\frac{m_p}{m} = 0.40$$

$$\frac{m}{W_0} = 0.45 \text{ kg/kW}$$

$$\frac{m}{S_1} = 60 \text{ kg/m}^2$$

$$M'_1 = 1.1$$

$$k = 1.1 \text{ and } 1.3$$

$$C_{s0} = 0.322 \text{ kg/kW h.}$$

V(km/h)	$C_s$
400	0.318
500	0.315
600	0.311
700	0.306
800	0.298

$$X = 500 \text{ km.}$$

The values of total mass thus obtained are plotted against design power disk-loading  $W_0/S_1$  in Figure 30.

Each curve is related to a value of the speed  $V$ . On such a curve the valid part is determined by the condition that the power  $W$  required for cruise must be equal to (or less than) the power delivered by the engine at its normal cruise power. It is clear that the best point is the point where the two powers are identical, as in this case there is no unnecessary engine weight. But in some cases it may be advantageous to utilize a reduced power in cruise, at the cost of some moderate extra-weight, for the sake of increased lifetime.

Let us concentrate now on the point where the two powers are identical, that is to say  $\gamma^* = 1$ . There is one such point on the graph at each speed. Generally these points do not coincide with the minimum mass value. But if we consider the whole graph it is possible to find one point (speed, power, disk-loading, mass) for which the equality of the available and required cruise power is obtained at a minimum mass point.

The aircraft defined in this way is the minimum mass aircraft for a preset value of payload, fuselage cross section and all the other parameters. It is important to notice that this minimum mass aircraft has a stated cruise speed which cannot be preset.

The same type of calculation has been applied (with other values of the weight parameter) to several values of the figure of Merit and two values of range: 500 and 1000 km. Each set of figures leads to one minimum mass aircraft which are compared in Figure 31. The important points to be noted are:

- (1) The improvement of the Figure of Merit (because of jet diffusion) has the following effects:
  - (a) an increase of the relative payload  $C_u/m$ ,
  - (b) a decrease of the total mass factor  $m/S_M$ ,  
(In the process, the absolute value of the payload  $C_u$  is nearly constant.)
  - (c) a decrease of the cruise speed  $V$ .



2. The increase in range has the following effects:

- (a) a decrease of the relative payload  $C_u/m$ ,
- (b) an increase of the total mass factor  $m/S_M$ ,
- (c) an increase of the power disk loading  $W_0/S_1$ ,
- (d) an increase of the cruise speed  $V$ .

One last point deserves a discussion: the range and payload being preset, the absolute minimum mass aircraft is generally not the best answer to the problem, as an increase of cruise speed is a factor which permits more traffic to be handled for a given overall cost even if the weight (and cost) of each aircraft of the fleet increases quickly with speed.

Special economical studies agree with the fact that the importance of the speed factor is more than the first power of  $V$ . A dependance on  $V^{1.4}$  seems to be a correct estimate.

In this case the overall economical efficiency parameter will be:

$$E = \frac{C_u}{m} \times V^{1.4} .$$

This new parameter is plotted in Figure 32 as function of the assumed static Figure of Merit  $M'_1$ . It is interesting to notice that the maximum efficiency  $E$  is *not* systematically obtained for the maximum  $M'_1$  value: an improvement from 0.9 to 1.1 is certainly beneficial, but a further increase to 1.25 has very little, and sometimes unfavorable influence.

This is fortunate for a figure of 1.1 seems to be the best possible that can be reached.

#### REFERENCES

- |                              |  |
|------------------------------|--|
| Chaplin, H.R.                | <i>Shrouded Propeller Thrust Ratio as Measure of Shroud and Propeller Static Performance.</i> David Taylor Model Basin, Aerodynamics Laboratory, TED No. TMB AD 3232, Aero Report No.951, January 1959 (ASTIA AD 212.203). |
| Sacks, A.H.<br>Burnell, J.A. | <i>Ducted Propellers. A Critical Review of the State of the Art.</i> Contract NONR 2677 (00). Advanced Research Division, Hiller Aircraft Corp. ARD 232, 1959.   |
| Theodorsen, Th.              | <i>Theoretical Investigation of Ducted Propeller Aerodynamics.</i> Contract No. DA 44 - 177 - TC - 606. Republic Aviation Corporation 10.8.1960.   |
| Lazareff, M.                 | <i>Hélices Carénées - Synthèse.</i> Unpublished Nord-Aviation Report No. ARA/NT/89/66, February 1967.  |

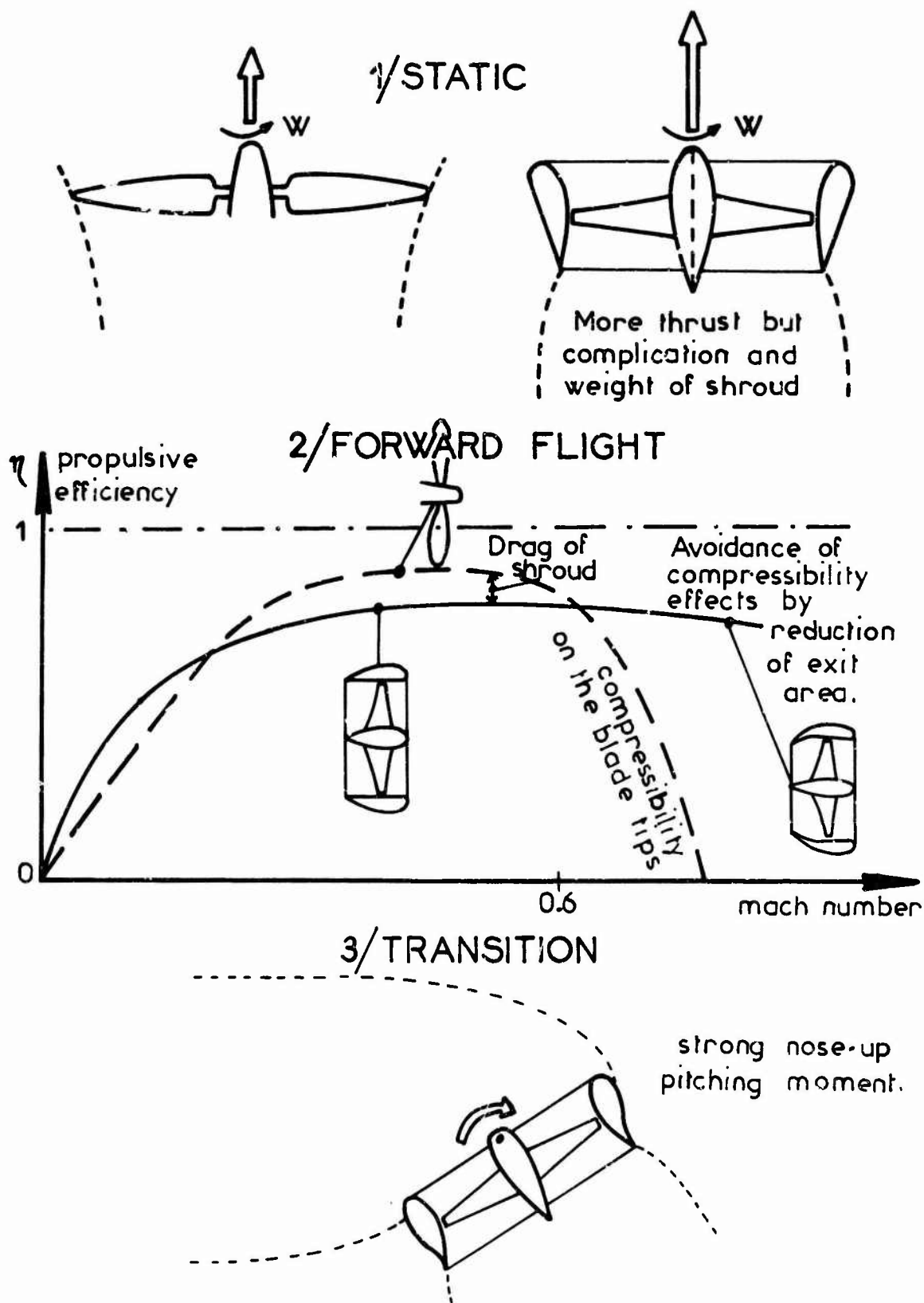


Fig.1 Summary

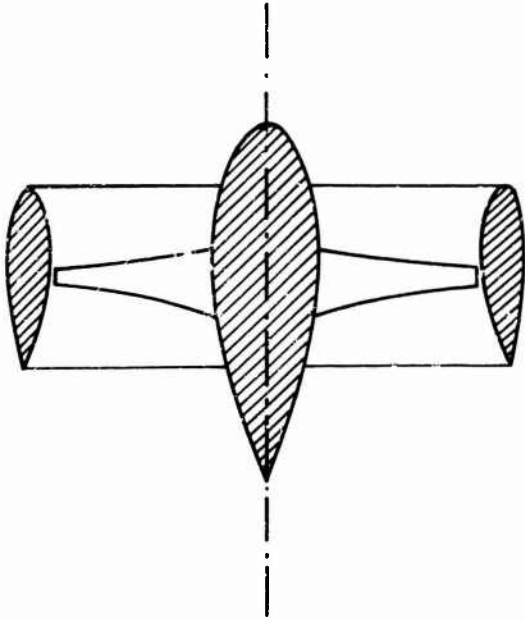


Fig.2 Average relative size of the shroud

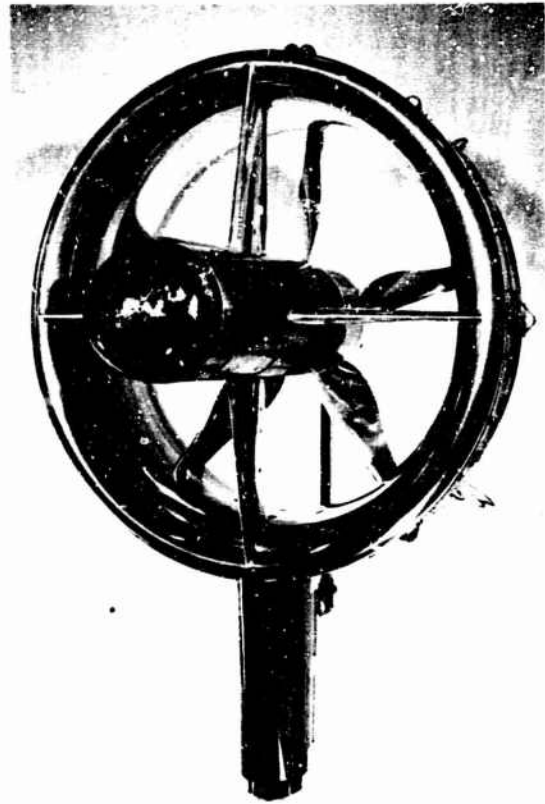


Figure 3

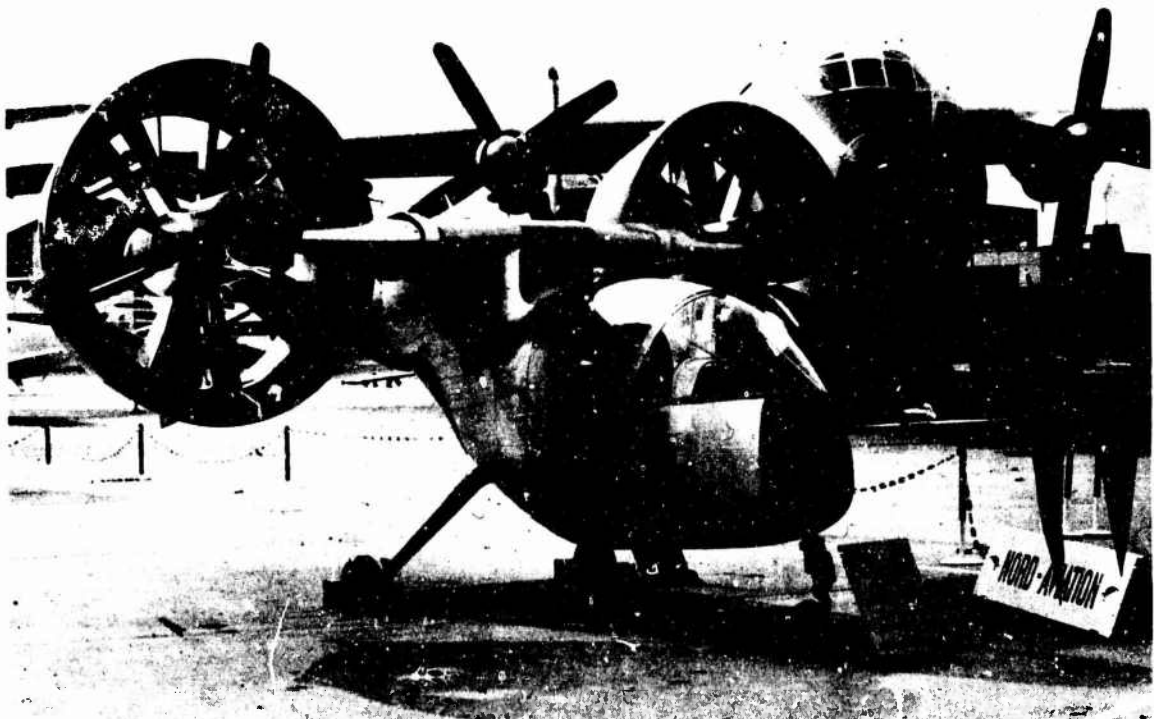


Figure 4

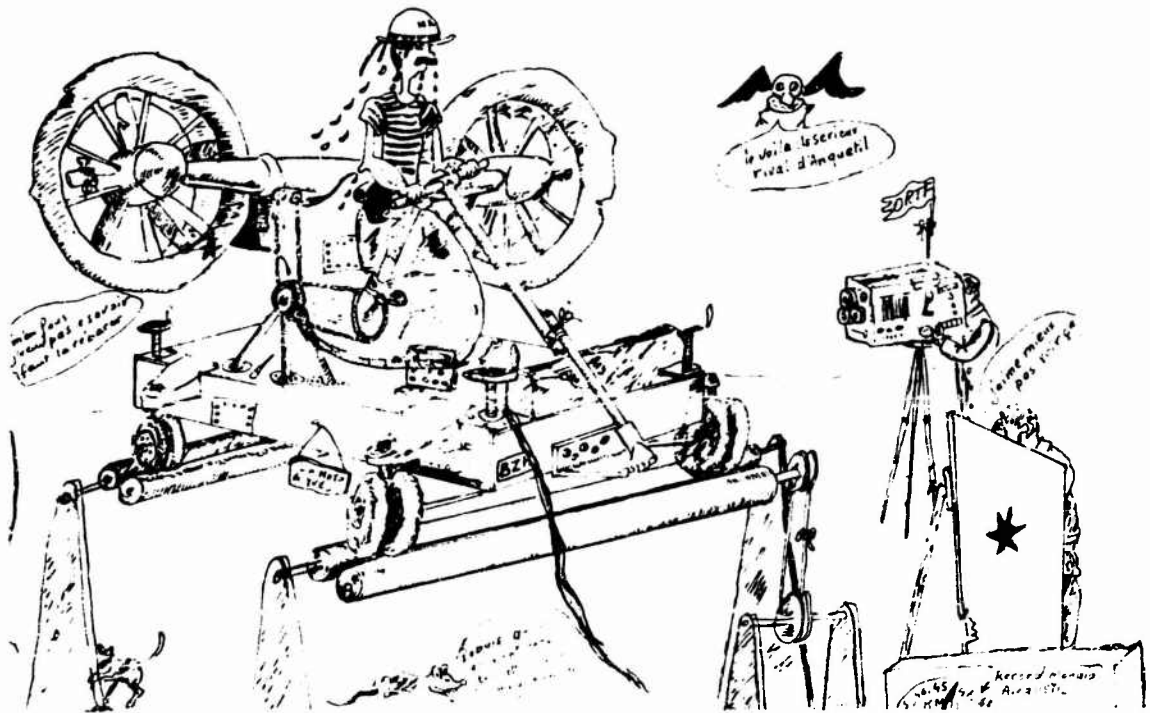


Fig.5 Artist's concept of the Nord 500

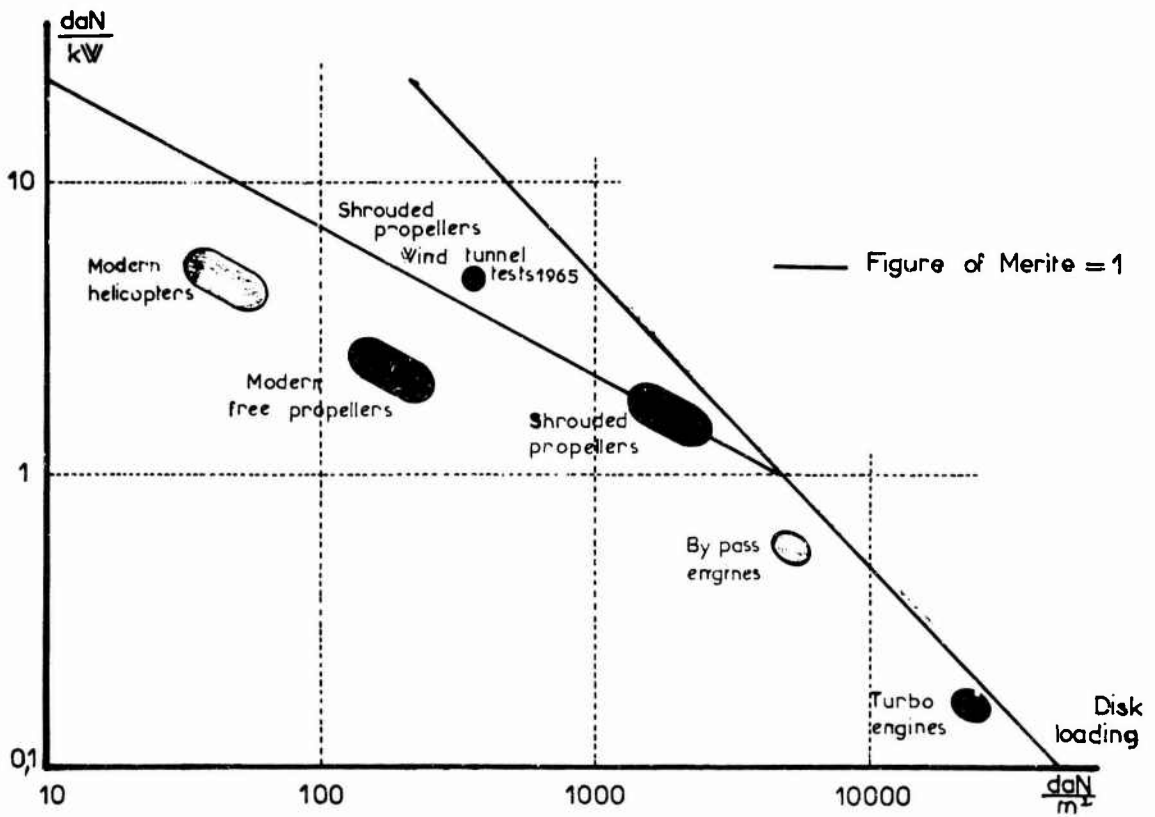


Fig.6 General disk loading graph

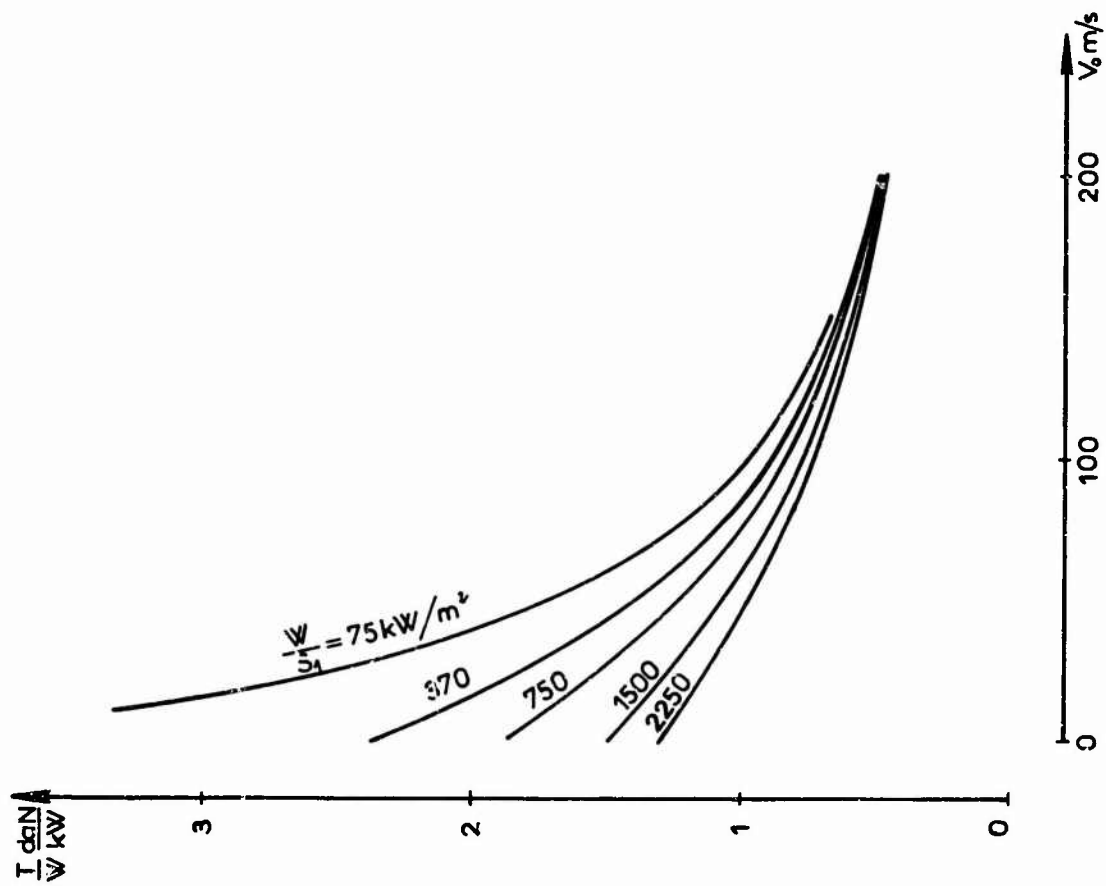


Fig. 8 Specific thrust in forward flight

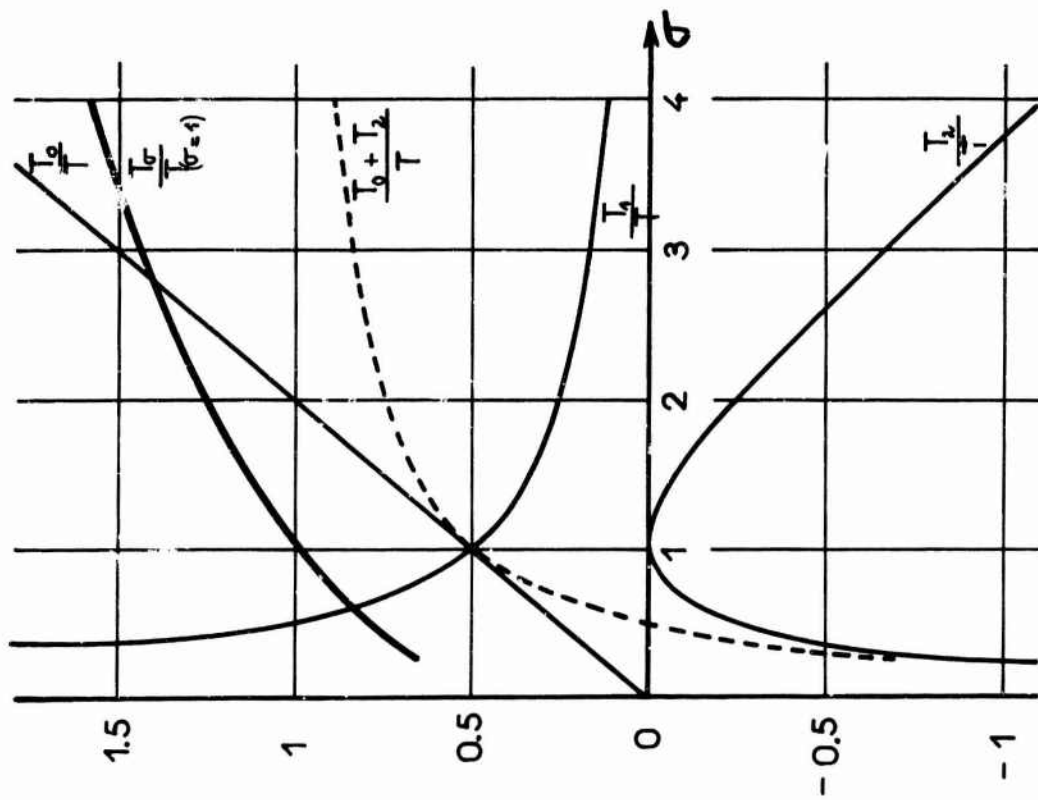


Fig. 7 Components of the total thrust

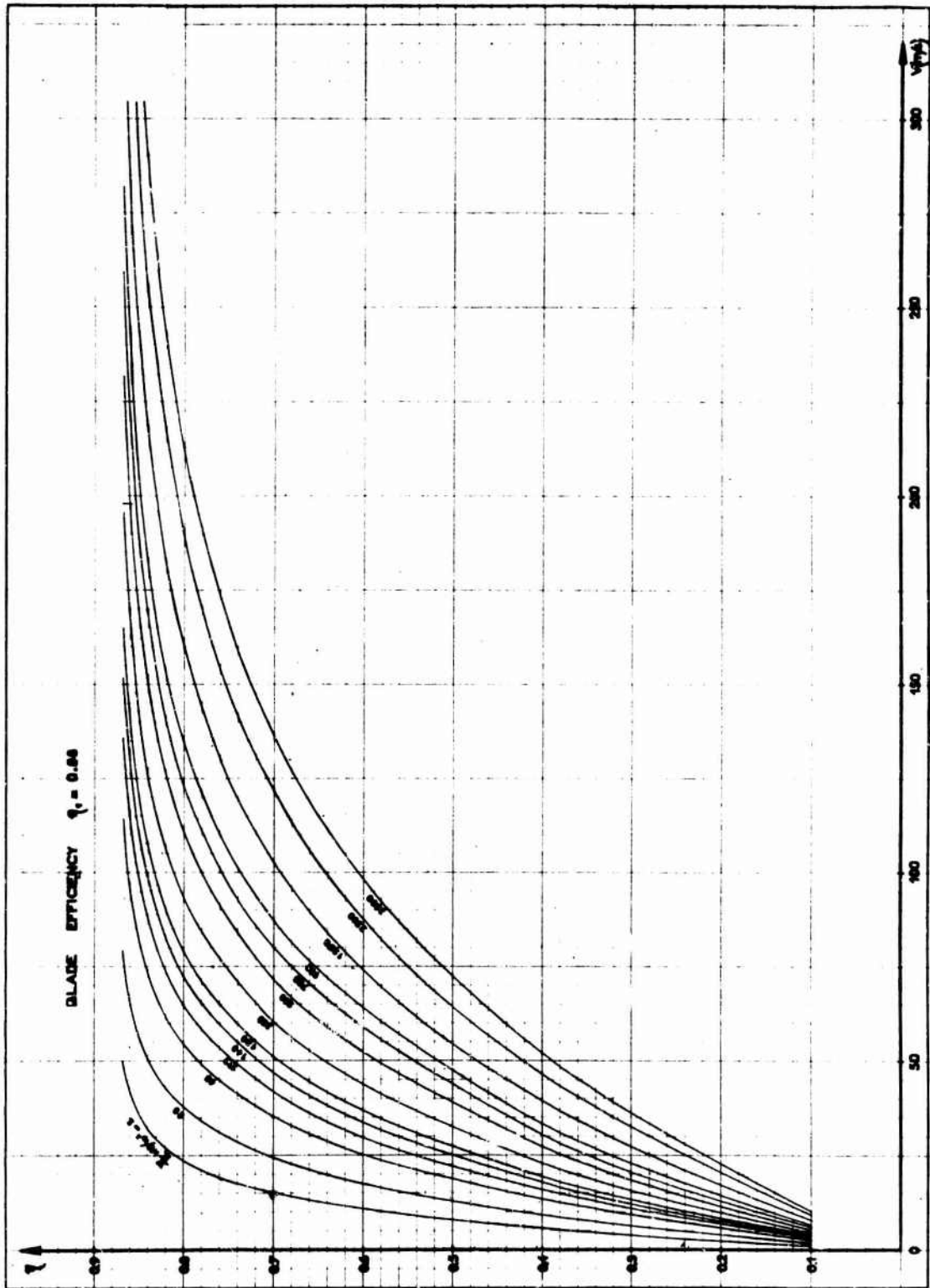


Fig. 3 Propulsive efficiency without shroud drag

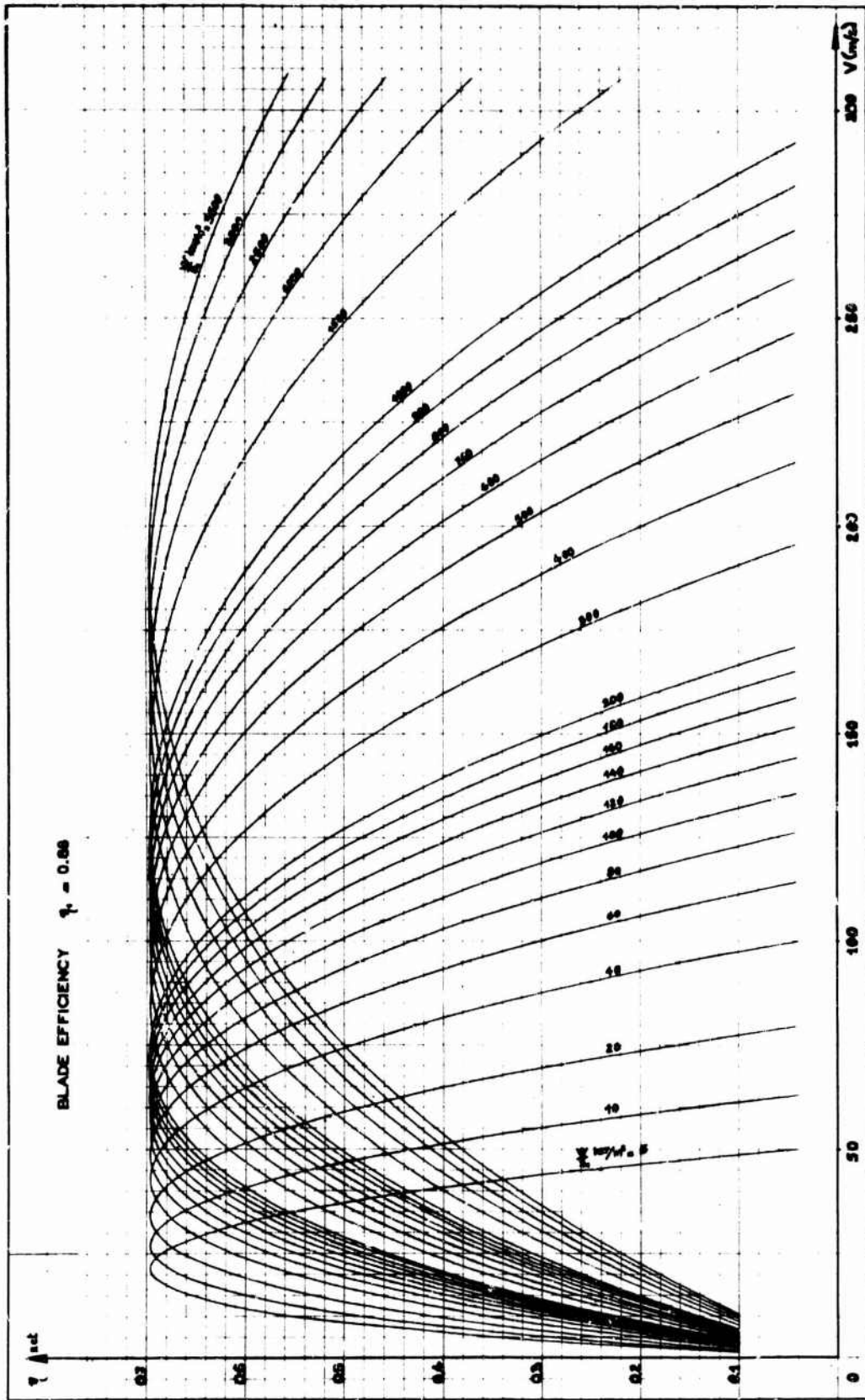


Fig.10 Propulsive efficiency including shroud drag

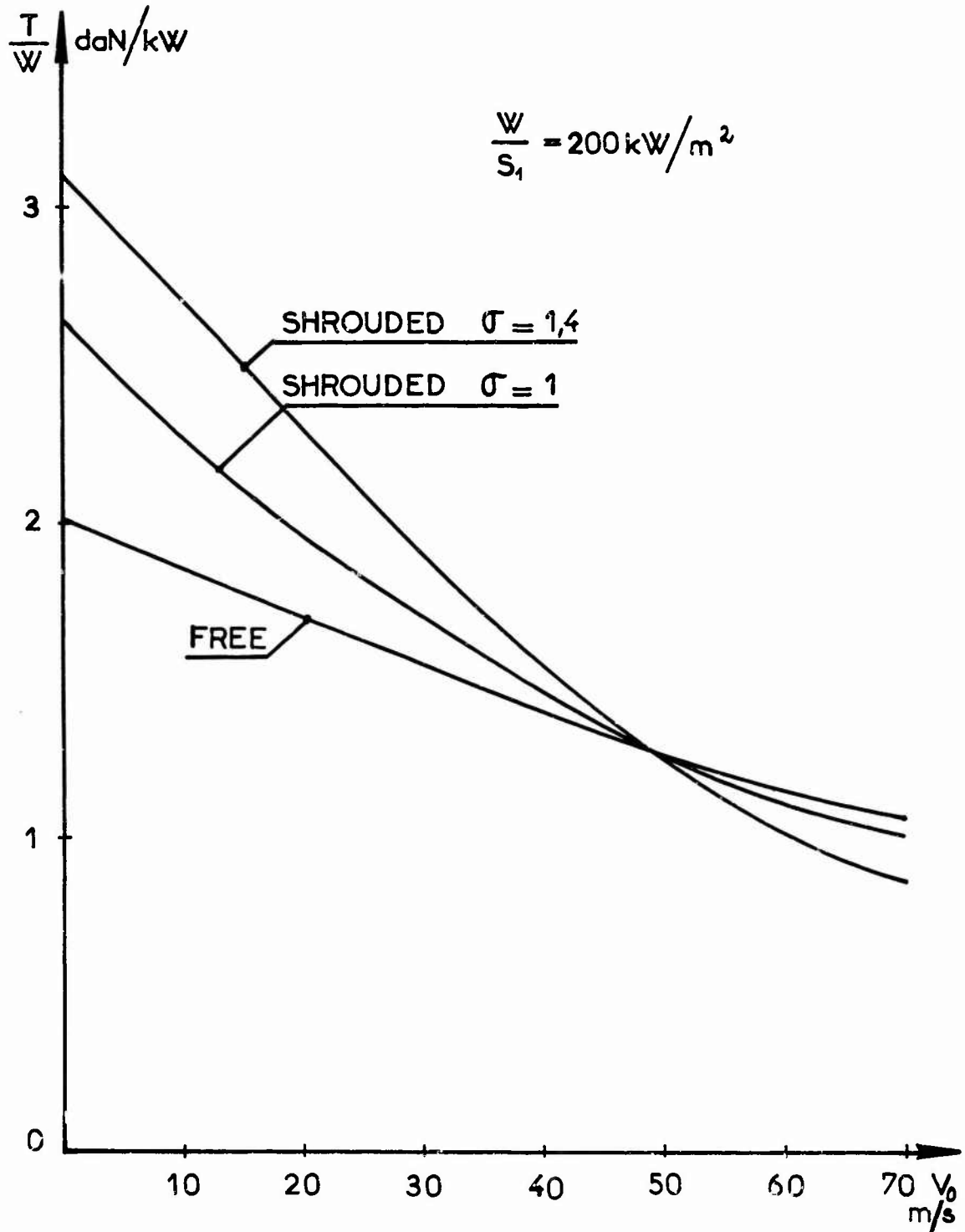


Fig. 11 Comparison with the free propeller and effect of diffusion



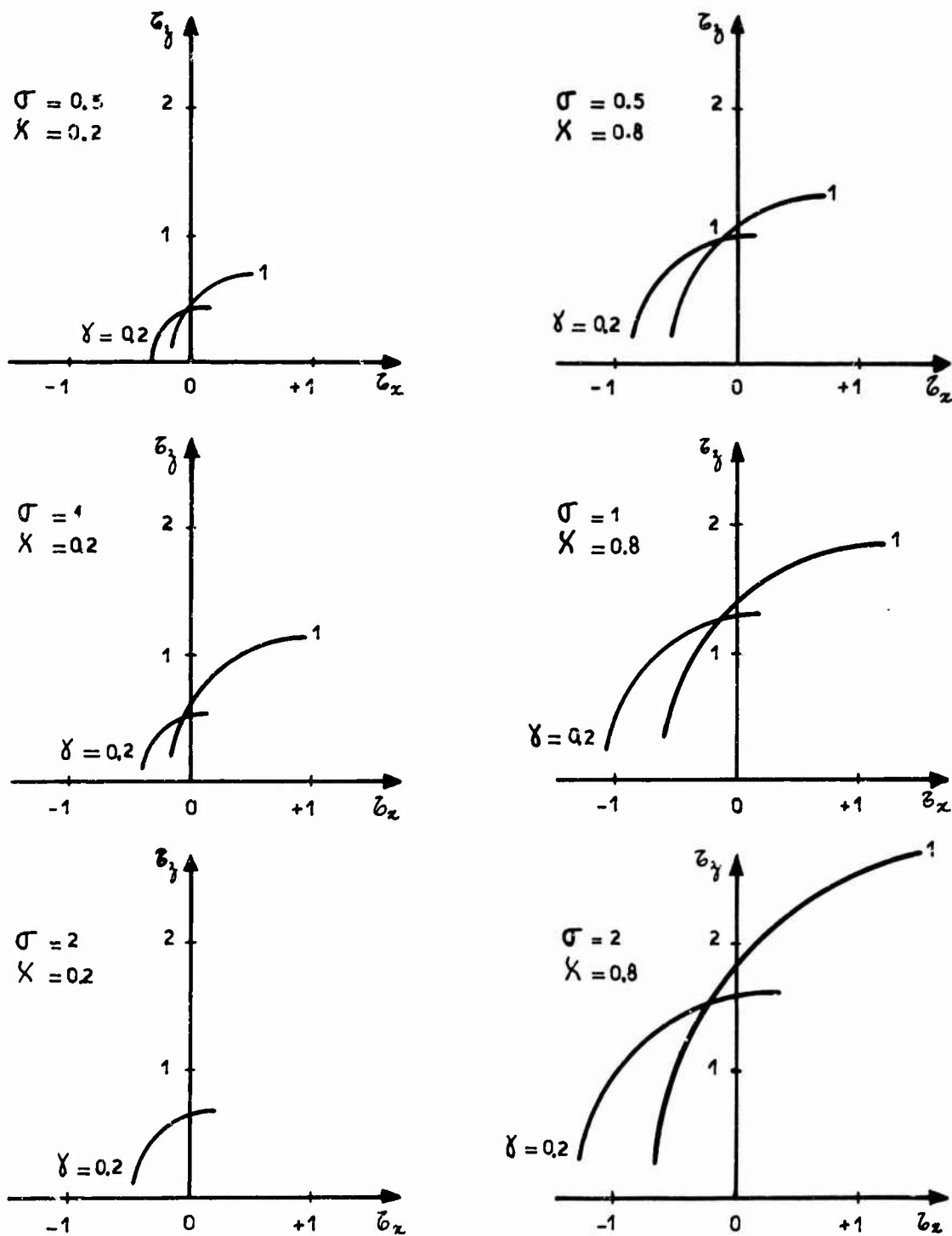


Fig.12 Polar curves of shrouded propellers, power on

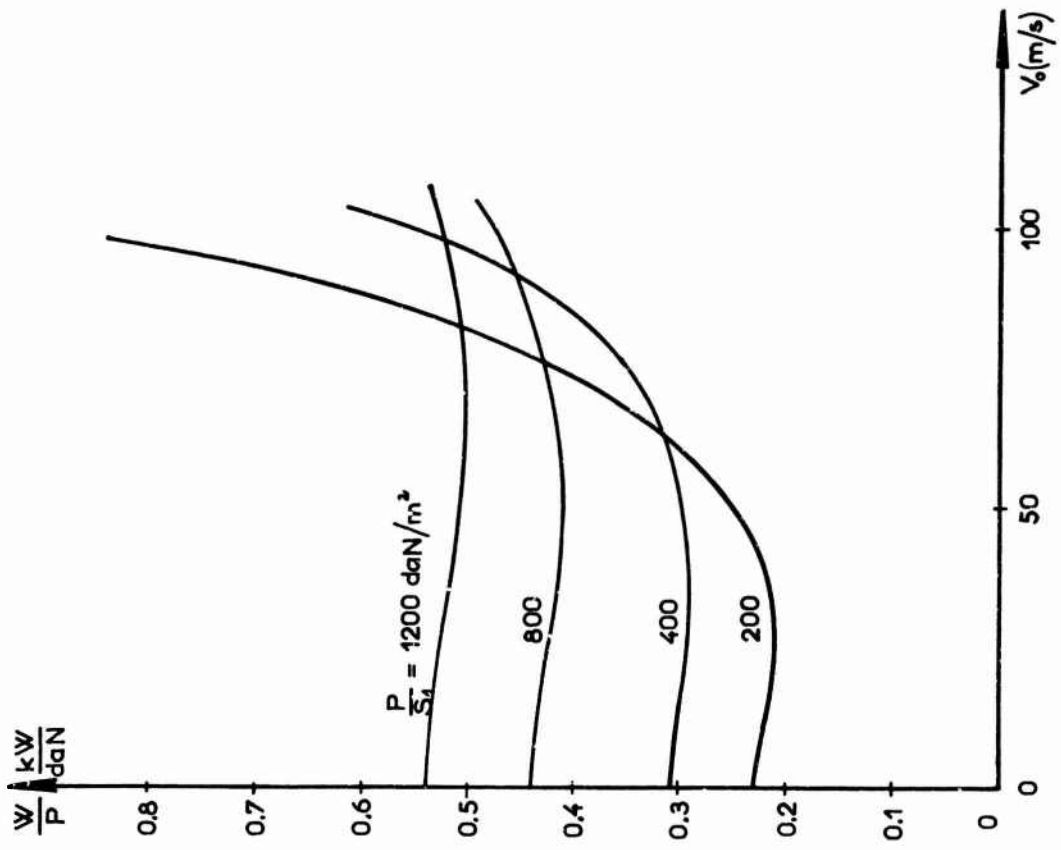


Fig. 14 Specific power, drag effect included

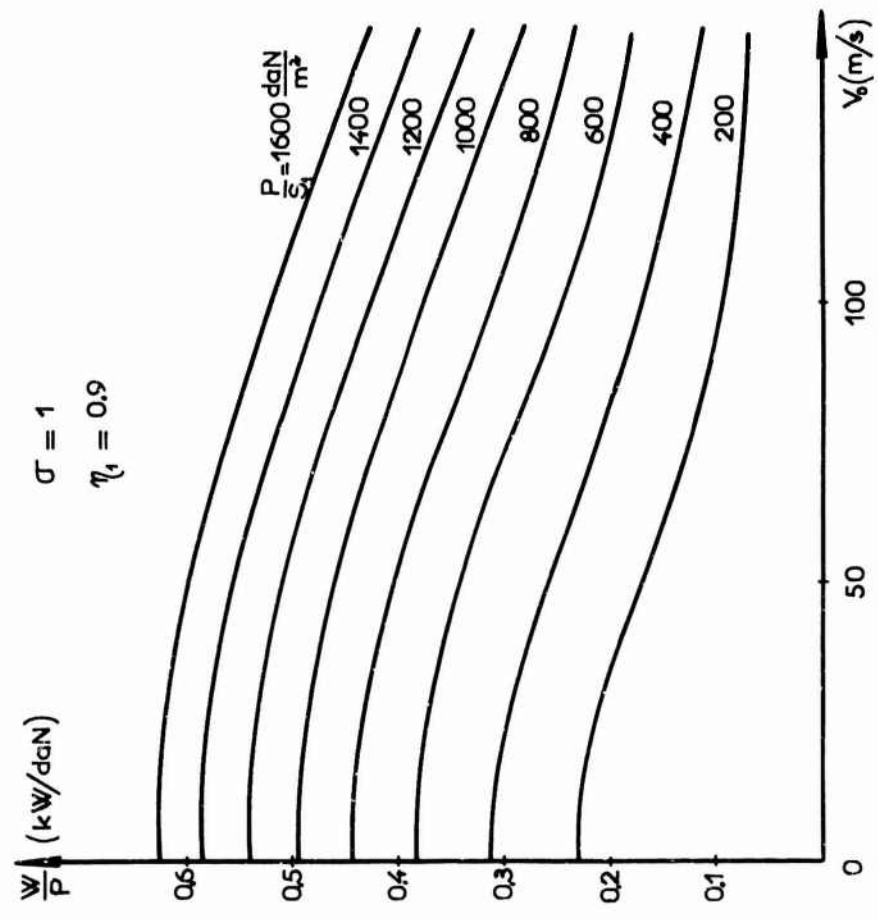


Fig. 13 Specific power (per unit weight)

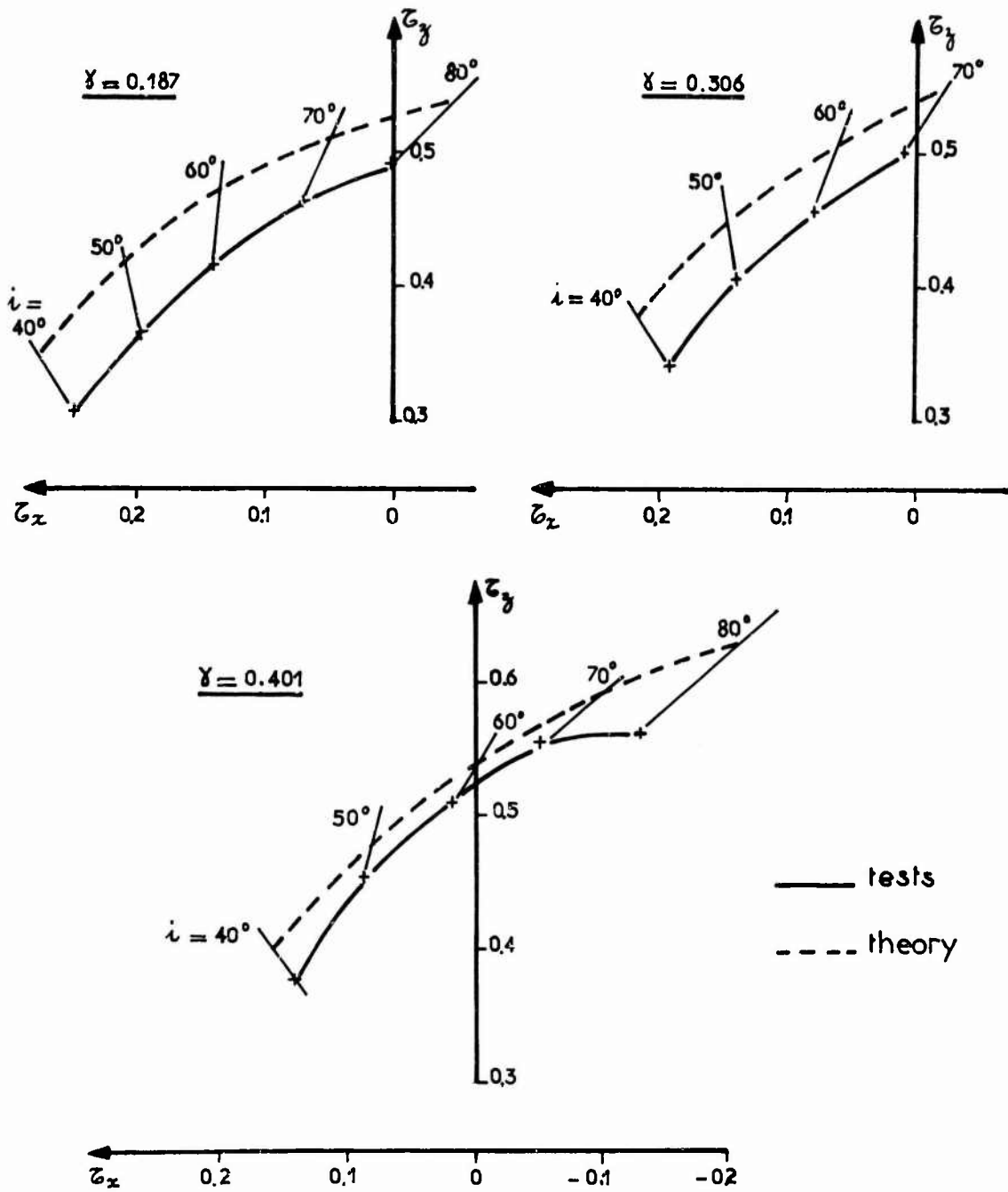


Fig. 15 Comparison of theoretical and experimental polars

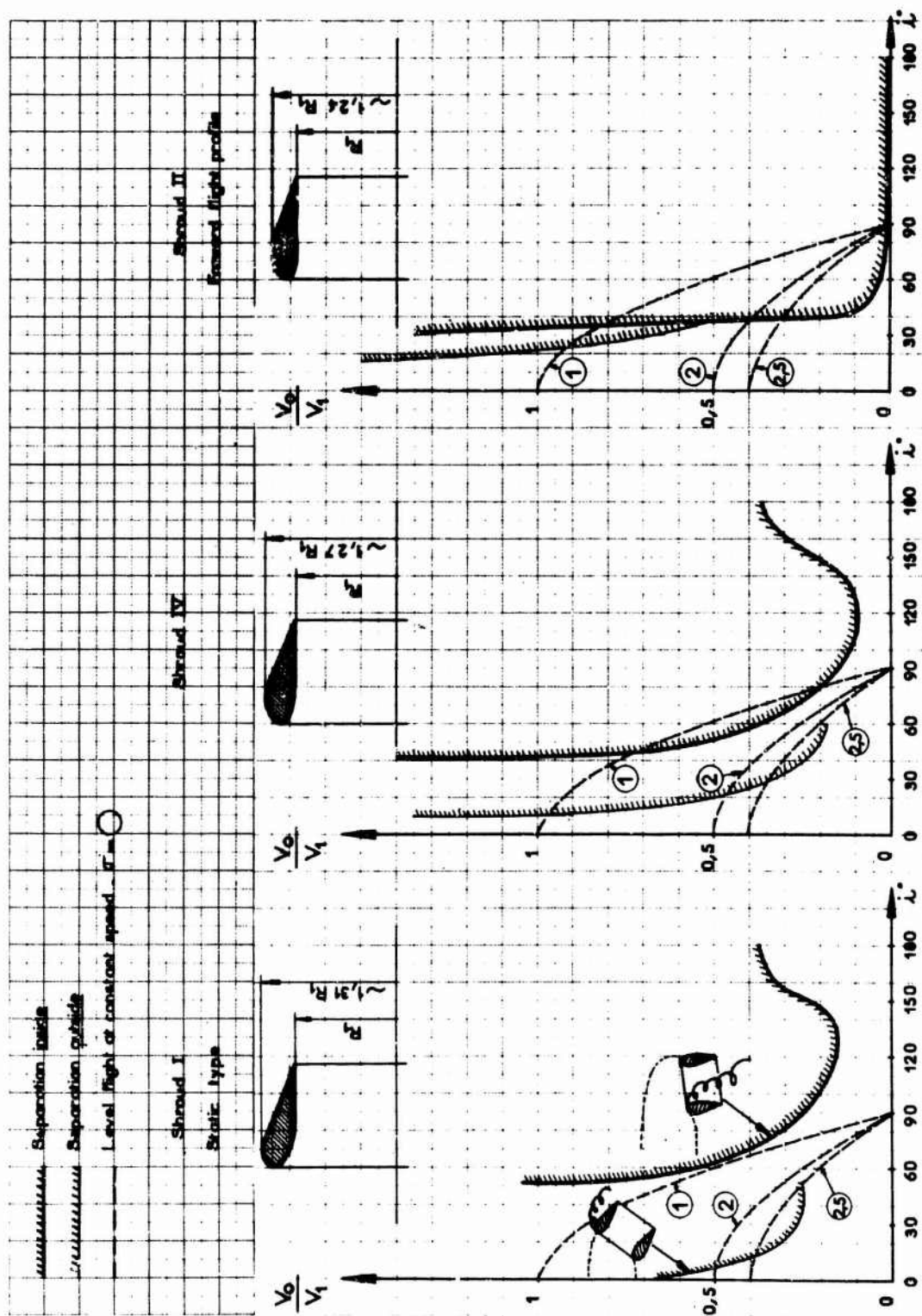


Fig. 16 Experimental limits of separation

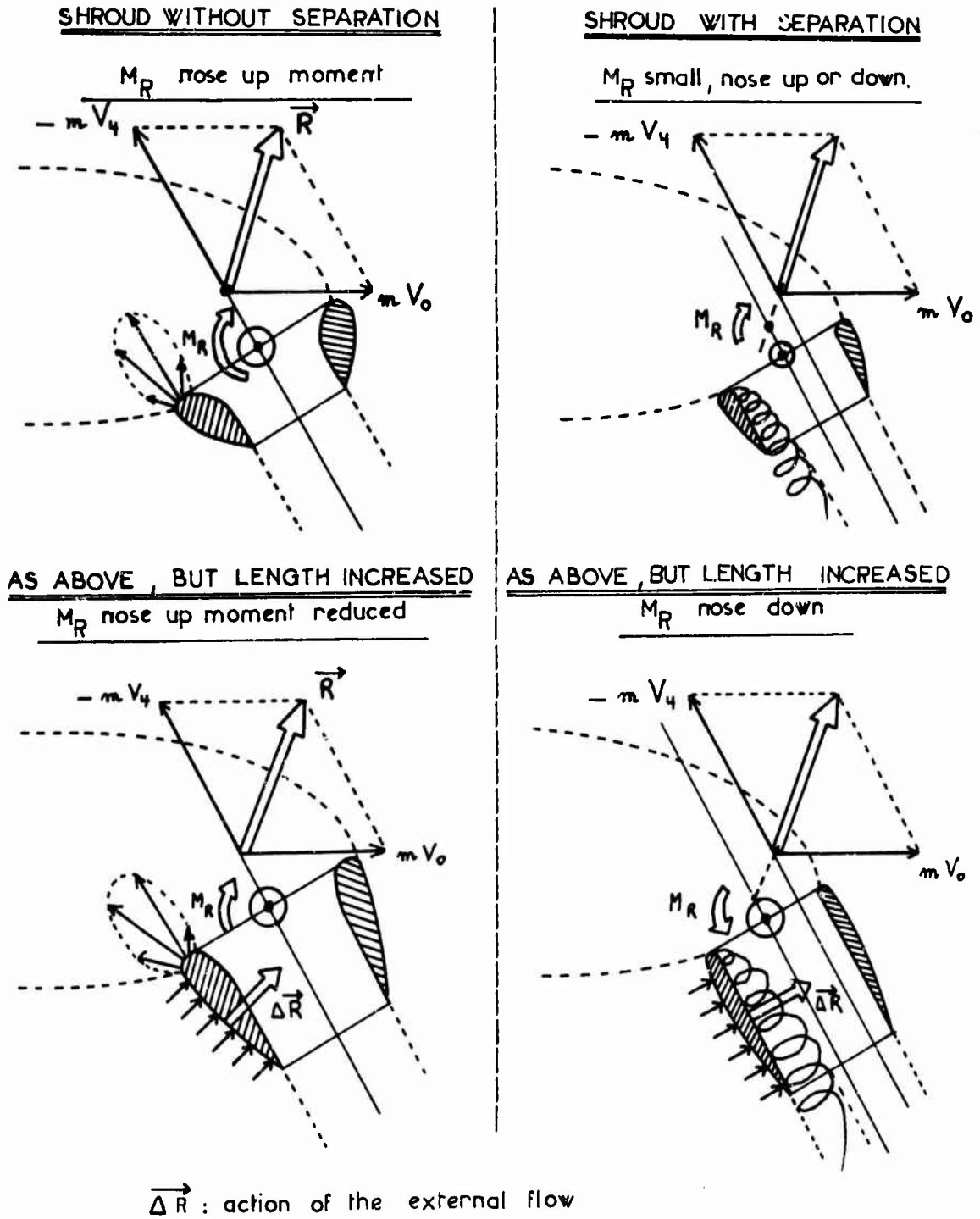


Fig.17 Physical explanation of the pitching moment

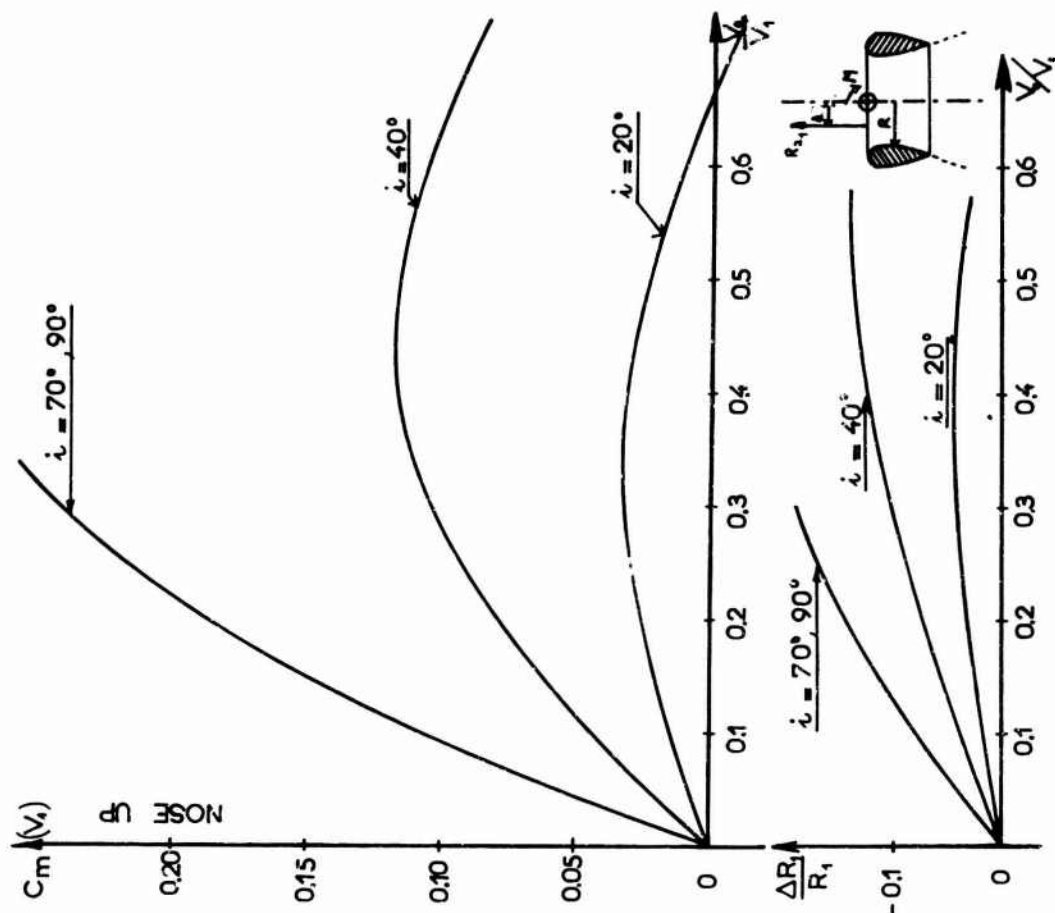


Fig. 19 Pitching moment on a shroud free from separation

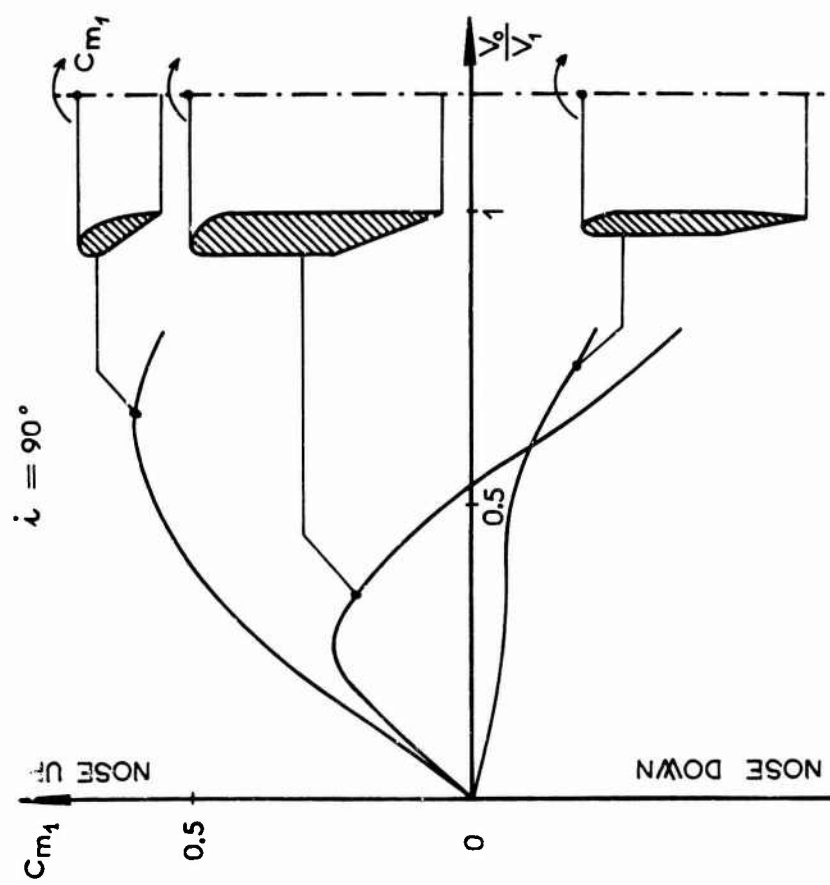


Fig. 18 Influence of the shape of the shroud on pitching moment

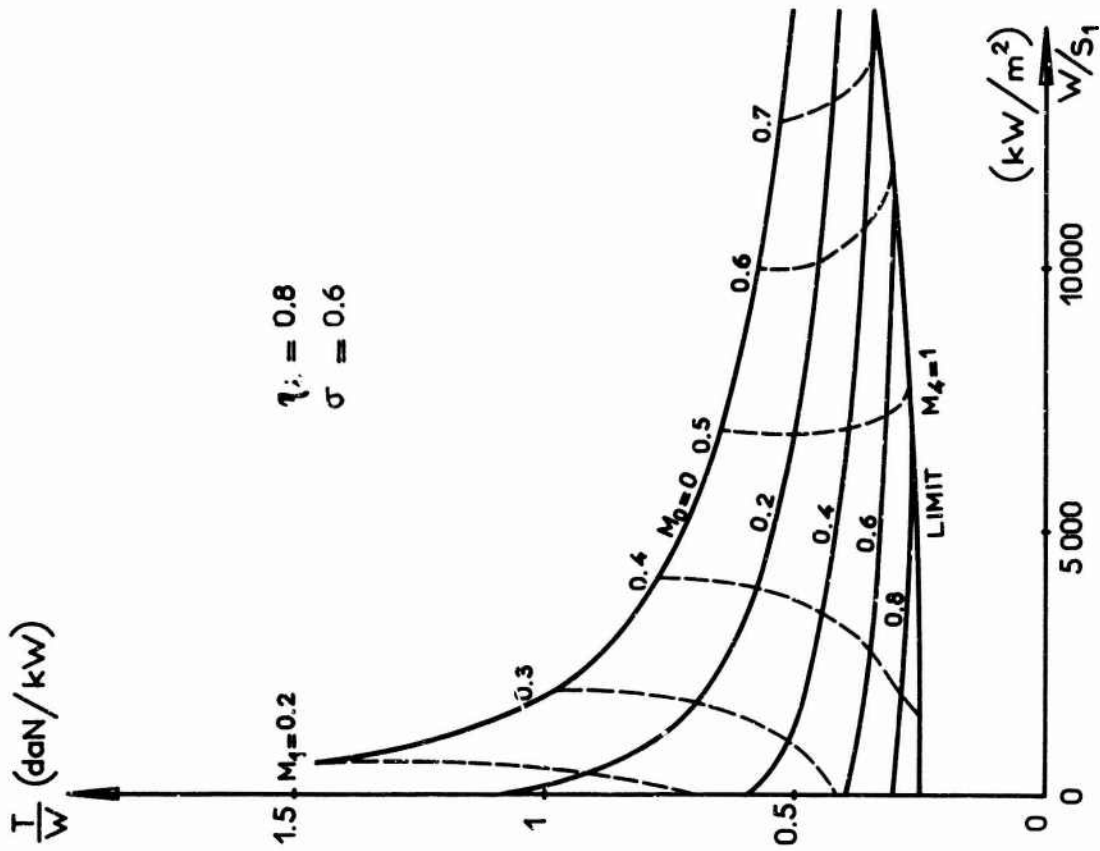


Fig. 21 Performance in forward flight. Compressible flow

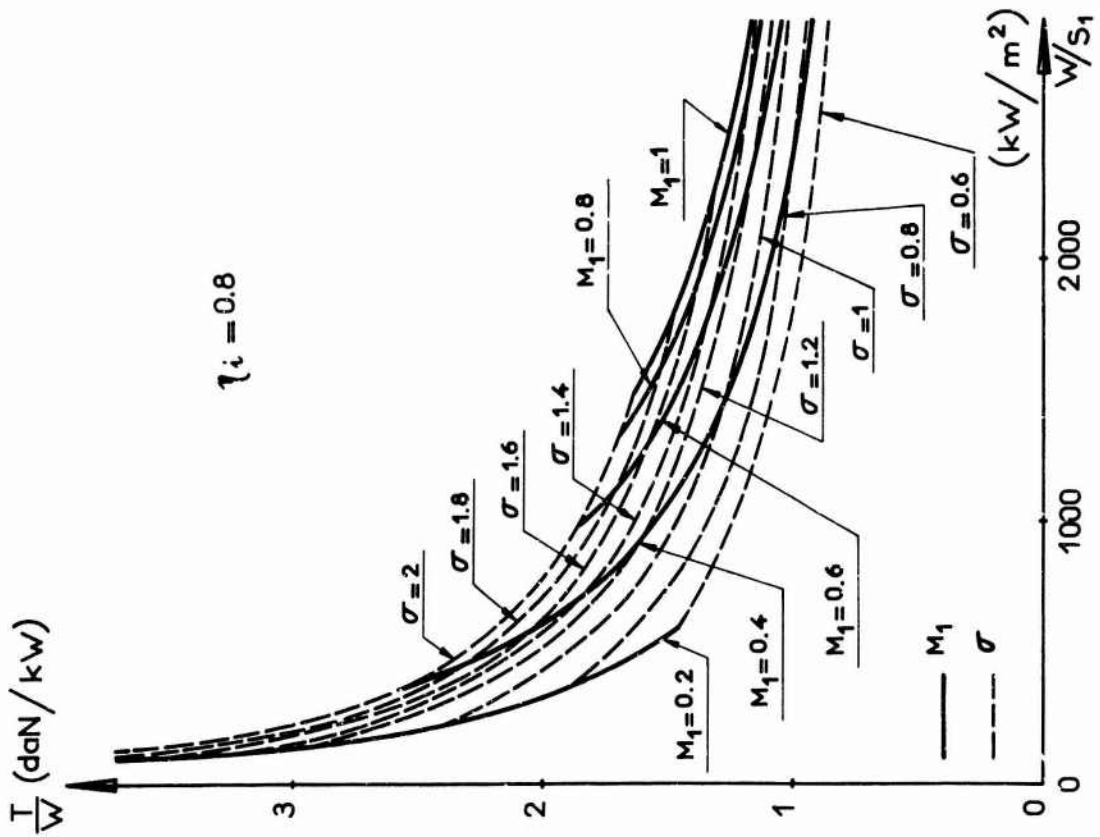


Fig. 20 Static performance. Compressible flow

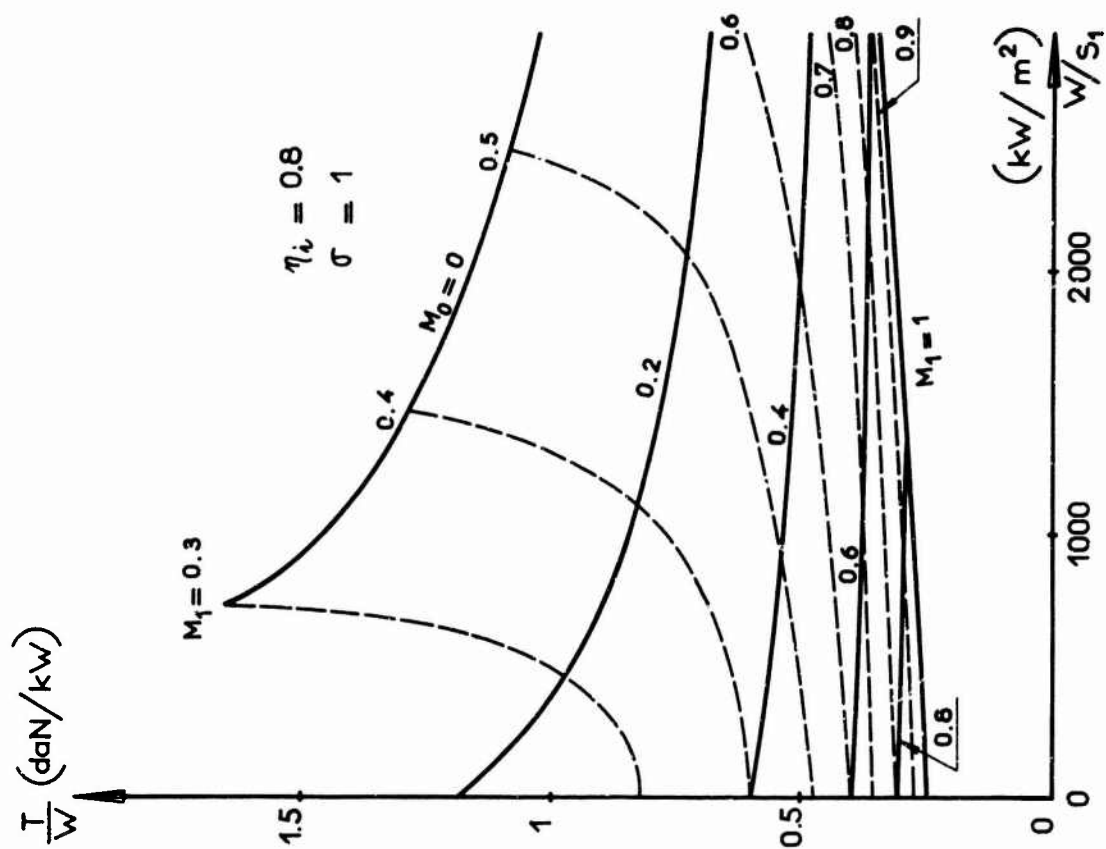


Fig. 22 Performance in forward flight. Compressible flow

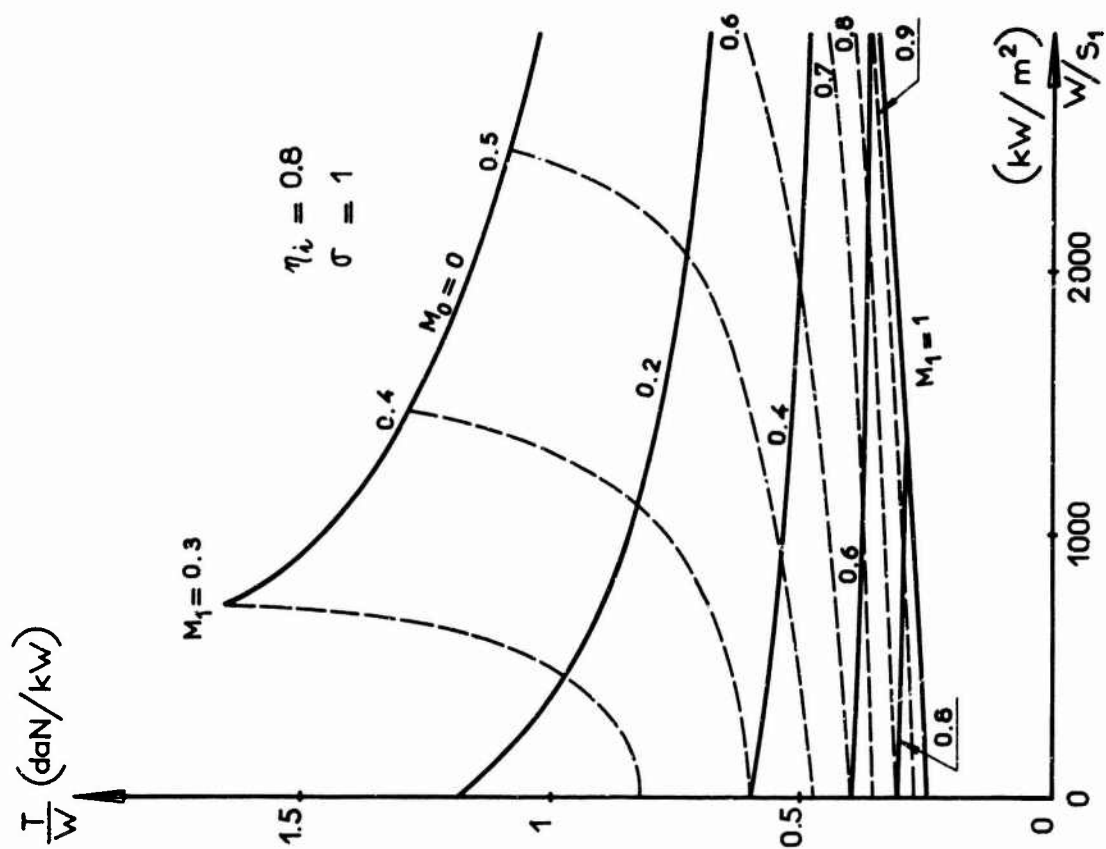


Fig. 23 Performance in forward flight. Compressible flow



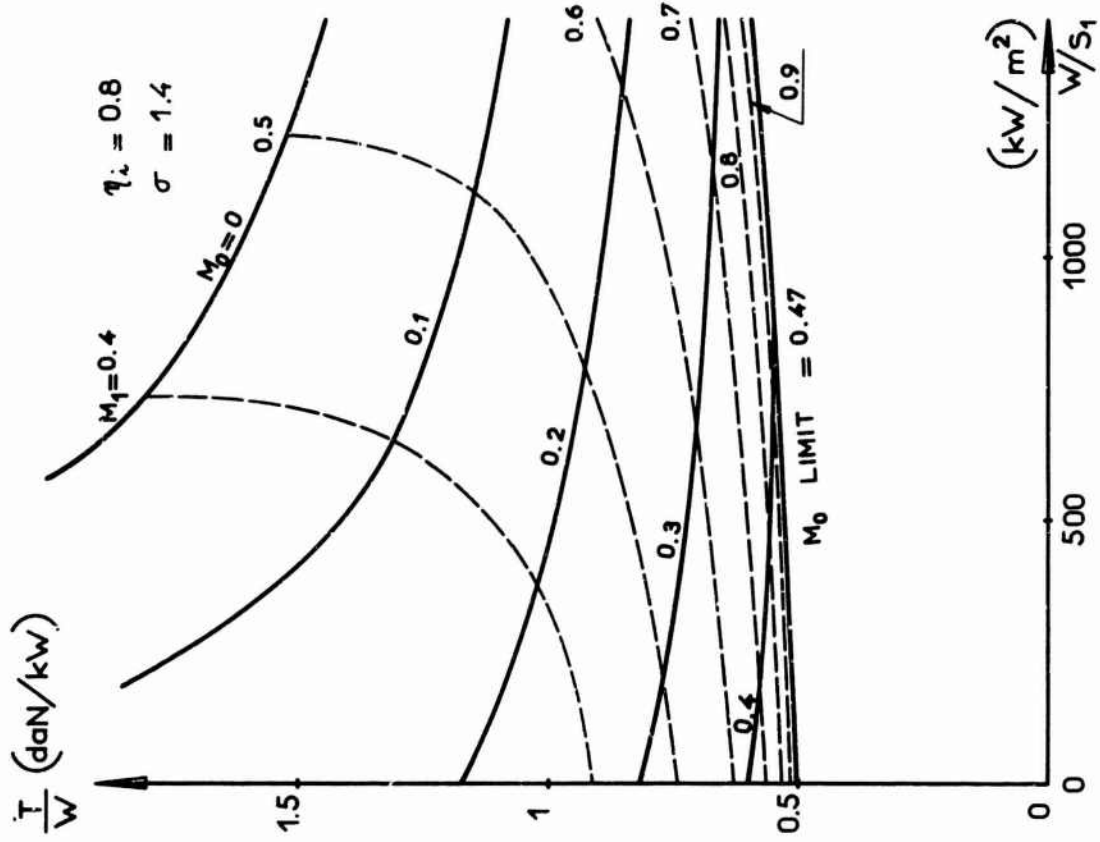


Fig. 25 Performance in forward flight. Compressible flow

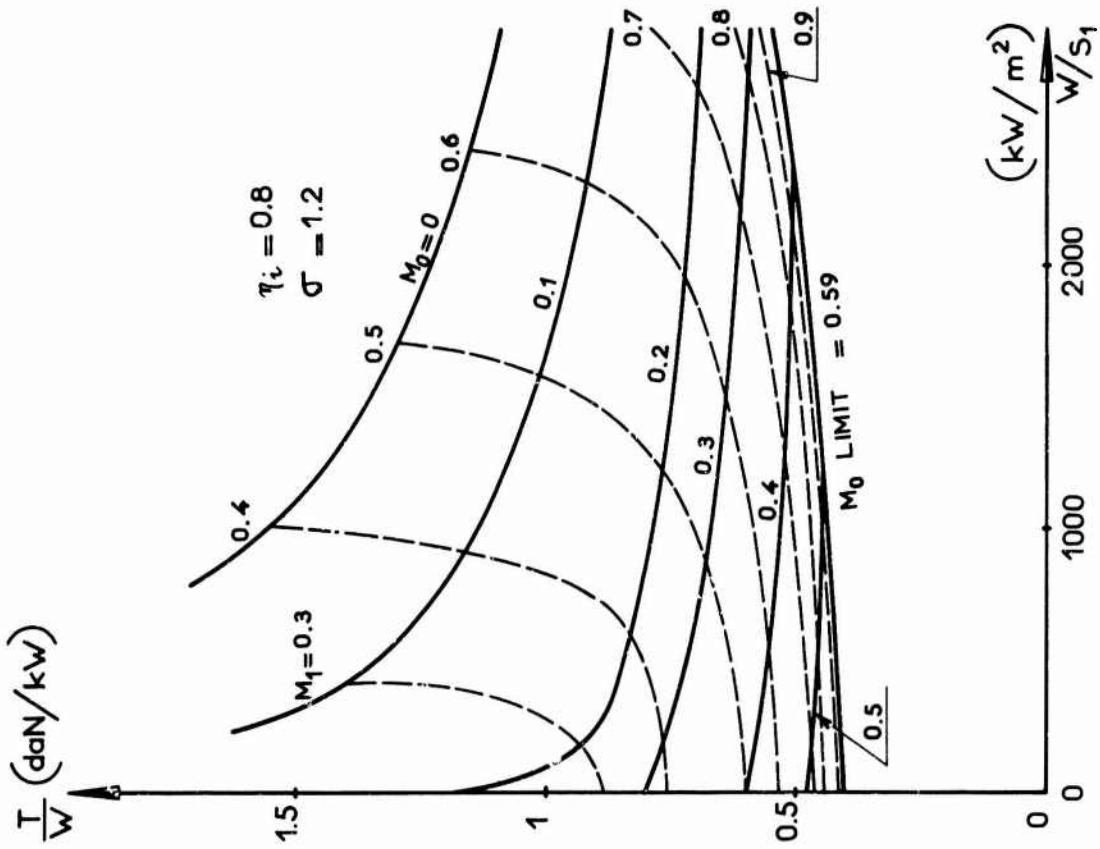


Fig. 24 Performance in forward flight. Compressible flow

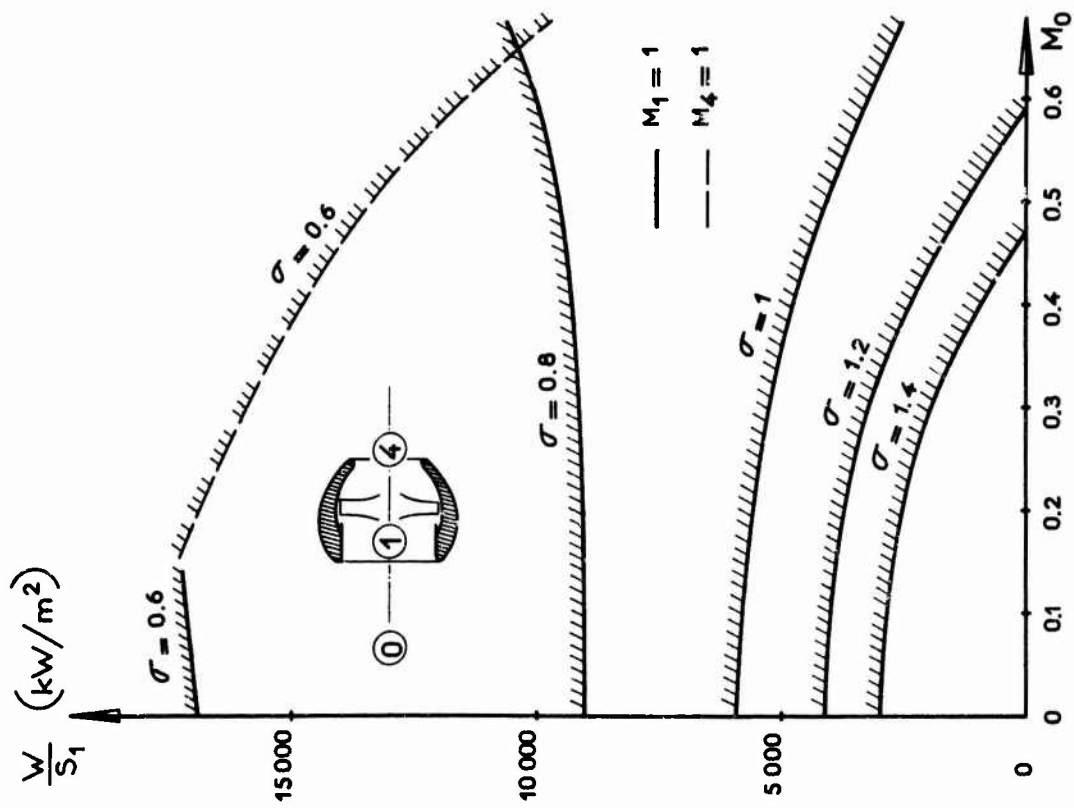


Fig. 26 Limiting conditions: Mach number 1 inside

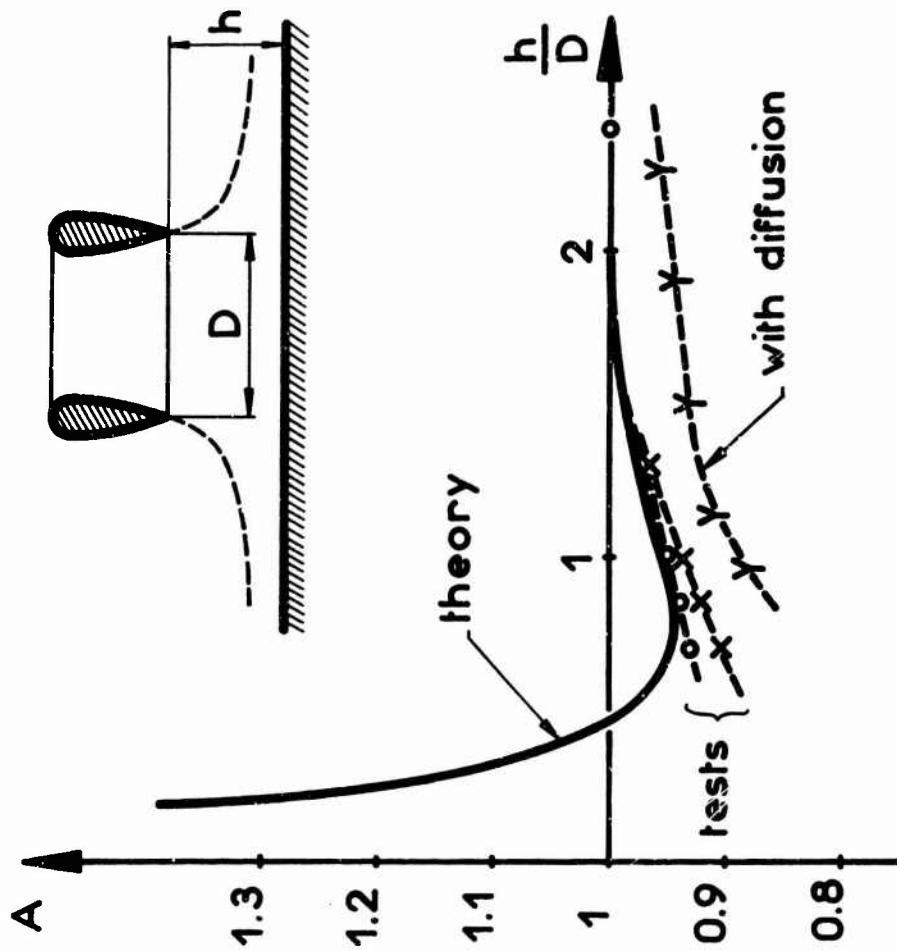


Fig. 27. Ground effect. Shrouded propeller alone

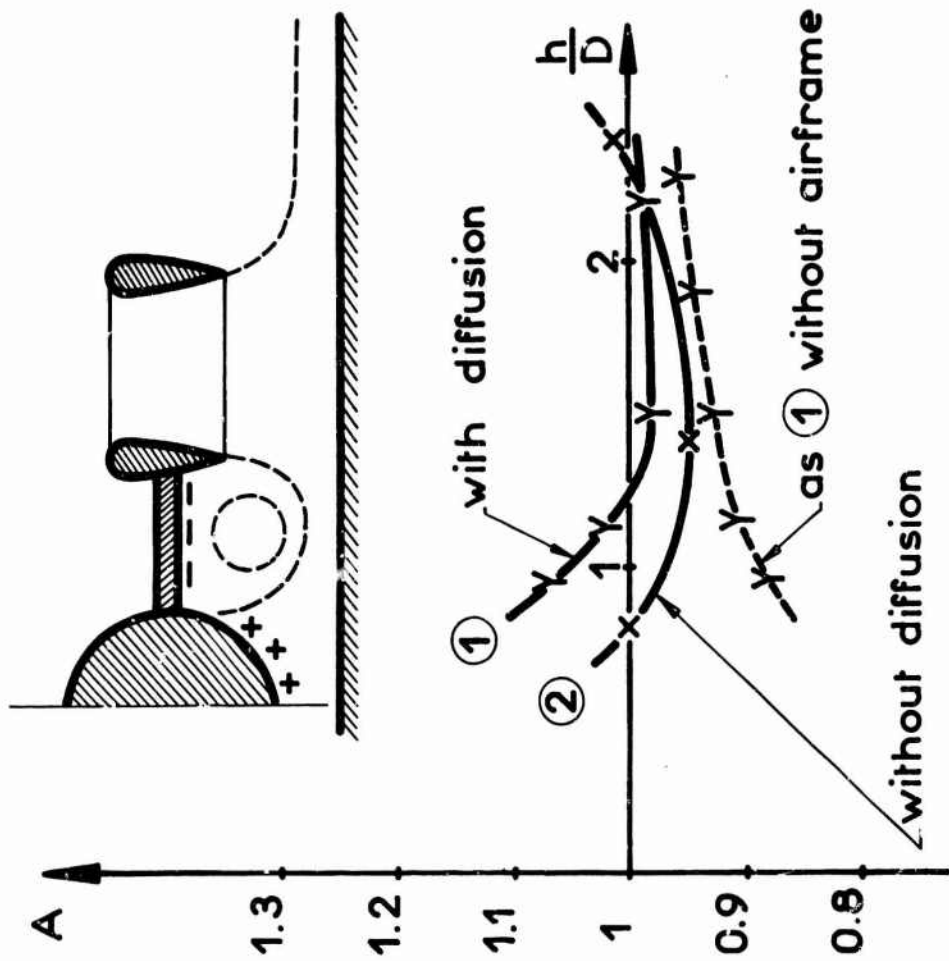


Fig. 28 Ground effect. Shrouded propeller with airframe

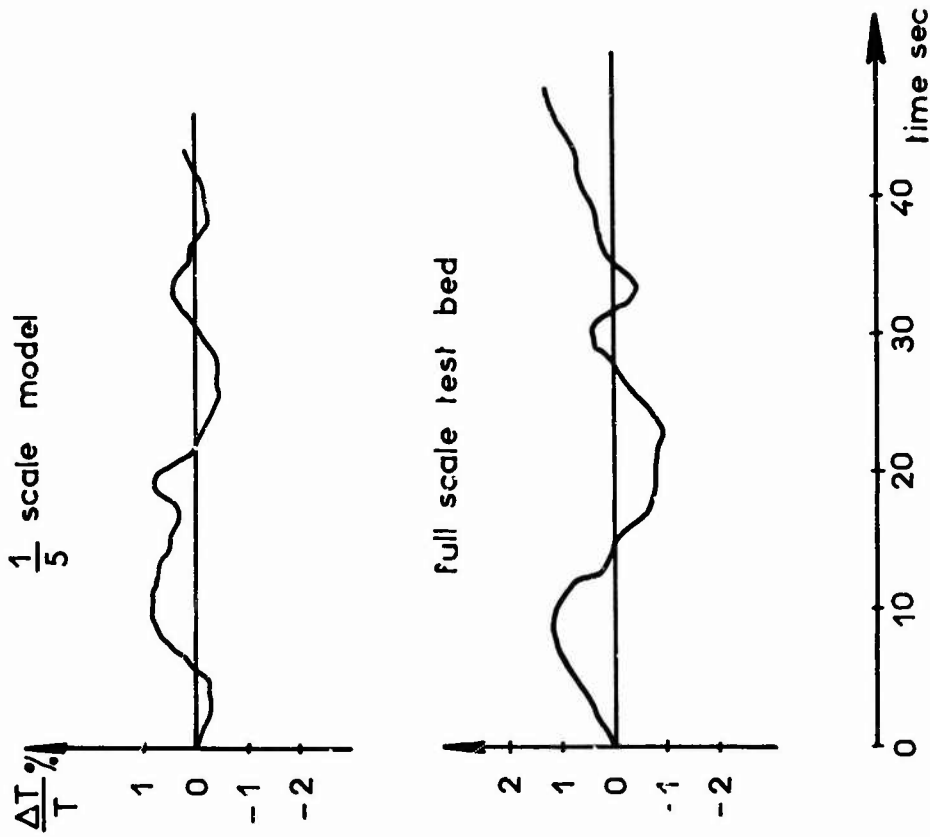


Fig. 29 Unsteady ground effect on the vertical thrust

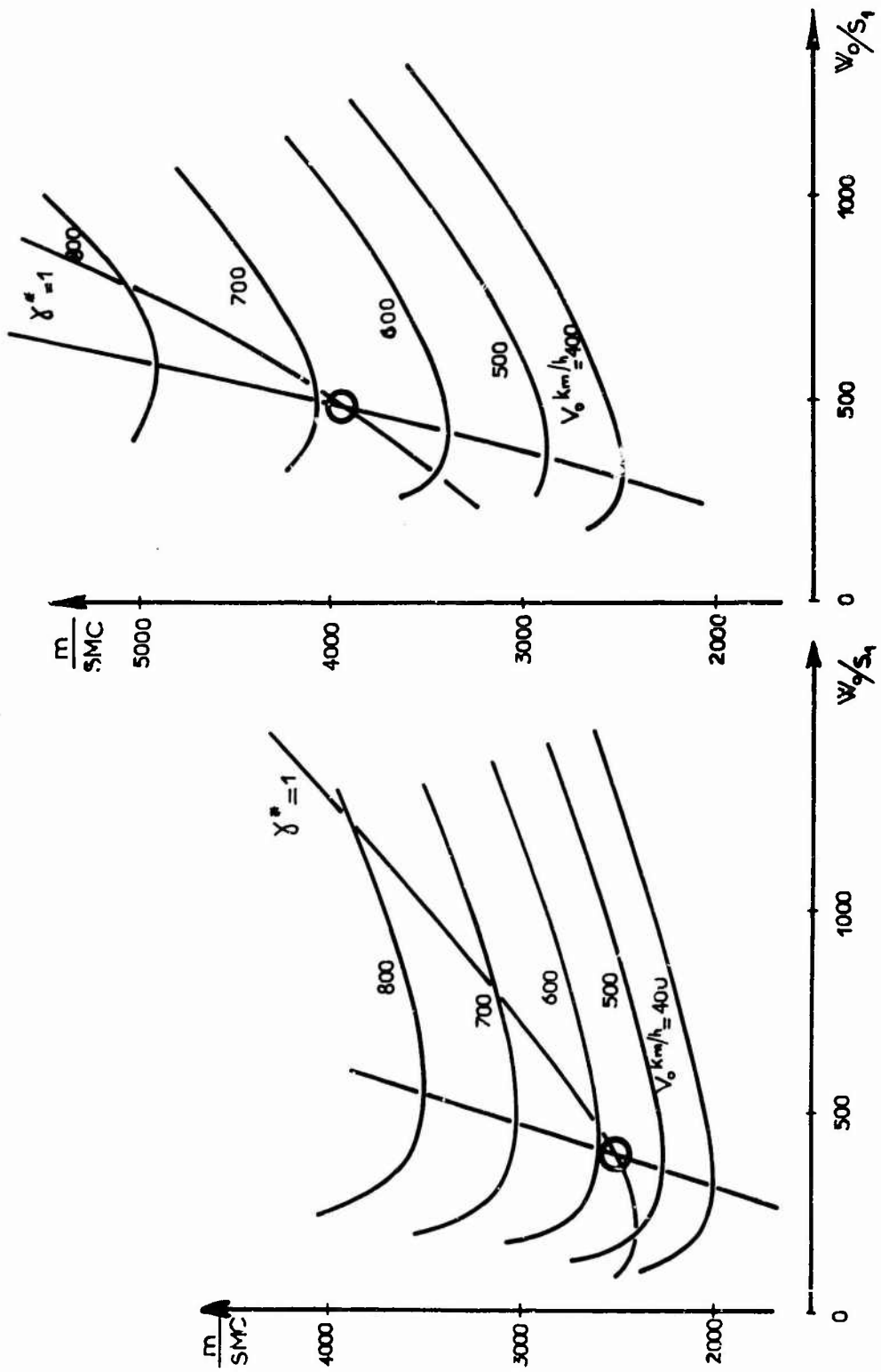


Fig. 30 Minimum mass curves

$C_x = 0.2$   
 $k = 1.1$

$m_p/m = 0.35$   
 $m_m/W_0 = 0.35 \text{ kg/kW}$   
 $m_r/S_1 = 40 \text{ kg/m}^2$   
 $C_u/S_M = 500 \text{ kg/m}^2$

$X(\text{km}) = \begin{cases} \text{---} & 500 \\ \text{—} & 1000 \end{cases}$

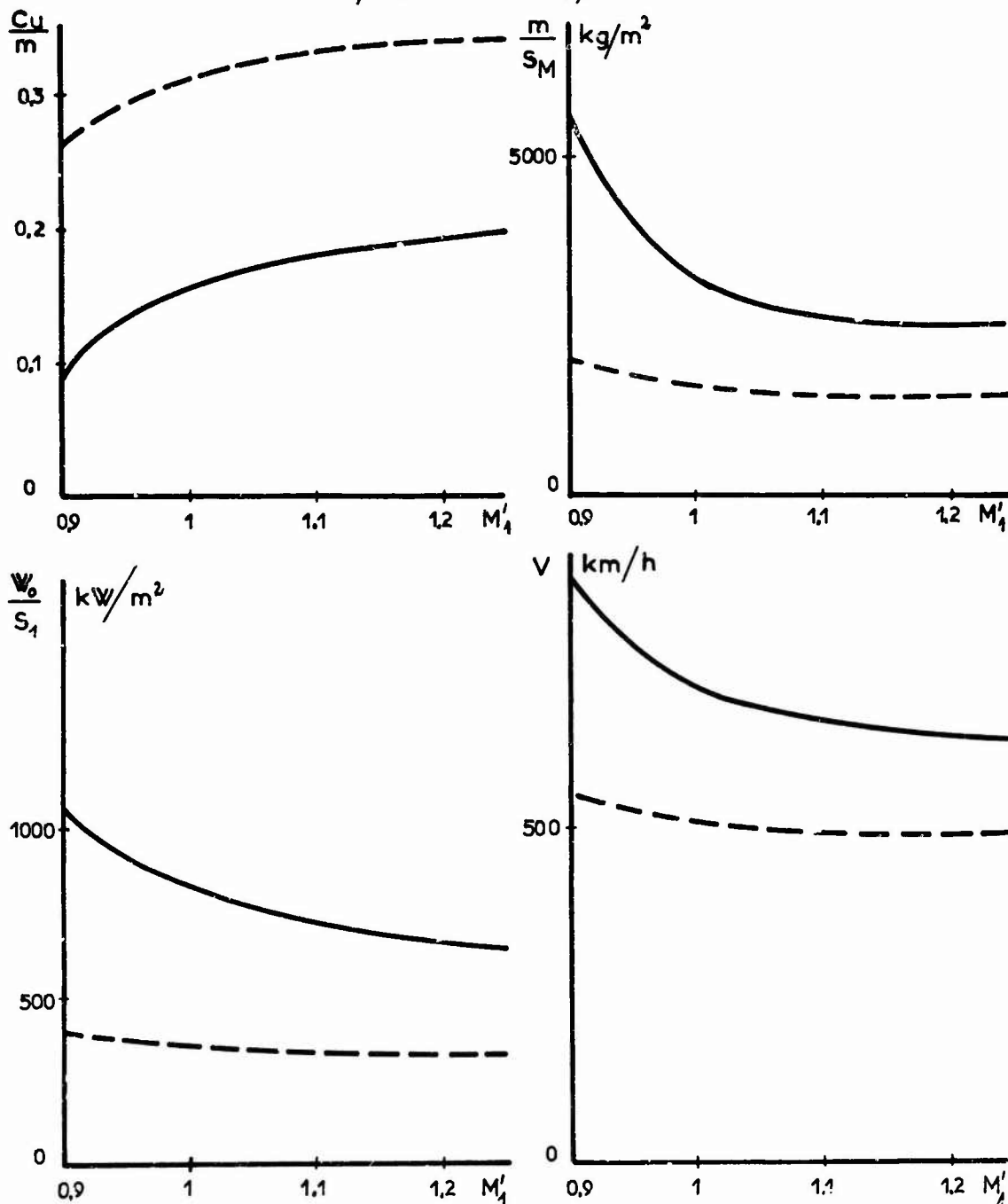


Fig.31 Minimum mass aircraft

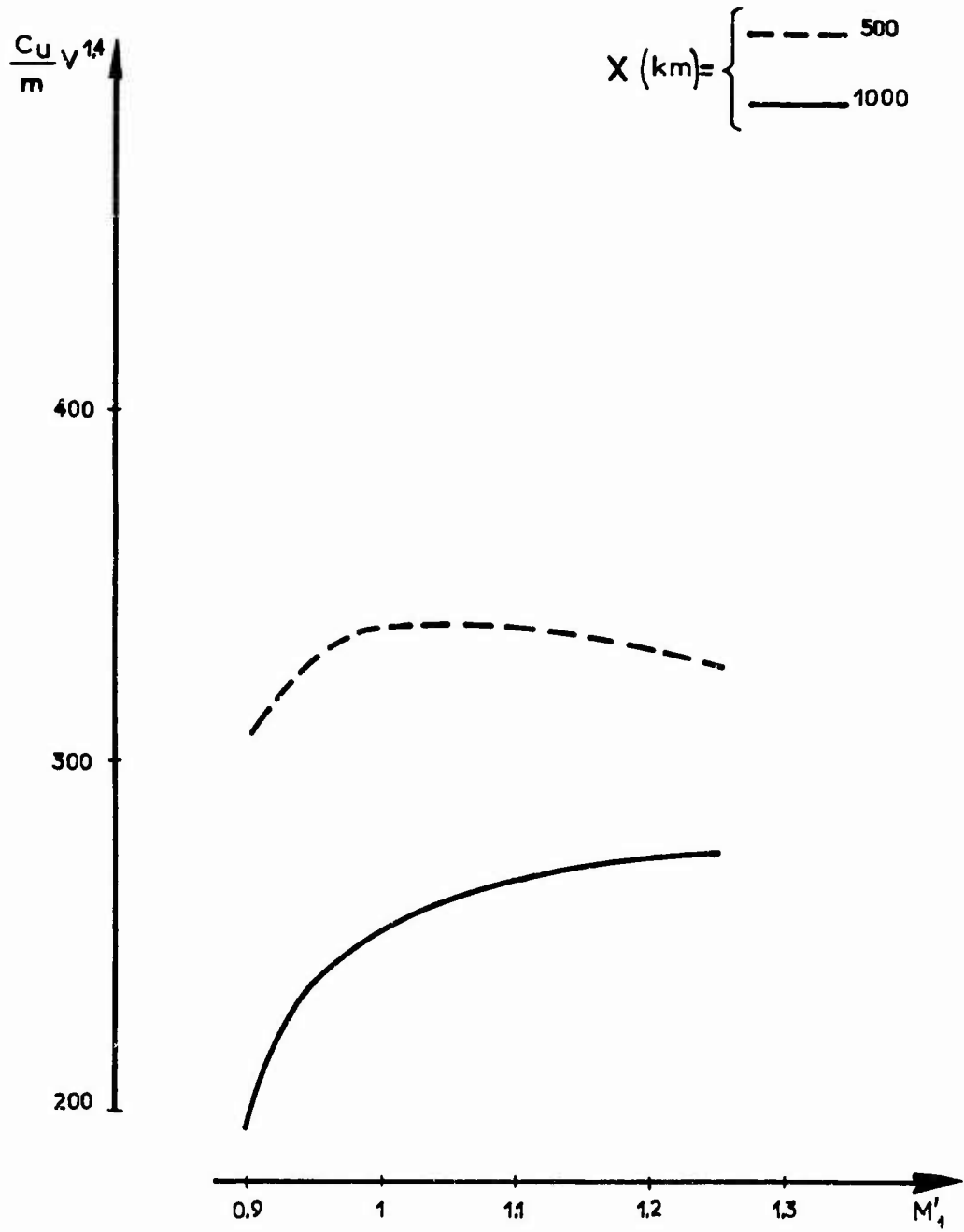


Fig.32 Economical efficiency of minimum mass aircraft

PAPER E

TURBO-JET/TURBO-FAN AIRCRAFT

by

John Williams

Aerodynamics Department, Royal Aircraft Establishment  
Farnborough, Hants, UK

## TURBO-JET/TURBO-FAN AIRCRAFT

John Williams

### 1. INTRODUCTION

#### 1.1 Jet and Fan VSTOL Aircraft Concepts

Simple jet deflection downwards to provide direct jet lift on an aircraft at take-off and landing was first studied on a modified Gloster Meteor fighter<sup>1</sup> over 20 years ago. Exploratory VTOL studies in respect of performance, stability and control at zero and low values of translation speed soon followed on hovering test vehicles, exemplified by the Rolls-Royce Flying-Bedstead lifted by two Nene turbojets, and the Hiller-Zimmerman Flying-Platform lifted by a five-foot diameter fan. Since then, accompanying the continuing increase in the thrust/weight and thrust/volume ratios of gas-turbine engines for aircraft propulsion, various jet and fan lift-engine configurations have been suggested to provide combat aircraft and transport aircraft with VSTOL capability. Several types of research and prototype aircraft have been built, and jet-lift VSTOL strike-fighters are now being produced in quantity for RAF service. Naturally, with specific aircraft projects, the preferred schemes have varied widely according to the power plants promised at the time, the aircraft role and mission postulated, and the personal experience or expectations of the particular project team involved. Also, for aerodynamic-structural-operational reasons or from personal preferences, the engine lifting systems may have been fixed inside the fuselage, the wings and extra pods, or been attached to the airframe so as to be able to tilt through large angles.

For simplicity, at least for the purpose of our aerodynamic analysis, relevant jet and fan lift-engines schemes may be divided broadly into four main groups with examples as quoted below:-

(a) *Light-weight lift-engines*, comprising pure jet or compact turbo-fan units installed in groups, intended to provide vertical lift for VSTOL purposes,<sup>26, 29</sup> though deflector systems or swivelling exits may be incorporated to expedite acceleration and deceleration during transition or to alleviate ground running problems. For example, starting with the RB.108, Rolls-Royce have developed pure jet lift-engines with thrust ranging from some 3,000 lb to 11,000 lb, and have improved the basic thrust/weight ratios from 9:1 to 25:1, with corresponding installed thrust/weight ratios from 5:1 to 15:1. Currently, compact self-contained turbo-fan lift-engines are being designed and developed with a variety of bypass ratios, providing efflux velocities down to 600 ft/sec. and with basic thrust/weight ratios of as high as 18:1. Aircraft already constructed have so far employed vertically mounted pure jet units with upper-surface intakes, such as in the fuselage of the Short SC.1 research aircraft and the prototype Mirage III V strike-fighter aircraft, as well as in the wing-mounted pods of the Do.31 transport research aircraft. However, sideways mounted engines with sideways facing intakes have also been proposed as in the HSA.129 submission for the NATO NBMR 4 military transport aircraft. Tilting lift-engines swung out from the fuselage for VSTOL, were also proposed for the US/FRG (AVS) VSTOL fighter project. Naturally, the thrust from the cruise engines may also be deflected towards the vertical to assist VTOL operation, though extra problems and performance penalties can be then introduced.

(b) *Vectored thrust (lift/cruise) jet engines* capable of thrust well in excess of that noted during conventional cruising flight and incorporating swivelling jet exits and



diverters, to provide both vertical lift and horizontal propulsion as demanded by the flight regime<sup>30</sup>. The Rolls-Royce (Bristol) Pegasus family of engines represents a well-proven practical example; with thrust approaching 20,000 lb and basic thrust/weight ratios (including vectoring nozzles) of the order 5:1. Horizontally mounted engines with front forward-facing intakes have so far been employed, such as in the fuselage of the original Hawker P.1127 prototype and the RAF Harrier strike-fighter aircraft<sup>33</sup>. For transport aircraft, such engines mounted in wing nacelles could provide STOL performance, as on the HS.681 transport aircraft project, with added groups of lift-engines in wing pods to provide VTOL performance<sup>31</sup>. The concept of tilting lift/cruise jet engines mounted at the wing-tips, as in the early Bell D.188 supersonic fighter mock-up and on the EWR-Sud VJ 101C experimental prototype now seems to have been abandoned.

(c) *Large lifting fans*, of relatively small depth compared with their diameter, usually driven by separate gas generators whose efflux could also be directed rearwards through a conventional nozzle for forward propulsion. Although practical, lift-fan and power plant integration and optimisation is not as far advanced as the pure-jet engine, a well tried example already exists in the General Electric J.85/lift-fan configuration<sup>50</sup>. As regards aircraft projects, vertical-mounted fan units with upper-surface intakes have so far usually been employed, e.g. in the wings as on the Ryan XV.5 research aircraft, and adjacent to the fuselage or propulsion engine pods as in some American project studies.

(d) *Ducted fan-propeller (lift/cruise) units* with separate gas or mechanical drive, employing either a tilting-duct layout in which the fan thrust axis tilts 90° for transition from hovering to conventional forward flight<sup>55</sup>, or a vectored thrust layout in which the fans remain in the cruise position at all times and their efflux is deflected downwards to provide direct lift for VTOL operation<sup>44</sup>. These are being discussed separately by Mr. M. Lazareff.

Mixed or intermediate arrangements of the above systems could more generally prove worthwhile for specific aircraft projects, particularly as regards the combination of jet or fan light-weight lift-engines with vectored thrust jet-engines, for combat or transport aircraft.

In addition to the problem of satisfactory engine development and engine installation for VSTOL aircraft, with minimum weight-penalty in the airframe, there are obviously a wider variety of special design considerations and problems arising from such engine/airframe integration, in order to achieve an acceptable and optimised aircraft in the VSTOL and transition modes, without unduly penalising cruise efficiency. The particular sensitivity of VSTOL aircraft performance to unpredicted aerodynamic losses or growth in weight estimates is worth special mention, along with the penalties for hot-and-high operation and prolonged hovering. Control, stability and safety requirements, together with the required or acceptable method of VSTOL operation, can have substantial repercussion on fuel requirements, payload and aircraft design weight. Here, we shall be more particularly concerned with the marked influence on the aircraft performance and stability, of the interaction between the air flow through the jet or fan engines and the external airflow about the airframe surfaces, under both static and forward-speed conditions.

*Rolling take-off and landing* procedures on VTOL aircraft designs (RTOL) can be useful to alleviate exhaust gas recirculation or ground erosion problems. But, for airfield distances less than 500 ft to clear 50 ft height (ground roll < 300 ft say), the wing aerodynamic lift gained thereby does not on balance confer a significant advantage. With greater distances, so-called STOL operation of VTOL aircraft designs can be profitable, at least for acceptable overload conditions.

*Special STOL aircraft*, employing jet or fan lift-engines to provide aircraft thrust/weight ratios of about 0.6, may of course be designed at the outset; e.g. the HS.681 jet-lift transport project. The efflux from the vectored cruise engines or pure lift-engines may then be directed away from the vertical at some optimum angle, depending on the

airframe lift and drag contributions at forward speed. However, aerodynamic augmentation of airframe lift and improvement of stability or manoeuvrability, by employing extra engine power to control the airflow over the wings and other aerodynamic surfaces, has obvious applicability for STOL in its own right. Such aerodynamic lift-augmentation schemes, which also could be usefully employed to improve the transition characteristics of VTOL aircraft, are being discussed separately by Prof. Fred Thomas.

## 1.2 Scope of Aerodynamic Discussion

Most jet and fan lift systems might nominally be expected to produce direct vertical and horizontal thrust roughly equal to the corresponding components of the rate of ejection of exhaust gas momentum. However, even *under static and zero-wind conditions*, the external airflows induced by the lifting jet or fan efflux over the airframe surface (including engine pods) can have noticeable effects on the installed lift and aircraft stability. These are especially marked near ground where there can be substantial circulation of the jet-induced free-air flow between the airframe lower surface and the ground. The intake flow is also then important, partly in that the sink-action affects the circulatory airflow pattern, but more especially in that re-ingestion of hot gas efflux may take place. Associated problems of interest include ground erosion due to the efflux impact pressure and temperature disturbed ambient conditions in the vicinity of the aircraft and possible intake ingestion of debris.

At forward speeds, or even statically in a natural wind, the lifting efflux can impose gross constraints on the external airflow past the airframe, with consequent influence on both aircraft performance and stability, during transition of VSTOL aircraft or VTOL manoeuvres, and also during STOL operation away from and near ground. The sink-action of intake flows have also proved important in relation to their influence on pressure distributions developed over airframe surfaces at forward speed, as well as from simple intake-momentum drag force considerations. An acceptable inlet flow distribution and pressure recovery has also to be provided for engine operation through the transition and for engine starting in forward flight, not merely during VTOL operation.

In the *conventional flight regime*, the aerodynamic penalties arising from the need to incorporate engine lifting systems have to be allowed for, apart from any airframe design restrictions arising from the need to minimise the aerodynamic interference effects with engine flow during non-conventional flight.

In the following sections, the detailed discussions relate mainly to research topics and examples with which the author has been directly concerned, at the Royal Aircraft Establishment<sup>2, 3, 4</sup>; a list of relevant published papers is included. Since only brief mention can be made of significant investigations elsewhere - particularly by NASA<sup>39</sup> the list of selected publications includes primarily review papers which themselves provide a substantial bibliography for further reference.

## 2. HOVERING FLIGHT

### 2.1 Basic Engine Considerations

In a practical installation, the performance of gas-turbine units can of course be reduced by factors which affect the basic engine performance, such as high-altitude, hot-day conditions, allowable ratings (continuous or emergency), and essential engine-air bleed requirements for control purposes or other services. The foregoing problems fall essentially within the province of engine research and development, and the performance effects tend to be closely associated with the particular engine design features<sup>29</sup>. The provision of satisfactory intake flow for the engine, together with the development of hot-gas recirculation flow fields, are items more directly of interest and will be considered in later sections.

The incorporation of some means of deflecting the jet efflux relative to the engine axis, either with lift engines (to help transition) or with lift/cruise engines, can introduce internal losses, while possible back pressure effects on the engine may have to be watched. For jet deflections up to  $\pm 15^\circ$  the thrust loss can be as little as 2%, even with a relatively simple deflector. For much greater deflections, elbow or cascade vanes incorporating contractions in the exit nozzle are likely to be needed. Typically, thrust losses can then be kept down to about 2%, though of course there is some added weight penalty. In practice, such thrust losses are again normally included in the basic specification of the engine performance.

## 2.2 Efflux Interference Effects on Airframe

The external flows induced over the airframe, due to entrainment of the ambient air by the jet (and fan) efflux, are relevant and important. Even under static conditions well away from ground, surface pressures below ambient are generated on the lower surface of the airframe surrounding the jet exit, thereby leading to a reduction in net lift  $L$ . For a simple circular planform with an elementary central round jet having a uniform efflux velocity distribution (Fig. 1) the lift reduction  $-\delta L$  can be about 2% of the jet efflux momentum  $T$  for a jet-exit to planform-diameter ratio  $d/D \equiv \sqrt{S_J/S} = 0.1$ , which is a practical minimum for a pure jet-lift fighter installation. But this proportional lift loss  $-\delta L/T$  becomes steadily smaller as the ratio  $d/D$  increases towards values more representative of turbo-fan or high bypass-ratio installation. If  $d/D$  exceeds 0.5, as is feasible for some large diameter fan installations, the lift-installation loss from this type of aerodynamic interference should be negligible.

The magnitude of the lift installation loss is directly related to the mixing rate close to the jet exit and hence to the decay rate of the jet potential core. The effects of jet turbulence and exit nozzle shape on the decay rate and the associated lift loss have been studied by NASA<sup>43</sup> with model and full-scale tests. An empirical correlation for the lift loss is suggested, in terms of the decay rate of the jet dynamic head  $q_x$  with the distance  $x$  from the exit, namely (Fig. 2)

$$\frac{\delta L}{T} = -0.009 [S/S_J]^{1/2} \left[ \frac{\partial(q_x/q_J)}{\partial(x/d_e)} \right]_{\max}^{1/2} \left[ \frac{d_e}{x} \right]_{\inf}^{1/2}$$

Here, "max" denotes the maximum rate of decay of the dynamic pressure in the jet, "inf" signifies the inflection point of the decay curve - at which this maximum decay rate occurs,  $d_e [= 2\sqrt{S_J/\pi}]$  is the equivalent diameter of the total exit area. It is evident that special nozzles (corrugated, etc.) designed to provide rapid mixing, in order to minimise ground erosion effects, will necessarily incur an additional installation penalty, possibly doubling the lift loss.

When many multiple jets are dispersed over the planform, the percentage lift loss might be expected to be greater than for the corresponding single jet of the same equivalent diameter-ratio  $\sqrt{S_J/S}$ . This would follow partly from the increased mixing rate, but also from the additional depression produced on the lower surface between the jets because of the constricting effect of the jets themselves on the entrained flow. Fortunately, this does not appear to be a strong effect, and the lift loss is unlikely to exceed 5% unless the jet exits are arranged in long rows or elongated narrow slots, thus tending to enclose a significant amount of the planform area. In the extreme case of the peripheral jet arrangements, the lift loss could rise to as much as 50% because of the so-called "tulip effect", while at least half the jet curtain may have to be vented to alleviate this lift loss appreciably.

### 3. LOW-SPEED FLIGHT AND TRANSITION

#### 3.1 Nature of Efflux Interference Effects with Mainstream Flow

To introduce the basic aerodynamic concepts of jet and fan efflux interference at forward speeds, it is helpful to consider first the behaviour and influence of a single cold circular jet emerging downwards at right angles to a plane wall (or airframe lower surface) into a mainstream. On leaving the nozzle, the jet is deflected downstream and rapidly distorts into a horse-shoe shape, with a pair of strong contra-rotating vortices which trail downstream at the outer edge of the jet (Fig.3), growing in size and strength with the increasing deflection along the jet. Typically, for a mainstream-speed/jet-speed ratio  $V_0/V_J = 1/10$ , the jet axis - defined from the line of maximum total head at local cross-sections - has deviated only about  $1/4d$  downstream of its static vertical path by a distance  $5d$  below the jet exit, where  $d$  denotes the jet exit diameter. The downstream deviation increases roughly as the cube of both the speed-ratio and the vertical distance. Flow visualisation studies imply that the trailing vortices are the dominant feature of the jet interference flow and are likely to be responsible for the major interference effects on the surface pressures, except perhaps close to the nozzle exit at low values of  $V_0/V_J$ . Detailed pressure measurements over the wall surface show extensive suction regions to the rear and side of the nozzle exit throughout the speed range (Fig.4); suction regions also predominate forward of the exit at values of  $V_0/V_J$  below about 0.2 though significant regions of positive pressure can arise there at higher speed-ratios.

A useful empirical expression for the jet path can be derived from direct measurements such as those by Jerdinson<sup>37</sup> and by Keffer and Baines<sup>38</sup> for a single circular jet issuing normally to a crossflow. Figure 5 shows the excellent agreement of the experimental results with a simple expression

$$\frac{X}{d} = 2.3 \left( \frac{Z}{d} \right)^3 \left( \frac{V_0}{V_J} \right)^3$$

where  $X$ ,  $Z$  are respectively the downstream and normal distances from the centre of the nozzle and  $d$  is the jet exit diameter. Further jet path studies have also been reported recently<sup>57</sup>. Unfortunately, the detailed flow mechanisms responsible for the actual deflection and distortion of the jet in a mainstream are still not fully understood. Pure inviscid-theory treatments for the jet paths cannot reasonably be formulated. Other analytical treatments have been suggested from time-to-time, by assuming that deflection is caused by cross-flow drag force on the jet, similar to the drag on a solid cylinder. Admittedly, these have nominally provided good agreement with experimental measurements, by introducing empirical values for the drag coefficient and reference cross-section areas. But the situation still remains fundamentally unsatisfactory.

#### 3.2 Theoretical Treatments of Efflux Interference

Early attempts at theoretical analysis of such complex jet interference effects involved either broad speculation or the fitting of "working formulae" to experimental results as an expediency, often without any realistic appeal to the fundamental mechanisms involved. For example, the simple circular cylinder analogy, with the jet replaced by a semi-infinite solid cylinder of about the same diameter as the jet exit, is soon seen to be totally inadequate, even for order of magnitude arguments. Figure 4 shows that the contours of constant static pressure  $C_p [= (p - p_0)/q_0]$  measured on the wall with the true jet are strongly dependent on speed-ratio, in contrast to the solid cylinder analogy. Moreover, they present vastly different distributions from those measured on the wall with a solid cylinder or the theoretical values for two-dimensional potential flow past a cylinder (Fig.6).

Some elaboration of the solid cylinder analogy approach can of course be formulated by introducing a variable geometry blockage (or line of doublets) along the jet axis, together with a line distribution of sinks along the axis to simulate entrainment into the jet.

Unfortunately, this implies the postulation of a physically acceptable blockage to give suction forces several times larger than with the simple circular cylinder, or the entrainment properties of the jet need to be arbitrarily specified as vastly greater than those under static conditions - which seems unlikely. Moreover, a variety of artificial constants seem necessary to achieve quantitative agreement over a reasonable range of speed-ratio. Such difficulties inhibited satisfactory theoretical development on this basis at RAE<sup>5</sup>. More recently, such an approach has been intensively developed with some success by Northrops<sup>51</sup>.

A more consistent and tractable framework<sup>5, 36</sup> has been formulated from "vortex sheet" representation of the jet to predict "far field" effects, consistent with the experimental observation of the strong and growing pair of trailing vortices. The jet deflection and curvature are then assumed to be solely related by inviscid theory to the differential pressure across the deflected jet sheet, whose path can be prescribed empirically. The corresponding distributions of bound and trailing vorticity along the jet path can thus be formulated, so that the induced velocity field and wall surface pressure distribution can be calculated by classical potential flow arguments using a "small-perturbation" approach. As discussed in the next section, there are of necessity some inherent assumptions in this theory which could be strongly criticised. But the fundamental concepts employed have some physical justification as a first approximation, while the theoretical results give reasonable predictions of the experimental pressure measurements on the plane wall considering the complexity of the flow field.

### 3.3 Vortex-Sheet Theory for Efflux Interference

The theory developed by Bradbury and Wood at RAE from an approach first suggested by Wooler<sup>36</sup>, adopts three major approximations:

- (a) The jet momentum flux  $J$  is assumed constant along the jet path.
- (b) The radial force on an element of the jet length  $\delta l$  is taken to be  $J \delta l/R$ , where the local radius of curvature  $R$  is defined empirically.
- (c) The mainstream flow near the jet is assumed to be predominantly along the local jet path direction and to have a mean velocity equal to the undisturbed mainstream velocity  $V_0$ .

This last assumption facilitates an analytical treatment similar to that of lifting-surface theory for finite wings. The surface of the jet plume can be dissected into a network of elementary segments  $\delta l \delta s$ , where  $s$  is the contour length around a transverse cross-section of the jet (Fig. 3). Then, following conventional arguments, the surface pressure force on the element is simulated by a bound vortex element of strength

$$\gamma \delta l \delta s = (\text{pressure force}) / \rho_0 V_0 .$$

In addition a trailing vortex filament of strength

$$(-\partial \gamma / \partial s) \delta l \delta s = -\delta l (\partial \gamma / \partial y) \delta y$$

is shed along the jet,  $y$  being the distance from the plane of symmetry. By contour integration around the cross-section of the jet, the inward normal force ( $=J \delta l/R$ ) on the element of the jet is, in vector notation, equal to

$$\delta l \oint \rho_0 \gamma \mathbf{V} \times \delta \mathbf{s} = (\rho_0 \mathbf{V}) \times \left( \delta l \oint \gamma \delta \mathbf{s} \right) .$$

where  $\mathbf{V}$  denotes a velocity vector of magnitude  $V_0$  in the local jet direction. Likewise, the local contribution to the trailing-vortex doublet strength

$$-\delta l \int y \frac{\partial \gamma}{\partial s} ds \equiv \delta l \int \gamma \frac{dy}{ds} ds = \frac{1}{\rho_0 V_0} \frac{J}{R} \delta l .$$

Hence, assuming that the trailing vorticity shed by each jet element follows the path of the jet, the total "doublet" strength of the trailing vorticity passing through an element position distance  $l$  from the jet-exit becomes

$$(1/\rho_0 V_0) \int_0^l (J/R) \delta l .$$

Now the magnitude and direction of the velocity induced by either a vortex or vortex-doublet element of length  $\delta l$  depends only on the orientation and strength  $\gamma \delta l$  of the element and on the distance of the point away from the element. Thus, at distances large compared with the cross-sectional dimensions of the jet, the velocity field induced by the surface distribution of vorticity of the jet element length  $\delta l$  will approximate to that due to a simple transverse bound-vortex element of strength  $(J \delta l / \rho_0 V_0 R)$ , together with a simple trailing vortex doublet element of strength

$$(J \delta l / \rho_0 V_0) \int_0^l (dl/R)$$

inclined along the local jet direction, both located at the local centre of the jet plume. Consequently, the computation of the velocity at such a "far-field" point outside the jet requires only knowledge of the path and momentum flux of the jet.

#### *Criticism of the basic theory*

Before discussing the major objections and some possible refinements to the basic theory, it is worth comparing theory and experiment for the case of the single circular jet issuing normally from an infinite plane wall into a mainstream. Estimates of the surface-pressure distribution on the wall, derived by the method outlined above with the empirical expression given in Section 3.1 for the jet path, reproduce effectively the shape and magnitude of the experimentally determined pressure-distribution contours, particularly at a velocity ratio  $V_0/V_J = 0.125$  (Fig. 4a). Thus the basic theory would appear to have some practical value and justify further refinement.

Unfortunately, the proposed mathematical model of the flow rests on a number of assumptions which, though plausible as a means of making the problem tractable, still have to be justified on fundamental grounds. For example, there is little justification for the development of an inviscid model of the flow, except perhaps by invoking classical arguments that the major region of the flow field can be treated in inviscid terms provided the boundary conditions take account of the viscous flow at the edge of the jet. A clarification of the fundamental mechanism by which the jet is deflected would be valuable for this purpose, as mentioned earlier. Next, the assumption of constant momentum flux along the jet, despite the entrainment of mainstream air, is as yet only supported by its successful application in jet-flap theory, together with broad classical arguments which are scarcely tenable in the present case of large deflections. The remaining major assumption, that the mainstream flow near the jet can be taken as moving predominantly along the local jet path direction with velocity  $V_0$ , is naturally questionable, even as a first approximation. It effectively implies that the jet is inclined at only a small angle to the undisturbed mainstream flow, whereas evaluation of the pressure distribution around a circular jet shows clearly that the bulk of the induced velocity is generated from jet regions where the jet angle is still large. Nevertheless, despite all these misgivings as regards the theoretical model, comparisons with experimental results so far available suggest that the theoretical estimates for the distribution of vorticity along the jet path are at least realistic as a useful working basis for analytical studies on jets emerging from an infinite wall.

#### *Extensions to the basic theory*

Thus far, the treatment has essentially been a "far-field" theory, since any point at which the induced velocity is calculated is assumed to be far distant from all parts of



the jet, the growth and distortion of the cross-sectional shape of the jet - as distinct from the jet path - then being shown to be of secondary importance. Naturally, in the "near-field" region close to the jet-exit, some allowance should be made for the initial jet shape and size and perhaps also for the entrainment of mainstream air into the jet. For a circular jet, a line of sink/source doublets could be taken to simulate the initial "shape-blockage" effects and a line of sinks to allow for the entrainment; the doublet strength being proportional to the jet diameter and the sink strength being defined to a first approximation by the known entrainment properties of a jet in still air. Such corrections have been examined and appear to have only a minor effect on the overall suction force generated on the wall. Further detailed measurements and correlation of jet paths and surface-pressure distributions are needed to establish more firmly the validity of the basic vortex-sheet theory, as well as to specify more precisely the nature of the "near-field" corrections and the significance of jet-exit geometry with regard to the prediction of the surface-pressure distribution induced on the wall.

Finally, the extension of the theory to the practical case of a *finite* wing with a jet issuing from the lower surface needs to be considered. At first sight, this could involve simply the computation of the downwash velocity field induced over the wing by the vortex system already defined in terms of the jet path and momentum flux, followed by the usual derivation of the wing-surface loading consistent with this downwash distribution. However, two important factors have so far discouraged progress along these lines. Firstly, theoretical methods currently available for estimating wing loadings seem quite inadequate to cope with the large downwash (and sidewash) variations induced by the jet vorticity. Secondly, recent RAE measurements on a simple wing, of rectangular planform (aspect-ratio 4.6) with a centrally located jet ( $d/c = 0.1, 0.15$ ), have revealed surface-pressure distributions which could not be explained even approximately by any linear theory as a simple extension of the solution for an infinite wall or flat-plate. Figure 7 shows the changes in wing upper-surface and lower-surface pressure distributions due to the jet efflux for the typical case of jet-diameter/chord = 0.15,  $V_0/V_J = 0.25$ . The jet efflux is seen to have only a small effect on the flow over the upper surface, but there is a region of strong positive pressure on the lower surface ahead of the jet which has no counterpart in the corresponding infinite flat-plate pressure distribution, e.g. Figure 4a. No surface vorticity distribution could be expected to produce such differences between the two sets of results.

Frankly, these are real problems which must be clarified and solved before the satisfactory estimation of jet (and fan) efflux interference effects on finite wings can proceed on more than a semiempirical basis as at present. Although valuable progress has been made by the formulation of the theoretical vortex-sheet framework discussed here, further attempts at development along such lines seem of doubtful value until the mechanisms of jet deflection and the growth of the vortex field are better understood, and until radical advances have been made in wing lifting-surface theory to allow for the unusual type of downwash field associated with a deflecting jet. Similar and perhaps even stronger criticisms can be directed at the full blockage/sink approach mentioned in Section 3.1.

### 3.4 Correlation Parameters for Efflux Interference

For basic analysis and correlation of jet (and fan) efflux interference effects on overall forces and moments, the non-dimensional increments in the lift  $\Delta L/T$ , pitching-moment  $\Delta M/TL$ , drag  $\Delta D/T$ , etc. arising from jet (or fan) operation can usefully be examined. Here, the reference jet thrust will be taken to be the measured total efflux momentum rate  $T$  or total installed static thrust  $T_1$  as convenient or available. As discussed in section 2, the latter may be two or three per cent smaller than the former. For a specific airframe and exit geometry, and for each prescribed attitude of the airframe to the mainstream direction, the non-dimensional force and moment increments ( $\Delta L/T$ , etc.) resulting with cold jets are primarily a function of the speed ratio  $V_0/V_J$ . From our experience, the further influence of jet efflux Reynolds number  $R_J (= V_J d/\nu)$  and model Reynolds number  $R_c (= V_0 \bar{c}/\nu)$  on jet interference effects appears to be of

second order. The influence of temperature and compressibility effects can reasonably be included by correlation on the basis of momentum ratio or an "effective speed-ratio"

$$(V_o/V_J)_e = (V_o/V_J) (\rho_o/\rho_J)^{1/2} .$$

rather than the simple speed-ratio, where  $\rho_o$  and  $\rho_J$  represent the mainstream and jet densities respectively. This follows from classical arguments that jet paths and jet induced flows tend to depend mainly on the momentum flux ratio for a prescribed geometry. Moreover, comparative pressure-plotting results for hot jets and cold jets emerging from a plane wall certainly support this assumption (Fig. 8), though admittedly our own quantitative evidence relates as yet only to temperatures up to 300°C and pressure-ratios up to choking with jet diameters of 1 inch.

The use of a jet momentum coefficient  $C_J [= T/q_o S]$  instead of  $(V_o/V_J)_e$  as a basis for correlation has some attractions, but has not such generality as in the analysis of jet-flap (and blowing BLC) results with thin jet sheets. For a round jet, the jet path geometry relative to the wing (or body) dimensions, varies with the relative size of the jet exit area to planform area  $S_J/S$  at a prescribed  $C_J$  value, and the jet interference effects vary likewise. The "vortex sheet" theory mentioned in Section 3.3 suggests that, if the jet path  $(X,Z)$  can be expressed in the form  $Xf(n)/d = \text{function} [Zf(n)/d]$  where  $f(n)$  is some function of  $n = (V_o/V_J)_e$ , then certain similarity laws will hold of the type

$$(\Delta L - \Delta L_o)/T = \text{function} [(S/S_J)^{1/2} f(n)] .$$

Here  $\Delta L$  and  $\Delta L_o$  signify the measured lift increments from jet operation under forward speed and static conditions respectively. This could lead to some unique correlating parameter, which is equivalent to  $C_J$  for jet-flap work, but here will involve an additional parameter such as  $(V_o/V_J)_e$ .

For example, the approximate relation given in Section 3.1 for the path  $(X,Z)$  of a single jet can be written as

$$Xn^{1.5}/d = \text{function} [Zn^{1.5}/d] .$$

Far-field vortex-sheet theory then implies that

$$(\Delta L - \Delta L_o)/T = \text{function} [(S_o/S_J)^{1/2} (V_o/V_J)_e^{3/2}] .$$

Thus, the ratio

$$(S_o/S_J)^{1/2} \cdot (V_o/V_J)_e .$$

or a "power coefficient"

$$(V_J/V_o)_e (T/q_o S) .$$

might be postulated as a simple correlation parameter, to take area-ratio as well as effective speed-ratio into account. But more evidence and analysis is needed to support this.

With non-uniform distributions, some equivalent mean jet velocity will need to be specified, or a distribution weighting-factor derived. The effects of special nozzle exit modifications, to accelerate mixing for the alleviation of ground erosion, or to alleviate hot-gas recirculation and noise, will also ultimately have to be examined and taken into account.



### 3.5 Basic Efflux Interference Effects on Airframe

#### *Simple wing configurations*

Early experimental results on a simple rectangular-wing model with a centrally located jet established that the lift increment  $\Delta L/T_1$  produced by operation of the jet falls steadily below its static value of unity as the speed ratio  $(V_0/V_J)$  is raised from zero (Fig.9). This lift loss is accompanied by the expected nose-up pitching-moments, again increasing as  $(V_0/V_J)$  is raised, partly because of the steady growth of the downward load from jet interference on the lower surface behind the jet and partly from rearward movement of the centre of this jet interference load; the increase in drag associated with the jet interference is only a small proportion of the installed thrust. The marked sensitivity of the jet interference effects to the value of  $S_J/S$ , the jet exit area to planform area ratio, is amply confirmed. At very low area ratios with  $\sqrt{(S_J/S)} < 0.04$ , admittedly of academic interest,  $\Delta L/T_1$  actually falls to zero! Fortunately, for more practical area ratios, the lift fall-off and accompanying nose-up moments are much less severe. For example, with  $\sqrt{(S_J/S)} \approx 0.1$ ,  $\Delta L/T_1$  here falls only to a minimum of 0.75 at about  $V_0/V_J = 0.2$ , and the nose-up moment then corresponds to about 0.1c forward shift of the static lift centre. The subsequent recovery of lift and eventual lift magnification at the higher speed-rat'os are accompanied by a substantial drag rise and are worth noting, at least from fundamental aspects, since the interference flow regime is probably vastly different from that at low speed-rat'os.

As regards jet disposition, rearward location of the jet exit naturally tends to alleviate the lift fall-off and the nose-up moments arising from jet interference, since the surface extent aft of the jet exit is reduced. Furthermore, with multiple jets, there is some evidence to suggest that the speed-ratio range over which the lift fall-off occurs can be much reduced and the subsequent lift augmentation much increased by the adoption of a spanwise row arrangement towards the rear of a wing instead of a close cluster, though the nose-up moments and drag interference simultaneously tend to increase at a given speed-ratio (Fig.9(b)). The jets may then act as a crude jet-flat or line-source on the wing lower surface and thereby generate extra lift by supercirculation, but significant areas of flow separation are likely to be present on the rear lower surface in practice. Such rearward positions could well warrant further aerodynamic study, possibly with some extra surface-flow control aft as well, as a method of providing favourable interference on lift and lift/drag ratio at practical speed-rat'os. Chordwise rows seem attractive in that the interference moments produced are much less than with a cluster of jet about the same centre, while the lift losses also tend to be slightly less (Fig.9b). In all these cases, variations of wing incidence does not seem to influence significantly the jet interference effects, except at high values of the speed-ratic.

#### *Simple body-wing configurations*

Even with lifting jets emerging from a body (pod, nacelle or fuselage) rather than a wing surface, the jet interference effects can still be significant, since there may be appreciable surface areas downstream of the jet exits, while the wing lower surface may also be close by. Such effects were examined first on a series of simple body models at RAE without and with unswept wings of various sizes. For example, with a single large lifting jet centrally located in a bluff body<sup>6</sup> [ $\sqrt{(S_J/S)} = 0.5$ ], the lift increment  $\Delta L/T_1$  due to jet operation decreases, roughly as  $(V_0/V_J)^2$  at first, falling from unity to 0.9 by  $(V_0/V_J) = 0.3$  and reaching a minimum of 0.73 by  $V_0/V_J = 0.6$  (Fig.10). With wings added, the initial fall is accelerated as the span is increased, being almost doubled for the high wing with  $\Lambda = 3.1$ , and trebled for the corresponding low wing; the lift minimum tends to occur earlier, but the subsequent lift recovery and augmentation are much increased. With such a relatively short body, the nose-up moments correspond to only a small movement of the static thrust centre, e.g. at  $V_0/V_J = 0.3$ ,  $\Delta m/T_1 d \approx 0.04$  and 0.06 for the body alone and for the low wing configuration respectively. The drag induced by jet efflux interference is likewise small and does not vary greatly with the wing configuration, e.g.  $\Delta D/T_1 \approx 0.02$  by  $V_0/V_J = 0.3$ .

Similar investigations on a more elongated pod with a smaller area ratio<sup>7</sup> [ $\sqrt{S_j/S} = 0.24$ ] show much more significant effects, particularly when the jet is located forward of the body centre (Fig.11). Again, rearward movement of the jet from  $x/l_b = 0.4$  to 0.6 provides some alleviation of lift losses and nose-up moments about the jet-exit centre. In this case, the addition of a *high* wing even further alleviates the lift loss, presumably because favourable wing circulation effects are induced, though this is accompanied by greater nose-up moments.

#### *Efflux interference alleviation*

From the preceding arguments, unfavourable efflux interference effects on lift could in principle be minimised, even made favourable, by rearward movement and special arrangements of the jet or fan exits. Favourable effects from using jet exit locations near to the under-surface of a deflected trailing-edge flap also have been demonstrated recently at NASA<sup>47</sup>. However, for complete practical aircraft such as will be discussed in later sections, trim and other layout considerations restrict the range of such possibilities. From a performance aspect, some improvement may be provided naturally by reducing the efflux-momentum (i.e.  $T_1$ ) as much as can be allowed by usable aerodynamic lift available from wing incidence at the appropriate forward speed.

Some alleviation of unfavourable efflux interference effects has been attempted also by the addition of streamwise fences to the lower surface of the airframe, along each side of the exit. In specifying such an arrangement, it seems important that the depth of the fence should be at least an exit diameter  $d$ , and the streamwise length at least  $2d$  so as to extend forward of the exit as well as bounding the sides (Fig.23). Flow visualisation studies suggest that the fences reduce the initial curvature of the jet, thus increasing the penetration of the jet and delaying the growth of the trailing-vortex flows. This is consistent with the apparent negligible effect of the fences at low velocity ratios, where the rate of deflection of the jet is inherently small.

### 3.6 Efflux Interference Problems on Jet-Lift Aircraft

#### *Scope of considerations*

With pure jet-engine arrangements, or fan-engines of *small* bypass ratio (order unity), the efflux interference effects on the airframe aerodynamics naturally tend to predominate over those from the intake flow. In fact, the intake-flow interference on lift is then usually negligible, while the order of magnitude of the drag and moment increments can probably be adequately assessed by consideration of the relevant rotation of the flow momentum vector at the inlet. The influence of forward speed (or relative wind) on intake efficiency and on basic lift-engine performance cannot of course be ignored as referred to in Sections 3.7 and 3.8, prior to consideration of high bypass-ratio fans when intake-flow interference effects on the airframe aerodynamics can become of comparable importance to those from the efflux.

For practical jet-lift V/STOL aircraft, values of  $(V_0/V_j)_e$  below about 0.3 are of primary concern during transition (or STOL). Higher values arising under transient conditions, while the engines are being started up or shut down, are mainly of interest from engine safety or reliability aspects rather than from aircraft performance or stability. The area ratio  $\sqrt{S_j/S}$  tends to lie between 0.1 or 0.2 for jet VTOL aircraft, but can be lower for STOL aircraft or higher for V/STOL aircraft employing injector schemes or turbo-fan units.

Although elementary jet-lift model experiments of the type already illustrated in the previous section can help establish basic aerodynamic features broad trends, with orders of magnitude as regards jet-efflux interference effects, closer simulation of practical lay-outs is certainly essential for aircraft design and project assessment purposes. Apart from providing adequate simulation of the jet disposition in the airframe, together with the jet exit and airframe geometry, inclination of the jet efflux to the airframe

may have to be varied. The influence of the attitude of the airframe to the mainstream, corresponding to aircraft motion or natural winds, also needs examination. As well as jet efflux interference effects on the main lifting surfaces (wing and body), the effects on the flow around the rear fuselage and empennage also have to be considered, particularly with regard to the demands of trim, stability and control throughout the flight range.

#### Lift losses

Some typical jet-interference lift losses and their sensitivity to practical layout changes are well illustrated by Figures 12 and 13, for a combat aircraft configuration with lift engines installed in the fuselage and with a delta wing. For example, the value of  $\Delta L/T_1$  due to jet operation for the low wing arrangement with a single large central jet-exit a close cluster [ $\sqrt{(S_J/S)} = 0.16$ ] falls from the datum static value of unity to 0.73 as the mainstream speed to jet speed ratio  $(V_o/V_J)_e$  is raised from 0 to 0.2, i.e. up to a flight speed of some 225 ft/sec for a choked jet. In this speed range, the lift loss is relatively independent of incidence and of fore-and-aft location of the wing within practical limits, and is roughly proportional to  $(V_o/V_J)_e^2$ , so that over  $8^\circ$  of incidence compensation is required, assuming a representative wing lift-incidence curve slope of 0.04 per degree. Comparison with the lift loss for the smaller jet-exit area [ $\sqrt{(S_J/S)} = 0.115$ ], when  $\Delta L/T_1$  falls even faster to about 0.55 by  $(V_o/V_J)_e = 0.2$ , demonstrates the sensitivity to area ratio on a practical arrangement. The most startling results arise for the low wing with four dispersed jets when, even with  $\sqrt{(S_J/S)} = 0.16$ ,  $\Delta L/T_1$  falls to as low as 0.5 at  $(V_o/V_J)_e = 0.2$ , the equivalent of about  $16^\circ$  of incidence! In contrast, the lift loss with two jets in-line astern is the same as for the single jet of the same area ratio. If the wing is located high instead of low on the fuselage, the lift losses become somewhat less but are still appreciable, e.g.  $\Delta L/T_1$  becomes about 0.65 for the high wing with four dispersed jets [ $\sqrt{(S_J/S)} = 0.16$ ]: the proportion of lift loss carried by the fuselage is then about two-thirds of the total.

For prediction purposes, it is interesting to compare the measured lift losses on the delta model, with the low wing and central jet configuration against the downward suction forces derived by integrating the pressure distributions over comparable areas on the plane wall model discussed earlier. Figure 14 shows that the lift losses measured on the delta model for  $\sqrt{(S_J/S)} = 0.115$  and 0.16 fit in reasonably with the pressure integrals quoted for area ratios of 0.1 and 0.2 on the plane wall. This tends to imply that the pressure distributions on the wing lower surface are likely to be similar to those on the plane wall. However, recent fundamental experiments on a finite chord wing have shown that the pressure distribution on the wing lower surface is in fact appreciably different, because of the development of strong positive pressure regions ahead of the jet.

Some lift-loss results for various values of  $\theta_J$ , the angle between the jet thrust vector and the longitudinal (fuselage) datum are shown in Figure 15 from tests on a lift/thrust model configuration with four swivelling exits in the fuselage. The lift-losses arising from jet-interference are again relatively independent of incidence. To facilitate direct comparison with corresponding results for pure lifting jet configurations, the lift values plotted here are  $\Delta L^*/T_1 = (\Delta L - \Delta L_o + T_1)/T_1$ , where  $T_1$  is the jet-exit momentum flux, while  $\Delta L$  and  $\Delta L_o$  represent the measured lift increments from jet operation at the prescribed angle  $\theta_J$  under forward speed and static conditions respectively; thus  $\Delta L^*/T_1 = 1$  when  $(V_o/V_J)_e = 0$ . The lift loss near  $\theta_J \simeq 90^\circ$  on this lift/thrust model, with its four jets in the sides of the fuselage and a high wing layout, are of the same order of magnitude as those for the delta model with four jets in the base of the fuselage and a high wing arrangement. Also, for  $\theta_J < 90^\circ$ , the lift loss is roughly proportional to  $\theta_J$  rather than to  $\sin \theta_J$  - which corresponds to the vertical component of jet momentum.

Contrasting with the delta, the lift-loss on the lift/thrust model is more nearly proportional to  $(V_o/V_J)_e$  rather than to  $(V_o/V_J)_e^2$ . Early on, from a prediction viewpoint, this seemed to be consistent with the simple argument that the jet flow merely induces a downwash velocity past the airframe, which combines with the mainstream velocity

to produce a reduction in the effective wing incidence and thereby a loss of lift at a prescribed geometric incidence. However, available wing pressure distributions on other models, as well as more detailed examination of fundamental concepts (see Section 6) completely refute such crude concepts. In general, moreover, there is no valid reason for assuming that the geometric incidence for maximum or usable lift is correspondingly higher, or that the wing high-lift performance does not deteriorate like the lift at low incidence. Nevertheless, the presence of the jet flow could in some circumstances alleviate (by *local* entrainment effects) flow separation tendencies on the upper surface of the nearby inboard wing. For example, the absence of any significant loss of  $C_{Lmax}$  on the lift/thrust model compared with loss in lift at fixed incidence seems to arise in this way.

Some NASA model results on a swept-wing combat aircraft configuration<sup>47</sup>, with three jet exits in-line along the fuselage just ahead of the wing and a further transverse pair (deflected cruise engines) just behind the wing, are also of special interest (Fig.17), in confirming the extreme sensitivity of efflux interference to exit locations.

For jet-lift V/STOL transport configurations, experimental results are extremely scarce. BAC small-scale experiments on a wide range of simple models<sup>35</sup> (Fig.18) imply similar jet-interference considerations to those already mentioned for combat aircraft layouts. Some RAE experiments on an elaborate swept-wing V/STOL transport model<sup>3</sup> show that significant jet-efflux interference effects can arise even from lift/thrust units in underslung nacelles. These effects vary appreciably with the line of action of the nacelle jets relative to the wing, with the jet angle, and also with the wing/flap configuration. While unfavourable jet interference effects on the wing lift can often occur, favourable effects can also arise with the high-lift trailing-edge flaps deflected, at least for rearward jet locations at low  $(V_o/V_j)_e$  values. Moreover, the nacelle load contributions, though much smaller than those on the wing, are often significant and of opposite sign.

#### *Pitching-moments*

Jet interference effects on the pitching-moments for the pure lift delta and the lift/thrust aircraft models are plotted in Figures 12,13 and 15 respectively as  $\Delta_m/T_i d_e$ , the effective forward movement of aircraft CG needed to trim for a thrust-weight ratio  $T_i/W$  of unity, in terms of an equivalent jet diameter  $d_e (= 2\sqrt{S_j/\pi})$ . For the delta model with the low wing configuration, the nose-up moments increase with reduction in area-ratio and dispersal from 1 to 4 jet-exits, like the lift losses. Thus, when  $(V_o/V_j)_e$  reaches 0.2,  $\Delta_m/T_i d_e$  becomes about 0.35 and 0.75 for single jets with  $\sqrt{S_j/S} = 0.115$  and 0.16 respectively, and about 0.5 for the four disposed jets at the higher area-ratio. However, note that the moment interference for the two jets in-line astern is relatively small. More generally, for low values of  $(V_o/V_j)_e$ , the interference moments are not only small but can also be nose-down, which is consistent with the plan-wall and wing pressure-plotting measurements. The adoption of a high wing instead of a low wing configuration again helps to alleviate the jet interference effect, but the major proportion of the moment is carried by the fuselage.

#### *Drag*

The aerodynamic drag at zero wing incidence seems to be relatively unaffected by the presence of the jets, while at positive incidence a small reduction in drag sometimes occurs which is consistent with the argument that the lift loss is generated by suction on the wing lower surface. The intake momentum drag in contrast becomes significant at the top-speed end of transition and has to be balanced by appropriate rearward vectoring of engine efflux.

#### *Tailplane contributions*

For practical configurations incorporating a tailplane behind the jets, additional consideration of jet interference effects on longitudinal trim and stability are necessary.

The strong vortex flows, which develop as a result of the rearward deflection and distortion of the lifting jets together with entrainment of the mainstream flow, produce a substantial downwash and sidewash field in the region aft of the jet-exits. The tailplane contribution to trim and stability will depend on its geometric shape (size, planform, anhedral, etc.) and its position in this velocity field. The downwash and sidewash will naturally depend on such factors as jet configuration, inclination of the jet-exit efflux to the mainstream direction, and the speed ratio. There is also a contribution from the vorticity shed by the lifting wing and any associated high-lift devices.

Some early studies using the lift/thrust model with and without an elementary tailplane (no anhedral) serve to illustrate the various aspects of possible problems. The tailplane contributions vary enormously with the height of the tail relative to the jets (Fig.16). In the region of the mid and low tailplane positions, the downwash field is clearly dominated by the jet interference effects, and the variations with incidence are such as to produce destabilising contributions from this simple tailplane. The variations of downwash angle across the tailplane span in its lower position demonstrate forcibly the large gradients present near the jet plume, and these are accompanied by similar large variations in sidewash angle. Further above the jet plume, where the spanwise variations are much smaller, the tailplane may still provide little or no contribution to longitudinal stability (under transition conditions). This arises because the inclination of the jet-exit efflux to the mainstream direction naturally increases with incidence, thus increasing both the penetration of the jet plume and the strength of the vortex flows, so that the strength of the downwash field is generally increased in the region of the tailplane. The variation  $d\epsilon/d\alpha$ , of the mean downwash angle with incidence, is in this case seen to be sensibly unity at the mid-tail position.

Such effects will inevitably arise in some measure under transition conditions whenever a tailplane is mounted directly behind lifting jets (or fans), unless the tailplane is so far above the path of the jets as to be clear of the downwash field, which may be objectionable for other reasons. Fortunately, such aircraft inherently have large longitudinal control powers installed to cope with vertical take-off and landing requirements, so these can help minimise transition stability problems, provided longitudinal trim requirements are not simultaneously large.

### 3.7 Lifting-Engine Intake-Flow Problems

For discussions of problems and special design features associated with the provision of satisfactory intake efficiency and intake-flow distributions, under both stationary and low-speed flight conditions, attention may be particularly directed to the following published studies.

Rolls-Royce	.....	Refs.26, 27
NASA	.....	Refs.43, 46, 48
NPL	.....	Refs.16, 18
DFL	.....	Ref.59
NRC	.....	Ref.61

### 3.8 Basic Intake Flow Interference Effects on Airframe

In attempting to analyse fan-lift performance variation with forward speed, intake efficiency and internal fan-flow considerations have to be taken into account, particularly since there can be substantial differences between full-scale and model fan behaviour. It is also worth noting that the intake mass-flow rate for a mechanically driven model fan chosen to simulate the correct efflux speed ratio  $(V_0/V_J)_e = \sqrt{(\rho_0 V_0^2 / \rho_J V_J^2)}$  and area ratio  $S_J/S_0$  at the exit is approximately  $\sqrt{(T_J/T_0)}$  times that for an actual turbo-fan engine, where  $T_J$  and  $T_0$  represent the mean efflux and ambient total-temperatures. Thus,

such a model fan tends to exaggerate the full-scale inlet flow and associated sink-action effects. More generally, with practical installations, engineering design limitations with respect to blade loading, tip Mach number, rotational speed, fan-drive demands etc., can be relevant to the fan characteristics through the transition. Such "ducted-fan" problems are not to be discussed here, but we need to bear them in mind when analysing or applying basic concepts or model test results.

From elementary ducted fan concepts, it can be argued that the sink-action of the intake-flow in rotating the mainstream-air momentum vector generates reduced pressures on the upstream side of the intake lip and increased pressures downstream. Thus, with simple superposition of sink flow and of basic mainstream flow past the airframe (assuming fore-and-aft symmetry), the fan shroud lift remains the same proportion (ideally  $\frac{1}{2}$ ) of the exit momentum  $\rho_j V_j^2 S_j$ . But the throughput velocity  $V_j$  and the fan pressure-rise contribution to lift can both vary significantly with the intake ram pressure depending on the particular fan-design characteristics. Even when the ducted-fan lift remains invariant with forward speed, the induced pressures on the inlet surface lead to a "sink-drag" ( $\Delta D \sim \rho_j V_j S_j V_o$ ), together with moments - nose-up for an upper surface intake - proportional to the sink drag and dependent on the geometry. Two-dimensional sink-in-wing arguments likewise imply that the induced lift change is small, unless the inlet is located very close to the wing trailing-edge so that the circulation is substantially affected; appreciable sink drag and moments again rise.

However, intake-flow interference effects at forward-speed seem to involve additional important physical properties often more favourable to lift than implied by the above elementary sink-action concepts. For example, three-dimensional upwash effects and associated circulation changes with upper-surface inlets seem to be significant. Unfortunately, analysis and synthesis of fan-lift results at forward speeds becomes especially difficult, because of the possible interplay between intake efficiency, fan characteristics intake-flow interference, efflux interference and basic airframe aerodynamics.

#### *Simple wing configurations*

Early experiments, at NPL<sup>17</sup> on simple-single-fan wings and at RAE<sup>8</sup> on a simple multi-fan wing, demonstrated forcibly the significance of the location, disposition and area-ratio of the fan ducts in the planform as regards the initial fall-off in lift and increased pitching moments with forward speed. The multi-fan results (Fig.20) also imply that lift augmentation, and reduced chordwise movement of the centre of total-lift with exit-speed ratio  $V_o/V_j$ , can be achieved by spanwise rows of fans only as far back as half-chord. Note that these latter experiments are complementary to those discussed earlier (Fig.9) on the simple rectangular-wing model with multi-jets.

#### *Simple body-wing configurations*

Some overall force measurements on a bluff-body model, with the fan occupying a large proportion of the body, provide perhaps the most striking demonstration of intake-flow interference effects when compared with results for the similar bluff-body model with jet efflux only (Fig.21). The favourable lift effects, associated apparently with the addition of fan intake-flow, increase remarkably as the span of the *high* wing is increased, again accompanied by large nose-up pitching moments.

Detailed pressure-plotting experiments, for example (Fig.22) on the twin-fan nacelle, have confirmed that significant suction can occur on a body installation, on the upper surface near the front of each intake-lip, and on the lower surface downstream of the front fan exit. The upper-surface intake-flow interference thus tends to alleviate the loss in lift arising from lower-surface efflux interference. But again, the accompanying nose-up pitching moments and drag are much increased by the intake-flow, the former far more than would be predicted by simple consideration of rotation of the intake momentum vector at the inlet. It may be also noted that the streamwise fences added to the lower



surface on either side of the fan duct exit alleviated the lift loss due to efflux interference (see Fig. 23, Section 3.5) though the nose-up pitching-moments were little reduced with the arrangement shown.

### 3.9 Intake-Flow/Efflux Interference Effects on Fan-Lift Aircraft

#### *Scope of considerations*

For fan-lift installations of all types, particularly those mounted in the vicinity of the wing, the sink action of the intakes as well as the exit efflux momentum contributes significantly to aerodynamic interference effects on the airframe. With upper surface intakes, pitching-moments are especially affected at forward speeds; with side-intakes, yawing moments can be correspondingly affected. Intake momentum drag effects, together with intake efficiency and the particular fan characteristics at forward speed, have also to be seriously assessed with respect to transition performance capabilities. Moreover, the substantial downwash and sidewash created at the tailplane by the fan-flow interference with the mainstream can also affect trim and stability; normally, a high tailplane would be favoured from merely VTOL transition considerations.

With practical fan-lift VTOL aircraft, values of  $V_0/V_j$  up to 0.5 are of concern during transition, somewhat higher than with pure jet installations. Again, the area ratio  $\sqrt{S_j/S}$  tends to rise to between about 0.25, and 0.35 for fan lift arrangements. With VTOL vehicles not inherently designed to take advantage of airframe lift at all during the flight regime, say a flying car with large lifting fans,  $\sqrt{S_j/S}$  may be as high as 0.5 or even closer to unity; then, the intake-flow effects would be of predominant interest.

#### *Multiple turbo-fan lift-engines in wing pods*

While the early experiments on lifting fans in bodies are instructive, the duct exit area was of necessity relatively small compared with the body planform area, because the fan units then available required installation space unduly large compared with the fan duct diameter. More recently, some four-fan pod experiments, with area-ratios more representative of practical multiple lift-engine pods, have been undertaken employing compact air-driven fans specially built for the purpose; here, the variation of fan-flow throughput with speed was negligible. The pod was mounted on a half-model wing of rectangular planform to facilitate variation of wing aspect-ratio and pod spanwise position (Fig. 24). For this four-fan pod arrangement, the lift loss due to fan flow interference effects appears less than 10% of the installed static thrust for low  $V_0/V_{j1}$  values and becomes a lift gain for  $V_0/V_{j1} > 0.2$ ; unfortunately, the experimental results are inaccurate for  $V_0/V_{j1} < 0.1$  because of tunnel-wall constraint effects. The model lift-incidence curve slope and the aerodynamic centre position are also little changed by the fan-flow interference effects, while the associated interference drag does not exceed the expected intake momentum drag. In contrast, the nose-up pitching-moments rise steadily as the speed-ratio is increased from zero; for example, by  $V_0/V_{j1} = 0.3$ , the nose-up moments correspond to a forward movement in static lift centre of almost  $0.2 \bar{c}$ , i.e. about two-thirds of a fan diameter.

With only the three rear fans operating, the fan-flow interference on lift (as a proportion of the appropriate total static thrust) appears to be more favourable than with all four fans, though the corresponding nose-up pitching-moment interference becomes relatively large, as seems reasonable in view of the extra "solid" upper surface ahead of the operating fan intakes. With only the three front fans operating, the fan-flow interference becomes relatively more unfavourable, presumably because of the extra "solid" lower surface behind the operating fan exits.

The low-speed aerodynamic behaviour of moderately swept-back wing VSTOL transport configurations can now be studied more thoroughly on the complex RAE model with blowing BLC on leading-edge and trailing-edge flaps, together with simulated efflux and intake-flow for cruise/lift engine nacelles and for multiple lift-engine pods attached to the wing<sup>3</sup>

### *Large-diameter fan configurations*

The extensive studies carried out at NASA are of special interest here; excellent reviews of this work already exist as References 44 and 46. Figure 25 shows some lift results for a layout with two lift-fans slung ahead of the wing and for another with six fans mounted in the wing as a spanwise row. These illustrate the appreciable effects of variation in forward speed on the fan lift, performance itself and on the fan-flow interference with the airframe loads. Broadly speaking, these NASA studies and others on representative aircraft layouts confirm the broad trends to be expected from the discussions in the preceding sections, as regards the dependence of efflux/intake-flow interference effects (unfavourable or favourable) on wing geometry, fan disc/planform area-ratio, and fan disposition in the airframe. But prediction of such effects in quantitative terms from a realistic physical framework rather than by limited extrapolation using tentative ad hoc working formula is still not possible.

### **3.10 Influence of Sideslip**

At low forward speed during transition, V/STOL aircraft will inevitably experience larger sideslip angles than during conventional take-off and landing. Moreover, flight research on the Short SC.1 aircraft has revealed that the required combination of roll and side-slip in a typical turning manoeuvre at very low speeds can cause severe handling difficulties, with larger than usual roll control being needed to ensure safe flight.

Recent tunnel tests at RAE on an SC.1 model<sup>10</sup> have revealed that large sideslip angles can produce important effects, even without engine-flow simulated. If the aircraft is at a positive incidence, sideslip angles of the order of  $45^\circ$  can cause the loss of the major part of the wing lift, even at zero roll angle. Secondly, and more important from the handling viewpoint, strong rolling moments develop as the aircraft rolls its forward wing either up or down, tending to increase the roll angle (Fig.26). These moments appear at positive as well as zero incidence, being even stronger if the fuselage is removed. The lateral movement of the centre-of-lift for the wing alone is also shown in Figure 26. Simple strip theory arguments, assuming that the sectional lift (at  $\beta = 90^\circ$ ) acts at the quarter-chord point, would predict that the centre of pressure (at  $\beta = 90^\circ$ ) should be at about 1/3 semi-span. This agrees well with measurements, thus suggesting that for low aspect-ratio deltas at least, rolling moments will occur as a result of conventional aerodynamic "lift-incidence" effects. The presence of a fuselage modifies the behaviour slightly, presumably due to shielding effects on the trailing wing, but strong rolling moments remain which can exceed the static roll control power of the aircraft (Fig.26).

The lifting efflux interference on the airframe loads in sideslip naturally can be expected to generate additional rolling moments, due to the suction induced on the airframe lower surface downwind of the exit; following arguments similar to those already discussed at length in connection with efflux interference at forward speeds. For a fuselage installation at least, these additional rolling moments can be expected to be in the sense of downloads on the trailing wing and some exploratory tests have confirmed this. It could also be argued that the variation with roll angle of the additional rolling moments due to efflux interference is likely to be much different and much less than the variation of the basic airframe contributions (without efflux). The "wing-lifting" effectiveness of jet-reaction controls at the wing tip may likewise be substantially reduced in sideslip, as has been confirmed by recent NASA tunnel tests.

Intake momentum effects in sideslip can also be significant, mainly from the reduced pressures arising on the upwind lip of the intake and increased pressures downstream associated with rotation of the inlet momentum vector. Thus, with upper surface intakes, additional rolling moments due to intake flow interference can occur in the sense of uploads/downloads on the leading/trailing wings; substantial side-forces can also arise particularly for turbo-fans of large bypass-ratio. With forward facing intakes, additional yawing moments and side-force can likewise result. The influence of sideslip or natural crosswinds on intake efficiency and flow distributions has also to be taken into account in relation to the basic lifting unit performance in all cases.



More generally, the influence of planform geometry, anhedral, wing height on the fuselage and lifting-engine disposition, at the unusually large angles of sideslip possible with V/STOL aircraft operation, are not yet predictable except in terms of broad physical arguments. Further study of these problem areas, for high aspect-ratio as well as low aspect ratio configurations, is certainly well warranted.

#### 4. GROUND PROXIMITY EFFECTS

##### 4.1 Centrally Located Exits - Efflux Interference

At take-off and landing, a single jet or a close cluster of jets emerging from the central area of a wing or body entrains the free air between the lower surface and the neighbouring ground, producing flow patterns like those of Figure 27, the induced velocities tending to increase steadily as the clearance between the wing and ground becomes smaller<sup>11</sup>. Surface pressures well below ambient are thereby generated on the lower surface, producing significant reductions in the net upward thrust or lift often accompanied by undesirable moments, of increasing magnitude with reduced ground clearance. For a particular planform and jet exit geometry, the non-dimensional ratio  $L/T$  of the net lift to the jet efflux momentum rate and corresponding non-dimensional moment coefficients can conveniently be examined as functions of the ratio of the jet exit ground clearance  $H$  to some planform linear dimension like an equivalent diameter  $D (= 2\sqrt{S/\pi})$ , the ratio of the jet exit diameter  $d$  to  $D$  or the jet exit area  $S_j$  to the planform area  $S$ , the jet Reynolds number  $R_j (= V_j d/\nu)$ , the jet Mach number  $M_j (= V_j/a)$  and the ratio of jet to ambient temperatures.

##### *Lift losses*

The lift-ratio  $L/T$  with a single jet decreases steadily from its free-air value as the ground clearance  $H/D$  is reduced. Typically, a simple delta-wing model of aspect-ratio 1.6 with a jet-diameter ratio  $d/D = 0.16$  could lose an additional 15% of its installed vertical lift  $T_1$  ( $L/T_1 = 0.85$ ) at a representative ground clearance  $H/D = 0.3$  (Fig. 29). Fortunately, such interference losses tend to become less severe as the ratio  $d/D$  is increased towards values more representative of turbo-fan or high bypass ratio installations. Model results obtained from simple circular planforms having a centrally located jet, with  $d/D$  ranging from 0.1 to 0.3, indicate that the lift-ratio  $L/T_1$  can be treated principally as a monotonic function of  $H/(D - d)$  see Figure 28. Further results on a range of triangular and rectangular planforms of aspect-ratio  $1/4$  to 4, with a single jet ( $d/D = 0.11$ ) at the centroid of area<sup>12</sup>, imply that correlation for variation in wing geometry is possible against the parameter  $H/(\bar{D} - d)$ , where

$$D = (1/\pi) \int_0^{2\pi} r d\theta$$

is an "angular-mean" diameter for the planform, as shown on Figure 28. Simple curve fitting suggests the following simple working formula for a normal jet:-

$$1 - (L/T_1) = 0.012 [H/(\bar{D} - d)]^{-2.3}$$

In extrapolating to full-scale conditions, the possible influence of efflux Reynolds number, Mach number and temperature-ratio have to be allowed for, though there seems no reason to expect significant changes on these counts. Recently, analyses from a few quantitative full-scale experiments near ground have become available. Some Northrop results<sup>52</sup> relate to a ground rig, with a J. 85 engine exhausting at temperatures of at least 500°C, from a 1 ft diameter nozzle in a square plate. Some NASA results<sup>47</sup> relate to flight tests on their X-14A research aircraft, together with some small-scale model checks. The curves reproduced in Figure 31 and 32 confirm that, for central clusters of exits, small-scale experiments should provide adequate representation of full-scale conditions, while the foregoing simple formula should give useful estimates of the lift losses due to ground proximity.

Similar quantitative correlations could now usefully be attempted for more general practical cases of wing-body combinations. On high wing configurations, with the efflux emerging from the lower surface of an underslung body, the lift losses are appreciably smaller than with low wing configurations - for the same exit clearance from the ground (see Fig.29). Also, it is now important to ascertain the influence of exit geometry, efflux velocity distribution, jet turbulence and rate of decay, and jet angle on the rate of entrainment of ambient air into the jet flow as it spreads radially after impact with the ground, to provide a reliable basis for general correlation of airframe lift losses due to ground proximity.

With large fans, where ground clearances of less than a diameter need to be considered, the back pressure due to ground proximity can of course affect the fan characteristics as well. For example, in RAE tests on a bluff-body model containing a single low-pressure fan with  $d/D = 0.5$ , the installed lift at a fixed fan rpm and blade setting increased some 10% close to ground ( $H/D = 0.5$ ) even though the fan mass flow throughout decreased by 10%; however, the power input to the fan was some 20% larger than away from ground. In contrast, with a more highly loaded or optimised fan, the presence of ground could produce blade stalling or deterioration of performance. Furthermore, the simulation at model scale of specific full-scale lifting fans presents serious difficulties, particularly with regard to adequate calibration and correlation in ground proximity.

The influence of aircraft attitude to the ground also needs to be considered. Provided the jet is located near the centroid of area, the variation of lift with pitch and roll about the jet centre seems unlikely to be significant compared with height effects. Otherwise, when the height of the centroid varies with attitude, the lift may well depend on the height of the centroid rather than that of the jet centre. Measurements of the lift loss on the aspect-ratio 1.6 delta-wing model with the jets normal to the planform tend to confirm this (Fig.30). More generally, the effect of jet deflection away from the normal to the planform is of interest, for example with the aircraft at incidence and the jets directed normal to the ground, while cross-winds or the relative wind due to a rolling take-off may also be important.

#### *Stability considerations*

Loss of lift near the ground, particularly severe with low-wing central-jet configurations, might perhaps be expected to produce appreciable handling problems during a vertical landing. However, flight experience on the Short SC.1 aircraft, which has a low-wing with a central cluster of four lift engines, has shown that this height instability is in fact easy to control. This is presumably due to the very rapid jet-engine response when running at high rpm and in some degree perhaps to the fact that the variation in interference lift with height remains monotonic. With high wing (or dispersed jet configurations) the lift variations though not necessarily monotonic are generally much smaller, so should not in themselves present any appreciable handling difficulties given rapid engine response.

Control of attitude near the ground, both in pitch and roll, seems likely to cause much more severe problems than height control. Even in the horizontal attitude ( $\alpha = \phi = 0$ ), low aspect-ratio central-jet configurations may experience some pitching moment due to any unequal fore-and-aft-distribution of lower surface area around the jet. Evidence from tests on delta-wings with aspect-ratios between  $\frac{1}{2}$  and 4, and with a jet located at 0.7 root chord, suggested that the aerodynamic requirements for longitudinal trim while hovering at a practical ground clearance ( $H/D \leq 0.3$ ) should not exceed 1% of the gross thrust applied at an arm of one mean chord from the jet, though the pitching moment increases rapidly as the ground clearance is reduced. For low aspect-ratio ( $< 2$ ), the moments are nose-up and are further increased when, from other aerodynamic considerations, the aircraft C.G. and hence the thrust centre locations are further forward in the planform. Thus, for practical configurations, an appreciable proportion of the available reaction control, which is usually determined by handling requirements out of ground effect, may be needed simply for longitudinal trim. Once again, as with height control, the pitching moment varies monotonically with height.

The limited amount of experimental data available on stability changes actually arising from pitch and roll near ground presents a most confused picture of the interference effects, so that it is difficult to draw general conclusions, even for central jet arrangements. For example, a circular wing with a single central jet ( $d/D = 0.1$ ) exhibited either stable or unstable moments depending on the ground clearance, though the moments remained stable for all ground clearances  $H/D$  above 0.25. On the other hand, a delta-wing of aspect-ratio 2.8 with a central jet ( $d/D = 0.1$ ) was stable in roll for all practical ground clearances<sup>11</sup>. There is a tendency towards instability in pitch (in addition to the basic nose-up moment at zero incidence), if the jet is positioned ahead of the centroid of area. For example, on the model of Figure 29 with the thrust-centre one jet diameter  $d$  ahead of the wing-area centroid ( $d/D = 0.16$ ), a nose-up moment was measured at  $H/D = 0.23$  which for trim, would require 6% of the gross thrust at an arm of one mean chord; moreover, the thrust required increased by 0.4% per degree change of attitude (Fig.30). These control moments are of the same order as the total control which would normally be available on a typical practical configuration.

#### *Alleviation of efflux interference*

The provision of substantial ground installations to duct all the gas efflux well away from the jet (or fan) lift aircraft, when standing on or hovering close to the ground, could eliminate the aerodynamic penalties and problems just discussed. But such installations may not be practical or possible except at complex VTOL sites. A simpler scheme for the alleviation of adverse ground effects on aerodynamic behaviour comprises parallel channels on the ground<sup>11</sup> (supporting a landing grid) to destroy the radial symmetry of both the jet spread after impingement and the subsequent entrained flow. Alternatively, a close-mesh grid (gauze sheet) located slightly above the ground can contain the jet spread after penetration and minimise the entrainment after impingement. For example, with a delta-wing model of aspect-ratio 2.8 and  $d/D = 0.1$  simulating the Short SC.1 aircraft configuration, the loss in lift can thereby be reduced from about 20% to 2% at a normal ground-clearance  $H/D \approx 0.3$  (Fig.33), while the accompanying nose-up pitching moments become negligible.

Other problems arising from ground proximity, have to be simultaneously borne in mind, such as hot gas recirculation into intakes, ground erosion and other ground environment considerations. These, together with the use of ground roll techniques and jet deflection away from the vertical as a means of alleviation will be discussed in later sections.

#### **4.2 Dispersed Multiple Exits - Efflux Interference**

With several jet (or fan) exits some distance apart, the flow regime in ground proximity becomes considerably modified and the effects naturally become far more complex. The jet streams now tend to meet on the ground between the exits so that surface pressures higher than ambient can occur from the consequent jet upflow on to the local wing and body areas above, in contrast to the outer low pressure areas (Fig.27). These effects tend to be much more marked if the dispersed jets emerge from the lower surface of an underslung body, i.e. with a high wing configuration, where the ground clearance of the central body area is much smaller than that of the wing area outside the body.

#### *Lift loss and increase*

The favourable uploads on the central surface areas between the jets due to ground proximity tend to counterbalance the lift losses due to the unfavourable downloads, outside, to an extent depending on the particular layout. For example, the triangular wing and body combination of Figure 29, with  $\sqrt{S_j/S} = 0.16$ , loses about 15% of its lift with a single central jet and low wing when  $H/D \approx 0.3$ , in addition to the installation loss discussed in Section 2. This ground effect loss becomes only 7% if the jet area comprises four spaced exits, as indicated on Figure 29, falling still further to 2% if the wing is then raised to the top of the body.

With four swivelling nozzles in the body, as on the Hawker P.112, prototype V/STOL strike aircraft, results are slightly better still; probably because the jet exits are at the outer edges of the body with a high wing. Such favourable lift effects can be further encouraged by incorporating vertical fences on the body lower surface to box in the area between the jets. By this means lift gains, amounting to several per cent of the installed thrust can be achieved at close ground clearances, as can be seen from the results obtained on this prototype P.1127 model with a typical fence arrangement (Fig.34). With multiple jet exits arranged in-line fore-and-aft along the body, lift losses in ground effect can be reduced by using a spaced double-row instead of a single row arrangement (see Fig.36). Even more radical improvements are then seen to be achieved by canting the exit nozzles outwards from the vertical since, at least for small deflections ( $\sim 10^\circ$ ), this effectively increases the area of upflow without unduly diminishing the strength (Fig.35).

The above illustrations are concerned primarily with fuselage installations, but similar arguments can be applied for lift variations in ground effect with jets or fans hung from the sides of the fuselage, buried in the wings, or located in wing pods. With such spacing of the exits, lift increments several per cent above the installed lift away from ground can be achieved at or near touchdown. However, any design arrangements likely to produce distributions of both low and high pressure on the airframe lower surface can be especially sensitive to altitude changes and to relative wind effects, leading to large lift reductions from the most favourable datum condition and aggravating any tendency to instability in pitch and roll. Simultaneously, the influence on hot-gas recirculation towards the intakes and on the impingement of relatively hot flow onto the aircraft lower surface needs to be assessed; together with the possible need of alleviating such conditions by the introduction of surface strakes and fences which are not of necessity favourable aerodynamically.

The thin peripheral jet represents of course an extreme example of favourable ground effect on lift, by the provision of a substantial cushion of air at pressures higher than ambient over most of the planform area inside the periphery. This offers the possible attraction of air-cushion take-off and landing (ACTOL) at low forward speeds, combined with other favourable effects during transition. Although some exploratory aerodynamic research on this concept was carried out at the RAE and elsewhere several years ago, much more extensive research is needed and many technical problems have to be solved, before this can be established as both profitable and practicable.

#### *Stability considerations*

With multiple dispersed jet configurations, the interference effects are much less predictable. Model experience has shown that the pitching moment variation with height is strongly dependent on the position in the planform and the inclination to the vertical of each individual jet, as well as the detailed lower surface geometry. Control of the central positive pressure region is possible by means of lower surface strakes or small variations in the various jet inclinations. However, this in turn affects not only the longitudinal trim but also the loss of lift, the stability in pitch and roll, and the recirculation of hot gas to the intakes. Hence, it seems inevitable that, for a given configuration, the final detailed geometry will be a design compromise between these various requirements, determined only after an elaborate model test programme. Moreover, some longitudinal trim change will remain to be coped with, particularly taking engine failure cases into account.

To illustrate the order of possible variations of aircraft pitching moment with ground-altitude as well as ground clearance, a few test results on a model of the P.1127 prototype configuration can be referred to in Figure 34. For configurations with much more widely-spaced jet or fan exits, the variations may be much larger, though admittedly the control moments available through thrust modulation on individual lifting units can also be large. Finally, it must again be stressed that only general trends can as yet be anticipated on multiple dispersed exit arrangements, and that the real behaviour is extremely sensitive to the detailed geometry.

### 4.3 Influence of Forward Speeds (STOL)

Efflux interference effects near the ground under static conditions have been discussed already in Sections 4.1 and 4.2. But it is important to recall that their nature and magnitude tend to be critically sensitive to aircraft geometry, attitude and ground clearance, together with jet disposition and inclination.

The combined effects of forward speed and ground effect, which concern us here, have so far been studied only on a limited number of models and it is difficult to draw any general quantitative conclusions from the results. Some RAE tunnel tests with four dispersed jets imply that, even with a very low mainstream dynamic head as appropriate to rolling take-off or natural winds  $[(V_o/V_j)_e \approx 0.05]$ , large changes in jet interference loads can occur because of modifications to the jet impact pattern on the fuselage undersurface. At higher speeds more appropriate to STOL  $[(V_o/V_j)_e \approx 0.1]$ , which for a vectored lift/thrust installation would normally be associated with some rearward as well as downward inclination of the jet nozzles, the jet efflux is deflected even further aft before striking the ground. The resulting upwash after impingement can then occur in the region of the tailplane causing trim and stability changes. Throughout this part of the speed range, the various parameters like incidence  $\alpha$ , speed-ratio  $(V_o/V_j)_e$ , jet angle  $\theta_j$  and ground clearance can all influence strongly the jet interference loads. At still higher speeds  $[(V_o/V_j)_e \approx 0.2]$ , the influence of ground on the aerodynamics tends to become favourable. The deflection of the jets by the mainstream is then completely modified by the ground proximity and the development of the strong vortex flows of the type encountered out of ground effect is curtailed. Thus the loss of lift at constant incidence is much reduced and the tailplane contribution to stability is much improved relative to the corresponding results away from ground. More generally, the aerodynamic influence of ground proximity on high-lift wings (with jet efflux present) also becomes important in relation to both performance and stability.

In interpreting wind-tunnel test data, it is especially important to realise that the true dynamic situation of STOL aircraft take-off and landing may not be adequately predicted by quasi-steady analysis based on stationary model experiments. Admittedly, spurious boundary-layer effects encountered with the conventional fixed ground-plate in tunnel experiments may be minimised or checked by using moving-belt ground rigs or other allied techniques. But, even assuming steady rates of aircraft climb and descent, their substantial contributions to the angle of incidence under STOL conditions may not be adequately simulated. For, as illustrated in Figure 38, the stationary model with the ground-plane parallel to the tunnel mainstream may be placed either at the correct attitude to the ground or at the correct angle of incidence - but not both. Tilting of the ground-plane relative to the tunnel mainstream is not acceptable, since unrepresentative pressure distributions would then arise about the inclined ground-plate in the tunnel. Finally, it should be also remembered that STOL operation within ground effect is essentially a transient phase, so that application of "stationary" model results and quasi-steady treatments also needs further justification on this count, by dynamic model tests and flight-tunnel comparisons.

### 4.4 Hot-Gas Ingestion

The effects of ground proximity on lifting jet (or fan) efflux paths and the entrained ambient air flows has already been considered in relation to the interference effects on airframe aerodynamics, while the sink action of the intake flow itself can also be expected to affect the circulatory flow pattern. Here, we are concerned with the related problem of ingestion by the intake of hot exhaust gases or of ambient air heated by the exhaust gas. This is troublesome because of the increased intake air temperatures rather than intake air contamination. The resulting percentage loss in engine thrust can be of the order of one-half the mean intake temperature rise in °C. Moreover, compressor stall can occur, either due to the very rapid rise in mean intake temperature, or due to the occurrence of hot local "streaks" at the intake face. Such a compressor stall would itself lead naturally to large thrust losses and spasmodic thrust variations, which could not be tolerated when manoeuvring near ground.

Under still-air stationary-aircraft conditions, the hot-gas ingestion can be primarily related to the "near-field" flow conditions, i.e. those in the immediate vicinity of the aircraft. Outside the area of impingement of a single jet (or close cluster of jets) on the ground, the jet plume continues to entrain surrounding air and to spread, with a resulting rapid decay in jet total head and temperature. Some of this heated air rises locally because of buoyancy forces outside the planform (Fig.37). More important effects arise with multiple dispersed jets, meeting on the ground between their exits, so that the resulting hot-gas fountains can pass near an intake and be inhaled, though some alleviation can be derived from the downflow of cool air induced by the jets. Rapid-mixing nozzles, primarily incorporated for reducing ground erosion, are helpful in this latter connection. Such near-field "fountain" effects can generate high intake temperatures and unevenness of the intake temperature distributions; but the temperature rise can vary markedly, from the order of 1% to 10% of the jet efflux temperatures, depending on the aircraft configuration and ground clearance. The relative positions of the multiple nozzles and the intakes seem particularly important (e.g. Fig.37), while small jet deflections and the addition of surface strakes can often produce substantial reductions of the intake temperature rise - at least for a limited range of operational conditions. The shielding of intakes provided by the wing (or other airframe surfaces) against recirculation of hot gas is also relevant, so that side-intakes tend to suffer far more than upper surface intakes.

With relative winds, the far-field flow conditions also begin to play a major role, since the spreading jet plume rolls up and blows back towards the aircraft just above ground level (Fig.37). Thus ingestion of this hot-gas cloud can occur unless the aircraft accelerates quickly enough. The maximum intake temperature rise tends to occur for relative winds of the order of 20 knots. Such far-field effects seem in most cases to be relatively insensitive to practical changes of aircraft configuration. However, hot-gas ingestion can be completely avoided at take-off by using a short ground-roll technique (RTOL), with the aircraft accelerated to 30 knots or more, depending on the particular configuration and the degree of rearward jet deflection feasible before lift-off.

The prediction of intake temperature, rise and distribution associated with hot-gas ingestion is not possible even qualitatively at this stage for new aircraft projects under practical operational conditions, without results from representative tests on sealed models including some under dynamic conditions, backed up by some full-scale correlation parameters include:-

(a) The momentum ratios of the several jets and relative wind  $(\rho_J V_J^2 / \rho_0 V_0^2)$ , as needed for aerodynamic interference considerations; there is still some debate as to whether momentum or mass-flow should be employed here as regards intake flow considerations.

(b) The ratios of the jet excess temperatures  $(\theta_J)$  above ambient.

(c) Buoyancy/momentum force ratios, as exemplified by the simplified ratio  $\rho_J V_J^2 T_J^2 / d \theta_J$  suggested by NGTE<sup>22</sup>.

(d) Jet efflux Reynolds numbers  $(V_J d / \nu)$  and Mach numbers  $(V_J / a)$ .

In interpreting model tests, the unit of time to which the model motions and flow development should be referred are directly proportional to the value of  $\rho_J^{1/2} V_J / d$  for the model<sup>22</sup>. When the model tests involve substantial scaling, large changes in one or more of the correlation parameters above will have to be accepted, while the choice may have to be strongly influenced by measurement difficulties. It can be argued that the buoyancy parameter may be ignored in relation to near-field fountain effects, but becomes of primary importance along with momentum ratios for far-field wind effects. Some examples of recent experimental results for typical configurations may be found in References 20, 21, 47 and 49.

## REFERENCES

## Royal Aircraft Establishment

1. Ashwood, P.F.  
Lean, D.                    *Flight Tests of a Meteor Aeroplane Fitted with Jet Deflection.* J.Roy.Ae.Soc. Vol.62, pp.539-561; 1958
2. Williams, J.                *Some British Research on the Aerodynamics of Powered Lift Systems.* J.Roy.Ae.Soc. Vol.64, pp.413-437; 1960
3. Williams, J.                *Recent Basic Research on V/STOL Aerodynamics at RAE.* Z. Flugwiss, Vol.14, pp.257-276; 1966
4. Williams, J.  
Butler, S.F.J.                *Aerodynamic Interference Effects with Jet-Lift V/STOL Aircraft Under Static and Forward-Speed Conditions.* Z. Flugwiss, Vol.15, pp.237-256; 1967
5. Bradbury, L.J.S.  
Wood, M.N.                    *The Static Pressure Around a Circular Jet Exhausting Normally From a Plane Wall into an Airstream.* ARC Current Paper 822; 1964
6. Trebble, W.J.G.             *Wind-Tunnel Experiments on a Lifting Jet in a Bluff Body With and Without Wings.* RAE Technical Note No.Aero 2971; 1964
7. Trebble, W.J.G.             *Wind-Tunnel Experiments on a Lifting Jet Body With and Without Wings.* ARC Current Paper 718; 1963
8. Wyatt, L.A.                 *Summary of Low-Speed Wind-Tunnel Tests on a Wing Fitted with Multiple Lifting Fans.* RAE Technical Report 67032; 1967
9. Trebble, W.J.G.  
Williams, J.                    *Exploratory Wind-Tunnel Investigations on a Bluff Body Containing a Lifting Fan.* ARC Current Paper 597; 1961
10. Trebble, W.J.G.            *Low-Speed Wind-Tunnel Investigation of the Roll Stability of a 1/5-Scale Model of the Short SC.1 at Large Sideslip Angles.* RAE Technical Report 67104; 1967
11. Wyatt, L.A.                 *Tests on the Loss of Vertical Jet Thrust due to Ground Effect on Two Simple VTOL Planforms, with Particular Reference to the Short SC.1 Aircraft.* ARC R & M 3313; 1963
12. Wyatt, L.A.                 *Static Tests on Ground Effect on Planforms Fitted with a Centrally-Located Round Lifting Jet.* ARC Current Paper 749; 1962

## National Physical Laboratory

13. Gregory, N.  
Walker, W.S.                 *Measurements of Lift and Ground Interference on a Lifting Fan Wing at Zero Forward Speed.* ARC R & M 3263; 1958
14. Gregory, N.                 *On the Representation of Fan-Wing Characteristics in a Form Suitable for the Analysis of Transition Motions with Results of Tests of an Aspect-Ratio = 1 Wing with Fan at 0.354 Chord.* ARC Current Paper 552; 1959



15. Gregory, N. *On the Effect of Fan and Thrust Engine Loading on the Transition of Power Requirements of a Fan-Wing.* ARC Current Paper 690; 1962
16. Gregory, N. et al. *The Effect of Forward-Speed on the Inlet Flow Distribution and Performance of a Lifting Fan Installed in a Wing.* ARC R & M 3388; 1962
17. Gregory, N. et al. *Wind-Tunnel Tests of a Wing Fitted with a Single Lifting Fan.* ARC R & M 3457; 1964
18. Gregory, N. Love, E.M. *Wind-Tunnel Tests on a Nacelle Fitted with Two Lifting Fans in Tandem.* ARC R & M 3494; 1966
19. Hackett, J.E. *Wind-Tunnel Tests on a Streamlined Fan-Lift Nacelle.* ARC R & M 3470; 1965

#### National Gas Turbine Establishment

20. Cox, M. Abbott, W.A. *Studies of the Flow Fields Created by Single Vertical Jets Directed Downwards Upon a Horizontal Surface.* ARC Current Paper 912; 1964
21. Abbott, W.A. *Studies of Flow Fields Created by Vertical and Inclined Jets When Stationary or Moving Over a Horizontal Surface.* ARC Current Paper 911; 1964
22. Cox, M. Abbott, W.A. *Jet Recirculation Effects in V/STOL Aircraft.* J.Sound Vib., Vol.3, pp.393-406; 1966

#### British Firms

23. Wilde, G.L. *Jet-Lift Engines and Power Plants for VTOL Aircraft.* J.Roy.Ae.Soc., Vol.69; 1961
24. Fearon, J.R.C. Norman, D.H. *VTOL and STOL: Simple Solutions to Some of the Operating Problems During Take-Off and Landing.* J.Roy.Ae.Soc., Vol.66, pp.67-76; 1962
25. Challier, W.O.W. Wilde, G.L. *Power Plants for V/STOL Aircraft.* AGARD; 1964
26. Wilde, G.L. Coplin, J.F. *Lift-Turbo Fans.* J.Roy.Ae.Soc., Vol.69, pp.553-566; 1965
27. Wiles, W.F. *Jet-Lift Intakes.* Agardograph 103 pt.2, pp.559-586; 1965
28. Dent, J.M. *Overcoming Ground Erosion Effects in the Operation of Jet-Lift Aircraft.* AGARD Flight Mechanics Panel Meeting; October 1965
29. Wilde, G.L. *Engines for VTOL STOL Application.* Proc.Intern.Cong. Subsonic Aeronautics, New York Acad.Sc.; April 1967
30. Bishop, R.A. *Developments in the V/STOL Power Plant Field.* Flight Journal; 27th August 1964



31. Brown, D.G.  
Jagger, D.H. *Military V/STOL Transport Aircraft: A Review of the Background to Current Jet-Lift Tactical Transport Proposals.* Aircraft Engineering Journal; May 1966
32. Kemp, E.D.G. *Studies of Exhaust Gas Recirculation for VTOL Aircraft.* AIAA Paper 67-439; 1967
33. Wilson, M. *Hawker Siddeley Harrier G.R. Mk.1.* Flight International Weekly; 2nd November 1967
34. Slenkier, T.K.  
et al. *Initial Studie of Jet-Lift Systems with Fan-Like Exhaust Characteristics for V/STOL Transport Aircraft.* AGARD C.P.22, Paper 14; 1967
35. Emslie, K. *Wind-Tunnel Tests on Models of VTOL Aircraft.* AIAA/R Ae.Soc./J.S.A.S.S. Joint Meeting, Los Angeles; November 1965
36. Wooler, P.G. *On the Flow Past a Circular Jet Exhausting at Right Angles From a Flat Plate or Wing.* J.R. Ae.Soc., Vol.71, pp.216-218; 1967

#### British Universities

37. Jordinson, R. *Flow in a Jet Directed Normally to the Wind.* ARC R & M 3074; 1956
38. Keffer, J.F.  
Baines, W.D. *The Round Turbulent Jet in a Cross-Wind.* J. Fluid Mech., Vol.15, pp.481-496; 1963

#### N. A. S. A.

39. - *Conference on V/STOL and STOL Aircraft.* NASA S.P.-116; 1966
40. Goldsmith, R.H.  
Hickey, D.H. *Characteristics of Aircraft with Lifting-Fan Propulsion Systems for V/STOL.* IAS Paper 63-27; 1963
41. Higgins, C.C.  
Wainwright, T.W. *Dynamic Pressure and Thrust Characteristics of Cold Jets Discharging From Several Exhaust Nozzles Designed for VTOL Downwash Suppression.* NASA T.N.2263; 1964
42. McKinney, M.O.  
et al. *Aerodynamics and Flying Qualities of Jet V/STOL Airplanes.* S.A.E. Paper 864A; 1964
43. Kuhn, R.E.  
McKinney, M.O. *NASA Research on the Aerodynamics of Jet VTOL Engine Installations.* Agardograph 103, pt.2, pp.689-713; 1965
44. McKinney, M.O.  
Newsom, W.A. *Fan V/STOL Aircraft.* Proc.Intern.Cong.Subsonic Aeronautics, New York Acad.Sc.; April 1967
45. Spreeman, K.P. *Free-Stream Interference Effects on Effectiveness of Control Jets Over the Wing Tip of a VTOL Aircraft Model.* NASA TND-4084; 1967
46. Hickey, D.H.  
Cook, W.L. *Aerodynamics of V/STOL Aircraft Powered by Lift-Fans.* AGARD C.P.22, Paper 15; 1967
47. Hammond, A.D.  
McLemore, H.C. *Hot Gas Ingestion and Jet Interference Effects.* AGARD Flight Mechanics Panel Meeting; September 1967

48. Przedpelski, Z.J. *Lift-Fan Technical Studies.* NASA CR-761; 1967
49. Kirk, J.V.  
Barrack, J.P. *Reingestion Characteristics and Inlet Flow Distortion of V/STOL Lift Engine Fighter Configurations.* AIAA Paper 68-78; 1968
- American Firms**
50. Dickard, H.E. *Lift-Fan V/STOL Propulsion and Airframe Integration.* Agardograph 103, pp.661-688; 1965
51. Wooler, P.T.  
et al. *The Pressure Distribution on a Rectangular Wing with the Jet Exhausting Normally Into an Airstream.* AIAA Paper 67-1; 1967
52. Hall, G.F. *Scaling of VTOL Aerodynamic Suck-Down Forces.* J.Aircraft, Vol.4, pp.393-394; 1967
53. Adarkar, D.B.  
Hall, G.R. *The "Fountain" Effect and VTOL Exhaust Ingestion.* AIAA Paper 68-79; 1968
54. Jenny, R.B. *Power Effects on Two-Fan-In-Fuselage Fighter Configuration.* AGARD C.P.22, Paper 19; 1967
55. Kutney, J.T. *Propulsion System Development for V/STOL Transports.* J.Aircraft, Vol.3, pp.489-497; 1966
- Germany**
56. Hartmann, A. See Reference No.34
57. Krowe, C.T.  
Riesebieter, R. *An Analytic and Experimental Study of Jet Deflection in a Cross-Flow.* AGARD C.P.22, Paper 16; 1967
58. Fütterer, H.  
Harms, L. *Jet Interference measurements on a VTOL-Model with Jet Simulation by Fans.* AGARD C.P.22, Paper 17; 1967
59. Göthert, R. *Inlet Measurements on a VTOL-Aircraft Model.* AGARD C.P.22, Paper 18; 1967
- France**
60. Deplante, H. *The Mirage III V V/STOL Fighter.* S.A.E./ASME Paper ; April 1964
- Canada**
61. Schaub, U.W. *Experimental Studies of VTOL Fan-In-Wing Inlets.* Agardograph 103, Part 2, pp.721-747; 1965

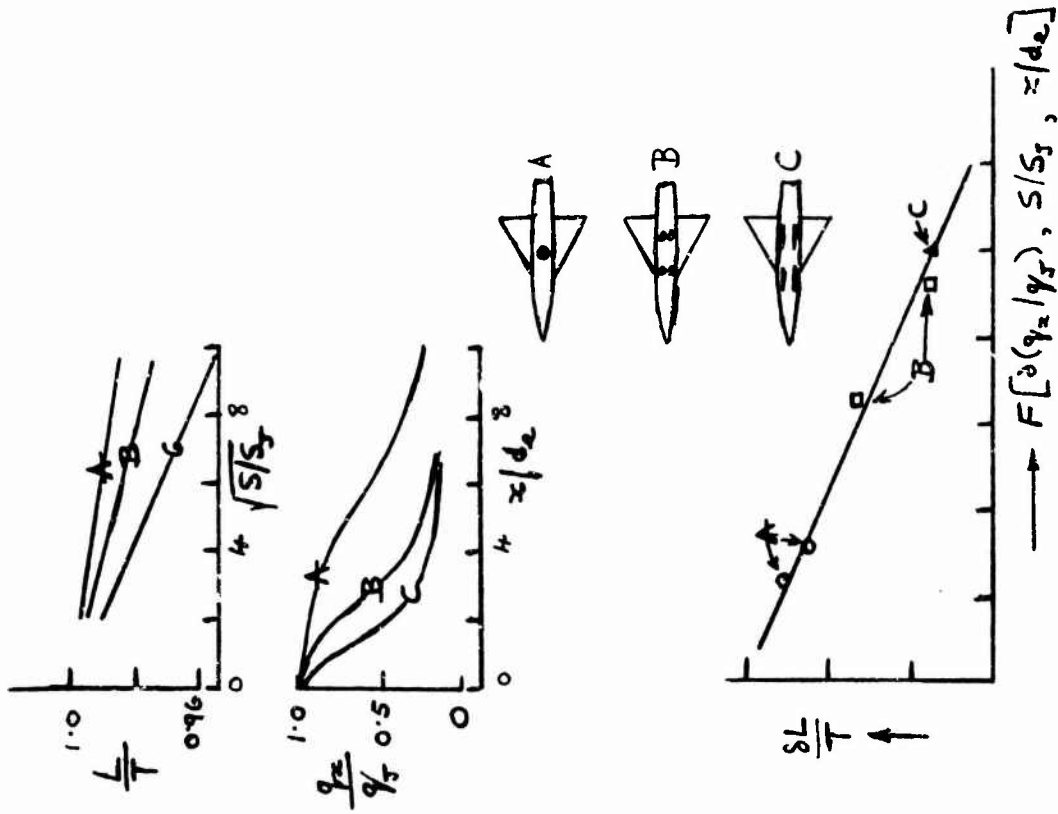


Fig. 2 NASA jet-decay/base-suction studies

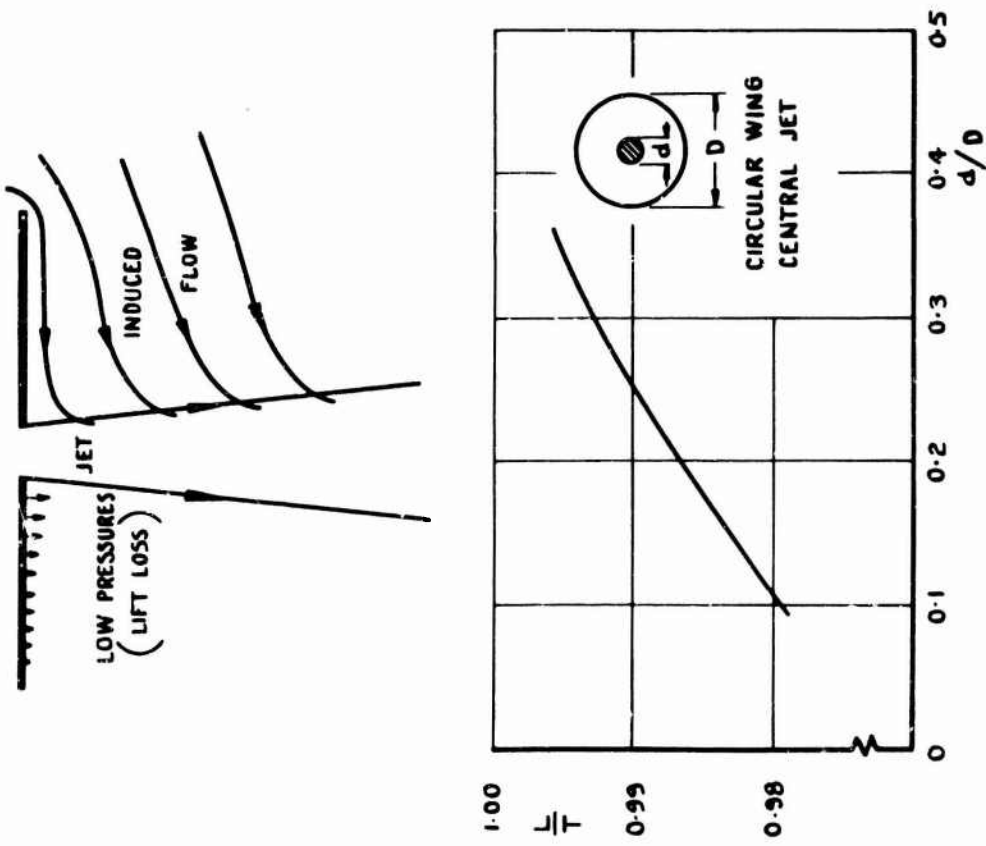


Fig. 1 Installed lift loss away from ground

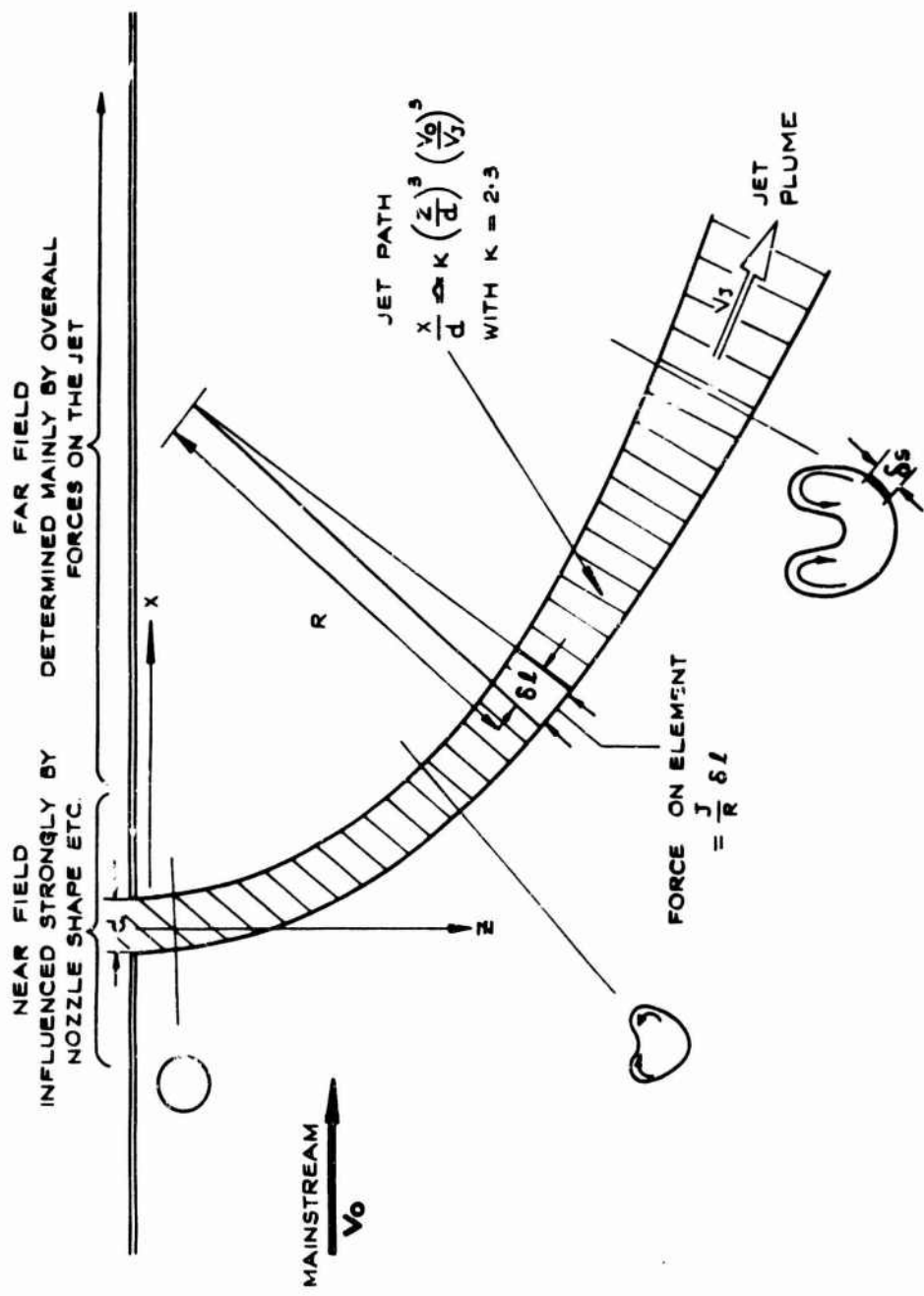


Fig. 3 Jet efflux into a mainstream

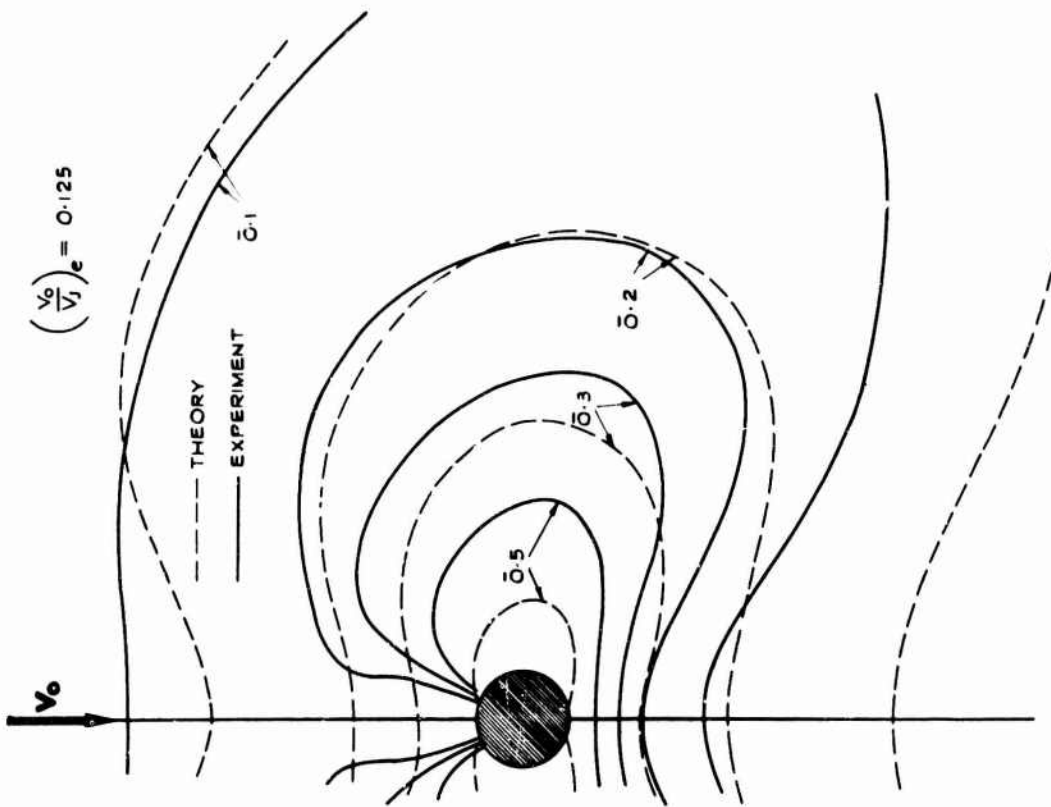


Fig. 4(a) Surface pressure contours with jet efflux from a plane wall

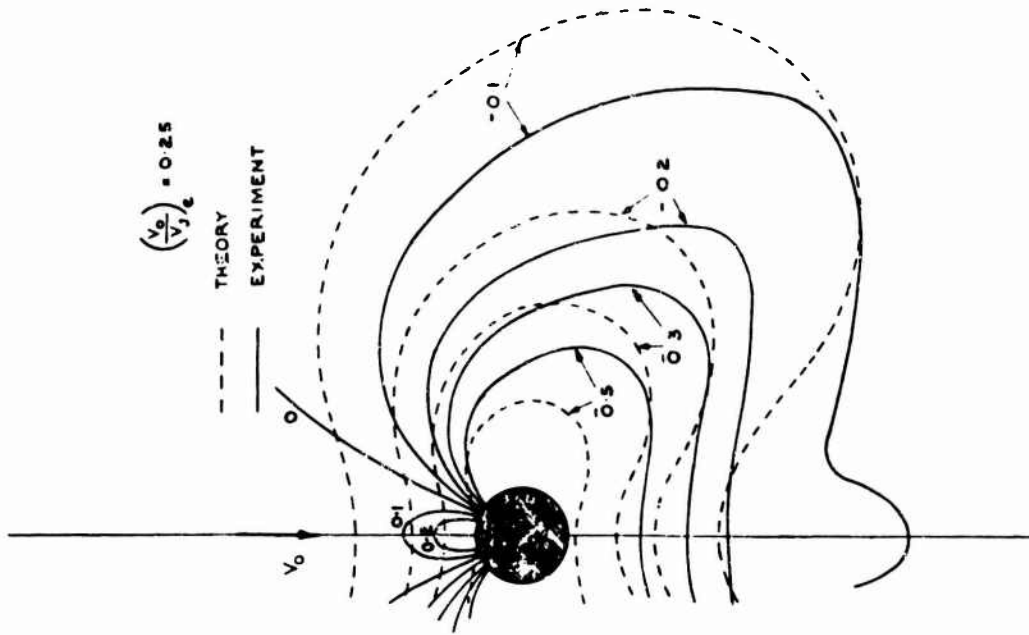


Fig. 4(b) Surface pressure contours with jet efflux from a plane wall



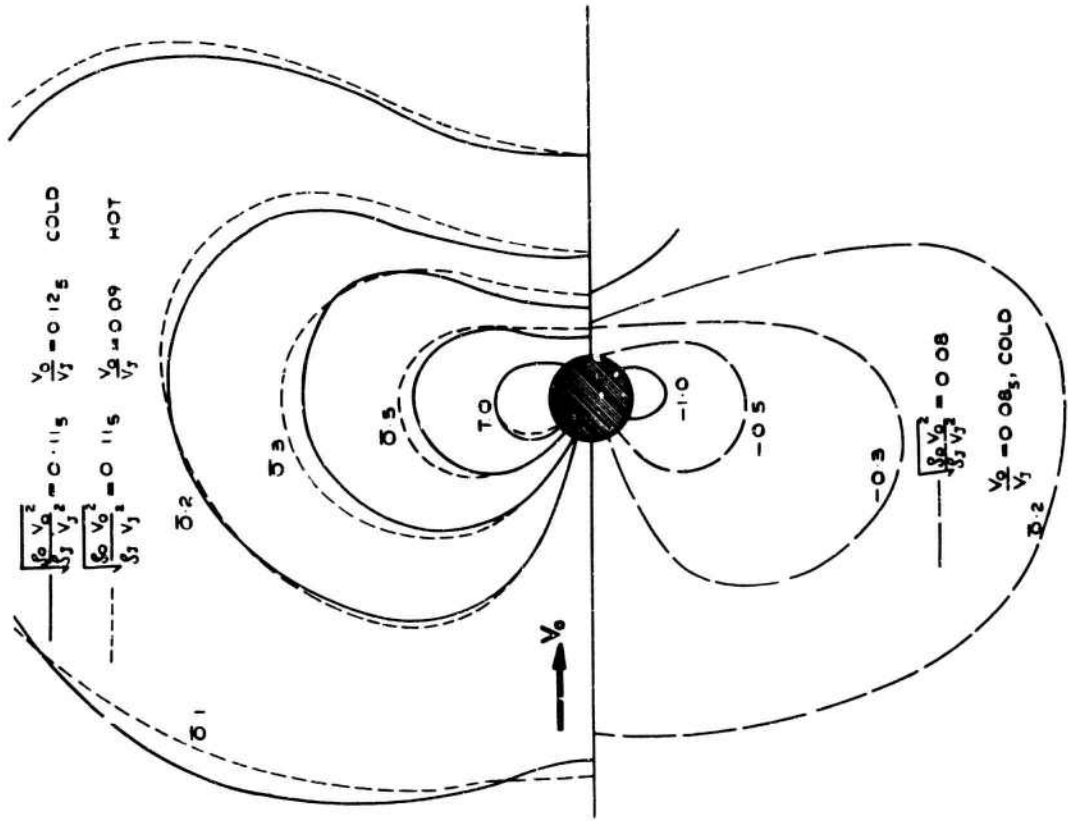


Fig. 8 Correlation of surface pressure distributions for hot and cold jets

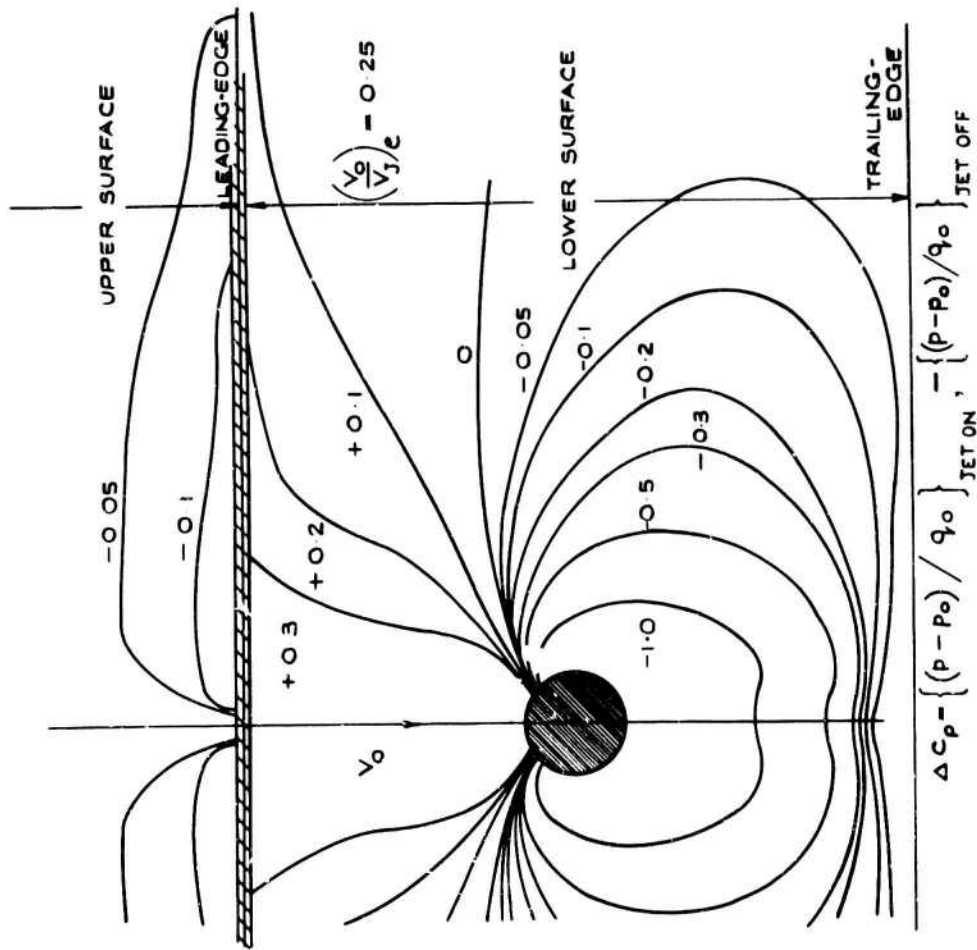


Fig. 7 Incremental pressure ( $\Delta C_p$ ) contours due to jet efflux from a rectangular wing

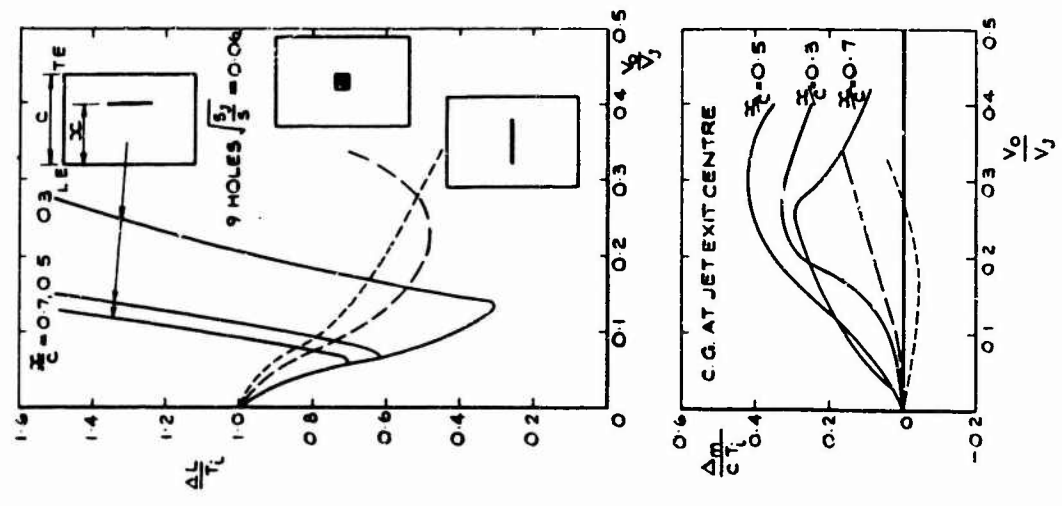


Fig. 9(b) Rectangular r-wing model with multi-jets

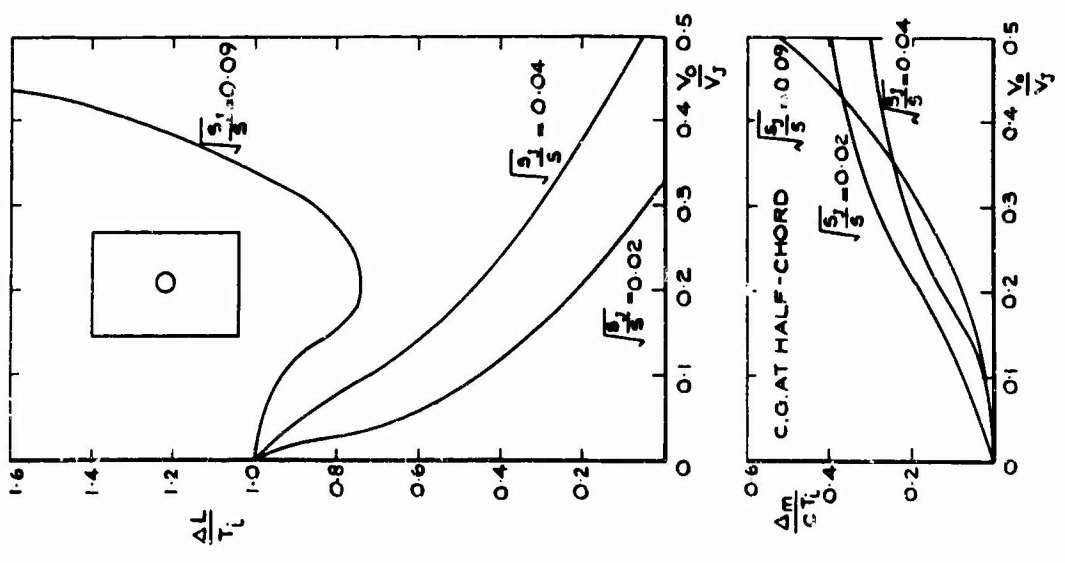


Fig. 9(a) Rectangular wing model with single central jet



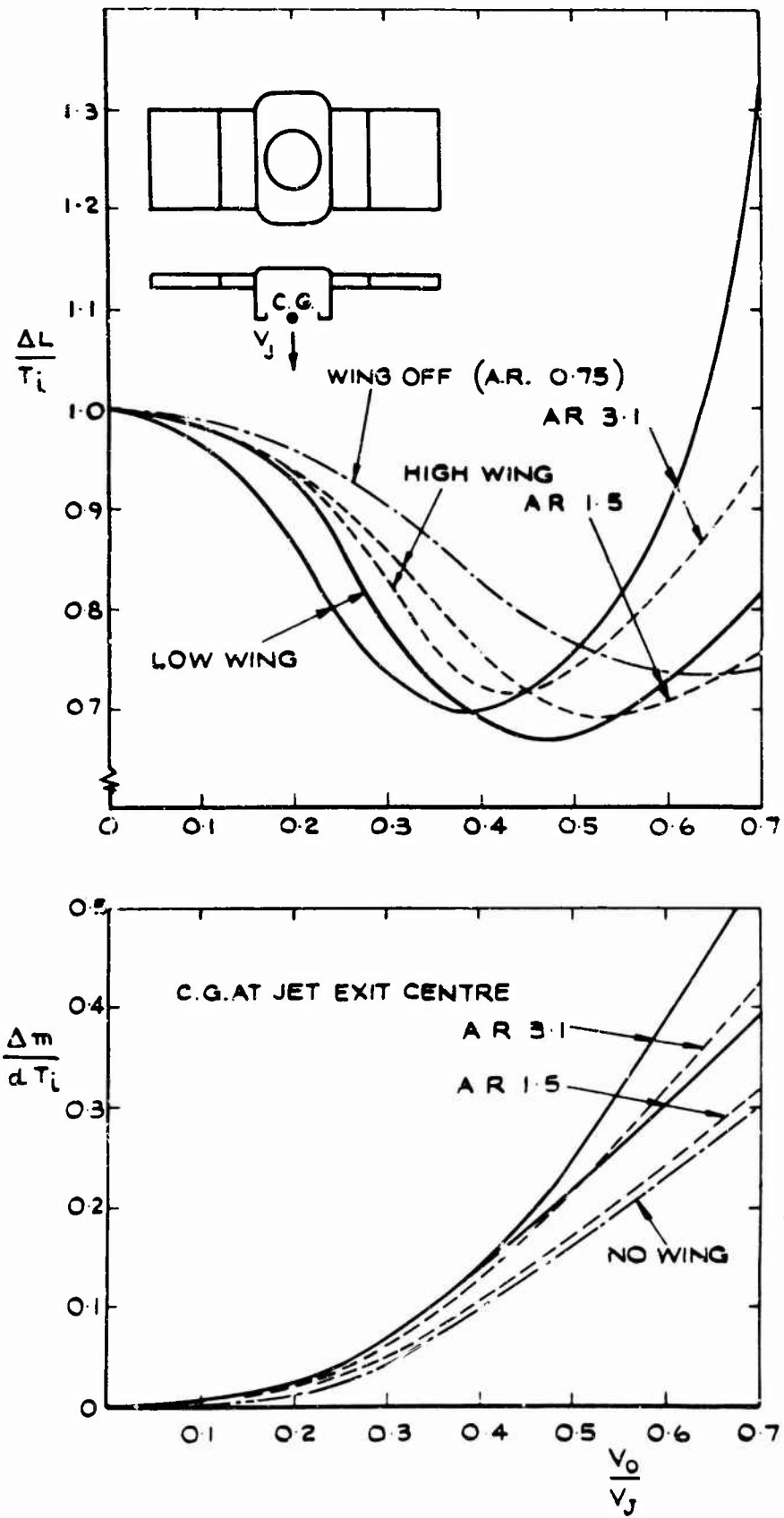


Fig. 10 Single-jet bluff body model

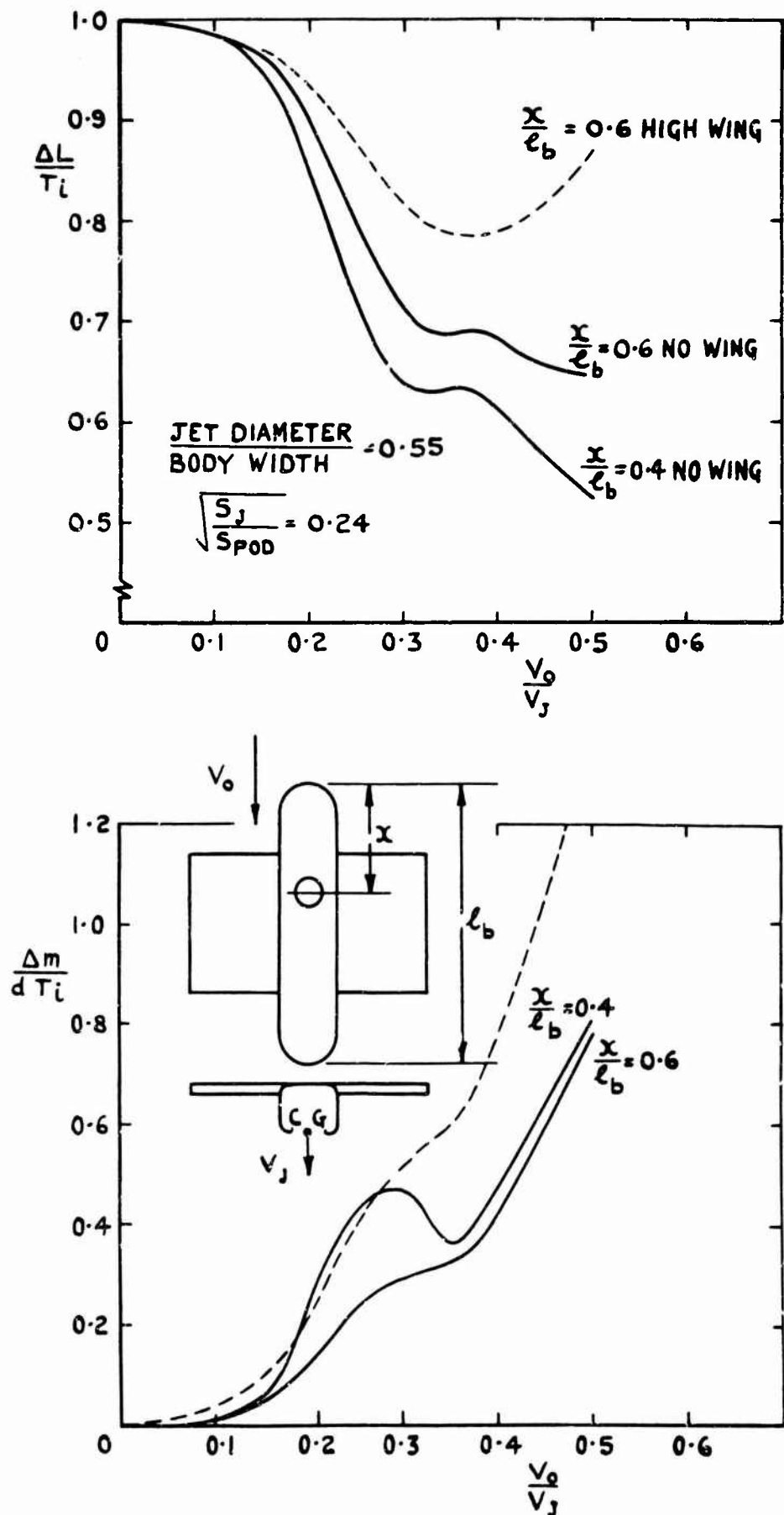


Fig. 11 Single-jet pod model

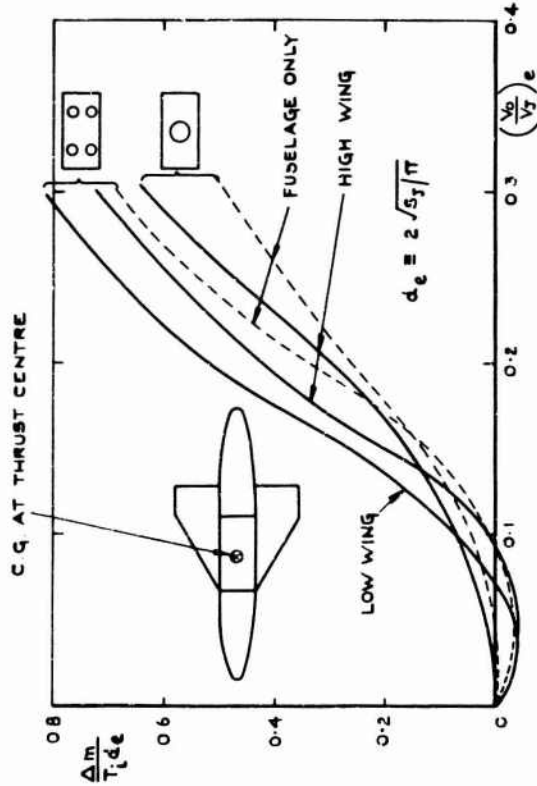
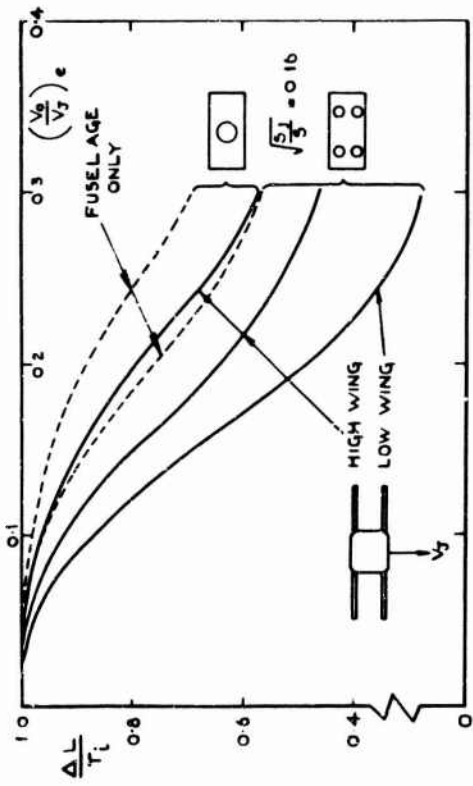


Fig. 13 Generalised delta-wing model. Effect of wing location

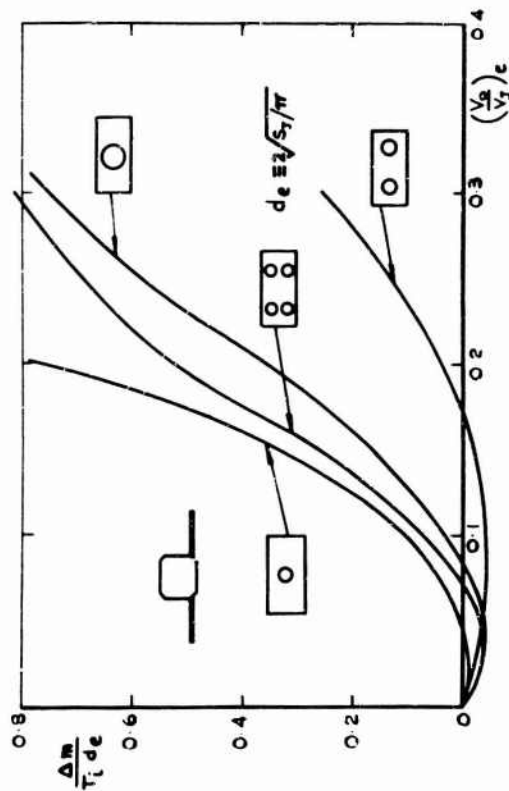
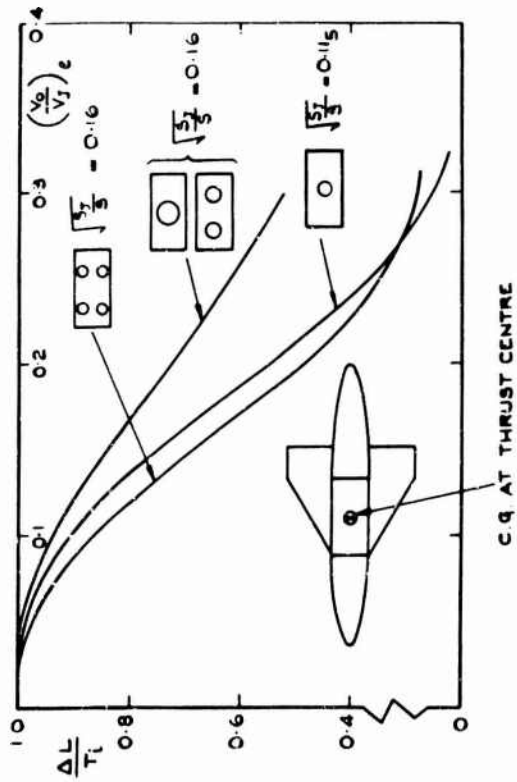


Fig. 12 Generalised delta wing model with low wing. Effect of jet size and disposition

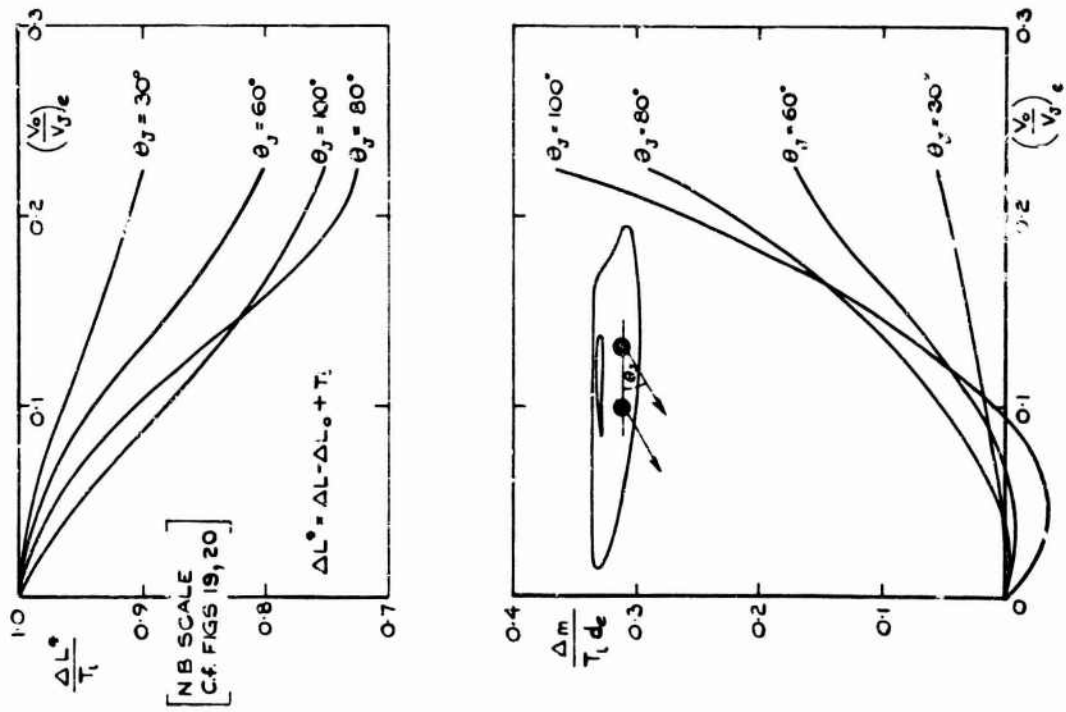


Fig. 15 Effect of variation of jet angle

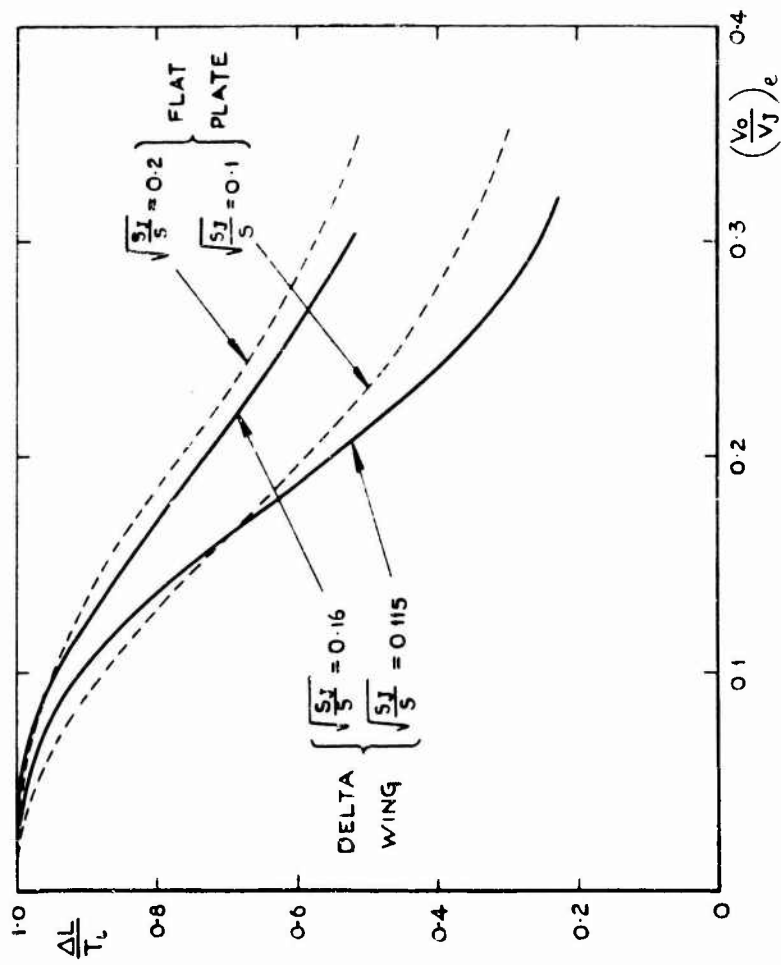


Fig. 14 Comparison of flat plate and delta results

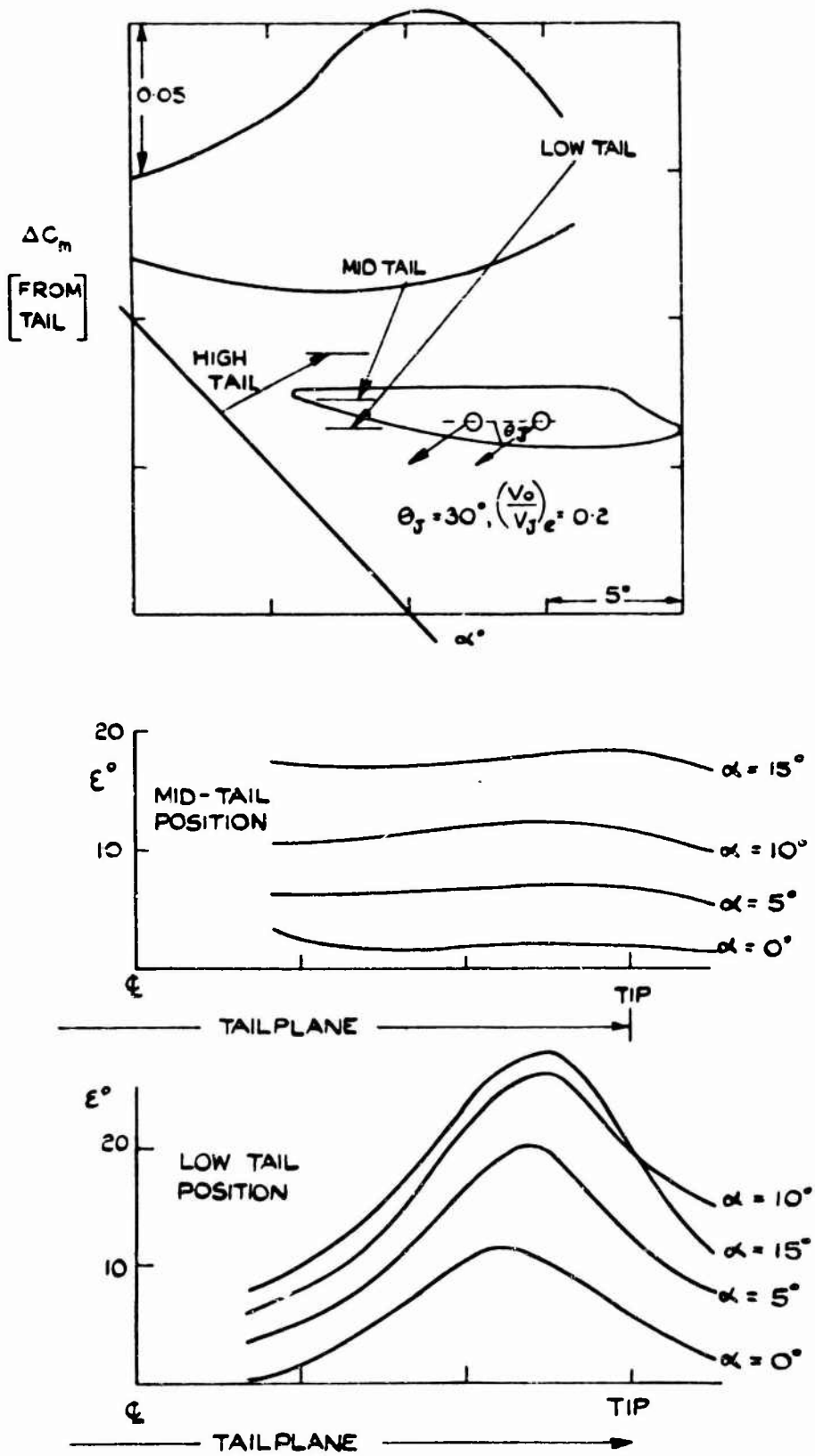


Fig.16 Jet efflux effects on tailplane

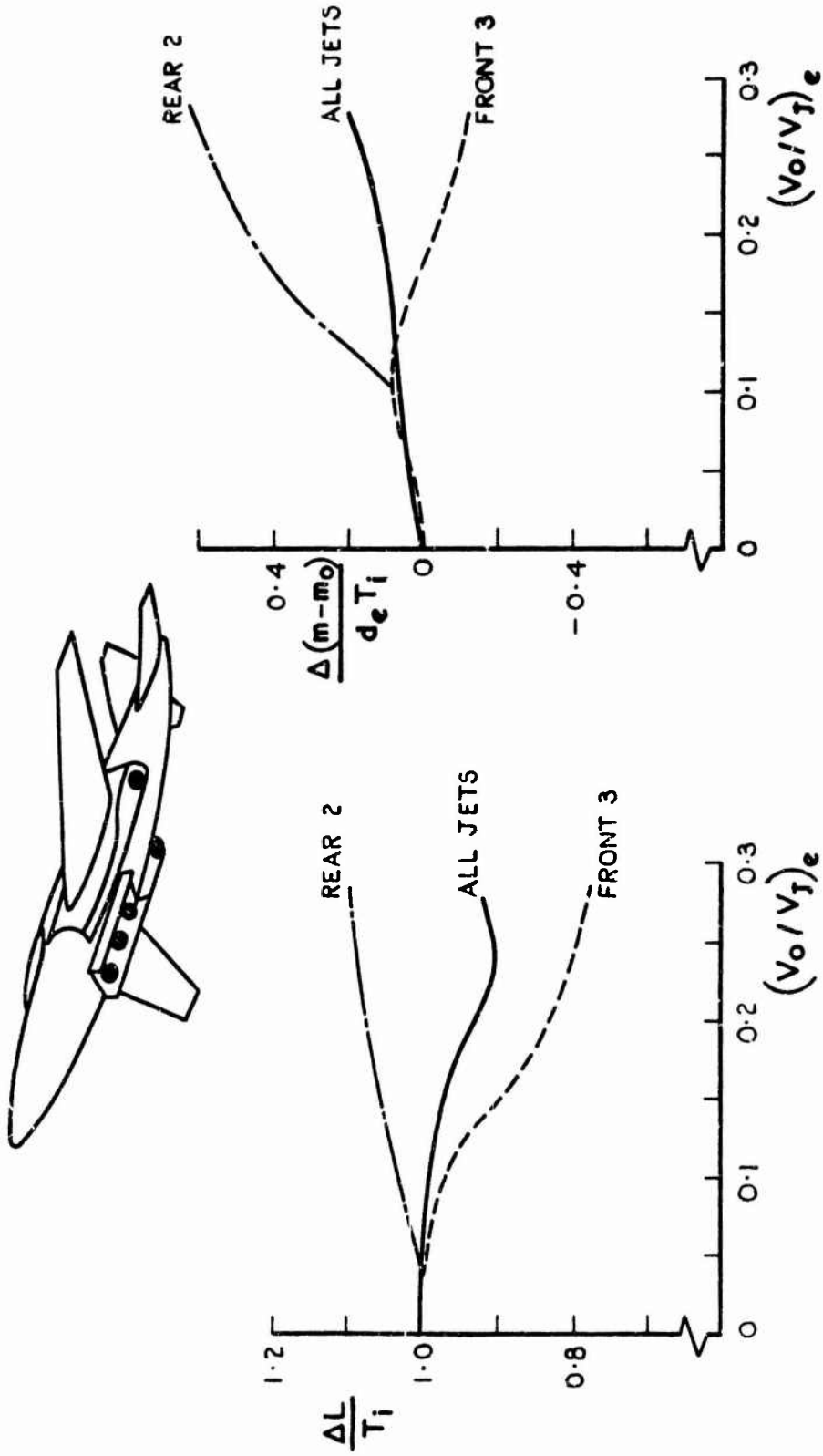


Fig. 17 NASA model tests on jet interference in transition

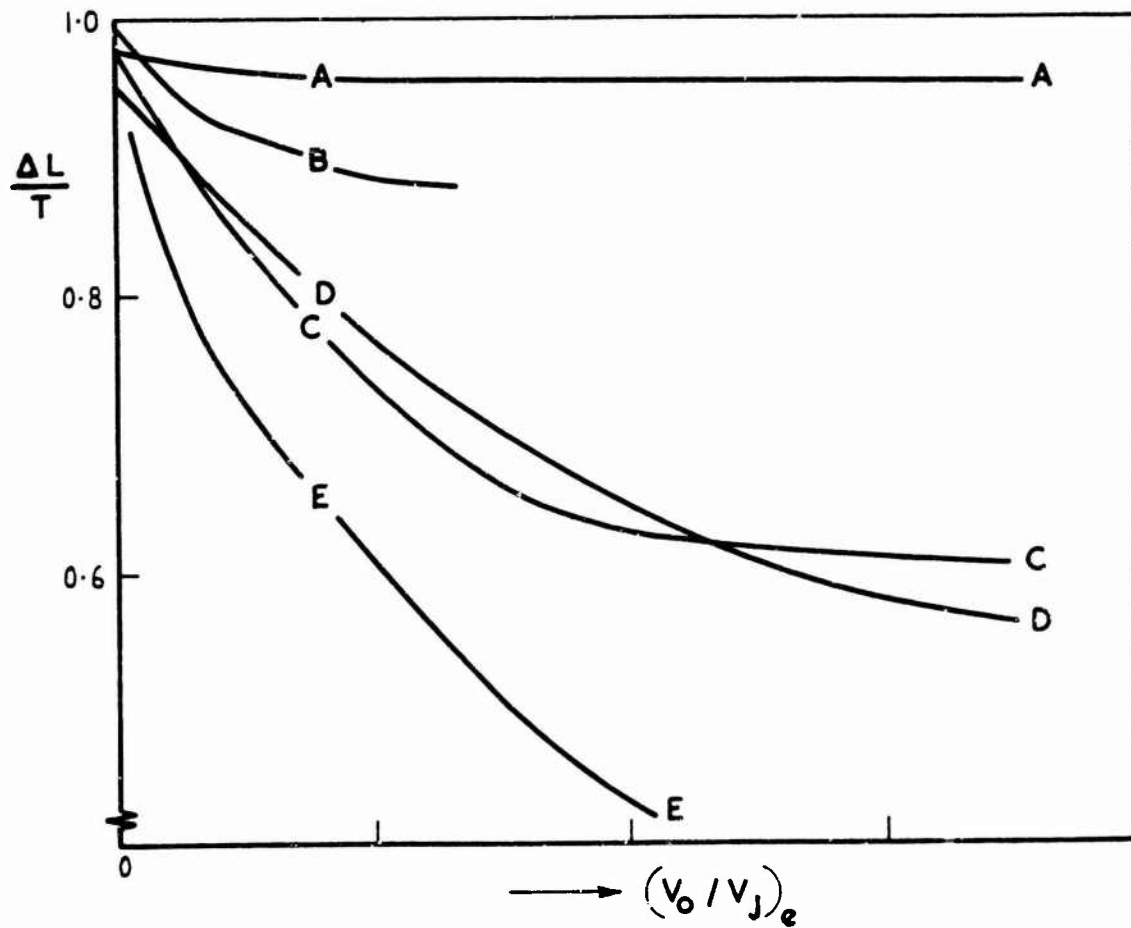
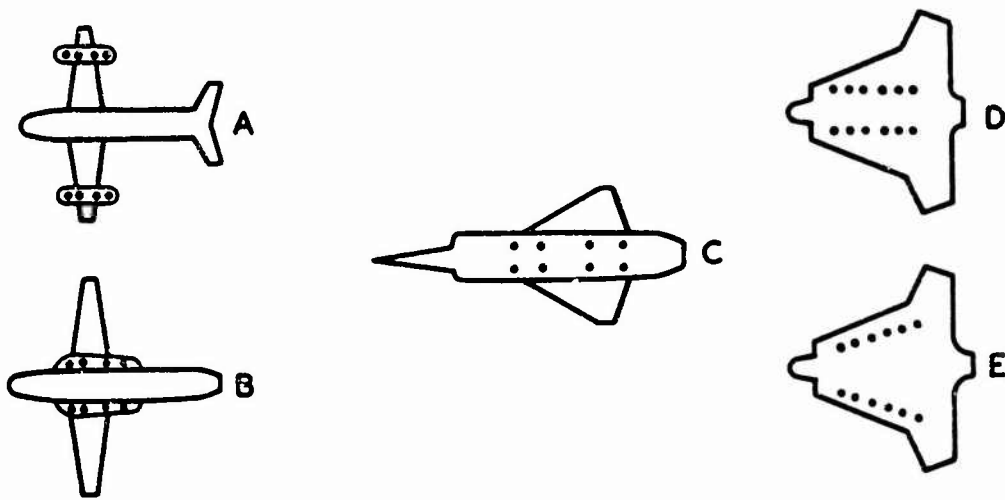


Fig. 18 BAC models with multiple jets in transition

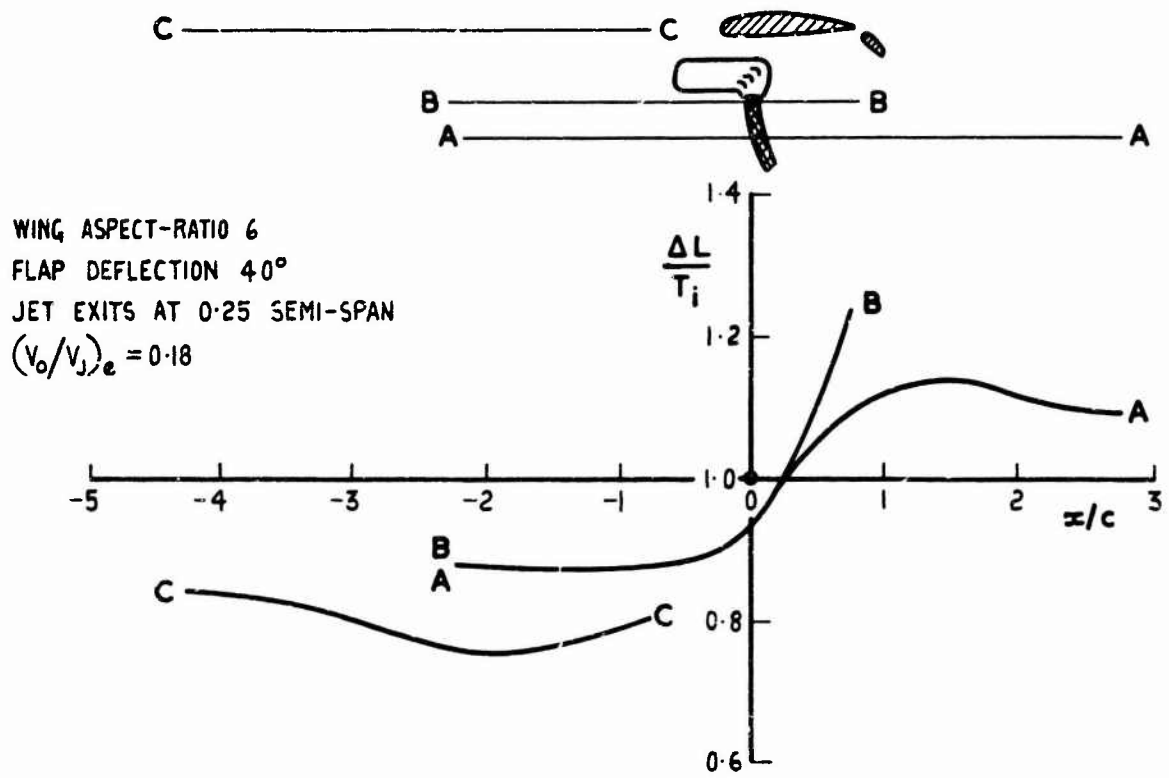


Fig. 19 NASA results on effect of jet-exit position



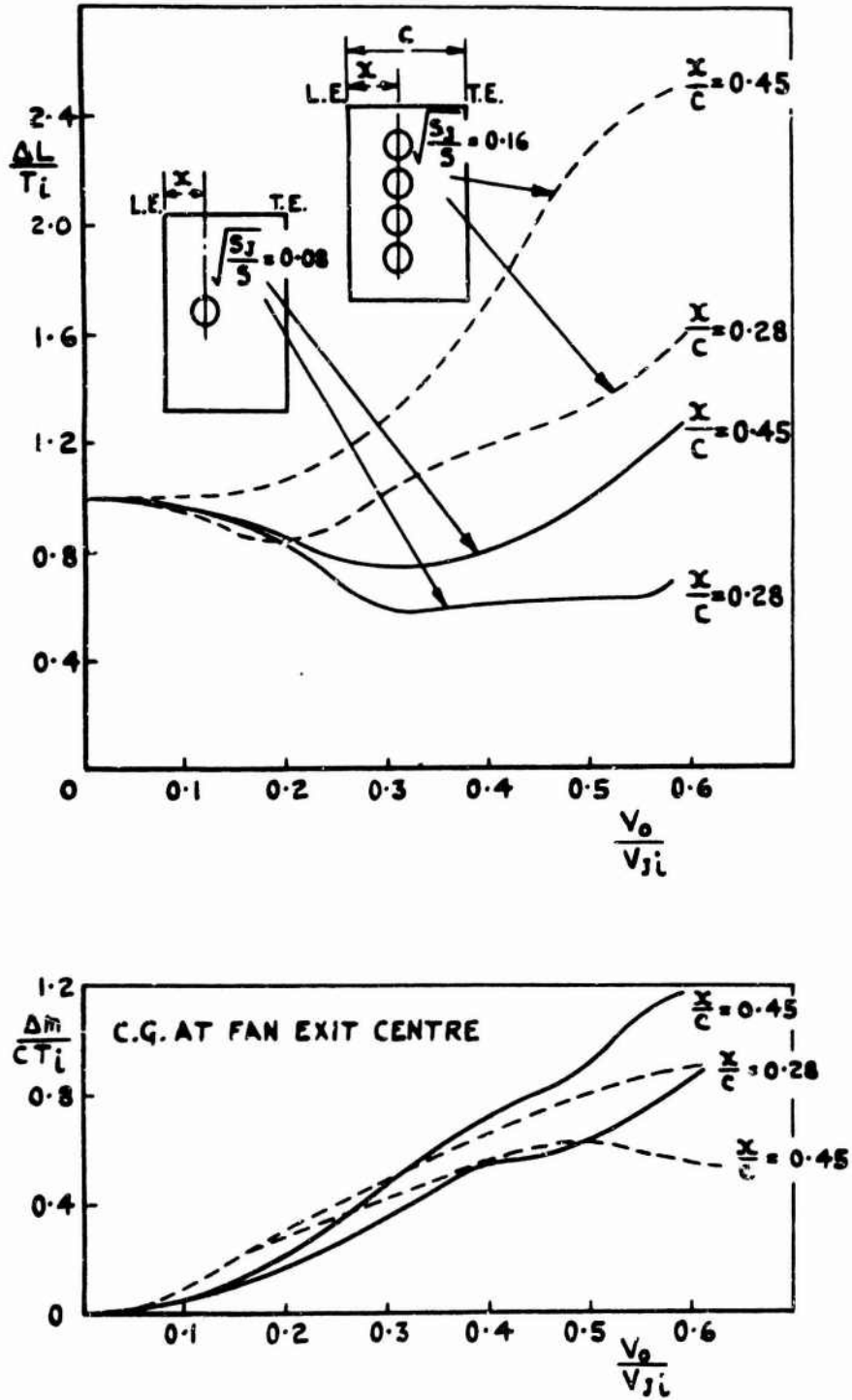


Fig. 20 Multi-fan rectangular wing model

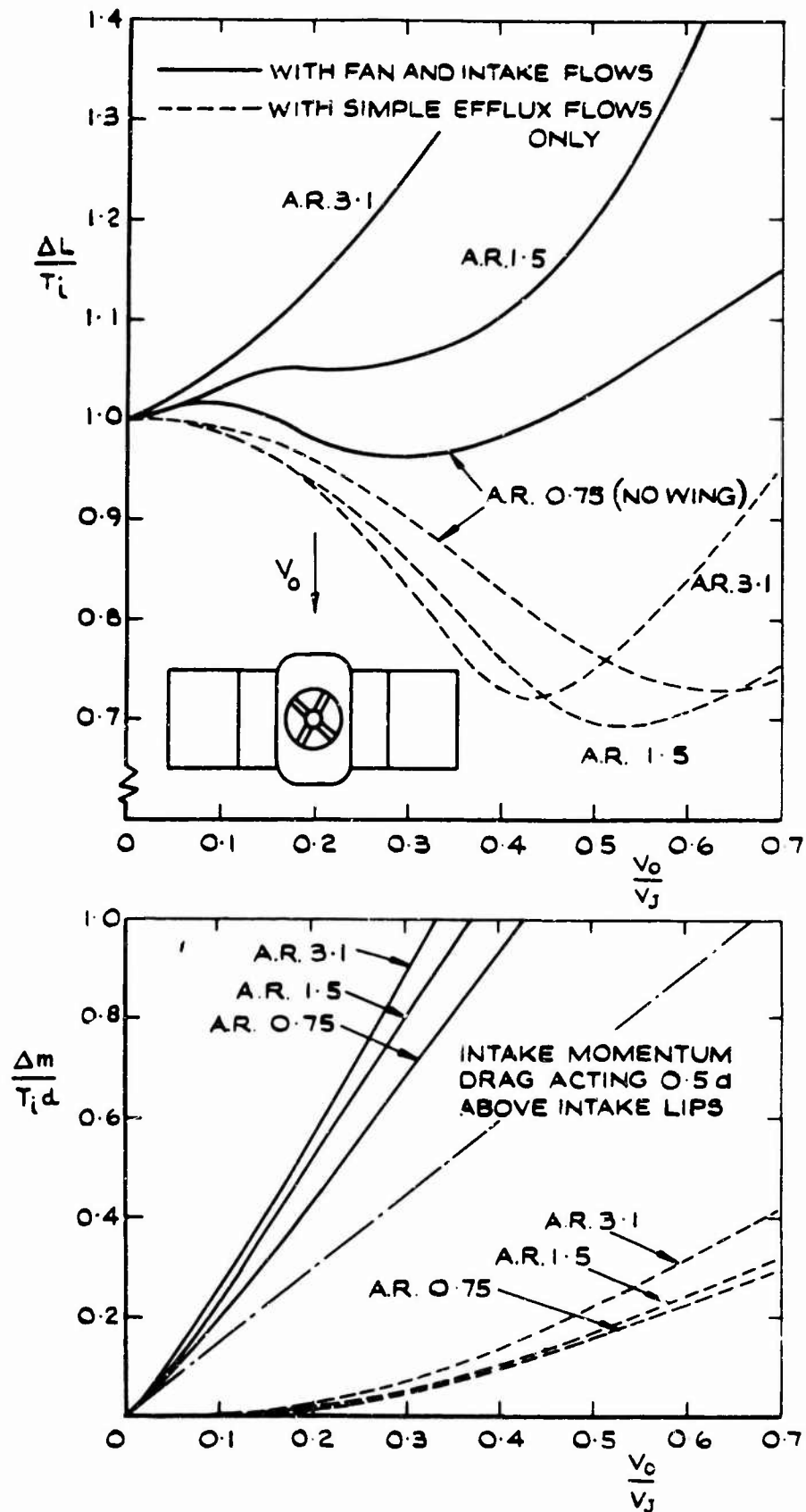


Fig. 21 Fan-flow and simple efflux effects on bluff body model with high wing

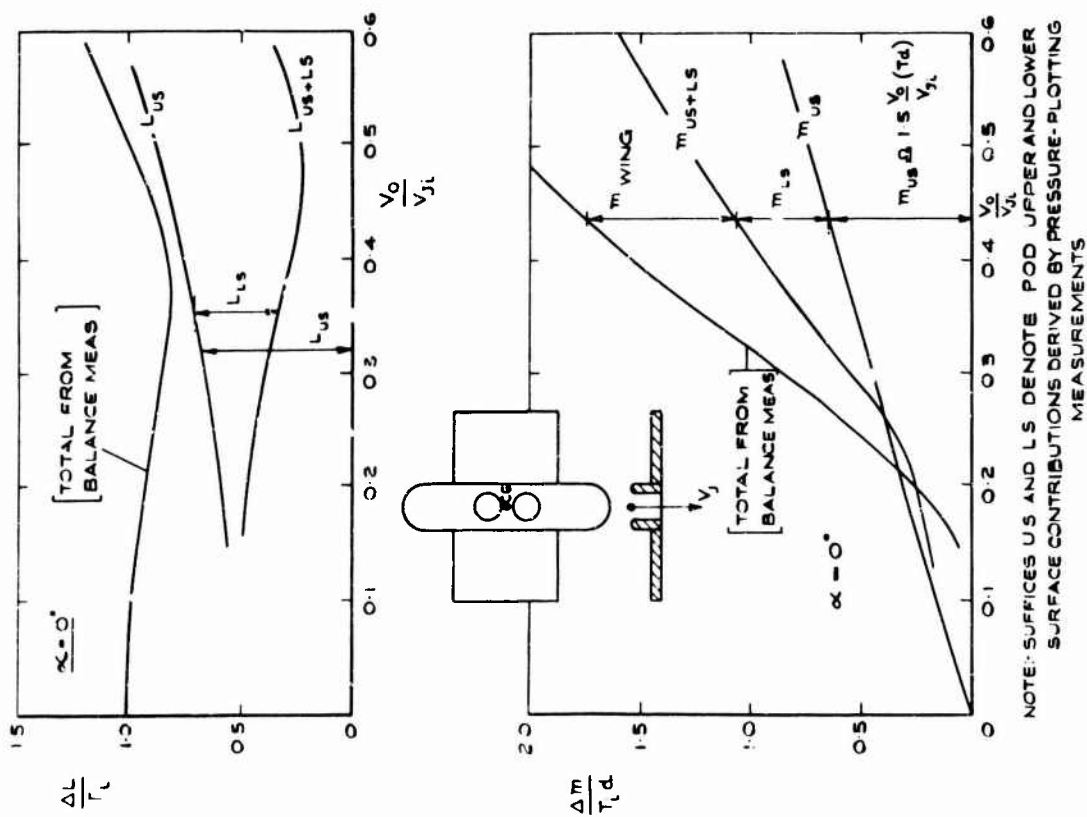


Fig. 22 Twin fan pod model with low wing

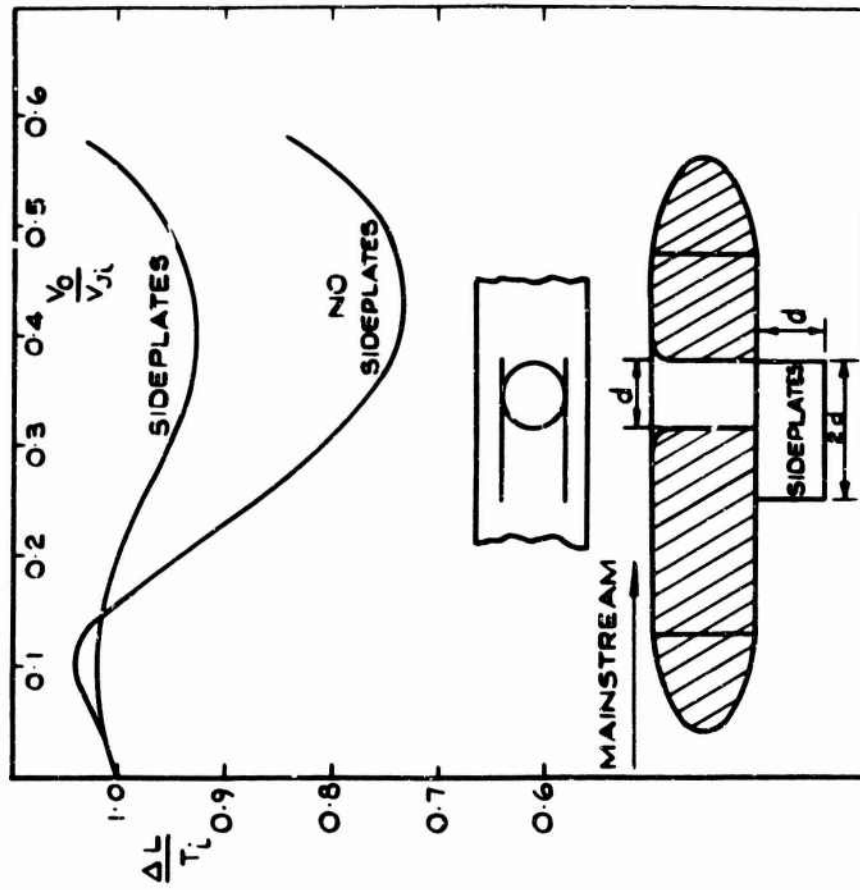


Fig. 23 Effect of sideplates on pod lift with rear fan

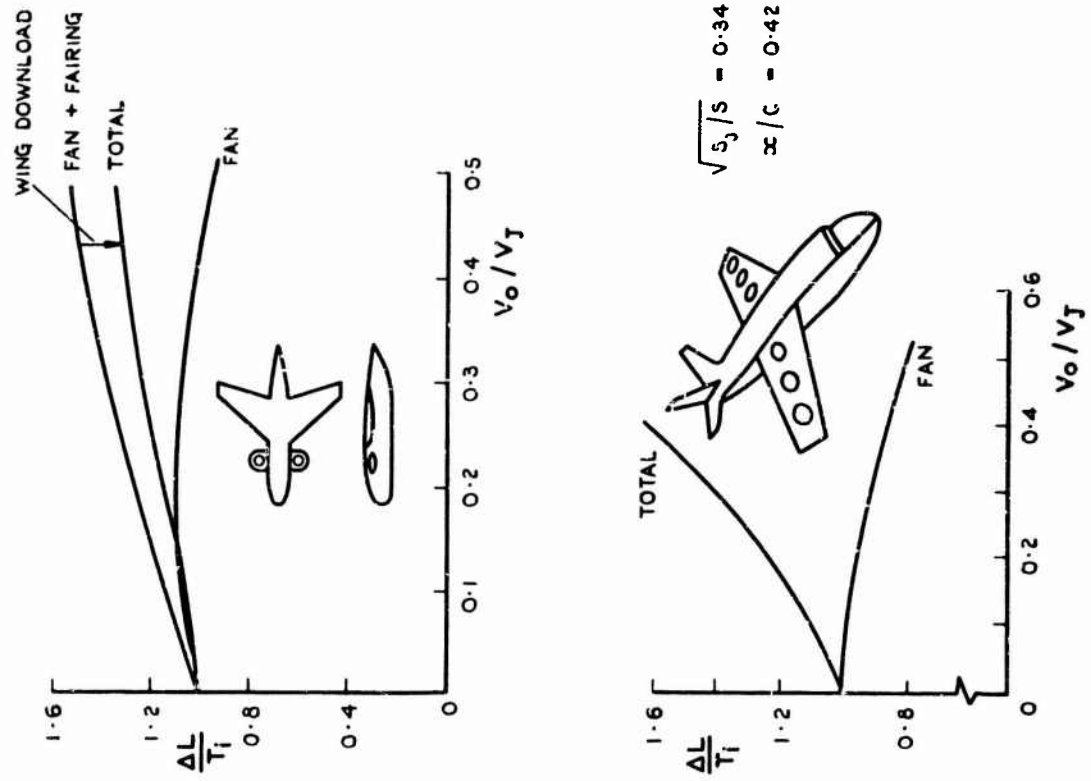


Fig. 25 NASA results on lifting fans

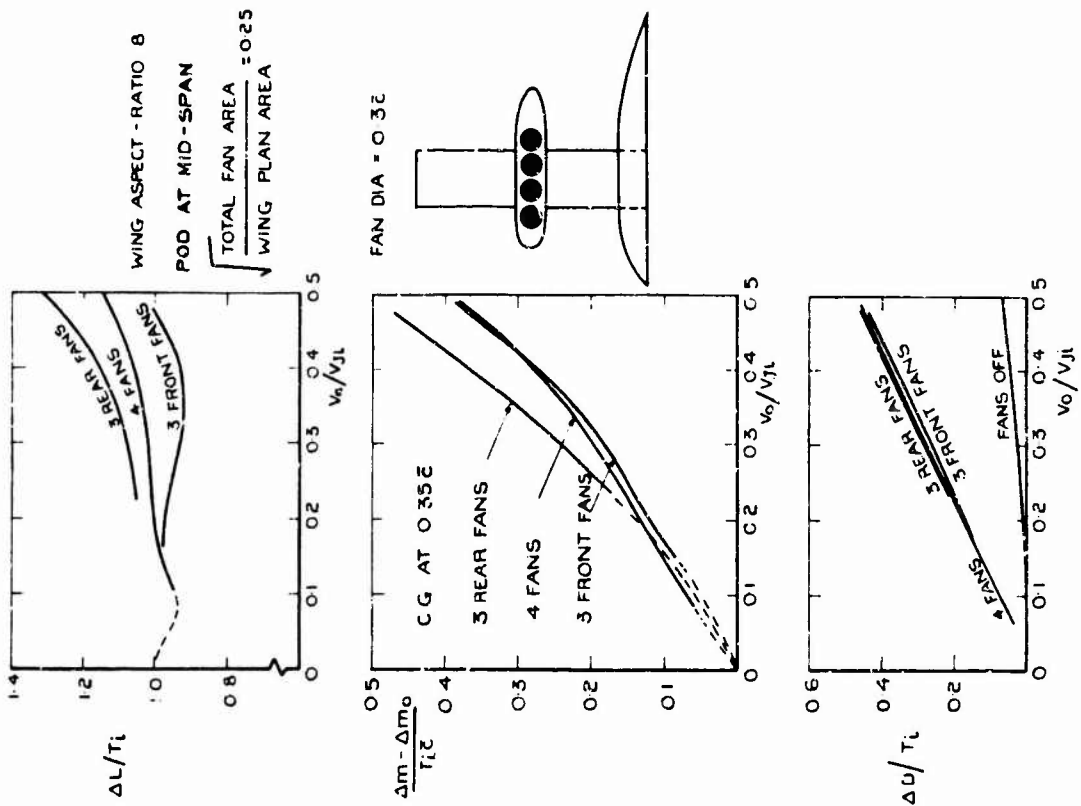


Fig. 24 Four-fan pod half-model results

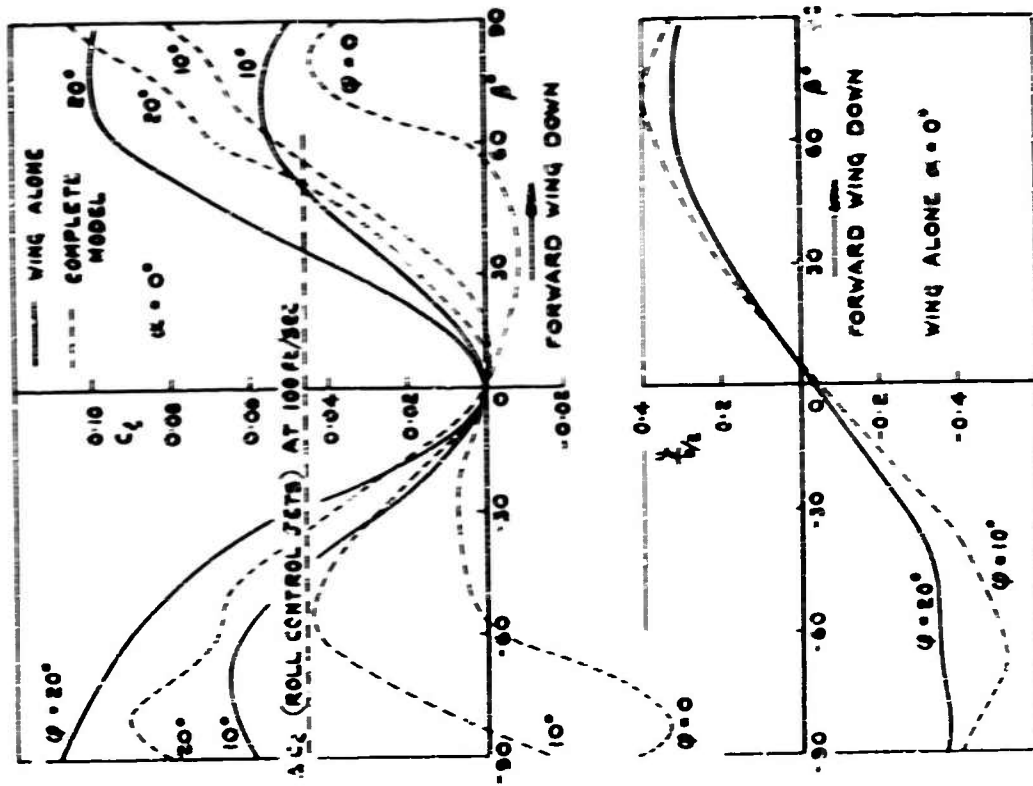


Fig. 20 Rolling moment due to sideslip and centre of pressure movement. Short B.C.1 model

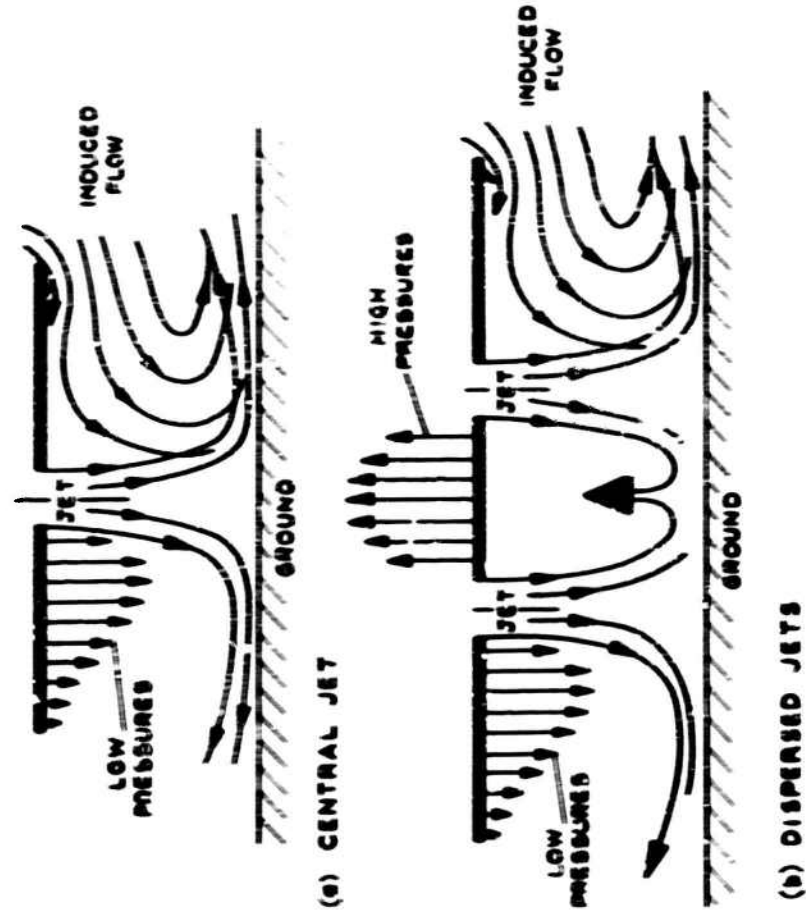


Fig. 27 Flow patterns near ground with central jet and with dispersed jets

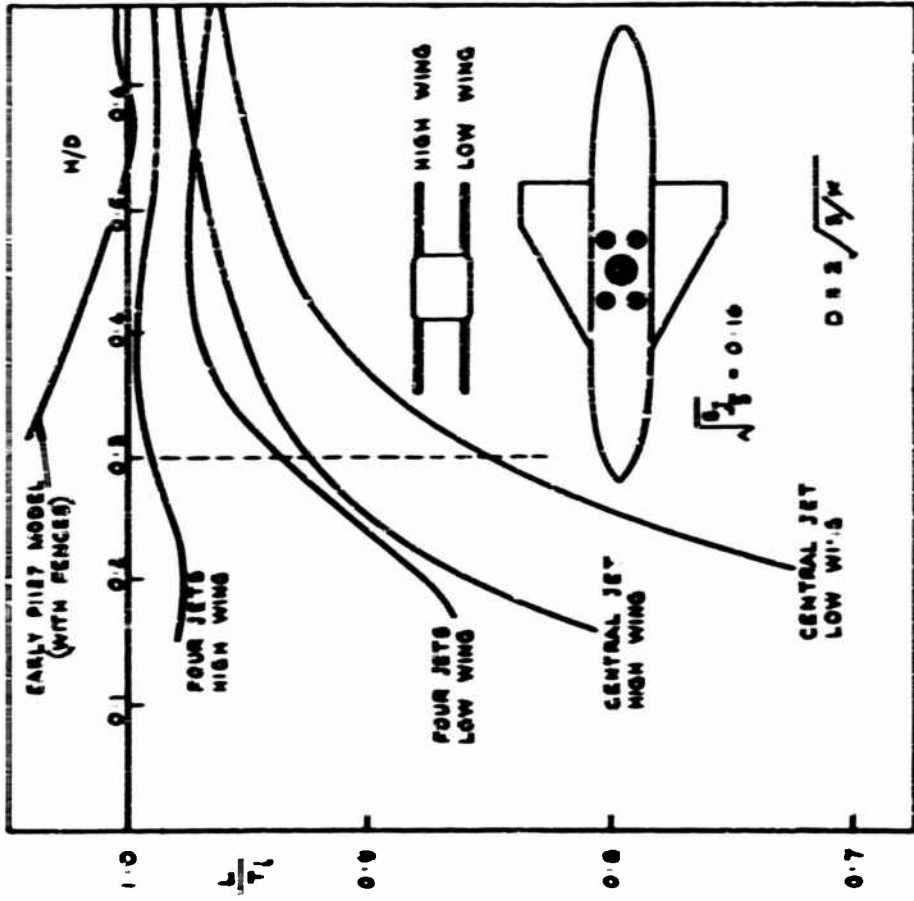


Fig. 20 Jet-efflux interference on lift near ground

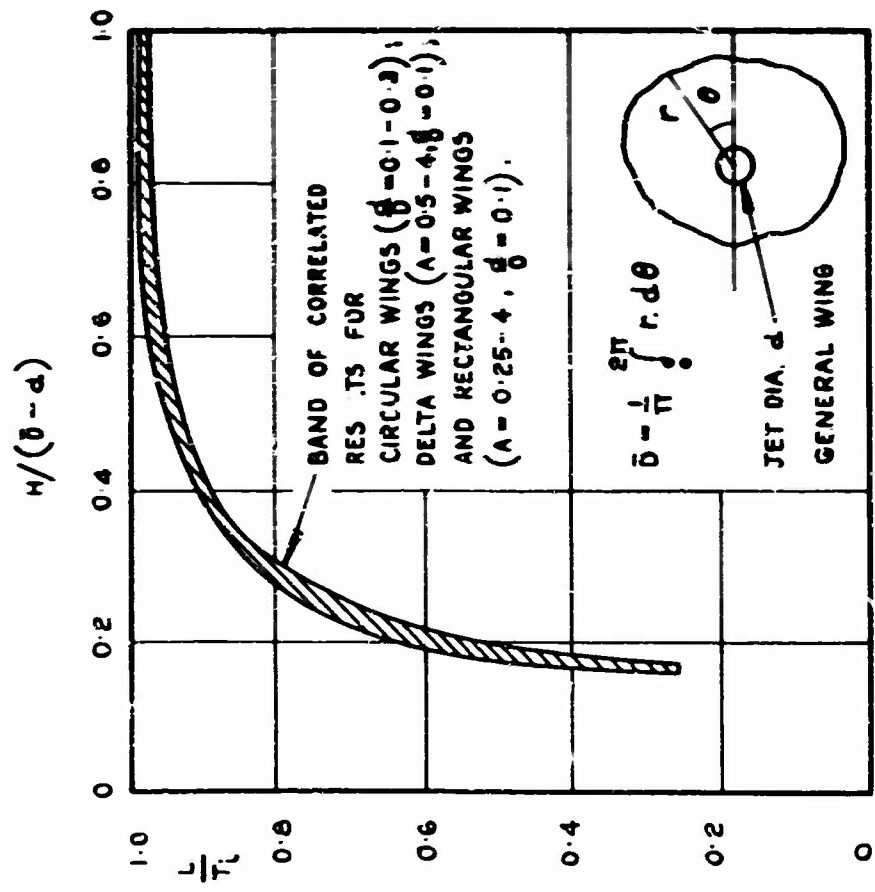
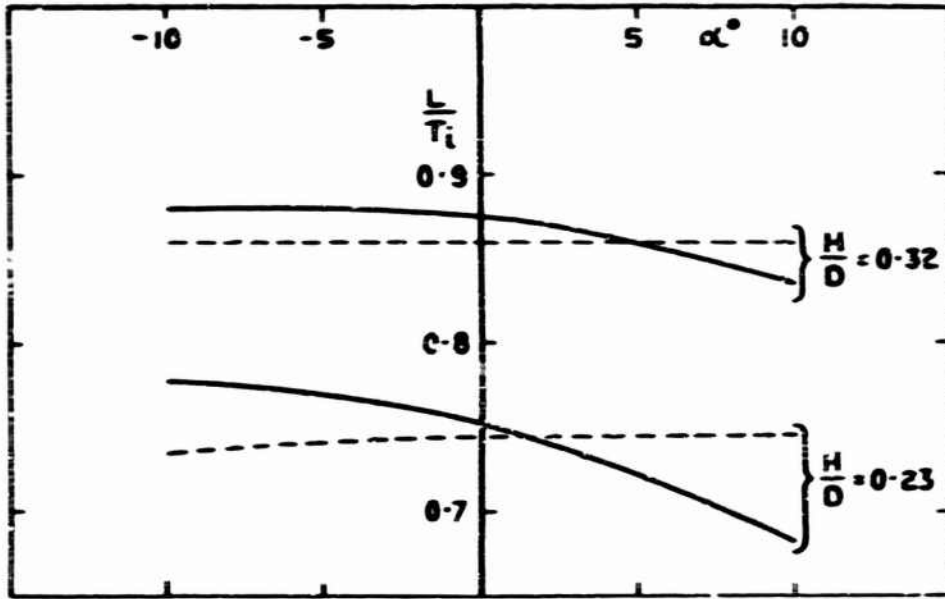


Fig. 28 Correlation of lift near ground for range of planforms with central jet



— WING CENTROID 1.1d BEHIND THRUST CENTRE  
 - - - WING CENTROID 0.5d AHEAD OF THRUST CENTRE

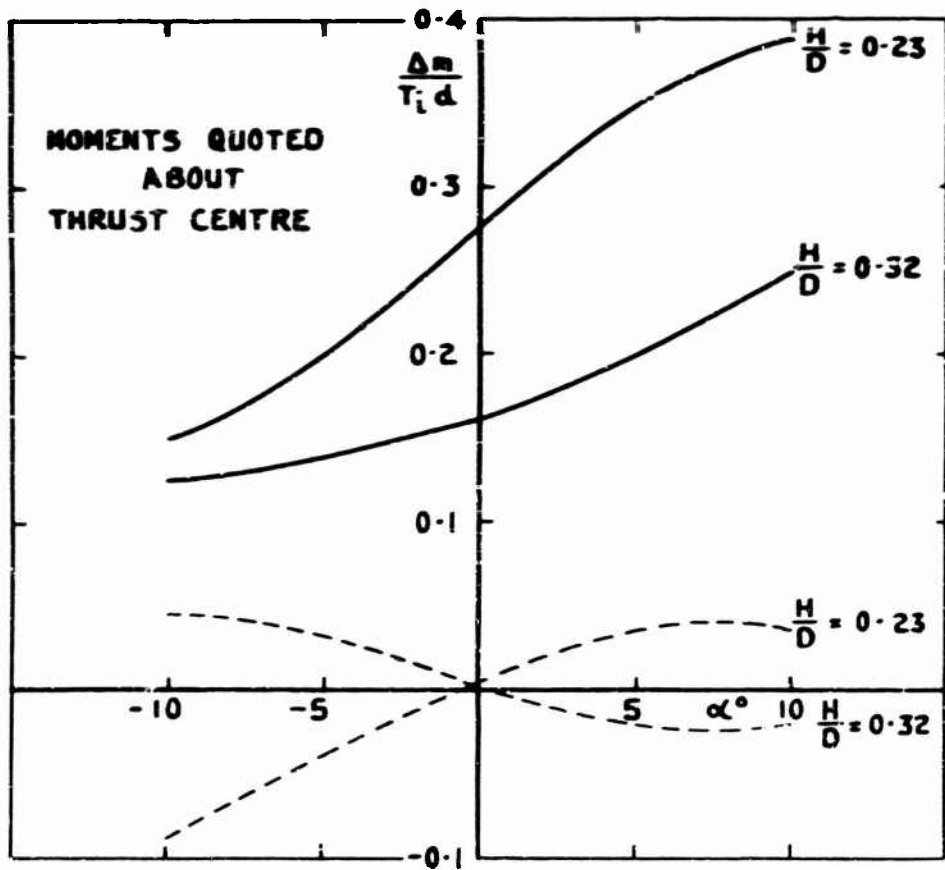


Fig. 30 Variation of jet-efflux interference with attitude near ground

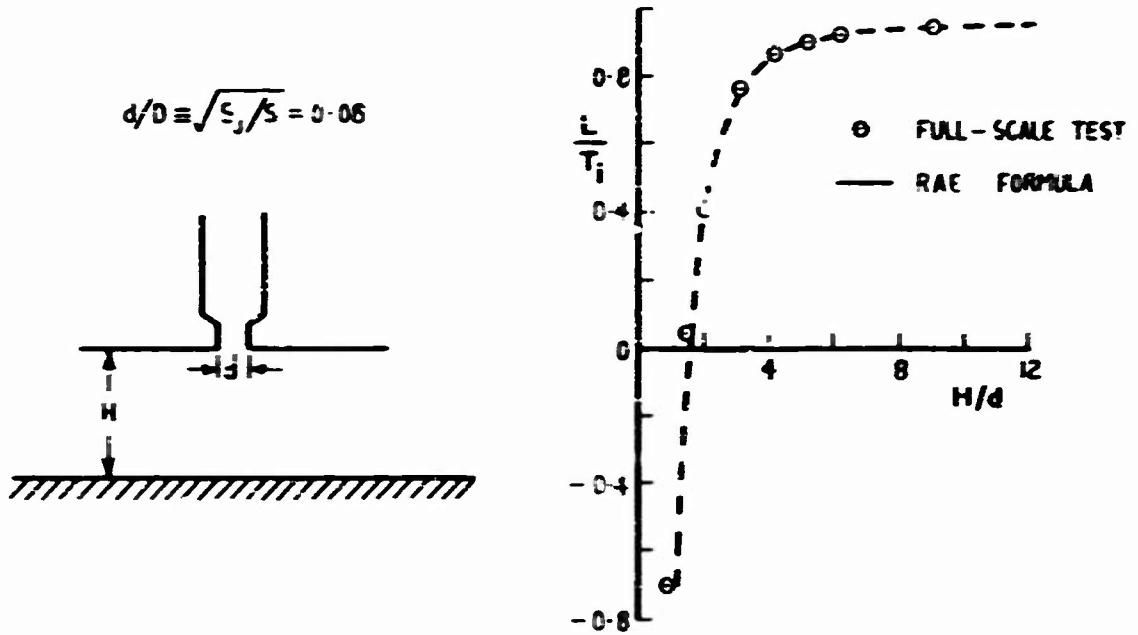


Fig. 31 Northrop full-scale results on jet interference near ground

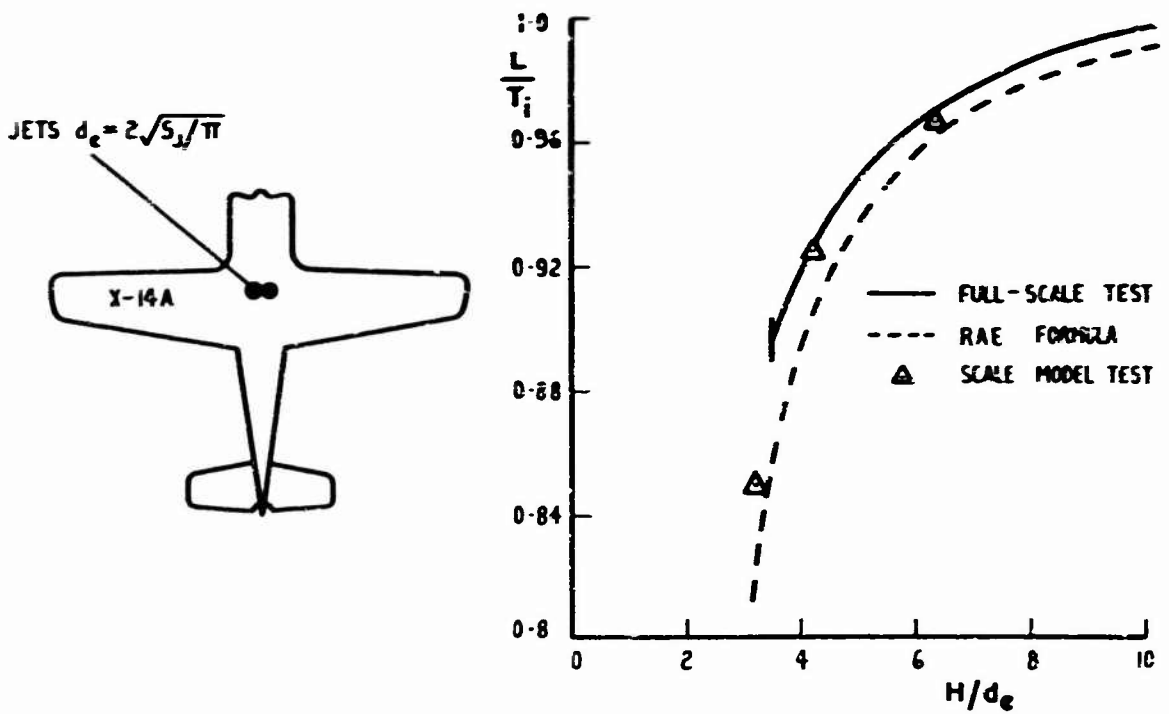


Fig. 32 NASA full-scale results on jet interference near ground



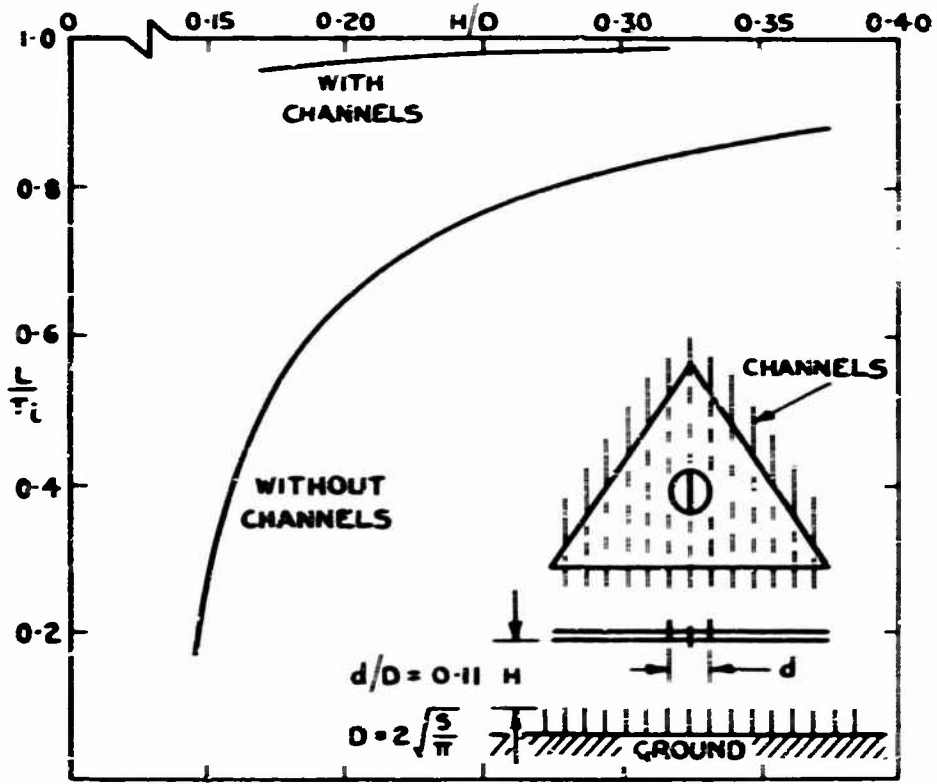


Fig. 33 Alleviation of lift loss near ground by channels

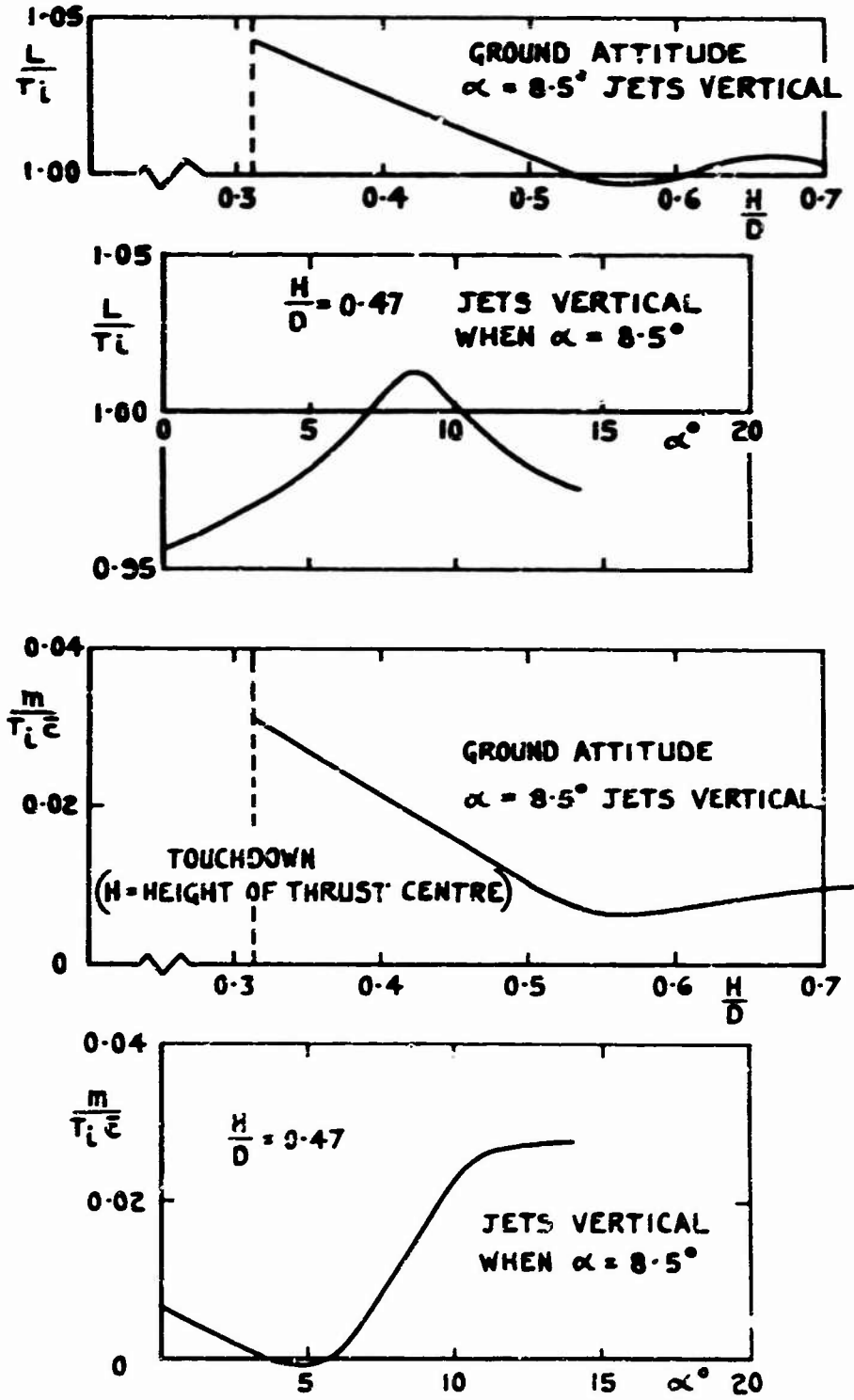


Fig. 34 Hawker P1127 prototype model static ground effects

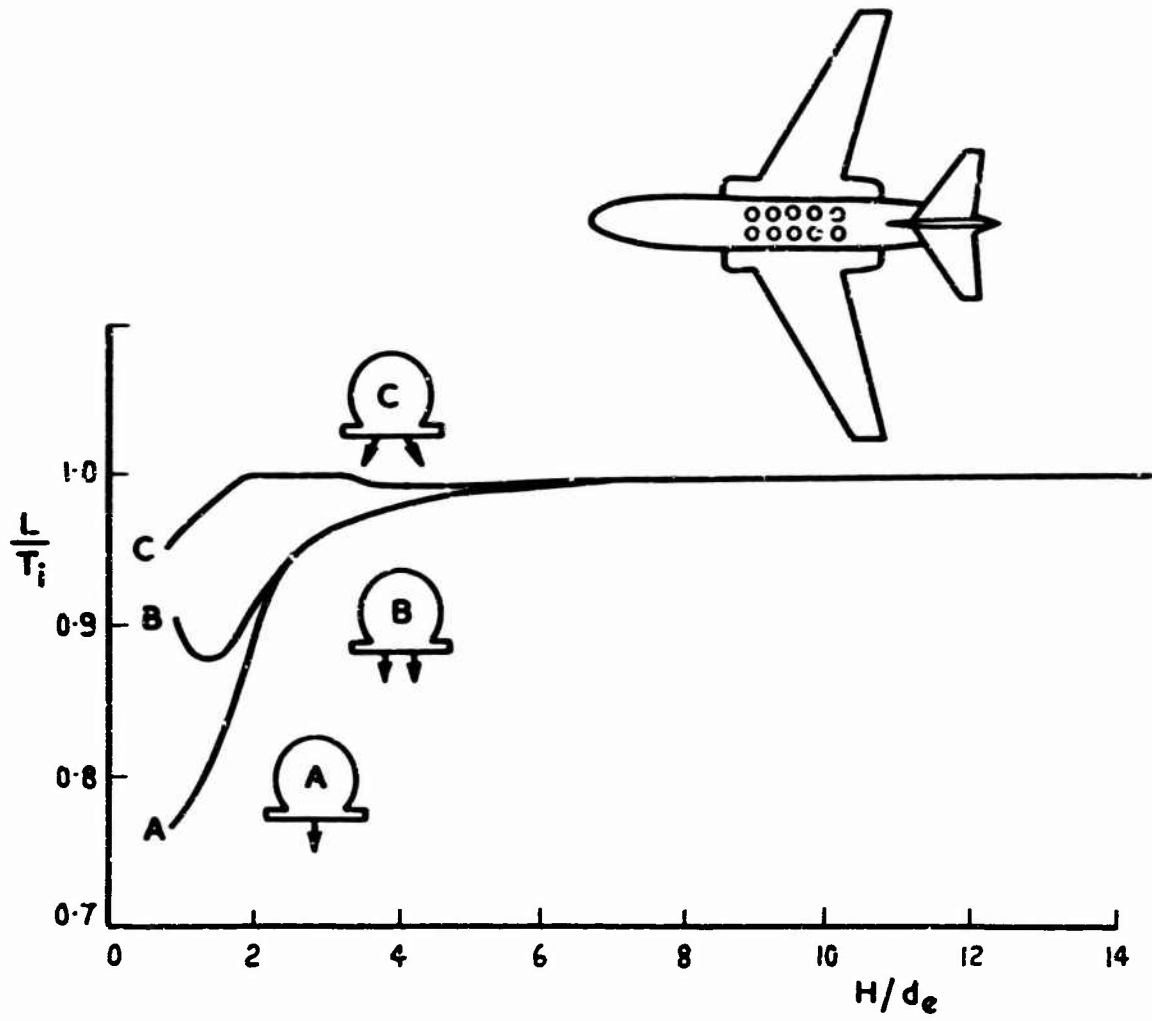


Fig. 35 NASA results with multiple jets near ground

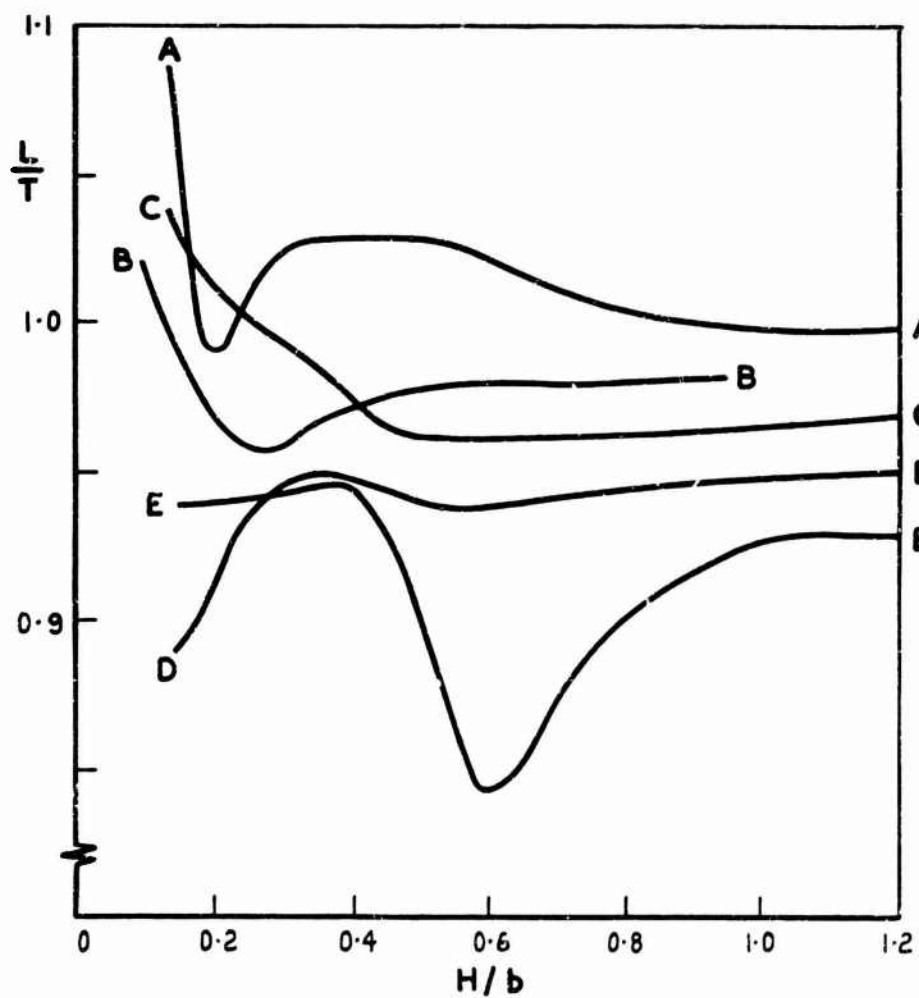
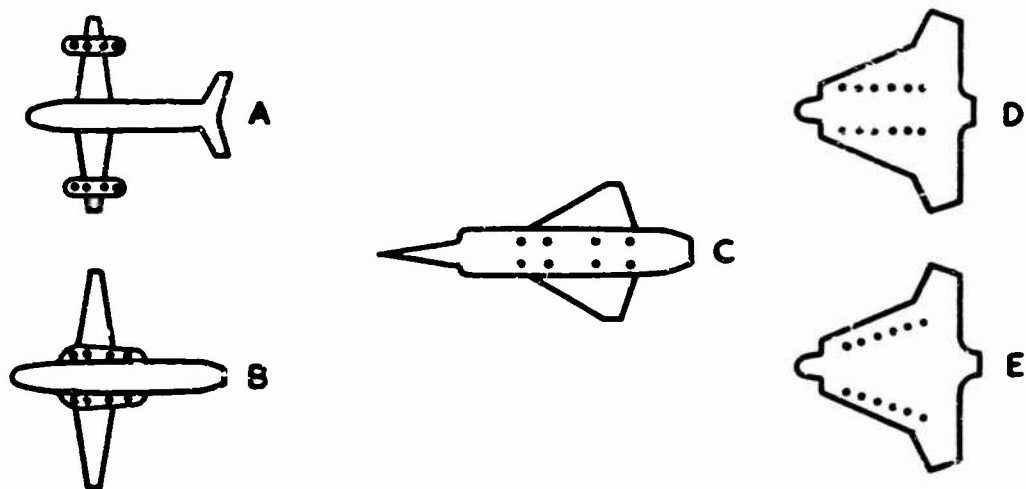


Fig. 36 BAC models with multiple jets near ground

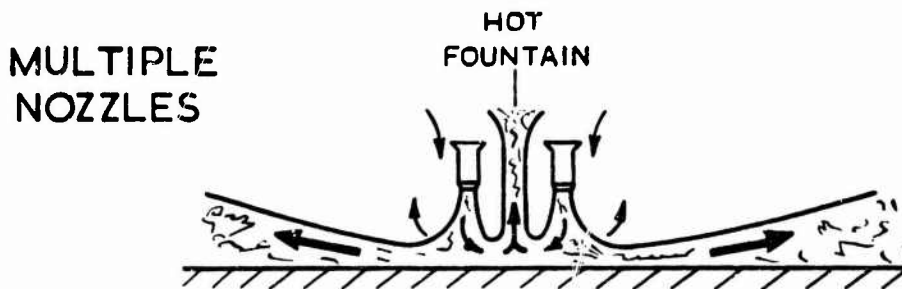
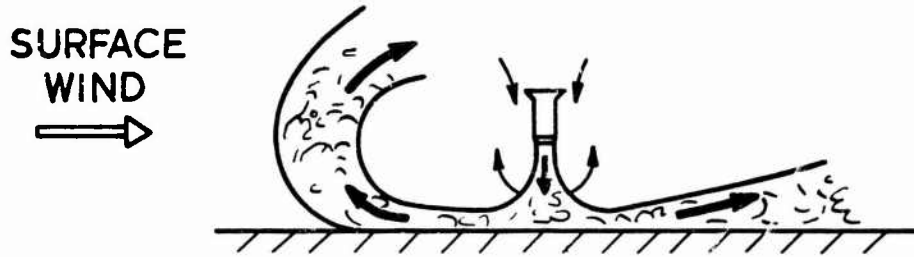
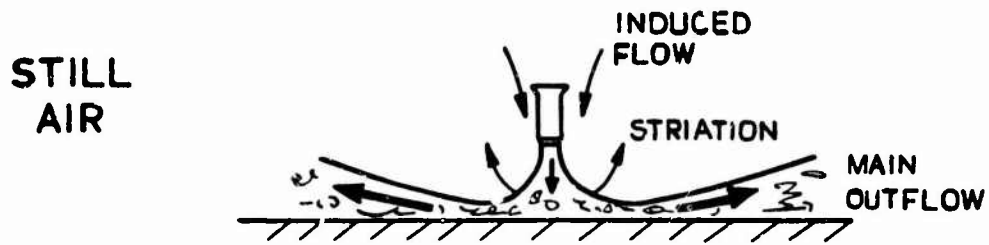


Fig. 37 Hot gas ingestion near ground

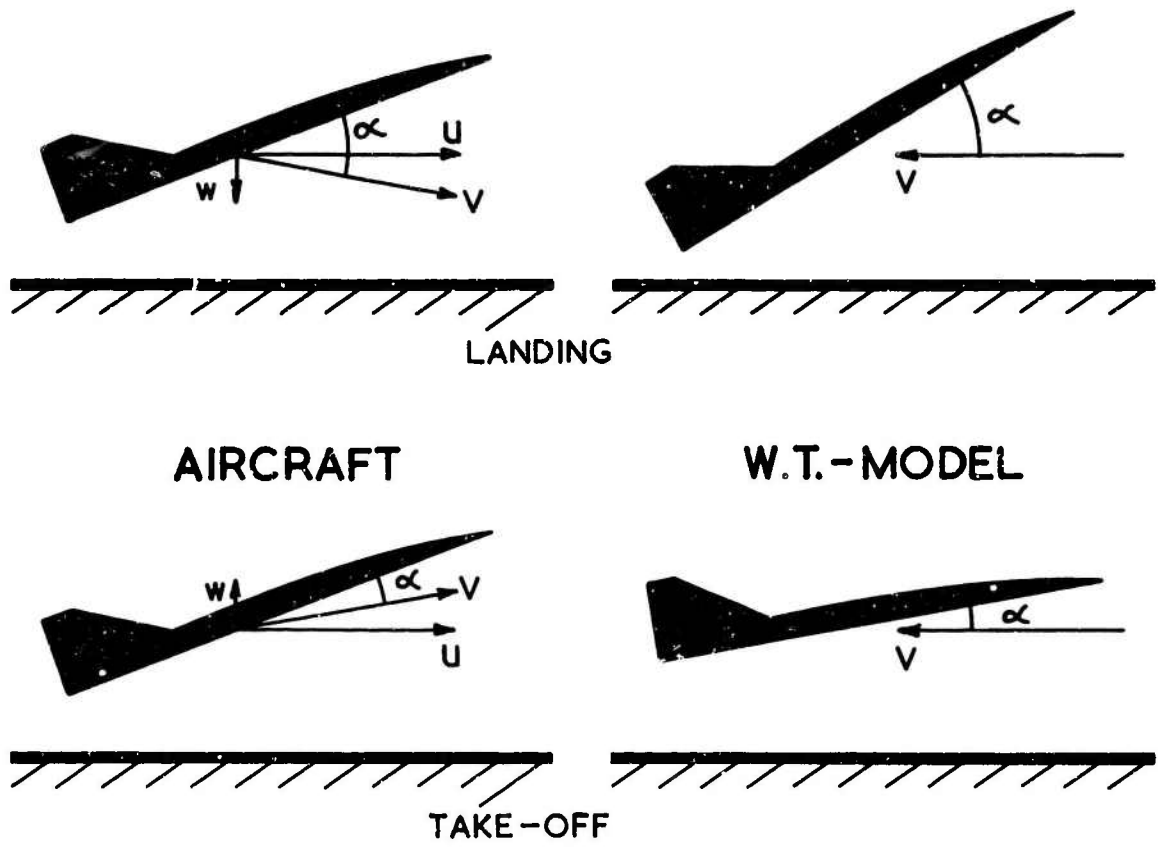


Figure 38

PAPER F

BOUNDARY LAYER AND CIRCULATION CONTROL FOR STOL AIRCRAFT

by

F. Thomas

Theoretical Dynamics Department, D.F.L. Germany

(Shortened version of a lecture given at the  
von Kármán Institute, Brussels, 15th May 1968)

#### SUMMARY

Successful wind tunnel and flight tests have clearly shown that very high lift coefficients can be achieved by using various methods of boundary layer and circulation control. Although most of our present day aeroplanes are still using conventional flap systems in order to increase the lift for take off and landing, rising wind loadings and more severe landing conditions will lead to a wide spread use of these modern lift systems in the future.

The lecture is intended to give a survey over the most important methods of increasing lift by boundary layer and circulation control. Experimental test methods, calculation procedures and practical applications for full scale aeroplanes will be described. Special attention is paid to boundary layer control by blowing.



## BOUNDARY LAYER AND CIRCULATION CONTROL FOR STOL AIRCRAFT

F. Thomas

### 1. INTRODUCTION

An aircraft is usually designed to fulfil certain prescribed requirements in the most economic way. In most cases a given payload has to be carried over a given range. This problem is described by the well known Breguet formula

$$R = \frac{V L}{b D} \log_e \frac{W_1}{W_2} \quad (1)$$

(R = range, V = speed, b = specific fuel consumption, L = lift, D = drag,  $W_1$  = weight at take off,  $W_2$  = weight at landing).

Without looking too close to the more subtle optimisation problem as a whole, we find from this formula, that range or payload of an aircraft of given size and engine thrust is improved by increasing L/D and speed.

In order to achieve high cruising speeds and at the same time lift coefficients in the vicinity of the optimum L/D values of the drag polar, it is necessary to choose a high wing loading W/S, because

$$V_{\text{cruise}} = \frac{2 W}{\rho S} \frac{1}{c_{L \text{ cruise}}} \quad (2)$$

The upper limit for the wing loading is normally dictated by the take off and landing requirements

$$V_{\text{min}} = \sqrt{\left( \frac{2 W}{\rho S} \frac{1}{c_{L \text{ max}}} \right)} \quad (3)$$

A low minimum speed requests either a low wing loading or a high value of  $c_{L \text{ max}}$ . The implications in the overall economy of the aeroplane have led to steadily increasing wing loadings. In order to keep the runway lengths within reasonable limits, the influence of the higher wing loading has to be compensated by higher maximum lift values. High maximum lift values are of special importance, if extremely short runways have to be used, for instance aircraft carriers or unprepared landing grounds. Aeroplanes which are able to take off or land on a runway of about 500 ft length with a 50 ft high obstacle at the end are defined as so called STOL (Short Take Off and Landing) aircraft.

Maximum lift coefficients for wing sections of medium thickness are limited to values of about 1.2 to 1.8. Very thin sharp nosed high speed wing sections do not even reach lift coefficients of 1. Various means to increase the lift of such aerofoils have been proposed in the past.

A great variety of mechanical flap systems is now in wide spread use. Lift coefficients up to 3.0 and more have been achieved by this method. The efficiency of mechanical flaps is limited, however, because steep adverse pressure gradients in the pressure

distribution lead to boundary layer separation, if too high angles of attack or too high angles of flap deflection are applied. Modern methods of boundary layer control by blowing or suction prevent these separations and lead thus to still higher lift coefficients.

Much research work has been performed in this field in the past. Starting from the first pre-war experiments at the Aerodynamische Versuchsanstalt Göttingen, the systematic tests of J. Williams and his collaborators at the Royal Aircraft Establishment, the contributions of Ph. Poisson-Quinton and his colleagues from ONERA, the work of NACA and of the Deutsche Forschungsanstalt für Luft- und Raumfahrt at Braunschweig have now led us to a fairly broad knowledge of the problems connected with boundary layer and flow control. A large number of full scale flight experiments and the practical application in production aeroplanes have clearly shown the merits and problems of the various artificial lift-augmentation systems.

The knowledge in this field has been described in various summarising surveys. The most important of these (see list of references) are the book of G.V. Lachmann<sup>1</sup>, several papers of J. Williams<sup>2,3,4,5,6</sup>, Ph. Poisson-Quinton<sup>7,8</sup> and H. Schlichting<sup>9,10</sup>, see also References 11, 12 and 13. A survey over the German contributions to the boundary layer and flow control problem has been given in a lecture at the von Kármán Institute in 1967 (see Reference 14).

The present lecture is intended to give an introductory survey over the problems of boundary layer and flow control. Starting with a description of the physical principles of boundary layer and flow control, the various methods of increasing lift are illustrated by typical test results. Further, the basic problems of wind-tunnel testing and theoretical calculation are mentioned. The practical application and some results of flight tests are finally discussed.

The reader, who is interested in a more detailed treatment of special questions will find this in the original papers of the various authors listed in the list of references. Most of the figures of this paper are also taken from these original papers.

## 2. VARIOUS METHODS FOR INCREASING MAXIMUM LIFT

### 2.1 Flow Mechanism in the Vicinity of a Separation Point

The wing section of an aeroplane has to combine low drag in the cruise attitude with high lift in the landing attitude. The simplest method to adapt the wing section to both conditions is to increase the angle of attack and to deflect a trailing edge flap in the landing attitude (see Figure 1). In this way we can use a low drag wing section for cruising. At high angles of attack and at high angles of flap deflection strong adverse pressure gradients occur near the wing nose and the flap hinge. Because of frictional losses the kinetic energy of the boundary layer material is not sufficient to overcome the pressure gradients and the flow separates from the wing surface. This is shown in Figure 2(a).

The separation of the flow indicates an upper limit for the attainable lift coefficients. There are two basic methods available for preventing separation and augmenting maximum lift:

- (a) Removing of the low energy material from the boundary layer by suction through slots or holes (Fig.2(b)).
- (b) Acceleration of the boundary layer, for instance by blowing high energy flow into the boundary layer (Fig.2(c)).

A typical example for the second type of boundary layer control (BLC) is the so-called slotted flap. Sound flow from the lower surface of the wing is led to the upper surface

through a properly shaped slot and accelerates the boundary layer there. Double or even triple slotted flaps have proved themselves very effective.

Another possibility to prevent boundary layer separation is the moving wall, for instance a rotating cylinder, which accelerates the boundary layer material in the direction of the main flow. The technical complexity of this method, however, makes a practical application difficult. A. A. Calderon<sup>15</sup> has recently investigated this method and recommends its application for high lift wings.

## 2.2 Boundary Layer Control by Suction

A much simpler method to avoid the separation of the flow consists in sucking the decelerated material of the boundary layer through holes or slots into the interior of the wing. In this way sound flow from outside of the boundary layer is drawn near to the wall (Fig. 2(b)). If the suction is strong enough the separation of the boundary layer can completely be avoided. The lift coefficients, which are predicted by potential flow theory can thus be achieved.

For practical applications, the energy for the suction has to be supplied by a separate power unit. In order to keep the required power as small as possible, we must find the most effective arrangement for the suction system. We have to aim for the highest possible lift increment with the least possible sucked in quantity of air. The latter is usually defined by the volume parameter

$$c_Q = \frac{Q}{V_\infty S},$$

where  $Q$  is the quantity of air sucked in,  $V_\infty$  the velocity of the main flow and  $S$  the wing area.

If the air is sucked through very small slots or through very fine holes, which are properly distributed in the region where separation is imminent, only very small volume parameters are necessary to prevent separation. Two typical examples are shown in Figures 3 and 4. Figure 3 shows how the distribution of the suction slot affects the required volume parameter  $c_Q$ , which is necessary to achieve a certain lift. In Figure 4 areas of perforated skin in the region of steep pressure gradients are used for suction. Appreciable lift increments were achieved, as it is shown by the wind tunnel results. An example for suction through one discrete slot is shown in Figure 5. Typical results of this wing are shown in Figures 6 and 7.

## 2.3 Boundary Layer Control by Blowing

The most important method of boundary layer control for practical applications is without doubt boundary layer control by blowing.

A very thin jet of high velocity is blown out of a narrow slot parallel to the wall. The slots are situated in the zone of high adverse pressure gradients near the knee of a trailing-edge or nose-flap or near the wing nose as it is shown in Figures 8 and 9. The intensity of the jet is defined by the momentum coefficient

$$c_\mu = \frac{m_j v_j}{\rho_\infty S},$$

where  $m_j$  is the mass flow per second and  $v_j$  the jet velocity.

The high velocity jet accelerates the fluid in the boundary layer and by mixing processes a boundary layer profile is developed, which can withstand the adverse pressure gradient for a considerable distance. If the momentum coefficient is large enough,

separation can completely be avoided. Typical examples for the lift increments obtained by this method are shown in Figures 10, 11 and 12. If the lift is plotted against  $c_{\mu}$  (see Figure 11), we can clearly distinguish two regions of different slope in each of the curves, at first a very steep lift increase until the theoretical lift after Glauert is reached and then a less steep further lift increase above the theoretical value, which is caused by supercirculation. The momentum coefficient  $c_{\mu A}$ , which is necessary to achieve the theoretically predicted lift depends strongly on the width of the blowing slot. This is shown in Figure 11. It is obviously better to blow with high pressure and high jet velocities through a very thin slot (about 1mm and less) instead of blowing large quantities of air through big slots with low pressure. This result was also found from boundary layer considerations (see Reference 16). Another reason to use high pressure air consists in the more continuous distribution of jet momentum along the span of a wing, which is very difficult to obtain with a low pressure system. In most practical applications a choked slot is used. A large number of further wind tunnel test results are accumulated in the various papers, which are listed in the list of references.

#### 2.4 Circulation Control by Blowing

In Figure 11 it was shown that the lift coefficient of an aerofoil can be increased beyond the theoretical value of the potential flow theory, if the momentum coefficient becomes higher than the critical value  $c_{\mu A}$ . This additional lift increment is much higher than the reaction force of the jet and this is due to super-circulation. The momentum of the additional momentum coefficient is equivalent to an enlargement of the mechanical flap. In a similar way lift can be produced by supercirculation, if simply a jet without any mechanical flap is blown out of a slot in the trailing edge of a wing section (see Figure 13). In the same figure is shown how such a "jet flap" changes the pressure distribution over the wing.

Whilst for BLC only a very small amount of air is blown through the slot, it is in principle possible to blow the whole thrust of the engines through the slot of a jet flapped aeroplane.

For a jet flapped aeroplane the ground effect may become very important. Considerable lift losses occur, if the wing comes too near to the ground. This is shown in Figure 14.

### 3. WIND TUNNEL TECHNIQUE

After the description of some of the physical principles of boundary layer and flow control a few words should be told about the problems of testing blowing and suction models in wind tunnels.

The difficulties of wind tunnel testing, when high  $c_{Lmax}$  values have to be measured, are well known. The problem is to combine high Reynolds numbers with small tunnel interference effects. These two conflicting requirements can only be fulfilled, if we can use a very big and if possible pressurised wind tunnel. In most other cases, we can only choose between low Reynolds number or high wind tunnel interference, which both lead to questionable results. This problem becomes very severe, when strong jet flaps have to be investigated.

An additional problem is connected with the air supply for blowing and suction models. The air has to be fed into (or out of) the model by a duct system in such a manner, that no forces from the supply system can actuate on the wind tunnel balance. For suction models flexible pipes have to be used and it is necessary to calibrate the balance very carefully in order to avoid any interferences. A typical test rig for suction models or for blowing models, which use low pressure air, is shown in Figure 15. A much more satisfactory arrangement can be used, if high pressure blowing is to be tested. In this case air bearing connectors can be used by which the air is fed into the model without transferring any forces to the balance. A typical test rig for three component measurements

is shown in Figure 16. The air bearing connector itself is shown in Figure 17. These elements are rather simple for three component measurements; they became very complicated for 6 component balances. Such air bearing connectors have been developed by the Royal Aircraft Establishment (see References 2, 17 and 18).

Additional problems arise, if ground effects have to be measured. For low lift coefficients it is normally sufficient to simulate the ground by a fixed plate in the wind tunnel, neglecting the effect of the boundary layer on this plate. For wings with blowing, especially for jet flapped wings, the ground effect is overestimated with a fixed plate and a moving ground has to be used in order to avoid the boundary layer effects on the ground, which can change the character of the flow completely in extreme cases. A typical comparison of results achieved with fixed and moving ground is shown in Figure 14. The installation of such a moving ground is rather complicated. An example is shown in Figure 16.

#### 4. THEORETICAL PREDICTION OF $c_{\mu A}$ , $c_{QA}$ AND PRESSURE DISTRIBUTION

A large number of experimental data concerning boundary layer and flow control have been accumulated in the past years. Although it is possible with the help of these results to design properly a BLC or jet flapped-wing by experience, it remains rather unsatisfactory, that a thorough theoretical treatment of the whole problem is still lacking.

Nevertheless, many special problems, such as the mixing processes of a wall jet and the boundary layer of a main flow have been dealt by various authors, for instance by P. Carrière, E. Eichelbrenner, Ph. Quinton-Poisson<sup>8</sup>, see also Reference 19 and 20, and there are first approaches to calculate the critical momentum coefficient and mass flow parameters for complete boundary layer control. The pressure distribution over a two-dimensional jet flapped wing has been calculated by D.A. Spence<sup>21</sup> and A. Das<sup>22</sup> has extended this theory to finite wings of arbitrary planform and momentum distribution. Typical examples are shown in Figures 18 and 19. W. Pechau<sup>23,24</sup> has calculated the most effective distribution of perforated area for boundary layer control by suction. Typical wings, which were designed with the help of this method are shown in Figures 4, 28 and 29.

A first attempt for the theoretical prediction of the critical momentum coefficient  $c_{\mu A}$  for complete boundary layer control was made by F. Thomas<sup>16</sup>. The idea of this method is demonstrated in Figures 20, 21 and 22. The momentum coefficient is expressed in form of a momentum thickness, and from systematic boundary layer measurements in the mixing region (Fig. 20) an empirical law for the mixing losses was found (Fig. 21). The remaining net momentum is then calculated by boundary layer theory (Fig. 22). A more detailed description of the method is given in Reference 16. Gersten and Löhr<sup>25</sup> have applied this method to combined boundary layer control at the wing nose and the trailing edge flap (Fig. 23). A remarkable result is the prediction of the influence of the slot width on the critical momentum coefficient. A similar method was developed for BLC by suction through a slot by K.O. Arnold<sup>26</sup>.

#### 5. PRACTICAL APPLICATION OF BLC AND JET FLAP FOR STOL AIRCRAFT

The methods for lift augmentation, which have been described in the preceding chapters are of different value, if their practical application is considered. Low power requirements, simplicity of design and maintenance, low weight and cost and high reliability are of great importance for any lift augmentation system. In this respect the leading edge slot and the single, double or triple slotted trailing edge flap have so many advantages, that they are still the mostly used system. Typical examples for this type of STOL aeroplanes are shown in Figure 24. Propeller slipstream and jet deflection (see Figure 25) are often combined with such flap systems.

Boundary layer control by suction and blowing are quite different in their practical application. Boundary layer control by suction was successfully investigated in flight test already in the late thirties. Typical results are shown in Figures 26 and 27. A large number of research aeroplanes of similar shape and size have been flight-tested since then (see Figures 28 and 29, and Reference 27). Although considerable reductions in take-off and landing distances were obtained, the suction system has never been applied to production aeroplanes. The reasons for this are several disadvantages of this system compared with the blowing system, for instance: a separate pump is required for the suction, the possible pressures are low and, therefore, very thick ducts are needed, the proper distribution of suction intensity is difficult to achieve, perforations are difficult to be manufactured and sensitive to rough treatment. Nearly all test aeroplanes have, therefore, been conventional aeroplanes with piston engines and rather thick aerofoils. The only exception known to the author were flight tests carried out with an F-86 fighter, which used suction through perforated area in the flap knee<sup>28,29</sup>.

Boundary layer control by blowing has considerable advantages especially for jet propelled aeroplanes. If the engine is properly chosen, there is no need of a special pump for the air supply because the blowing air is simply taken away from the compressor of the engine. The blowing air has rather a high pressure so that thin ducts are possible. High temperatures of the air avoid icing problems and if choked slots are applied there is no problem to obtain the proper momentum distribution along span. The simplicity and effectiveness of this reliable system has led to a wide spread use in production aeroplanes. A typical example is shown in Figure 30. A thorough description of the investigation of the BLC system for a Marine fighter aircraft is given by Poisson-Quinton and Jacquignon<sup>30</sup> (see also Figure 31). Further examples are described by J. Williams and S.F.J. Butler<sup>6</sup>, see also Reference 31, 32 and 33.

The advantage of using boundary layer control instead of double slotted flaps is shown in Figures 32 and 33 for a typical transport aeroplane (see also Reference 34).

A special research aircraft for the investigation of the jet flap scheme has been built and tested by Hunting Aircraft. Although useful results were obtained it seems not likely that a pure jet flap aeroplane will be produced in the near future. Most aeroplanes with BLC by blowing produce, however, a considerable amount of additional lift by super-circulation.

## 6. SUMMARY

It was neither intended nor possible to give a complete account of the rather wide field of boundary layer and flow control within this short lecture. The main idea of the lecture was to give an introduction into this field, which helps the non-specialist to recognize the basic problems and the possibilities of boundary layer and flow control for aircraft design. The various problems such as the physical behaviour of the boundary layer with suction or blowing, wind tunnel techniques, ground effect, theoretical approaches and practical applications were demonstrated with a series of more or less arbitrarily chosen figures from various authors. The possibility of using many already existing figures of the Aerodynamics Institute of DFL Braunschweig explains the fact, that in this paper a rather large proportion of the presented examples and results are of German origin. I should like, therefore, to draw the attention of the reader to the list of references, which, although by no means complete, will help to find access to the large amount of work which was not specially mentioned here.

## REFERENCES

1. Lachmann, G.V. *Boundary Layer and Flow Control, Vol.I.* Pergamon Press, 1961.
2. Anscombe, A.  
Williams, J. *Some Comments on High Lift Testing in Wind Tunnels with Particular Reference to Jet-Blowing Models.* AGARD Report 63, 1956, Journ. Roy. Aero. Soc. Vol.61, 1957, pp.529-540.
3. Williams, J. *British Research on Boundary Layer Control for High Lift by Blowing.* Z. Flugwiss, Vol.6, 1958, pp.143-150.
4. Williams, J. *British Research on the Jet-Flap Scheme.* Z. Flugwiss. Vol.6, 1958, pp.170-176.
5. Williams, J. *Some British Research on the Basic Aerodynamics of Powered Lift Systems.* Journ. Roy. Aero. Soc. Vol.64, 1960, pp.413-432.
6. Williams, J.  
Butler, S.F.J. *Aerodynamic Aspects of Boundary-Layer Control for High Lift at Low Speeds.* Journ. Roy. Aero. Soc. Vol.67, 1963, pp.201-223.
7. Poisson-Quinton, Ph. *Einige Physikalische Betrachtungen über das Ausblasen an Tragflügeln.* Jahrb. WGL 1956, pp.29-51. Techn. Sci. Aero. No.4, 1956.
8. Carrière, P.  
et al. *Contribution Théorique et Expérimentale à l'Etude du Contrôle de la Couche Limite par Soufflage.* Advances in the Aeronautical Sciences. Proceedings of the First International Congress in the Aeronautical Sciences, Madrid 1958, Pergamon Press, 1958, Vol.II, pp.620-661.
9. Schlichting, H. *Absaugung in der Aerodynamik.* Jahrb. WGL' 1956, pp.19-28.
10. Schlichting, H. *Aerodynamische Probleme des Höchstauftriebes.* Proceedings of the International Council of the Aeronautical Sciences, 1964, pp.275-303. Lecture at the third ICAS-Congress, 1962, Stockholm.
- 10a. *Aerodynamic Problems of High Lift.* DFL Report No.190, 1962.
11. Gersten, K. *Bericht über die englischen Forschungsarbeiten über Höchstauftrieb.* Aus "Höchstauftrieb" AVA Forschungsbericht Nr. 60-10, 1960, pp.4-29. Bericht über die Sitzung des Ausschusses "Aerodynamik" der Wissenschaftlichen Gesellschaft für Luftfahrt am 20/21.6.1960 in Göttingen.
12. Puffert, H. *Ueber die Erhöhung des Maximalauftriebes durch Ausblasen unter besonderer Berücksichtigung der französischen Forschungsarbeiten.* Aus "Höchstauftrieb" AVA Forschungsbericht Nr. 60-10, 1960, pp.30-73.
13. Thomas, F. *Uebersicht über die amerikanischen Forschungsarbeiten über Höchstauftrieb.* Aus "Höchstauftrieb" AVA Forschungsbericht Nr. 60-10, 1960, pp.74-100.

14. Thomas, F. *Some German Contributions to the Research on Boundary Layer and Circulation Control.* AGARD VKI Lecture series on Boundary-Layer and Circulation Control, 10-14 April, 1967. Von Kármán Institute for Fluid Dynamics, Course Note 63.
15. Calderon, A. A. *Rotating Cylinder Flaps for V/STOL Aircraft.* Aircraft Eng. Vol.36, 1964, pp.304-309.
16. Thomas, F. *Untersuchungen über die Erhöhung des Auftriebes von Tragflügeln mittels Grenzschichtbeeinflussung durch Ausblasen.* Z. Flugwiss. Vol.10, 1962, pp.46-65.
- 16a. *Boundary-Layer Control for increasing Lift by Blowing.* AIAA Journal, Vol.3, 1965, pp.967-968.
17. Williams, J.  
Butler, S.F.J. *Recent Developments in Low-Speed Wind-Tunnel Techniques for V/STOL and High-Lift Model Testing.* Z. Flugwiss, Vol.13, 1965, pp.73-89.
18. Arnold, K.O. *Messung der aerodynamischen Beiwerte an Modellen mit Ausblasung.* WGLR Bericht 8/63, 1963.
19. Thomas, F. *Untersuchungen über die Grenzschicht an einer Wand stromabwärts von einem Ausblasespalt.* Abhandlg. der Braunschweig. Wiss. Ges. Vol.15, 1963, pp.1-17. DFL Report 168.
20. Kruka, V.  
Eskinazi, S. *The Wall Jet in a Moving Stream.* Syracuse University Research Institute. Report No. ME 937-6309F, 1963.
21. Spence, D. A. *The Lift Coefficient of a Thin Jet-Flapped Wing.* Proc. Roy. Soc. London (A) 238, 1956, pp.46-68. *The Lift of a Blowing Wing in a Parallel Stream.* J. Aeron. Sci. Vol.23, 1956, pp.92-94.
22. Das, A. *Tragflächentheorie für Tragflügel mit Strahlklappen.* Jahrbuch der WGL 1960, pp.112-133.
23. Pechau, W. *Ein Näherungsverfahren zur Berechnung der ebenen und rotationssymmetrischen turbulenten Grenzschicht mit beliebiger Absaugung oder Ausblasung.* Jahrbuch der WGL 1958, pp.81-92; see also AGARD Report 259, 1960.
24. Schlichting, H.  
Pechau, W. *Auftriebserhöhung von Tragflügeln durch kontinuierlich verteilte Absaugung.* Z. Flugwiss. Vol.7, 1959, pp.113-119.
25. Gersten, K.  
Löhr, R. *Untersuchungen über die Auftriebserhöhung eines Tragflügels bei gleichzeitigem Ausblasen an der Hinterkantenklappe und an der Profilnase.* DFL Bericht 189, 1962; see also Estratto dai Rendiconti del V Congresso Aeronautico Europeo, Venezia 12-15 settembre, 1962.
26. Arnold, K.O. *Untersuchungen über die Auftriebserhöhung eines Klappenflügels durch Schlitzabsaugung.* Z. Flugwiss. Vol.15, 1967, pp.36-56.
27. Cornish, J.J. *Some Aerodynamic and Operational Problems of STOL Aircraft with Boundary-Layer Control.* J. Aircraft, Vol.2, 1965, pp.78-86.



28. Cook, W.L.  
et al. *Area-Suction Boundary Layer Control as Applied to the Trailing Edge Flaps of a 35° Swept Wing Airplane.* NACA Report 1370, 1958.
29. Holzhauser, C.A.  
Bray, R.S. *Wind-Tunnel and Flight Investigations of the Use of Leading-Edge Area Suction for the Purpose of Increasing the Maximum Lift Coefficient of a 35° Swept-Wing Airplane.* NACA Report 1276, 1956.
30. Poisson-Quinton, Ph.  
Jacquignon, M. *Qualités de Vol et Hypersustentation des Ailes en Fleche. Application en Vol au Soufflage de la Couche Limite sur l'Avion Dassault "Etendard IV Marine".* Jahrbuch der WGL 1960, pp.149-163.
31. Kelly, M.W.  
et al. *Blowing Type Boundary Layer Control as Applied to the Trailing Edge Flaps of a 35° Swept-Wing Airplane.* NACA Report 1369, 1958.
32. Kelly, M.W.  
et al. *Full Scale Wind-Tunnel Tests of a Low-Aspect-Ratio, Straight Wing Airplane with Blowing Boundary Layer Control on Leading and Trailing Edges.* F-104. NASA TN D-135, 1959.
33. Maki, R.L.  
Giulianetti, D.J. *Low Speed Wind-Tunnel Investigation of Blowing Boundary Layer Control on Leading and Trailing Edge Flaps of a Full Scale Low Aspect Ratio 42° Swept Wing Airplane Configuration.* NASA TN D-16, 1959.
34. Streit, G.  
Thomas, F. *Experimentelle und Theoretische Untersuchungen an Ausblaseflügeln und ihre Anwendung beim Flugzeugentwurf.* Jahrbuch der WGLR 1962, pp.119-132.
35. Schwarz, F. *Flugversuche am Baumuster RW 3a mit Grenzschichtabsaugung zur Steigerung des Höchstauftriebes.* Z. Flugwiss. Vol.11, 1963, pp.142-149.
36. Schwarz, F.  
Wuest, W. *Flugversuche am Baumuster Do 27 mit Grenzschichtabsaugung zur Steigerung des Höchstauftriebes.* AVA Göttingen Forschungsbericht 63-02, 1963.
37. Wuest, W. *Druckverteilungen am Profil NACA 747 A 315 (Gö 817) mit Absaugung.* Bericht 60 A 18 der AVA Göttingen, 1960.
38. Malavard, L.  
Lepage, L. *Principes et Resultats de Calculs d'Ailes a Jet par Analogies Rheoelectriques.* La Recherche Aeronautique No.77, 1960, pp.3-17.
39. Pankhurst, R.C.  
et al. *Wind Tunnel Tests of the Stalling Properties of an 8% Thick Symmetrical Section with Nose Suction Through a Porous Surface.* ARC R & M 2666, 1953.

## TEXT FOR FIGURES

Fig. 1 Various methods to increase the lift by boundary layer control

- a) High angle of attack
- A)  $c_{L \max}$  without high lift aids
  - B)  $c_{L \max}$  with high lift aids
  - ① slat
  - ② nose-flap
  - ③ BLC by suction
  - ④ BLC by blowing
- b) High angle of trailing edge flap deflection
- A) without trailing edge flap deflection
  - B) with trailing edge flap deflection
  - C) with trailing edge flap deflection and BLC
  - ① slotted trailing edge flap
  - ② BLC by suction
  - ③ BLC by blowing

Fig. 2 Boundary layer in the vicinity of a separation point without and with BLC

- a) without BLC
- b) prevention of separation by suction
- c) prevention of separation by blowing
- $\delta$  = boundary layer thickness
- A = Separation :  $(du/dy)_w = 0$

Fig. 3 Lift increment  $\Delta c_{L \max}$  for various positions of suction ar<sup>39</sup>Fig. 4 Lift increment of aerofoil G5 817 with distributed suction from wind tunnel tests (W. Wuest<sup>37</sup>)

$$c_Q = Q/SV_\infty$$

—○—  $c_Q = 0$

—+—  $c_Q = 0.003$

—△—  $c_Q = 0.006$

Fig. 5 Cross section of a NACA 66<sub>4</sub> A 421 wing model with one suction slot at the trailing edge flap. (K.O. Arnold<sup>26</sup>)

- a) interchangeable trailing edge ( $s = 1.5 \text{ mm}$ ,  $\Delta \tilde{x} = 20 \text{ mm}$ )
- b) suction chamber
- c) spacer
- d) transition wires
- e) sealing

Fig. 6 Results of three-component measurements of a NACA 66<sub>u</sub> A 421 suction wing. (K.O. Arnold<sup>26</sup>)

$c_a$	$c_q$
○	0
△	0.0144
●	0.0180
□	0.0262
◇	0.0292
▲	0.0351

Fig. 7 Lift curve  $c_{L0}(\gamma_k)$  without suction and  $c_{LA}(\gamma_k)$  without separation for a NACA 66<sub>u</sub> A 421 suction wing (K.O. Arnold<sup>26</sup>).

— . —	Theory after M. Glauert
— ○ —	$\alpha$ - 1°
— □ —	4°
— ◇ —	9°
— △ —	14°

Fig. 8 Typical positions of blowing slots

- blowing slot at the nose of the profile
- blowing slot at the nose of the trailing edge flap
- blowing slot in front of the trailing edge flap
- pressure distribution in potential flow
- region of adverse pressure gradients

Fig. 9 Effect of blowing over the trailing edge flap.

- separated flow without blowing
- attached flow with blowing
- pressure distribution with (1) and without (2) blowing
- flow mechanism near the blowing slot

Fig. 10 Increase of lift by blowing over the trailing edge flap (J. Williams<sup>3</sup>).

Fig. 11 a) Lift increase by blowing over the trailing edge flap for  $\alpha = \text{const}$  (F. Thomas<sup>16</sup>)

—  $\Delta c_{Lth}$  after H. Glauert.

- Comparison of the critical momentum coefficient  $c_{\mu A}(\gamma_k)$  with other results:
 

□	J. Williams <sup>3</sup>	$s/c = 0.33 \times 10^{-3}$
△ ◇ ▽	ONERA <sup>8</sup>	$= 0.25 \times 10^{-3}$
▲ ▼	ONERA <sup>7</sup>	
○	F. Thomas <sup>16</sup>	$= 1.7 \times 10^{-3}$
///	Schwier <sup>7</sup>	$= 5 \sim 7 \times 10^{-3}$

Fig. 12 Effect of blowing at the nose and at the trailing edge flap on lift and pitching moment for a NACA 0010 wing section with  $\tau_k = 60^\circ$  flap deflection (K. Gersten and R. Löhner<sup>25</sup>).

—●—	$c_{\mu N} = 0$
—□—	0.01
—■—	0.05
—▽—	0.10
—▼—	0.20

Fig. 13 Pressure distribution of a jet-flapped aerofoil

- a) without blowing
- b) with blowing

Fig. 14 Ground effect for blowing wings (K. Gersten and R. Löhner<sup>25</sup>)

$c_\mu$	0	0.6	1.0	2.0
Moving Ground	○	□	△	◇
Fixed Ground		■	▲	◆

Fig. 15 Test rig for suction and blowing of low pressure air (K. O. Arnold<sup>18</sup>).

- a) blower  $\Delta p_g = 1800 \text{ kp/m}^2$  ;  $Q = 23 \text{ m}^3/\text{min}$
- b) mass flow meter
- c) pipe for calibration
- d) throttles
- e) flexible pipe

Fig. 16 Test rig for high pressure blowing including ground effect. (K. Gersten and R. Löhner<sup>25</sup>).

- a) wing
- b) air bearing connector (see Fig. 17).
- c) contact indicator
- d) valves for  $c_{\mu K}$  and  $c_{\mu N}$
- e) endplate
- f) moving belt
- g) wing NACA 0010 with nose and flap blowing  $c_k/c = 0.257$  ;  $s_N/c = 0.0017$  ;  $s_k/c = 0.0018$  .

Fig. 17 Air bearing connector for three-component measurements (F. Thomas<sup>16</sup>).

- a) air bearing (0.06 mm)
- b) connected with wing and balance
- c) fixed to the ground
- d) contact indicator

Fig.18 Lift and pitching moment for a rectangular wing with jet flap (A.Das<sup>22</sup>).  
aspect ratio  $A = 4.5$ , jet angle  $\eta_j = 30^\circ$

—○— Experiment  $c_\mu = \frac{\rho_j v_j^2 b s}{q_\infty S}$   
- - - - Theory

Fig.19 Lift distribution of a delta wing with jet flap

a) Total lift  $c_L$  depending on  $c_\mu$

① after A.Das<sup>22</sup>, aspect ratio  $A = 1.88$ .

② after Malavard<sup>38</sup>, aspect ratio  $A = 2.32$ .

b) Lift distribution for delta wing with  $A = 1.88$

① with constant jet velocity  $v_j$  along span

② with constant momentum coefficient  $c_\mu \sim v_j^2 s/c$  along span.

Fig.20 Velocity profiles in the boundary layer behind a blowing slot for a velocity ratio of  $v_j/U_\infty = 8$  (F.Thomas<sup>16</sup>).

Momentum loss thickness :

$$\nu(x) \rho_\infty U_\infty^2 = \int_0^\infty \rho u (U_\infty - u) dy$$

Augmentation of momentum thickness due to jet :

$$\nu_j = -\frac{1}{2} c_\mu c \left( 1 - \frac{U_\infty}{v_j} \right)$$

Fig.21 Momentum efficiency  $\eta_\mu$  of the blowing jet as a function of the velocity ratio  $v_j/U_\infty$  (F.Thomas<sup>16</sup>)

$$\eta_\mu(x) = \frac{\nu(x) - \nu_0(x)}{\nu_j}$$

①	②	③	$v_j/U_\infty$	$s = 1.3 \text{ mm}$
▽			2	
□		■	3	① $U_\infty = 40 \text{ m/s}$
◇	◆		4	② = 20 m/s
△	▲	▲	6	③ = 120 m/s
	▼		8	

○ flapped wing with  $\eta_k = 0$  and  $s = 0.5 \text{ mm}$

Fig. 22 Estimation of the critical momentum coefficient  $c_{\mu A}$  for avoiding separation on the flap (F. Thomas<sup>16</sup>).

A. separation without blowing

$$\text{total momentum input: } v_{js}^2 = 0.5(1 - \bar{U}/v_j)c_{\mu A}c$$

$$\text{required net input: } v_G^2 = 0.85(1 - \bar{U}/v_j)v_{js}^2$$

critical momentum coefficient

$$c_{\mu A} = 2 \frac{v_G^2}{c} \frac{1}{0.85(1 - \bar{U}/v_j)^2}$$

$v_G^2$  is calculated by boundary layer theory.

Fig. 23 Estimation of the critical momentum coefficients  $c_{\mu NA}$  and  $c_{\mu KA}$  for nose and trailing edge blowing (K. Gersten and R. Löhr<sup>25</sup>).

A. separation point

B. blowing slit

S. stagnation point

Fig. 24 Take off and landing distances for the Do 27 (single engine) and Do 28 (twin engine) STOL-Aeroplanes with fixed slat and slotted trailing edge flaps.

Fig. 25 Various jet deflection systems.

Fig. 26 First flight tests with boundary layer control at Göttingen 1938.

Fig. 27 Results of flights with suction for three STOL Aeroplanes at Göttingen 1938.

- - - - without suction

——— with suction

Fig. 28 Flight test results for the RW 3a aeroplane with nose suction. (F. Schwarz<sup>35</sup>).

Fig. 29 Flight test results for the Dornier Do 27 aeroplane with nose suction. (F. Schwarz and W. Wuest<sup>36</sup>).

$\eta$  = flap deflection

$$c_Q = Q/V_\infty S$$

$$\eta_k = 0^\circ: \begin{cases} \circ & c_Q = 0 \\ + & = 1.5 \times 10^{-3} \\ \Delta & = 2.04 \times 10^{-3} \end{cases}$$

$$\eta_k = 45^\circ: \begin{cases} \circ & c_Q = 0 \\ \Delta & = 2.04 \times 10^{-3} \end{cases}$$

Fig. 30 Lift augmentation by BLC at the nose and the trailing edge flap for the F-104 aircraft. (M.W. Kelly, W.H. Tolhurst, Jr., R. L. Maki<sup>32</sup>).

Fig.31 Wind tunnel results for the "Etendard IV M" aeroplane with BLC by blowing (Ph.Poisson-Quinton and M.Jacquignon<sup>30</sup>).

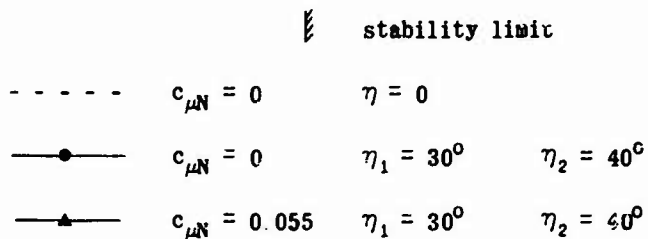


Fig.32 Take off and landing distance depending on thrust used for blowing for a typical transport aeroplane with an aspect ratio of  $A = 8$ , wing loading  $W/S = 300$   $\text{kp/m}^2$  and total thrust per weight ratio of  $T + T_B/W = 50\%$  (G.Streit and F.Thomas<sup>34</sup>).

- a) take off distance
- b) ground roll distance
- c) landing distance with flare out:  $T = 0$
- d) landing distance without flare out:  $T \neq 0$ ;  $\theta = 120^\circ$

Fig.33 Take off and landing distance depending on total thrust for a typical transport aeroplane with an aspect ratio of  $A = 8$  and wing loading  $W/S = 300$   $\text{kp/m}^2$ . (G.Streit and F.Thomas<sup>34</sup>).

- a) plain flaps with blowing
  - b) double slotted flaps without blowing
- |         |   |
|---------|---|
| ————    | with flare out: $T = 0$                   |
| — . . — | no flare out: $T \neq 0$ ; $\theta = 120$ |

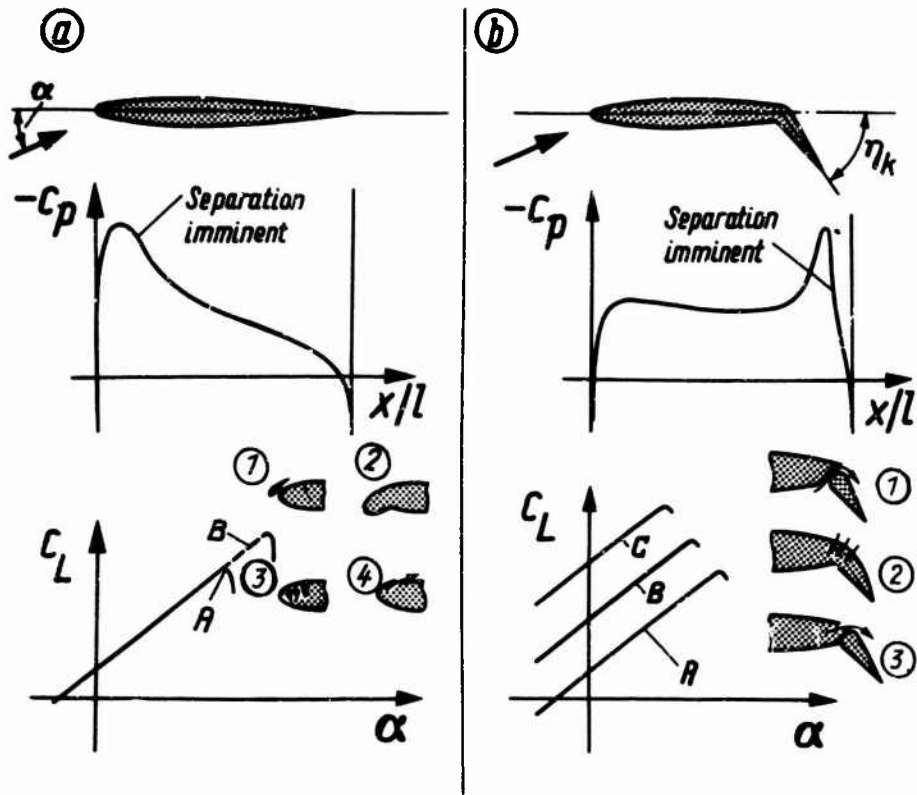


Figure 1

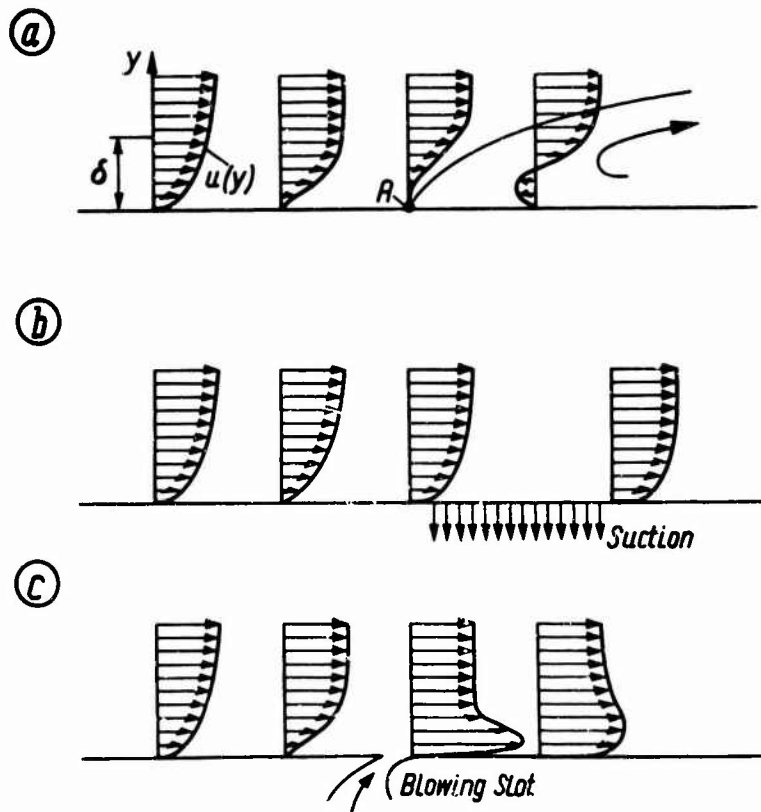


Figure 2



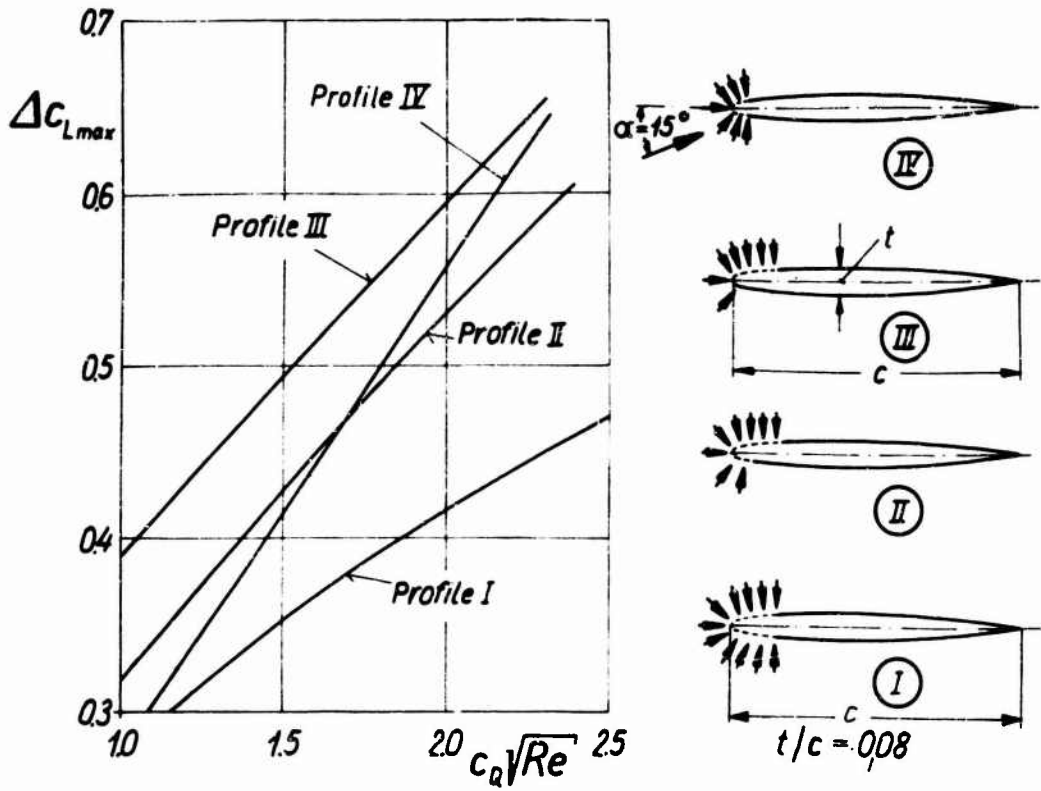


Figure 3

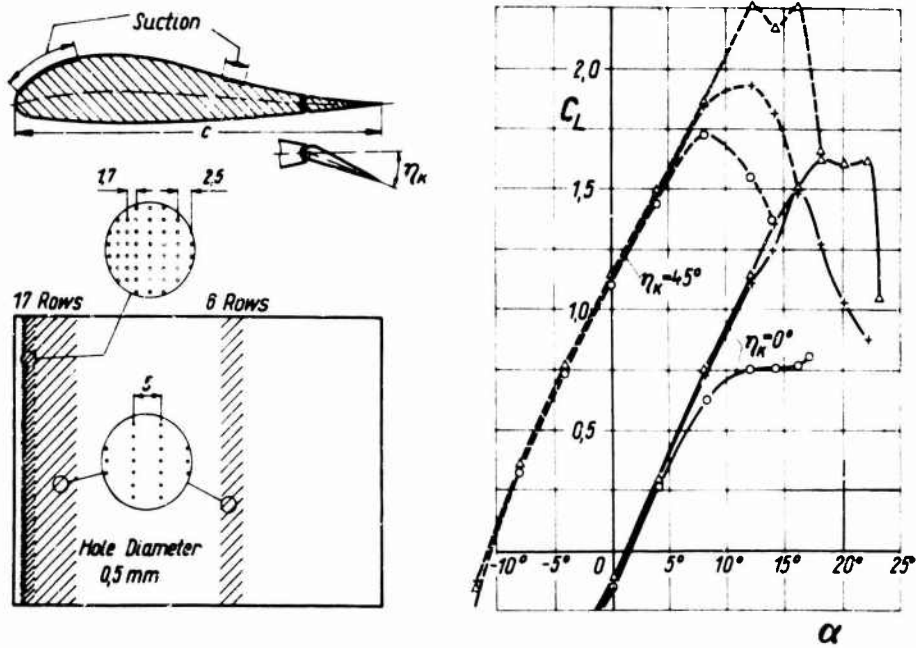


Figure 4

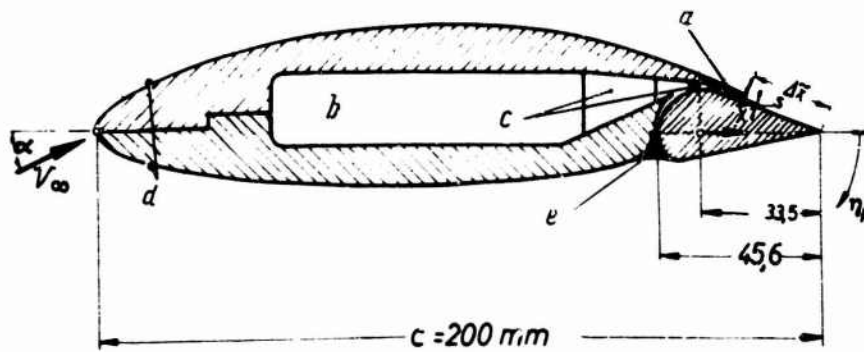


Figure 5

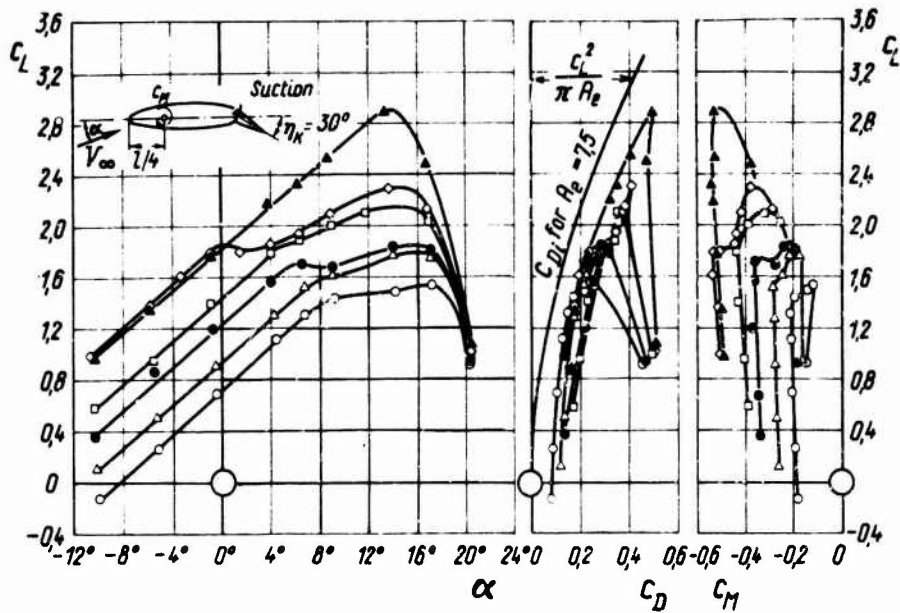


Figure 6

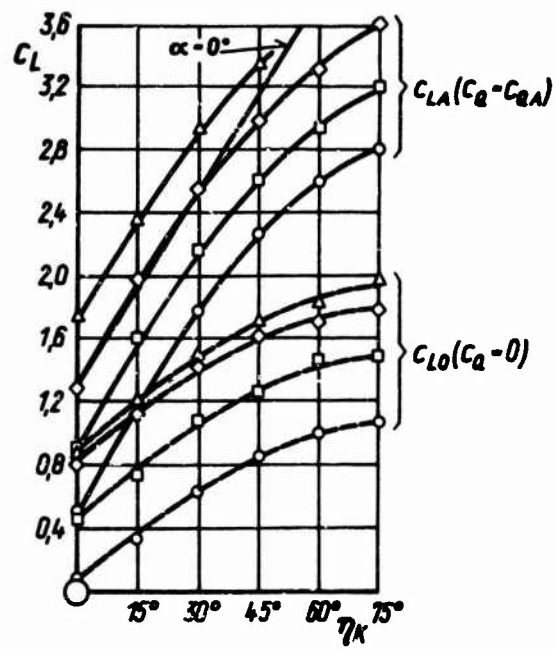


Figure 7

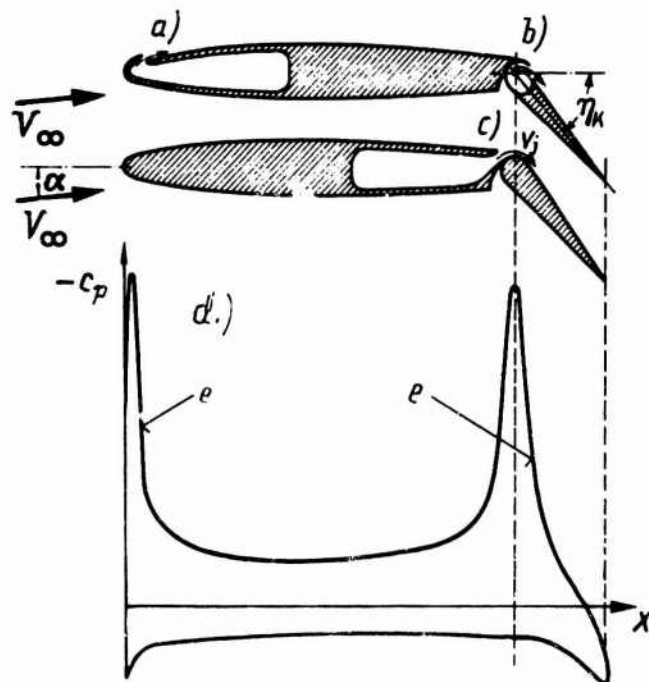


Figure 8

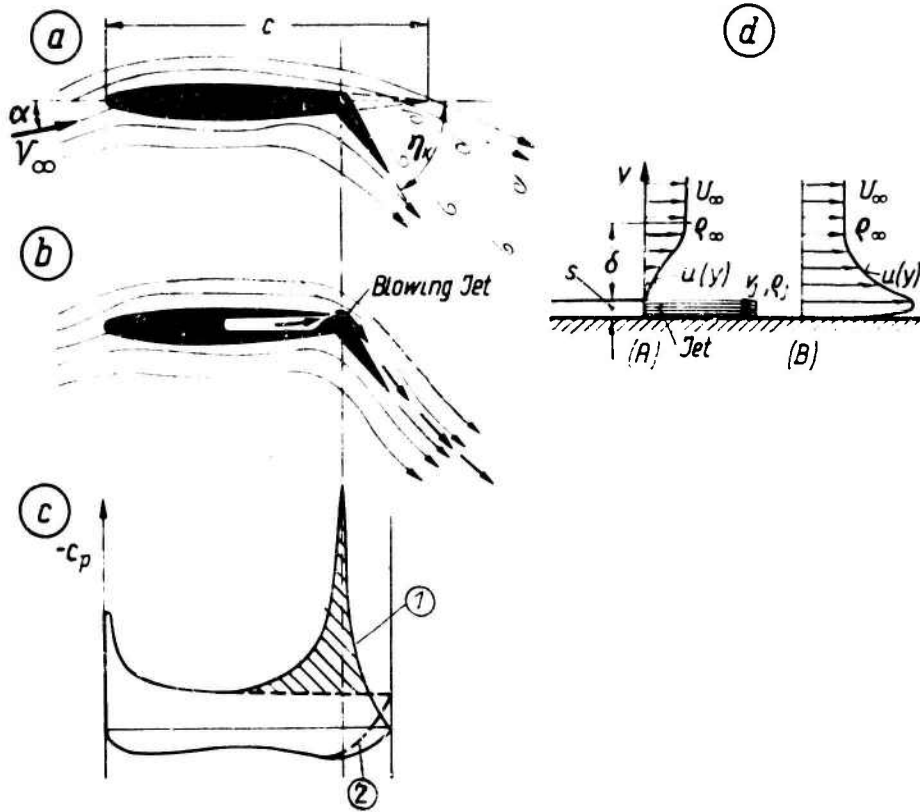


Figure 9

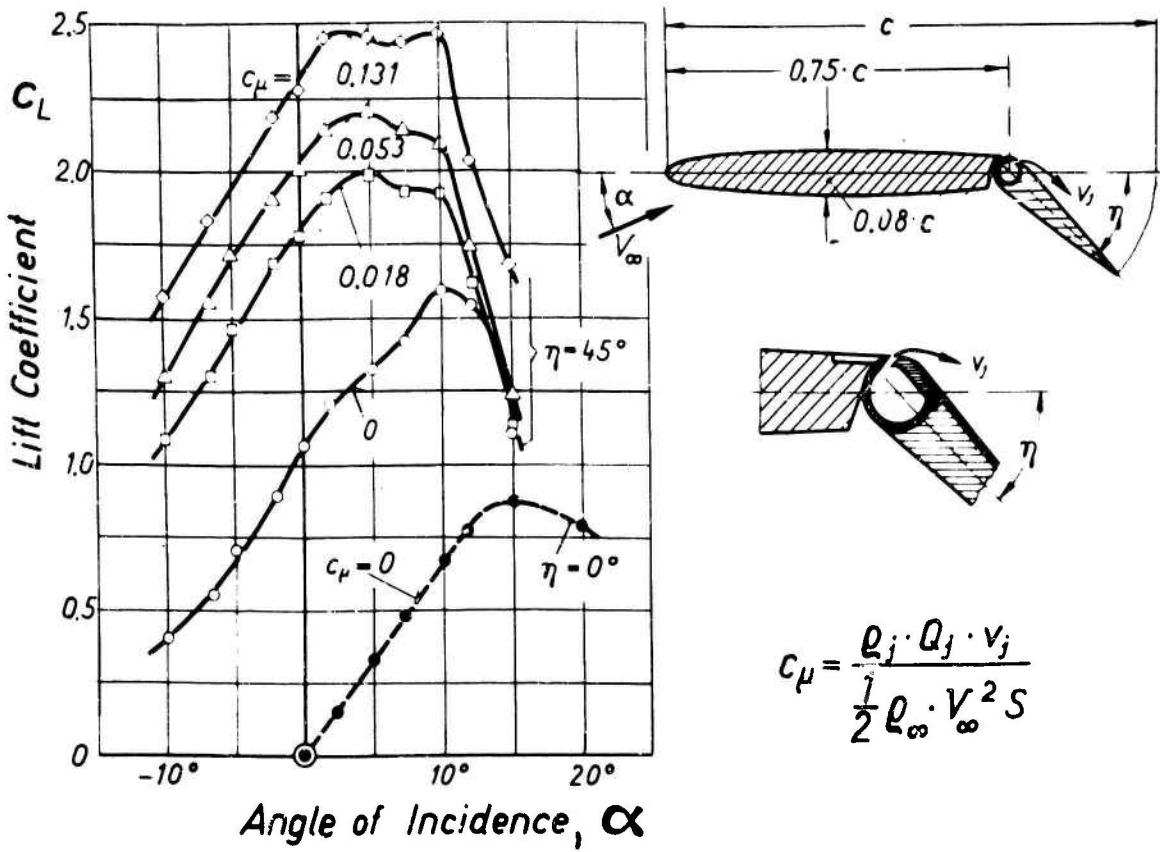


Figure 10

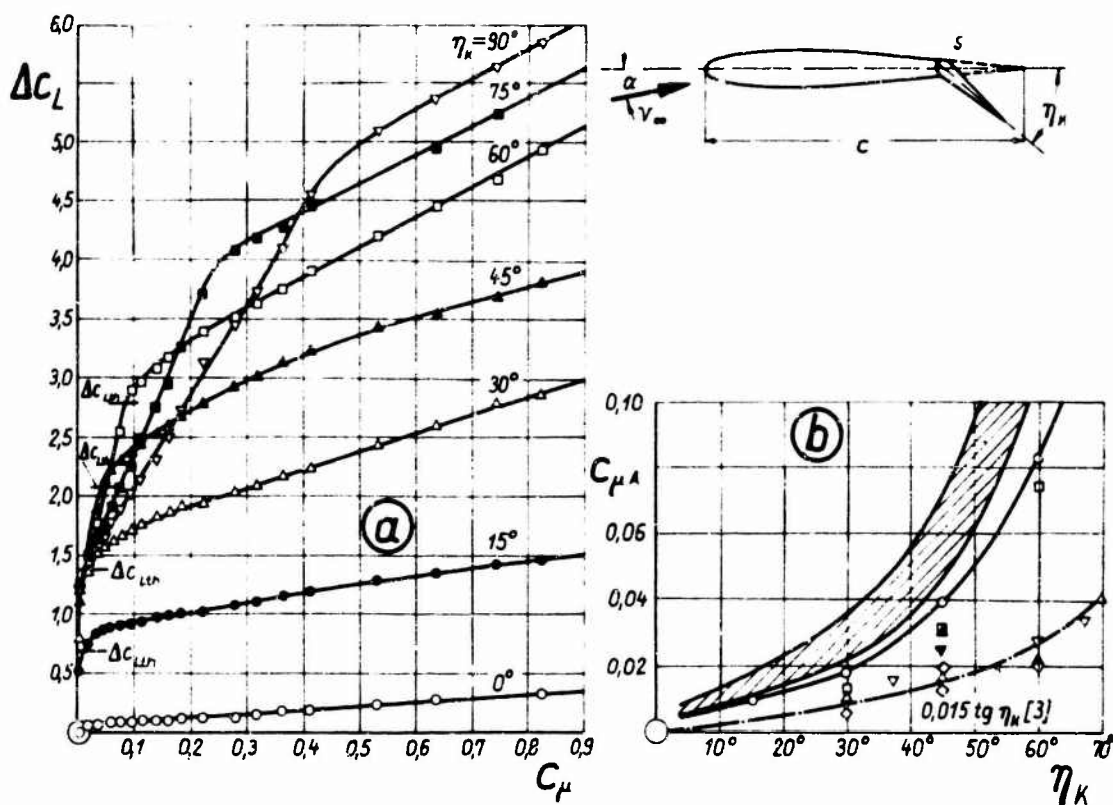


Figure 11

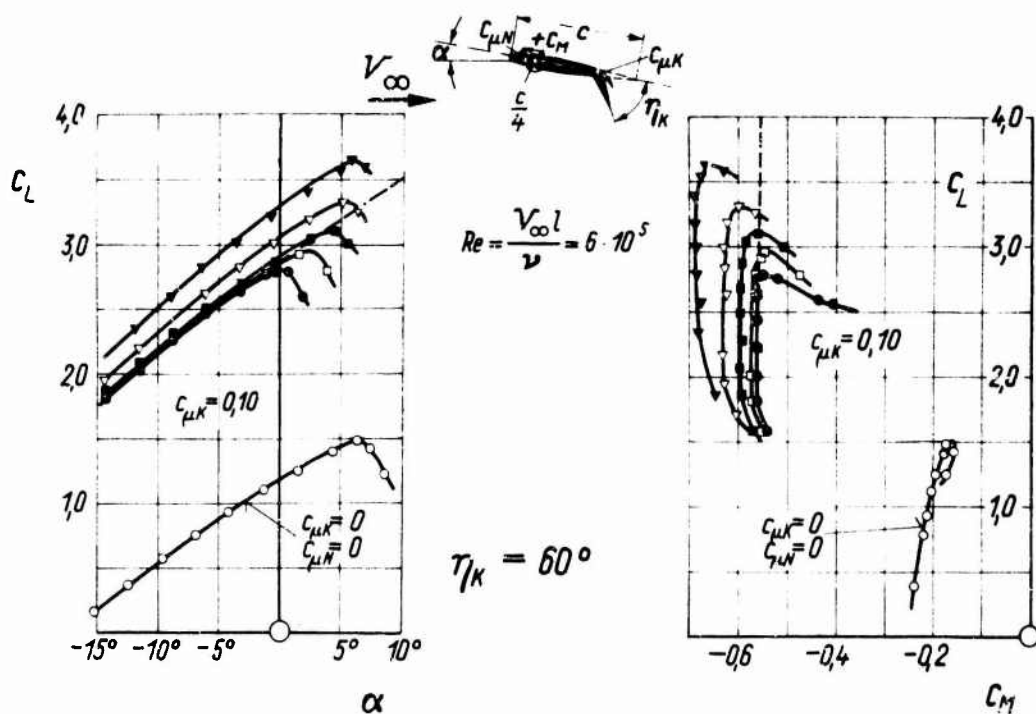


Figure 12

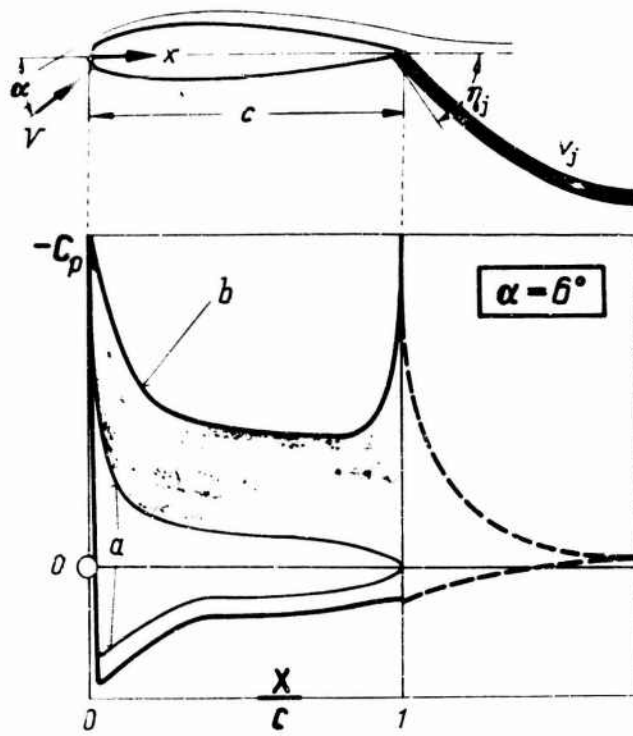


Figure 13

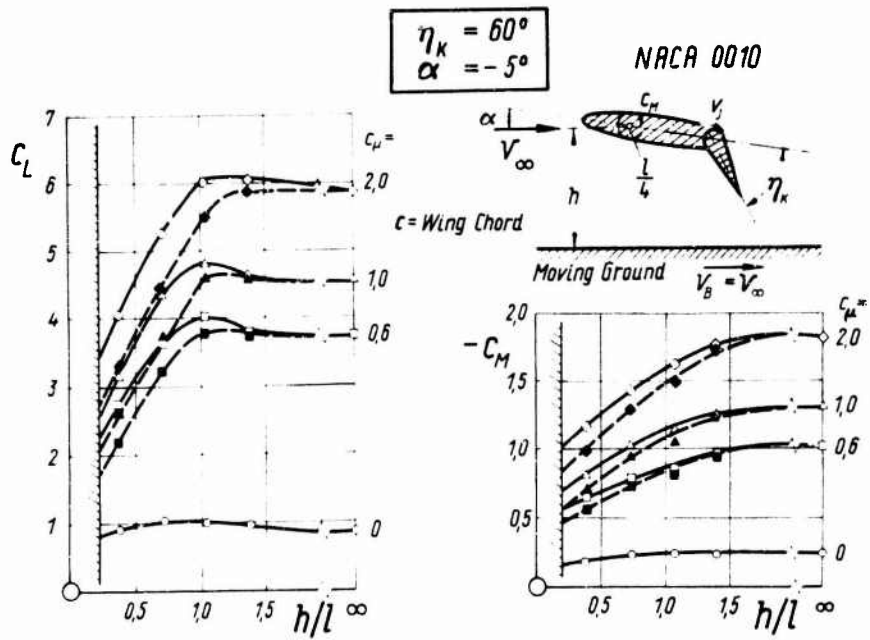


Figure 14

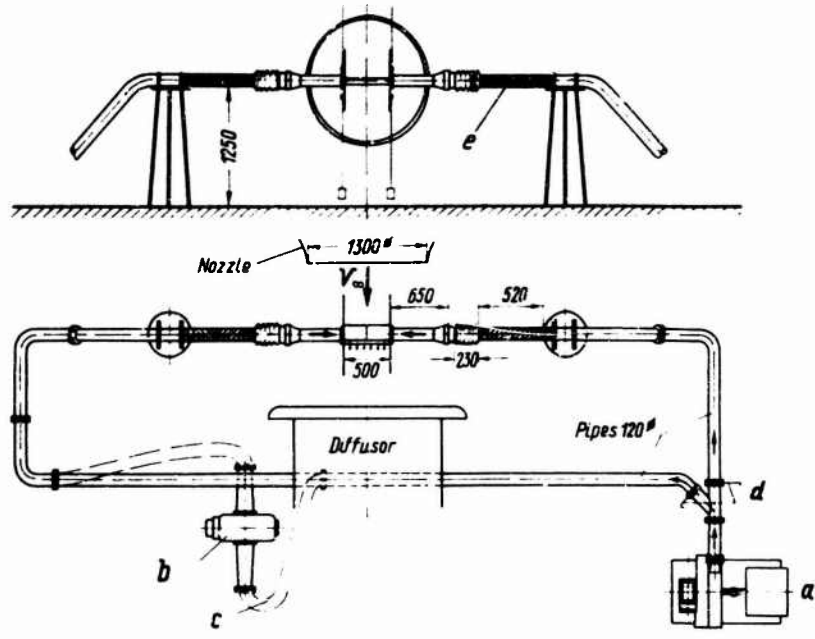


Figure 15

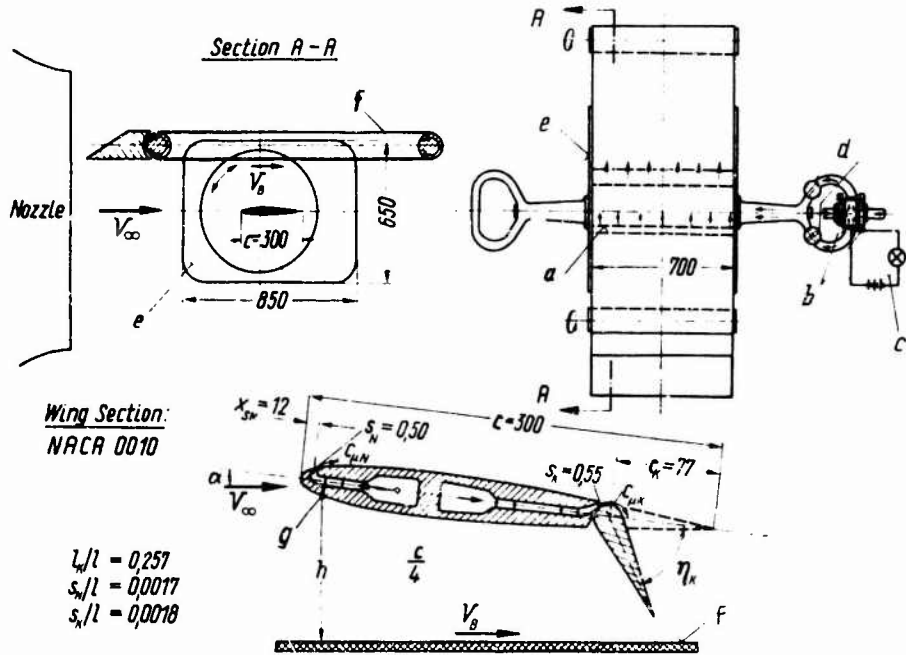


Figure 16

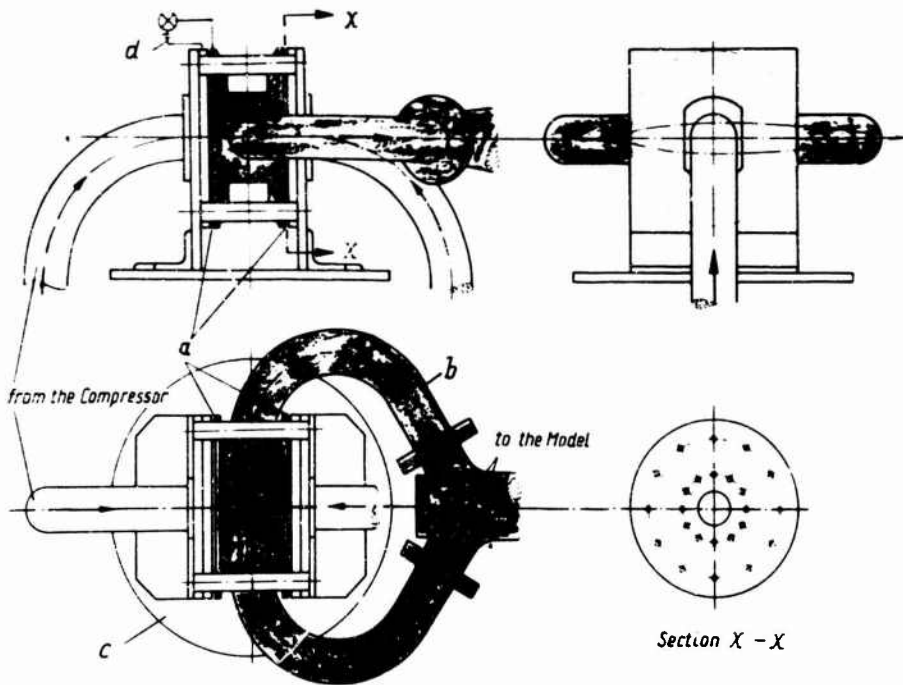


Figure 17

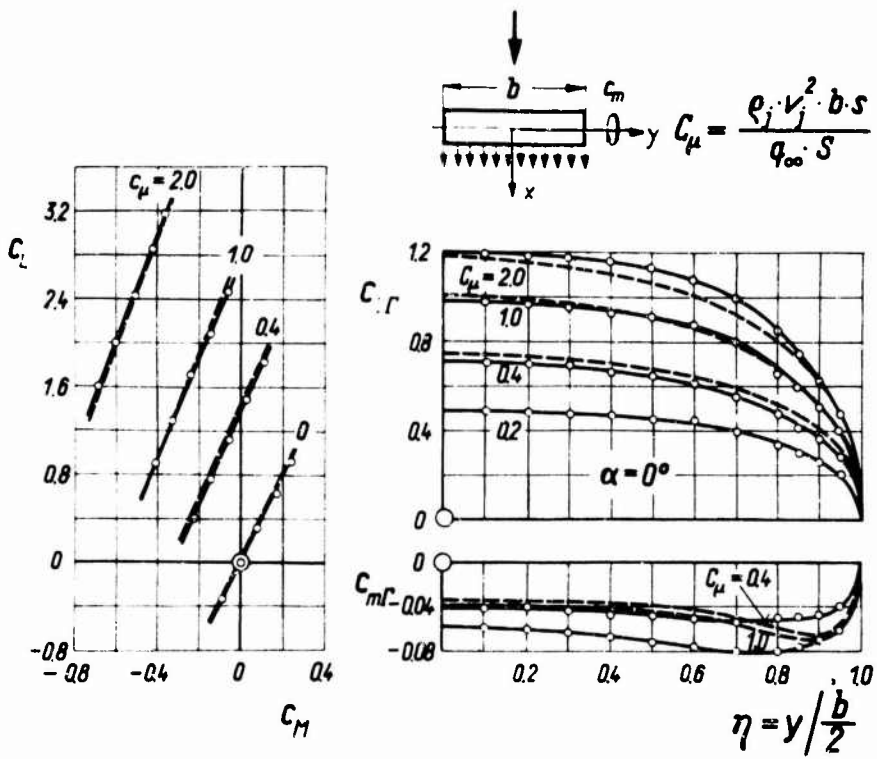


Figure 18



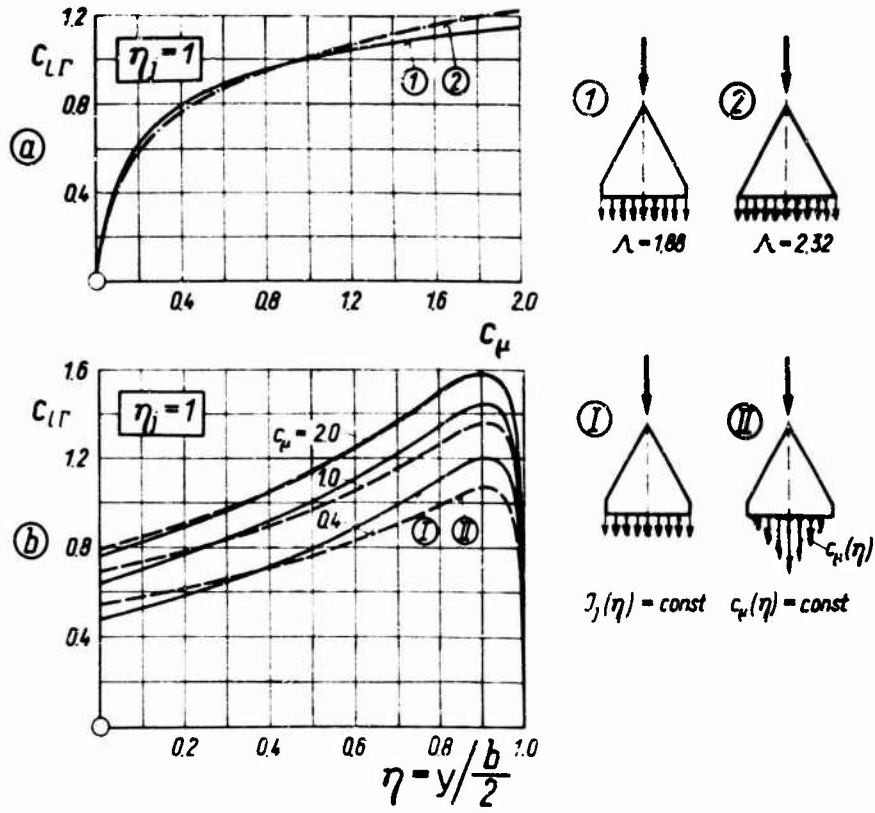


Figure 19

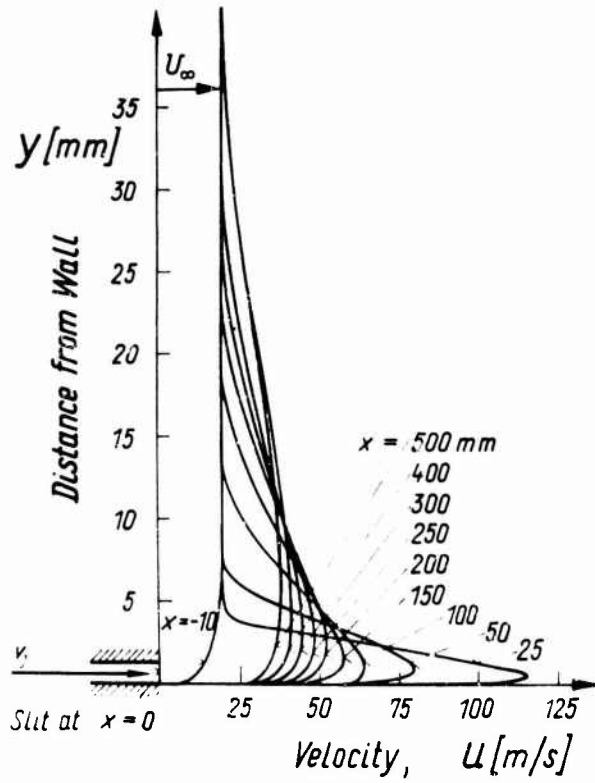


Figure 20

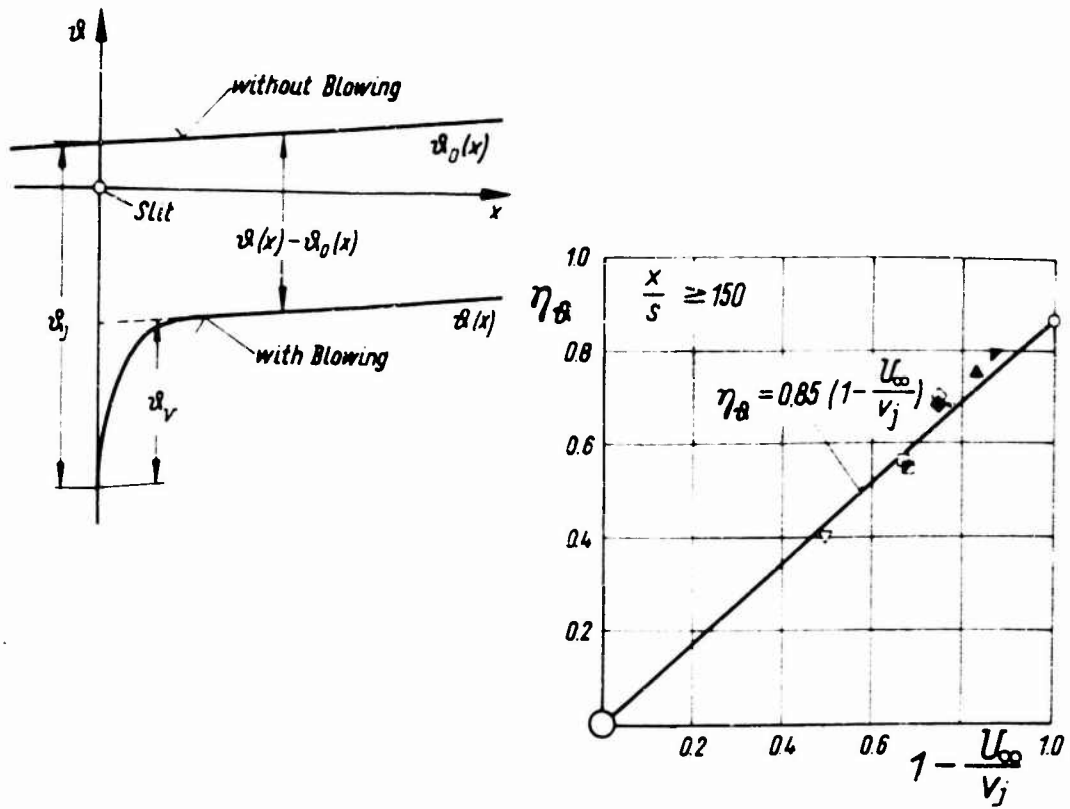


Figure 21

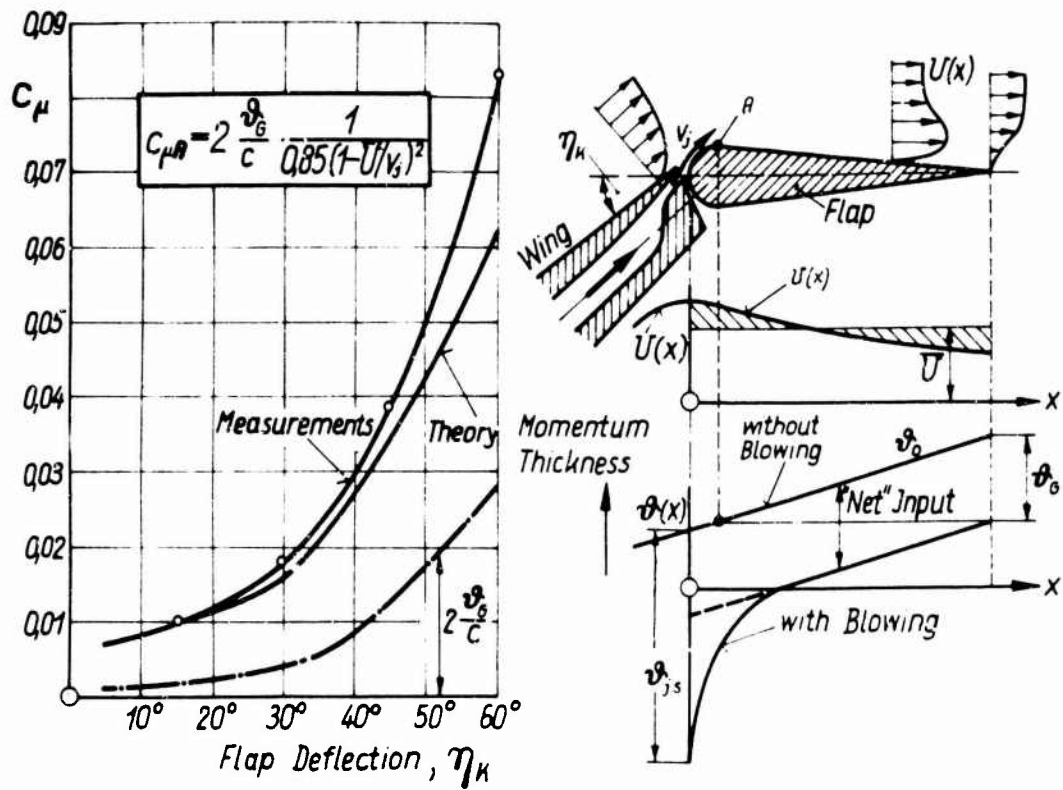


Figure 22

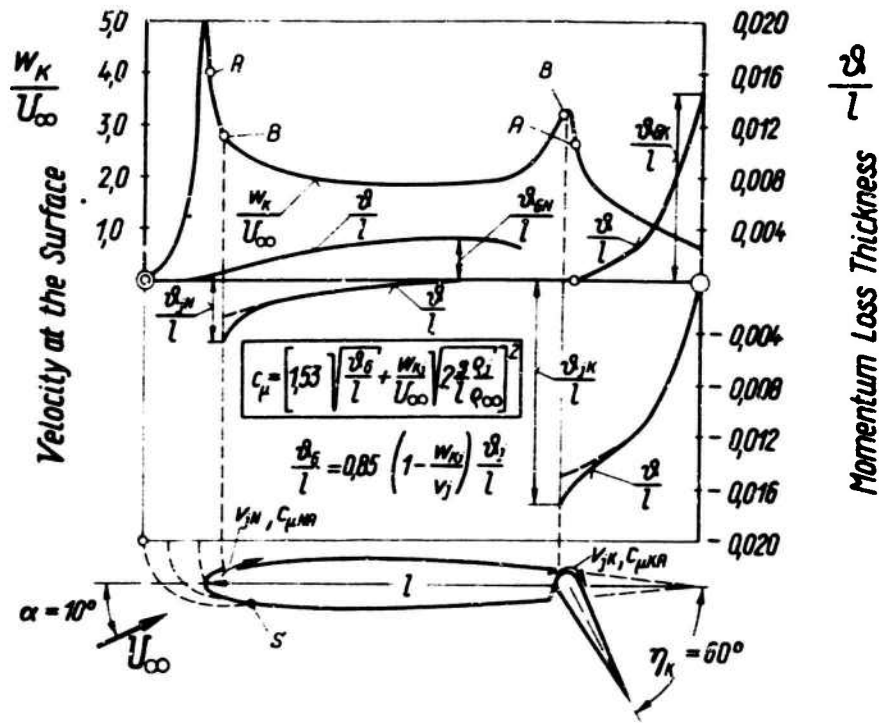


Figure 23

DO 27

DO 28



$G = 1500 \text{ kp}$     $V = 205 \text{ km/h}$   
 $N = 274 \text{ PS}$     $G/F = 77 \text{ kp/m}^2$

$G = 2450 \text{ kp}$     $V = 248 \text{ km/h}$   
 $N = 2254 \text{ PS}$     $G/F = 109,5 \text{ kp/m}^2$

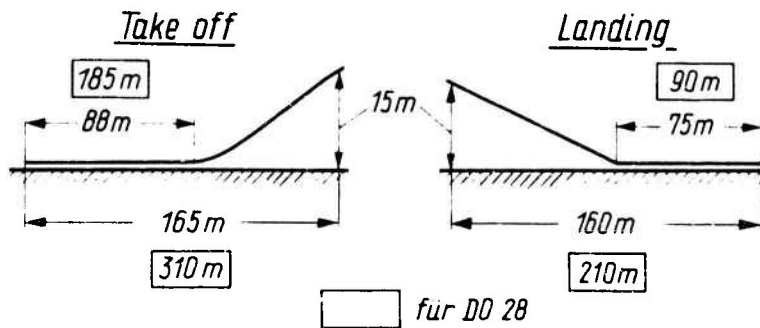


Figure 24

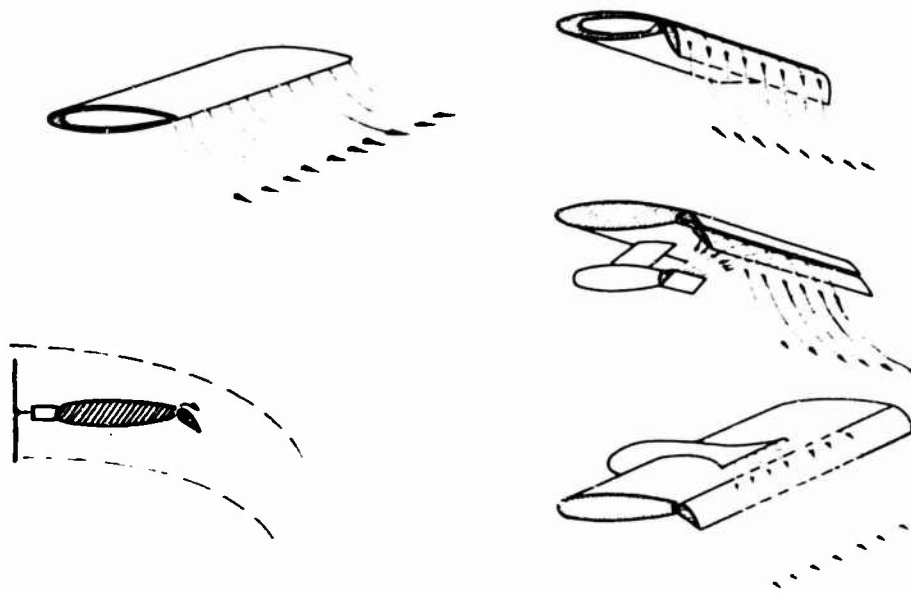


Figure 25



*Without Suction*



*With Suction*

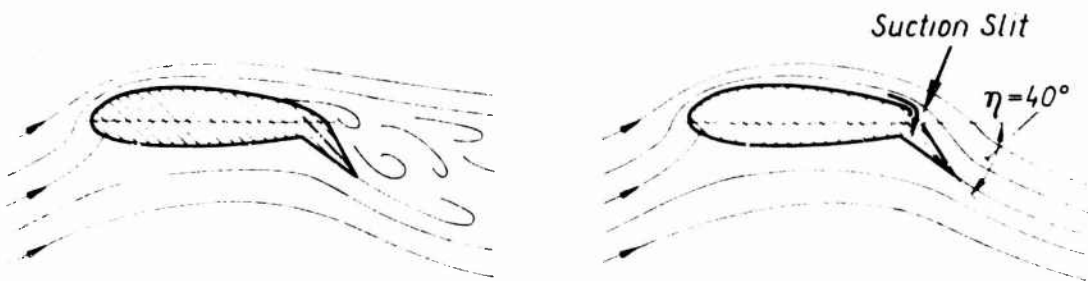


Figure 26

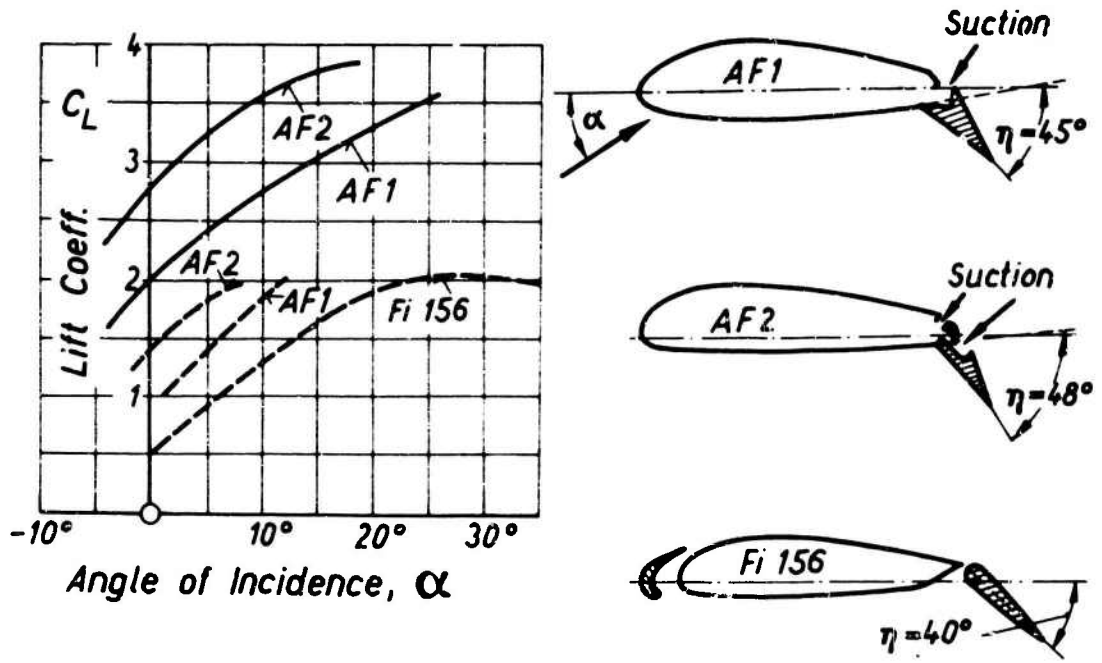


Figure 27

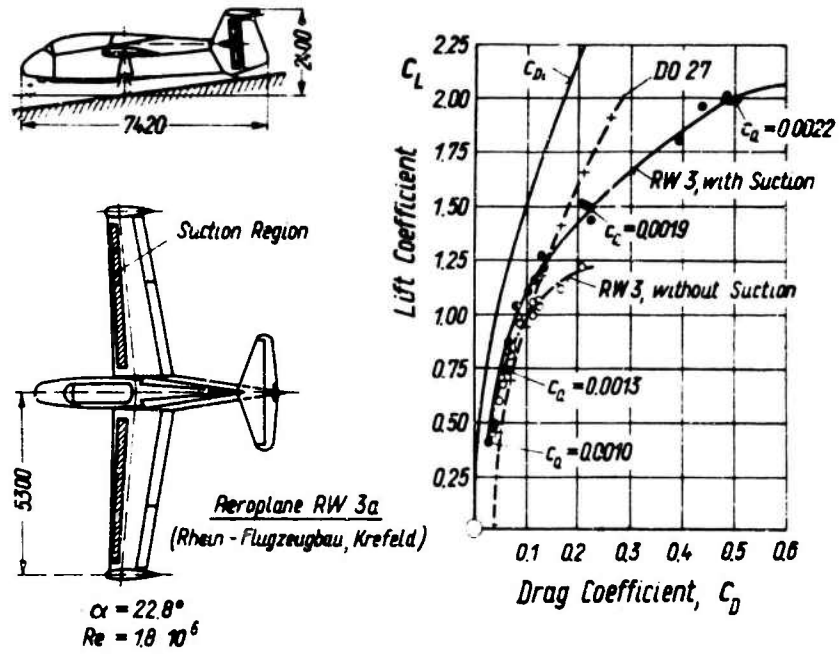


Figure 28

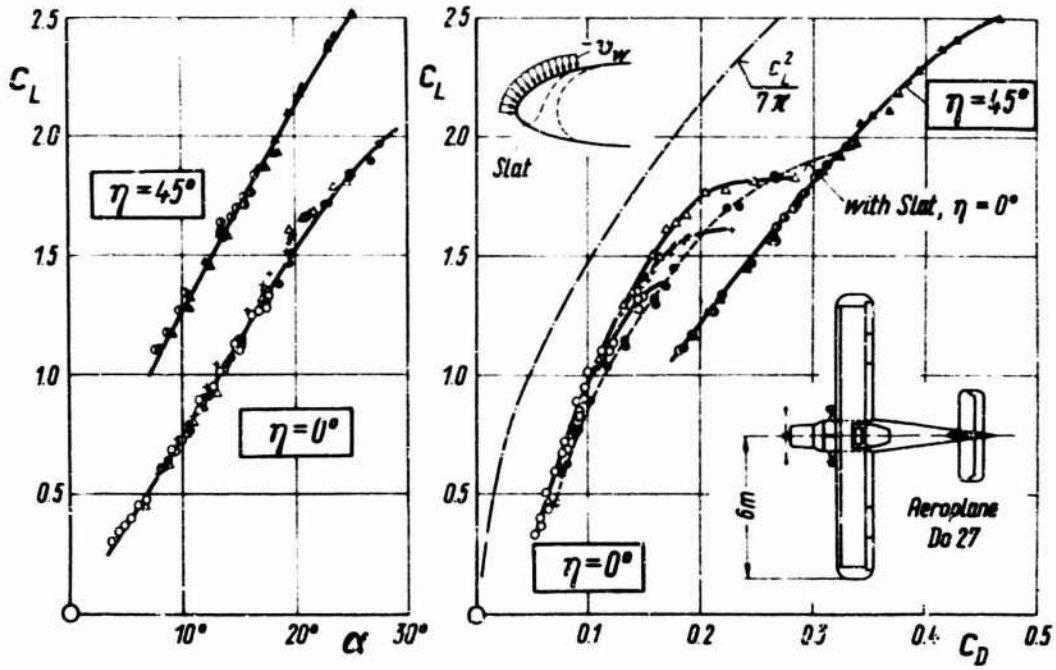


Figure 29

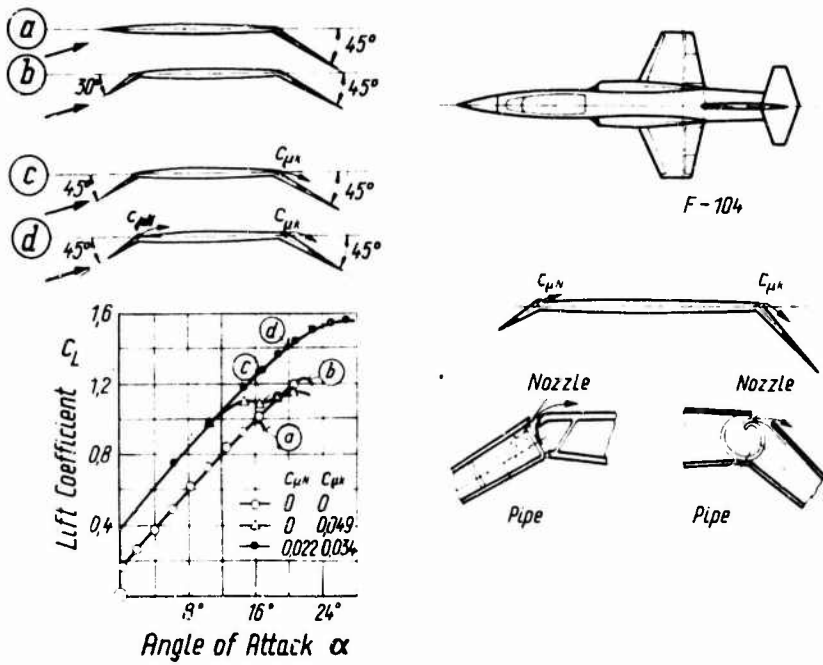


Figure 30

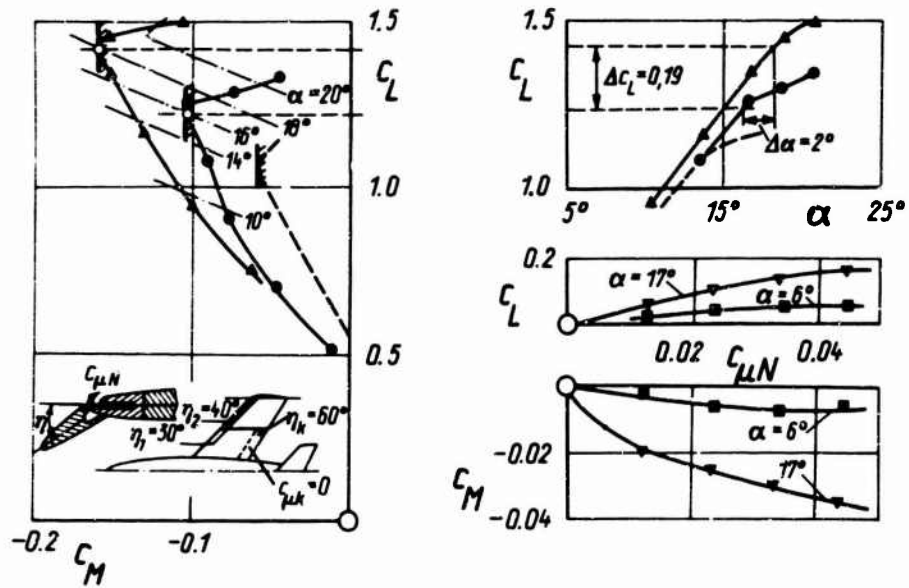


Figure 31

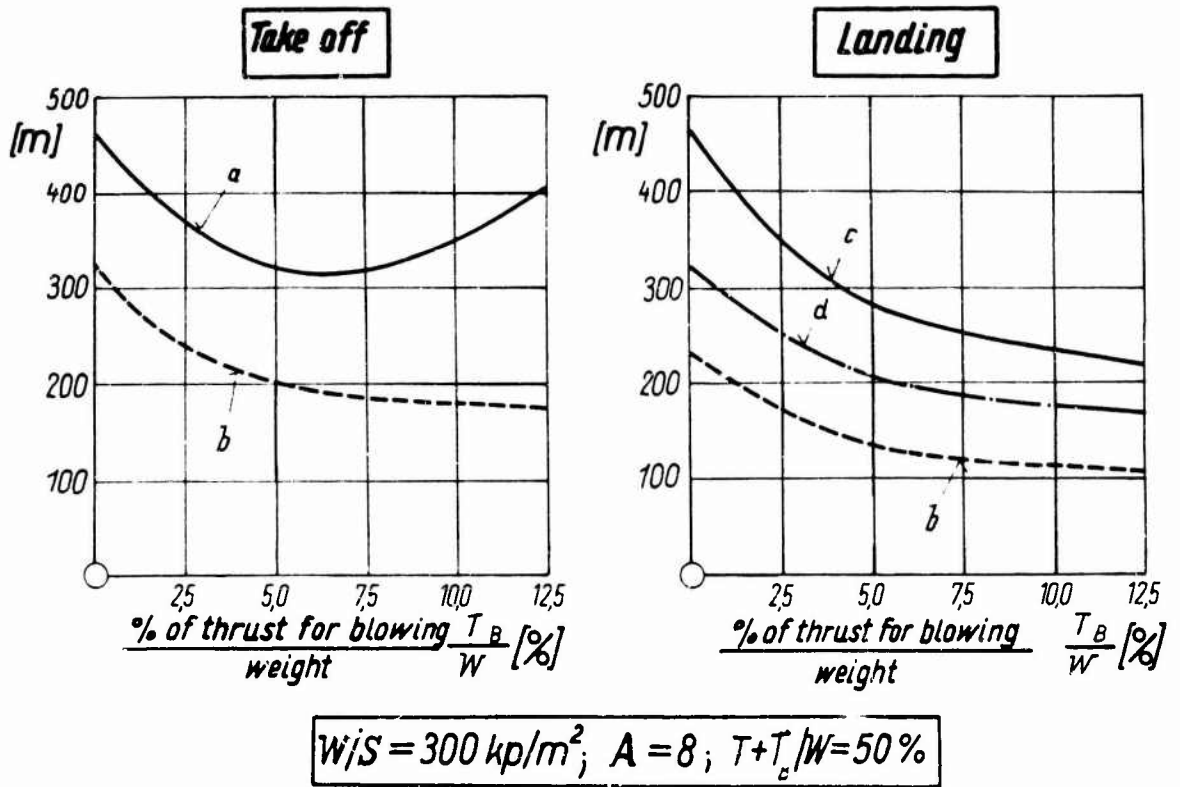


Figure 32

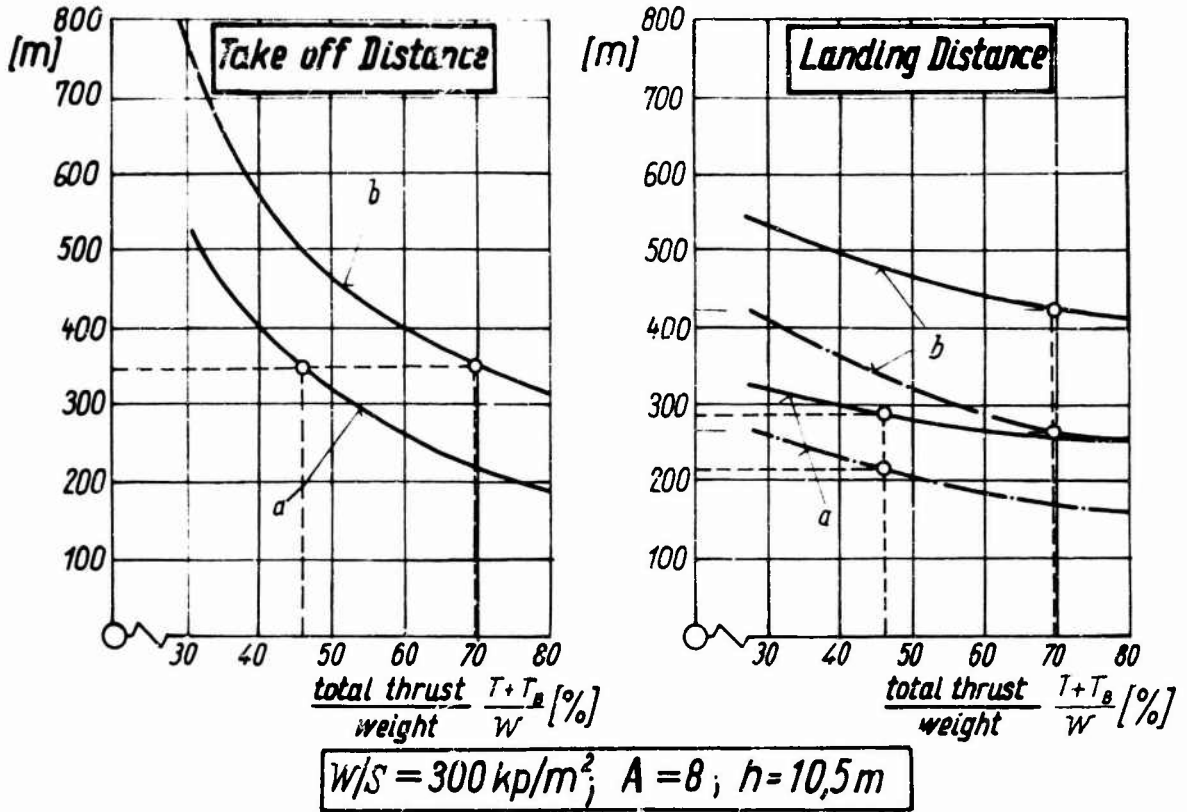


Figure 33



PAPER G

TECHNIQUES FOR THE AERODYNAMIC TESTING OF  
V/STOL MODELS

by

W. J. G. Trebble

Aerodynamics Department, Royal Aircraft Establishment  
Farnborough, Hants, UK

## TECHNIQUES FOR THE AERODYNAMIC TESTING OF V/STOL MODELS

W. J. G. Trebble

### 1. INTRODUCTION

Wind tunnel testing of aerofoils, scaled aircraft models or their components dates back half a century and has been well established as a flexible and profitable method for carrying out essential basic research and guiding development. Throughout this period, there has been a continued improvement in test techniques to achieve satisfactory mainstream flow over the models, to facilitate accurate force measurements and pressure plotting, and to ensure adequate corrections for differences between models mounted in a tunnel and the full-scale aircraft in free flight. The advent of the V/STOL concept during the last two decades has demanded the development of specialised and novel techniques for model testing including complex model and rig designs to allow air to be ejected from or sucked into models. Appropriate test methods will be outlined below, for obvious reasons, the discussion will be mainly based on research in the United Kingdom though it is appreciated that parallel developments have been taking place elsewhere in Europe as well as in the USA.

Attention is mainly concentrated on techniques required for lifting-jet or lifting-fan research though some mention is also made of the problems encountered with propeller driven V/STOL concepts. The need for adequate ground simulation is also considered as well as the desirability of special tunnels for V/STOL and high-lift research.

### 2. JET-BLOWING RIGS

For tunnel testing full-scale V/STOL aircraft or large models, the pumping system for blowing or suction can be installed in the model. However, most V/STOL testing must of necessity take place in relatively small tunnels using external air supplies which require the development of air-connectors which neither put physical constraints on the balance nor unduly interfere with the mainstream flow.

#### 2.1 Complete Model Rigs

A tunnel equipped with a virtual-centre platform type balance is the simplest to adapt for V/STOL testing as, for this type of balance, frictionless mountings about the pivot are unnecessary. Figure 1 shows a typical model arrangement in which an air-bearing connector (Fig.2) is located below the tunnel and is thus isolated from strut deflections. Alternative types of connector that may be used are canvas sleeves (Fig.3), metallic bellows (Fig.4) or a mercury seal (Fig.5). With all these systems care must be taken to avoid large induced mass flows up the strut-guard and to use air at constant temperature.

Systems have also been developed for passing air into models suspended from conventional balances where constraints about the pivot point cannot be tolerated. One method<sup>2</sup> (Fig.6) is to mount an air-bearing on the axis of rotation of the model but outside the tunnel. The air connector from this air-bearing to the model passes over the tunnel and the pipe inside the tunnel is left exposed to the mainstream flow so that the model incidence can be varied. Figures 7-10 show models used on this rig which has the disadvantage of large corrections to drag and pitching moment arising from the supply-pipe.

An alternative supply system<sup>3</sup> (Fig.11) is to pass air from a ring-main supply below the tunnel into eight equally spaced flexible tubes and hence into the base of the strut leading to the pressure-box (Fig.12) inside the model. This system is amenable to the provision of a strut-guard but a separate angle piece must be inserted in the air-supply for each incidence tested.

## 2.2 Half-Models

Half-models have the advantages that they can be made at larger scale than complete models and that the air feed problem is greatly simplified though, of course, the effects of sideslip cannot be studied. Two typical half-model rigs are illustrated in Figures 13 and 14 for a conventional three-component balance and for a platform type virtual-centre balance respectively. The tunnel wall is used as a reflection plate but to keep the wing out of the boundary layer, either the fuselage width is increased or a false wall is mounted a little distance from the tunnel wall. In the latter case care must be taken to correctly monitor the flow past the model in a similar manner to that used for ground-effect measurements (see Section 4).

## 2.3 Composite Rigs

In V/STOL testing, slight inaccuracies in the measurement of the jet thrust can seriously affect accuracy with which the interference effects on the airframe can be determined. Consequently there is a need to know the airframe loads separately from the overall forces and moments. These can conveniently be obtained by supporting the fuselage shell and wings on a strain-gauge balance mounted on top of the variable incidence head of the supply strut (Fig.15). If lifting-jets are carried on pods, it may be more advantageous to mount them separately from an overhead balance whilst the main model is supported on the lower balance (Fig.16).

## 2.4 Strain-Gauge Balance Problems

Unless a platform type balance is available, strain-gauge balance rigs may well be preferable for V/STOL testing, particularly for six-component measurements. The possibility of a variety of alternative support arrangements is a very attractive proposition from tare and interference considerations. Nevertheless there are problems such as reduced accuracy, balance interactions and zero drift which could be extremely troublesome if the temperature of the air supply was significantly different from ambient.

An internal strain-gauge balance has been used for tests on a propeller slipstream model<sup>15</sup> (Fig.17) with blown trailing-edge flaps (Fig.18) mounted on a braced vertical support tube attached to a turntable in the RAE 24 ft tunnel (Fig.19). With the air supply near ambient temperature the system worked very well but serious zero drifts were observed when high flow rates were pushed through the model as the higher pressurisation raised the temperature of the supply air to 20°C above ambient.

More recently a strain-gauge balance has been incorporated in a shielded vertical strut<sup>6</sup> (Fig.20) for testing the Jet-Nacelle model (Fig.16). It was designed as a virtual-centre balance with the gauges located at stations for which the moduli were proportional to the distance from the virtual centre but; on initial test, large interactions were observed between the various components and repositioning of various gauges was necessary to reduce these interactions to an acceptable level. The associated air-connector (Fig.21) has been designed to deliver air with no net vertical or horizontal momentum.

### 3. JET EFFLUX AND INTAKE SIMULATION

#### 3.1 Basic Considerations

Experience suggests that the parameter which must be correctly represented is  $\rho_0 V_0^2 / \rho_j V_j^2$  where  $V_0$  and  $V_j$  are the velocities of the main stream and efflux and  $\rho_0$  and  $\rho_j$  are their respective densities; the effects of jet Reynolds number, jet to mainstream temperature ratio and jet pressure ratio appear to be of second order. However, the size and position of the jet relative to the surrounding planform is of crucial importance on the aerodynamic interferences. For intake representation, some distortion of inlet shape may be necessary at low Reynolds number to correctly simulate the inlet flow conditions.

#### 3.2 Blowing Duct Nozzle Design

Blowing nozzles for jet-lift representation are quite complex as large mass-flow rates must be smoothly ejected from short nozzle lengths (2 diameters or less). High pressure air must be fed to a pressure-box inside the model and adequate baffling incorporated down-stream from the pressure-box to ensure reasonably uniform flow in the efflux. Some simple pressure chambers are illustrated in Figure 22 in which plenum chambers are incorporated in the design. Baffles were used in conjunction with resistance gauzes and a contraction ahead of the nozzle to give efflux distributions within  $\pm 5\%$  of the mean jet velocity.

For the P 1127 model (Fig. 23), no plenum chamber was feasible and the air supply from the vertical strut was divided to provide the appropriate feed to the four rotatable nozzles. To ensure adequate representation, each nozzle had two sets of resistance gauzes and an area contraction of 1.3:1 in the final turning cascade. With rotateable nozzles, the uniformity of the efflux must be verified throughout the angle range.

On the Jet-Nacelle model<sup>4</sup> (Figs. 24 and 25), each main wing constituted a pressure-box designed to pass 5 lb/sec at 10 atmospheres absolute through the slender hollow pylons to the nacelles. A variety of internal baffling arrangements have proved necessary according to the nozzle configuration but for the case of the single large-nozzle nacelles, it was also necessary to insert a honeycomb in the nozzle.

#### 3.3 Injector Units

Injector units provide a convenient way to simultaneously represent the intake and exit flows in jet nacelles. However, reduced exit velocities must be accepted if reasonable amounts of intake flow are to be induced by the injector and consequently mainstream speeds are lower to cover the same speed-ratio range. The reductions in jet efflux and mainstream speeds must not be so severe that the thrusts and interference loads cannot be measured accurately enough.

The injector nacelle unit consists essentially of a cylindrical mixing tube (Fig. 26) fed with compressed air ejected from slots in the trailing-edges of a cartwheel spoke arrangement of elliptic tubes near the front of the mixing tube. At the design pressure-ratio of  $3\frac{1}{2}$  atmospheres absolute, a mean efflux velocity of 650 ft/sec is attainable.

#### 3.4 Model Fan Units

At RAE model fans have been used simply as a means of providing simultaneously both upper surface intake suction and lower surface jet efflux and no attempt has been made to represent specific configurations.

Early experiments<sup>3</sup> were made using electric motors to drive fans in fuselages and nacelles (Fig. 27) and efflux velocities of some 120 ft/sec were available from 1 ft diameter ducts using a 6 h.p. motor. The motor-fan unit, having a length of one foot, was too long to fit vertically into a model wing and a scheme of driving fans through bevel

gears from a horizontally mounted motor has been devised<sup>9</sup> (Fig.28). By judicious location of the motors, multiple fan systems have been represented.

Unfortunately, even with this latter system, electric motor units occupy large volumes inside the model but air-driven turbine fans have now been developed with a casing width little greater than the fan diameter (Fig.29 and 30). Mean efflux velocities of 300 ft/sec are available from 6 inch diameter hub driven turbine fans with air supplied at 4 atmospheres absolute. Smaller fans of 3 inch diameter are now available but these are tip driven.

More recently the use of hydraulic motors has received favourable attention<sup>10</sup>. In the past such motors have been rejected because of the difficulty of supplying fluid at 2000 to 3000 lb/in<sup>2</sup> without imposing physical constraints and also because of doubts as to whether the speed can be adequately controlled. Research on small motors (Fig.31) has shown that these problems are not insurmountable and that torques of up to 140 lb/in can be obtained from motors as small as 3½ inches diameter and 4 inches long at rotational speeds from 0-6000 r.p.m. A typical pump-motor circuit is illustrated in Figure 32 where two pumps in parallel are used to drive a single motor. One pump has a fixed stroke whilst the other has variable stroke so that any motor speed between the sum and difference of the pump speeds can be obtained. The entire drive system is extremely compact (Fig.33) compared with the control system required for electric motors or the compressors required for turbines. The problem of frictionless connections in the supply system can be overcome by the use of flexible ball and socket joints which have been successfully used in the two layouts shown in Figure 34

### 3.5 Air-Cushion-Vehicles<sup>11</sup> (Fig.35)

The adequate representation of A.C.Vs is very difficult as the aerodynamics of the upper and lower surfaces as well as the internal aerodynamics are so intimately connected that inaccurate representation of one design feature could affect the aerodynamics of distant components. In order to fully understand the aerodynamics it is recommended that three models should be built, viz:-

- (a) an intake model for the upper surface aerodynamics;
  - (b) an efflux model to study the air-cushion;
- and (c) a composite model to check the interference effects.

### 3.6 Jet-Nacelle Model Design (Fig.24)

The jet-nacelle model already mentioned is an extremely complex model and its design is worthy of further study. Propulsive, lift/thrust and pure-lift jet units can be disposed in underslung nacelles. The high aspect-ratio wing of moderate sweepback is provided with knee blowing slots for leading-edge and trailing-edge flaps (Fig.36). As the hollow wings are used as ducts to transport compressed air to the nacelles the boundary layer control (BLC) ducts are incorporated in the flaps. Great care is necessary to minimise distortion in the BLC nozzles which are tapered from 0.004 to 0.008 in at the trailing edge (TE) and from 0.002 to 0.004 in at the leading edge, the width being regulated with graded spacers.

## 4. GROUND SIMULATION

Over the years many techniques have been developed for the investigation of ground effect on models. These have generally used a stationary reflection plate and some doubt has always arisen from the presence of the plate boundary layer which does not simulate full-scale conditions. To overcome this difficulty, an elaborate moving-belt ground rig (Fig.37) has been developed at RAE<sup>12</sup> for running at speeds up to 90 ft/sec over a pair of one foot diameter rollers located 9½ feet apart in an 11½ x 8½ ft tunnel (Fig.38). As a lower balance is used, models are inverted and the lower surface of the rig is the "ground". The endless moving-belt of 3/16 in overall thickness is 7 ft 10 in wide and 22 ft long;

the outer panels of the 11½ ft wide rig are stationary. In order to ensure flat running, suction must be applied to hold the ground onto the main box construction of the rig not only to overcome the gravitational effects but also to counter local negative pressure regions arising from aerodynamic interference effects. Boundary layer characteristics above the moving-ground (Fig.39) are very close to those pertaining to flight conditions.

The belt speed can accurately be determined by using an electronic timer to measure the time interval for a narrow metallic mirror attached to the belt to move between two photo-electric cell units on the backing plate. Wind speed is more difficult to determine accurately and involves a detailed calibration of both air-passages with pitot-static tubes before a model is installed and then monitoring the flow-rate in the "scrap" part of the tunnel when the model is rigged; model drag will force more air into the "non-operating" passage. The relevant air speed at the model can then be determined provided the mass-flow rate ahead of the ground is also known.

This moving-ground rig has been used for investigations on a variety of models (Fig.40) and the ground effect on lift for these configurations, with the ground moving and stationary, can be seen in Figures 41-45. Overall these results justify the use of a fixed ground-plate over a much wider range than could reasonably have been expected. Only in the extreme Jet-Flap<sup>13, 14</sup> case is the presence of the extraneous boundary layer seen to significantly influence the ground effect on the aerodynamics. It would therefore be preferable, in general, to make the tests on a conventional ground-board at higher values of the Reynolds number but if  $C_L$  -values in excess of 5 are required from a blown-flap configuration then a moving-belt rig should be used.

## 5. WIND-TUNNELS AND OTHER FACILITIES

### 5.1 Restrictions Imposed by Use of Conventional Tunnels

Most V/STOL research has been made in tunnels of cross-section between 10 × 7 and 13 × 9 ft with the result that Reynolds numbers are of necessity rather low so that tunnel interference effects can be kept to a tolerable level. In USA Heyson has made a theoretical investigation of V/STOL model corrections and has concluded that it is the fore and aft variation of wall induced interference rather than its absolute size that is the main limitation on model size. This limits the span of a V/STOL model to less than half the tunnel width as against the two thirds usually regarded as acceptable for conventional models.

Although high Reynolds number is a very desirable feature it should not be attained by testing at excessive speed, particularly if leading-edge flap blowing is being investigated as this may result in serious errors in the measured  $C_L$  -values (Fig.46). The explanation for this is that extremely low pressure regions can be carried on the wing at high  $C_L$  and thus locally very high air velocities may accrue leading to compressibility effects at the higher test speeds even though the free-stream Mach-Number is as low as 0.2 (Fig.47).

### 5.2 V/STOL Tunnels

The first attempts to provide special facilities for V/STOL testing involved the installation of a second test section in the return circuit of existing wind-tunnels as for example in the NASA Langley 10 × 7 ft tunnel which now also has a 17 ft square section. For such modifications great care must be taken to ensure that the flow is of acceptable quality in both test sections.

During the past few years special V/STOL tunnels have been constructed such as the BAC 18 ft square tunnel and the Hawker Siddeley 15 ft square tunnel in England. For economic reasons both have been built out in the open and, as they are of the non-return circuit type, this has resulted in some limitation of their use in adverse weather conditions.

Tunnels of a more sophisticated nature are now under active consideration and one of the main parameters influencing their design is the test Reynolds number which should be at least  $6 \times 10^6$  based on wing chord for high lift representation<sup>15</sup>. This would imply the need for a tunnel 20 x 20 ft with a top speed of 300-350 ft/sec and the capability of pressurisation up to 3 atmospheres absolute (Fig.48). For flexible VTOL testing a larger atmospheric tunnel would be preferable and a section 30 x 20 ft is suggested with a working speed range from 15 ft/sec to 250 ft/sec (Fig.49). A second, larger test section could also be incorporated in the design for very low speed research. A tunnel of this type was put into operation by the Lockheed Georgia Company at Marietta last year.

### 5.3 Tracks

The idea of making aerodynamic measurements on a moving model in still air rather than on a stationary model in an air-stream is by no means new and outdoor facilities of this type have been in existence for many years (e.g. at Pendine Sands in UK or China Lake, California USA). In each case several miles of accurately laid railway line has provided a track for a high-speed sledge which is normally rocket-powered but the natural air-currents in the atmosphere would preclude their use at the low speeds required for V/STOL on any but the calmest days. On the other hand, an enclosed facility requires a very long building so that steady conditions can be attained for a significant period of time. For either type of facility extremely smooth running is essential if the aerodynamic loads are not to be obscured by the transient gravitational loads imposed by the track.

A 750 ft long track enclosed in a building 35 ft high and 30 ft wide has been built at Princeton University<sup>19</sup> primarily to investigate the behaviour of freely pivoted dynamic models but it can also be used for steady state measurements on restrained models. For dynamic similarity, the ratio of gravitational to aerodynamic forces must be the same as for the full-scale vehicle whilst the radius of gyration must also be correctly scaled. The resultant motions are then in a "quickened" time scale which is proportional to the square root of the linear scale (i.e. for a ninth scale model, an event would occur in one third the time taken full-scale) and hence velocities must be represented at only a third of the full-scale value. The track can be operated at steady speeds up to 40 ft/sec but additionally, at lower speeds, horizontal accelerations as high as 0.6g can be represented. Power is transmitted via rails and by bushes to three-phase electric motors in the model which drive either propellers or fans. This track has proved to be very useful and models representing helicopters, tilt-wing VTOLs and Gound Effect Machines have been successfully tested at model weights between 20 and 50 lb.

### 5.4 Whirling Arm

The old N.P.L. whirling arm has recently been installed at the College of Aeronautics specifically for research on "ram wings"<sup>16</sup> but such a facility could also be used for research on V/STOL models, particularly for studies of the effects of gusts and transient conditions. Unfortunately, the device has certain inherent problems of which the most important is that the low pressure wake shed by the rotating arm reduces the air speed being represented to a value significantly less than the physical speed of the model. Also, of course, the circular track implies a spanwise velocity gradient and, furthermore, corrections must be applied for the centrifugal forces.

## 6. PROPELLERS

### 6.1 Deflected Slipstream and Tilt-Wing

Various models have been built to represent these methods of attaining V/STOL flight on propeller aircraft. At RAE a composite model (Fig.51 and 52) was built with 4 1½-in diameter propellers individually driven by 7 h.p. electric motors carried in nacelles under the wing; for propeller models, the scale is usually determined by the size of motor available as this fixes the minimum size of the nacelles. The wing is equipped with

a 50% chord sliding flap and a 30% chord slotted flap for the deflected slipstream configuration but the sliding flap is locked closed for the tilt-wing representation. With the balance below the model (or above if the model is inverted) it is not practical to represent  $90^\circ$  tilt as the slipstream would then be blowing directly onto the balance but test have been made at deflections of up to  $60^\circ$ .

## 6.2 Measurement of Propeller Torque and Thrust

For V/STOL operation propellers must be designed to operate efficiently at much lower forward speeds than those pertaining to conventional aircraft and, for air-cushion-vehicles, some parts of the flight plan require efficient thrust control even in a tail wind. It is therefore necessary to investigate propeller characteristics on a rig such as that shown in Figure 53 which shows a 1500 h.p. variable frequency electric motor mounted in a nacelle on a pylon in the RAE 24 ft tunnel. The normal drag balance is used to measure the propeller thrust whilst the power absorption is measured on wattmeters with due allowance made for electric losses of the motor.

On a smaller scale, model characteristics have been determined by the use of the rig illustrated in Figure 54. A small electric motor is carried on two ball-races inside a nacelle and a strain-gauge link from the motor to the outer casing permits the measurement of torque. The complex hub fittings (Fig.55) allow a selection of predetermined blade angles to be set but these cannot be varied during a test-run.

## 6.3 Tunnel Interference

Tunnel walls can cause severe constraints on the large core slip-stream generated by rotors at large angles of sideslip and, at the University of Washington, Rae<sup>17</sup> has made a detailed study of the limiting conditions that can be truly represented for a given propeller-tunnel geometry (Fig.56). This research shows that, at very low forward speeds, there is some forward movement of the flow along the tunnel floor and interferences involving flow breakdown must be assumed to be present and these are not amenable to theoretical treatment.

In addition to wall-constraint effects, some uncertainty arises in any wind-tunnel propeller investigation from the possibility that the pressure field generated by the propellers may upset the reference pressure system used to determine the air speed. The use of a 1.6 ft diameter propeller in an  $11\frac{1}{2} \times 8\frac{1}{2}$  ft tunnel at RAE has shown that this can create large errors in the speed determination when the propeller is deflected (Figs.57 and 58). It is recommended that the pressure tapings should be in the roof if the propellers are yawed and in the sides when the propellers are pitched.

## 7. OSCILLATORY AERODYNAMIC DERIVATIVES

The study of the aerodynamic damping on V/STOL models can be made either by using a free oscillation or a forced oscillation technique but whichever method is used, there is the problem of passing large quantities of air into an oscillating model. This requires a frictionless air-support assembly capable of movement through a range of some  $\pm 6^\circ$  without varying the flow rate. One such device for measurement of damping in yaw (Fig.59) has an inner component attached rigidly to the model support strut (which is firmly earthed) and an outer component moving with the model. Vertical forces are supported by two annular air-bearing surfaces in the lower part of the assembly whilst horizontal forces are sustained by two tapered bearings at the top of the assembly; pitching and rolling moments are sustained jointly by all four bearings.

For the free oscillation technique, springs, attached to the wall, are connected by thin piano wires to flexure hinges on the tail spar; a range of spring size enables variations to be made in the period of oscillation. An air-gap transducer is used to indicate the model angular position and the amplified output indicates the decay of the yawing oscillation on an ultra-violet recorder.



In practice it has been found that the aerodynamic damping is dependent on the amplitude of oscillation and consequently forced oscillations of constant amplitude are desirable. A rig has been developed at RAE<sup>18</sup> in which the model is constrained to oscillate in a sinusoidal motion and the instantaneous loads on a strain-gauge balance are plotted against time on an electronic recorder which simultaneously indicates the rotational position of the model. Aerodynamic stiffness and damping are obtained by resolving the balance outputs into components in phase with and in quadrature with the motion.

#### ACKNOWLEDGEMENTS

The author has freely drawn on the experience and test results of past and present members of the Low-Speed Tunnels Division at RAE to whom he is greatly indebted. Particular mention should be made of the work of Dr J. Williams and Mr S.F.J. Butler whose excellent papers<sup>1</sup> have formed the basis of this lecture.

#### REFERENCES

1. Williams, J.  
Butler, S.F.J. *Recent Developments in Low-Speed Wind-Tunnel Techniques for V/STOL and High-Lift Model Testing.* Z. Flugwiss, Vol.13, pp.73-89; 1965.
2. Trebble, W.J.G. *Exploratory Investigation of the Effects of Blowing From the Leading Edge of a Delta Wing.* ARC R & M 3518; 1966.
3. Trebble, W.J.G. *Wind-Tunnel Experiments of a Simple Lifting-Jet Body With and Without Wings.* ARC Current Paper 718
4. Eyre, R.C.W.  
Butler, S.F.J. *Low Speed Wind Tunnel Tests on an A.R. 8 Swept Wing Subsonic Transport Research Model With BLC Blowing Over Nose and Rear Flaps For High-Lift.* RAE Tech. Rep. 67112; 1967.
5. Eyre, R.C.W. *Description of Model and Test Rig For Flap Blowing Tests With Slipstream in the 24 ft Wind-Tunnel.* RAE Tech. Note Aero 2919; 1963.
6. Foster, D.N.  
Eyre, R.C.W. *The Development of a Vertical Strain-Gauge Balance Strut For Jet Blowing V/STOL Models.* RAE Tech. Rep. 66240; 1966
7. Wood, N.N.  
Howard, J.B.M. *The Development of Injector Units For Lift-Jet Engine Simulation on Low-Speed Tunnel Models.* ARC R & M 3464; 1965.
8. Trebble, W.J.G.  
Williams, J. *Exploratory Investigations of a Bluff Body Containing a Lifting Fan.* ARC Current Paper 597; 1961.
9. Wyatt, L.A. *Preliminary Note on Wind-Tunnel Tests of a Wing Fitted With Lifting Fans.* RAE Tech. Note Aero 2643; 1959.
10. England, K.J. *A Hydraulic Transmission System For Powered Wind-Tunnel Models.* RAE Tech. Rep. 66224; 1966.
11. Trebble, W.J.G. *Low-Speed Wind-Tunnel Tests on a 1/6th Scale Model of an Air-Cushion-Vehicle (Britten-Norman Cushion Craft C.C.2).* RAE Tech. Rep. 66383; 1966.

12. Butler, S.F.J.  
et al. *A Moving-Belt Rig For Ground Simulation in Low-Speed Wind-Tunnels.* ARC R & M 3451; 1963.
13. Butler, S.F.J.  
et al. *Six-Component Low-Speed Tunnel-Tests of Jet-Flap Complete Models, With Variation of Aspect-Ratio, Dihedral and Sweep-Back, Including the Influence of Ground Proximity.* ARC R & M 3441; 1961.
14. Butler, S.F.J.  
et al. *Low-Speed Tunnel Tests of an Aspect Ratio 9 Jet-Flap Complete Model With Ground Simulation by Moving-Belt Rig.* RAE Tech. Note 2957; 1964.
15. Williams, J. *Recent Basic Research on V/STOL Aerodynamics at RAE.* Z. Flugwiss, Vol.14, pp.257-276; 1966.
16. Kummur, P.E. *The College of Aeronautics Whirling Arm Initial Development Tests.* Unpublished Coll. Ae. Paper
17. Rae, W.H. *An Experimental Investigation of the Effect of Test Section Geometry on the Maximum Size Rotor That Can be Tested in a Closed Throat Wind Tunnel.* AIAA Paper No.66-376; 1966.
18. Owen, T.B.  
Cox, A.P. *Some Low-Speed Wind-Tunnel Techniques For the Measurement of Oscillatory Aerodynamic Derivatives on Jet-Blowing Models.* J. Sound Vib., Vol.4, pp.507-525; 1966.
19. Curtiss, H.C.  
et al. *The Princeton Dynamic Model Track.* AIAA Aerodynamic Testing Conference, Washington, 9-10 March 1968.

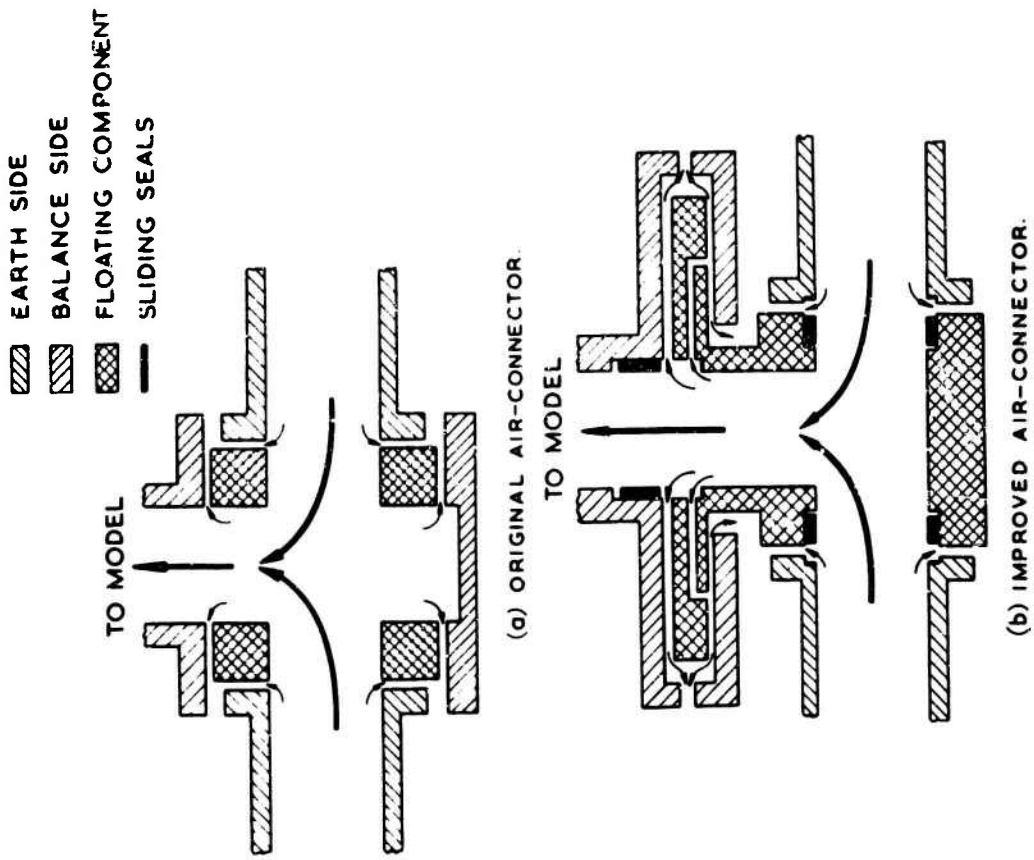


Fig. 2 Air-bearing connectors for RAE virtual-centre balance rig

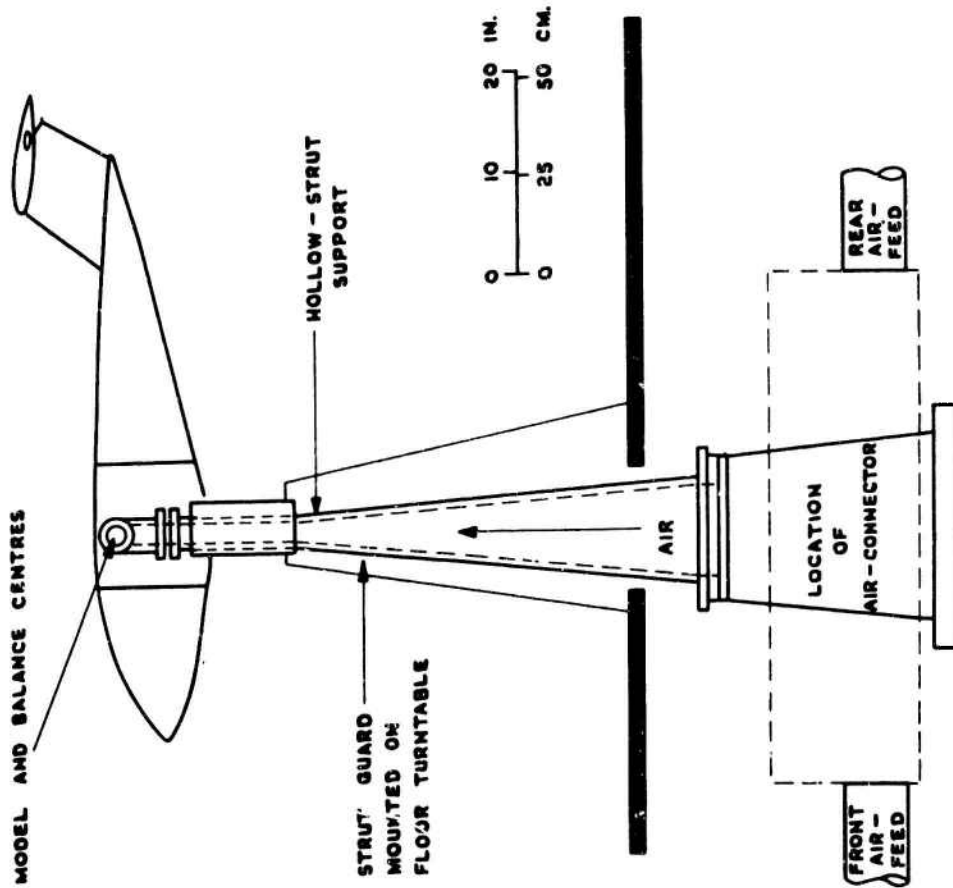


Fig. 1 RAE complete-model rig

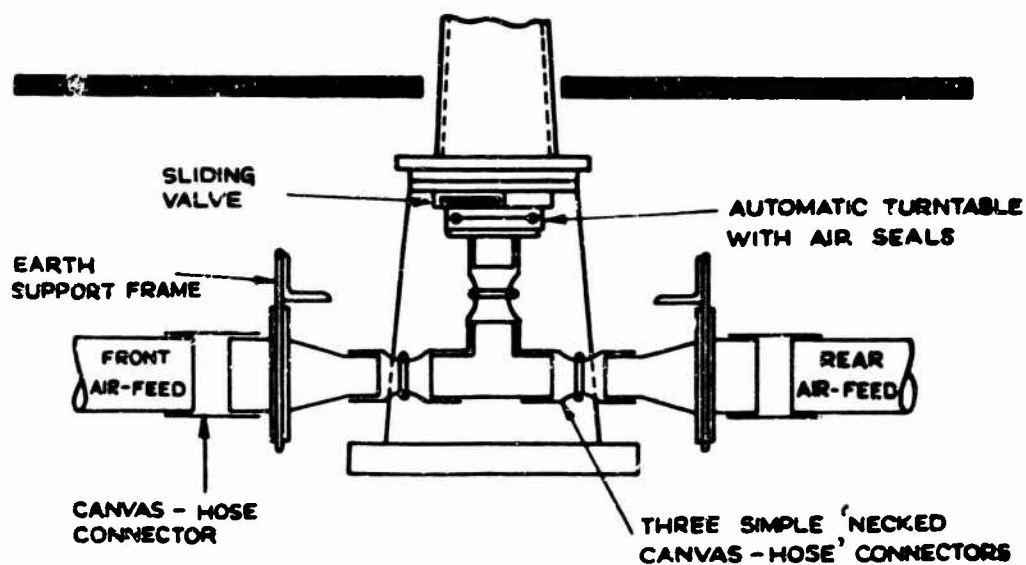


Fig. 3 Multiple simple-connector system for a virtual-centre balance rig

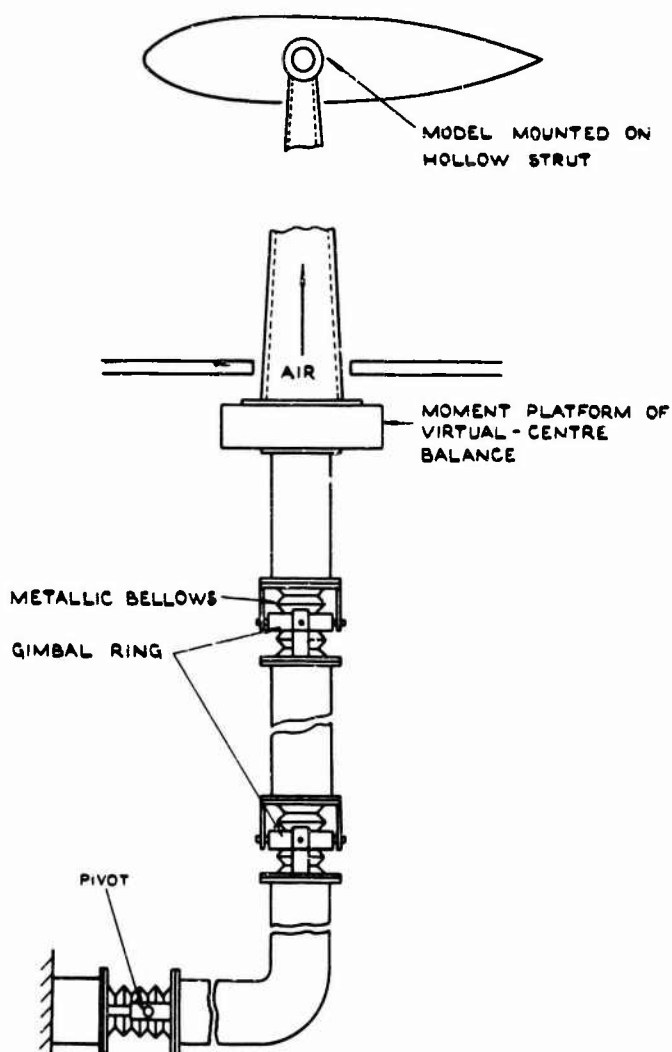


Fig. 4 Arrangement of metallic bellows for virtual-centre balance rig. (David Taylor Model Basin, USA)

MODEL SUPPORTED FROM BALANCE  
IN A CONVENTIONAL MANNER

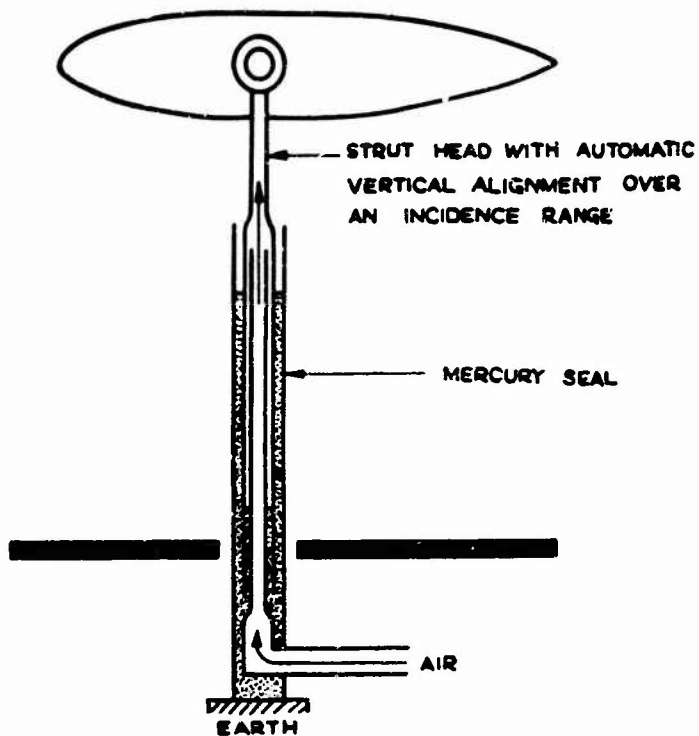


Fig. 5 Complete-model rig with mercury-seal connector

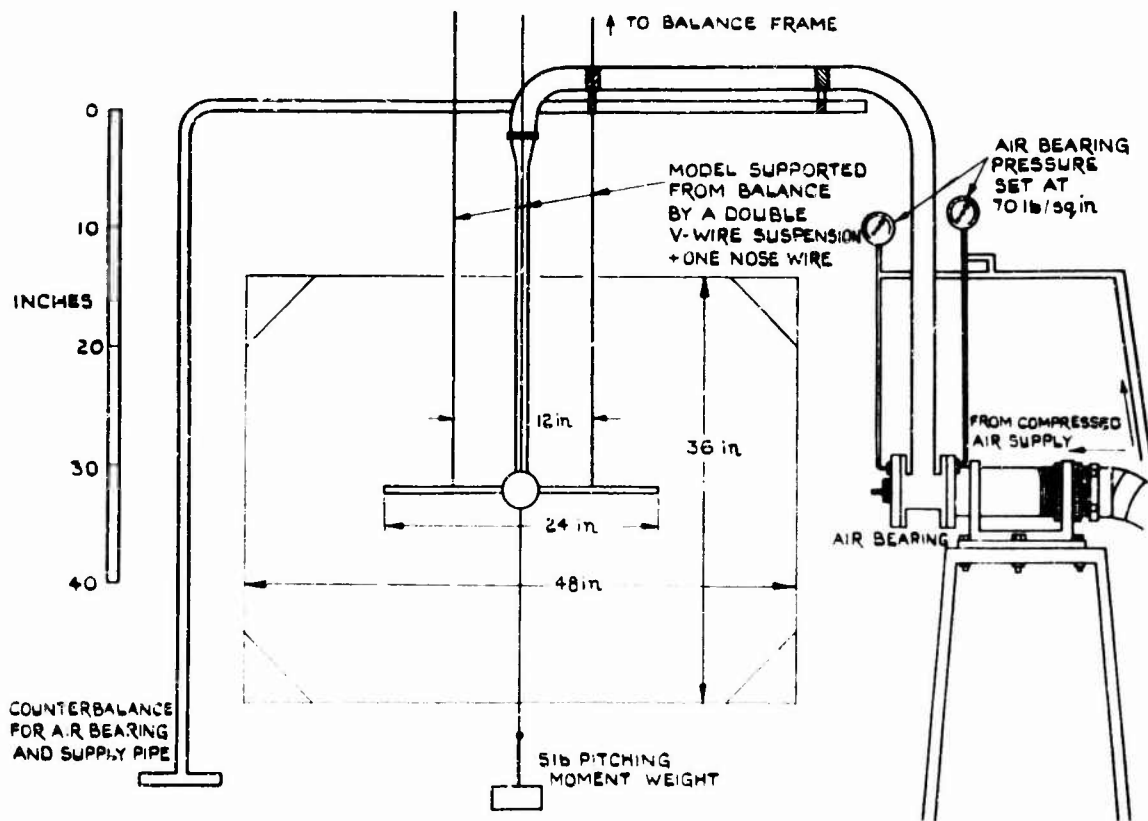


Fig. 6 Model installation in RAE 4 ft x 3 ft wind tunnel

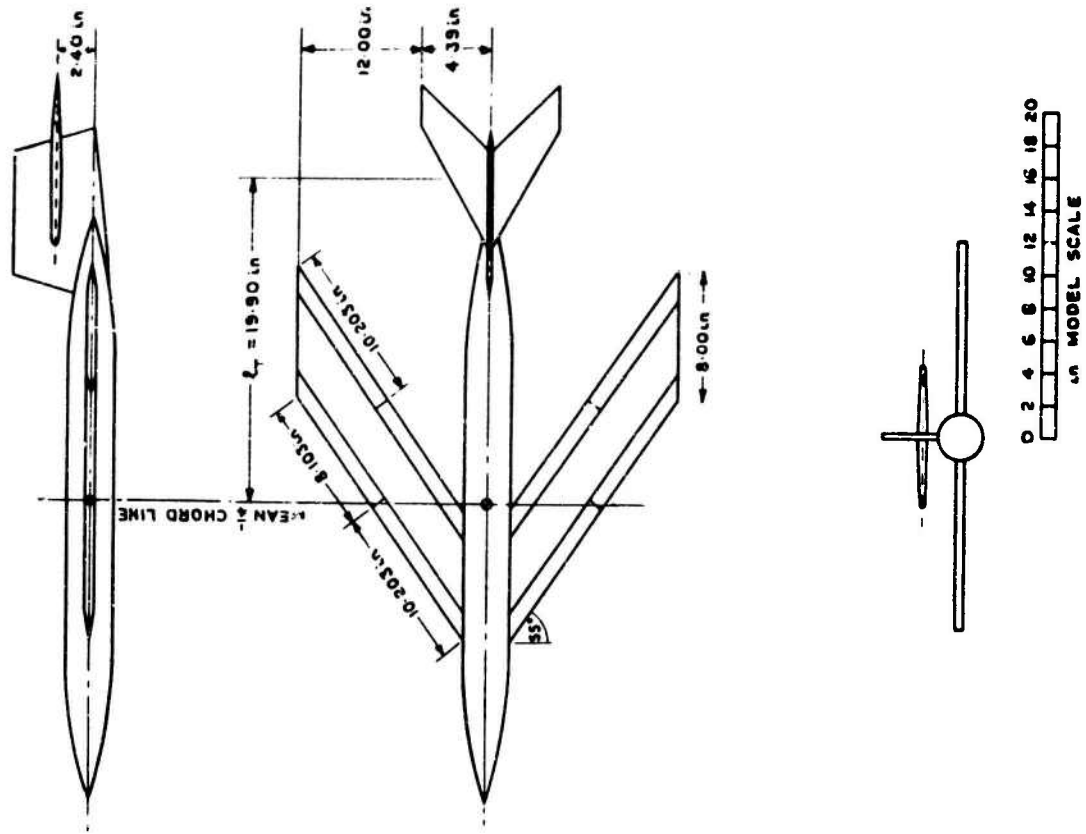


Fig. 8 G.A. of model

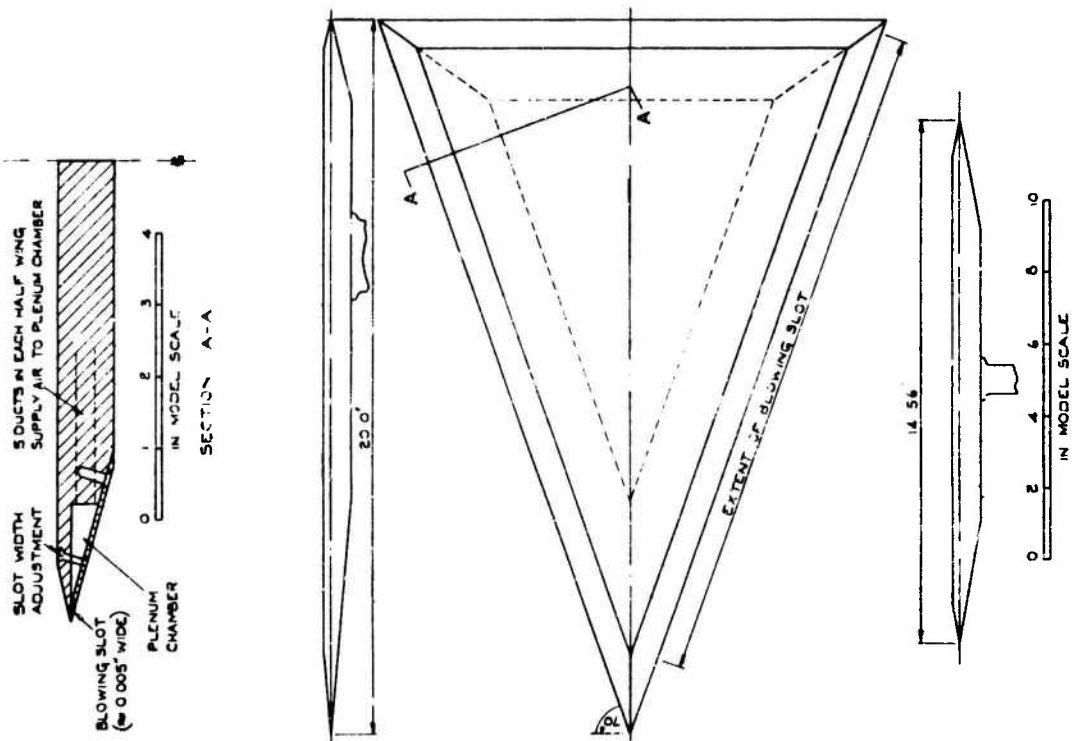
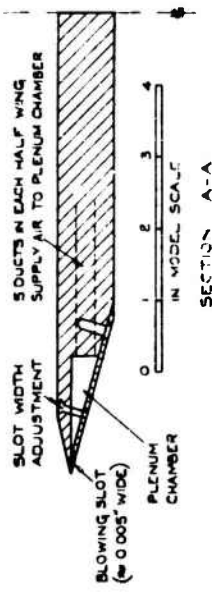


Fig. 7 G.A. of delta wing



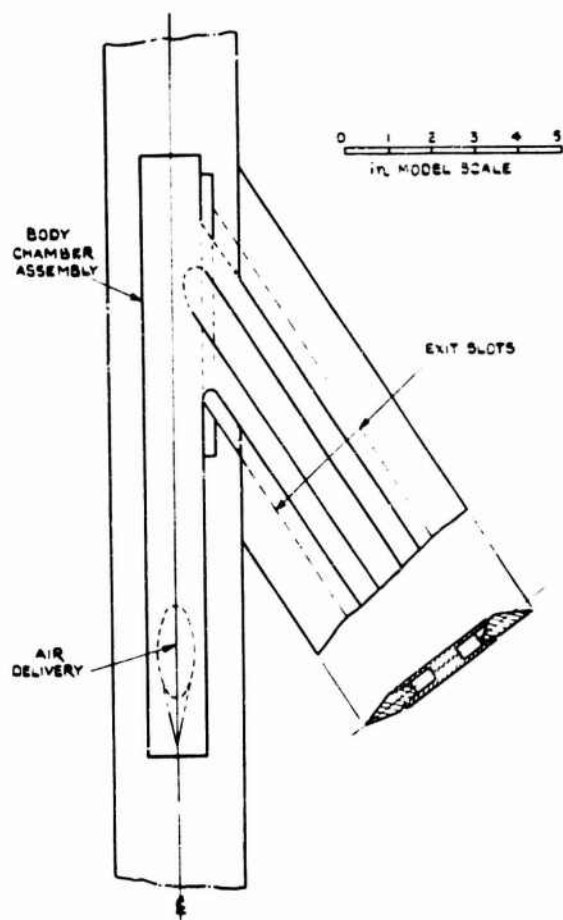


Fig. 9 Details of internal air ducting

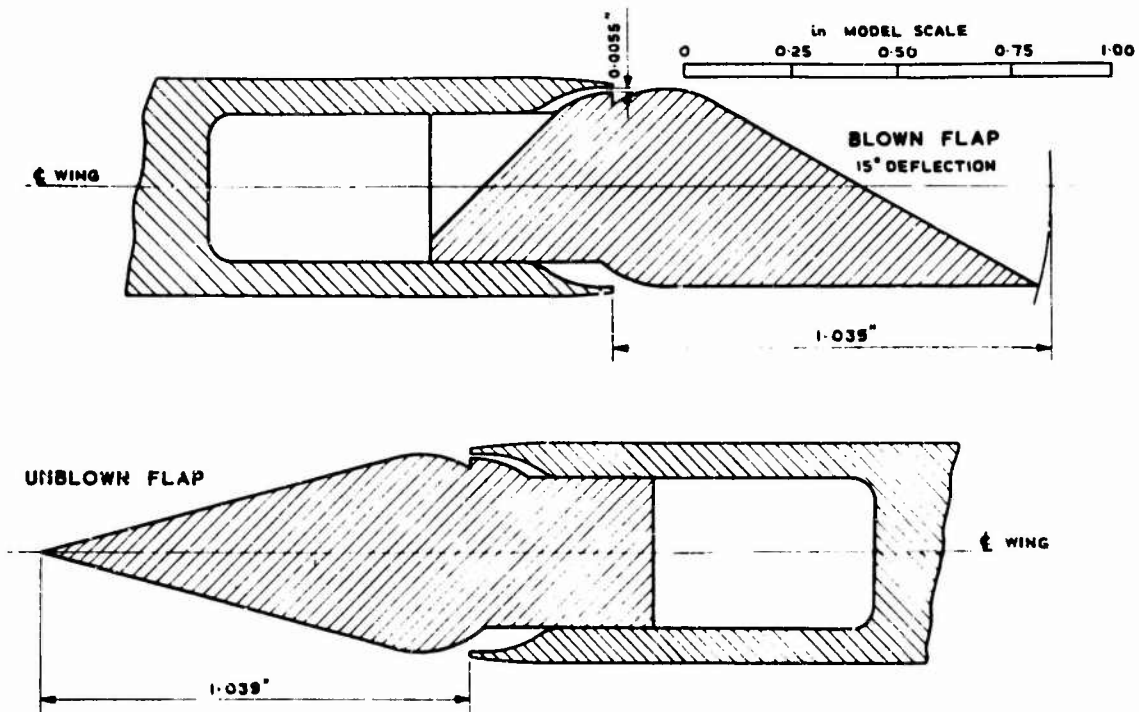
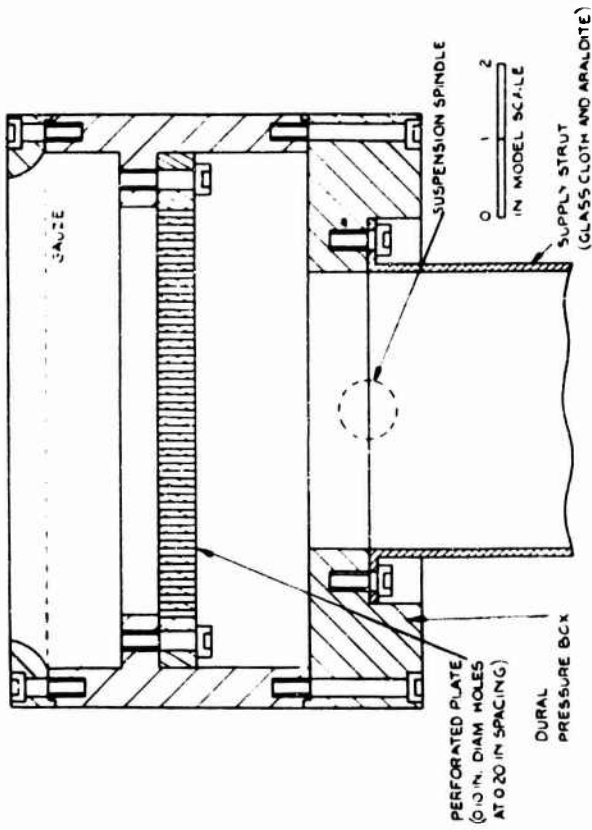


Fig. 10 Details of flaps and blowing nozzles



q) PRESSURE-BOX FOR ZERO INCIDENCE TESTS

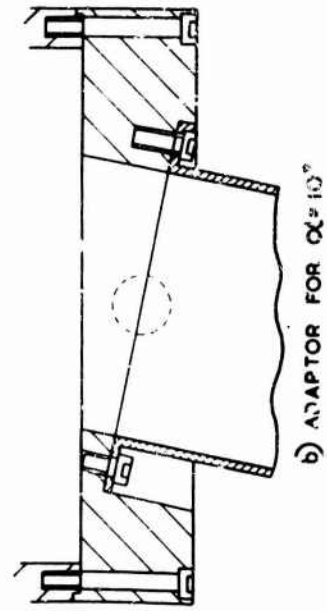


Fig. 12 Section through centre of pressure-box

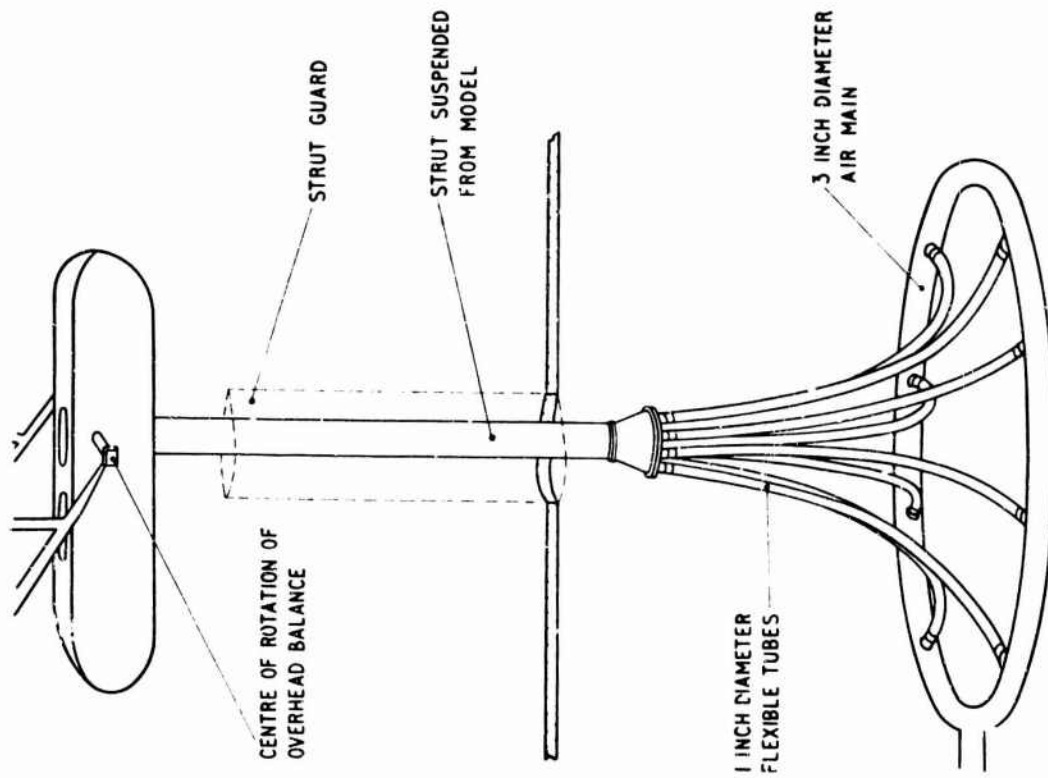


Fig. 11 RAE complete-model conventional-balance rig with simple flexible connectors



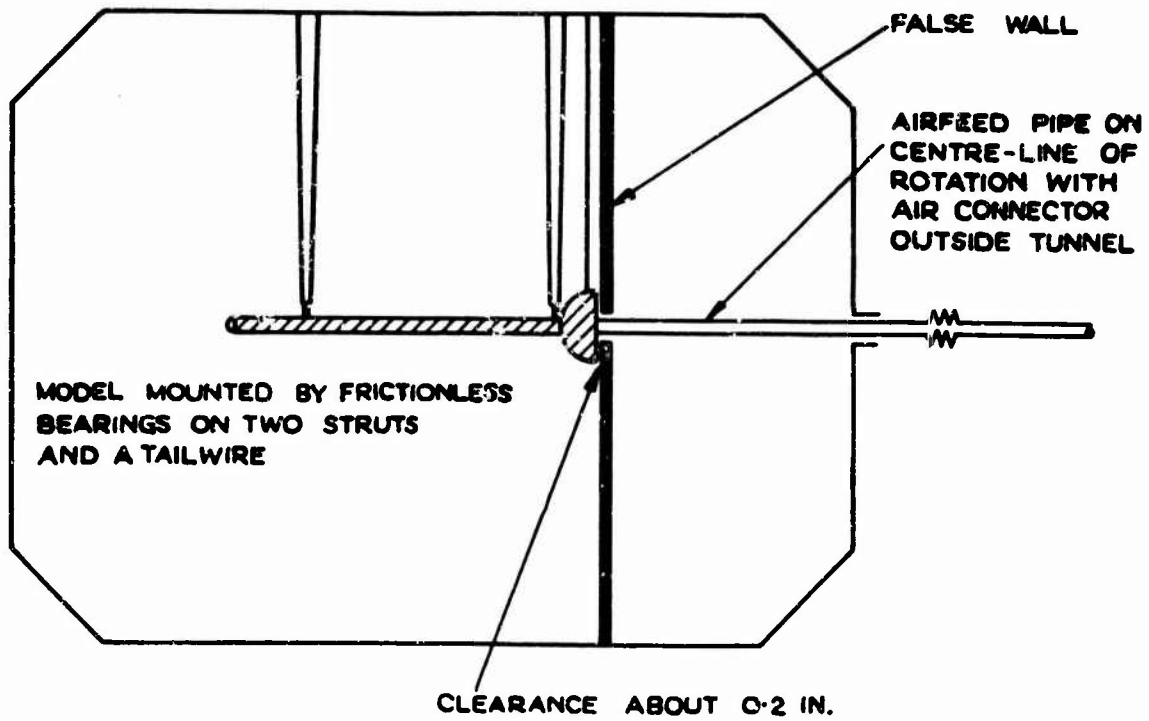


Fig. 13 Horizontal half-model rig for a conventional overhead balance (NPL)

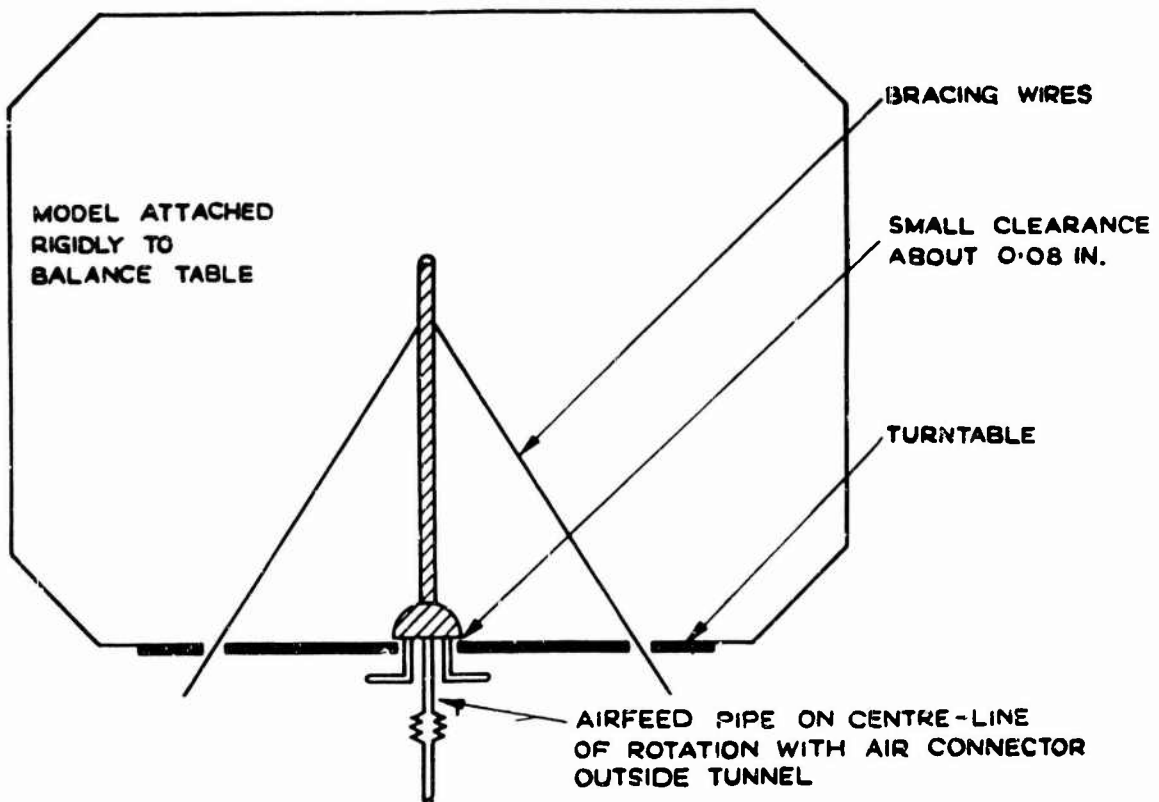


Fig. 14 Vertical half-model rig for a virtual-centre floor balance (RAE)

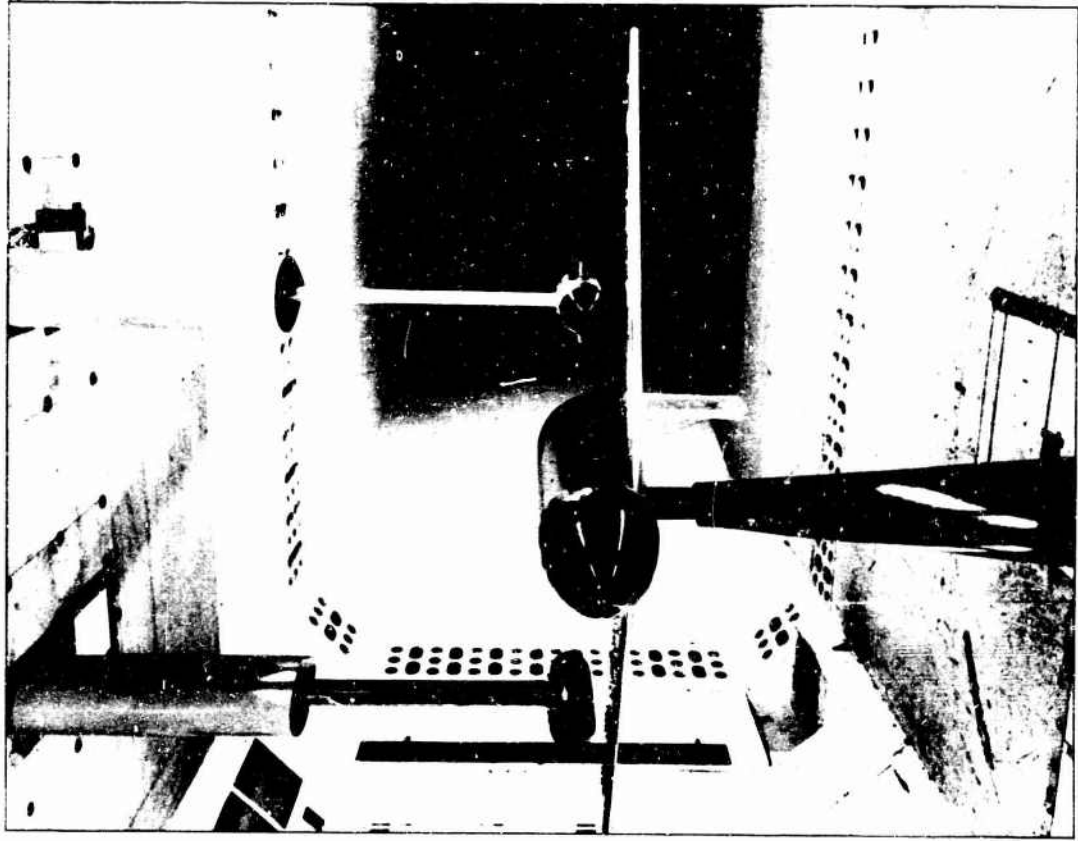


Fig. 16 Composite-model rig for jet-nacelle model

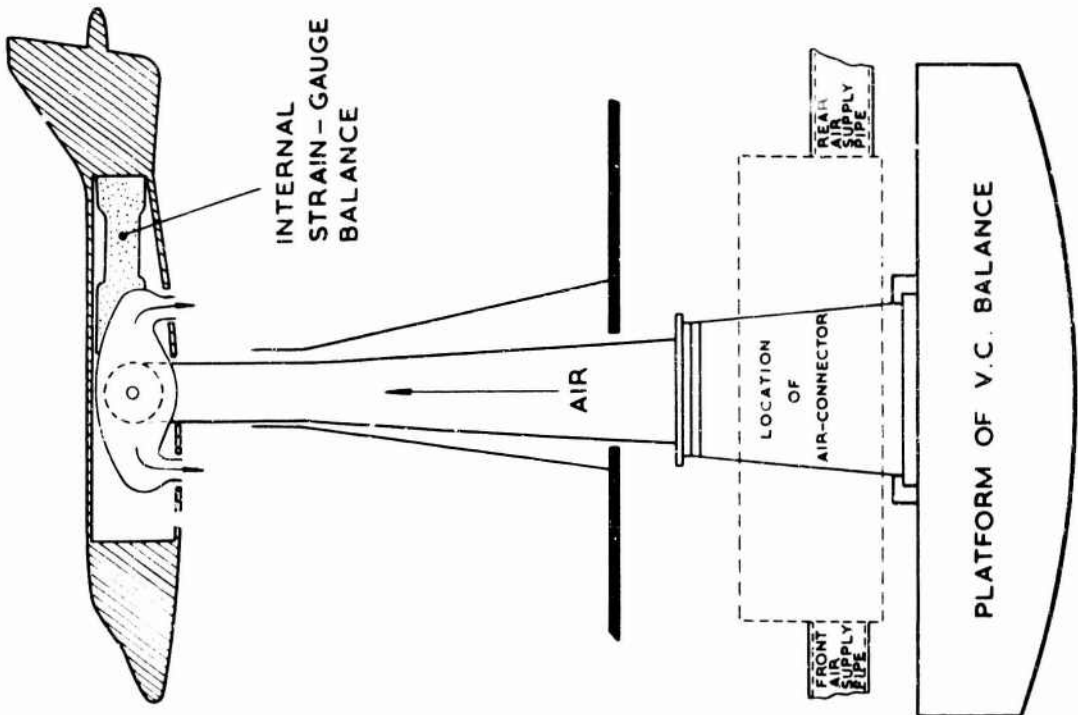


Fig. 15 Composite-model rig for RAE virtual-centre balance

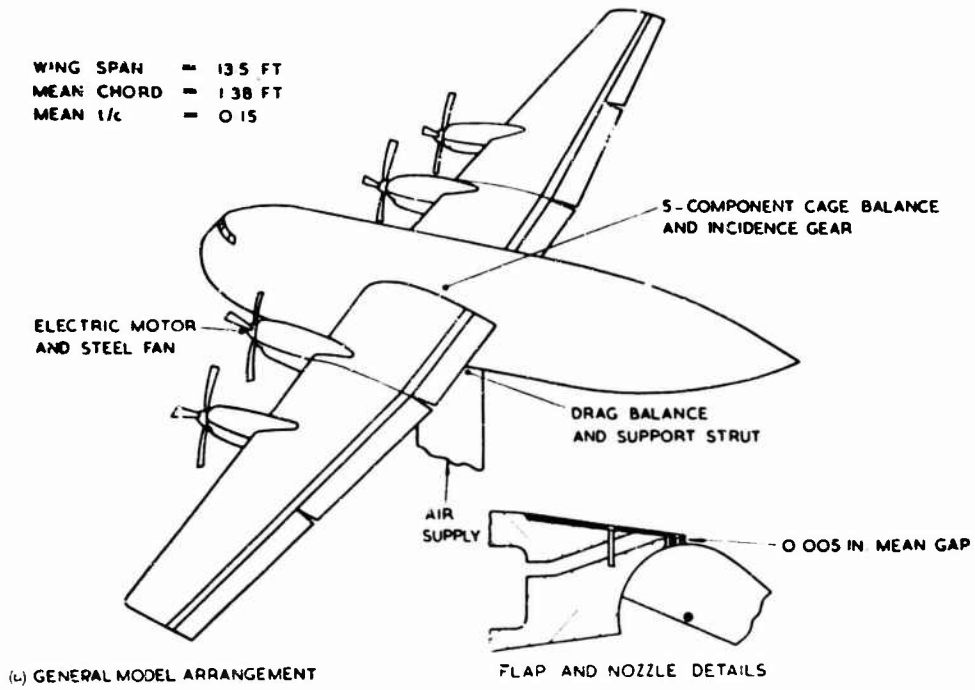
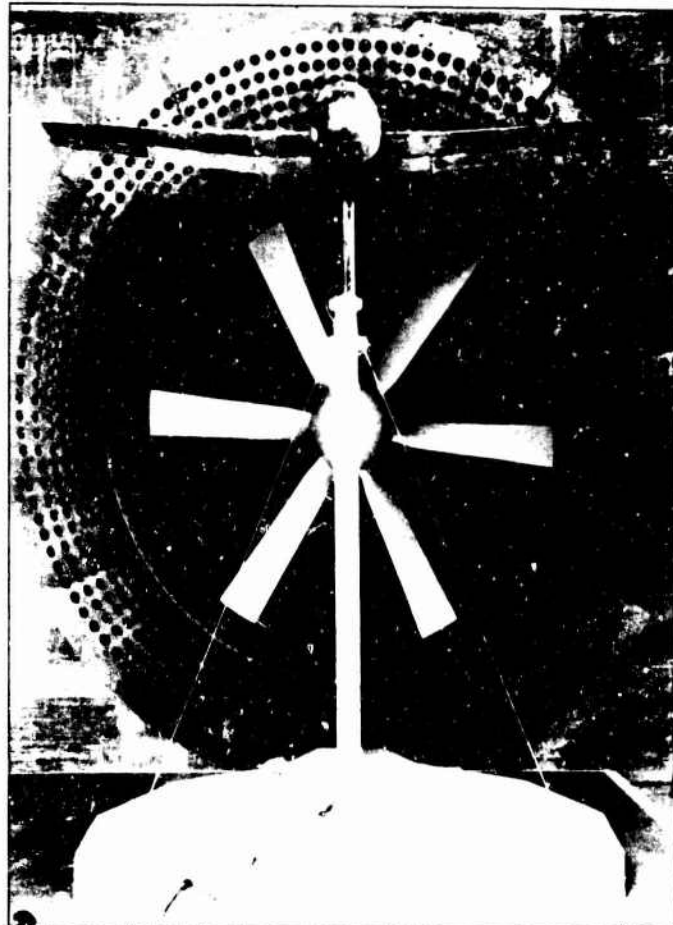


Fig. 17 Aspect-ratio 10 model with trailing-edge flap blowing and propeller slipstream



(b) 2-FT TUNNEL RIG

Fig. 18 Aspect-ratio 10 model with trailing-edge flap blowing and propeller slipstream

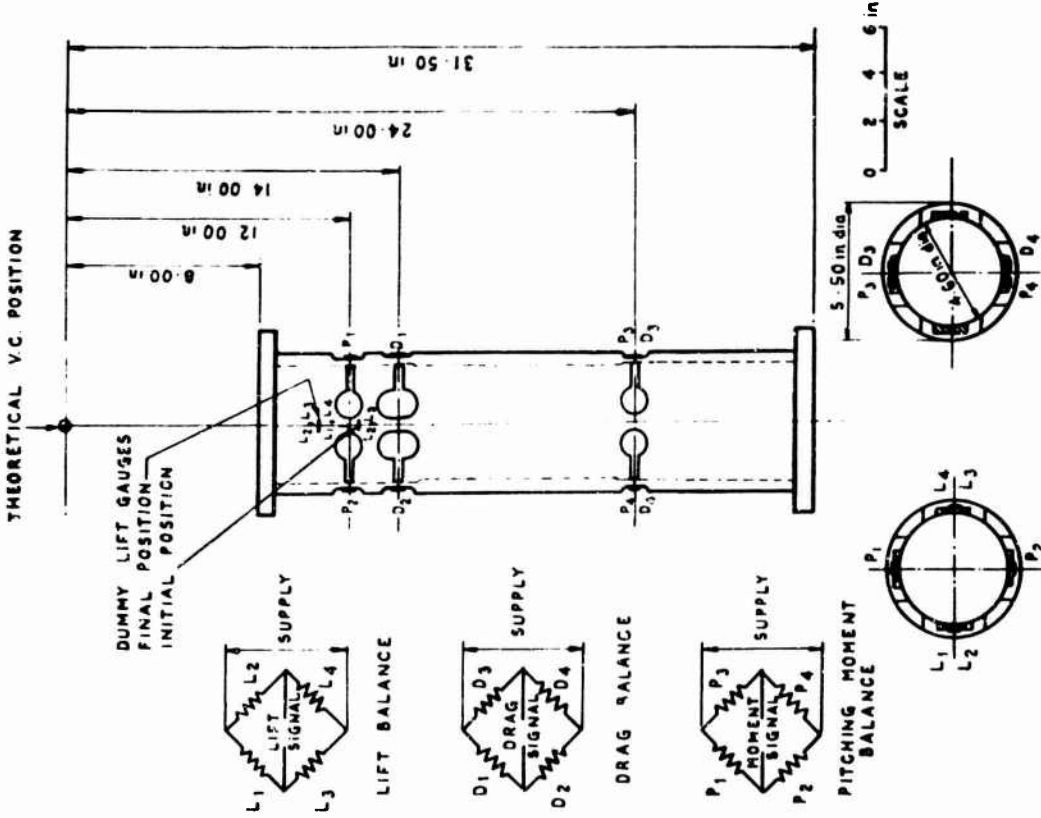


Fig. 20 Strain-gauge balance

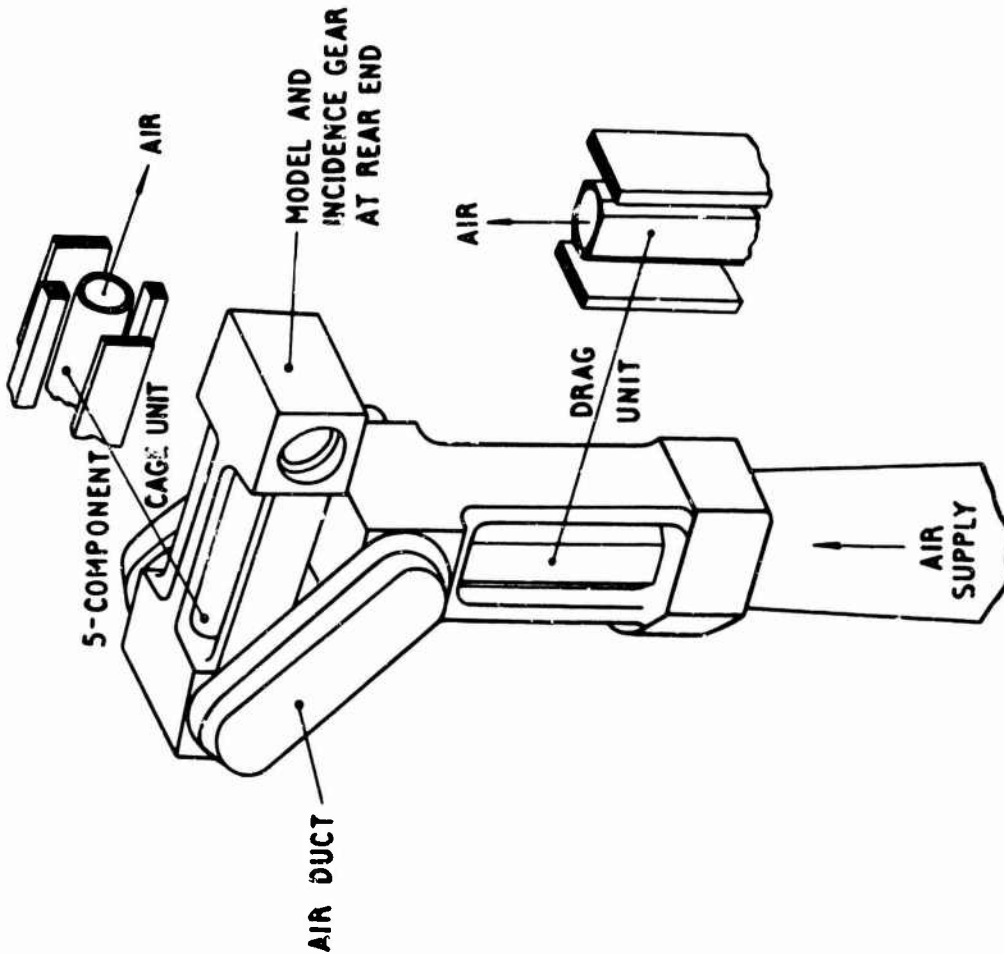


Fig. 19 Six-component strain-gauge balance for aspect-ratio 10 model with trailing-edge flap blowing

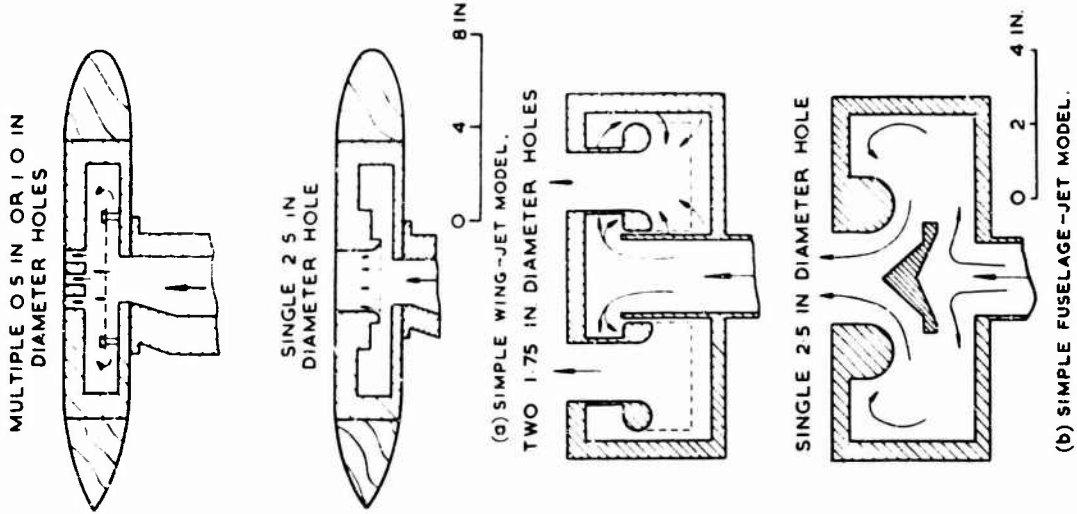


Fig. 22 Pressure chamber and nozzle details for elementary jet-lift models

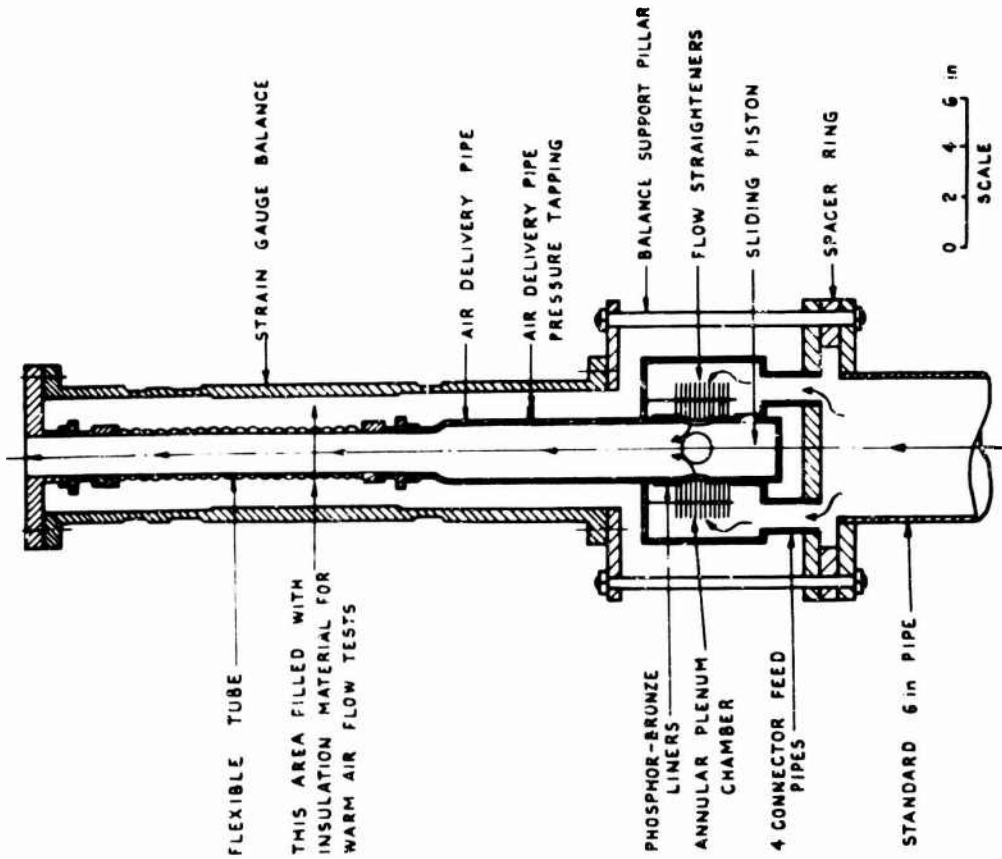
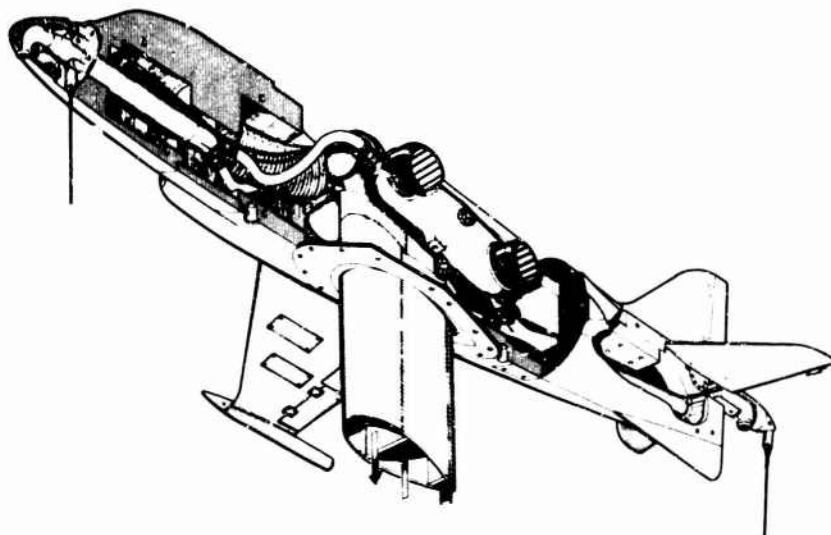
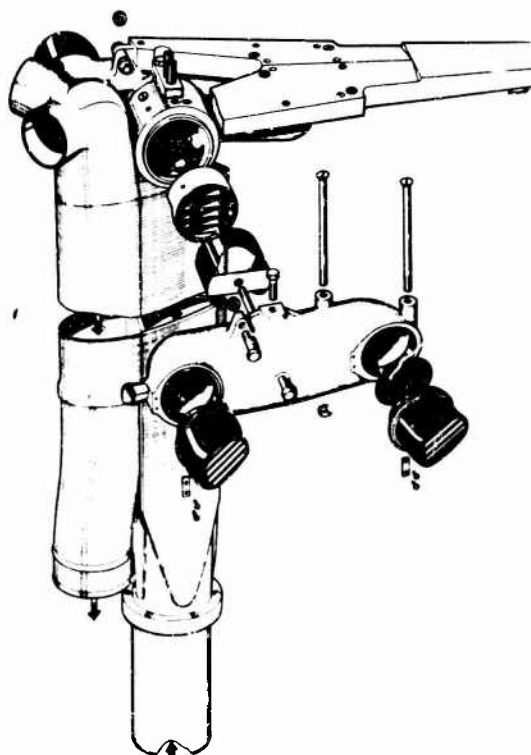


Fig. 21 Details of air connector

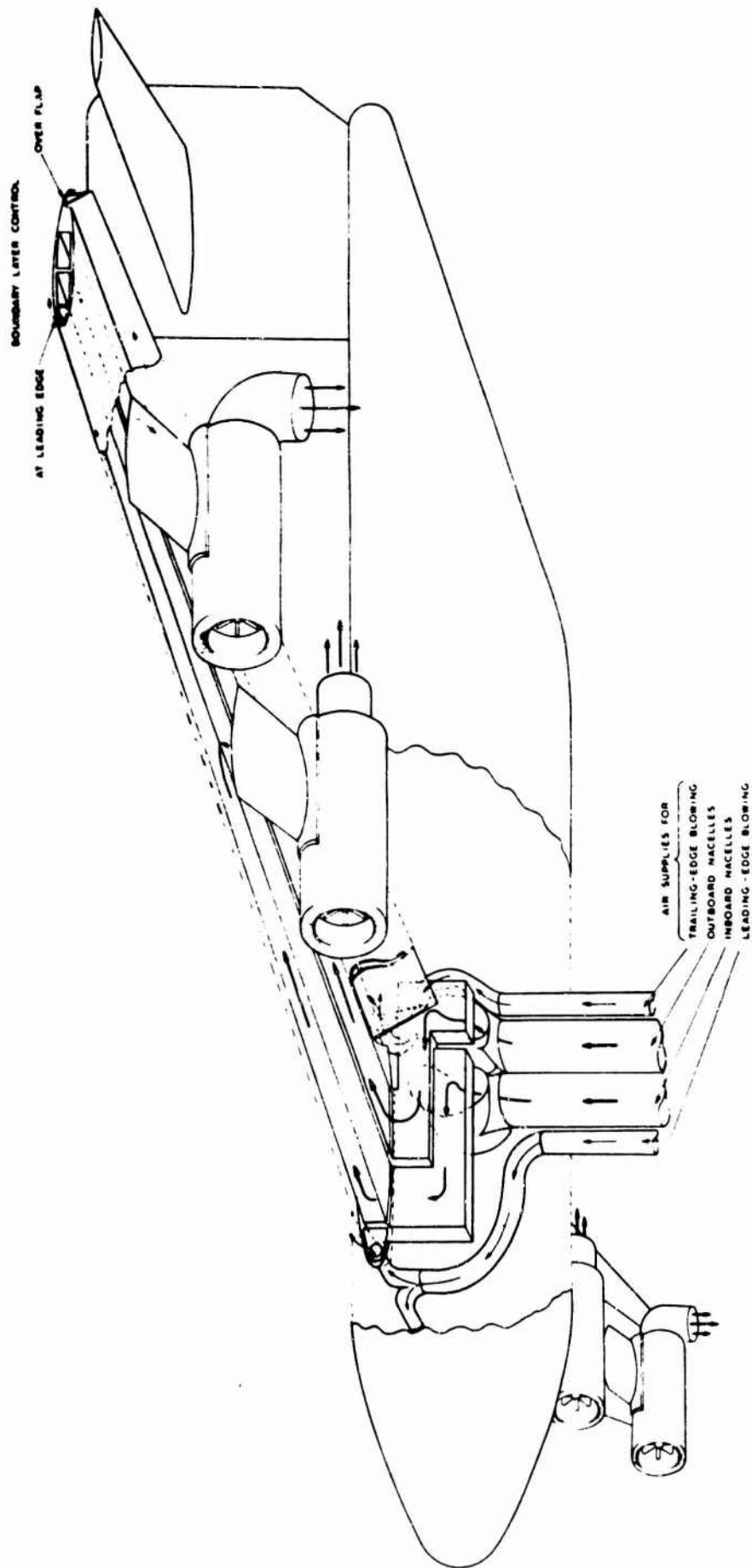


(a) GENERAL MODEL ARRANGEMENT



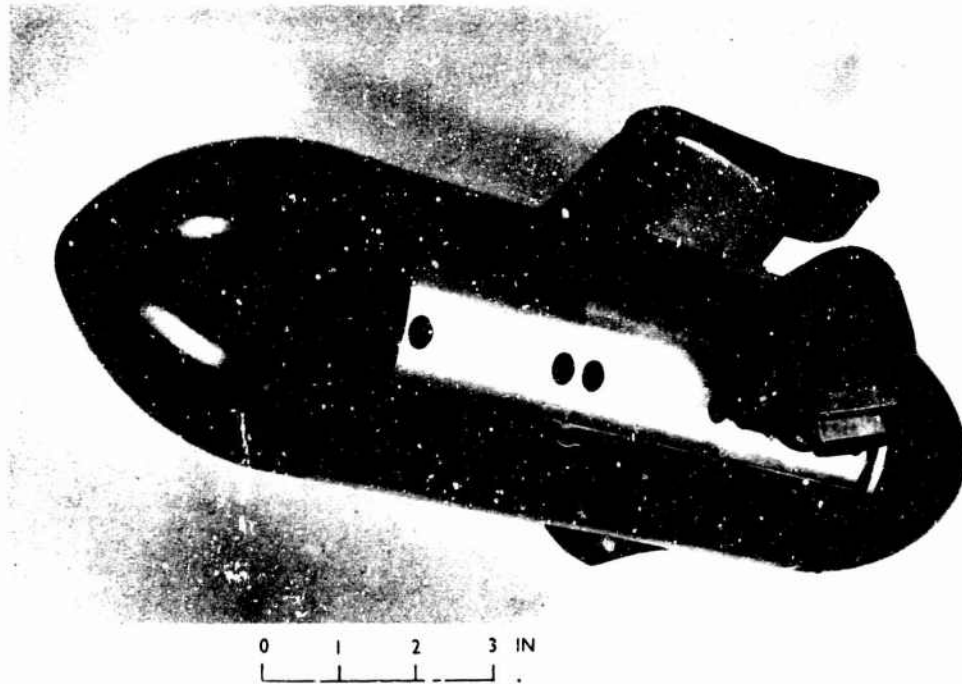
(b) DUCTING AND NOZZLE DETAILS

Fig. 23 Hawker P.1127, 1/10th scale model

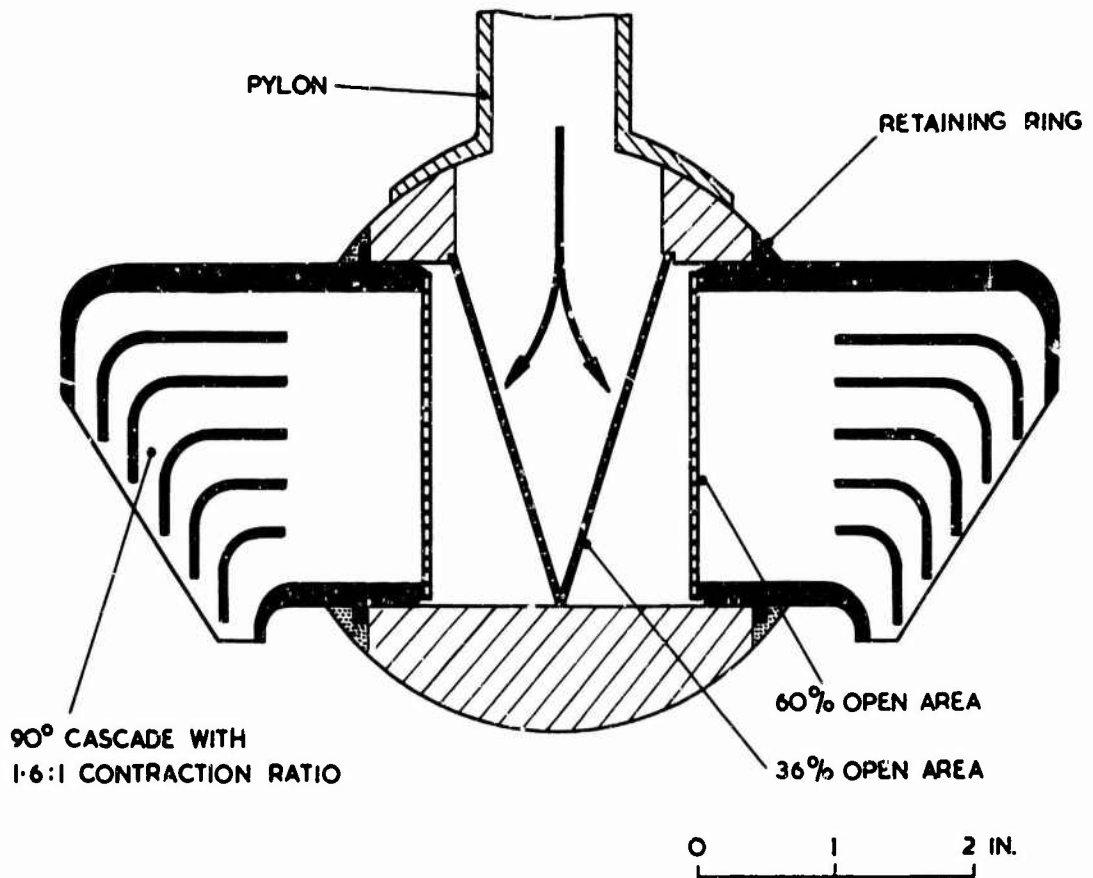


(c) GENERAL MODEL ARRANGEMENT

Fig. 24 RAE subsonic-transport jet-nacelle research model



(a) GENERAL VIEW



(b) PRESSURE CHAMBER AND NOZZLE DETAILS

Fig. 25 Typical ejector nacelle for jet-efflux simulation



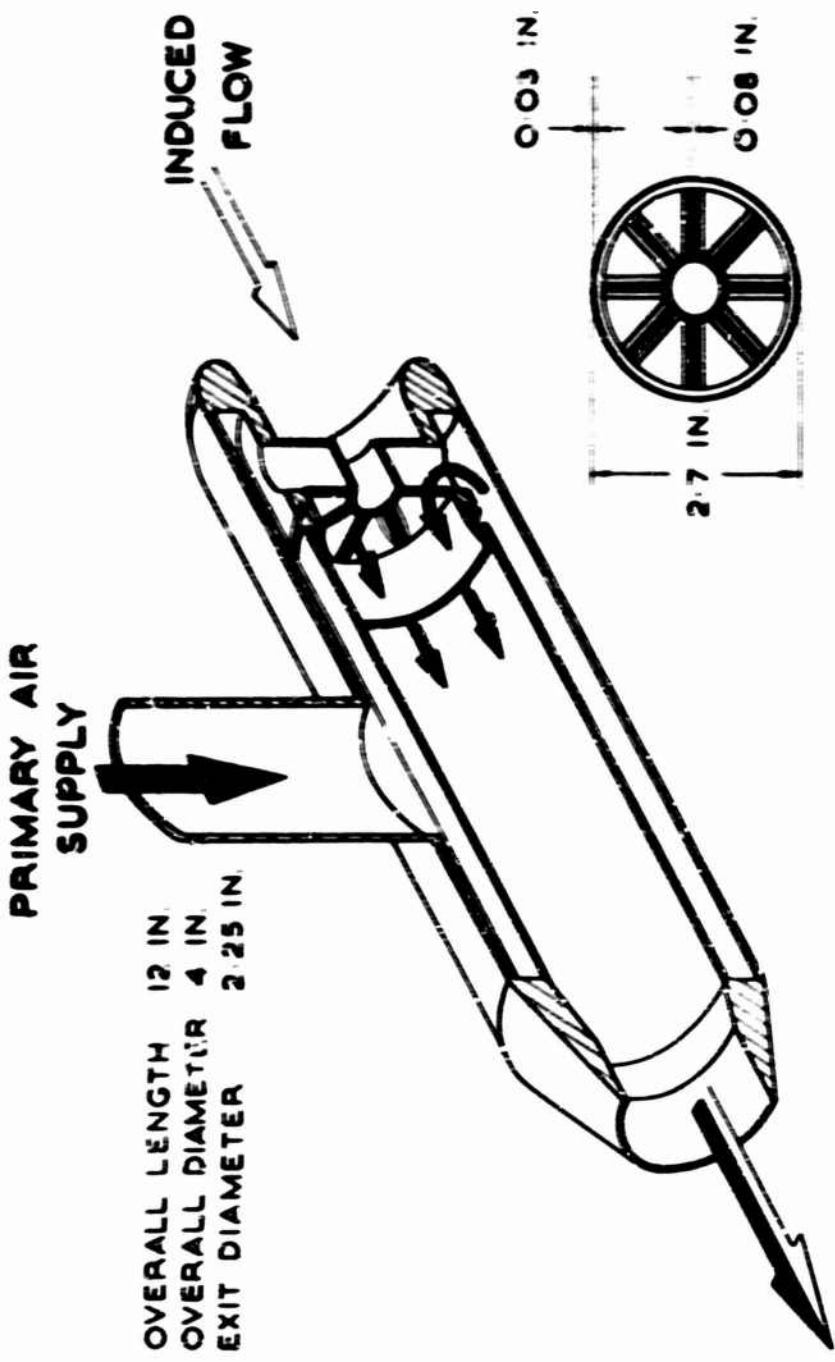


Fig. 26 Typical injector nozzle for jet efflux and intake-flow stimulation

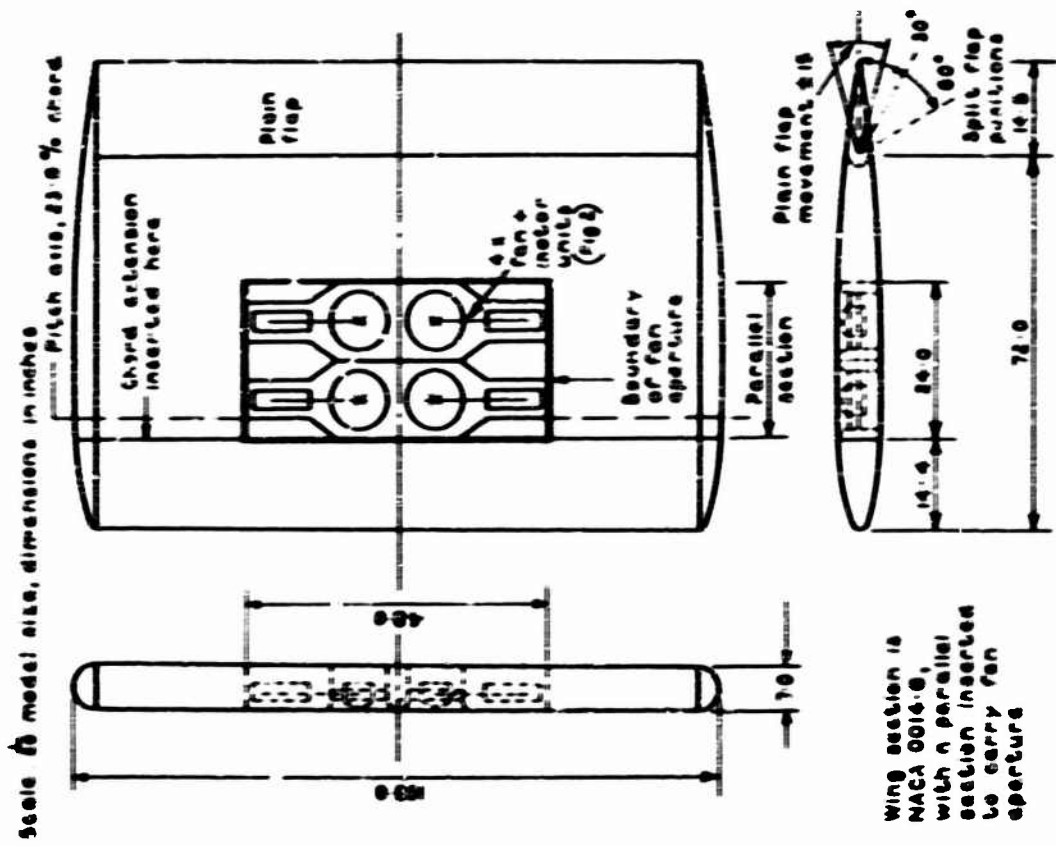


Fig. 26 G.A. of model for low-speed wind-tunnel tests on wing fitted with multiple lifting fans

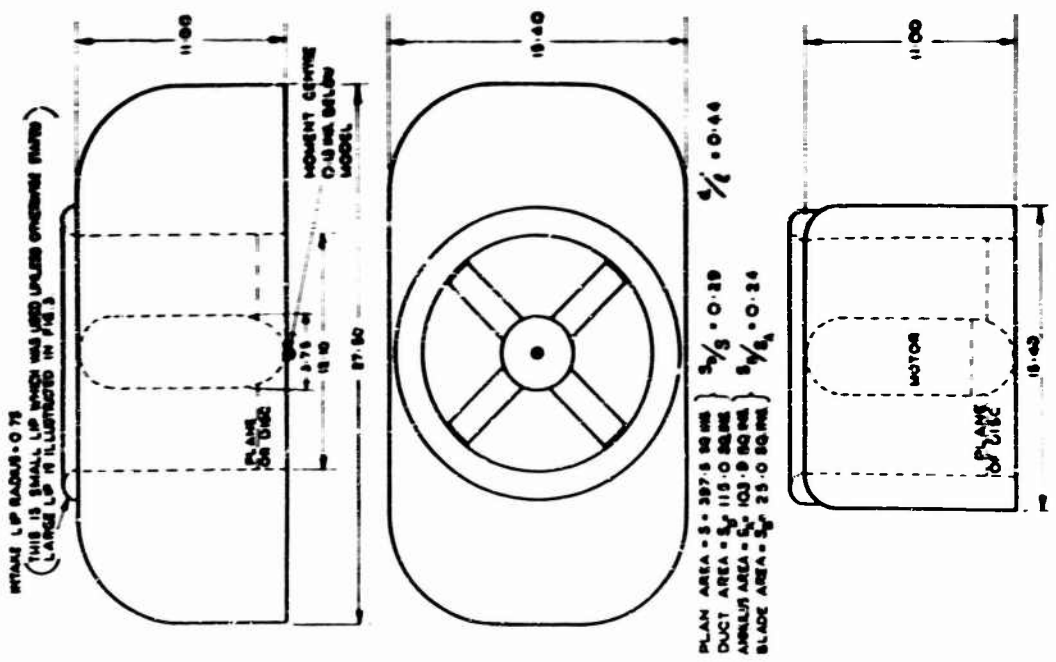
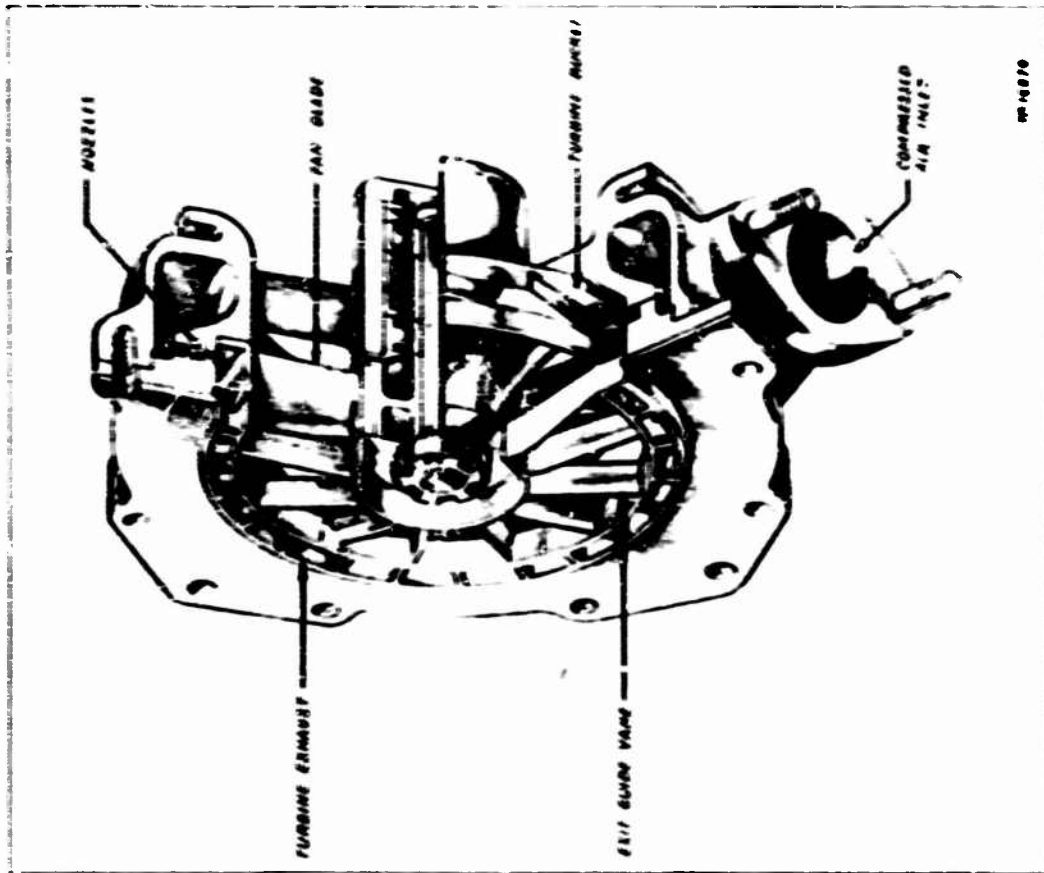


Fig. 27 G.A. of basic model configuration. [Scale =  $\frac{1}{2}$ ; all dimensions are given in inches]



10-10070

(b) 2 1/2" DIAMETER MODEL FAN

Fig. 30 Duty-rotol air driven fans



(a) 4" DIAMETER MODEL FAN

Fig. 29 Duty-rotol air driven fans

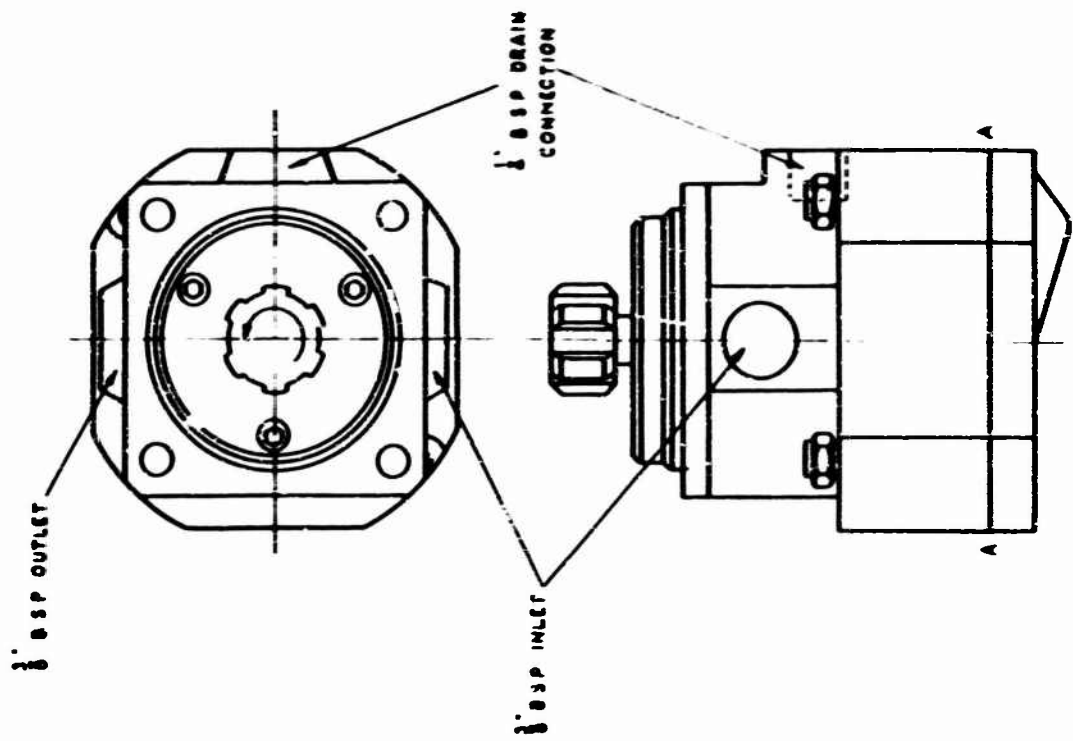


Fig. 31 Hydraulic pump/motor unit (full scale)

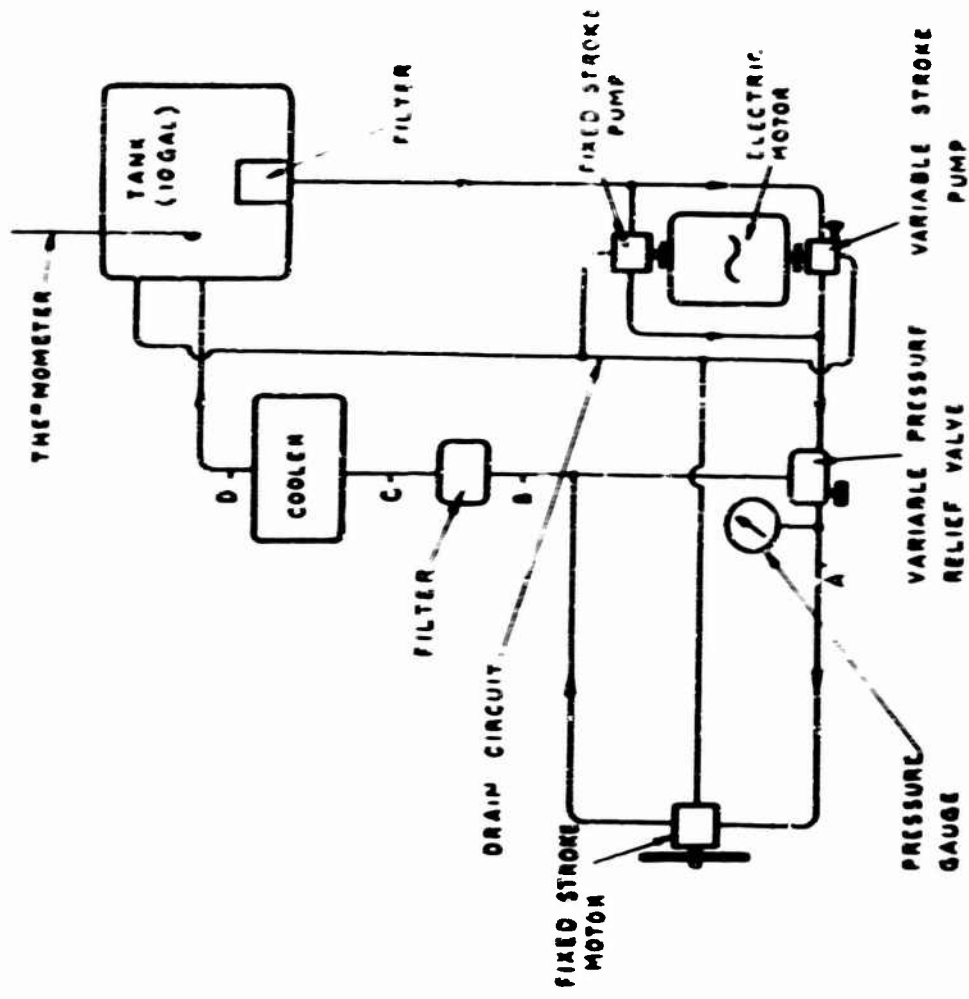


Fig. 32 Pump - motor circuit

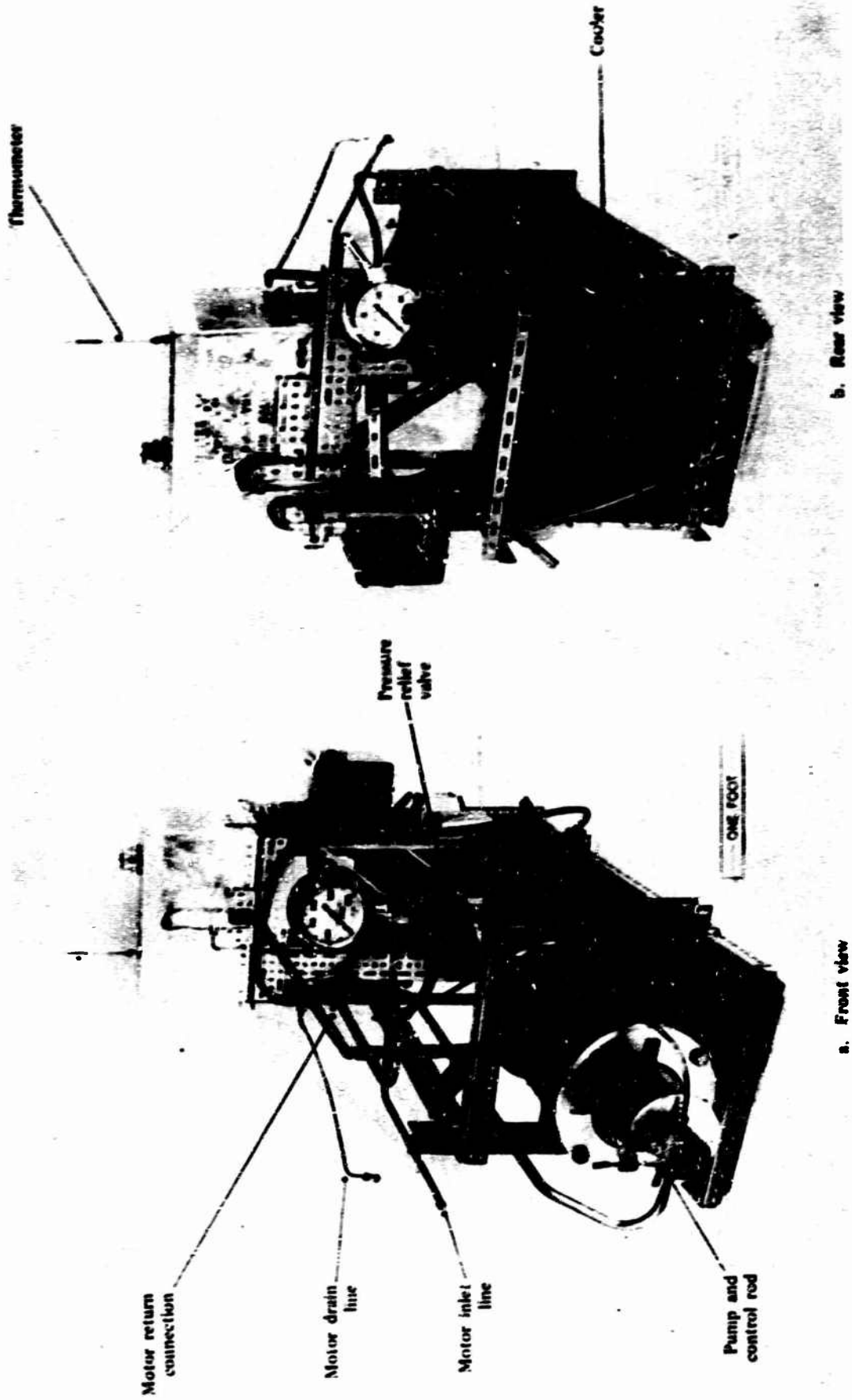


Fig. 33 Arrangement of pumping and control unit

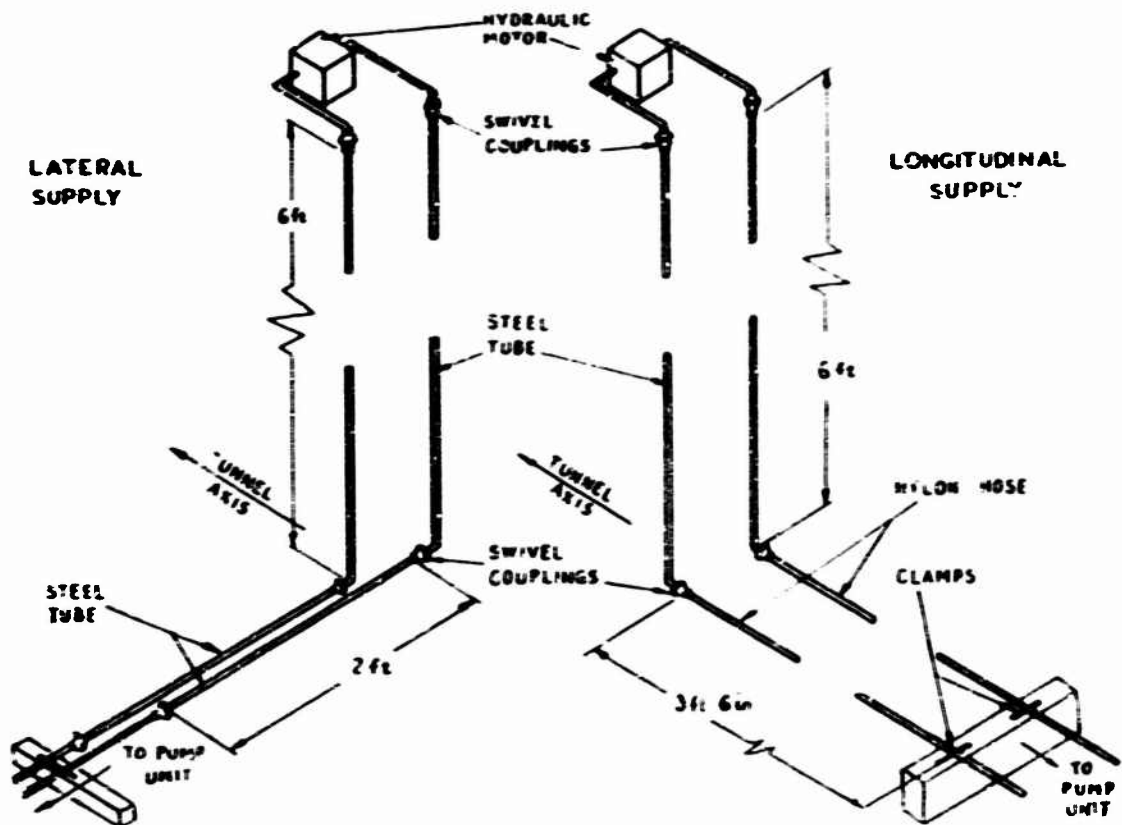


Fig. 34 Hydraulic connections used in balance interference tests

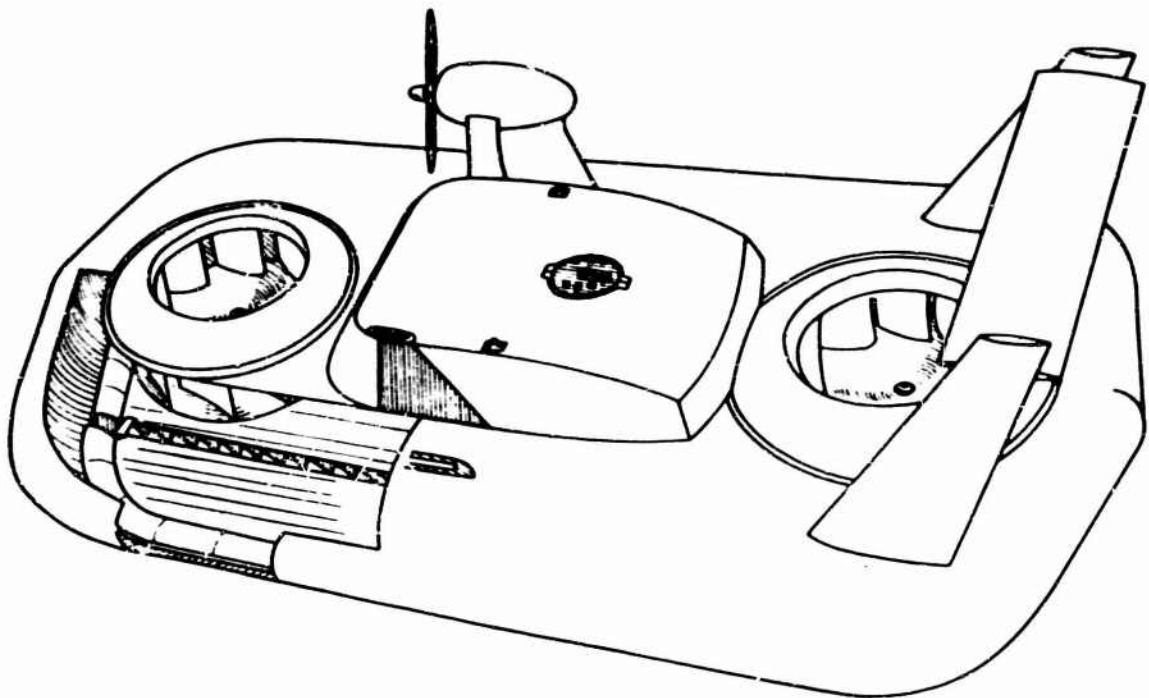


Fig. 35 Schematic view of model. Note:- port nacelle and propeller not shown

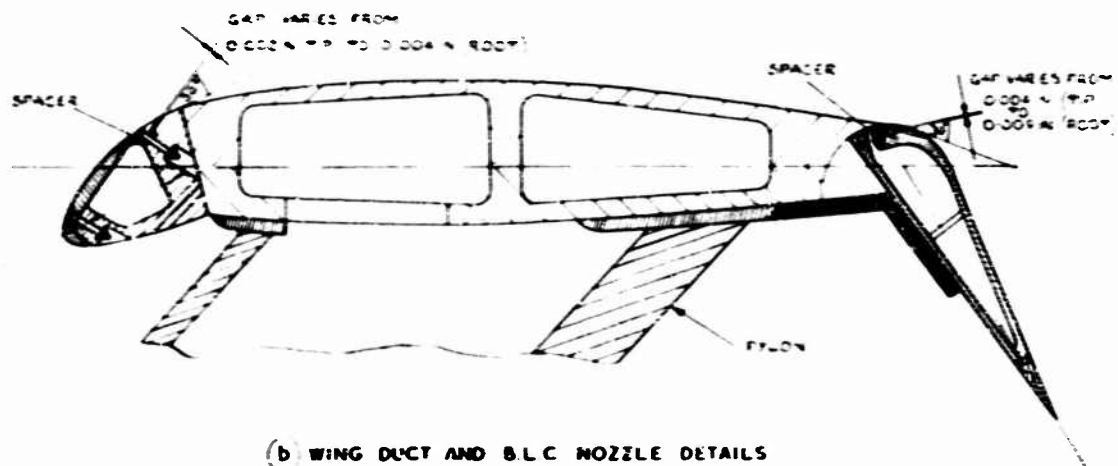


Fig. 36 RAE subsonic-transport jet-nacelle research model

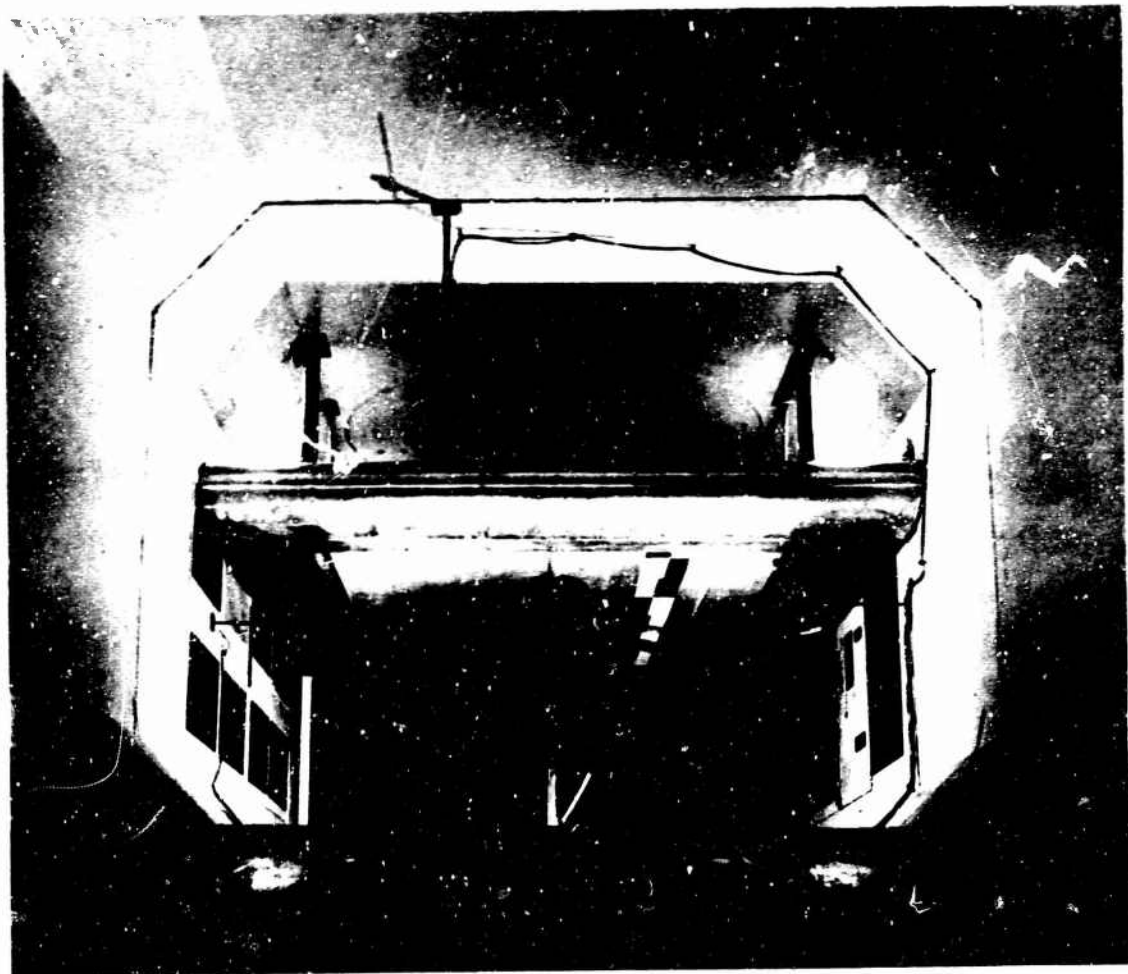


Fig. 37 Moving-belt ground rig RAE 11½ ft x 8½ ft tunnel

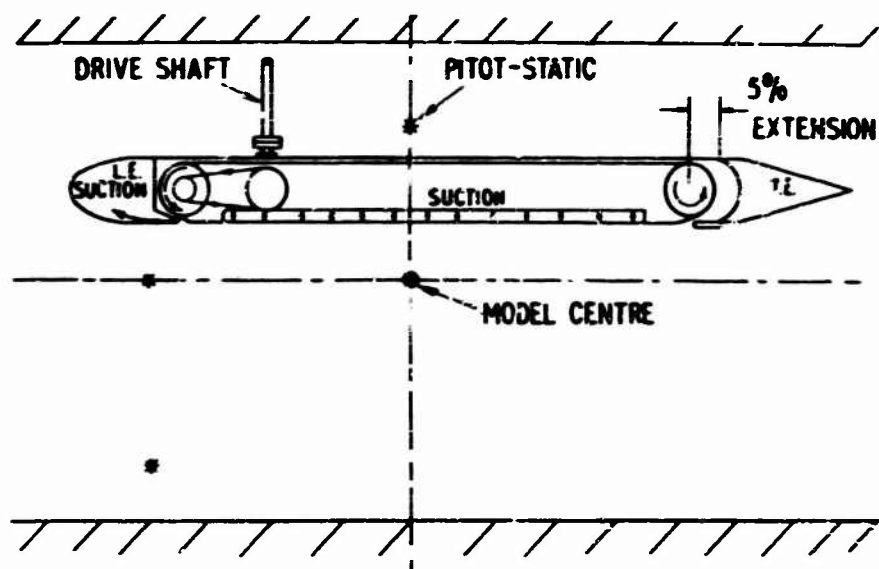


Fig. 38 Section of moving-belt ground rig

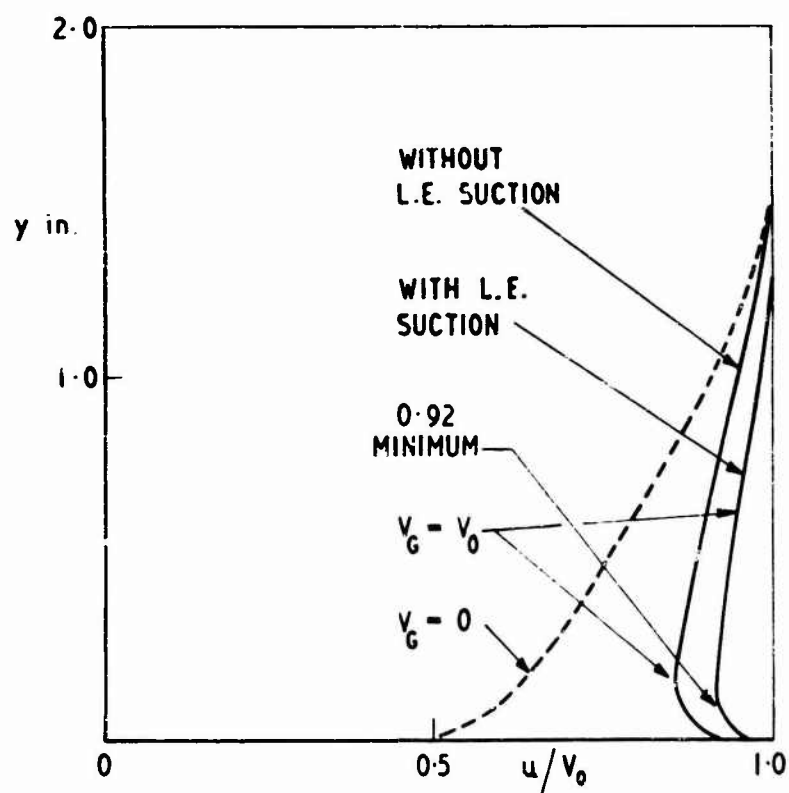


Fig. 39 Ground boundary-layer profiles on moving-belt



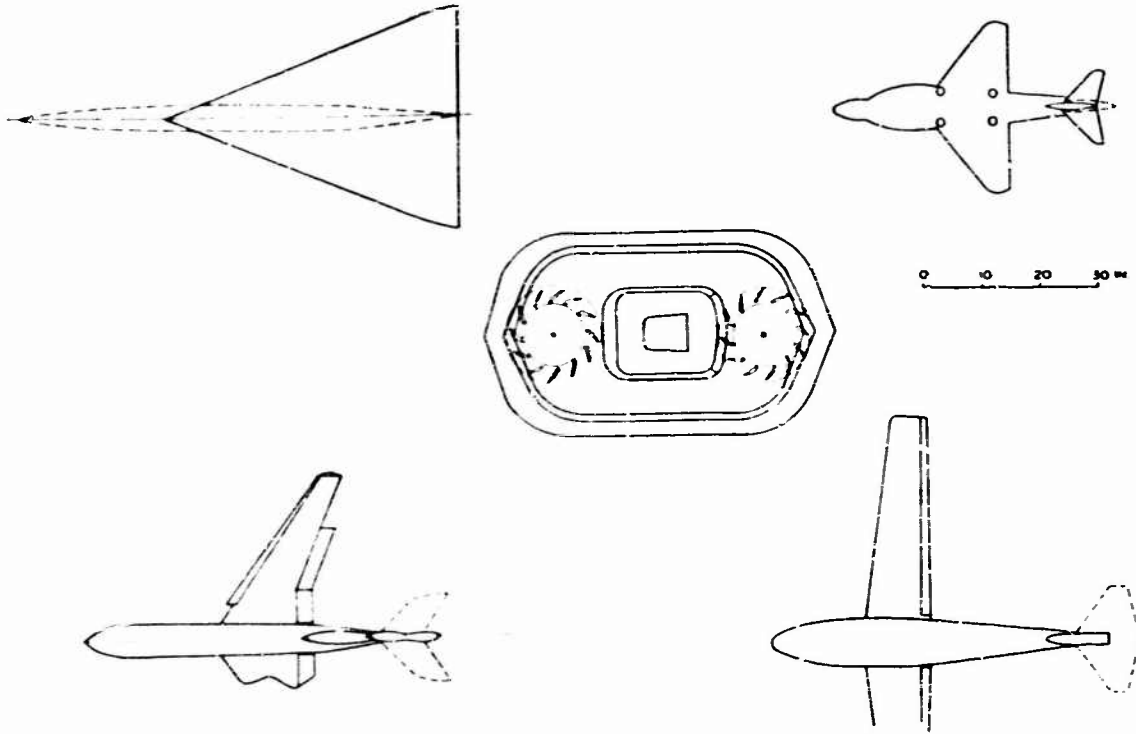


Fig. 40 Model configurations tested with moving-belt ground rig

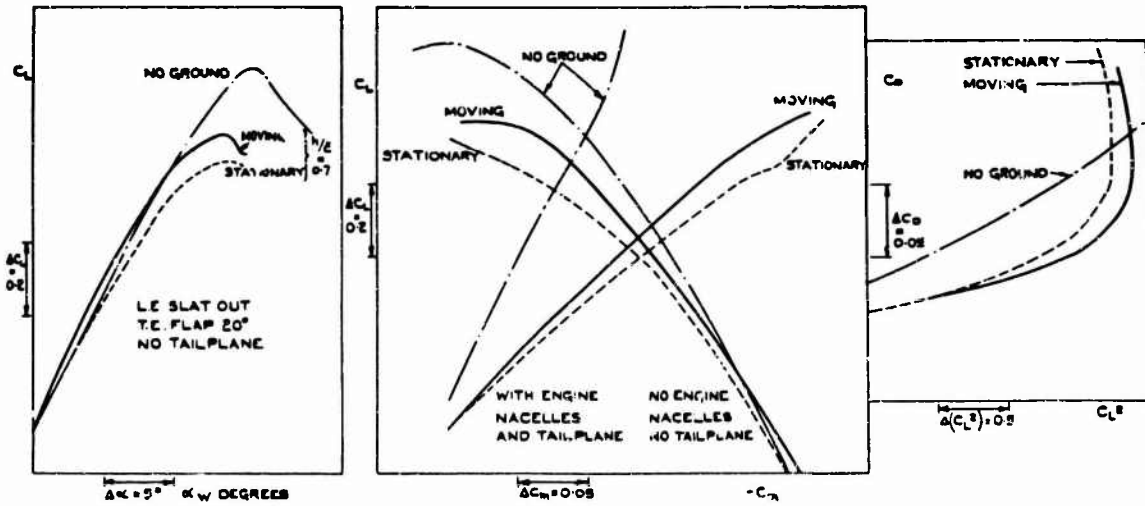


Fig. 41 Ground effect comparisons for subsonic jet-transport configuration

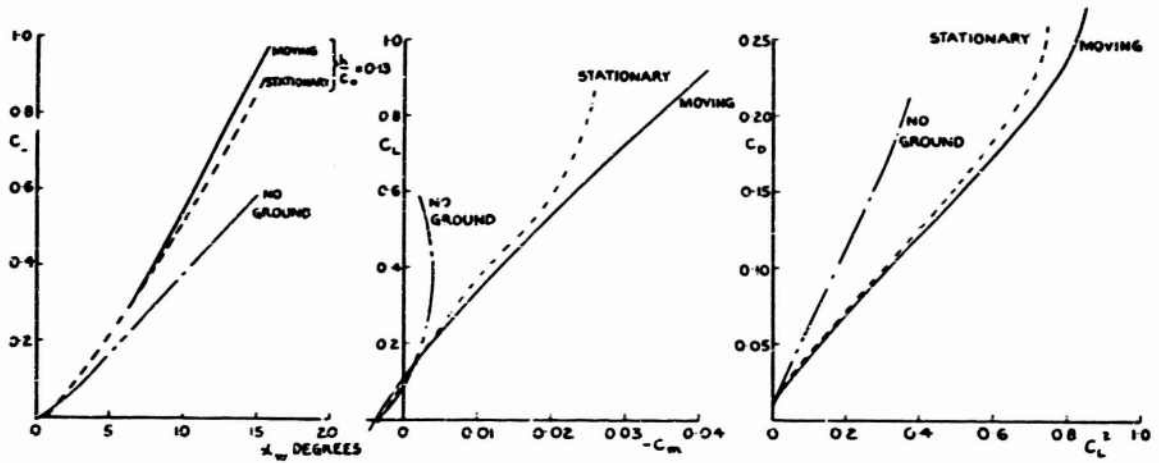


Fig. 42 Ground effect comparisons for slender wing

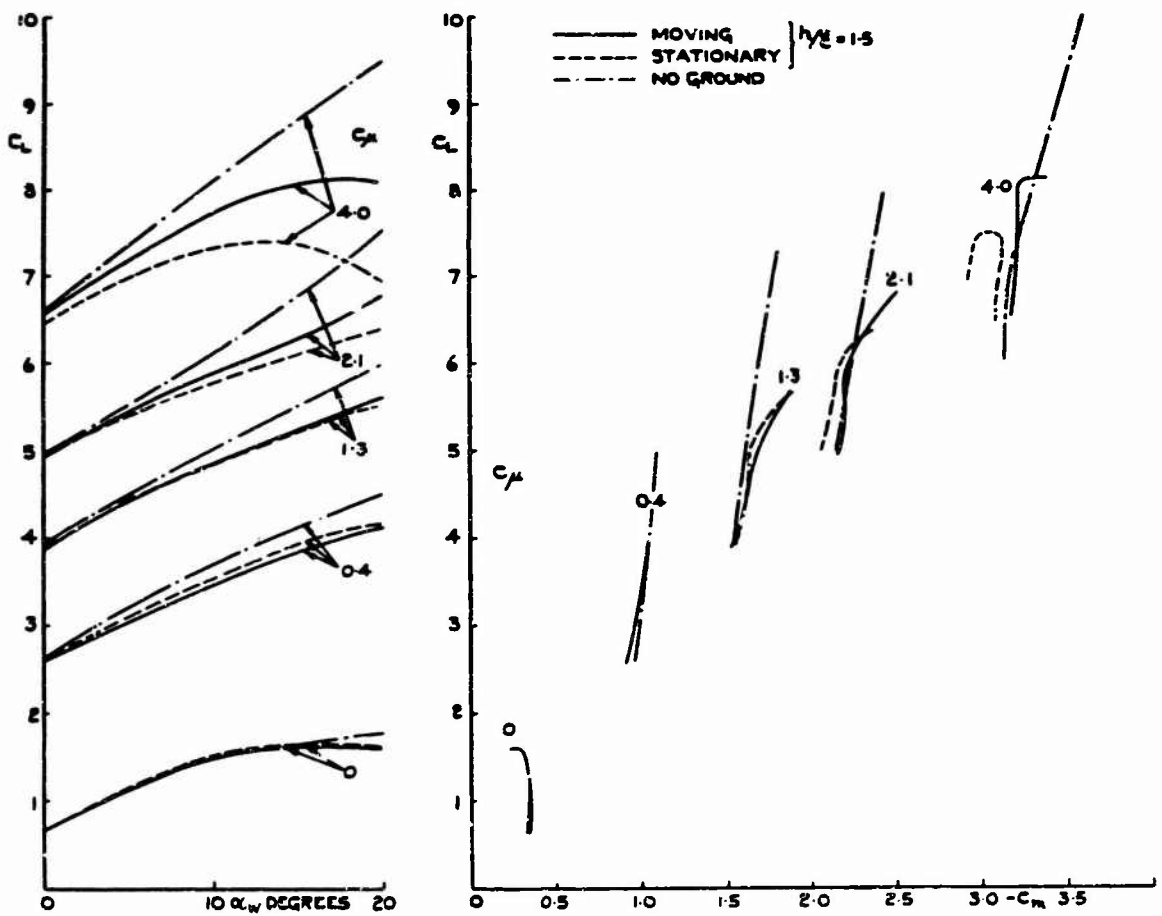


Fig. 43 Ground effect comparisons for jet-flap wing

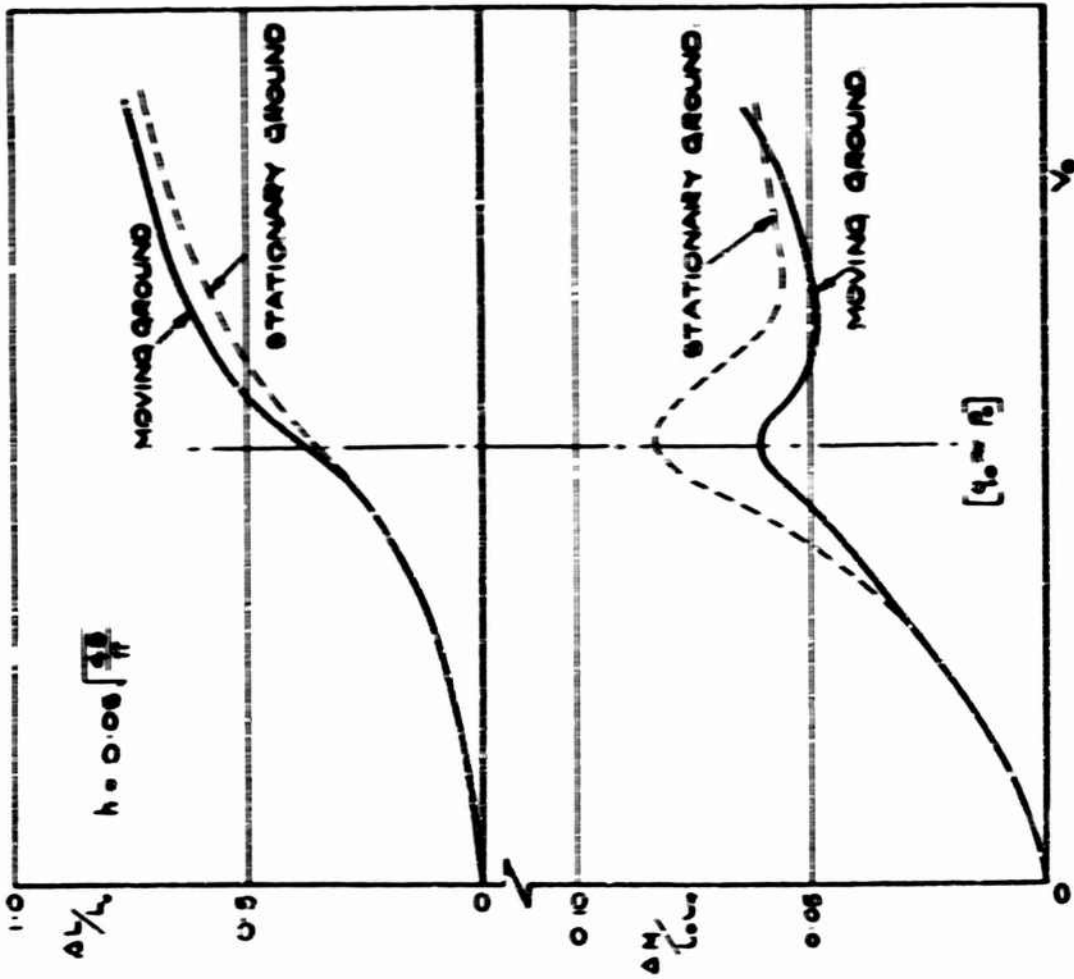


Fig. 44 Ground effect comparisons for air-cushion vehicle

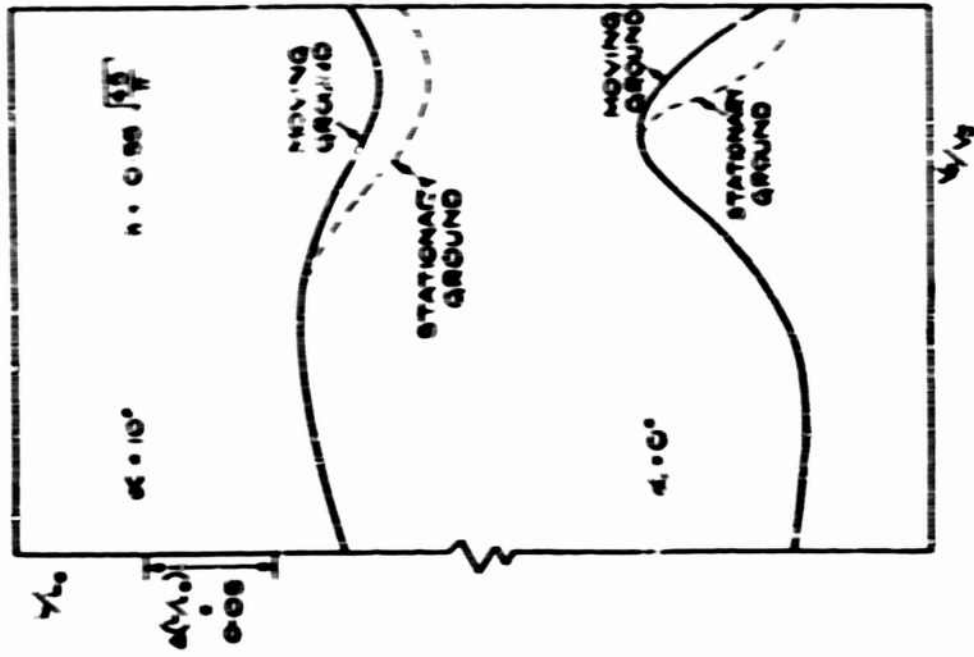


Fig. 45 Ground effect comparisons for jet-lift mode

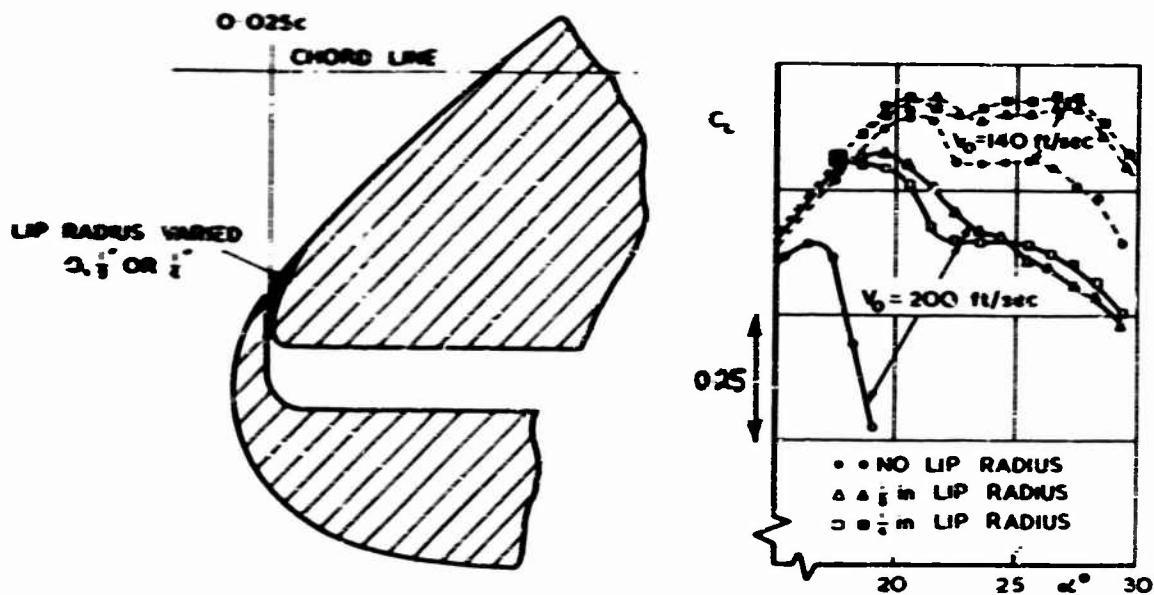


Fig. 46 Effect of slot geometry and test speed on  $C_L$ .  $G_{\mu_N} = 0.334$ ,  $C_{\mu_R} = 0.065$

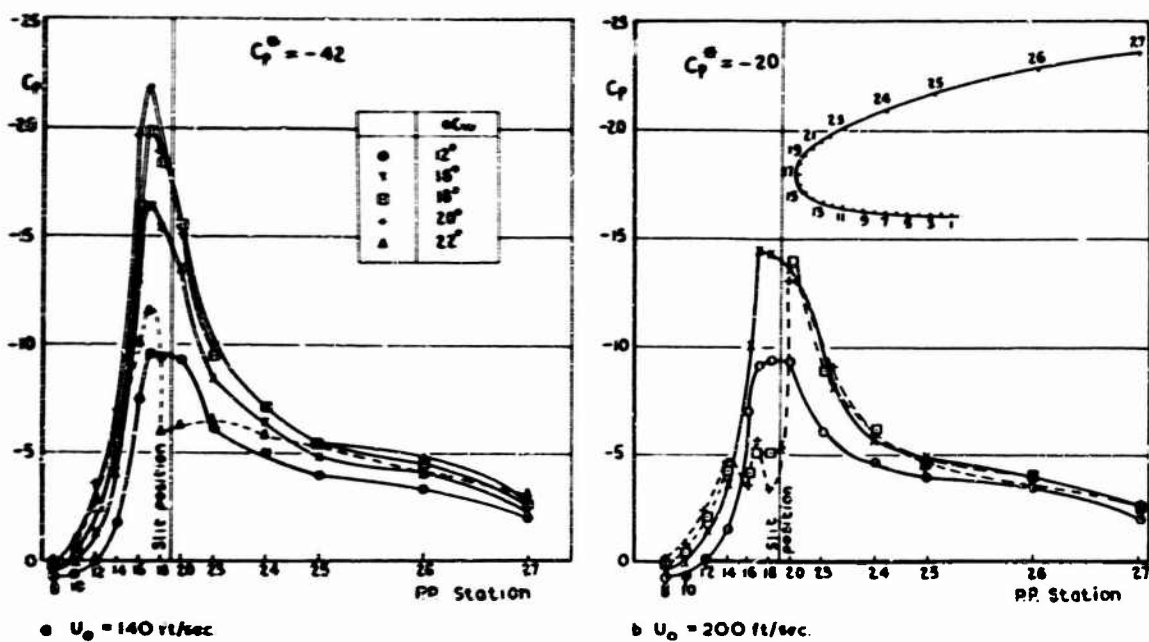


Fig. 47 The effect of mainstream speed on pressure distributions at 75% semispan, with L.E. blowing. Original L.E. arrangement, configuration  $D_1$ .  $\beta = 30^\circ$ ,  $\xi = 20^\circ$ ,  $C_{\mu_N} = 0.024$ ,  $C_{\mu_R} = 0.04$

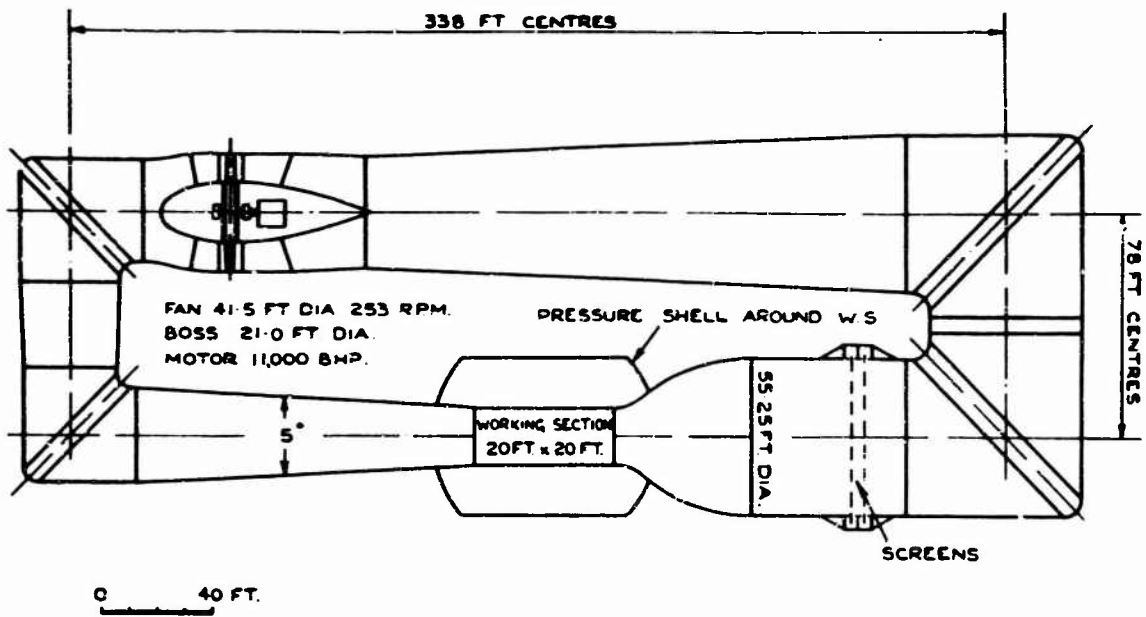


Fig. 48 Possible 20 ft x 20 ft high-lift/V/STOL pressurised wind-tunnel

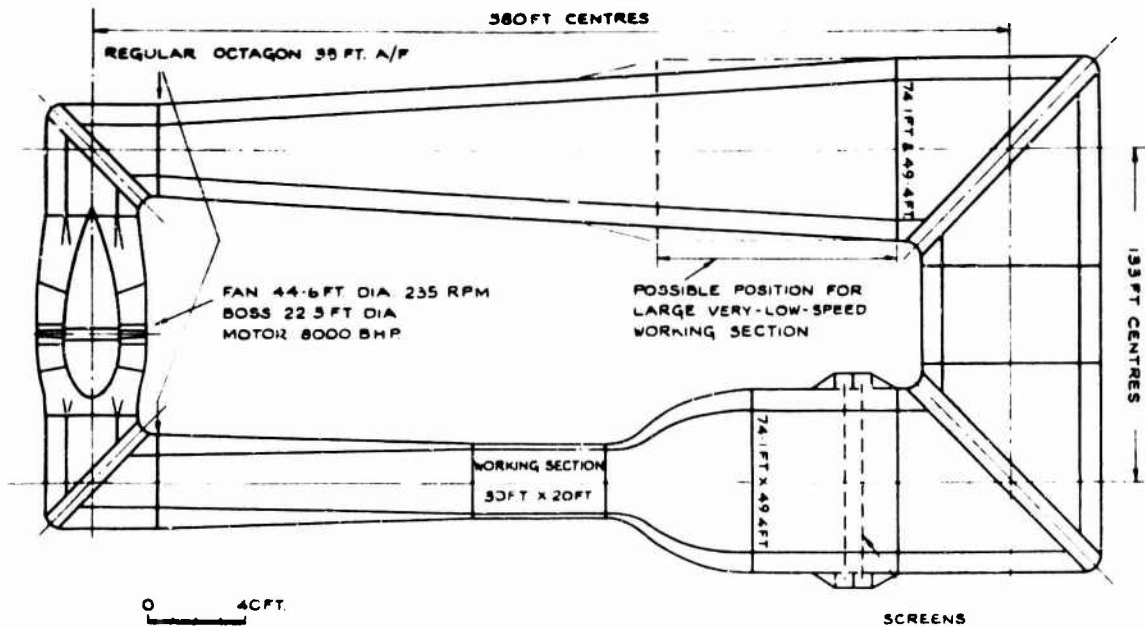


Fig. 49 Possible 30 ft x 20 ft V/STOL/high-lift "atmospheric" wind-tunnel

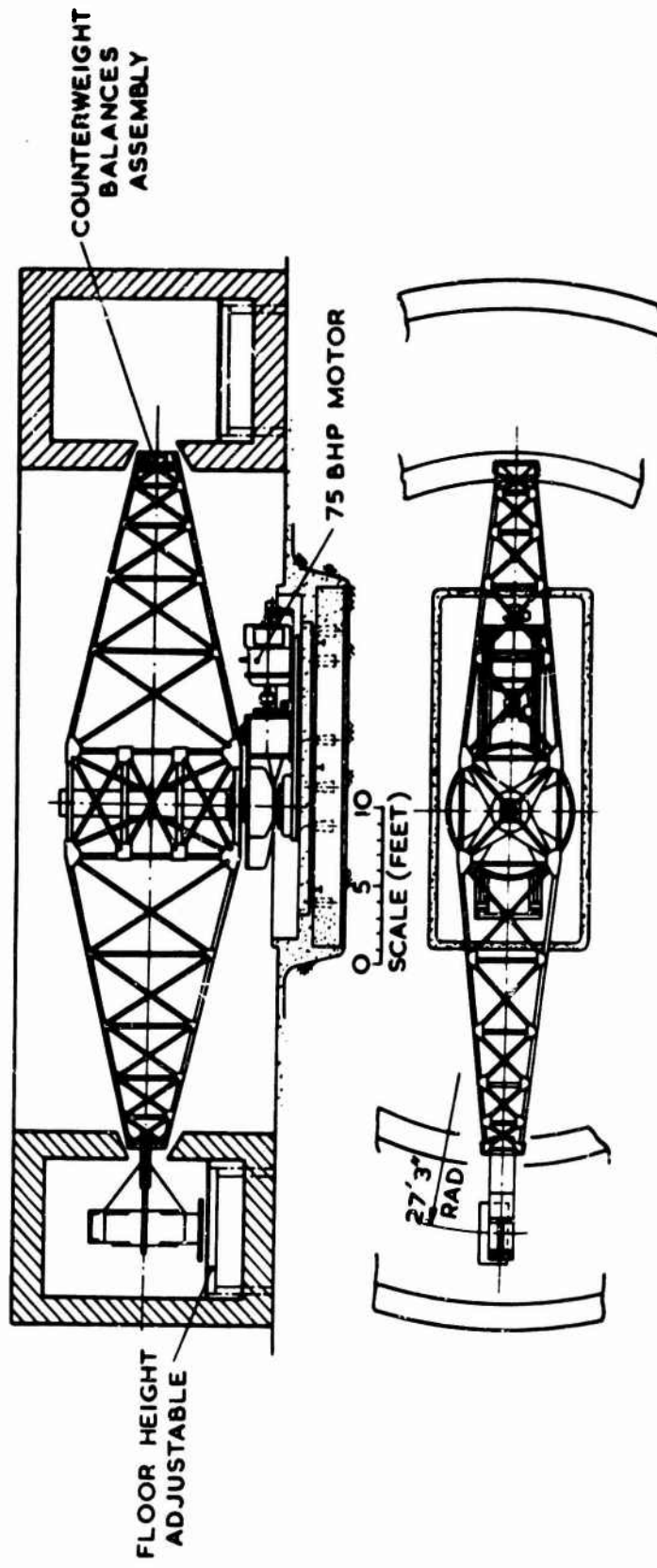


Fig. 50 Whirling arm for aerodynamic research

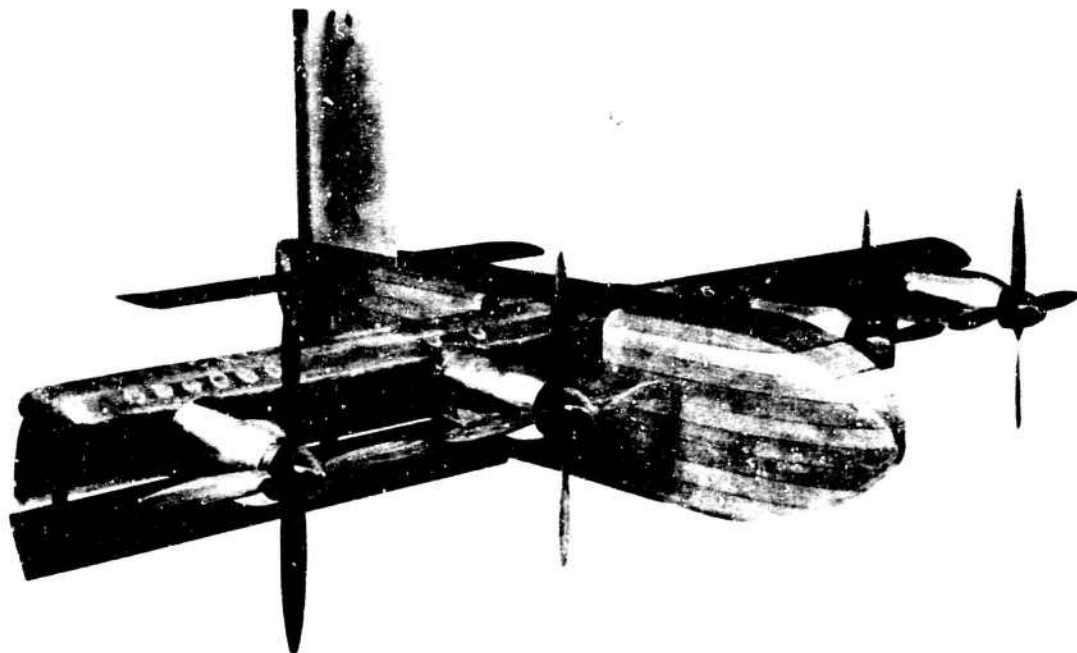


Fig. 51 Deflected slipstream model

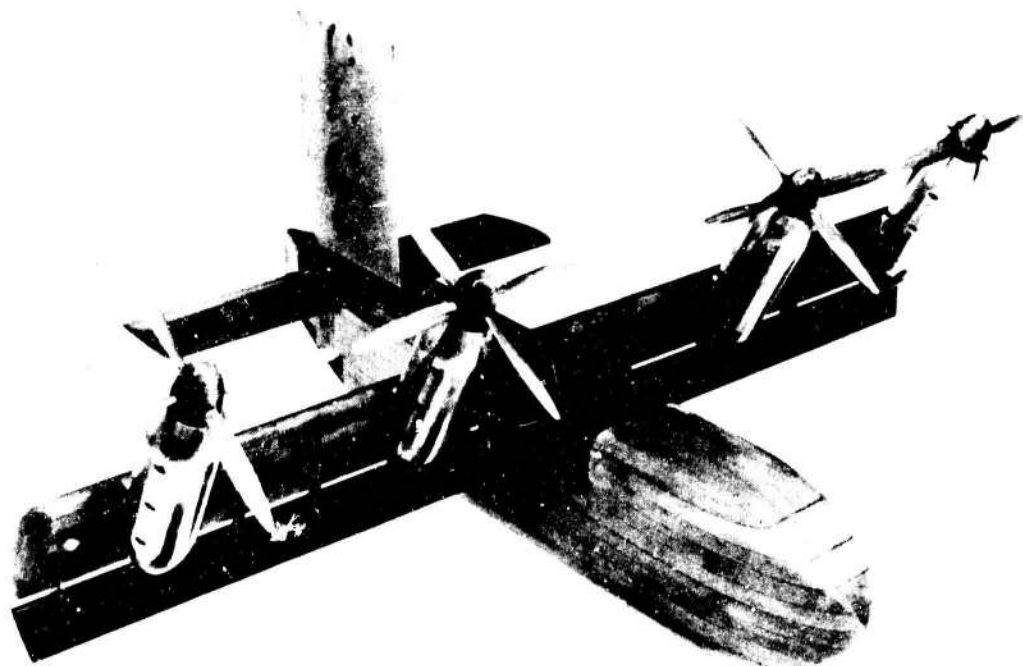


Fig. 52 Tilt-wing model

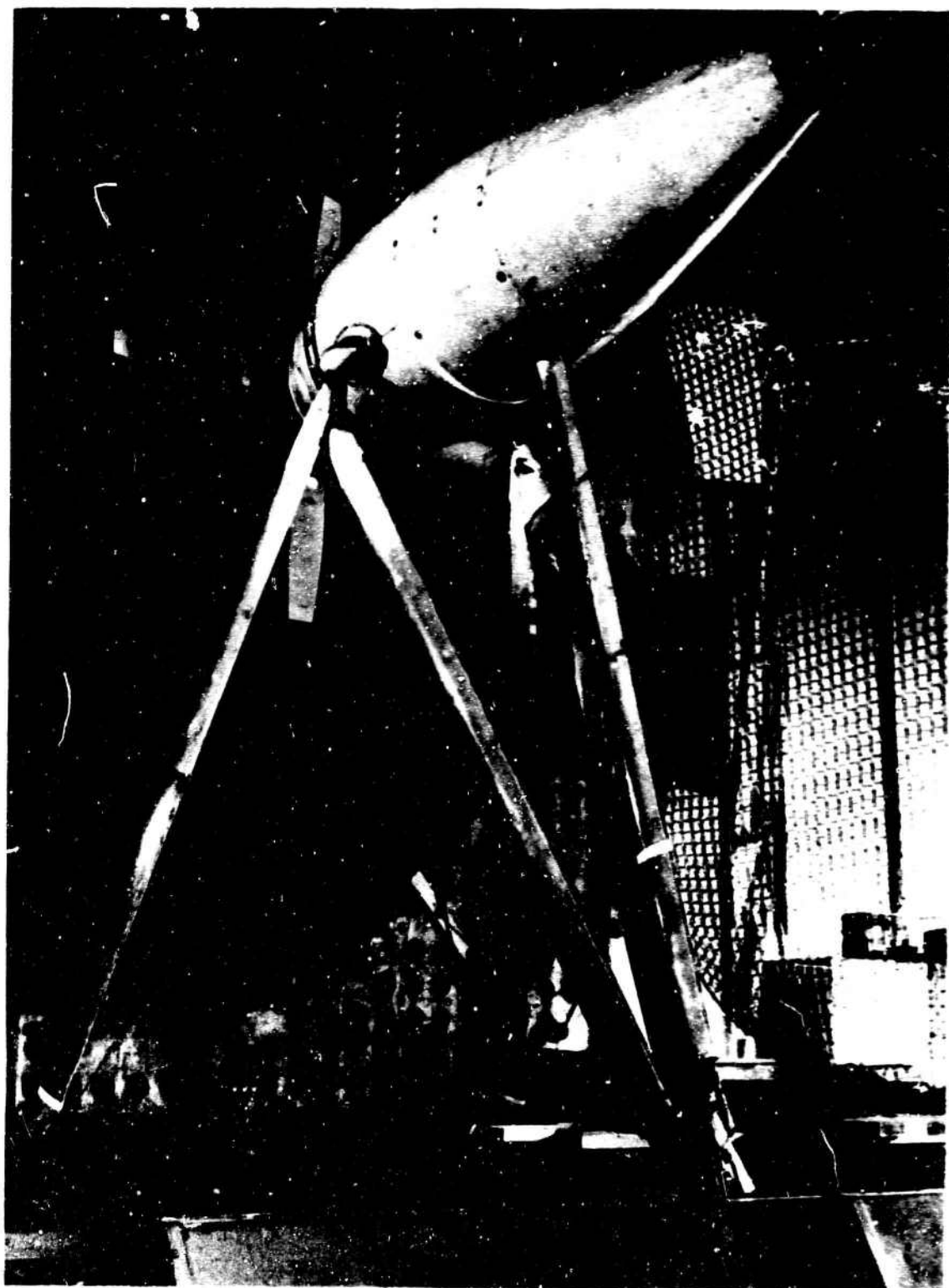


Fig. 53 Propeller test rig



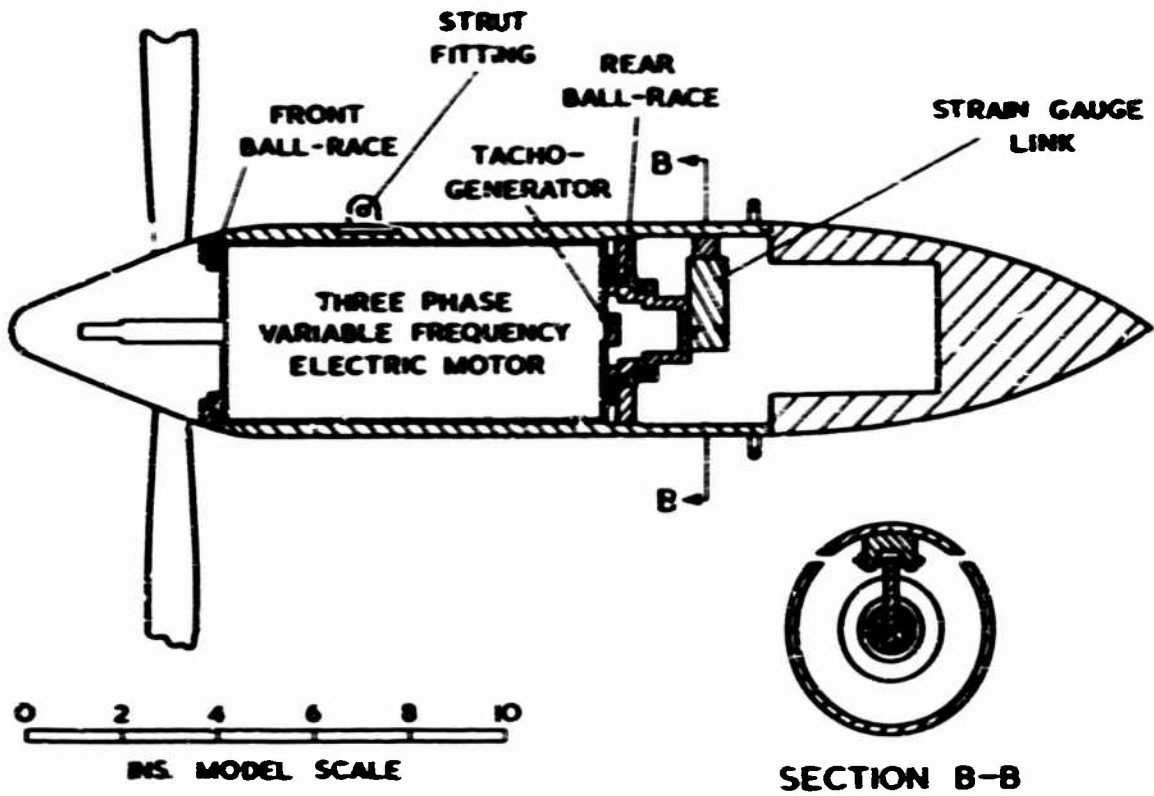


Fig. 54 G.A. of torque case

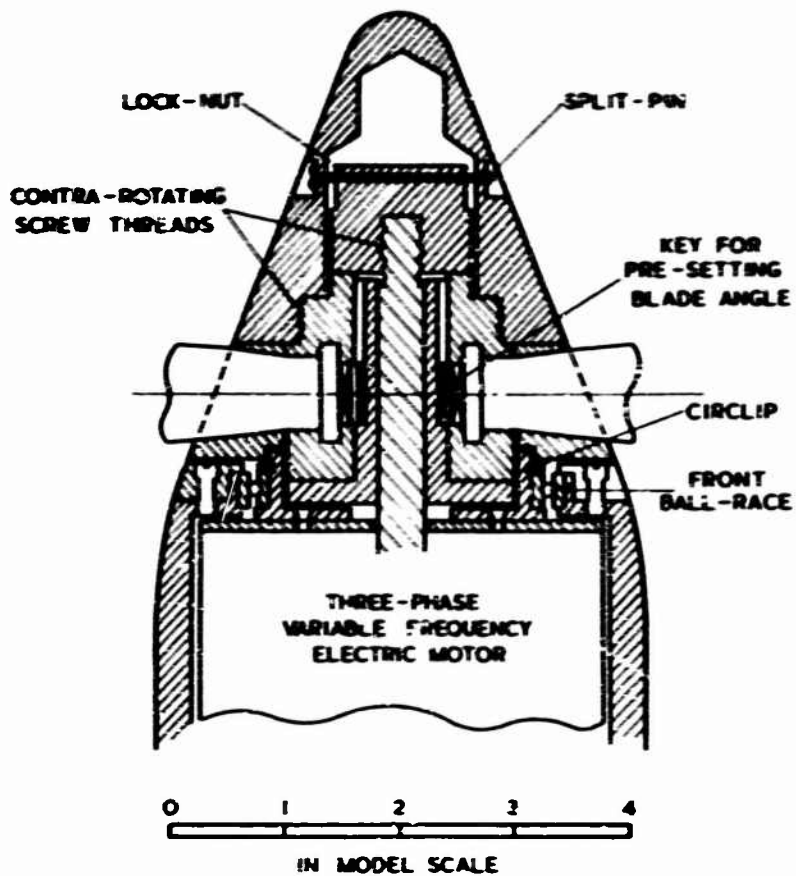


Fig. 55 Details of propeller hub assembly

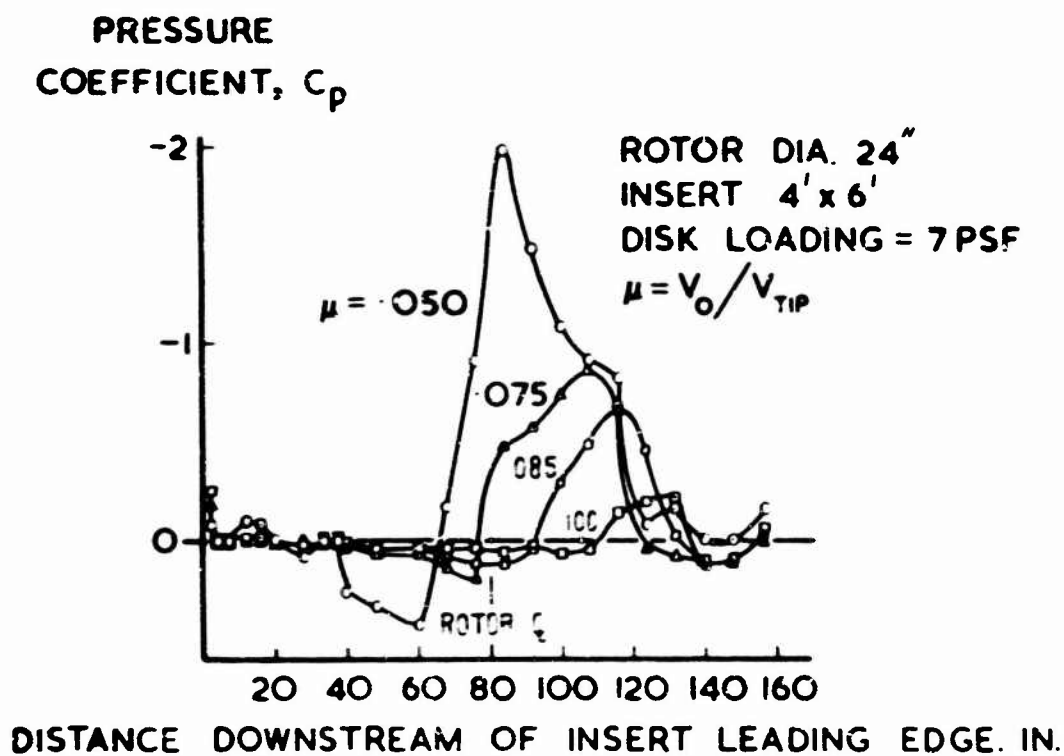


Fig. 56(a) Variation of pressure coefficient along wall under advancing blade

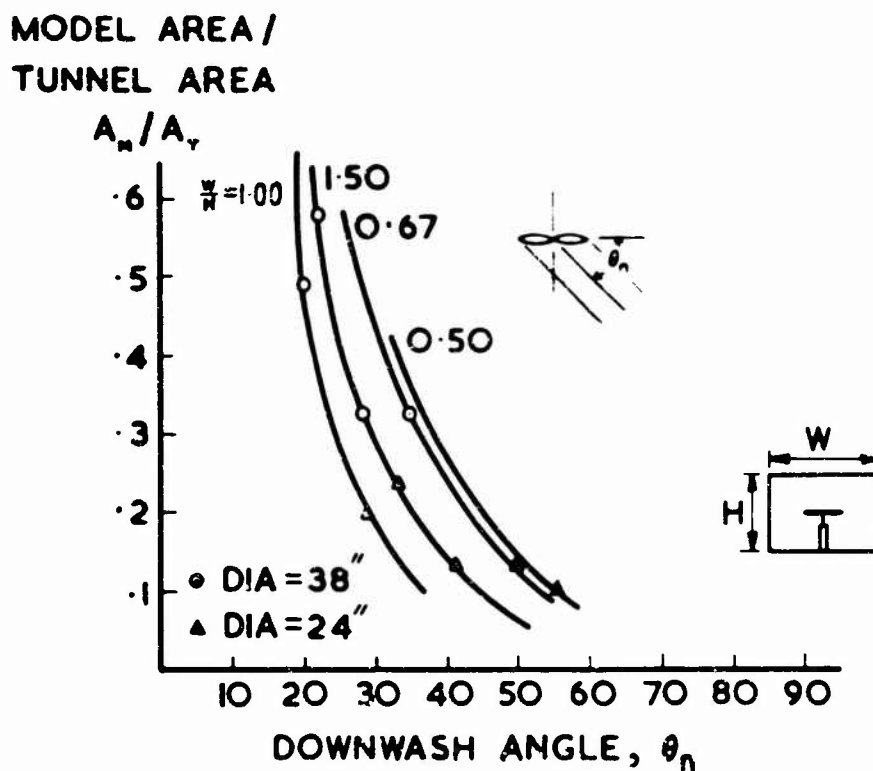


Fig. 56(b) Estimated limit of rotor downwash angle for various rectangular wind tunnels

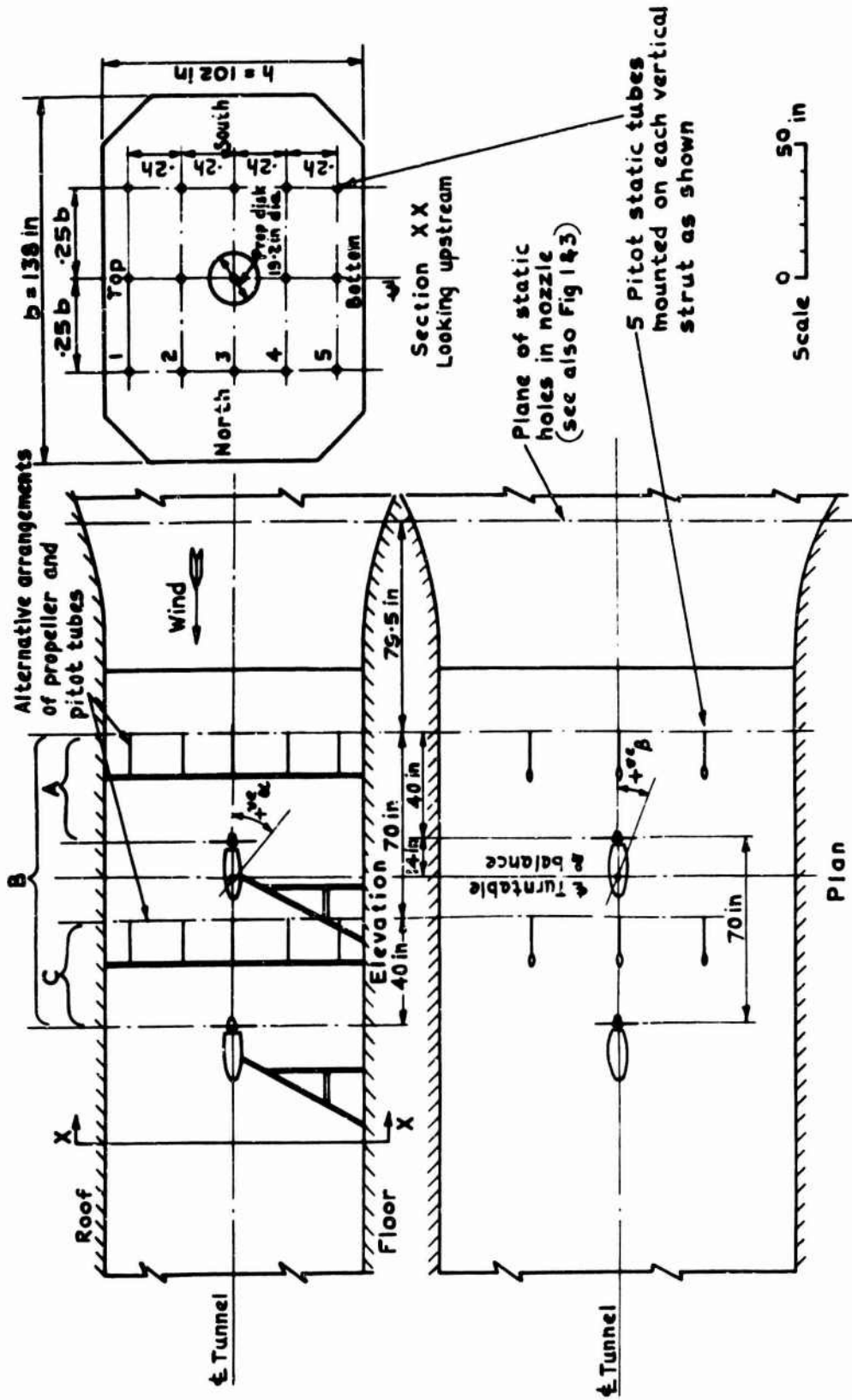


Fig. 57 Details of test arrangements in tunnel working section

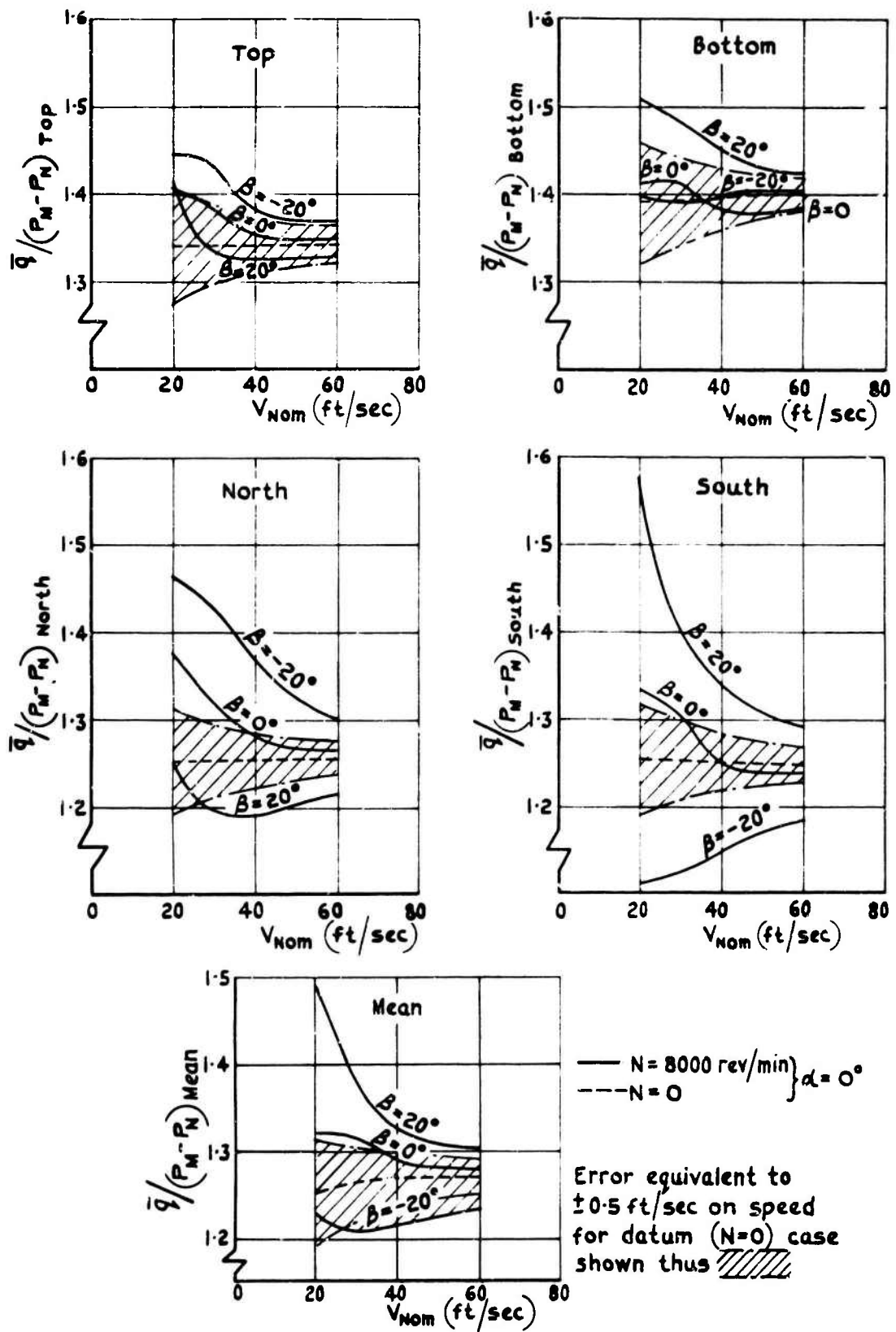


Fig. 58 Effect of yawed propeller on mean dynamic head in W.S. in terms of  $(P_M - P_N)$ -arrangement A

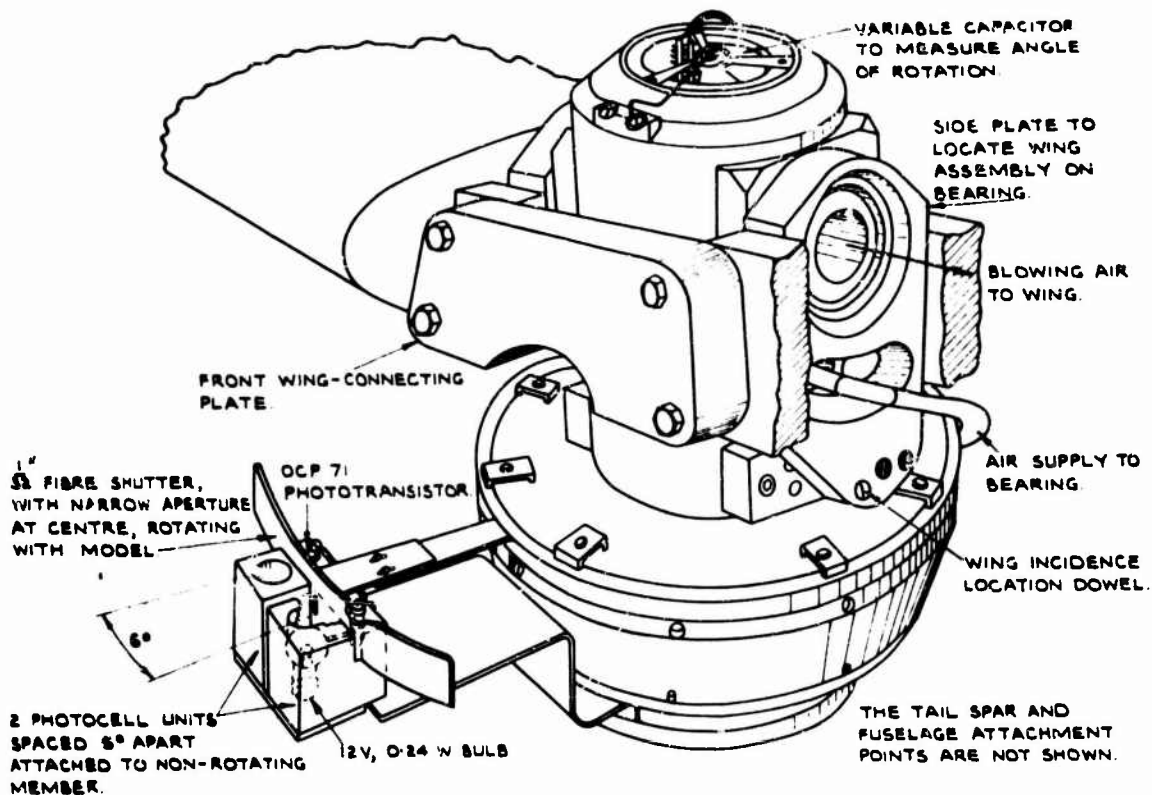


Fig. 59 Details of air-bearing installation and automatic calibration equipment

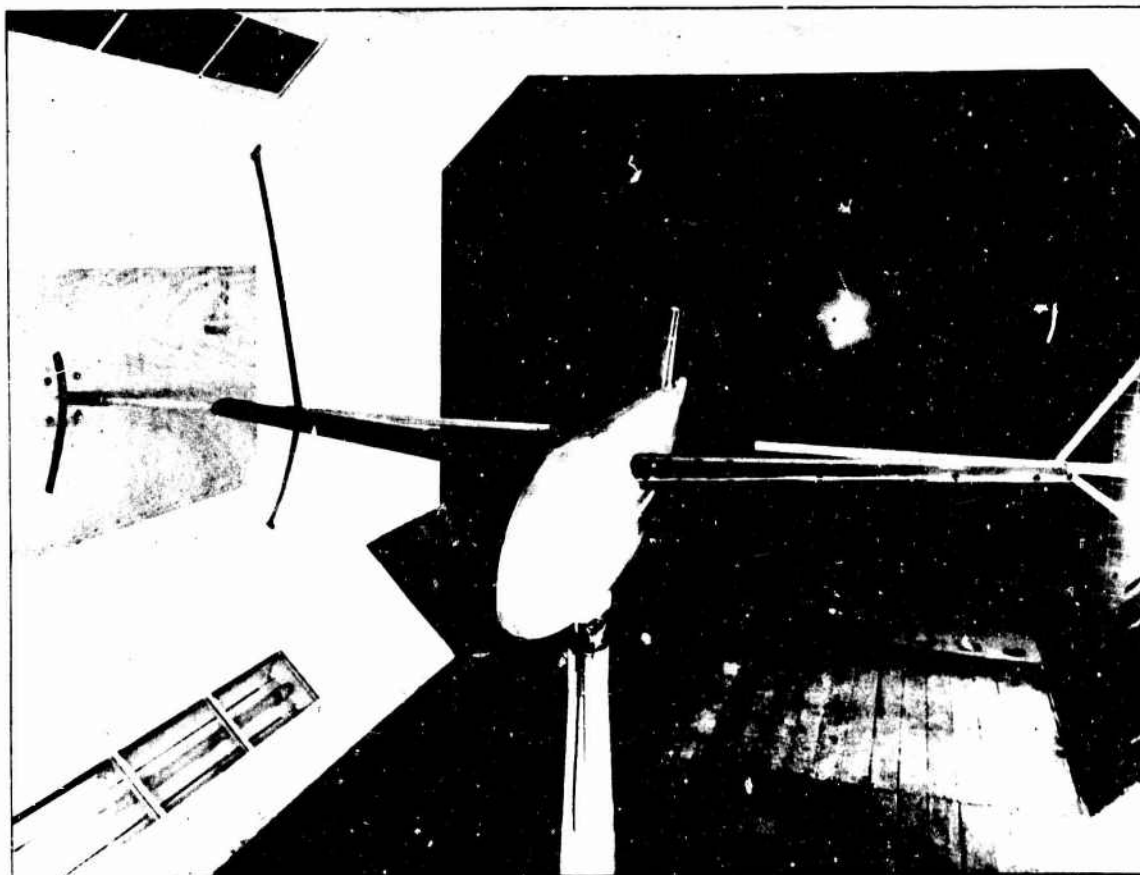


Fig. 60 A.R.9 jet-flap model in the RAE No. 1 11½ ft wind tunnel

PAPER N

FLIGHT TESTING AND V/STOL HANDLING REQUIREMENTS

by

Paul P. Yaggy

Technical Director  
US Army Aeronautical Research Laboratory  
Moffett Field, California

## NOTATION

Several symbols defined in the text are not included in the following list:

$\ddot{y}$	translational acceleration
$C_{L\alpha}$	lift curve slope, lift due to angle of attack
$\delta$	control deflection
$\Delta\delta$	control deflection
$e$	error signal
$F$	stick force
$f(s)$	aerodynamic function
$I_x$	roll inertia
$I_y$	yaw inertia
$\alpha$	dust angle
$L_q$	control power
$L_r$	dihedral effect, roll due to sideslip
$M_{\alpha}$	static stability, pitching moment due to angle of attack
$M_{\dot{\alpha}}$	speed stability, pitching moment per velocity
$\zeta$	damping ratio
$\phi$	roll angle
$\dot{\phi}$	roll rate
$W$	gross weight
$\omega_n$	natural frequency
<i>Subscripts</i>	
a	aileron
e	elevator
ss	steady state

## FLIGHT TESTING AND V/STOL HANDLING REQUIREMENTS

Paul F. Yaggy

### 1. V/STOL FLIGHT AND SIMULATOR TESTING TECHNIQUES

#### 1.1 Concepts of Simulation

Whenever one is to venture into an unknown region or into an unknown experience about which little is known and where the unexpected can be disastrous, it is always prudent first to attempt exposure to a pseudo-experience wherein the parameters of the environment can be explored in a safe manner. V/STOL flight represented such an unknown environment at its inception some ten years ago. It was perhaps fortunate that the strong interest shown in V/STOL flight at that time was accompanied by a tremendous expansion of the area of space flight research as well as in pushing back the barriers of high speed flight. In particular, it was not possible to progressively encounter the rigors of space flight without being subjected at once to the complete environment. Whereas the areas of V/STOL and high speed flight could be probed by incremental decreases and increases in flight speed, space flight demanded a short period steady acceleration which thrusts the human pilot immediately into the full rigors of his task. As a result capable researchers began to develop realistic means by which simulation of the environment and the associated tasks could be accomplished to permit exposure to these elements without the risk of total subjection to the actual environment.

It is not meant to imply that simulation is a new art, but rather that the degree of sophistication which was begun in the fifties for aircraft simulation was well beyond that which had been accomplished in any previous time period. The use of simulators to aid the designer must be viewed in the same light as the use of any model, whether structural, aerodynamic, or other to provide the necessary information for design purposes while the design decisions are being made. A classical example of this procedure is the technique used by the Wright Brothers in the designing of their successful airplane. A diagram of their design technique is shown in Figure 1. Following the desire to fly, a review of the available knowledge was made, the vehicle was designed and constructed, and the pilot-vehicle compatibility problem was investigated in flight using unpowered gliders. The results evaluated were then fed back in the manner shown and the process was repeated until a satisfactory vehicle was developed. Accounts of these efforts can be found in Reference 1, 2 and 3.

It is not meant to imply in the preceding statements that V/STOL flight is only ten years of age. VTOL flight, represented primarily in the helicopter, dates back to the early part of the century. STOL flight is a subject of definition and many light weight aircraft operate at speeds well below those for which we are striving in present STOL vehicles. Definitions relating to these areas will be discussed in subsequent sections. The historical event to which we are referring for the last ten year period is that sudden flurry which produced a large number of flight test beds and a considerable expenditure of research effort in an attempt to bring into fruition successful V/STOL operational vehicles performing in both military and civil missions. It is lamentable that, with few exceptions, we have not yet accomplished that task.

In our present consideration of simulation let us consider a parallel process to that of the Wright Brothers, in that what we want to do with the flight simulator is to present the problem to the pilot-experimenter in such a form that he can identify and assess its



specifics, and give a subjective rating of his ability to carry out the analogous problems in flight. A model of the flight simulator concept is shown in Figure 2. Use of equipments such as this expedites this experimental approach. The block diagram indicates other relationships that must be considered during the design process. In this simulation process we make use of the man himself as the *controlling element*, not a mathematical representation of him. As long as we are considering the man in the loop we must be able to represent to him a vehicle in which we can control the response characteristics of the vehicle and to vary them at will; we must be able to control those factors represented by extravehicular disturbances. The vehicle response quantities must be fed back to the operator in such a fashion as to readily indicate the status of the vehicle and to provide the necessary cues for conducting the required task. These response quantities fall in the categories of visual, kinesthetic and aural cues. In addition, the environmental stress effects must be included to properly represent the requirements of the task or mission.

The use of such equipment as this, of course, requires highly motivated human subjects with experience as an experimental test pilot to provide the subjective information required. It should be recognized that there are many researchers and developers working in the areas of guidance and control, and human factors who are becoming more and more desirous of removing the subjective pilot from the aircraft control loop and providing systems which will accomplish the rigorous demands of flight control by automatic means through automatic stabilization and control systems. There is little doubt such control systems are on the horizon and that eventually they will be employed. The exact time of their entry on the operational scene cannot be predicted; however, the reliability of such systems will necessarily be demonstrated with the human pilot still in the loop as safety monitor. Therefore, it is considered reasonable that at least the next generation and possibly two generations of aircraft will require handling qualities which are suitable for the human operator in all modes of flight. For this reason, efforts in improved flight simulation and the development of handling qualities for human operators are now and will be continued.

In designing V/STOL vehicles which must cope with large variations in their operating environment, it is necessary to consider the effect on the human pilot of the variations of the vehicle response characteristics over its entire operating envelope. A decision regarding the acceptability of these response characteristics from the pilot's standpoint must be based upon terms that can be applied directly to the human. This is accomplished by considering vehicle response characteristics as functions of time and expressing the response characteristics in terms of those quantities that directly affect the pilot's assessment of the motion. These terms include the time dependence of the motions and the interactions of all the forces imposed on the pilot. For example, the longitudinal stick-fixed response characteristics of an aircraft are approximated by a fourth-order constant-coefficient linear differential equation. This equation describes motions which are ordinarily the combination of two oscillations, and can be factored into two second-order equations which can be expressed in terms of gains, natural frequencies, and damping ratios. These latter quantities are the actual dynamic descriptors of the vehicle. Generalized experimental and/or analytical determinations of the allowable ranges of these factors for various tasks have built up a body of knowledge that enables the designer to predict whether the expected operation of his vehicle is close to or far away from regions of unacceptability and to isolate the vehicle characteristics shown on the diagram of Figure 3. This approach leads to definitions of flying qualities requirements on a static and dynamic parameter basis. We shall deal with this subject in subsequent sections.

The interpretation of Figure 3 is simply that if we wind up in the good sections well away from the boundaries for all expected cases, then adequate performance is assured and further simulation is not required. However, if the expected operation is close to a boundary then the precise task to be carried out must be considered before the location of the boundary can be determined. This simply means that general shapes of the boundaries can be determined from a systems simulation and analysis of the problem on a generalized task basis, but precise definition of boundaries depends on the exact task expected. In

cases where comparable operational experience exists, or prior simulation has defined or mapped the region of acceptable or unacceptable behavior, simulation is used objectively to investigate those areas where predicted operation in this case expected concern. Otherwise only the general shapes of the boundaries can be determined from simulations of the problem on a generalized task basis.

In a paper presented before the Fluid and Flight Mechanics Panel of AGARD in January 1963 (Ref.4), George Cooper of the NASA-Ames Research Center evolved a system of classification of flight simulators that evaluates their usage. This classification is still generally accepted in simulations technology. His original comments are quoted.

"The primary breakdown into rudimentary, basic, and advanced simulators reflects increasing sophistication and realism, but without explicitly defined boundaries. The simulators are also classed as either part-task or whole-task, again reflecting the simulator's sophistication and whether only discrete parts or most of the problem is included. This separation into part-task or whole-task simulators is not explicit but it is convenient, particularly if used in conjunction with the concept of self-initiated tasks versus mission-oriented tasks. The method of evaluation used is seen to vary from primarily subjective pilot opinion to primarily task performance based on fairly complete criteria. Application to handling qualities may range from a few basic parameters on the rudimentary simulator through increasing computational complexity and degrees of freedom on the basic simulator, to the very accurate representation of a complete vehicle with the advanced simulator. Results range from very qualitative to quantitative and relatable to flight. The so-called advanced simulator is included for completeness but has not yet been applied to research problems. Its possible application is only conjectured at this time but theoretically it should provide more directly applicable data in the areas of minimum acceptable handling qualities and operating problems."

It is worthy of note that five years after the presentation of this paper the advanced simulator is at least in some degree becoming a reality. To what degree this will ultimately be realized is not known. An example of a more advanced simulation technique presently being used in V/STOL research efforts is the six-degree-of-freedom simulator at the NASA-Ames Research Center shown in Figure 4. Also at NASA-Ames under construction is an advanced aircraft simulator capable of simulation for such tasks as the supersonic transport as well as utility in other areas. Although these probably represent the greatest degree of simulation for aircraft purposes at the present time many other simulators have been constructed throughout the world and are being utilized meaningfully in the development of various aircraft.

The full range of simulators is useful, since every application does not require the same degree of sophistication. When one knows the use or application required of the results as well as the type of results (qualitative and/or quantitative) desired, one may determine the type of simulator (rudimentary, basic or advanced) that is required as well as the kind of task that must be considered and the corresponding method of evaluation. The more precise and realistic in the flight sense the type of information required, the more complete must be the simulation with the ultimate limit being reached in the actual flight situation.

In actually performing the simulation process, after the selection of the type of simulator has been made, the actual establishment of the simulation must be done. Equations of motion defining the kinetic relationships with the system must be determined, and the equation of motion programmed on the analog computers which control the simulator equipment must be provided for both the vehicle response computation and the vehicle response feedback information. The test pilot and the designer must work out the test procedure. At that time, a validation must be accomplished by the operator to be sure he has bridged the gap between the real-life situation and the simulator situation. It is at this point that the experience of the pilot becomes absolutely essential, since his subjective evaluation determines the adequacy of the simulation. Once the adequacy has been established experimentation can begin. The results are analyzed on the basis of a subjective pilot opinion rating scheme which controls the variation of the parameters within the test.

A few examples will serve to demonstrate the usefulness of the flight simulator in demonstrating flight capability and assessing flight handling qualities. It is emphasized that these are only cursory and are not intended to represent a complete analysis of the simulations concept or the techniques which can or may be employed. The reader is referenced to the literature (in particular, Reference 5) wherein a vast amount of information can be obtained concerning flight simulation techniques.

Early attempts at simulation were confined primarily to fixed base simulators; i.e. those which do not have motion cues. In their most simple application these devices utilized cathode ray tubes and meter displays as control factors. By increasing the complexity of the simulation, and thereby making the situation more real, it was found possible to obtain information ordinarily considered accessible only in actual flight.

The next degree of sophistication was to add a visual display to add realism to the simulated situation. As an example let us consider the landing approach simulator. From this simulation quantities such as touchdown rates of descent and landing distance from runway thresholds were obtained. Pilot opinion of such simulations was that they very faithfully represented the real situation. Although the exact rates obtained from simulations with visual cues tended to be somewhat conservative, the general shape of the curves were similar and indicated that the difficulty of the task was being represented to a fair degree of accuracy. These results demonstrated that sophistication and realism of the simulation process enabled the acquisition of data of a more quantitative nature.

The pilot will utilize all the information available to him to achieve and maintain control of the vehicle. Therefore, it is necessary to properly represent these feedback quantities to him for a realistic appraisal of the capabilities of the airplane. Such factors as visual cues in the form of instruments, kinesthetic cues in the form of tactile and body forces and aural cues in the terms of engine power, vibration and air noises are useful to the pilot in assessing his situation. It was found that the use of body forces to increase realism and augment the visual cues was extremely important. Examples are given in Reference 6 which demonstrate that motion feedback can be of help to the pilot in exercising control in the simulated condition but that it also can be a deterrent factor to his ability for control. A brief summary of these two conditions illustrates the point.

The first example is a deflected slipstream VTOL vehicle. Its characteristics are shown in Figure 5. The range of conditions studied were from 0 to 55 knots. Any point on Figure 5 represents an available steady flight condition. The upper boundary is fixed by wing stall and control available. The lower boundary is imposed by structural limits of the flap. The wind tunnel data alone dictated the operational range. On a fixed-base simulator the pilots found it very difficult or impossible to complete the transition, but when pitch and roll motions were added to the cockpit these motion cues enabled the pilots to explore the transition region and a comfortable transition boundary was established which, with the flap limit as the lower boundary, designated a corridor through which the aircraft could be flown by careful attention to flap speed and angle of attack. Subsequent flight experience supported the conclusions.

The second example of the effects of motion feedback considers a large tilt wing vehicle in hover. This study was primarily concerned with roll control. The simulation was in three degrees of freedom including vertical and lateral translation and roll. The tasks were to lift off into hover, move laterally, and land. A comparison of conditions with a fixed cockpit and roll freedom included in the cockpit is shown in Figures 6 and 7. The erratic movements and larger lateral velocities with the fixed cockpit simulation and the more regular movements and lower lateral velocities with roll motion feedback conclusively demonstrate the advantage of the motion cues. These two examples illustrate that fixed cockpit studies tend to be conservative. One important conclusion which can be drawn is that if the task can be performed on a fixed base simulator it can probably be considered unimportant.

In some cases the presence of motion cues renders the control of the vehicle more difficult even though these cues result in more realistic flight situations being presented to the pilot. A task designed to stress the capability of the pilot to quickly change angle of bank of an aircraft necessitates an overall maneuverability of the aircraft (a problem of long standing). Experiments were made on both a fixed-base simulator and a rolling simulator. Boundaries defining ranges of satisfactory, acceptable, and unacceptable characteristics were determined and are presented in Figure 2. It can be seen that at values of the rolling parameter of approximately ten radians per second, the effects of motion feedback reduce the acceptable region. It can be assumed that larger angular accelerations in roll hinder the pilot's ability to control precisely. The overall comparison of the results of these moving simulator tests compared very well with flight results.

Thus it is seen that the presence of motion cues can both help and hinder the pilot in performing his task. The use of motion feedback will always increase the realism to the pilot and unload him so that a better assessment of the flight task can be made. However, it is important to remember that in the use of motion feedback, motion artifacts (such as unwanted motion about an axis perpendicular to the axis of concern) can compromise the problem and decrease the region of acceptability.

Other areas of importance in simulation are stick-force feedback, the representation of the overall response in the control system and the faithful representation of control system responses both time and forcewise. Failure of stability augmentation systems can cause dangerous out-of-trim conditions or divergent oscillatory behavior that can result in exceeding structural limitations of the airframe before the pilot has time to adapt to this new dynamic situation. Therefore, it is extremely important to represent the control system in all its functional complexity so that transients inherent in the systems to be controlled can be properly assessed by the pilot in judging the overall controllability characteristics of the aircraft.

In summary, the concept of simulation is to provide to the greatest degree possible, a representation of the environment including as many cues and feedback responses as possible to duplicate the actual flight situation. This has been accomplished to a sizable degree in present day simulators. The utilization of these simulators in assessing the handling qualities of V/STOL aircraft has been meaningful and gratifying. However, it is emphasized that a considerable amount of sophistication in the employment and interpretation of simulator results is yet to be accomplished. The flight testing of V/STOL aircraft is extremely difficult because of the extremely low speeds which are desired and the highly critical effects of extra-vehicular forces as well as power loss. It is desirable to continue research to obtain a higher degree of sophistication in the simulation utilization; in particular, the ability to assess scaling factors and to establish the handling qualities of large V/STOL vehicles utilizing the experience gained on small scale test beds.

This cursory approach to the concepts of simulation indicates its importance in the design and development of V/STOL aircraft whether these aircraft are to be piloted by humans or controlled by automatic systems. The importance of simulation in the continued development of not only V/STOL but all forms of flight vehicles should be appreciated. For further information concerning the varieties of simulators which are utilized the reader is referred to Reference 5.

## 1.2 Flight/Simulator Correlation

A basic axiom of simulation is that the simulation is only as good as the degree to which it faithfully represents the actual environment which it is desired to simulate. Evaluation of the simulation can only be obtained by direct comparison with that environment. Therefore, it becomes obvious that confidence in simulators can only be obtained through a continued amassing of a variety of experience which demonstrates its adequacy. There is nothing strange or mysterious about this process; it applies to every learning function. The attempts to demonstrate flight/simulator correlation have been orderly and

are continuing with the result that an ever increasing confidence in flight simulation is being realized.

The economies of simulation should be appreciated by the aerodynamicist and he should strive to capitalize upon their usefulness in accomplishing the research and development task. The construction and testing of flight vehicles is an extremely costly operation. The demonstration of the adequacy of a given design can be accomplished at considerably less cost by the use of simulators. It will be increasingly important to take advantage of these cost savings as the sophistication of flight vehicles such as the V/STOL vehicle increases. It is obvious that once perturbation methods have been established, the confirmation of a given flight condition in a safe regime can then establish the basis for the simulation model. Perturbations about that point on the simulator can be made on a broad matrix form to ascertain the potential limits and acceptable flight envelope for the vehicle. With this vast display, only limited flight tests need be made to demonstrate the adequacy of the trends and gradients established in the perturbed cycles. Not only is a considerable savings in cost of flight operations realized but confirmation of the gradients will more clearly establish the limitations of the flight envelope and will serve to establish for the pilot those regions which he should avoid as unsafe operations. Further, the establishment of these limitations by flight testing which is of course a necessity can be done in an orderly and knowledgeable manner, thus avoiding the loss of valuable resources represented in experienced test pilots and high cost equipment.

In this manner, the piloted simulator has become a valuable aid in flight test programs. It will be well for us to consider one of many examples of the vital support of flight research provided by the simulators. In an attempt to reduce the roll control power in a hovering jet-lift VTOL aircraft, it was planned to install a movable vane in the engine exhaust to vector the thrust, thereby producing sideward translation without rolling the aircraft. A schematic representation of this desired capability is shown in Figure 9.

It was necessary to know (1) how to control the vane from the cockpit (that is, by a thumb controller or by the stick deflection) and (2) how much to deflect the vane for satisfactory maneuvering. Information was obtained regarding these questions by a study on the piloted simulator which was shown in Figure 4. The cab of this simulator is free to travel within a cube of approximately eighteen feet on a side and with angular motion capability of  $\pm 45^\circ$  about all axes. According to pilots' comments, the overall motion capability of this simulator closely corresponds to actual hovering flight.

The results of the simulator study in which three methods of control were used are presented in Figure 10. The two obvious conclusions which can be reached from these data are that the vane improved (lower number) the pilot rating and programming the vane as a function of bank angle was not as desirable as actuating the vane by a thumb controller on the top of the stick. Both bang-bang and proportional controller methods were evaluated for possible flight application. The simulator tests indicated that a lateral acceleration of approximately  $0.1g$  would be the maximum desired for rapidly positioning a VTOL aircraft. In addition, attitude stabilization in roll was desired to reduce the effects of inadvertent upsets caused either by the pilot or by gusts. Subsequent flight tests with the vane installed on the X-14A VTOL aircraft which is shown in Figure 11 have borne out trends shown by the simulator. The flight tests also confirmed the simulation in that they emphasized the need for attitude stabilization when the vane is used for control. The thumb controller method of regulating the vane, established by the six-degree-of-freedom simulator studies, was adequate and remained essentially unchanged for the flight program. It is emphasized again however, that even when sophisticated, multi-motion piloted simulators are used, experience always has shown the need for flight validation.

### 1.3 Ground Test Stands

The use of ground base test rigs for pre-flight assessment of V/STOL aircraft has found considerable favor in many countries. These rigs are utilized for essentially four types of investigations. These are:



- (a) To provide a functional check of the control systems used in hovering flight including SAS failure and engine out.
- (b) To study ingestion and recirculation problems due to engine exhaust or lift systems.
- (c) To measure hover performance in and out of ground effect.
- (d) To check engine operation, calibration of various equipment, and initial pilot familiarization.

Perhaps the best means of obtaining an appreciation for the role which the ground base test rig plays in the development of V/STOL aircraft is to consider several examples which are currently being employed. First, we shall consider a rig adjustable only in height which was utilized for evaluating the XV-5A fan-in-wing VTOL aircraft. This rig was utilized at the NASA-Ames Research Center and is pictured in Figure 12. Before flight of the aircraft it was tested on the stand at various heights above the ground to assess the importance of ground proximity. These tests revealed that close to the ground, an erratic rolling oscillation was produced by recirculation of the exhaust from the nose fan which is used to provide longitudinal balance of the aircraft. The XV-5A aircraft is controlled laterally by means of louvers at the wing fan-exit which close off the fan exhaust differentially to produce a rolling moment. Measurements made on the ground test rig of the available control moment indicated that lateral control would be only marginal. Subsequent checks of the control system indicated that the system deflected under dynamic pressure from the fan exhaust. Therefore, a more rigid system was installed before the flight tests were begun. The unsteady behavior in ground effect was confirmed by the flight tests, but the difficulty of operating in this region had been alleviated by making the roll control power adequate and by use of attitude stabilization techniques. It is possible that in this case serious damage if not fatality could have resulted if flight tests had been attempted without these meaningful measurements.

The foregoing example employed only adjustable height in the test rig. More sophisticated ground base rigs with more motion freedom have been used. Of particular interest is the rig shown in Figure 13, used for testing the VJ-101-X2 in West Germany. This rig is of a telescoping type with a mounting capable of angular freedom in roll, pitch and yaw. The most desirable configuration is to have the pivot as close to the center of gravity of the aircraft as possible to avoid large static moments when the aircraft is tipped. The maximum free movement which is restricted by cable is  $\pm 25^\circ$  in pitch and roll and  $\pm 8^\circ$  in yaw. The unique aspect of this type of rig is that it is possible to "fly" the aircraft on the telescope and this is done each time any change is made or maintenance is performed on the control system, including the stability augmentation system. This type of control rig provides a safe means of checking such items as the time constants of the control system (thrust modulation is used for pitch and roll in the VJ-101), hard over failures in the SAS, the effect of one engine thrust loss, and the difficulty of flying as a system fails progressively from an attitude command, to a rate-damped, and finally an acceleration system. It is ironic indeed that if the VJ-101-X1 had been checked on this telescope prior to its last flight, loss of the aircraft could have been precluded. The crash resulted from the yaw gyro which was installed with the wrong polarity. Although the flight was made as a conventional airplane with no hovering intended, the yaw gyro which in conventional flight serves as a yaw damper, caused a divergent Dutch roll oscillation.

The Dornier Do 31 flying hovering rig was also tested on a ground base rig. This rig had full angular motion within the prescribed limits but did not have the freedom in vertical height capability. It would be well to point out that the inclusion of freedom in vertical height, other than ground adjustability, is somewhat a subject of question regarding its adequacy of simulation because of the large inertias which must be accelerated in the vertical direction. It would be possible to properly simulate the inertias of the aircraft with the rig, but the cost of providing such capability is very high. The ability to utilize the ground test rig in the Do 31 program was credited by the test pilot Mr. D. Wood and others of the Dornier GmbH with being one of the most important factors in

enabling the successful program which has been demonstrated. A picture of the Do 31 hover rig mounted on the test stand is shown in Figure 14.

In summary, ground base test rigs have been extremely useful for examining potential control problems for hovering flight and for checking the functioning of the entire aircraft in a partial-flight environment. Their inherent limited motion capabilities however, limit the use of ground base rigs in determining the desired values of control power needed for hovering. It is probable that the ground base rig will continue to grow in sophistication as VTOL aircraft become more complex.

#### 1.4 Flight Testing at Altitude

Flight testing techniques of experimental concepts for V/STOL aircraft have taken two forms. The first utilizes airborne test rigs usually capable only of the hover portions of flight which are utilized to evaluate the specific problems of this flight regime. The second consists of the experimental aircraft itself which takes on varying degrees of sophistication depending upon its intent in an overall program. In the 1950's a rather large quantity of small, light-weight experimental V/STOL aircraft were built in several countries with a particularly large portion in the United States under the Tri-Service evaluation program. Many of the details of these aircraft and their characteristics are contained in Reference 7.

Airborne test rigs were first used in the 1950's. The Rolls-Royce flying bedstead was tested in the United Kingdom and the Coleopter in France. Both served to prove the practicability of attitude control for VTOL flight. In more recent times, the airborne test rig has been used as a flying simulator in the development of hover and low speed handling qualities requirements and as a test bed for the propulsion and control systems hardware which ultimately are installed in a specific aircraft.

An example of a flying simulator is represented in the North American FS-1 "Hover Buggy" which is shown in Figure 15. This vehicle is built with a cruciform shape to enable the installation of both longitudinal and lateral controls at the extremities of the crossarms. It has a twenty-two foot span and is powered by two GE-YJ-85-1 turbo-jet engines. The gross weight of the vehicle at its takeoff weight is approximately 3400 pounds. Angular stability and control about each axis is provided by compressor bleed air in a continuous flow reaction control system. The electronic package provides variable stability and control features which allow control power, control sensitivity, rate damping, and attitude stabilization to be studied systematically in a real world environment. The North American Aviation Corporation has recently completed tests to determine hover and low speed control power requirements for various control systems. The FS-1 hover rig has essentially no aerodynamic surfaces and the pilots report essentially neutral stability about all axes. It has been suggested that this type of vehicle could be used to define control power requirements for maneuvering. Also suggestions have been made for much larger multi-engine rigs of this type to help answer the controversial question of the effect of aircraft size and inertia on control power requirements. Initial results with the FS-1 rig indicate that it can be very useful as a flying simulator for comparing the effect of various control system parameters on a specific maneuvering task. However, its small size limits its usefulness for settling the aircraft size control power question for at least two reasons. First, it does not take into account the control requirements for offsetting the effects of upsets and gusts acting on the aerodynamic surfaces. Second, even though inertia can be increased by adding weights there are unknown effects of angular acceleration on the pilot. Since the pilot is usually displaced farther from the center of gravity as the aircraft grows in size, the amount of control power desired for pitch and yaw will undoubtedly be influenced by this factor. The roll axis, which has been of greatest interest from the designers standpoint, would be influenced to a lesser extent since the pilot is usually located close to the roll axis regardless of aircraft size. Exceptions to this occur in specialized aircraft such as the Sikorsky S-64 where the pilot is relatively far below the center of gravity.

The second example of the utilization of airborne test rigs is that of the Dornier Do 31 experimental program. The initial vehicle used in this program was a hover rig which had pilot and engine displacements in positions where they were envisioned in the final aircraft. The airborne control rig, the large hovering rig and the Do 31 experimental aircraft are shown in Figure 16 extracted from Reference 8. In the upper photo, it is seen that, as was the case for the FS-1, the rig has no aerodynamic surfaces and serves well to evaluate the control power requirements for maneuvering based on one power system and inertias. In this case, the actual inertias of the aircraft can be well simulated as well as the response on the pilot who is now located in the position where he will be in the aircraft. The generalization of such a rig of course would require the ability to change the pilot's location as well as the arrangement of engines and inertias of the overall system.

In the case of the Do 31 program, a more sophisticated airborne test rig was produced whereby the aerodynamic characteristics could be evaluated in conjunction with the inertial control requirements. This rig is that one which was shown in Figure 14 on the ground test rig. It is typical of those used in West Germany for developing such aircraft as the VJ-101, and the VAK-191B as well as the Do 31. These rigs are used essentially for research on the control systems hardware and the propulsion system which ultimately will be installed on the actual aircraft. The advantages of such rigs as these are that they will have encountered the real life environment of noise and vibration in free flight and such items as control system gains and time constants will have been adjusted for optimum performance. Both the rigs for the VJ-101 and the Do 31 have proved to be extremely valuable in the development of the actual aircraft. They have much more potential for research on control system requirements for large jet VTOL transport than do the less sophisticated hovering rigs. It is seen that the Do 31 hovering rig is in most aspects an aerodynamic duplication of the flight vehicle and would have realistic trim, upset and ground effect disturbances typical of a large jet-lift transport.

It can be seen that airborne test rigs have great value for assisting in the development of complex VTOL aircraft. However, safety considerations limit their capability in the same manner as aircraft to investigate control requirements in areas of low control power, hard over SAS failures and engine failures. As discussed previously, these requirements are best investigated on a multi-motion, ground-base piloted simulator. The upper limits of hovering flight, (i.e. the transition to aerodynamic flight from engine supported flight) also cannot be studied with airborne test rigs.

It is at this point that the consideration of the actual experimental aircraft begins. Generally the aircraft is designed to fly initially in the conventional aircraft mode. Takeoffs and landings are performed in the converted configuration as a conventional aircraft. Conversions are then attempted in the reverse procedure back toward the hover mode. Progressive steps are taken during each flight and the results evaluated to maintain safety in the program. The performance of these portions of the program at altitude enable recovery from an inadvertent upset without catastrophic results. This technique has been found extremely useful by the pilots. Its only drawback is a lack of reference at the slow forward speeds which are being investigated. However, many pilots owe their lives to this technique which would have resulted in fatality if the upsets which were experienced had been encountered in proximity to the ground.

In the Do 31 program it was possible to use the large hovering rig to explore the range from 0 to 40 knots while the experimental aircraft tests were made beginning at 170 knots progressing downward until the complete flight range was closed. This program has been most successful and has demonstrated the capability of developing a relatively large-scale VTOL transport. It is hoped that current efforts which are being undertaken will enable a flight/simulator correlation of this aircraft to be made. The results of such a coupling will have the greatest of value in evaluating the handling qualities requirements for this class of aircraft.



In flight testing at altitude, it has been found beneficial to utilize a chase aircraft to monitor the test. The observations which can be made from the chase aircraft by trained observers not only contribute to the safety of the operation, but provide valuable data for analysis of flight records. The coupling of these observations with the reactions which are continuously spoken by the pilot, contribute greatly toward the total evaluation of the mission. In most systems either onboard recording or telemetering is employed to complete the acquisition of necessary data. Instrumentation requirements will be discussed in Section 2.1.

Let us now consider in greatest detail two particular flight testing techniques. The first concerns measurements of control power in hover. The amount of control power required for hover of VTOL aircraft has been a controversial issue. VTOL aircraft are particularly sensitive to control power requirements because there is usually a direct trade off between performance and the amount of control power required for the hover. The control power required can be evaluated by (1) measuring attitude changes directly with an attitude gyro, (2) integrating angular rate, and (3) measuring angular acceleration. All three are important and must be included, since angular acceleration measurements give only the moment available and do not include the effects of the time constant. Various techniques have been used to measure angular acceleration but the control reversal method is generally preferred. This method is portrayed graphically in Figure 17. Utilizing this method of measurement of rolling acceleration, the aircraft is initially banked in a direction opposite of that for the measured responses to assure that the lateral control input is constant at the time angular acceleration is measured, and to reach higher angular accelerations at smaller bank angles. The stick grip is usually fitted with a chain stop to aid in keeping control inputs constant and to provide means of obtaining prescribed partial control positions.

Even when the reversal technique is utilized, large bank angles can occur for high response systems and the use of the chain stop which restricts the available control power can make control power measurements somewhat hazardous when performed while hovering near the ground. Therefore, these types of tests are usually performed at approximately 2000 ft of altitude. There are limitations to the technique of testing at altitude, however. A lack of good position information noted earlier makes it difficult to avoid sideward or fore and aft translation. Not only does this affect the accuracy of control-power measurements, but upsets can occur. It can be assumed generally that the larger the aircraft and the higher its wing loading, the greater the altitude must be to afford a safe recovery from possible upsets. This is unattractive from performance aspects.

Another technique which is permissible by testing at altitude is the investigation of stalling behavior. This requirement has been emphasized by such problems as the T-tail subsonic transport aircraft. Investigations of this sort have made use of such techniques as flow visualization utilizing atmospheric conditions favorable for condensation in vortex flow, and by the emission of smoke into the vortex pattern as was accomplished by the RAE Bedford in the United Kingdom on the HP115 slender delta wing research aircraft. Utilization of these flow visualization techniques enables a better understanding of the high lift benefits which are realized from such phenomena as the stable vortex flow associated with sharp, highly-swept leading edges on the wings. Utilization of the visualization technique together with such well known methods as tufting the upper wing surface, enable a tracing of the vortex flow and provide a better comprehension of the mechanisms at the onset of stall. Such problems as asymmetric stall producing roll off can be studied to good advantage by these techniques. It is also possible to evaluate the interaction between aircraft components as, for example, between the wing and the tail.

A few general comments concerning the methods of establishing static stability and trim characteristics, maneuver stability, and dynamic characteristics are in order but cannot be dealt with in detail in this presentation. Therefore the reader is referenced to the literature for additional information. A general comment concerning all three of these items is that of obtaining data by slowly varying a given parameter, such as airspeed or sideslip angle, while recording continuously with time that parameter and the

other associated parameters. Cross-plotting the appropriate parameters at frequent time intervals yields a well-defined curve showing the stability slopes. A considerable saving of flight time results from this technique. An example is that of determining directional stability at a given condition which can be defined completely over  $\pm 30^\circ$  sideslip range in about two minutes of flight, whereas if steady conditions were established and recorded at a sufficient number of discrete sideslip angles, many times this amount of flight time would have been necessary. Generally, the rates must be limited to about  $1^\circ$  per second for angular changes or to 1 knot per second for airspeed changes to prevent dynamic effects from showing up in the measurements. By making a sweep from trim to the maximum change in one direction, then back through trim to the maximum change in the opposite direction and then back to trim again, data curves will reveal the effects of too rapid rate of change as a hysteresis loop.

Speed stability must be determined for no change of power setting or configuration. The slope of the curve of stick position plotted against airspeed will then be indicative of the moment change of the aircraft due to inadvertent airspeed changes. It is very difficult to obtain speed stability curves at low airspeeds because of the resultant vertical velocities which accompany the technique described. This is because the vertical velocity is generally very sensitive to power changes for V/STOL aircraft. The accelerating and decelerating effects due to inertia have a strong influence on the vertical velocity induced at a given airspeed with attendant large variations in control position.

Directional stability and dihedral effects can generally be obtained at the same time by performing sideslips while recording the pedal and stick lateral movements. In ranges where the weathercock stability is positive, data taken during slow continuous variation of sideslip angles generally provide a well-defined stability curve. When the aircraft is unstable directionally, large amounts of scatter appear and well-defined slopes are difficult to obtain. Under these conditions, the range of instability can generally be demonstrated by establishing a sideslip angle in the unstable range, fixing the controls and recording the subsequent limit of divergence of the aircraft in sideslip angle and/or heading, and yawing velocity. This can be a dangerous technique if the range of instability is over a very wide regime of flight since control power can degenerate to where it is not powerful enough to overcome the unstable moments.

Trim changes and power effects generally require a systematic coverage of most of the flight envelope of the aircraft. With conventional aircraft it has generally been found sufficient to maintain constant airspeed while power and/or configuration changes were made. With the VTOL types however, because of the additional variables involved, additional techniques must be used to completely cover the various possible combinations of angle of attack, power, airspeed, and configuration that could be obtained in a conversion flight range. Techniques include maintaining level flight and constant fuselage attitude throughout the airspeed range while converting from hover to cruise configuration, holding power and fuselage attitude constant while the conversion is accomplished at varying rates, and holding both airspeed and fuselage angle of attack constant while the power (that is, vertical velocity) is varied throughout the feasible range. The first two tend to highlight trim variations in the conversion range and provide data which could be used to establish transition corridor limits. The third defines the usable range of descent or climb angles through establishing, in particular, limiting rates of descent for given airspeeds or conversion angles. This technique reveals such criteria as limiting rates of descent due to stall and limits due to deterioration of stability characteristics which result in erratic uncontrollable motions of the aircraft. Consideration must also be given to operation on the back side (that is, unstable variation with speed) portion of the power required curve. It has been established that by use of the proper technique, landing approaches can be made in the low speed range under conditions where unstable power variation with speed is present. This capability must be demonstrated for V/STOL aircraft if optimum handling qualities are to be maintained.

Maneuver stability characteristics of VTOL configurations at low speed generally involve flight procedure which has been applied to the helicopter. For example, longitudinal pull

and hold test maneuvers to document maneuver characteristics or divergence tendencies are used rather than the more conventional wind-up turn procedure at the lower airspeeds where high angular rates are present. For small bank angles and  $\phi$  turns, normal acceleration and pitching angular velocity are the important parameters. At higher speeds, where significant changes in lift can be made by changing angle of attack, maneuver stability characteristics appreciated by the pilot can be related to the buildup of a normal acceleration following a pull and hold of the longitudinal control. At lower speeds, where a change in attitude of the aircraft does not produce appreciable lift or change in flight path, the buildup and peaking of the pitch angular velocity becomes the primary parameter. In either case the basic criterion for maneuver stability is that evidence be present in the time histories, within ten seconds of the start of the maneuver, of the eventual peaking of the normal acceleration and/or pitching angular velocity. Although the time history of these parameters are not in themselves the specific characteristics the pilot appreciates, experience has shown that the specific shape of these time histories can be correlated with the pilot's opinion of the characteristics of the aircraft in general maneuvering and rough air flights, and provides a numerical representation of the maneuver stability characteristics.

Dynamic characteristics are separated into longitudinal and lateral directional. Modified longitudinal oscillations tend to involve simultaneous changes in airspeed, altitude, and angle of attack. Thus it is difficult to delineate the oscillatory characteristics of the VMI configurations, particularly at low airspeeds, with respect to the classical concepts of short period and phugoid oscillations. Two distinct techniques are used in flight to produce oscillations. The first involves an abrupt control pulse intended to produce a disturbance in angle of attack or attitude at constant airspeed. The second also involves a control pulse but of a longer duration intended to produce a disturbance of airspeed. In each case, the resulting oscillation can generally be defined with respect to period and damping by the recorded time histories of the normal acceleration and pitching angular velocity. In some cases, any control-induced oscillation expands at such a rate as to appear almost a pure divergence in the initial cycle. In the presence of static instabilities, control pulses can result in a pure divergence. Situations such as this make it difficult to obtain a time history of any length sufficient for quantitative means to define stability characteristics. In this case, it is desirable to supplement these data by obtaining records in both smooth and moderately rough air wherever the pilot flies the control as long as he can tolerate and the ensuing buildup of attitude of the aircraft are recorded.

Lateral directional handling qualities, in addition to static stability and Dutch roll oscillations, include primarily the characteristics during partial-fixed turns. In the case of unsatisfactory characteristics, time histories show the roll angular velocity reversed within a few seconds after the control input or what appears to be the beginning of an expanding oscillation. In marginal cases, the roll angular velocity rate history is non-reversing and, although it reduces to zero, its roll velocity is built up in the opposite direction.

### 1.5 Flight Testing as Ground Effect

Testing as presented to the ground is a rather a operation for aircraft of mixed handling characteristics since there is little or no time for recovery from disturbances upset or the onset of unexpected angular and translational motions. However, the necessity to evaluate in ground effect some wind tunnel results. As an example, the effect of ground proximity on the lift and pitching moment characteristics of low aspect ratio wings as a significant design consideration in computing their take-off and landing characteristics. The increase in lift through the ground effect is beneficial in reducing ground roll for this type of aircraft. However, pitching moment changes and reversals affect the pilot's perception of control in landing flare and rotation at take-off. As a good consideration, it is important to measure ground effect properly in evaluating low aspect ratio designs so that a comparison can be made between wind tunnel results and flight

Another example of the problems of ground proximity is that of V-STOL aircraft with highly deflected slipstream using large flap systems. Flight tests of the XZ-35 aircraft were of great concern when evaluating the effects near the ground because of the large changes in pitching moment which occurred and the effects of recirculation on the performance of the propeller. The effects of reingestion as well as recirculation will be discussed below.

Two flight test techniques have been developed for the purposes of measuring ground effect. One method, which is presented in Reference 9, is to make a level "fly-by" at various heights above the ground at various air speeds. This method relies wholly on onboard measurements of aircraft acceleration, thrust, and attitude for calculating lift and drag. A special camera facing downward from the undersurface of the fuselage is used to measure aircraft height, rate of change in height, ground speed and pitch attitude. This method has two inherent deficiencies. First, it requires a large number of passes, one for each height and airspeed of interest. Second, repeatability is poor because of inaccuracies in measuring such characteristics as angle of attack and thrust. Further, the reduction of data from the camera is extremely time consuming and tedious.

The second technique for measuring ground effect is the external tracking of the aircraft while it makes steady descents at constant angle of attack and power setting. The aircraft flares caused by ground effect will cause a change in drag which in turn produces a change in airspeed, and the change in pitching moment which accompanies the change in airspeed will require longitudinal control to hold a constant angle of attack. Such a technique was utilized in tests of the B-71 aircraft and showed a non-linearity of lift coefficient with ground proximity. The results may be found in Reference 10. This method holds promise of improved accuracy but does have limitations. First, the initial sink rate and power setting must be established such so wind and thermal effects of the atmosphere must be small so that the aircraft can maintain an equilibrium glide slope. Second, the pilot must maintain a constant angle of attack, usually from signals on an indicator difficult to track and which may have a flow induced error as a function of ground height. Data reduction again is tedious and subject to the usual errors of reading the aircraft's position and attitude in each fall.

Experience has shown that both methods lack repeatability and are greatly subject to the effects of atmospheric turbulence and pilot proficiency in performing the required maneuvers. There is much need for improvement in the data reduction technique and more experience is required, particularly with high aspect ratio aircraft to improve these techniques.

A problem which plagues all V-STOL aircraft because of their high downwash velocities is that of recirculation of slipstream and exhaust after impingement with the ground while in ground effect. Reference 11 reports unsteady flight behavior of the XZ-142 tilt wing aircraft in landing approach at speeds of the order of 25 knots. Characteristic of this unsteady behavior was a strong loss of lift and weakened directional and lateral controllability. This problem was attributed to spitting of the deflected propeller slipstream in such a manner that it began to precede the aircraft and recirculate into the incoming flow. This phenomenon was similar to that of the XZ-35 aircraft which was mentioned earlier. This ground effect phenomenon had been predicted since it had been encountered in wind tunnel tests. However, it is difficult to establish the limitation of low speed operation in flight. One of the XZ-142 aircraft was damaged in attempting to evaluate this phenomenon.

One form of evaluation for a better understanding of flow characteristics in ground effect is performed by attempting to visualize the flow phenomenon of recirculation and ingestion. Utilizing the XZ-35 deflected slipstream aircraft, flights were made over the runway which had been dusted with Royal Purple extinguishing powder. Flights were made at a constant attitude and airspeed. In Figure 18(a), the flight speed exceeds that of the recirculated slipstream and the disturbance remains aft of the wing leading edge. In Figure 18(b) the velocity of the aircraft is less than that of the recirculated slipstream

and the disturbed area, indicated by the dust cloud, precedes somewhat ahead of the aircraft, even out of ground effect. In Figure 18(c) where the attempt was made to assess the same condition in ground effect, the airspeed was too low to prevent a landing even though power was applied as rapidly as possible. These results indicated that as airspeed is decreased, the deflected slipstream is recirculated through the propeller disc as turbulent air causing a partial loss of thrust and turning effectiveness. Flying over the Ansul powder at gradually reduced speeds would make it possible to predict when the recirculated flow would affect the lift of the aircraft.

This problem is common to the jet-lift aircraft as well as to the deflected slipstream aircraft. In the jet aircraft, the effects are compounded by the reingestion of exhaust gas into the engine inlet which degrades the engine performance. The Ansul powder technique could not be applied to the jet-lift VTOL aircraft since the powder dispersed too rapidly and flow patterns were not visible. Tests utilizing crushed nut shells also were tried but without success. The use of Corvis oil in the jet exhaust, which has been useful in thrust reversal tests, completely engulfed the aircraft in a cloud of smoke and flow patterns were not discernible. To the present time the best picture of flow patterns for jet aircraft has been obtained over a wet runway, utilizing the recirculation of the water as a flow visualization technique. Improved testing techniques are needed to explore more safely the STOL limitations of V/STOL aircraft. Flow visualization methods are not a good solution because they have not proved successful for all types of aircraft.

#### 1.6 Variable Stability Aircraft

Variable stability aircraft have been used in varying degrees of sophistication for many years. They have made large contributions to the establishment of handling qualities criteria. However, as new generations of transport aircraft have been entering into the consideration of V/STOL capability, new problems in low speed operation have been generated. Consider for example attempts to predict characteristics of the Lockheed C5-A aircraft, particularly if STOL capabilities were envisioned as a capability. The handling qualities of these new large transport-type aircraft can be expected to be quite different from those of present airplanes, even in their conventional design. Some requirements such as dynamic longitudinal stability which have been based chiefly on fighter experience, prove to be unduly restrictive while other characteristics seem to be not restrictive enough.

While at present the problems of predicting the handling qualities of low speed, large aircraft are receiving major attention, it should not be forgotten that the variable stability aircraft still finds its uses in trying to evaluate the characteristics and handling quality requirements of more accepted aircraft in which there has been greater experience. As an example, the reader is referred to Reference 12 which describes a variable stability helicopter utilized for simulation of VTOL handling qualities. Examples of variable stability aircraft being used for examining problems of large aircraft are the Cornell B-26 aircraft described in Reference 13, the Lockheed Jetstar described in Reference 14, and the Boeing 367-80 described in Reference 15. These variable stability aircraft differ in type and size ranging from the propeller driven B-26 at 35,000 pounds gross weight to the jet transport 707 at 175,000 pounds. The validity of the results when a small aircraft is used to simulate the low frequency longitudinal dynamics of the large, high-inertia aircraft such as the C5-A type naturally comes into question. The small aircraft must be forced into a much lower frequency than its natural frequency and providing valid, long period response data is tied directly to the type of variable stability system used.

Currently, variable stability systems have been mechanized either by (1) a response feedback or (2) a model controlled system. Descriptions of these systems can be found by the reader in Reference 14 which is a model controlled system and Reference 16 which is a response feedback system employed in the X-22 aircraft. The response feedback technique senses the aircraft response variables and transmits these as commands to the control surface actuators. Thus the aircraft's aerodynamic stability parameters can be changed



artificially by generating forces and moments proportional to the aircraft responses. In the model control technique, an onboard computer programmed to simulate the model aircraft's aerodynamic parameters is employed. Thus the pilot flies the model through the computer and the feedback loops force the airplane response to match those of the model. Each variable stability technique has its limitations. The response feedback system, although the earliest in use, is limited by (1) accurate knowledge of the basic aircraft's aerodynamic characteristics and (2) frequent inflight calibration to check the values of aerodynamic parameters being simulated. Processes for evaluating the aerodynamic parameters from the aircraft responses are tedious and in certain cases inherently inaccurate although an analog computer can relieve this somewhat. Simulation of the large-inertia, long-period large aircraft for example, requires gains of the response feedback system to be maintained with great accuracy to cancel the basic aircraft's short period as gross weight and center of gravity change due to fuel use. On the other hand, the model following technique for simulating the short period modes requires higher feedback gains to keep the errors between the basic aircraft response and the model output small. The use of high gains is limited by system noise, instabilities and non-linearities. In addition, applying model following to a flexible aircraft requires the gains to be limited to avoid exciting structural modes. Limiting the gains reduces the accuracy of the simulation.

A further aspect of using variable stability aircraft in flight simulation has to do with cost. Large aircraft with complex systems are inherently expensive to operate and one must limit the number of flight hours devoted to a program. In some large scale programs the costs run to figures as high as many hundreds of thousands of US dollars for one flight. A prudent view is that flight simulation be complemented as largely as possible by ground based simulation. As discussed previously, by the use of simulators a broader matrix of parameters including those "unsafe for flight" can be accomplished without the cost and risks of the flight tests.

An example of the use of this approach, given in Reference 17, was used to study the longitudinal control requirements for a very large aircraft such as the C5-A utilizing the Boeing 367-80. The results in Figure 16 illustrate that ground based simulator results covered a broad range of pitching moments due to angle of attack, and the flight test points served as validation of the trends established by ground based simulators. The lack of flight test points in the region of low stability where long periods are encountered reflects the difficulty of operation in this area.

Variable stability aircraft have contributed valuable assistance in aiding the development of new aircraft designs. However they are limited in their capability to define the effects of aircraft size including the aerodynamic parameters peculiar to large aircraft, and the effect of pilot position. In particular, small, variable-stability aircraft fail to reproduce realistic translational accelerations, and sophisticated ground based simulators must be considered to study this effect.

The presentations concerning flight testing techniques in this section have borrowed heavily from Reference 18 by Anderson and Schroers and recognition is given to their endeavours.

## 2. SPECIAL RESEARCH AND SAFETY REQUIREMENTS

### 2.1 Special Instrumentation Requirements

The subject of special instrumentation for V/STOL flight testing divides itself generally into three areas of consideration. These are, (1) Instrumentation essential to the flight mission, (2) Instrumentation required for evaluating the test objectives and (3) Instrumentation associated with variable stability systems. Any one of these topics is a course of study in itself. Only a brief treatment will be afforded each in these notes.

The very low velocities associated with V/STOL flight have required additional displays on the pilot instrument panel of angle of attack and angle of yaw and a much more sensi-

tive indication of flight velocity. Other requirements peculiar to a given installation exist such as for example the tilt angle of wings, ducts, or shafts, but these will not be treated in any detail in this presentation. It has been found advantageous in some installations to include an instantaneous reading of vertical velocity when the aircraft is particularly susceptible to rapid changes in vertical velocity with power setting. This is generally accomplished by means of combining a pressure signal and an accelerometer signal to provide the instantaneous reading. The problems of supplying adequate displays of angle of attack, angle of yaw and velocity have received considerable attention. Generally, the means employed to determine the angles is by counter-balanced, freely-turning vanes which are aligned by the action of the air on the vanes. These vanes are generally coupled with a transmitting autosyn capable of deflection over the full range to be measured. The important aspects of the autosyn receiver are that it be of sufficient sensitivity and that it have low friction. The most important consideration regarding the use of such equipment as this is that it be in a position on the aircraft to indicate the true angulation relative to the freestream. For some types of aircraft, this is extremely difficult because of the significant induced effects of the particular device used for generating vertical lift such as rotors, lift engines, propellers, etc. Frequently the vane devices are mounted on long cylindrical booms to project them sufficiently far ahead of the aircraft to escape these effects. It should be noted that satisfactory solution of the problem of presenting sufficiently adequate angular information has not yet been obtained although those devices which have been used have provided sufficient information to enable the tests to be made.

With respect to the measurement of airspeed, although many devices have been employed to attempt a better presentation, it yet remains for a completely acceptable system to enter upon the scene. Currently, efforts are being made by several researchers using new techniques which have much greater sensitivity to airspeed variations and better indication of flow angulation than anything yet in use. In the past, shielded, double-ended pressure pickups have been employed in an interconnected manner to provide an average pressure difference reading. Utilizing this technique the forward facing pickup gives the total pressure while the rearward facing pickup supplies low-pressure reference information. If the flow reverses, the pickups interchange function. Display information to be utilized with this equipment is commercially available and generally is satisfactory. For the low airspeeds which are involved, it is often necessary to supply temperature compensated equipment because of the high sensitivities which are required. Such equipment has been developed. It is important to note that very often it has been found necessary to provide dual systems for airspeed indication since the sensitivity of the system required for the low speed indication precludes its utilization at the higher flight speeds. It is likely that this requirement will continue with the high sensitivity system being automatically disabled as the airspeed increases.

Additional research is being pursued to generate devices which can be installed on lifting surfaces to indicate their effective angle of attack. Since this information is that which is really required and desired from a flight control standpoint, it will have considerably more significance than the freestream flow direction angles supposed to be indicated by the vanes. Through the use of such equipment on the lifting surface, proximity to stall and the avoidance of incipient divergent conditions may be permitted. The application of hot-wire anemometry is particularly interesting from this standpoint.

It is necessary to adequately document all of the pertinent information regarding surface positions, angular rates, translational velocities, atmospheric conditions and power settings which are associated with a given V/STOL flight test. To accomplish this a variety of equipment is necessary. Most of this equipment, much of which was designed specially for application to V/STOL flight testing, is available in satisfactory form on a commercial basis. The majority of this equipment is of the optical recording type such as air-damped accelerometers, turn meters which utilize electric driven gyros, magnetically and liquid damped angular velocity recorders, and recording tachometers. In addition to this equipment, linear and circular control position transmitters, photo panel data recorders and strain gage control information recorders are provided. In some more modern

installations, the information which would be recorded by onboard devices such as photo panels and oscillographs is telemetered by methods such as FM/FM pulse code modulated systems whereby rapid transmission of data on a time-sharing basis can be accomplished. This type of system is extremely valuable since it allows immediate analysis of the data by computational means on the ground and a more adequate monitoring of the program. In addition, in the event of damage to the aircraft, valuable flight information is not lost. A description of the equipment such as is generally utilized for flight test of V/STOL aircraft can be found in Reference 19. In Table I, extracted from Reference 19, are shown many of the characteristics sought in V/STOL testing, the technique employed, data recorded, and the manner of data presentation.

Finally, we shall consider the instrumentation required for variable stability systems. Perhaps one of the best descriptions of the variable stability system is contained in Reference 20 wherein the variable stability system proposed and being prepared for the X-22A tilt duct aircraft is described. A few basic diagrams and some description will be borrowed from this reference to make this presentation. A typical diagram of a basic loop for the variable stability system is shown in Figure 20.

A variable stability airplane may be defined as an airplane equipped with an automatic-control system in such a way that significant parameters of the airplane's motion and control, in or about one or more axes, may be altered in flight in a predictable manner. An auxiliary but very necessary part of the automatic-control system is an adjustable "artificial feel" system for each axis of variable stability. For example, a three-axis variable stability airplane might be capable of changing the frequencies and damping of the controlled airplane about the pitching, rolling and yawing axes, and at the same time changing the coupling that exists between these axes from that which exists in the basic airplane. The artificial feel system is important because it provides coupling between the pilot and the airplane and it is the closed-loop pilot-airplane system that is of primary interest in the use of a variable stability airplane, whether that use be research, training or education. "Flying qualities" is the term used to describe the suitability from the pilot's viewpoint of the closed-loop pilot-airplane system for a specific task.

The mechanization of a variable stability system involves (1) a provision in each controlled axis for taking hold of the airplane's flight control system with a servo of adequate power capable of responding to system electrical signals, (2) a system of sensors and signal processing equipment adequate for the design goals of the system which can measure all of the airplane response variables of interest, and (3) an artificial-feel system which permits changing control force gradients, non-linearity such as breakout forces or preload, and gearing between the aerodynamic flight controls and the pilot's inputs.

The X-22A variable stability system is a response-feedback system. It is a four axis system; thrust, pitch, roll and yaw. It is not possible to describe all of the many factors of this system; these can be found in the reference if the reader desires to pursue them. It will suffice for our purposes here to consider only the complexity which is associated with such a highly sophisticated system as that in the X-22A. It is obvious that lesser sophistication and fewer axes can be considered in any aircraft equipped with a variable stability system. For example, a system employing only variable stability in yaw to study that mode uncoupled is possible.

Let us consider as an example of a complex multi-axis system, the variable stability system for the pitch axis of the X-22A aircraft. A diagram of this system is shown in Figure 21. After passing through the function generators and manual gain controls, signals corresponding to the various airplane response and control system variables are summed to provide the signal  $\delta \delta_c$ . This signal represents the incremental command to the VSS pitch servo with two different compensations available. The derivative term  $\delta \dot{\delta}_c$  provides compensation for control system lags while the term  $\delta \delta_c / (1 + \tau_c s)$  provides a variable static gain to account for changes in elevator effectiveness with duct exit dynamic pressure. The other two input signals summed with the compensated  $\delta \delta_c$  signal, are



alternate methods provided to eliminate control system transients and airplane trim disturbances when the VSS is engaged. These signals remain constant after engaging the VSS. The manual balance circuit provides a back up for the automatic balance and also has considerable utility for system monitoring and trouble shooting. During VSS operations the SAS is effectively locked by causing the two servos of the dual-redundant system to cancel at the mechanical summing point downstream from the VSS servo. By this means, failures in the locked out SAS will be detected if the cancellation is within tolerances, yet for normal operations the VSS will not have to compensate for the SAS. The upper right corner of Figure 21 shows the generation of the reference duct angle  $\alpha_{ref}$  for transition and an  $\alpha_{in}$  for fixed operating point operation. When the VSS fly-by-wire switch in the input to the summing amplifier is in the fly-by-wire position, the pitch servo is commanded only by the evaluation pilot's stick position without any feedback of response variables. The source of each response feedback and control systems signal is shown on Figure 21 and its purpose is given in Table II.

Instrumentation technology for variable stability systems is a special field in itself and requires a high degree of competence on the part of those who utilize it. The miniaturization of solid state equipment has contributed greatly toward its sophistication and the ability to employ it in research aircraft without large weight penalties.

## 2.2 Pilot Safety Considerations

The considerations of safety in flight have been dealt with in some degree under the section describing the simulators wherein the use of the simulator to adequately define flight safety boundaries prior to flight was portrayed. Many times it is possible to simulate the characteristics of a new aircraft on a variable stability aircraft to give in-flight familiarization with the characteristics of the test vehicle before the vehicle is flown. These pre-flight flights generally are flown with relative safety since another pilot is in the second cockpit who could take over with normal controls if necessary.

The sequence of test flights should be arranged in such a manner as to gradually expand the envelope of flight conditions. Stresses and amounts of control used for trim and maneuvers must be monitored on a flight to flight basis during the feeling out process. The establishment of safe boundaries within the limit of trim in accelerating flight and the limits of controllability with respect to flow separation in reduced power segments, directional capabilities, and limits of the instabilities must be established. Once these are established perturbations within these ranges can be accomplished with relative safety.

Currently, most V-STOL aircraft are being fitted with emergency ejection equipment for pilot protection in the event of catastrophic failure. This equipment generally has capabilities for zero altitude recovery and for rapid deployment of recovery devices to provide survival even in the event of ejection in the inverted position at altitude. Obviously there are conditions for which this equipment cannot guarantee satisfactory escape. Therefore, it is necessary to schedule the test program in such a manner as to preclude the necessity for ejection in these conditions if at all possible. Experimentation at altitude in the low speed regimes of flight as described previously, contribute towards avoiding this kind of emergency condition.

Further considerations involve proper arrangement of the cockpit with regard to displays and controls. It has been found extremely important to provide adequate and proper arrangement to prevent the inadvertent actuation of various special equipment and to guarantee the pilot necessary information quickly on the instrument panel without the need to search for the desired variable. Human factors engineering plays a great part in the solution of these problems and in the proper consideration for pilot safety.

## 2.3 Special Airframe and Propulsion Needs

The most important aspect of airframe and propulsion needs in the V-STOL aircraft is that of the coupling which is required to perform the special capabilities of V-STOL.

flight. Control of the aircraft in the low speed regime requires integration of airframe aerodynamic controls and those of the particular propulsion system that is being used to supply the vertical force to support the aircraft. Many times, aerodynamic controls can be made more effective by properly locating them within the efflux of propulsion lifting systems. It is essential for the controls to respond with proper time constants in addition to being of sufficient power if proper control is to be realized. Thus, the configuration and arrangement of the airframe must give special consideration to these needs.

The propulsion system must be capable of supplying not only that power required to support the aircraft in vertical flight and that required through the transition, but also of providing trim, control and maneuver capability. This capability is provided by many different schemes in the different types of aircraft being employed. Pure jet reaction controls often times are used which are powered from a compressor bleed or from the hot gas system. Sometimes augmenters are used with these systems to increase the ratio of control power available to required engine power. The various types of rotary wing devices employed on V/STOL aircraft which are used for control and trim represent an augmentation of this sort.

The propulsion unit utilized in V/STOL aircraft must have proper time constants in its response to control if it is to perform the control functions normally required. Droops in the acceleration curve must be minimized or eliminated if the engine is to be used for such characteristics as direct lift control which have been shown to be desirable for many STOL and VTOL missions. If a continuous bleed system is used for trim and control, it must be assured that the system is capable of producing the necessary control power at all engine settings.

Particular attention must be given to the interactions between the airframe and propulsion installations. The engines and augmented propulsion devices to supply vertical lift often times react with surrounding airframe components to produce adverse reactions resulting in increased control power or poor performance. These must be avoided if possible. Of particular concern is the possibility of stall or other separated flow phenomena induced by these interactions in particular modes of flight, where the resulting moments or forces may occur with such rapidity as to be uncontrollable or with such force as to exceed the capability of the control system.

Finally, it must be assured that the propulsion system provides sufficient capability in thrust to weight ratio to meet the necessary requirements for handling and control in all flight regimes within the operating flight envelope. This will be discussed in more detail in the next section.

#### 2.4 Redundancy

The term redundancy can be applied to many aspects of the V/STOL flight testing and landing qualities assessment. We shall consider the following in brief: stability augmentation systems, instrumentation systems and propulsion.

The use of redundancy in SAS systems primarily is of concern where failures of that system can produce dangerous out-of-trim conditions (hard-over failures) or divergent oscillatory behavior that can result in exceeding structural limitations of the airframes before the pilot has time to adapt to this new dynamic situation. If the failure can be handled on a gradual degradation basis without imposing this type of problem on the pilot, redundancy is not essential. However, redundancy where it can be provided at reasonable cost may often pay for itself in the ability to continue the flight test program without interruption once the aircraft is airborne.

Redundancy in the instrumentation of the aircraft and in the instrumentation for recording pertinent flight characteristics for evaluation must be based on the impact of the failure of this equipment for safety of flight and test performance. In the case of basic flight instrumentation, reasonably good reliability can be assured as a result of utiliza-

tion of equipment of proven capability and little need exists for redundancy. For the instrumentation used for flight evaluation, the redundancy must be based on the reliability of the equipment involved, and the impact of the loss of this information or the need to terminate a test because of instrumentation failure. These considerations vary from configuration to configuration and must be assessed independently for each program. In dual piloted aircraft redundancy of instrumentation is considered to be essential for those aircraft which have a variable stability system. The provision of such duality, as noted previously, prevents entry into restricted flight regimes without the knowledge of the test pilot and provides the second pilot with the capability of overriding such control inputs as may be disastrous.

The duplication of actuators to flight controls often times is employed to avoid the loss of an aircraft in unexperienced conditions in the event of system failure. Such a provision was made on the X-22A aircraft where a dual hydraulic system was installed. The irony of that installation is that even the redundancy did not preclude a catastrophic failure, since both systems failed almost simultaneously. The cause of these failures was due to the vibrational environment in which they were operating. It is important to assess properly the environment since it has a strong bearing on the necessity for redundancy.

Redundancy in the propulsion systems involves simply the provision of adequate power to provide for an engine-out condition (multi engine configuration). If a vehicle is being constructed solely for research purposes, such redundancy usually is considered of sufficient importance that it is included. If the vehicle is being constructed for prototype purposes, the mission application will generally dictate the amount of redundancy in propulsion which is to be installed. Generally for civil aircraft, the regulations are such that engine-out conditions must be met and redundancy is mandatory. For military installations sometimes the risk element is the determining factor and redundancy is not provided.

## 2.5 Tether Rigs

The use of tether rigs in the initial phases of flight demonstration to restrict the motions to those which will not cause catastrophic failure has sometimes lead to undue restriction in the development of the particular configuration. The categorization of tether rigs in this case does not apply to the ground test stands which were described in Section 1.3. Tethers are necessary on those stands to restrict the angular motions to those which can be safely handled and have little adverse effect.

Many developers have resorted to the tether rig and many have successfully employed this technique. Generally, the procedure which is used is to restrict the angular and translational motions in such a manner that the aircraft is returned to the ground in an upright position in the event of the onset of upsetting moments or sudden translational forces of greater magnitude than can be controlled by the pilot. In practice, the tethers are kept short at the beginning of the investigation and are gradually lengthened to provide more freedom as confidence is gained in the control capability.

It has been found however, that tether rigs can unduly compromise the evaluation of the control capability and may lengthen the time required for flight demonstration in hover. A particular instance in which this occurred was the demonstration of the VZ-4 ducted fan aircraft. During the tethered tests, severe and uncontrollable erratic motions of the aircraft appeared to exist and the aircraft would pull sharply against the tether. The developer suspected this problem and by screwing up his courage took off the tethers and attempted a free flight hover. It was discovered that the restraints on the vehicle caused by the tether were basically responsible for the seemingly uncontrollable condition, as a result of the moments and forces put into the airframe by pulling against the tether limit. The first flight without the tethers confirmed the capability of the control system and the test was able to proceed. Thus, the application of tethers for testing purposes must be used carefully and judiciously. This is not meant to infer that tether rigs should not be employed. However, the results obtained utilizing these rigs must be a subject of careful interpretation.

### 3. SPECIFICATIONS OF HANDLING QUALITIES

#### 3.1 Terminology

A considerable amount of confusion has existed regarding the terminology employed in V/STOL flight testing and handling qualities assessments. Recently, the US Air Force sponsored an Ad Hoc V/STOL terminology committee which generated a listing of some pertinent terms which have been given as wide a dissemination as possible for comment. This listing is included here for familiarization of the reader with such terms as are defined. It is emphasized that this list is not complete nor is it necessarily entirely correct. However, it does represent the most recent attempt for standardization of terminology. A revision of this list with appropriate additions will be released by the AGARD Handling Qualities Committee in a publication to be prepared soon which will not only contain this listing, but will serve to update the basic document of Reference 21 published by AGARD concerning V/STOL handling qualities.

#### V/STOL TERMINOLOGY

##### Basic Letter Terms

VTOL - Abbreviation for vertical takeoff and landing. Pronounced by letter or as a word and used as an attributive adjective designating heavier-than-air aircraft which have VTOL capability.

STOL - Abbreviation for short takeoff and landing. Pronounced by letter or as a word and used as an attributive adjective designating heavier-than-air aircraft which have STOL capability.

V/STOL - Abbreviation for vertical and short takeoff and landing. Pronounced by letter or as a word and used as an attributive adjective designating aircraft which have both VTOL and STOL capability.

ATOL - Abbreviation for airplane-type takeoff and landing. Pronounced by letter or as a word and used as an attributive adjective designating a takeoff and landing in which lift is derived primarily by the forward flight dynamic pressure ( $q$ ) acting on non-rotating aerodynamic surfaces (wings).

##### Flight Regimes

Powered Lift Flight Regime - That flight regime of any aircraft in which controlled, level flight is possible below the power off stall speed and in which part or all of the lift and/or control moments are derived directly from power plant(s).

Hovering Flight - Flight primarily supported by power plant(s) derived lift.

Hover - To remain stationary relative to the air mass.

Spot Hover - To remain stationary relative to a point on the ground.

Translation - Horizontal movement in any direction relative to a fixed point.

Air Taxi - Forward translations in close proximity to the ground, in the powered lift flight regime.

Transition Flight - Flight at airspeeds below the power off stall speed, where lift is derived both from power plant(s) and the dynamic pressure ( $q$ ) resulting from forward flight.

Transition - The act of going from the powered lift flight regime to the aerodynamic flight regime and vice versa.

Conversion - The act of making the configuration changes to a VTOL, STOL or V/STOL aircraft necessary to go from the appropriate takeoff configuration to the aerodynamic flight regime.

Reconversion - The act of making the configuration changes to a VTOL, STOL or V/STOL aircraft necessary to go from the aerodynamic flight regime to the appropriate landing configuration.

Aerodynamic Flight Regime (Conventional Flight Regime) - Flight supported primarily by the forward flight dynamic pressure ( $q$ ) acting on nonrevolving aerodynamic surfaces (wings) at airspeeds above the power off stall speed.

#### Aircraft Capabilities

VTOL Capability - The capability of an aircraft to make vertical takeoffs and landings over a 50 ft obstacle with zero ground roll, where there is not over one aircraft major dimension clearance between the aircraft and the obstacle.

Maximum VTOL Weight - The maximum weight at which an aircraft has VTOL capability.

STOL Capability - The capability of an aircraft to make takeoffs and landings over a 50 ft obstacle is not over 1000 ft total distance.

Maximum STOL Weight - The maximum weight at which STOL capability is possible.

V/STOL Capability - The capability of an aircraft to meet both VTOL and STOL requirements.

#### Maneuvers

Air Run Takeoff (ARTO) - A takeoff using the technique of a vertical lift-off followed immediately by a forward acceleration in ground effect.

Air Run Landing (ARL) - A landing using the technique of a final deceleration in ground effect, followed immediately by a vertical touchdown.

Verticircuit - A vertical takeoff, conversion, reconversion, and a vertical landing.

#### Special Terms

Conversion Angle (CA) - The angle measured from the longitudinal axis of the aircraft to some meaningful reference in the lift mechanism. This angle is approximately 90 degrees in hover and approximately zero degrees in aerodynamic flight. (NOTE: This is a general term. The name of the angle will vary with types of aircraft, such as duct angle tilt angle, vector angle, wing/flap angles, etc.).

Conversion Speed - The minimum speed for aerodynamic flight.

Ground Effect - Any effect on the aircraft performance, stability and control or systems operation due to its proximity to the ground, caused by the aircraft itself.

IGE - Abbreviation for in ground effect.

OGE - Abbreviation for out of ground effect.

Ground Cushion - The phenomena of increased buoyancy experienced close to the ground.

Height Velocity Diagram (Deadman's Zone) - That height and airspeed envelope in the powered lift flight regime which defines unsafe operations in the event of power plant failure.

Recirculation - The phenomenon in which engine exhaust or propeller-/fan-generated windblast remains in or returns to the immediate proximity of the aircraft.

Reingestion - Ingestion of engine thrust or propeller-/fan-generated windblast into the engine inlet(s), usually occurring in ground effect.

Transition Envelope - That portion of the aircraft's flight envelope in which trimmed, controllable flight is possible in the powered lift flight regime. The envelope is defined by such factors as airspeed, height, rate of climb or descent, conversion angle, power, control margins, angle of attack, etc.

Downwash - The downward component of power plant(s) derived windblast directly under the aircraft.

Groundwash - The outward flow of the power plant(s) derived windblast over the ground.

#### Engineering Terms

Rate Damping - The negative reciprocal of the time taken to reach 63% of the final steady state angular or linear velocity resulting from a step control input.

Control Displacement - The displacement from trim of the pilot's control element in the cockpit.

Control Effectiveness - The capability of trimming and maneuvering the aircraft throughout its design envelope.

Control Power - The maximum angular or linear acceleration for full control displacement from any trim condition.

Control Response - The change in aircraft attitude, position, or height in one second from the initiation of a specified control displacement, usually determined for both one inch and full control displacements.

Control Sensitivity - The initial angular or linear acceleration per unit step control displacement from a given trim condition.

Damping Ratio - Ratio of actual damping to critical damping (exponential attenuation envelope for oscillatory modes).

Rate Response - The stabilized angular or linear rate per unit control displacement from any trim condition.

Control System Time Constant - The time required for a control moment to reach 63% of its commanded value after a step control displacement from a trim condition.

Control Force Sensitivity - Control sensitivity per unit applied control force.

Control Lag - Any time delay experienced between control application and initial aircraft response.

Control Authority - The amount of power a given input has over a control system, usually expressed in percent, force, or displacement.



### 3.2 Application of Pilot Rating Scale

It should be recognized that handling qualities are, by their very nature, difficult to define, difficult to measure and always somewhat subjective. There is a need for a standardization of the subjective aspects which, in basic content, are the pilot evaluation reports regarding the handling qualities experienced during any given mission. Prior to the introduction of such rating scales the engineer was dependent upon those adjectives and descriptive phrases considered most applicable by a given individual pilot. A lack of uniform interpretation was often encountered. In 1957 a single rating scale was proposed and subsequently used extensively. This scale was proposed by George Cooper of NASA-Ames Research Center and was appropriately called the Cooper Scale. It emphasized the need for more uniform methods for assessing aircraft handling qualities through qualitative pilot opinion. However, the most widely accepted has been the Cooper or NASA Scale. This scale is presented in Figure 22 where it may be seen that numerical ratings from 1 to 10 are assigned to various descriptive phrases with the lower number being the most desirable. Despite the wide acceptance of this scale, it has deficiencies for some applications as do all other accepted scales.

Recently, it has come under consideration that a single scale should be devised which would both clarify the use of such scales and provide an improved basis for the qualitative evaluation of handling qualities. From consideration of the various categories from which the pilot may select a rating, a revised scale is presently being developed and clarifying descriptions are being devised to provide for individual ratings.

The original Cooper Scale first introduced the basic framework that defines specific boundaries relative to mission accomplishment. Specific category adjectives - Satisfactory, Unsatisfactory, and Unacceptable - were related to grades of quality through both the numerical ratings and the description. The mode of flight as represented by normal operation, emergency operation and no operation was also associated with the categories for illustrative purposes. Confusion resulted from this approach as well as from the references to normal and emergency operations under the numerical rating description for 5 and 6. In effect, two possible boundaries are shown - acceptable for normal and acceptable for emergency operation.

The lack of definition of the emergency condition was confusing to some. A better term might have been limited operation even though this would still require definition under the mission. The doubtful terms with respect to mission completion were introduced to emphasize the difficulty in determining exactly the acceptable boundary.

The inclusion of the term optimum for pilot rating of 1 has virtually eliminated its use as in any category a pilot is always expecting something better to come along and therefore is reluctant to rate an existing situation as optimum. The use of the ratings in the Unacceptable category have been considered to arise too often. These situations may be academic for a specific vehicle but when a systematic variation of stability and control parameters is sought for many vehicles, separation within the Unacceptable range is desired.

The most important factors in the use of these scales of pilot rating are (1) definition of mission, task and simulation situations and, (2) pilot comment. It is obvious that the objectives and criteria of a given handling qualities program and a clear definition of the mission involved must be thoroughly understood by the pilot participant. This requires that specific definitive tasks and maneuvers be selected which will assist the pilot in evaluating handling qualities for the mission. Simulation is always involved to some degree and therefore an understanding of what is left out of a program as well as what is left in must be reached between the pilot and the engineer. The pilot must be able to use all his knowledge and experience to provide a rating which includes all considerations pertinent to the mission whether simulated in the task or not.

The pilot's comments are essential since the use of a single numerical rating cannot possibly represent the entire qualitative assessment. It can be determined from the comments which the pilot makes whether objections on the part of the pilot are related to the mission, or resulted from some extraneous uncontrolled factor in the execution of the experiment, or resulted from the individual pilot's focusing on different emphasis to various aspects of the mission. The use of questionnaires as an aid in obtaining supplementary pilot comments is often very beneficial.

Figure 23 illustrates the decisions which lead to a particular rating. This is in essence a flow chart to enable tracing of the series of dichotomous decisions which the pilot must make in arriving at a final rating. At the bottom of this figure is shown the new scale which is being proposed to replace that used in current rating systems. The use of the letter prefix differentiates the acceptable from the unacceptable ranges. Further, the use of A1 which is generally accepted in technical jargon as being the top or best, clearly indicates that it is considered to be the best; confusion had arisen by use of a simple numerical scale where one might expect that the higher number represents more capability.

The general categorization may be accomplished in a reasonably simple fashion as shown. However, major category descriptions must be supplied which clearly delineate the intent and purpose of each rating. These ratings and their descriptive phrases are shown in Figure 24. It is emphasized that this is not an accepted scale, but is currently being considered for adoption with revisions, if necessary.

The use of the pilot rating scale, together with the quantitative measurements which can be made provide the design engineer with the necessary information to determine the adequacy of the handling qualities inherent in his vehicle. Because of the subjective nature of the pilot rating scale it is currently being proposed by the AGARD Handling Qualities Committee that a distinction be made between V/STOL handling qualities criteria and handling qualities requirements. One consideration of the material presented in Reference 21 has been that it is a mixture of criteria and requirements so that the user tends to interpret the meaning to suit his purpose. Criteria can be defined as standards for judging. They are intended to provide qualitative background information. For example, roll-control criteria should not only point out the magnitude of the desired bank-angle change, but should also make it clear that control power must be sufficient to maneuver in particular tasks and to provide control for trim and disturbances as well. Criteria could and should serve as a guide in establishing specifications or requirements for a given aircraft.

Requirements are quantitative measures of particular flight characteristics of a particular vehicle. They should be easily measurable in flight and be related as directly as possible to the pilot's impression of the aircraft's behavior. They are specifications against which to assess production aircraft. Requirements for one class of aircraft should not be used as a yardstick for another class of aircraft. First must come the meaningful criteria before requirements can be defined.

### 3.3 Mechanical Characteristics of Control Systems

The specification of the characteristics of the control system necessary to guarantee proper handling characteristics of V/STOL aircraft as well as the specifications of the handling qualities themselves was begun in the 1950's. To a great extent these handling qualities specifications were derived from those which had been formulated for helicopters and consequently are not directly applicable to many of the configurations which have been evolved since that time. The first attempt at formal presentation of these handling qualities criteria was made by Anderson in Reference 22 in 1960. Subsequent to the publishing of that paper, in 1962 a working group on V/STOL handling qualities was established by the AGARD Flight Mechanics Panel to formulate recommendations for V/STOL handling qualities. These were published as mentioned earlier in Reference 21. They were based essentially on the material from Reference 22, Reference 23, and Reference 24. It was



recognized by the working group at the time that the specifications which were laid down were sketchy and based on conjecture in many cases rather than on fact. Reference 21 made recommendations for yearly updating of the criteria set forth. Many papers have been published since that time regarding the various aspects of specifications of control systems and handling qualities. However, it is only at present, some six years later that a new committee has been appointed to update the requirements set forth in the AGARD 408 publication.

Since a myriad of publications have been published on the subject of control and handling requirements, it will not be possible to provide a complete updating or review in a short presentation such as these notes. Therefore, since Reference 21 is still the basic document for handling qualities specification, discussion will center about its requirements and comments concerning the opinions for updating will be offered. These comments are gathered from many sources but are primarily furnished from Reference 25 and members of the group working on the rewrite of Reference 21.

The primary consideration of the mechanical characteristics of the control system is that the force-feel of the system as felt by the pilot should not result in objectionable handling qualities at any speed or in any configuration covered by the handling qualities criteria as set forth. In particular, the effects of centering, breakout force, feel, pre-load, friction, free-play, etc., should not result in objectionable flight characteristics or permit large departures from trim conditions with controls free. There should be no undesirable variations in the control force gradients of the longitudinal, lateral, or directional controls. Consideration must also be given to any single failure in powered or boosted systems, artificial trim devices or stability augmentation systems such that the characteristics of the control system as felt by the pilot shall not result in unacceptable flying qualities in the configurations and flight conditions appropriate to emergency operation.

The breakout forces, including friction, feel, pre-load, etc., have been specified to be within the limits shown in Table III. These forces of course must be those measured at the pilot's control in flight or conditions resembling those in flight as closely as possible. These forces have been specified irrespective of size and regardless of the use of a stick or a wheel type control. The height control is permitted to be either a conventional throttle or a helicopter collective-pitch stick.

In addition to specification of the breakout forces, the gradient of force control with stick movement has also been specified to be positive. Further, the maximum movement of control stick has been recommended to be about  $\pm 4$  inches for longitudinal control and  $\pm 3$  inches for lateral and directional control. With these conditions, the total force for the first inch of travel from trim is specified to be not less than the breakout force and equal to or greater than the slope for the remaining stick travel to the limit. For VTOL operation, longitudinal and lateral force gradients of between 1 and 2.5 pounds per inch are considered desirable. For the directional control, the gradient should be between 5 and 15 pounds per inch. A failure in the power control system should permit any maneuver within the design flight envelope to be accomplished with control forces not exceeding 40 pounds longitudinally, 20 pounds laterally and 80 pounds directionally. Current opinion questions the need to make the exact value of the gradients mandatory as long as the maximum forces are not exceeded and adequate control is realized without pilot objection.

The characteristics of height control systems are to be such that the control remains fixed at all times unless moved by the pilot or some automatic system. Adjustable friction locks are desirable, but the limiting forces specified in Table III should be achieved with any friction damper off. A failure in the power control or stability augmentation system should not affect this specification.

Mechanical characteristics of control linkages for power control shall be such as to insure freedom from objectionable flight characteristics including difficulty in trimming

or tendency toward pilot induced oscillations. Failure of a power control or stability augmentation system shall not affect this requirement.

Free play in each cockpit control is to be minimized and in no case exceed  $\pm 1\%$  of total travel. Upon a failure in power control or stability augmentation system, free play shall not exceed  $\pm 3\%$  of total travel.

Wheel throw for wheel type controls shall provide the full lateral control recommended readily with one hand operation and should not exceed  $60^\circ$  in each direction.

Trim systems are recommended to be continuously adjustable throughout the flight range and may be of the press and release type. All trimming devices should maintain indefinitely a setting selected by the pilot unless actuated by an automatic system. Following any failure of a trim system, permanent out-of-trim forces must not exceed ten pounds longitudinally, seven pounds laterally and forty pounds directionally at any speed up to the conversion speed.

For thrust vector control systems, any device acceptable to the pilot has been recommended. However, any selected setting of the thrust vector control should be maintained indefinitely without attention from the pilot. It should be possible for the pilot to select the angular setting for hovering without reference to an indicator. Acceleration and deceleration during the transition should not be limited by the rate at which the thrust vector can be rotated, not should the performance and repeatability of the takeoff maneuver. After failure of the power system it should still be possible to actuate the system necessary for transition.

In addition to the above considerations, the moment generators installed in the aircraft control system which respond to the pilot controller must be designed such that they have minimum dead band and time lag following the input of a signal. It is assumed in this discussion that such capability is provided.

It is readily seen that the intent of these recommendations is to provide a control system which does not impede the capability of the pilot to provide smooth actuation of the controls and that does not require more than minimum attention from the pilot during the VTOL and transition flight regimes. Since the preparation of the recommendations presented here, additional research has been accomplished which indicates certain changes may be desirable. In particular, the desirability of incorporating non-linearities into the control system has been considered. The importance of this capability will be discussed in Section 4. Further, the type of controller to be employed has received some attention. In some cases, a sidearm controller has been substituted for either the wheel or the stick and is found to be acceptable. The controller dead band, breakout forces and control gradients are obviously affected by the type of control which is used. This subject together with many others which have been presented are matters of controversy at the present time and are receiving considerable discussion in the presentation of the revision of these recommendations.

The inability to predict the size-scaling factors on both the mechanical control characteristics and the handling qualities requirements has presented a considerable challenge in formulating a general set of standards. Numerous analytical flight and simulator studies have been directed in improving the understanding of V/STOL handling qualities since the preparation of References 21 and 22. It is indeed a challenging task to convert information from many of these studies to general handling qualities criteria because, for the most part, the results have been particularly difficult to generalize since the total control requirements depend on many interrelated factors.

### 3.4 Longitudinal Axis

#### 3.4.1 Static Stability

The prime objective of V/STOL aircraft is that they be capable of operation from restricted spaces. Handling qualities specifications recommended to date attempt to insure

that capability. In the case of emergency operation following a single failure, this capability is to be retained and the greatest degradation should allow the pilot to safely escape. In this regard the instability of the basic aircraft shall not be so great that during any longitudinal maneuver within the design flight envelope the input of the SAS to provide apparent stability together with the pilot's input at any time leaves less than 50% of the nominal longitudinal control moment for recovery. This specification of the numerical value of 50% has been brought into question upon reconsideration, since this value may be excessive depending upon the frequency of disturbance from which recovery is being attempted.

Reference 21 states that with the most critical loading for all steady forward flight conditions in which the aircraft might be operating continuously, including all the conditions listed in Table IV, the aircraft shall possess positive static longitudinal control position and control force stability with respect to speed. Further, the variation of control position and force with forward speed at constant power settings shall be a smooth curve over the complete speed range appropriate. This capability should be demonstrated over the out-of-trim range shown in the table with the aircraft trimmed at the referenced speed. Some degree of instability is allowable if the flight condition is infinitely a short period, provided the condition is not objectionable to the pilot. Following a failure in the longitudinal SAS, longitudinal instability with respect to speed can be tolerated provided the instrument approach and landing is not compromised, and no less than 50% of available control moment and pitch is available for recovery.

In general, the flight conditions specified in Table IV are those for which effectiveness about all three axes are to be demonstrated satisfactorily. The specifications laid down apply only up to the conversion speed. The conversion speed definition varies of course with the configuration. Since there is no conversion in a helicopter, this speed essentially represents the top speed. For a tilt wing it may represent a condition with the wing at zero tilt. The same may apply to tilt rotors and tilt ducts. For fan-in-wing aircraft, or direct jet lift aircraft, it may be defined as the speed at which all louvers are closed and/or all nozzles converted from vertical to horizontal position. This variation in configuration and therefore definitive flight conditions, is illustrative of the difficulty in generating specific handling qualities specifications applying to all V/STOL aircraft.

Probably no one would question that both fixed and stick free stability with respect to speed are desirable. Such stability is represented in Figure 25. However, even conventional aircraft have been designed with only stick free static stability in the landing approach. These aircraft have been found to be unacceptable under conditions for instrument flight, particularly in rough air. Speed stability is particularly important for V/STOL aircraft because these aircraft are operated at speeds where drag increases with decreasing speed, which make flight-path control difficult. On the other hand, many investigations have pointed out the adverse effects of having too much speed stability ( $M_u$ ). The presence of too much speed stability causes excessive response to horizontal gusts, increases the requirement for angular velocity damping ( $M_q$ ), and for tilt wing or tilt duct aircraft limits the usable speed range at a given wing/duct angle.

Angle of attack stability must also be considered. The operation of STOL aircraft such as the BLC C130, the Breguet 941 and the UF-XS reveals that the pilot uses angle of attack as a reference during approach, and wants the aircraft to return to the reference angle of attack as well as the reference airspeed when the aircraft is disturbed. The operational angle of attack range is limited by angle of attack instability, as for example in the P 1127 aircraft where the limit is only  $8^\circ$ , which in turn limits the maximum allowable glide angle to only  $10^\circ$  in the landing approach. The XV-4 aircraft had angle of attack instability as well as marginal longitudinal control power. This aircraft crashed, possibly as a result of this deficiency. The XV-5A and the Balzac aircraft also have angle of attack instability which limits operation in transition.

Thus, it is seen that additional consideration is required to obtain a more definitive set of specifications which will guarantee longitudinal control throughout the flight regime. The general specification for all types of aircraft may be difficult to define.

The recommendations of Reference 21 state that the general aspects of maneuver stability shall be retained at all conditions up to and including the most critical loading. A pull force on the stick should produce increased normal acceleration and nose up pitching velocity and the variation of stick force should increase approximately linearly with normal acceleration and/or pitching velocity. It is specified that longitudinal control force gradient should never be less than 3 pounds per g nor more than 20. The longitudinal control system should be generally insensitive to gusts and height control inputs. Criteria are established in the event of failure in the longitudinal SAS to specify the amount of control moment remaining for maneuver and the allowable stick forces. In general, 50% of nominal control moment is to be retained for recovery from disturbances following failure. The importance of retaining adequate control power for maneuver cannot be overemphasized. However, the amount of control moment required for this purpose may well be a function of aircraft size and class of aircraft.

The transient response characteristics of maneuvering flight are also specified in terms of the normal acceleration and the rate of pitch or angular velocity which is realized after sudden inputs of the longitudinal control. The performance is specified in terms of the concavity of both the angular velocity and normal acceleration curves which must be turned downward at no more than two seconds following the start of the specified maneuver. This characteristic is illustrated in Figure 26. The maneuver specified is that to produce 0.2 radians per second pitching rate within 3 seconds, or to develop a normal acceleration of approximately 1.2 g within 3 seconds. This specification is considered to be generally applicable and reasonable.

There should of course be no objectionable time delay in the development of angular velocity in response to the pilot's control input. Angular acceleration should be in the proper direction within 0.2 second after initiation of longitudinal control application.

### 3.4.2 Dynamic Stability

The specifications concerning longitudinal dynamic stability in Reference 21 are meager. In general, they state that damping characteristics following a single disturbance should be not less than those given by the normal flight curve of Figure 27 and that no tendency for small amplitude oscillations to persist should be present; also indicated in Figure 27 is the allowable curve for single failure. Further, there should be no tendency for sustained or uncontrollable oscillation resulting from the effort of the pilot to maintain a steady flight path or to maneuver the aircraft within its flight envelope (pilot-induced oscillations). This condition should apply following a failure of power controllers or the stability augmentation system. Further, it is specified that the cockpit control should exhibit deadbeat characteristics following a release from abrupt deflection.

There has been a lack of adequate criteria for the short period and the long period (phugoid) modes for V/STOL aircraft and for the conventional aircraft as well, particularly in the period range around 8 to 12 seconds. In Reference 26 it was shown that requirements for STOL aircraft in terms of a period-damping relationship are not directly related to the criteria from there to a pilot. In any landing approach of a VTOL or conventional aircraft, the pilot is concerned primarily with controlling flight path angle; however, the factors which affect control depend upon the aircraft type. Recent studies reported in Reference 27 for conventional aircraft with high aspect ratios indicated that the lift-curve slope  $C_{L\alpha}$  and the normal acceleration variation with angle of attack  $N_\alpha$  terms, as well as frequency-damping parameters, affect flight path control. It is interesting that for aircraft with lower aspect ratios such as the F-8C Crusader, flight path control in carrier approaches was markedly improved with the direct lift type of control which, in a sense, is a means of increasing  $C_{L\alpha}$ . Since landing approaches for V/STOL aircraft are made with very low effective  $C_{L\alpha}$ , engine power is used as a direct lift

control. It is apparent that factors in addition to period damping must be considered in arriving at dynamic-stability boundaries for V/STOL aircraft. Some of the current VTOL aircraft such as the P 1127 and VJ-101C which appear to need improved damping in STOL approaches, particularly for instrument operation, may actually need more lift control. The interplay of these factors is inadequately defined for V/STOL aircraft and should be studied with greater emphasis as soon as more sophisticated variable stability VTOL aircraft become available.

### 3.4.3 Control Response Requirements

Satisfactory longitudinal control power and sensitivity for maneuvering while hovering in still air with minimal effects of external disturbances are believed to be assured by the recommendations in Table V according to Reference 21. Specifications are also given regarding the aircraft response as a function of control displacement from trim with the provision that these shall obtain at all speeds up to conversion including a 1000 ft per minute descent. Additional specifications regarding control response requirements cover the effectiveness of the control in maneuvering flight, take-off and landing, and longitudinal trim. In general, these specifications guarantee the ability to develop the limiting attitudes or incidences consistent with the operational flight envelope and to provide adequate margins for maneuver in excess of all trim conditions for the various flight conditions cited. The trim effectiveness should allow for reducing all longitudinal control forces to zero within the flight conditions specified in Table IV. Limitations are placed on the longitudinal stick force which limits these forces for normal operation to 10 pounds pull or 5 pounds push, with momentary allowances up to 20 pounds pull and 10 pounds push. Emergency conditions are also specified.

Longitudinal response in damping and hover have been found from flight experience to be generally less severe than roll control requirements. For some VTOL types such as the X-14A and the P 1127, flight experience has shown little need for damping augmentation; in fact, zero angular rate damping can be tolerated in VFR operation. However, this statement is not generally applicable since analytical studies reported in Reference 28 and flight tests in Reference 29 have indicated that for some configurations such as the tilting duct types where the speed stability parameter  $M_u$  is large, both damping and increased control power will be required, particularly for IFR and rough air operation.

## 3.5 Lateral Axis

### 3.5.1 Static Stability

The recommendations made regarding static lateral stability criteria in Reference 21 specify that up to sideslip angles which might be required in normal tactical use of configurations specified for longitudinal stability, basic lateral instability shall not be so great as to preclude the retention of at least 50% of nominal lateral control moment for recovery. (The same comment regarding frequency of the disturbance applies as was made in the longitudinal case.) The aircraft shall provide positive control-fixed dihedral effect (left lateral control deflection needed during left sideslip and vice-versa). (This requirement should apply to both sideslip and crosswind). The positive dihedral effect should be limited so that no more than 50% of the nominal rolling moment is used for trim. No condition should leave less than 50% of the nominal lateral control moment for recovery. These requirements apply generally whether the controls are fixed or free. Control forces should not exceed 10 pounds for stick or wheel except under failure conditions when 20 pounds is allowed.

Reconsideration of these requirements have prompted the following comments in addition to the two parenthetical comments in the preceding paragraph. The roll control must be powerful enough to serve a number of functions. Lateral control is needed for trimming, for controlling upset and for maneuvering. Unfortunately it has not been easy to separate these individual needs and to the pilot, the amount of lateral control needed appears as a total requirement. Upon examination however, the pilot rating of a given configuration

reflects consideration for all the aforementioned aspects. Values of trim control power needed can be calculated from the geometry of the vehicle and the static stability values. Power needed for upset and maneuver, being not only affected by the configuration, but by the aircraft size and specific maneuvers required in the gust environment, must be known. Upsets, in addition, are a function of self-induced flows. Some of these factors which affect roll control power requirements are considered in the following paragraph.

Size effects, both from upset and maneuver standpoints, are indicated in Figure 28. One can assume that the maneuver requirement will be essentially similar for similar types of aircraft for the same mission or task even though the weight may vary considerably. However, it is also logical to assume the basic level of maneuvering control power required will be generally lower for larger size aircraft such as transports since the task itself will not require large and rapid maneuvers. This suggests that the total control power required for maneuvering should be specified for V/STOL aircraft by classes as is done for conventional aircraft. With respect to the effect on engine power plant, total control required for maneuvering can be divided further into (1) steady state or long term aspects to offset aerodynamic effects (speed stability,  $M_u$ , or rolling moment due to sideslip velocity,  $L_v$ ) when operating in steady winds and (2) the short term control inputs required to reposition the aircraft. The steady trim requirements are a function of configuration and the short term input is largely a function of the control system used. It can also be seen from these curves that, at the lower gross weights, gusts and self-induced disturbances dominate demands for control power, while at the higher gross weights the maneuvering tasks dictate the amount needed.

It is well to ask at this point how well this description of size fits with available data. Control power values that have been used in operating various VTOL aircraft are compared in Figure 29 with the sizing formula  $(W + 1000)^{1/3}$ . The example aircraft do not appear to follow any scaling rule; as an example the X-14A has 1/4 the weight of the P 1127 but requires less control power. Also, the control power values for the various aircraft are larger than the AGARD formula which is basically a maneuvering requirement. Assuming for simplicity that the same maneuvering task is applicable to each aircraft, the P 1127 requires high control power for trim to offset a very large dihedral effect ( $L_v$ ) as does the XV-5A, the Balzac and the Mirage III-V. The SC-1 also has recently been shown to have a large  $L_v$  requirement at higher angles of attack. The low control power value appears adequate for the VJ-101C when an attitude stability system is used. However, the control power is nominally rated at 1.2 radians/second<sup>2</sup> but actually seven radians/second<sup>2</sup> is available if one is willing to reduce power completely on one engine. The lateral trim control required for this aircraft is very small and gust upsets are minimized by the attitude stability system. For the X-19A, roll control power was adequate although there were a number of mechanical control systems problems with this aircraft. The XC-142 has 1.2 radians/second<sup>2</sup> available in roll which is judged ample for hovering but may not be entirely satisfactory at slow speeds. During STOL operation at speeds below about 25 knots ground effect and recirculation disturbances can exceed the control available as evidenced by the landing accident in 1965.

Thus, it is seen that considerable lack of depth in the present criteria for lateral control exists. The control power requirement is obviously not well defined by the present AGARD formula.

### 3.5.2 Dynamic Stability

The present recommendations from Reference 21 are that lateral oscillations should exhibit characteristics the same as those recommended for longitudinal oscillations. Spiral stability is to be positive for all normal flight conditions up to the conversion speed. In the event of a failure in the SAS, negative spiral stability can be permitted provided the rate of divergence at the trim conditions is not so great that when controls are released in a steady 10° bank turn established from trimmed laterally level flight, the bank angle is doubled in less than 20 seconds.



There should be no objectionable time delay in the response to lateral control application. In any case angular acceleration should be in the proper direction within 0.2 seconds after initiation of pilot control application.

### 3.5.3 Control Response Requirements

The same conditions are applied to the lateral control response for the same flight conditions as specified for longitudinal control (Table IV). The response for full control input is recommended to be not less than  $10^\circ$  in the first second and the response for the first inch of control displacement from trim should, for both the normal and single failure cases, be equal to or greater than the response per inch of remaining travel. This recommendation is general throughout the specifications of Reference 21 to provide feel to the pilot and to reduce the tendency towards excessive sensitivity near the neutral position. It is further recommended that the lateral response not be so large as to cause a tendency for the pilot to overcontrol. The limit for this case is established to the response which produces no more than  $20^\circ$  in the first second for one inch of control deflection. The recommended lateral response in damping characteristics are shown in Table VI. Peak lateral control forces are specified as not to exceed 20 pounds in transition nor 10 pounds in hover. The lateral control effectiveness should be sufficiently great in combination with other normal means of control to balance the aircraft laterally during all flight and ground handling operations, and specifically when demonstrating directional control effectiveness. In addition to all other requirements, it is recommended that 50% of the roll control power be available for lateral maneuver. Changes in lateral control forces needed to trim any operationally necessary or normal configuration should be as small as possible, and in any case not exceed 3 pounds. The emergency conditions will allow 10 pounds. The trimming devices should be capable of reducing the lateral control forces to zero with zero sideslip in all configurations and flight conditions specified in Table IV.

In considering these requirements from Reference 21, it has been suggested in a number of studies that control power levels may be reduced when engine thrust is vectored to produce translation instead of tilting the aircraft in roll. This subject was discussed earlier as an example in Section 1.3. A translational control has obvious advantages for large aircraft where large roll inertia severely limits the angular response. The results of the simulator study were presented in Figure 10 in terms of pilot rating of roll control power required for various methods of translational vane control. The task for each type of control was to reposition the aircraft laterally as rapidly as desired in a gust-free environment and with no aerodynamic inputs. Stick sensitivity and roll damping were set at optimized values. It can be observed in Figure 10 that for the lower range of control powers, programming the vane as a function of bank angle reduced the angular acceleration requirements for a given pilot rating but did not achieve a satisfactory pilot rating. This quickening in side acceleration is similar to the cyclic effect in a helicopter rotor. When the vane was actuated by a thumb controller on top of the stick, angular acceleration requirements were markedly reduced as would be expected, since for these tests there was little tendency for the pilot to produce bank upsets. Flight tests with the vane on the X-14A VTOL aircraft bear out trends shown by the simulator tests. More operational flight experience must be obtained however to establish a tradeoff between vane control and bank angle control to account for upsets and trim requirements. Further work needs to be directed at IFR tasks where lateral positioning is more demanding.

## 3.6 Directional Axis

### 3.6.1 Static Stability

Reference 21 states that static directional stability with both controls fixed or free shall be such that right rudder pedal deflection from the laterally level straight flight condition is required to produce left sideslip. For angles of sideslip between  $\pm 15^\circ$  from laterally level, straight flight, the variation of sideslip angle with pedal force shall be essentially linear. An increase in pedal deflection should always be needed to produce

increase in sideslip. Again, it is recommended that 50% of nominal control moment be available for recovery. The rate of divergence due to directional instability should be limited; the rate of yaw divergence two seconds after a  $5^\circ$  sideslip displacement should not require more than 50% of the control moment available to return the aircraft to trim, nor should the rate of divergence double the size of the bank angle in less than three seconds for the uncorrected condition. Negative dihedral and negative directional stability defects shall not occur simultaneously.

### 3.6.2 Dynamic Stability

Directional oscillations should exhibit characteristics the same as those recommended for longitudinal oscillations. Time delays shall be the same as for the lateral case. Little more is said in Reference 21 concerning the dynamic directional stability.

### 3.6.3 Control Response Requirements

The aircraft is to possess the directional response and yaw angular velocity damping characteristics indicated in Table VII, at the most critical combination of both weight and moment of inertia, both in and out of ground effect. For all-weather operations it is recommended that the response be up to twice these values. The same requirement pertains to force gradients and stick movement as for the other axes. These conditions are to be retained for all operating and power conditions up to 500 ft per minute rate of descent. At normal STOL velocity or VTOL instrument approach velocity, there should not be a tendency for the pilot to overcontrol as a result of high directional response.

The directional control in hover is specified to permit, at the most critical combination of weight and moment of inertia, a  $360^\circ$  turn in either direction while hovering in the designated wind condition. At the most critical azimuth relative to the wind, application of full directional control shall meet the displacement in Table VII. It is specified that at least 50% of the nominal directional control remain after all trim requirements are met. (This requirement is believed by some to be excessive). The same directional control effectiveness is required for taking off, landing and taxiing as in hovering. The change in directional control force due to change in trim is prescribed not to exceed 10 pounds for the rudder. (This also is believed conservative). As with the other controls the trimming devices should be capable of reducing the directional control forces to zero with zero sideslip in all flight conditions and configurations.

Early experience with helicopters established the requirements for large values of directional control power in Reference 21. These values were necessary primarily because of the large directional trim change with power peculiar to single rotor aircraft. Recent experience with most VTOL aircraft has indicated that very low yaw response is acceptable, emphasizing again the importance of examining in detail the individual components making up the requirement for total control power. Even though for v/STOL aircraft the yaw axis requires only a fraction of the total control power required for roll and pitch, flight experience has shown that some additional factors are significant. These are (1) adequate control for upsets such as the XC-142 has encountered in ground effect in STOL landings must be considered for some designs, (2) a change in rudder effectiveness with height above the ground can be undesirable as evidenced by the landing accident with the XC-142, (3) non-linear directional characteristics are undesirable, primarily because of engine inlet moments; some jet VTOL configurations such as the P 1127 and XV-5A require non-linear rudder inputs when turning out of the wind. Pilots seem willing to accept poor response but object very strongly to the non-linear behavior. The present requirements in Reference 21 state only that it should be possible to turn  $360^\circ$  and non-linear aspects are not adequately covered.

## 3.7 Height Control

### 3.7.1 Thrust/Weight Requirements

The primary aspect of hovering and vertical flight is in the height control. However, a few brief comments concerning other aspects will be made before consideration of the



height control in detail. The effects of downwash ground interference are specified by Reference 21 to be such as to not result in unsatisfactory characteristics while hovering in any designated wind conditions. For all conditions up to the disappearance of ground effect, there should be no objectionable feedback of unsteady aerodynamic forces on control surfaces to the cockpit controls, nor any additional undesirable response from this source. Hovering precision should be maintained over any given point within a three-foot radius circle without acquiring a translational velocity in excess of two feet/second in any horizontal direction. This should be accomplished without undue pilot skill. Attitude control power, ability to trim, stalling or buffeting, or engine malfunction due to intake flow conditions or recirculation of exhaust gases shall not limit the rate of vertical ascent or descent that can be used, within the specified limits. (It should be added that this should be accomplished for any heading relative to the wind.)

With regard to height control, Reference 21 specifies that it should be possible to maintain satisfactory control of vertical speed with  $\pm 1$  foot/second by use of the height control while hovering in still air at all design hovering altitudes and ground clearances both in and out of ground effect with less than  $\pm \frac{1}{2}$  inch of control movement. The vertical thrust margin is specified in terms of thrust to weight ratio as 1.05 for take off and 1.15 for landing under the most adverse specified altitude-temperature conditions. Fifty percent of the available control power should be the maximum used simultaneously about all three axes to permit maneuver control. In addition, during take off application of full control about any one axis with 50% application about the remaining axes should not reduce the vertical thrust to less than the weight (or a thrust to weight ratio of 1). The pilot should be able to obtain full control power about all three axes simultaneously although the thrust margin in this condition is not specified.

The vertical thrust response during the final stages of a vertical landing is specified to be such that after step input of the height control the lift increase is 60% of the demand increase in no more than 0.3 second. (This time constant will be discussed in detail subsequently). For demonstration purposes it is specified that the demanded increase should be 10% of the landing weight at any power setting between hovering and 1000 ft per minute rate of descent, in the most adverse conditions for the power unit.

Since the time that these recommendations were prepared, several investigations have been made regarding the thrust/weight ratio requirements for adequate height control in the hovering and vertical flight regimes. Two of these have been selected for demonstrating the need for revision of the specifications in Reference 21. The first is a study made utilizing a vertical height simulator shown in Figures 30 and 21. This simulator is capable of accelerations of  $\pm 2g$  and maximum velocities of  $\pm 20$  feet/second, operating over a total height capability of 100 ft. The controller sensitivity is linear and fixed 0.1 g per inch of travel as measured along an arc at the hand grip. The maximum downward acceleration provides a 0g or free fall condition with the controller bottomed. This system is controlled by an analog computer to provide the desired simulation. A minimum response to a command step input is of the order of 0.07 seconds first-order time lag.

Generally these tests indicated that minimum upward acceleration for normal operation for typical hovering maneuvers should be about 1.06 g and the minimum level for acceptable safe operation about 1.02 to 1.03g. For normal operation, minimum damping level is highly dependent on control system time constant particularly during operation at high thrust to weight ratios. These results are presented in Reference 30.

The second and more recent investigation was made utilizing a variable stability helicopter. The results of which are presented in Reference 31. In general these results tend to confirm the results from Reference 30. Based on a primary evaluation task beginning with a rapid transition from hover to forward flight, a racetrack pattern at an altitude of about 400 ft, and a straight-in approach using approximately a 500 ft per minute rate of descent terminating in a 50 ft hover at the starting point, the following results and conclusions were drawn. Acceleration from hover and the subsequent climb out imposed the most stringent requirement on thrust to weight ratio. For normal operations

as reflected by the primary evaluation task the minimum satisfactory level of thrust to weight ratio is 1.09 providing other parameters are within a range which permits a climb capability of at least 600 ft per minute. If only the approach task is considered, including a flare and landing, satisfactory operation is possible for thrust to weight ratios as low as 1.03 if the normal velocity damping level is equal to or greater than -0.25/second. It should be noted that a primary difference between the two examples given is that for the latter case the damping was the value just stated, while for the former case damping was zero.

Now let us make a comparison with the AGARD recommendations just quoted from Reference 21 and the results obtained in these two investigations. The AGARD recommendation suggests that the optimum control sensitivity is on the order of 0.15 g per inch of control movement. This requirement was confirmed by the tests of Reference 31. However, such was not the case for the specification of thrust to weight ratio. In Figure 32 the results of Reference 31 are compared with the AGARD specification. In making the comparison, it has been assumed that the take off requirement of Reference 21 corresponds to the acceleration and climb results of the present study and further that the landing requirement of Reference 21 corresponds to arresting descent rates at the bottom of the approach. Inspection of the two figures in Figure 32 indicates that Reference 21 requires a much greater thrust to weight ratio for landing than for take off. This is seen to be contrary to the results of the present investigation which, except for zero damping, always requires a greater thrust to weight ratio for acceleration and climb out (that is, the take off) than for arresting descent rates (that is, the landing); for zero damping, the thrust to weight requirements of the present investigation are identical for the two tasks. It is concluded from these tests therefore that the requirement for an adequate acceleration and climb capability places the greatest demand on thrust to weight ratio. It is recognized of course that the minimum satisfactory thrust to weight ratio for the acceleration and climbout task would vary somewhat with specific mission constraints such as field size, exposure time, and the height of surrounding obstacles. Caution should be exercised in applying these acceleration and climb results to operations wherein the specific mission constraints are either much more or much less stringent than those represented by the primary evaluation task of Reference 31. This task might be considered as corresponding to a transport type operation.

These and other studies show the interrelation between thrust to weight ratio and vertical height damping and provide a basis for reasonably sound requirements for both take off and landing. The thrust margins needed for simultaneous control about several axes however, have not been covered adequately.

Reference 21 specifies that the thrust to weight ratio should not be less than 1 when full control is applied about one axis, with 50% control applied about the remaining axes. It is possible that this is very conservative in light of actual VTOL experience. For example the P 1127 operating with a demand bleed system and the VJ-101C with a thrust modulation control system have been found to be acceptable in spite of the fact that thrust to weight values less than 1 occur during pronounced control activity. This appears to be possible because the control inputs are needed for only a short time. How much altitude loss can be permitted is difficult to answer without more operational experience. Studies have shown that simultaneous control inputs in roll and pitch usually occur as discrete large control deflections for a short time. A revision of the requirement should probably recognize that altitude may be lost for some specific time period. In addition since large controlled inputs are held for only a short time, engine over-temperature may be acceptable for that time period.

Finally, the specification of vertical height control of  $\pm 1$  ft per second which may be required for missions such as rescue missions certainly need not be exercised for all missions in V/STOL vehicles. Height control to date has not proved a large problem on VTOL aircraft and vertical height damping has not been required even for aircraft with suck-down and unsteady ground effects. A factor now missing from the criteria in Reference 21, and perhaps which should be considered, is the non-linear trim change near the

ground. For example, the P 1127 aircraft has a nose-down tendency in ground effect which changes in magnitude with aircraft attitude, becoming larger as the aircraft noses down. In this sense, precision of height control and pitch could prove to be a problem for some designs, for example, those which obtain height control by a combination of lift engines and deflected cruise engines. The thrust response of the lift engines would undoubtedly be better than the cruise engines and lift-pitch coupling could result. In addition when the forward lift engines are used for roll control, the total thrust change results in a pitch change. This problem could be more severe in ground effect.

### 3.7.2 Effects of Time Constant

Time constants for first-order time delay in thrust response were investigated in the tests of both References 30 and 31. These results were found to be in reasonable agreement as shown in Figure 33 extracted from Reference 31. The agreement is considered reasonable when the difference in damping as indicated on the figure is noted. It is easily seen that the allowance for 0.3 second delay in Reference 21 with regard to vertical thrust response can result in a degradation of approximately one unit in pilot rating. These time delays presented relatively little problem for operation at higher altitudes in the variable stability helicopter. Although the pilot was able to maintain control of the aircraft for even the largest time delays simulated, for time delays greater than 0.5 second he found it necessary to alter his normal control technique for landing in order to reduce overcontrolling to a point where a reasonably safe touch down could be made. Either a hover at 50 ft with a constant low sink rate from there to the ground unchecked, or a control dither method was necessary to assure safe landing. Either of these is considered to be unacceptable for routine flight operation. The addition of a position indicator for the height control served as a lead-information device for the pilot and improved his capability with larger time delays. This method could be utilized but is not recommended at present.

The investigators in Reference 30 concluded that as long as the control system time constant remained below 0.37 second, acceptable control of altitude could be maintained in the event of artificial vertical velocity damper failure. They noted that velocity response plays an important part in the determination of minimum acceptable control power. Operation is sluggish and velocity limited for take off in the high damping case and there is inadequate arrest of high velocity sink rates for landing in the low damping case. Tests of hovering steadiness at zero velocity damping indicate the pilot tends to overcontrol at time constants above 0.6 second and the task requires his full attention at 1.2 seconds. This is apparent from the pilot ratings in Figure 33 where it is seen that the curve intersects the unacceptable boundary at approximately 1.1 seconds delay.

From these cursory considerations of the special cases of handling qualities requirements, it is obvious that a great deal of confusion yet exists in the methods by which the specifications can be generated in a manner that may find general application. Considerable improvement has been made as a result of tests, some of which have been presented here and many which are yet in progress. It is anticipated that the current effort to rewrite the AGARD Report No. 408 will reflect considerable advancement in understanding of the handling qualities problem since the first writing. However, it is obvious that a considerable amount of research is yet to be accomplished before adequate definitions are obtained for application to all classes of V/STOL aircraft.

## 4. AUTO-STABILIZATION REQUIREMENTS

### 4.1 Description of Types of SAS

The majority of the material presented in this section was extracted from the excellent presentation of Reference 32. A wealth of basic information regarding stability augmentation systems can be found in Reference 33 which was prepared by the Instrumentation Laboratory of the Massachusetts Institute of Technology. It is only fair to state that the

design and utilization of SAS systems is highly complex and filled with many aspects of an art rather than a pure science as of this time. A considerable amount of research will be required before a complete systemization of auto-stabilization requirements will be realized.

There are many types and forms of stability augmentation systems. We shall restrict our interest to three basic systems upon which most current systems lay their foundation. These are the acceleration, the rate and the attitude systems.

In Figure 34, a representation of an automatic stabilization system for a VTOL aircraft which requires attitude change in order to translate is portrayed. This type of aircraft is characterized by having the thrust vector fixed in relation to the aircraft. Thus translation can be accomplished only by rotation of the entire vehicle. It is seen from Figure 34 that the inputs through the control system consist of the pilot's command and the stabilization feedback from the airframe. The pilot's command may be shaped in any form desirable by means which shall be discussed later. The integration of these two pieces of information is then fed into the control system to provide the stabilization desired.

The descriptive elements of the three systems to be considered are shown in Figure 35. It can be seen that the acceleration system has no stabilizing feedbacks. As its time history grows, stick deflection produces steady-state acceleration and the pilot must provide the stability and angular rate damping while controlling his attitude. The control system variables pertinent to this system are control power and control sensitivity.

The rate system is built upon the acceleration system to which is added an angular rate feedback. With this modification stick deflections now produce steady-state rate. The pilot must provide attitude stability to control attitude but he does not have to worry about excessive rate buildup. Thus he has been relieved of one task in his workload. The variables associated with the rate system are control power, control sensitivity and damping. The damping in the system is simply the gain in the rate feedback loop.

The attitude system goes one additional step beyond the rate system by incorporating into that system an attitude feedback in addition to the rate feedback. For this system the pilot controller commands steady-state attitude proportional to stick deflection and all stabilizing requirements are provided automatically. The variables which describe the attitude system are control power, control sensitivity, damping and frequency. The frequency here refers to the undamped natural frequency of the system. It is a commonly used measure of the stability of a second-order system. More precisely, the frequency is equal to the square root of the gain in the attitude feedback loop. Frequency and damping together are both necessary to define the actual oscillatory characteristics of an attitude system. This is illustrated by the time history at the bottom of Figure 35 which is typical of a somewhat underdamped case. If frequency were increased the oscillations could be made to disappear.

Further sophistication of these systems could be made as, for example the inclusion of another feedback loop representing velocity over the ground could provide a constant translational velocity system with stick command. One more step could be included to represent the ground position which would then create the capability to move to and maintain a given position over the ground as a function of stick command. Thus, it is seen that sophistication of the system can continue almost at the whim of the designer. It should be remembered however, that problems of reliability and failure plague complex systems. This will be discussed in detail in a later section.

#### 4.2 Effects of Type of Control

As a means of comparing the effects of various types of control systems let us again borrow from Reference 32 which describes a series of tests made for the three control systems described in Section 4.1. These tests were performed on the six-degree-of-freedom

simulator described in Section 1. The conditions for the majority of the tests are shown in Figure 36. Simplicity was stressed in these tests to insure a basic understanding before subjecting each control system to complex conditions. For example, rather than attempting to optimize control stick geometry and force characteristics, a representative set of values was selected and held constant throughout the tests. Systematic data were generated for the roll axis only, even though the simulator was operated in the six-degree mode. The roll axis was considered to be more important since it is usually more critical than the pitch or yaw axis. Further, roll axis data should qualitatively apply to the pitch axis. For this reason, the pitch axis parameters were varied identically with the roll axis parameters throughout the tests. The roll axis was permanently maintained as a satisfactory rate system. The results represent a sampling of three pilots.

The simulator tasks were designed as a general hover task and a general maneuver task. No attempt was made to define tasks which would be universally representative of actual flight conditions, since this is unimportant for establishing a common basis for system comparison. The hover task was divided into two parts - precision hovering at a point in space and precision altitude changes to simulate take off and landing. The maneuver task consisted of translational start-stops and roll reversals. The precision hover task involved the pilot's ability to hover a given system within limits on the order of  $\pm 2$  ft. Maneuvering for the start-stop mission involved rapid motion from one hover point to another over 15 ft distances. These conditions are more critical than those probable in actual flight. Thus, the results presented here should not be applied in an absolute quantitative sense.

Parameters were optimized at control power equal to two radians/second<sup>2</sup>, in order to minimize any influence on the results; stick travel was limited to  $\pm 5$  inches. Most comparisons were made in calm air with a brief comparison for the presence of random disturbances.

Figure 37 shows the variation of pilot rating over a wide range of control sensitivity for the acceleration system. The optimum range lies between 0.4 and 0.8 radians/second<sup>2</sup>/inch. No other variables are available to optimize for the acceleration system; however, this type of test was useful to determine optimum control sensitivity for the rate system, and later on for the attitude system. The results shown here served as a starting point since the acceleration system can be considered as a rate system with zero damping.

The results for the rate system are shown in Figure 38 which shows the effect of damping on the optimum sensitivity range. The band was drawn through the optimum sensitivity ranges found at various levels of constant damping. Zero intercepts on the damping axis correspond to the acceleration system. Increasing the damping did not change the optimum sensitivity range until high damping values of about -5 per second were reached. Above that value increases of sensitivity were required to compensate for sluggish response. This result can be understood due to the relationship for roll sensitivity as a steady-state rate divided by the control displacement and is the ratio of the attitude feedback to the rate damping. For damping less than -2 per second, problems similar to those with the acceleration system became apparent. For damping greater than -5 per second the rate system was felt to be overly tight in response. From the optimum ranges for the rate system a starting point for discussion of the attitude system is found.

Results concerning optimum control sensitivity, optimum damping and optimum frequency for the attitude system are contained in Figures 39, 40 and 41 respectively. Sensitivity and damping were found to be interdependent variables and the results of Figures 39 and 40 should be interpreted accordingly; in Figure 39 damping has been optimized according to its variation shown in Figure 40 and vice versa.

Figure 39 shows the variation in optimum control sensitivity with frequency; intercepts for zero frequency correspond to the optimum sensitivity range for the rate system. This is discussed in Figure 38. The optimum sensitivity at first remains constant with increase in frequency up to values of about 3 radians/second. Beyond that value the sensitivity

had to be increased to overcome increasing stability of the system. The equation in Figure 39 expresses the relationship of bank angle sensitivity to control sensitivity and frequency, where bank angle sensitivity is the steady state bank angle per inch of stick deflection. This sensitivity must approach infinity as frequency goes to zero, since the bank angle sensitivity for a rate system, which is zero frequency, is infinite. It is seen that at high values of frequency, optimum control sensitivity decreases in a manner which causes bank angle sensitivity to approach a constant range for about 0.04 to 0.06 radians per inch. Frequencies less than 3 radians per second cause the pilot to be concerned about control sensitivity, not bank angle sensitivity. The desired acceleration was about the same for all three systems.

In Figure 40, the variation of optimum damping with frequency is indicated. The intercepts at zero frequency represent the values required for a rate system. The damping parameter used is the damping to inertia ratio, not the conventional damping ratio normally used to describe second-order systems of this type. Values of the conventional damping ratio appear as lines of constant slope in Figure 40. Up to about 3 radians per second, optimum damping to inertia ratio is relatively constant with frequency; the pilot is more concerned with basic level of damping than the overshoot or undershoot characteristics which occur as a function of conventional damping ratio. Above 3 radians per second overshoot must be considered and optimum damping appears to be asymptotic to a constant conventional damping ratio of about 0.5.

Figure 41 shows optimum frequency for the attitude system. At various levels of constant control power, pilot ratings were obtained as frequency was varied over a range from 0 to 4 radians per second. Control sensitivity and damping were set to optimum values prior to evaluation. Contrary to the expectation that optimum frequency might decrease with control power in order to avoid bank angle limitations, for control powers greater than 0.5 optimum frequency was found to lie in a constant band between 1.4 and 2.6 radians per second. Frequencies below 1.4 radians per second require too much attention from the pilot to control attitude; above 2.6 radians per second the system was overstable. An increase in the control sensitivity to improve maneuvering made the system overly sensitive in hover.

A comparison of the various systems for calm air conditions is shown in Figure 42. The acceleration system is seen to be unsatisfactory for the simulator task regardless of control power. The workload placed on the pilot was primarily responsible for the rating. Comparison of all three systems indicates that not only does progressive addition of stabilization improve handling qualities, but, also allows significant reductions of control power. The tendency of the rate and altitude systems to converge at very high control powers is misleading since pilots seldom give ratings better than 2.

The possibility of improving the attitude system by reducing the control power to still lower levels and still retaining superior handling qualities can best be considered by understanding the factors which affect the control power requirements of this linear attitude system in general. Figure 43 presents a summarization of the attitude hold system with the restrictive boundaries indicated. The variation of control power requirements with frequency in order to maintain constant levels of handling qualities appear to be shaped by the influence of four factors, as are indicated by the various boundaries. Minimum frequency appears to be at about 2 radians per second. In this region, control powers appear to depend primarily on maneuvering response or more precisely attitude response. This means that there is a level of control power below which attitude response is inadequate for maneuvering requirements of the tasks. (The minimum acceptable rating for a satisfactory system is a pilot rating of  $3\frac{1}{2}$  as indicated). At frequencies just above the optimum, insufficient bank angle becomes a factor. For the linear attitude systems, maximum bank angle is determined by the ratio of maximum control power to frequency squared. Control power must be increased accordingly to maintain whatever bank-angle capability is required to perform a given task. Otherwise maneuverability would suffer because of inadequate horizontal force generation. At high frequencies the attitude system eventually becomes uncomfortable to the pilot. Since system stiffness is the basic objection at this point, no amount of control power will solve the situation.



### 4.3 Linear Versus Non-Linear Systems

The linear systems described above are based on the concept of proportional control and linear stabilization feedback. Proportional control means simply that the output of the pilot's controller varies linearly with his input.

Tests were also performed, as reported in Reference 32, for a non-linear variation of the attitude system. This system is also referred to as an attitude system with saturation. The non-linear system combined both non-proportional control and non-linear feedback in a manner such that large control inputs by the pilot had a temporary cancelling effect on the feedback signals. This principle is described below.

Since it is evident from the foregoing presentation that control power reductions are possible only for those attitude systems in the frequency range from about 2 to 3 radians per second, the margin for improvement is based upon the potential for non-linearizing the current system. A limit is imposed by the extent by which the inadequate response and insufficient bank angle problems can be overcome. Non-linear systems can be devised in a limitless variety. The reasons for selecting the one discussed here were that first, the inadequate response problem is one which lends itself readily to the use of non-proportional control of the pilot's stick and second, the problem of insufficient bank angle suggests the use of non-linear stabilization feedback. Non-linearity in control systems is essentially a tailoring process and must take into account the incompatible demands of the VTOL task. An efficient control system must be adaptive to both the stability requirements for hovering and the response requirements for maneuvering.

The saturation system attempted here is based on the principle of providing the pilot's control with more acceleration command than is actually available in the control system itself. Diagrams comparing the saturation system with a linear system of equal power are shown in Figure 44. The linear system is typical of a low control power system with optimized sensitivity, but with relatively wide spaced stops on the control travel. With the linear system the pilot can never command the control system to produce more than its available moment or acceleration. With the saturation system, large inputs from the pilot's control have the effect of saturating the control system at its maximum output. A condition which temporarily produces pure acceleration. Once the feedback signals become large enough to counteract the control input the control system unsaturates and behaves like a linear system. Large quick inputs produce saturation; large slow inputs do not. Three points are attractive for this configuration. First, it provides maximum initial response for the large quick control inputs typical of rapid maneuvering; second, the system retains a constant level of static stability upon reaching any steady-state bank angle; third, the saturation system provides a simple method for increasing maximum bank angle without increasing control power. The saturation system with a ratio of 3 will provide a maximum bank angle three times that of a linear system with the same available power.

The important results of this attempt are shown quite simply in Figure 45. It is indicated that saturation allows a relatively insignificant control power reduction of about 10%. However, saturation also results in an upward shift of optimum frequency so that when the factors of upset are taken into account, the effective reduction might be more of the order of 15%.

Benefits of saturation or non-linearity result primarily from increased bank angle. However, a degrading phase-lag characteristic between pilot input and aircraft response occurs which is aggravated by the amount of saturation. Therefore, it is important to realize that saturation should not be used unless a bank angle problem exists in the first place. Even then its benefits are limited to the point where phase-lag begins to dominate.

The benefits of the approach are obvious and reductions in control power will depend primarily on the development of better non-linear methods of optimizing response. This may prove to be very difficult. As with most systems, the benefits do not come without

the problems which, in this case, are represented by the phase-lag dangers characteristic of the saturation system.

#### 4.4 Effects of Disturbances

It must be realized that simply to provide control power sufficient for hovering and maneuvering in calm air can court disaster. In reality control must be powerful enough to also satisfy the requirements for trim and that for controlling upsets or disturbances. Total control power is not necessarily the simple addition of these elements, which would be unduly conservative, nor is it the control power equated to the most critical requirements. A practical design accounts for the critical case with some margin to allow limited operation in the others. A satisfactory design requires information about the individual effects of hovering and maneuvering, trim, and upset or disturbances.

Generally, control power required for trim depends on the aircraft's aerodynamic and mechanical configuration. This can usually be calculated using static stability information and is essentially a problem of statics. The analysis of disturbance effects on the other hand is complicated by dynamic considerations requiring knowledge about an aircraft's susceptibility to upset. Configuration, of course, is important, but now the aircraft's size (mass and inertia) must be taken into account. The nature of the disturbance itself is important. For example the type of disturbance typically encountered in gusty air may be quite different from that due to ground effect and recirculation, and it is not always clear which is the most critical.

A preliminary look was taken at this problem as reported in Reference 32 for the three systems discussed. The results are shown in Figure 46. The type of random input supplied is also indicated in that figure. Frequency was found to have only a minor effect on the pilot rating. The parameter of most significance was found to be the ratio of peak disturbance acceleration to control power. The degradation in pilot rating with increasing disturbance intensity is shown. A single curve for the attitude system at a higher frequency is also indicated. Precision maneuvering tasks were the only tasks considered. The acceleration system hovers poorly in calm air and is strongly affected by disturbances. The rate system has relatively good rating for calm air hovering and can tolerate peak disturbances of about 15% of the available control power before becoming unsatisfactory. The attitude systems exhibit not only the best calm air performance but also the lowest susceptibility to disturbance.

Even though the disturbance toleration of the optimum attitude system appears more than adequate for practical applications, there may be instances when disturbance effects dictate an even higher degree of stability. The curve for a natural frequency of 4 radians per second has been included to demonstrate the effect of added stabilization. This frequency is considered to be impractical for linear attitude systems for the reasons demonstrated in Figure 41. It is here demonstrated that practical amounts of stabilization combined with low inherent configuration susceptibility to upsets could result in a vehicle with no apparent sensitivity to disturbances.

#### 4.5 System Failures

Adding complexity to the control system increases the possibility of failures. For this reason alone past designs have stressed simplicity to such an extent that handling qualities have often been compromised. For the modern aircraft, handling qualities must be recognized to be as important to overall safety as control system reliability. Figure 42 contains some interesting implications regarding failures. If, for example, a satisfactory attitude system indicated as a pilot rating of  $3\frac{1}{2}$  should experience a failure in its attitude feedback loop, it would revert to a rate system with a pilot rating of about 5. This is because its sensitivity and damping are essentially the same as those for the rate system shown in the same figure. By the same reasoning, if a satisfactory attitude system lost both its feedback loops, it would revert to an acceptable, for emergency operations only acceleration system. The only case not shown here is the one for a



failure of the damping loop in the attitude system. Such a failure produces an undesirable oscillation but is nevertheless acceptable for emergency operation.

It is interesting to note that the transients involved in sudden failure were not found to overtax the pilot's ability to recognize and adapt to a degraded system in sufficient time to avoid loss of control.

#### REFERENCES

1. Pritchard, J.L. *The Wright Brothers and the Royal Aeronautical Society - A Survey and Tribute.* Jour. Roy. Aero. Soc., Vol. 57, No. 516, December, 1953.
2. Relf, E.F. *Aerodynamic Work, From the Library Reviews of the Papers of Wilbur and Orville Wright.* Jour. Roy. Aer. Soc., Vol. 59, No. 529, January, 1955.
3. Draper, C.S. *Flight Control, 43rd Wilbur Wright Memorial Lecture.* Jour. Roy. Aero. Soc., Vol. 59, No. 535, July, 1955.
4. Cooper, G.E. *The Use of Piloted Flight Simulators in Take-Off and Landing Research.* Paper presented to the Take-off and Landing Specialists Meeting, Flight Mechanics Panel of AGARD, Paris, France, January, 1963.
5. - *Agardograph 99, 1964, Simulation for Aerospace Research, NATO AGARD.*
6. Heinle, D.R. *The Use of Piloted Simulators in the Study of VTOL Flight.* NASA Conference on V/STOL Aircraft, Langley Research Center, November, 1960.
7. - *NASA Conference on V/STOL Aircraft - A compilation of Papers Presented, November, 1960.*
8. Gittner, U. et al. *Interaction Between Airframe Powerplant Integration and Hot Gas Ingestion for Jet-Lift V/STOL Transport Aircraft.* AGARD 31st Flight Mechanics Panel Meeting, September, 1967.
9. Rolls, L.S.  
Koenig, D.G. *Flight Measured Ground Effect on a Low Aspect Ratio Ogee Wing Including a Comparison with Wind Tunnel Results.* NASA TN D-3431, 1966.
10. Schweikhard, W. *A Method for In-Flight Measurement of Ground Effect on Fixed Wing Aircraft.* AIAA Paper, 66-468, 1966.
11. Ransone, R.K.  
Jones, G.E. *XC-142A V/STOL Transport Tri-Service Limited Category I. Evaluation,* FTC-TR-65-27, AFFTC, 1966.
12. Garren, J.F. Jr.  
Kelly, J.R. *Application of the Model Technique to a Variable Stability Helicopter for Simulation of VTOL Handling Qualities.* AGARD Report 515, October, 1965.
13. Rhoads, D.W. *In Flight Simulation and Pilot Evaluation of the Landing Approach Flying Qualities of a Supersonic Transport Airplane.* Cornell Aero. Lab. Rep. TM-2091-F-1, 1966.

14. Berry, D.T.  
Deets, D.A. *Design, Development and Utilization of a General Purpose Airborne Simulator.* AGARD Rep. 529, 1966.
15. Schade, R.O.  
Crane, H.L. *Low Speed Flight Investigation of a Jet Transport with a Powered-Lift Boundary-Layer Control System.* AGARD Paper 503, AGARD Flight Mechanics Panel, Paris, France, 1965.
16. Beilman, J.L. *X-22A Variable Stability System.* 1st National V/STOL Aircraft Symposium, Amer. Hel. Soc., November, 1965.
17. Condit, P.M.  
et al. *In Flight and Ground-Based Simulation of Handling Qualities of Very Large Airplanes in Landing Approach.* NASA Report CR-635, 1966.
18. Anderson, S.B.  
Schroers, L.G. *A Review of Facilities and Test Techniques Used in Low Speed Flight.* Aerospace Proceedings ICAS, April, 1967.
19. Tapscott, R.J. *Flight Test Techniques and Instrumentation for VTOL Aircraft.* AGARD Report 319, April, 1961.
20. Beilman, J.L. *X-22A Variable Stability System.* 1st National V/STOL Aircraft Symposium, Amer. Hel. Soc., November, 1965.
21. - *Recommendations for V/STOL Handling Qualities.* AGARD Rep. 408, October, 1962.
22. Anderson, S.B. *An Examination of Handling Qualities Criteria for V/STOL Aircraft.* NASA TN D-331, July, 1960.
23. - *General Specification for Helicopter Flying and Ground Handling Qualities.* MIL-H-8501A, September, 1961.
24. - *NASA Conference on V/STOL Aircraft - A Compilation of Papers Presented,* November, 1960.
25. Anderson, S.B. *Considerations for Revision of V/STOL Handling Qualities Criteria.* NASA Conference on V/STOL and STOL Aircraft, April, 1966.
26. Curry, P.R.  
Matthews, J.T. Jr. *Suggested Requirements for V/STOL Flying Qualities.* USAAML 65-45, RTM37, US Army Aviation Materiel Laboratories, June, 1965.
27. Shomber, H.A.  
Gertsen, W.M. *Longitudinal Handling Qualities Criteria: An Evaluation.* AIAA Paper 65-780, 1965.
28. Stapleford, R.L.  
et al. *An Analytical Study of V/STOL Handling Qualities in Hover and Transition.* AFFDL-TR-65-73, October, 1965.
29. Kelly, H.L.  
Champine, R.A. *Flight Operating Problems and Aerodynamic and Performance Characteristics of a Fixed Wing, Tilt-Duct.* VTOL Research Aircraft, NASA TN D-1802, 1963.
30. Gerdes, R.M. *A Piloted Motion Simulator Investigation of VTOL Height Control Requirements.* NASA TN D-2451, August, 1964.

31. Kelly, J.R.  
et al. *Flight Investigation of V/STOL Height-Control Requirements for Hovering and Low-Speed Flight Under Visual Conditions.* NASA TN D-3977, May, 1967.
32. Grief, R.K.  
et al. *VTOL Control System Studies on a Six-Degree-of-Freedom Motion Simulator.* Aerospace Proceedings, ICAS, Vol.II, September, 1966.
33. *Advanced Flight Control System Concepts for VTOL Aircraft.* TRECOM TR 64-50, October, 1964.

TABLE I  
Summary of Characteristics Measured During Flight Study

<i>Characteristic</i>	<i>Technique</i>	<i>Data Recorded</i>	<i>Presentation of Data</i>
Initial response to control	Step inputs of varying magnitude	Control positions; aircraft angular velocities	Angular acceleration versus control deflection; angular velocity damping values
Speed stability	Slow variation of airspeed about trim (power, configuration, other variables held constant)	Stick longitudinal motion; airspeed	Plots of stick longitudinal positions as function of airspeed
Directional stability; directional effect	Slow variation of sideslip angle at constant airspeed (rate of change of sideslip angle less than 1°/sec)	Pedal and stick lateral motions; sideslip angle	Plots of pedal and stick lateral positions as functions of sideslip angle
Trim changes and power effects; aerodynamic flow characteristics	Conversion in level flight with fuselage attitude constant; conversion with constant power and fuselage attitude; power variation at constant airspeed and conversion angle	Power; aircraft angular velocity; angle of attack; stick and pedal motion; camera record of tuft action on various surfaces	Cross plots of airspeed, vertical velocity (see Figure 5)
Maneuver stability	Pull-up maneuver; wind-up turn	Stick motion; normal acceleration; pitch angular velocity	Time histories of normal acceleration and/or pitch angular velocity
Dynamic stability	Abrupt control pulse; airspeed disturbance; fixed controls	Control motion; airspeed; angle of attack; angular velocity	Variation of periods and damping with flight condition.

TABLE II  
Function of Gains. Pitch Axis

Feedback Variable	Source	Purpose
$\bar{\omega}$	Integrated incremental normal acceleration	To vary $M_{\omega}$ for all flight conditions. Changes short period frequency and damping ratio in cruise flight. Changes short period and long period modes in transition. Equivalent to $M_{\alpha}$
$\dot{\alpha}$	Differentiated signal from angle of attack vane	To vary $M_{\alpha}^*$ . Changes short period damping in cruise and transition.
$\bar{q}$	Rate gyro signal plus derivative	To vary $M_{\dot{q}}$ . Pitch damper in cruise and transition. $\dot{q}$ used for lead compensation.
$\delta_{aug}^2$	Elevon pickoff excited by elevon pickoff	Vary nonlinear change in pitching moments due to elevon deflection, especially to compensate (remove) effect present in basic aircraft.
$\Delta u$	Airspeed systems	To vary $M_{\dot{u}}$ in fixed operating point mode only. Influences phugoid frequency in cruise flight and both high and low frequency roots in hover.
$\dot{u}_j$	Differentiated signal from airspeed systems	To vary $M_{\dot{u}}$ . Effective in stabilizing the long period mode in forward flight.
$\Delta \lambda$	Error between actual duct angle and reference duct angle	Variation of pitching moment with duct angle; provides linear variation with duct angle of trim stick position versus velocity in transition.
$\alpha_{V_0}(u)$	Function Generator	To generate a moment-required-to-trim function that differs from that of the basic aircraft. Influences elevator stick position through transition.
$\Delta B_c$	Error between actual collective pitch and reference collective pitch	Dynamic control cross-coupling. Used for decoupling basic X-22A.
$\Delta e_c$	Pilot's control displacement or control force	Variable elevator gearing, $M_{\delta_e}$ .
$\epsilon$	Attitude gyro	To vary $M_{\epsilon}$ . Very powerful in stabilizing the long period mode for all flight conditions. Increases frequency of short period mode. Pitch loop of attitude stabilization system.
$\bar{\delta}_{BS}$	Collective pitch stick with variable lag	Control cross-coupling. To vary $M_{B_c}$
$\alpha_V$	Angle of attack vane	To vary $M_{\alpha}$ . Primary influence is on short period mode for all flight conditions. Affects stability of long period mode in transition.

TABLE III

Control	Normal operation (lb)	After failure of appropriate power control system (lb)
Longitudinal	0.5 - 2.5	< 5
Lateral	0.5 - 2.0	< 4
Directional	1.0 - 10.0	< 15
Height — stick	1.0 - 3.0	< 5
— throttle	1.0 - 3.0	< 3

TABLE IV

$V_{Con}$	Conversion speed
$V_{MO}$	Minimum operating speed. For multi-engined aircraft only. The minimum speed at which performance and control are adequate to make a safe landing at the desired point with the critical engine failed.
$V_{TOSS}$	Take-off safety speed. For multi-engined aircraft only. The minimum speed during take-off at which, after failure of the critical engine, performance and control are adequate either to continue flight and make a normal landing or to make an immediate emergency landing.
$V_{PA}$	Normal power approach speed for STOL aircraft, or a speed which could be used on an instrument approach in a VTOL aircraft (assuming that a constant approach speed technique is used).
$V_{MP}$	Speed for minimum power or minimum thrust - approximately the loiter speed or best climb speed. It is of interest only if it is less than $V_{Con}$ .
<i>Steady flight trim conditions for static longitudinal stability demonstration</i>	
1. Hovering	
2. $V_{Con}$	power for level flight
3. $V_{MO}$	power for 500 ft/min descent
4. $V_{PA}$	a. power for level flight b. power for 500 ft/min descent
5. $V_{TOSS}$	take-off power
6. $V_{MP}$	a. normal rated power b. power for level flight
<i>Speed ranges for demonstration</i>	
(1)	Speed range for hovering is zero to the designated wind speed.
(2)	Speed range for the remaining conditions is $\pm 20\%$ of the trim speed or $\pm 20$ knots, whichever is greater.

TABLE V

## Longitudinal Response and Damping Characteristics in Hovering Flight

	Response for full control input (degrees in first sec)	Response for first inch of control displacement (degrees in first sec)	Damping (lb ft/rad/sec)
Normal Conditions	$300/(W+1000)^{1/3}$	$75/(W+1000)^{1/3}$	$15(I_y)^{0.7}$
After a single failure in a p.c.s. or s.a.s.	$180/(W+1000)^{1/3}$	$45/(W+1000)^{1/3}$	$8(I_y)^{0.7}$
W = aircraft weight in lb. $I_y$ = pitching moment of inertia in slugs ft <sup>2</sup> .			

TABLE VI

## Lateral Response and Damping Characteristics

	Response for full control input (degrees in first sec)	Response for first inch of control displacement (degrees in first sec)	Damping (lb ft/rad/sec)
Normal Conditions	$300/(W+1000)^{1/3}$	$100/(W+1000)^{1/3}$	$25(I_x)^{0.7}$
After a single failure in a p.c.s. or s.a.s.	$300/(W+1000)^{1/3}$ (same as normal case)	$100/(W+1000)^{1/3}$ (same as normal case)	$18(I_x)^{0.7}$
W = aircraft weight in lb. $I_x$ = rolling moment of inertia in slugs ft <sup>2</sup> .			

TABLE VII

## Directional Response and Damping Characteristics in Hovering Flight

	Response for full control input (degrees in first sec)	Response for first inch of control displacement (degrees in first sec)	Damping (lb ft/rad/sec)
Normal Conditions	$180/(W+1000)^{1/3}$	$60/(W+1000)^{1/3}$	$27(I_z)^{0.7}$
After a single failure in a p.c.s. or s.a.s.	$180/(W+1000)^{1/3}$ (same as normal case)	$60/(W+1000)^{1/3}$ (same as normal case)	$14(I_z)^{0.7}$
W = aircraft weight in lb. $I_z$ = yawing moment of inertia in slugs ft <sup>2</sup> .			

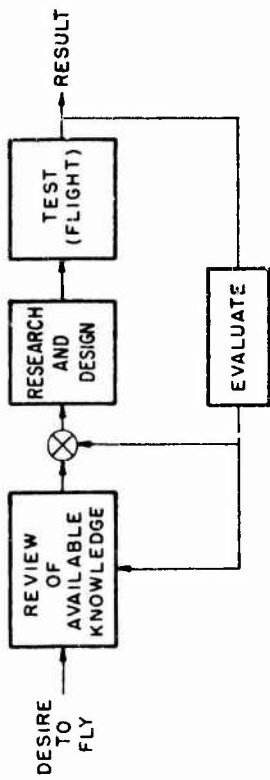


Fig. 1 Block diagram of Wright Brothers vehicle design technique.

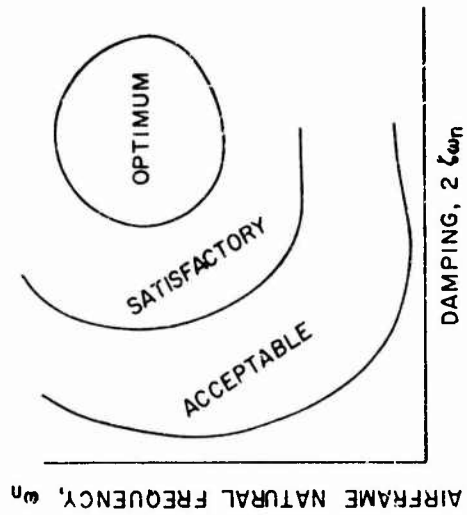


Fig. 3 Typical diagram showing regions of acceptability for short-period longitudinal control case of aircraft

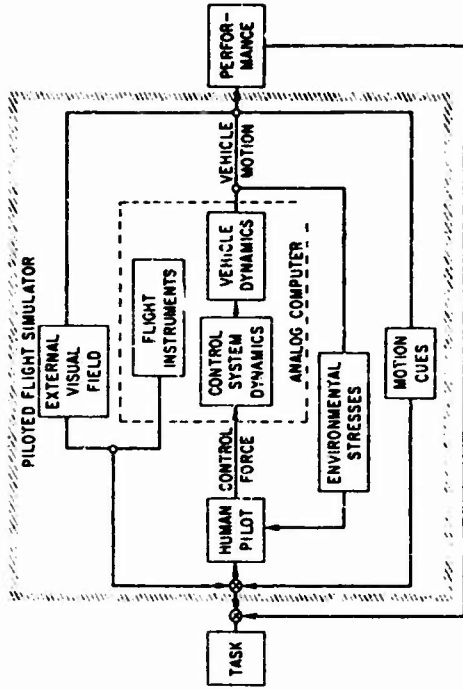


Figure 2



Fig. 4 Ames six-degree-of-freedom simulator



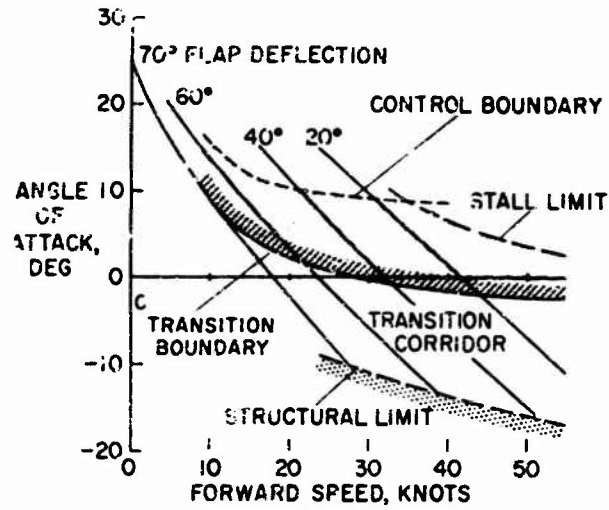


Fig. 5 Transition boundaries of deflected slipstream aircraft from simulator studies

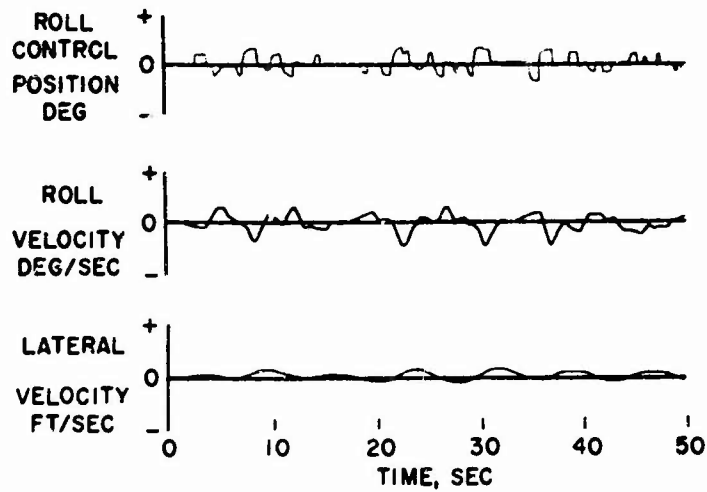


Fig. 6 Lateral control in hover. Fixed cockpit

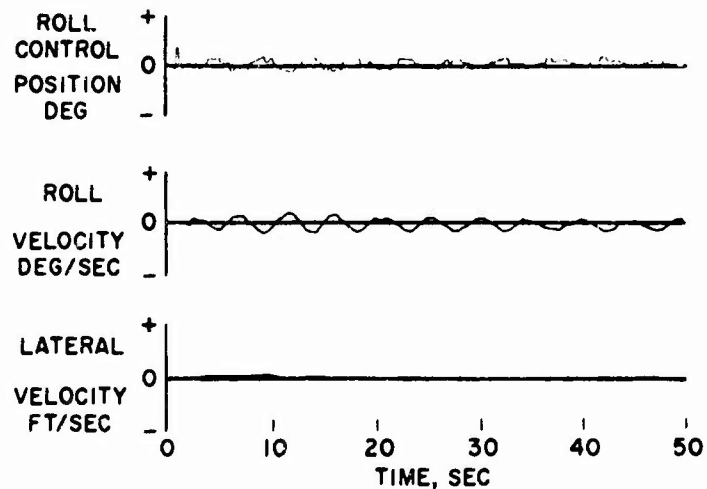


Fig. 7 Lateral control in hover. Moving cockpit

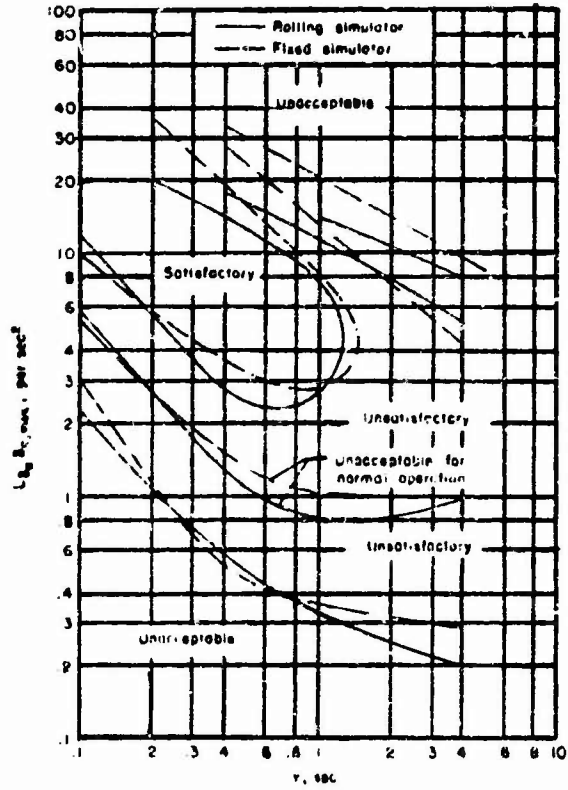


Fig. 8 Comparison of pilot opinion boundaries obtained from the fixed and moving flight simulators

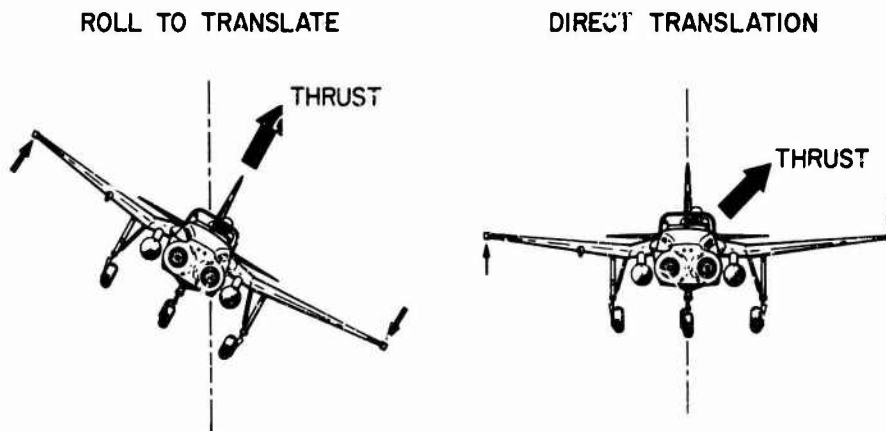


Fig. 9 Translational control methods. X-14A

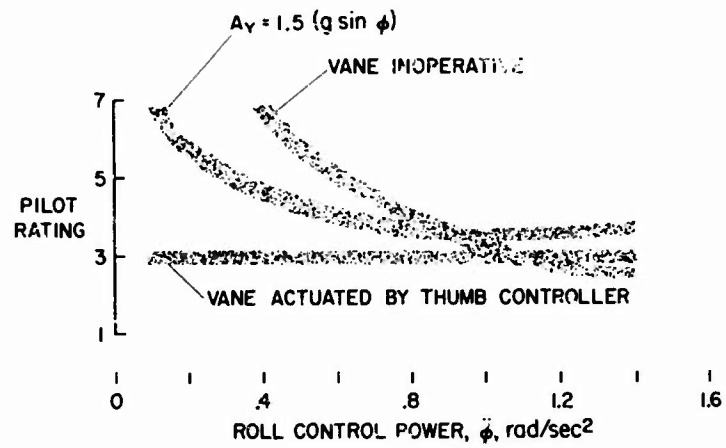


Fig.10 Effect of lateral acceleration vane on control power for hovering



Fig.11 X-14A VTOL Test vehicle

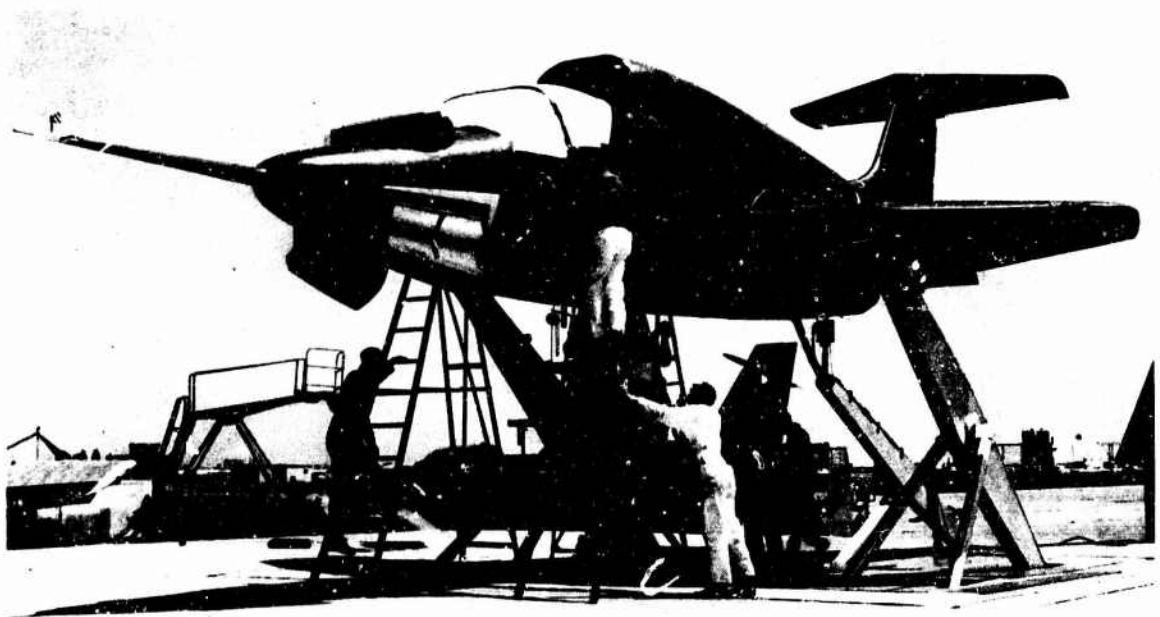


Figure 12

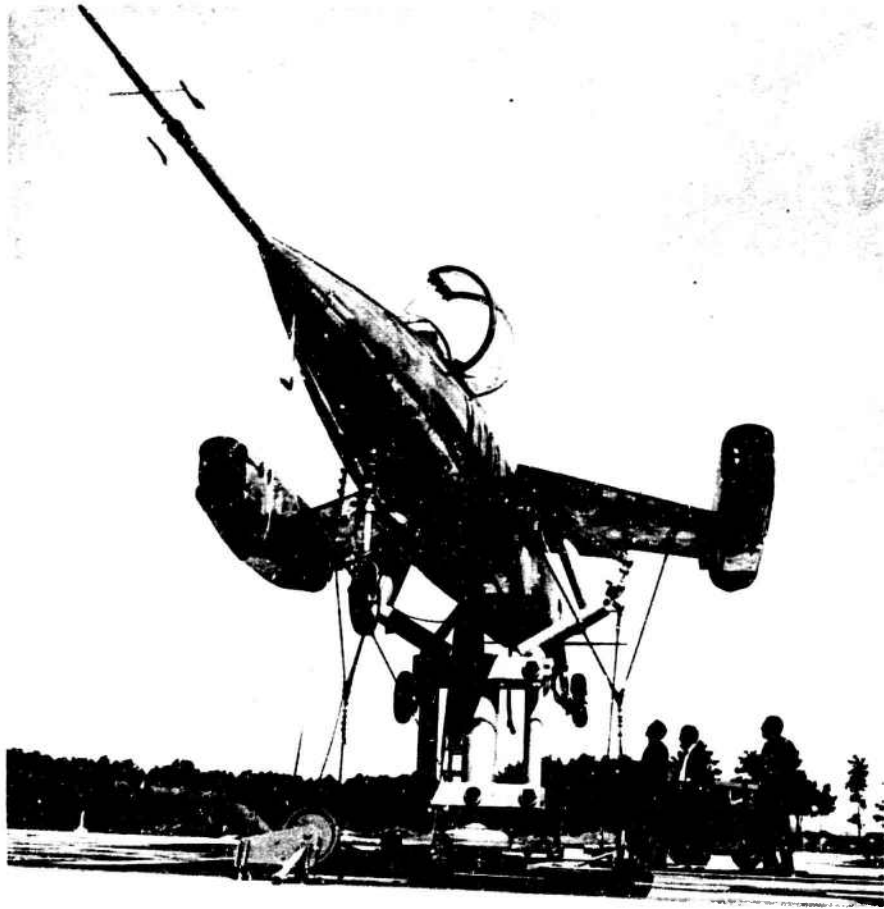


Figure 13

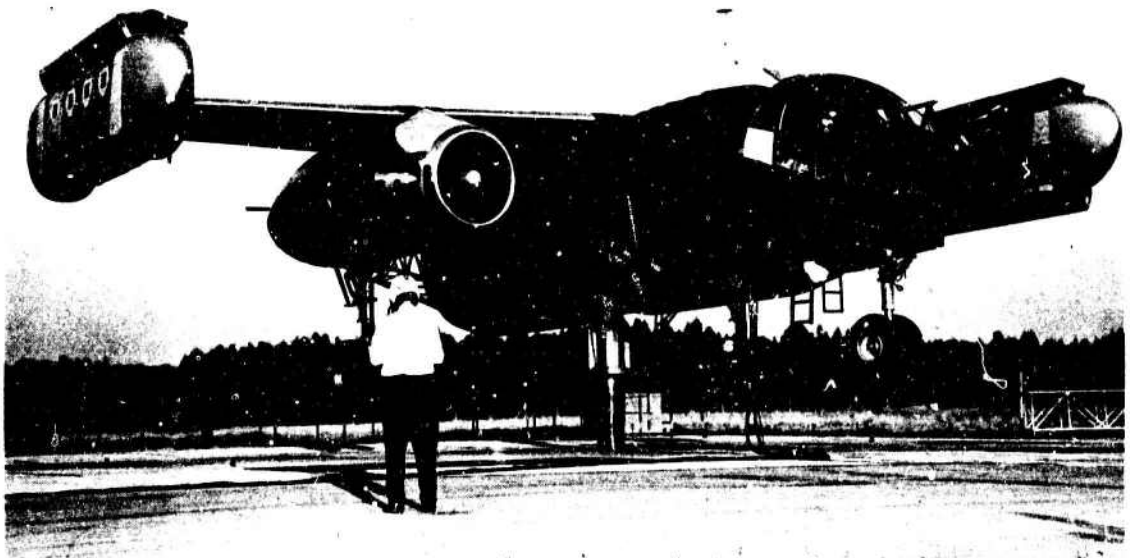


Figure 14

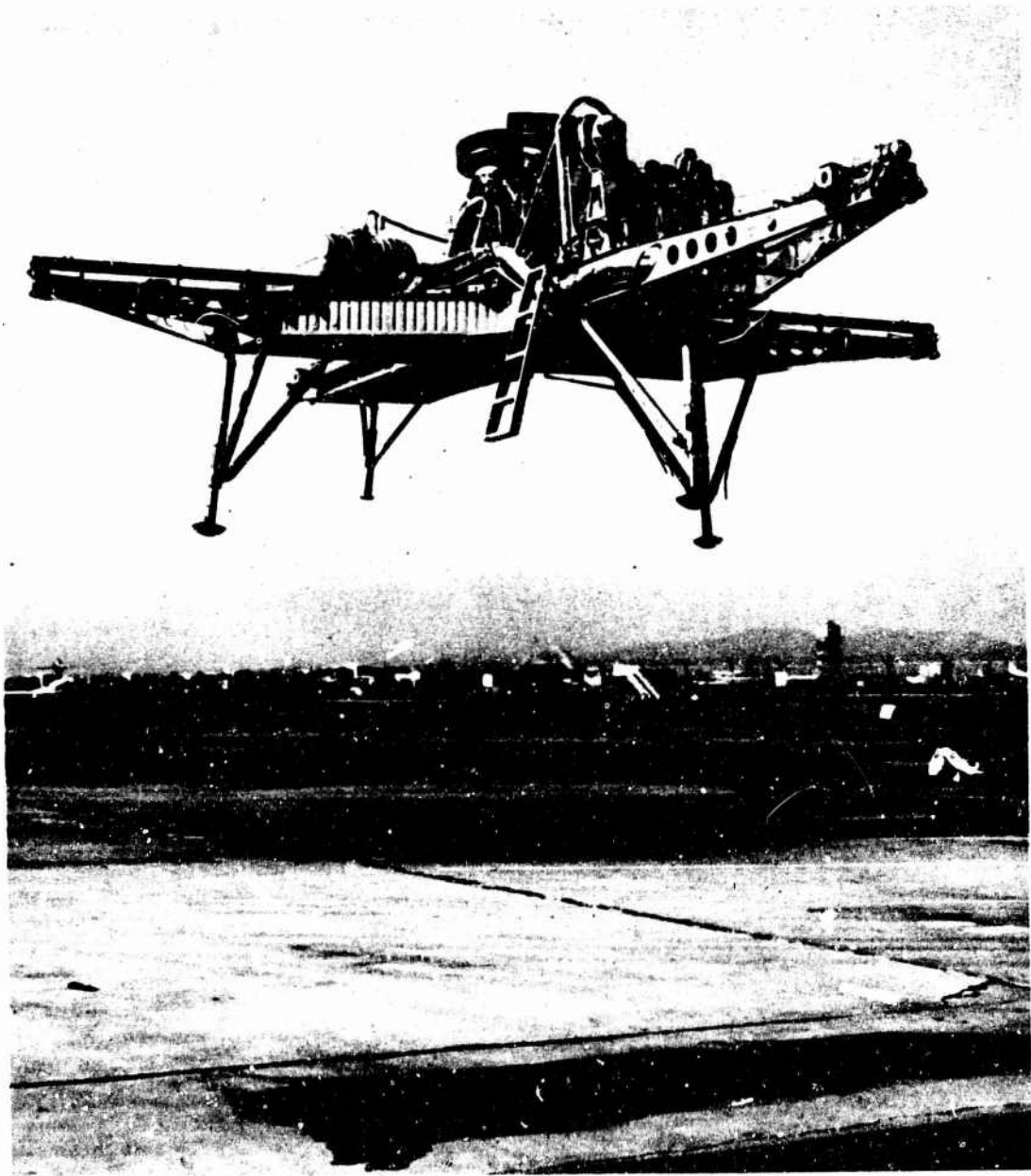


Figure 15

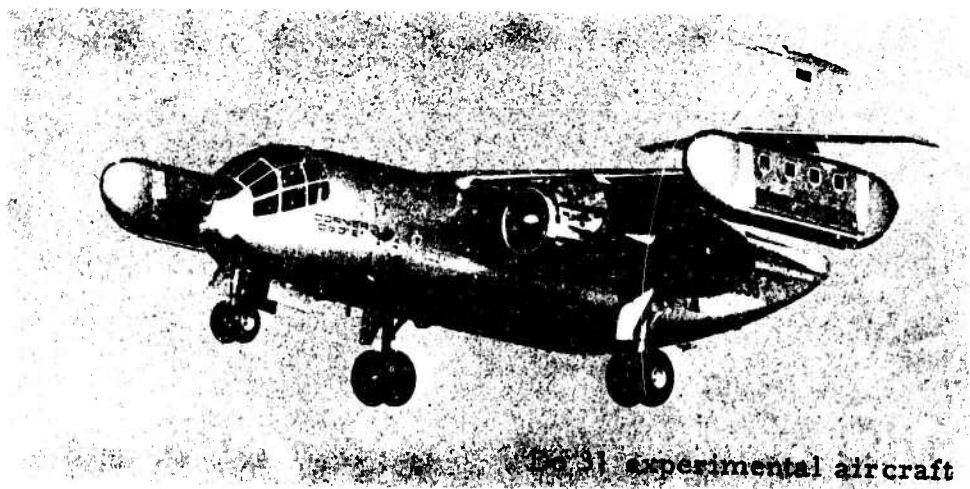
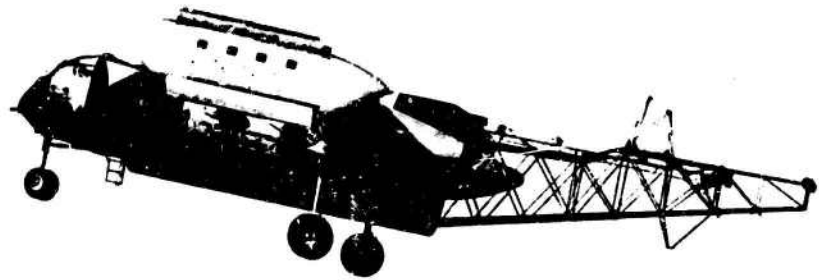
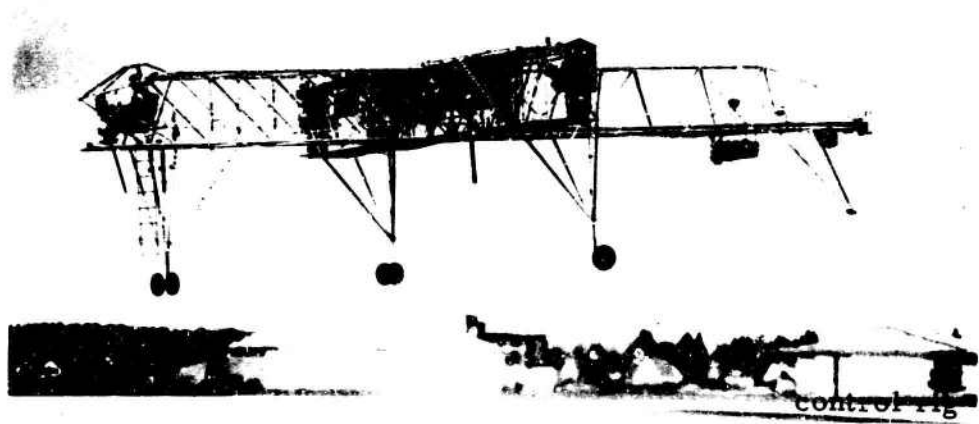


Fig. 16 Do 31 Experimental program

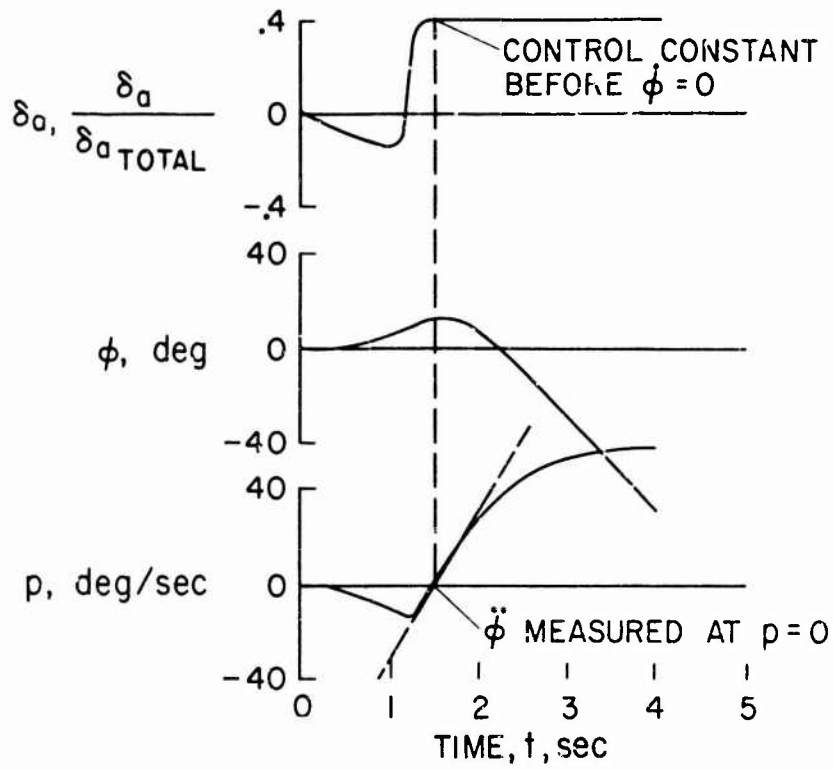
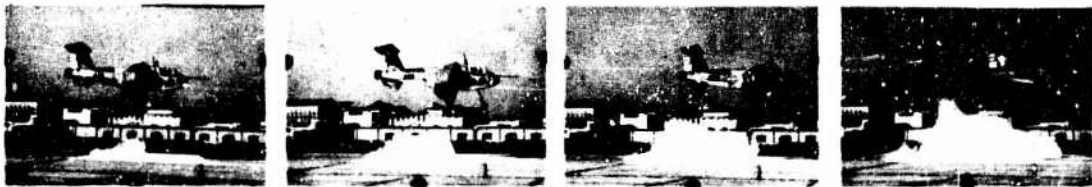
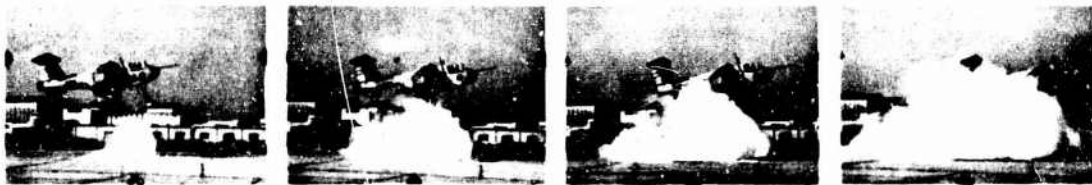


Figure 17



(a) 24 knots; 1.8 PROPELLER DIAMETERS ABOVE GROUND; POWER FOR LEVEL FLIGHT; OUT OF GROUND EFFECT



(b) 8 knots; 1.8 PROPELLER DIAMETERS ABOVE GROUND; MAXIMUM POWER; OUT OF GROUND EFFECT



(c) 8 knots; 1.0 PROPELLER DIAMETER ABOVE GROUND; MAXIMUM POWER; IN GROUND EFFECT

Figure 18

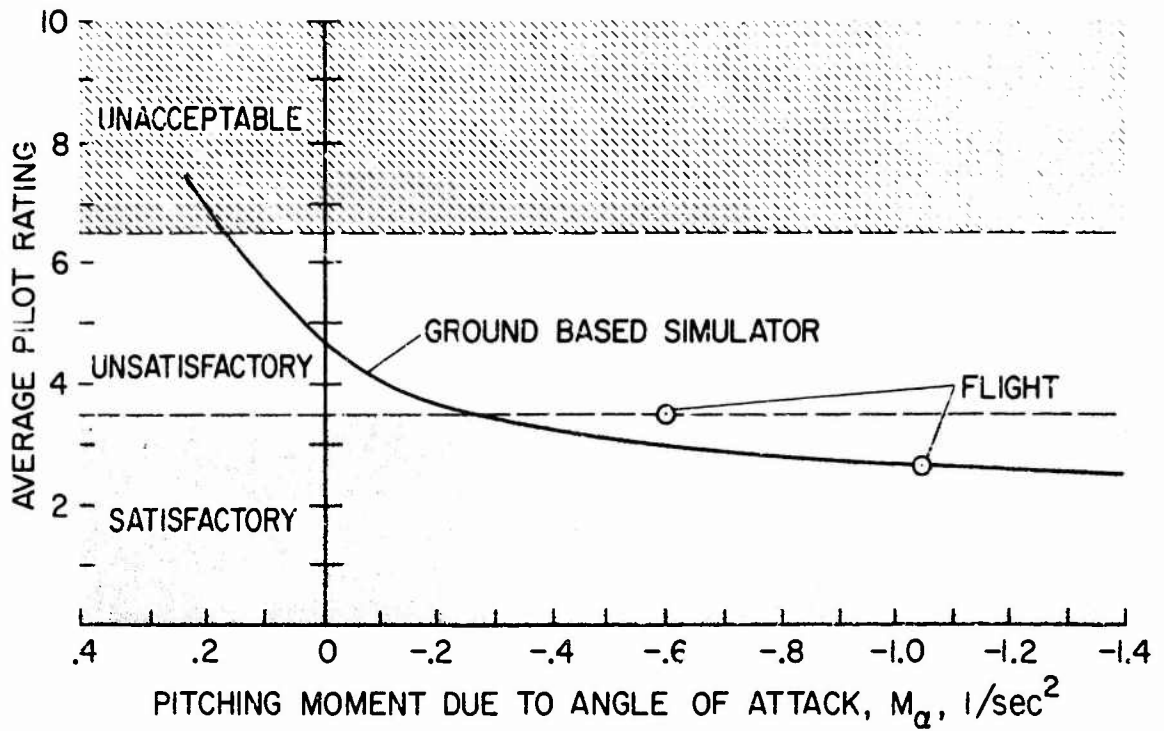


Figure 19

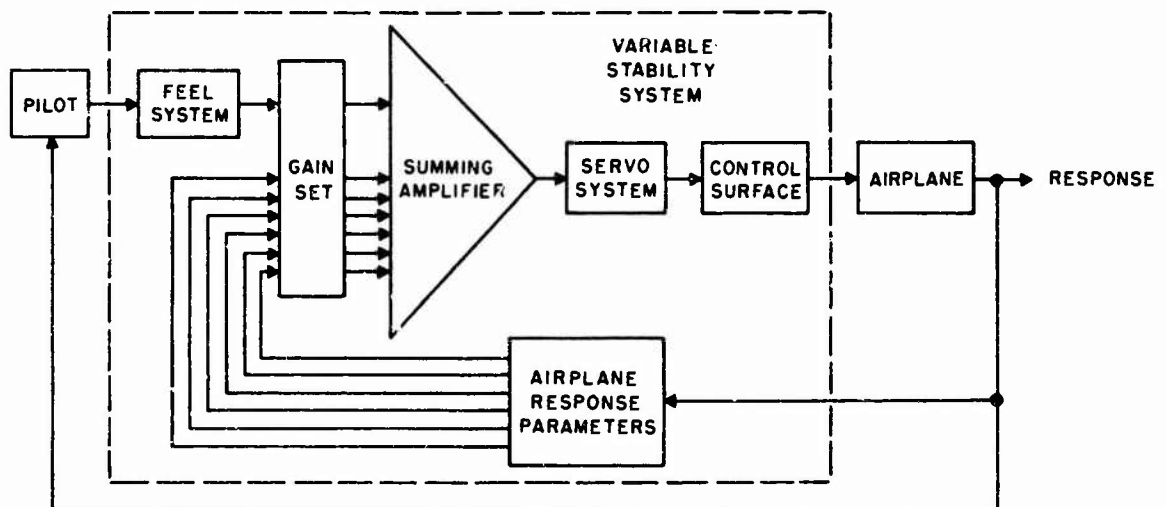


Fig.20 Basic loops of a variable stability system



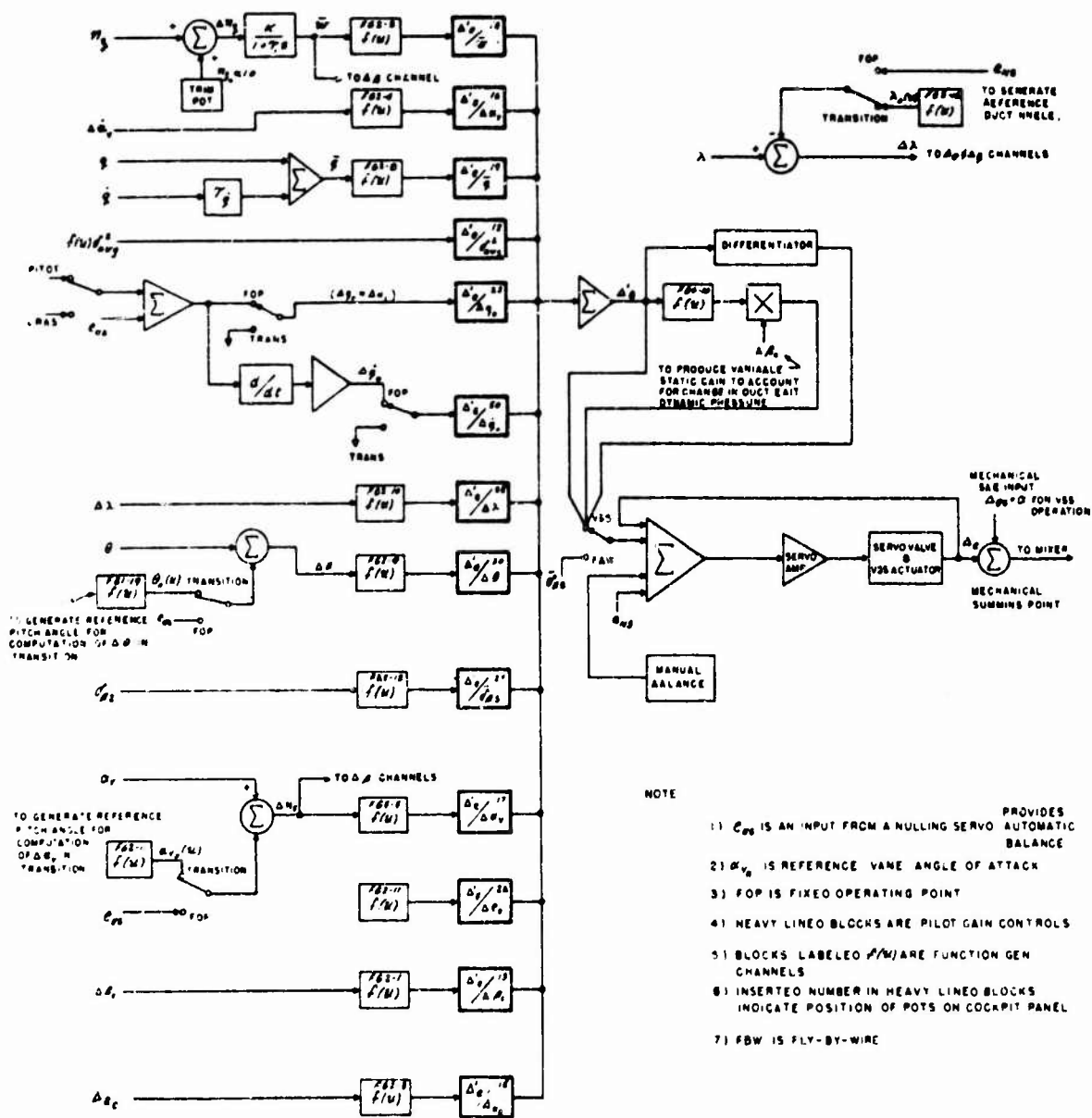


Fig.21 Variable stability and control system functional block diagram. Pitch control

	ADJECTIVE RATING	NUMERICAL RATING	DESCRIPTION	PRIMARY MISSION ACCOMPLISHED?	CAN BE LANDED
<b>NORMAL OPERATION</b>	Satisfactory	1	Excellent, includes optimum	Yes	Yes
		2	Good, pleasant to fly	Yes	Yes
		3	Satisfactory, but with some mildly unpleasant characteristics	Yes	Yes
<b>EMERGENCY OPERATION</b>	Unsatisfactory	4	Acceptable, but with unpleasant characteristics	Yes	Yes
		5	Unacceptable for normal operation	Doubtful	Yes
		6	Acceptable for emergency condition only*	Doubtful	Yes
<b>NO OPERATION</b>	Unacceptable	7	Unacceptable even for emergency condition *	No	Doubtful
		8	Unacceptable - dangerous	No	No
		9	Unacceptable - uncontrollable	No	No
		10	x!@...!! Did not get back to report	What mission?	

\*(Failure of a stability augments)

Fig. 22 Original pilot rating system

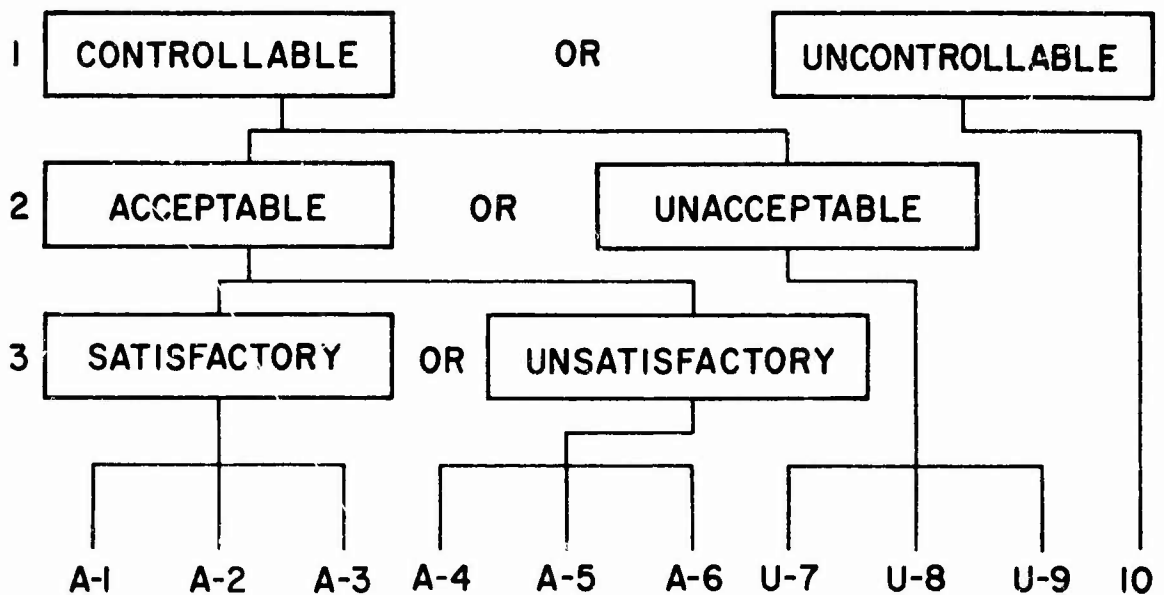


Fig. 23 Series of decisions leading to a rating

<p><u>EXCELLENT, HIGHLY DESIRABLE</u></p>	<p><u>SATISFACTORY</u> MEETS ALL REQUIREMENTS AND EXPECTATIONS. GOOD ENOUGH WITHOUT IMPROVEMENT. CLEARLY ADEQUATE FOR MISSION.</p>	<p><u>ACCEPTABLE</u> MAY HAVE DEFICIENCIES WHICH WARRANT IMPROVEMENT BUT ADEQUATE FOR MISSION.</p>	<p><u>CONTROL LABLE</u> CAPABLE OF BEING CONTROLLED OR MANAGED IN CONTEXT OF MISSION, WITH AVAILABLE PILOT ATTENTION.</p>	A1
<p><u>GOOD, PLEASANT, WELL BEHAVED</u></p>	<p><u>UNSATISFACTORY</u> RELUCTANTLY ACCEPTABLE DEFICIENCIES WHICH WARRANT IMPROVEMENT. PERFORMANCE ADEQUATE FOR MISSION WITH FEASIBLE PILOT COMPENSATION.</p>	<p><u>UNACCEPTABLE</u> DEFICIENCIES WHICH REQUIRE MANDATORY IMPROVEMENT. INADEQUATE PERFORMANCE FOR MISSION EVEN WITH MAXIMUM FEASIBLE PILOT COMPENSATION.</p>	<p><u>UNCONTROL LABLE</u> CONTROL WILL BE LOST DURING SOME PORTION OF MISSION</p>	A2
<p><u>FAIR, SOME MILDLY UNPLEASANT CHARACTERISTICS. GOOD ENOUGH FOR MISSION WITHOUT IMPROVEMENT.</u></p>	<p><u>UNSATISFACTORY</u> RELUCTANTLY ACCEPTABLE DEFICIENCIES WHICH WARRANT IMPROVEMENT. PERFORMANCE ADEQUATE FOR MISSION WITH FEASIBLE PILOT COMPENSATION.</p>	<p><u>UNACCEPTABLE</u> DEFICIENCIES WHICH REQUIRE MANDATORY IMPROVEMENT. INADEQUATE PERFORMANCE FOR MISSION EVEN WITH MAXIMUM FEASIBLE PILOT COMPENSATION.</p>	<p><u>UNCONTROL LABLE</u> CONTROL WILL BE LOST DURING SOME PORTION OF MISSION</p>	A3
<p><u>SOME MINOR BUT ANNOYING DEFICIENCIES. IMPROVEMENT IS REQUESTED. EFFECT ON PERFORMANCE IS EASILY COMPENSATED FOR BY PILOT.</u></p>	<p><u>UNSATISFACTORY</u> RELUCTANTLY ACCEPTABLE DEFICIENCIES WHICH WARRANT IMPROVEMENT. PERFORMANCE ADEQUATE FOR MISSION WITH FEASIBLE PILOT COMPENSATION.</p>	<p><u>UNACCEPTABLE</u> DEFICIENCIES WHICH REQUIRE MANDATORY IMPROVEMENT. INADEQUATE PERFORMANCE FOR MISSION EVEN WITH MAXIMUM FEASIBLE PILOT COMPENSATION.</p>	<p><u>UNCONTROL LABLE</u> CONTROL WILL BE LOST DURING SOME PORTION OF MISSION</p>	A4
<p><u>MODERATELY OBJECTIONABLE DEFICIENCIES. IMPROVEMENT IS NEEDED. REASONABLE PERFORMANCE REQUIRES CONSIDERABLE PILOT COMPENSATION.</u></p>	<p><u>UNSATISFACTORY</u> RELUCTANTLY ACCEPTABLE DEFICIENCIES WHICH WARRANT IMPROVEMENT. PERFORMANCE ADEQUATE FOR MISSION WITH FEASIBLE PILOT COMPENSATION.</p>	<p><u>UNACCEPTABLE</u> DEFICIENCIES WHICH REQUIRE MANDATORY IMPROVEMENT. INADEQUATE PERFORMANCE FOR MISSION EVEN WITH MAXIMUM FEASIBLE PILOT COMPENSATION.</p>	<p><u>UNCONTROL LABLE</u> CONTROL WILL BE LOST DURING SOME PORTION OF MISSION</p>	A5
<p><u>VERY OBJECTIONABLE DEFICIENCIES. MAJOR IMPROVEMENTS ARE NEEDED. REQUIRES BEST AVAILABLE PILOT COMPENSATION TO ACHIEVE ACCEPTABLE PERFORMANCE.</u></p>	<p><u>UNSATISFACTORY</u> RELUCTANTLY ACCEPTABLE DEFICIENCIES WHICH WARRANT IMPROVEMENT. PERFORMANCE ADEQUATE FOR MISSION WITH FEASIBLE PILOT COMPENSATION.</p>	<p><u>UNACCEPTABLE</u> DEFICIENCIES WHICH REQUIRE MANDATORY IMPROVEMENT. INADEQUATE PERFORMANCE FOR MISSION EVEN WITH MAXIMUM FEASIBLE PILOT COMPENSATION.</p>	<p><u>UNCONTROL LABLE</u> CONTROL WILL BE LOST DURING SOME PORTION OF MISSION</p>	A6
<p><u>MAJOR DEFICIENCIES WHICH REQUIRE MANDATORY IMPROVEMENT FOR ACCEPTANCE. CONTROL LABLE. PERFORMANCE INADEQUATE FOR MISSION, OR PILOT COMPENSATION REQUIRED FOR MINIMUM ACCEPTABLE PERFORMANCE IN MISSION IS TOO HIGH.</u></p>	<p><u>UNSATISFACTORY</u> RELUCTANTLY ACCEPTABLE DEFICIENCIES WHICH WARRANT IMPROVEMENT. PERFORMANCE ADEQUATE FOR MISSION WITH FEASIBLE PILOT COMPENSATION.</p>	<p><u>UNACCEPTABLE</u> DEFICIENCIES WHICH REQUIRE MANDATORY IMPROVEMENT. INADEQUATE PERFORMANCE FOR MISSION EVEN WITH MAXIMUM FEASIBLE PILOT COMPENSATION.</p>	<p><u>UNCONTROL LABLE</u> CONTROL WILL BE LOST DURING SOME PORTION OF MISSION</p>	U7
<p><u>CONTROL LABLE WITH DIFFICULTY. REQUIRES SUBSTANTIAL PILOT SKILL AND ATTENTION TO RETAIN CONTROL AND CONTINUE MISSION</u></p>	<p><u>UNSATISFACTORY</u> RELUCTANTLY ACCEPTABLE DEFICIENCIES WHICH WARRANT IMPROVEMENT. PERFORMANCE ADEQUATE FOR MISSION WITH FEASIBLE PILOT COMPENSATION.</p>	<p><u>UNACCEPTABLE</u> DEFICIENCIES WHICH REQUIRE MANDATORY IMPROVEMENT. INADEQUATE PERFORMANCE FOR MISSION EVEN WITH MAXIMUM FEASIBLE PILOT COMPENSATION.</p>	<p><u>UNCONTROL LABLE</u> CONTROL WILL BE LOST DURING SOME PORTION OF MISSION</p>	U8
<p><u>MARGINALLY CONTROL LABLE IN MISSION. REQUIRES MAXIMUM AVAILABLE PILOT SKILL AND ATTENTION TO RETAIN CONTROL.</u></p>	<p><u>UNSATISFACTORY</u> RELUCTANTLY ACCEPTABLE DEFICIENCIES WHICH WARRANT IMPROVEMENT. PERFORMANCE ADEQUATE FOR MISSION WITH FEASIBLE PILOT COMPENSATION.</p>	<p><u>UNACCEPTABLE</u> DEFICIENCIES WHICH REQUIRE MANDATORY IMPROVEMENT. INADEQUATE PERFORMANCE FOR MISSION EVEN WITH MAXIMUM FEASIBLE PILOT COMPENSATION.</p>	<p><u>UNCONTROL LABLE</u> CONTROL WILL BE LOST DURING SOME PORTION OF MISSION</p>	U9
<p><u>UNCONTROL LABLE IN MISSION.</u></p>	<p><u>UNSATISFACTORY</u> RELUCTANTLY ACCEPTABLE DEFICIENCIES WHICH WARRANT IMPROVEMENT. PERFORMANCE ADEQUATE FOR MISSION WITH FEASIBLE PILOT COMPENSATION.</p>	<p><u>UNACCEPTABLE</u> DEFICIENCIES WHICH REQUIRE MANDATORY IMPROVEMENT. INADEQUATE PERFORMANCE FOR MISSION EVEN WITH MAXIMUM FEASIBLE PILOT COMPENSATION.</p>	<p><u>UNCONTROL LABLE</u> CONTROL WILL BE LOST DURING SOME PORTION OF MISSION</p>	10

Fig. 24 Revised pilot rating scale

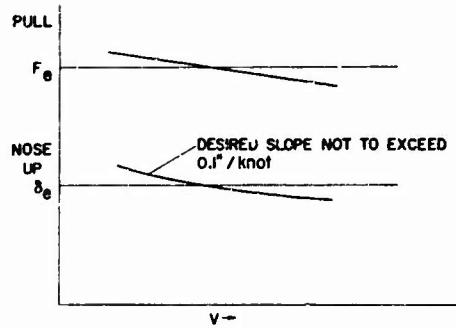


Fig. 25 Longitudinal stability characteristics. Low speed

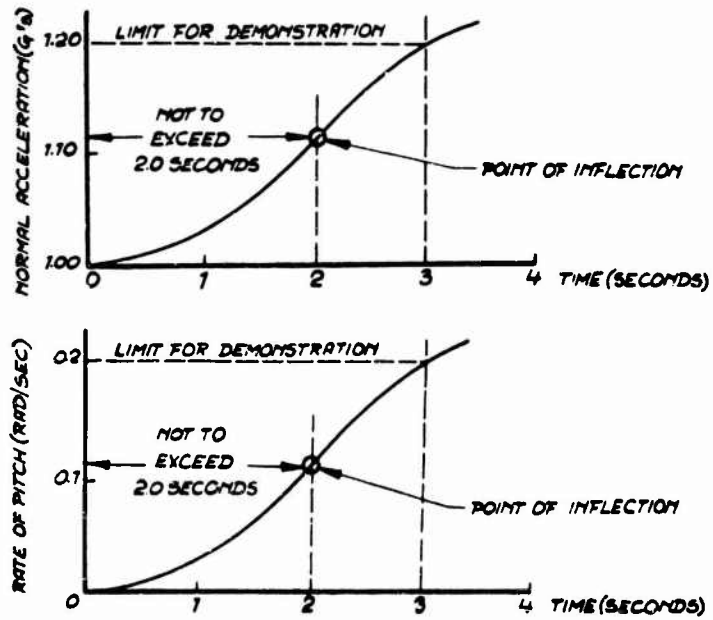


Figure 26

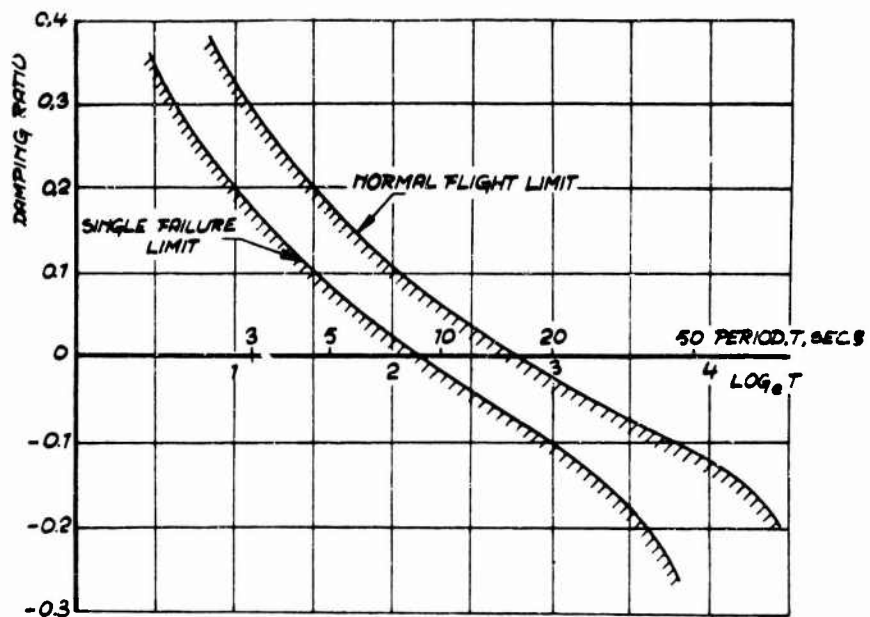


Figure 27

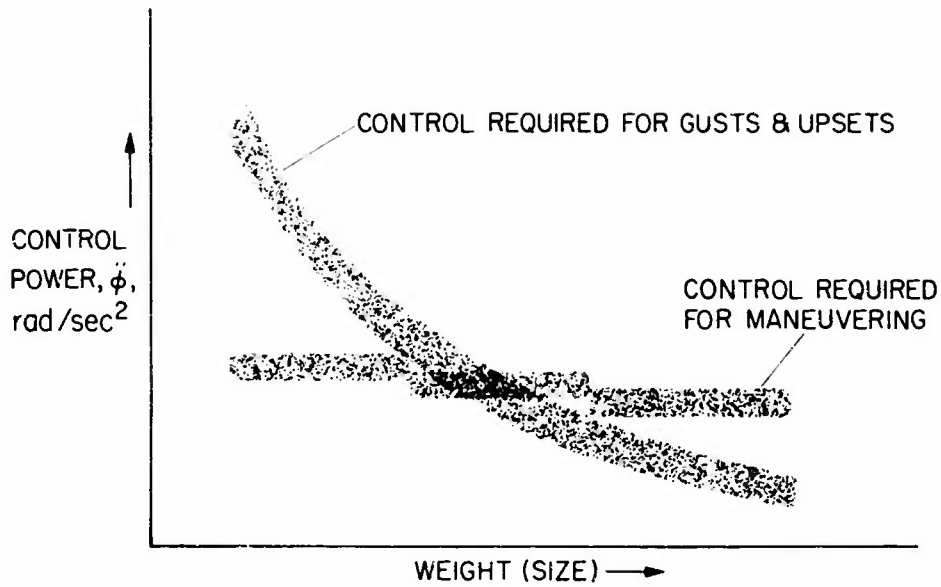


Fig. 28 Control power trends with weight

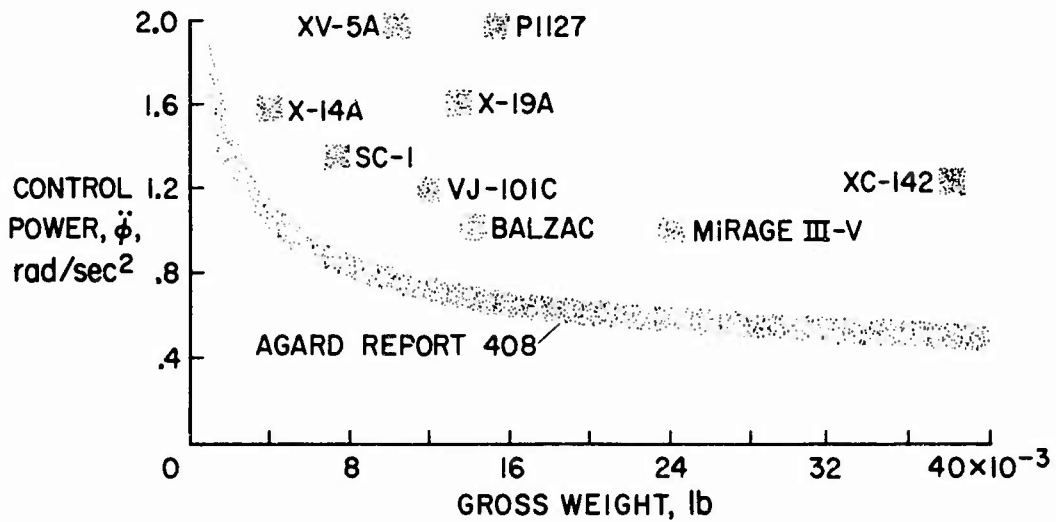


Fig. 29 Comparison of VTOL aircraft roll control power with AGARD requirement

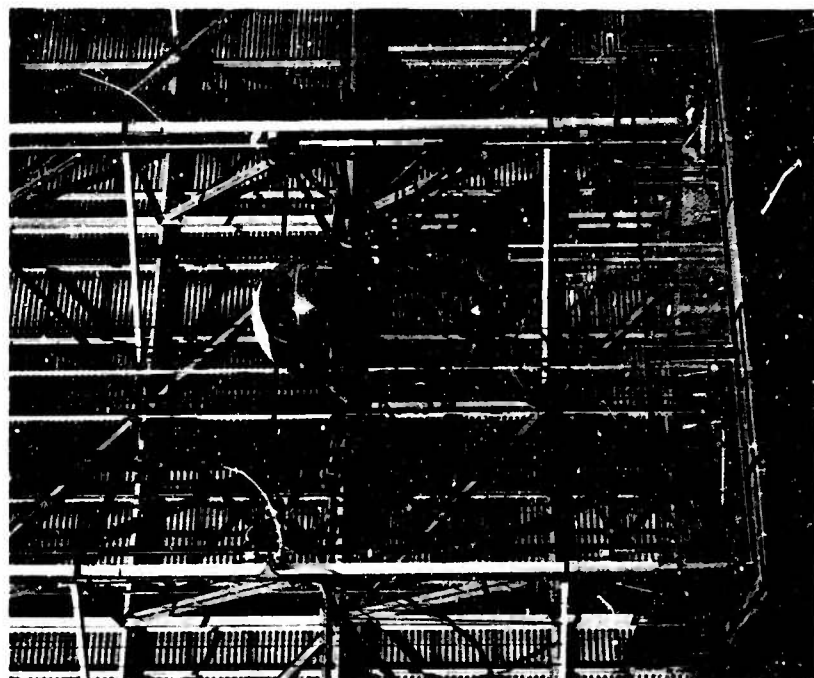


Figure 31

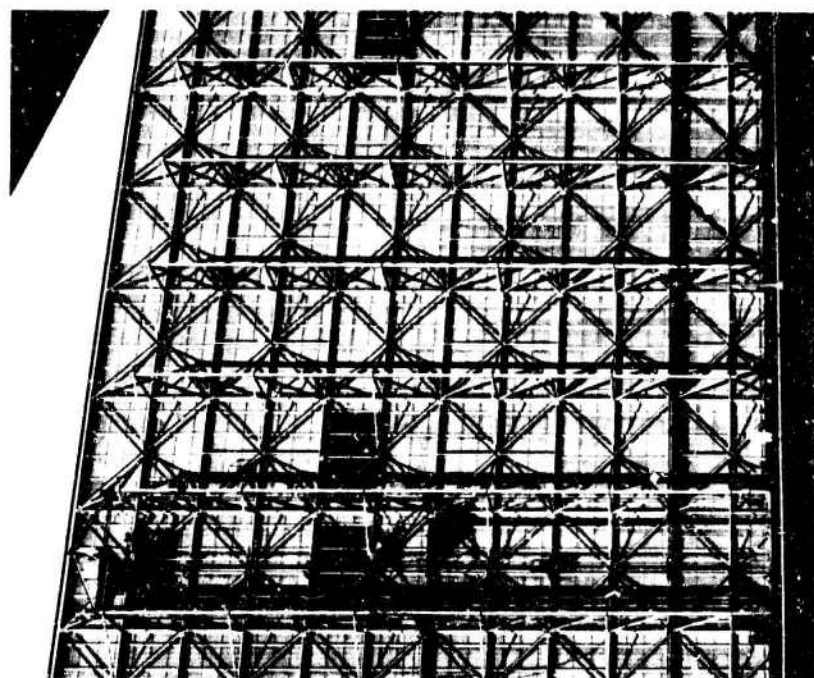


Figure 30

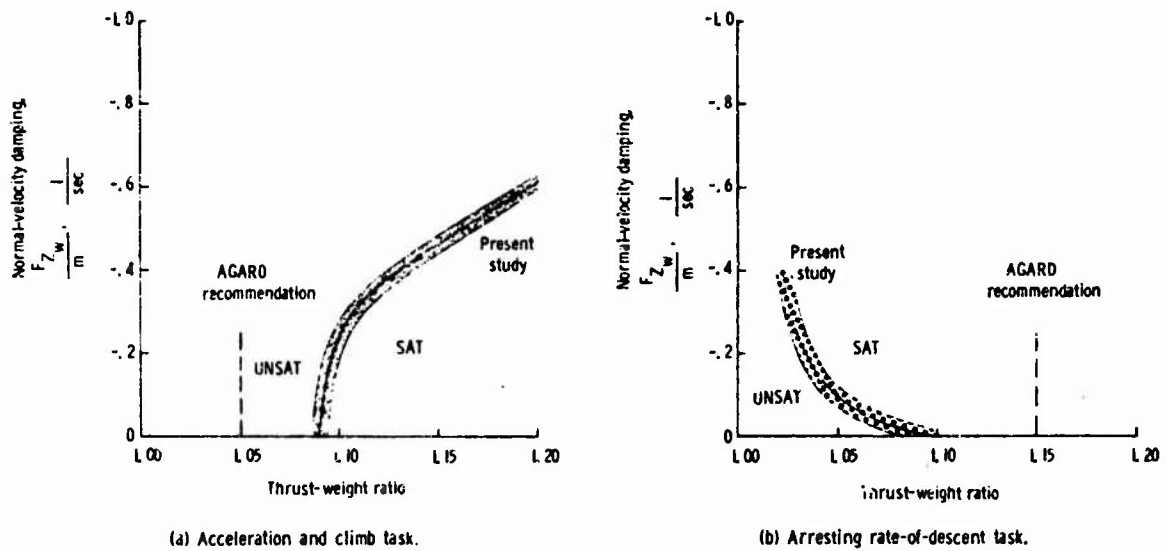


Fig. 32 Comparison of thrust-weight results with current criteria

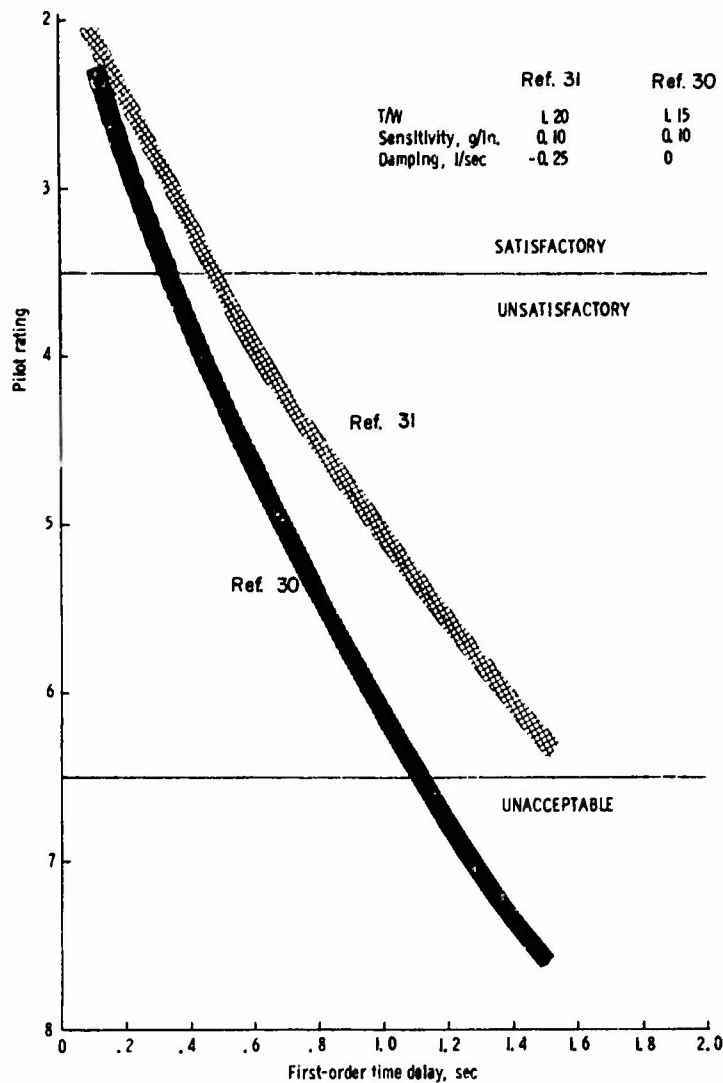


Fig. 33 Variation of pilot rating with thrust response time delay for vertical touchdowns

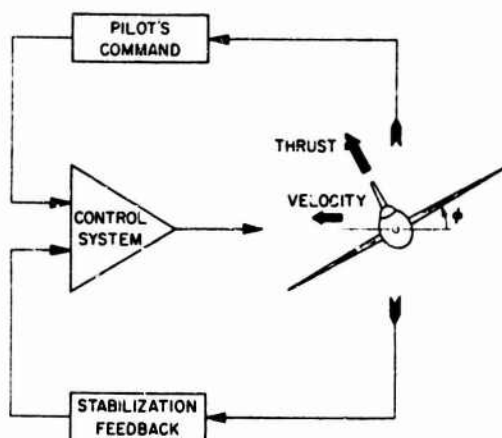


Fig. 34 VTOL control systems using attitude change for horizontal translation

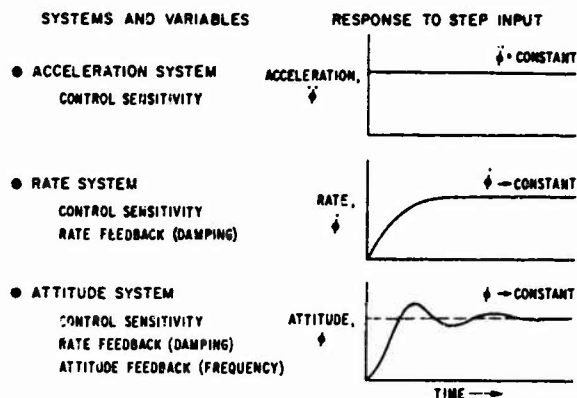


Fig. 35 Types of systems tested. All systems linear

- CALM AIR (NO GUSTS, CROSSWINDS, OR GROUND EFFECT)
- IDEAL SYSTEMS (NO ACTUATOR DYNAMICS, ETC.)
- NO GYROSCOPICS OR CROSS COUPLING
- CONSTANT CONTROL GEOMETRY

	MAXIMUM CONTROL DEFLECTION, in.	FORCE GRADIENT, lb/in.	BREAKOUT FRICTION, lb	
ROLL	±5	1.8	1	} CENTER STICK
PITCH	±5	1.8	1	
YAW	±2.5	0	6	} RUDDER PEDALS
THRUSTLE	FIGHTER TYPE QUADRANT			

Fig. 36 Test conditions

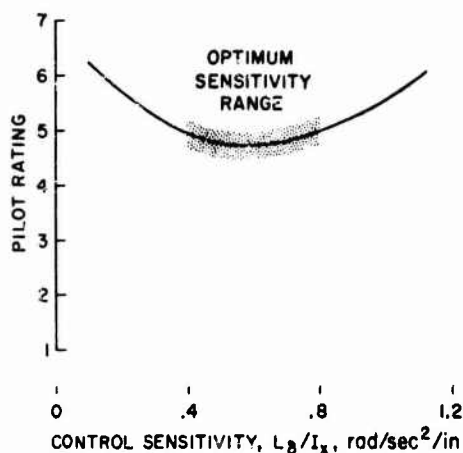


Fig. 37 Acceleration system. Effect of control sensitivity on pilot rating



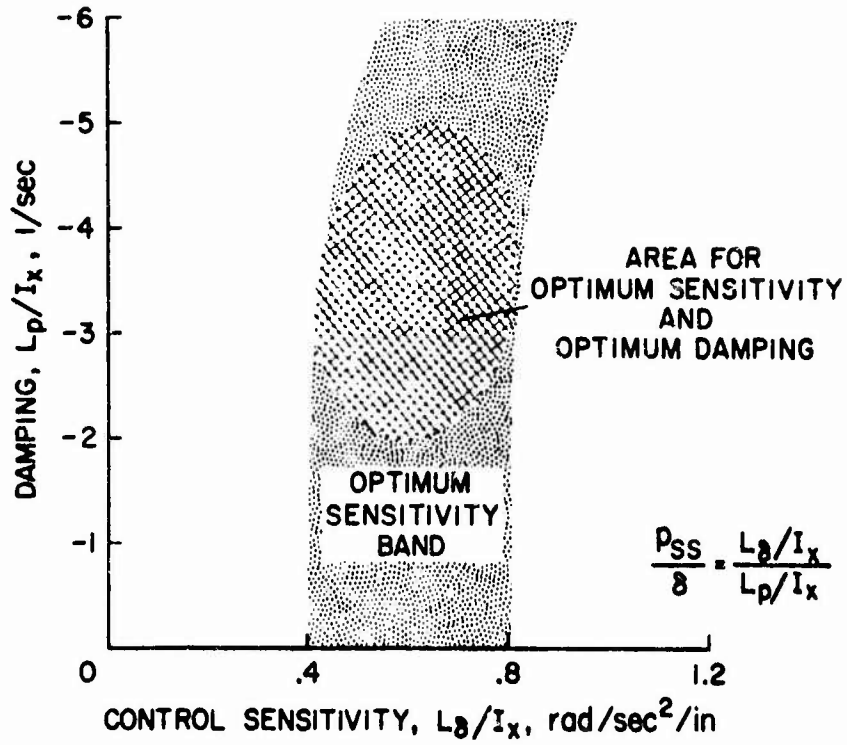


Fig. 38 Rate systems. Variation of optimum control sensitivity with damping (including range of optimum damping)

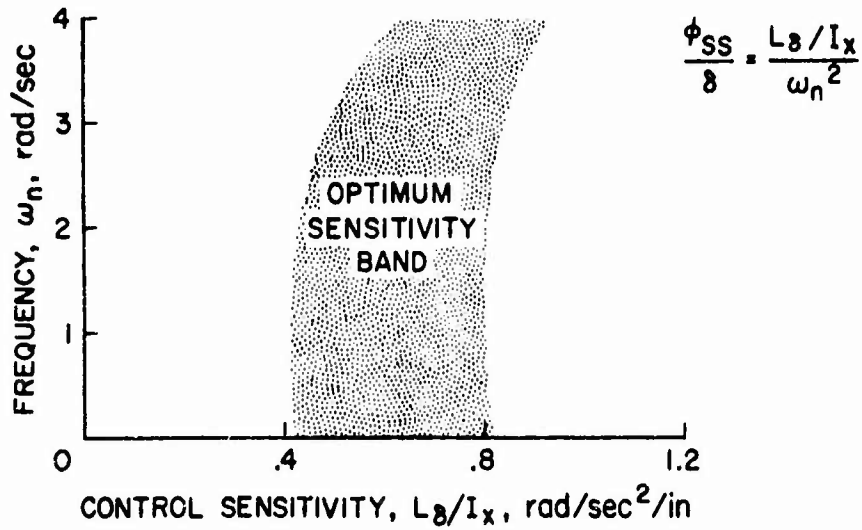


Fig. 39 Attitude systems. Variation of optimum control sensitivity with frequency

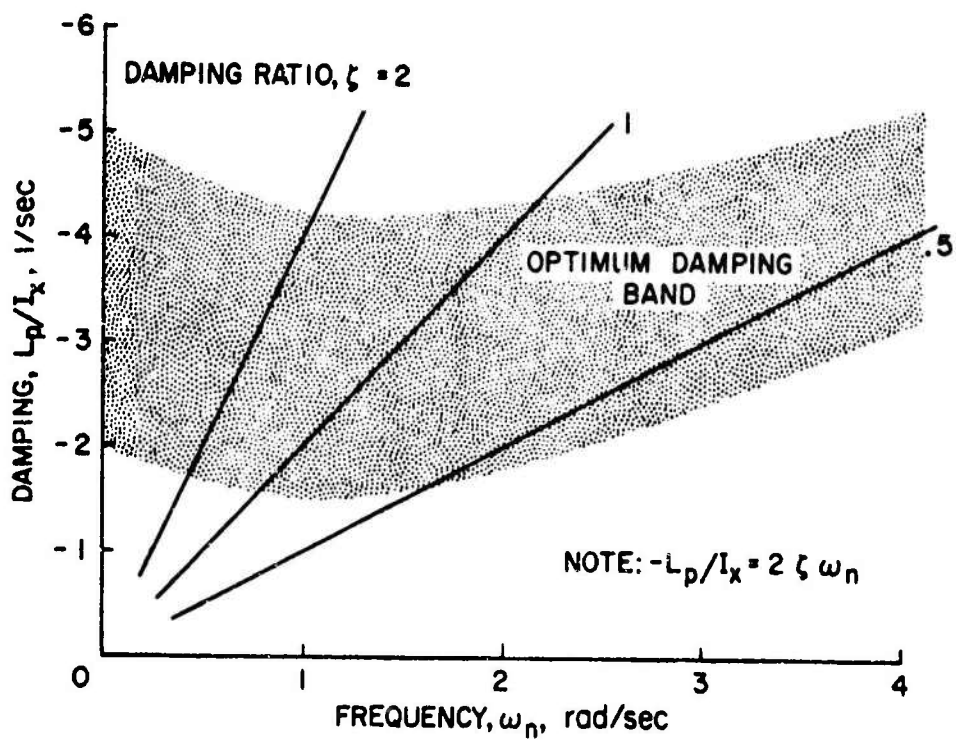


Fig.40 Attitude systems. Variation of optimum damping with frequency

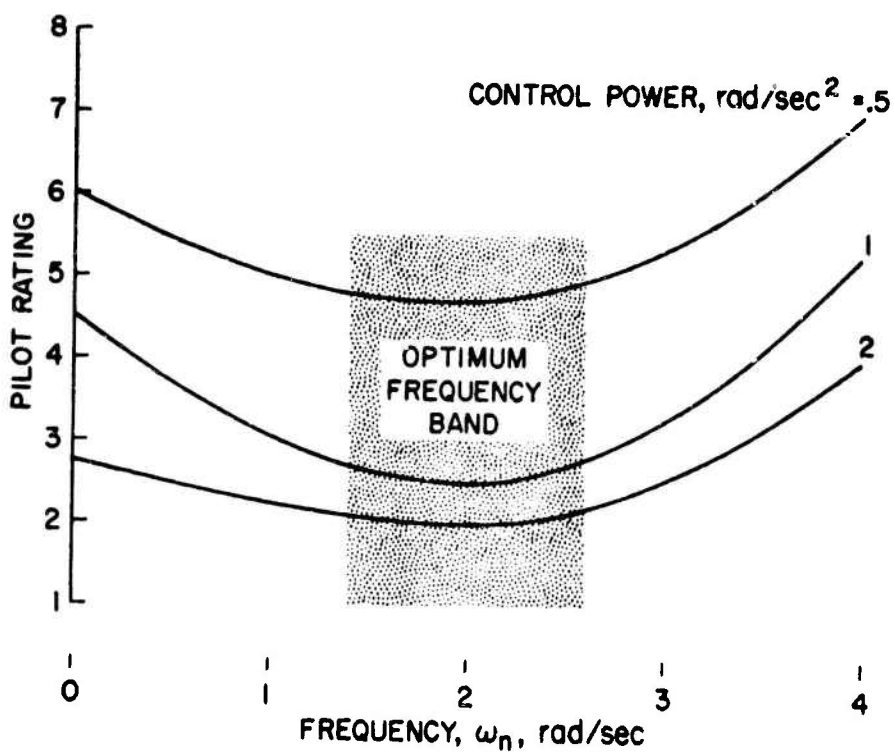


Fig.41 Attitude systems. Determination of optimum frequency

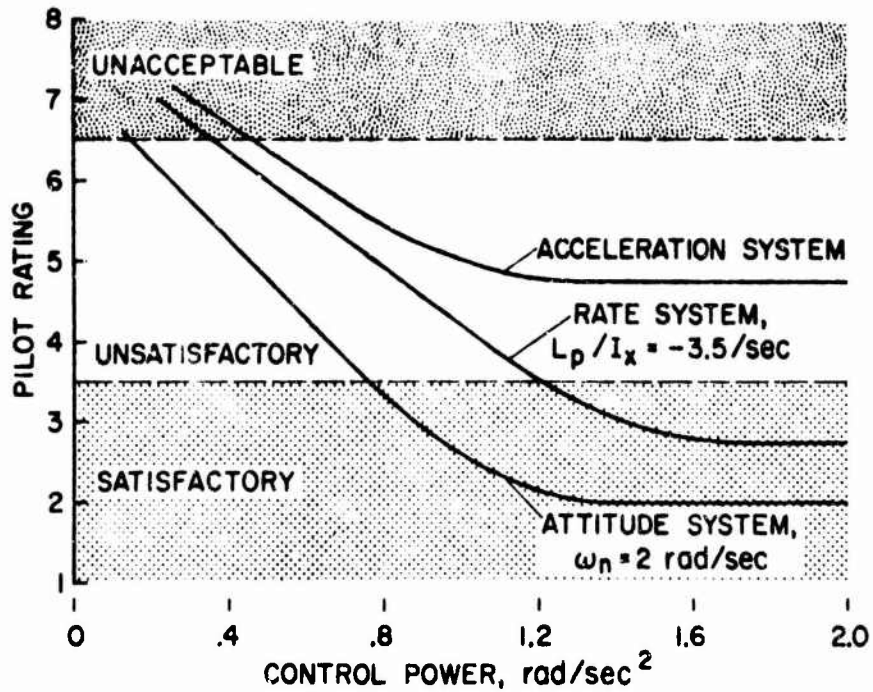


Fig. 42 Comparison of the acceleration, rate and attitude systems. Linear systems with all variables optimized

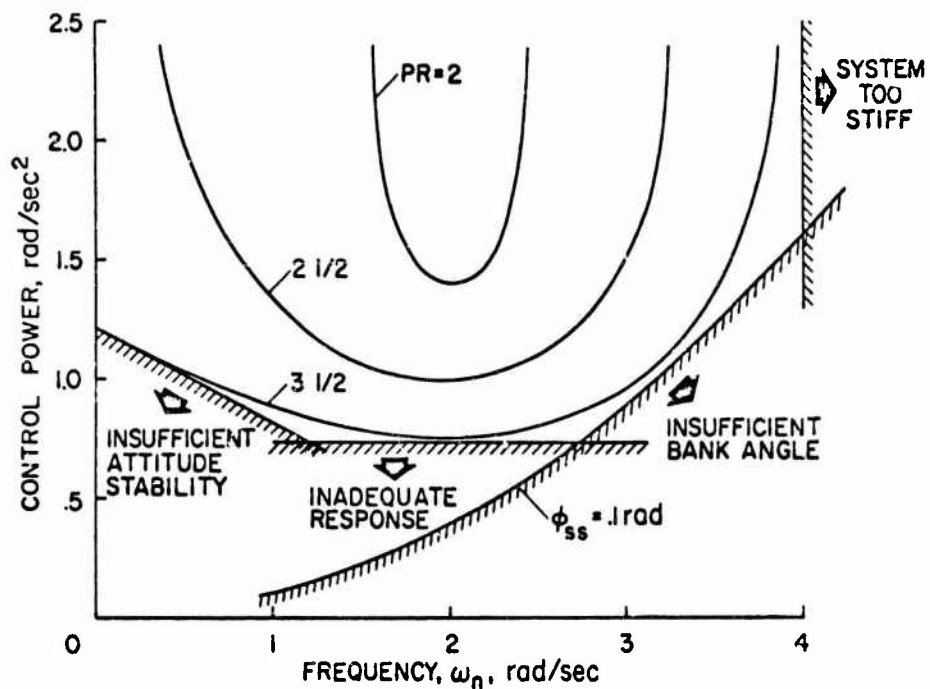


Fig. 43 Attitude systems. Factors affecting control power requirements

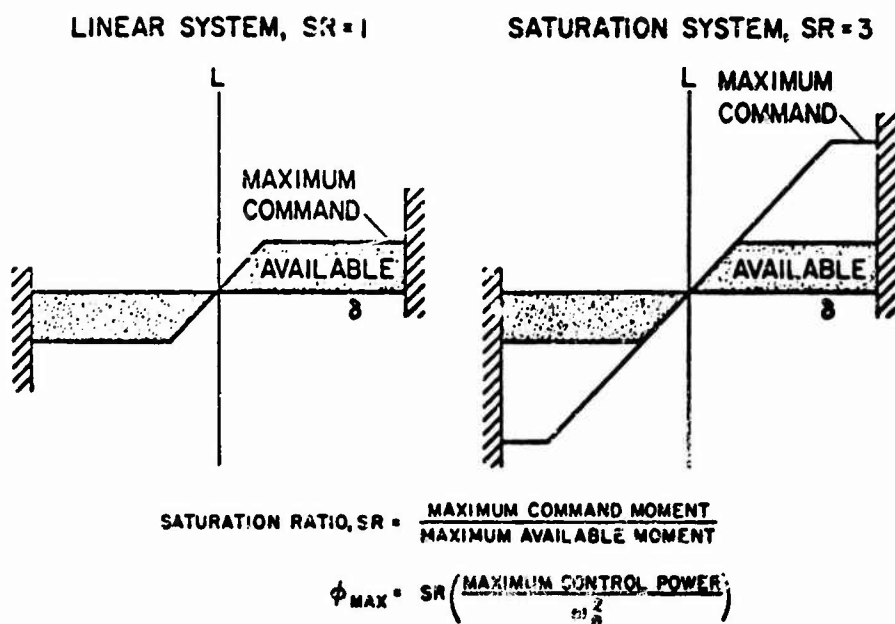


Fig.44 Description of saturation control. Moment versus control deflection

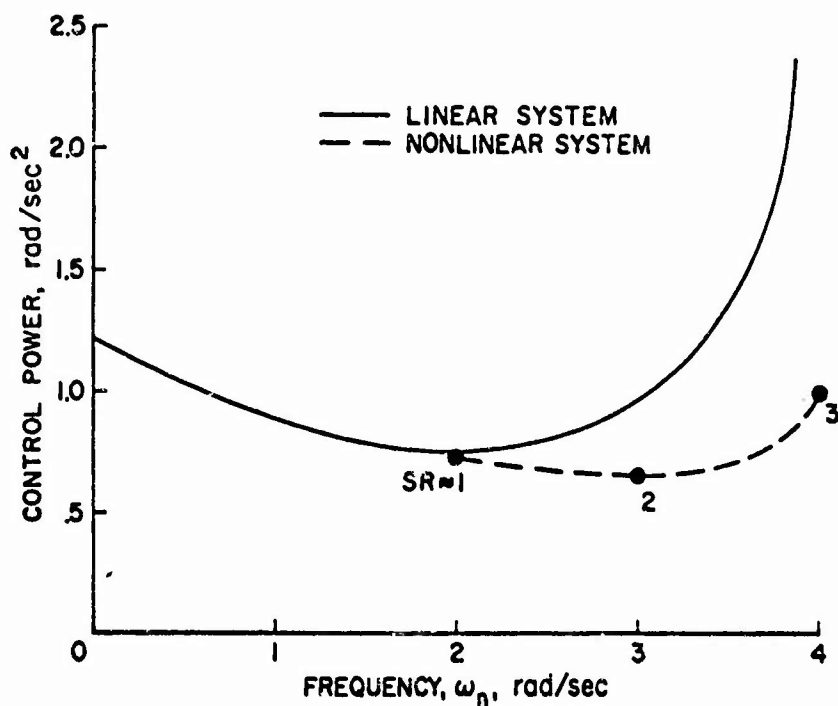


Fig.45 Attitude systems. Effect of saturation-type nonlinearity on control power required for  $PR = 3\frac{1}{2}$

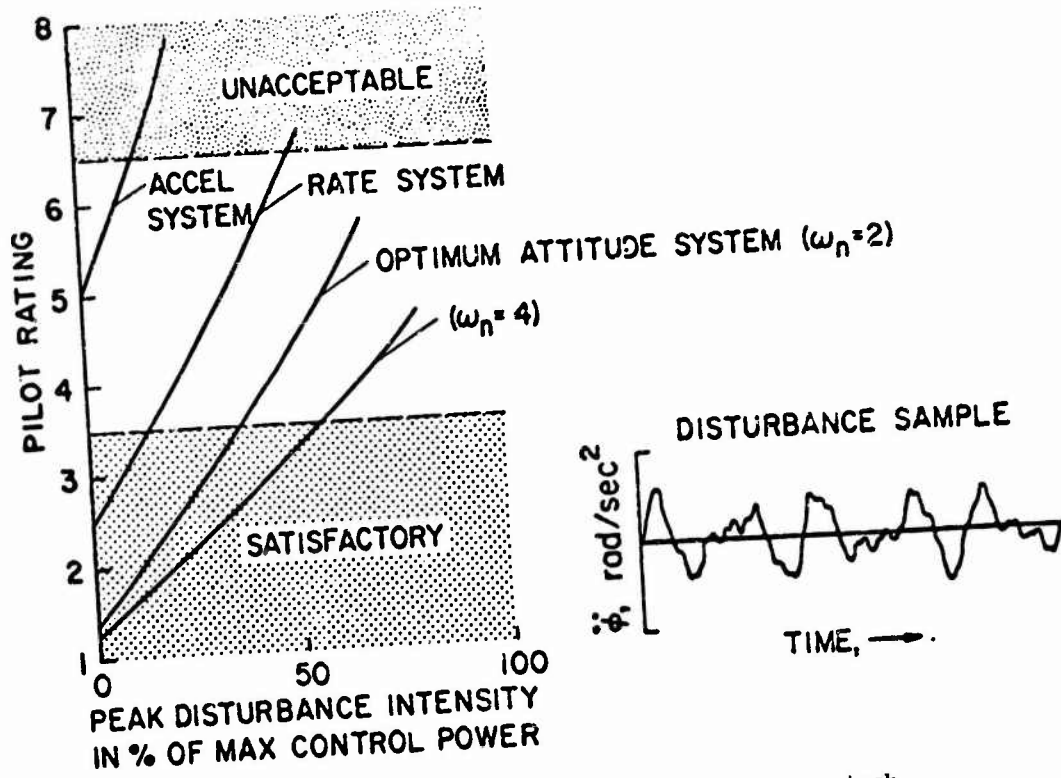


Fig. 46 Effect of disturbance. Precision hover task

Information regarding the availability of further copies of AGARD publications may be obtained from

The Scientific Publications Officer,  
Advisory Group for Aerospace Research and Development,  
7, rue Ancelle,  
92 Neuilly-sur-Seine,  
France.